

Development of Homogeneous First Row Metal Catalysts
(Fe, Mn, Co) For Organic Transformations and Bond Activation

By

Chandrani Ghosh

A Dissertation Presented in Partial Fulfillment
of the Requirements for the Degree of
Doctor of Philosophy

Approved July 2018 by the
Graduate Supervisory Committee

Ryan J. Trovitch, Chair
Don Seo
Ana Moore

Arizona State University
August 2018

ABSTRACT

Transition metals have been extensively employed to address various challenges related to catalytic organic transformations, small molecule activation, and energy storage over the last few decades. Inspired by recent catalytic advances mediated by redox non-innocent pyridine diimine (PDI) and α -diimine (DI) ligand supported transition metals, our group has designed new PDI and DI ligands by modifying the imine substituents to feature donor atoms. My doctoral research is focused on the development of PDI and DI ligand supported low valent first row metal complexes (Mn, Fe, Co) and their application in bond activation reactions and the hydrofunctionalization of unsaturated bonds.

First two chapters of this dissertation are centered on the synthesis and application of redox non-innocent ligand supported low valent iron complexes. Notably, reduction of a DI-based iron dibromide led to the formation of a low valent iron dinitrogen compound. This compound was found to undergo a sequential C-H and C-P bond activation processes upon heating to form a dimeric compound. The plausible mechanism for dimer formation is also described here.

Inspired by the excellent carbonyl hydrosilylation activity of our previously reported Mn catalyst, ($^{\text{Ph}_2\text{PPr}}$ PDI)Mn, attempts were made to synthesize second generation Mn catalyst, which is described in the third chapter. Reduction of ($^{\text{PyEt}}$ PDI)MnCl₂ furnished a deprotonated backbone methyl group containing Mn compound [$^{\text{PyEt}}$ PDEA)Mn] whereas reduction of ($^{\text{Ph}_2\text{PEt}}$ PDI)MnCl₂ produced a dimeric compound, [$^{\text{Ph}_2\text{PEt}}$ PDI)Mn]₂. Both compounds were characterized by NMR spectroscopy and XRD analysis. Hydrosilylation of aldehydes and ketones have been studied using [$^{\text{PyEt}}$ PDEA)Mn] as a pre-catalyst. Similarly, 14 different aldehydes and 6 different

formates were successfully hydrosilylated using $[(^{\text{Ph}_2\text{PEt}}\text{PDI})\text{Mn}]_2$ as a pre-catalyst.

Encouraged by the limited number of cobalt catalysts for nitrile hydroboration, we sought to develop a cobalt catalyst that is active for hydroboration under mild conditions, which is discussed in the last chapter. Treatment of $(^{\text{PyEt}}\text{PDI})\text{CoCl}_2$ with excess NaEt_3BH furnished a diamagnetic Co(I) complex $[(^{\text{PyEt}}\text{PDIH})\text{Co}]$, which exhibits a reduced imine functionality. Having this compound characterized, a broad substrate scope for both nitriles and imines have been investigated. The operative mechanism for nitrile dihydroboration has been investigated based on the outcomes of a series of stoichiometric reactions using NMR spectroscopy.

Dedicated to

*My parents
Nisit Kumar Ghosh
&
Bina Ghosh*

ACKNOWLEDGMENTS

From the beginning of my doctoral research journey, I met many great people who made this work successfully accomplished. First and foremost, I would like to strongly acknowledge my advisor Prof. Ryan J. Trovitch for his continual support. He is very approachable and always willing to answer my question even during his busy schedules. He directed and inspired me towards the new projects one after another. With his intelligence, critical thinking he always motivates me to pursuing my future career in science. Besides the research work in the lab, he also put lots of effort to improve my writing, presentation and professional skills, which led this dissertation and defense presentation in a successful direction. It is my pleasure that I joined his research lab and got a chance to work with him.

I would like to thank our crystallographer at School of Molecular Sciences, Dr. Thomas L. Groy without whom, many structural questions related my synthesized compounds would have been unanswered. Throughout my research, he helped me always with solving the crystal structures and teaching me the entire single crystal X-ray diffraction technique with patience. I would like to thank also Dr. Marco Flores for his input on EPR experiments related to my manganese projects. I am also thankful to Dr. Brian Cherry for his help in running different NMR experiments and also his insight on the outcomes the experimental results. I am fortunate to have Prof. Don Seo and Prof Ana Moore as my Ph.D. committee members who put lots of insights on my dissertation and also Prof. Anne K. Jones and Prof. George Wolf as my oral examination committee members.

Additionally, there is a list of other scientists outside the Arizona State University who made a significant contribution in my work. I would like to acknowledge Prof. Amanda C. Bowman at Colorado College for her time to perform DFT calculations on the iron compounds, in my first paper. I am also thankful to Prof. Paul Chirik for giving the opportunity to perform Mössbauer experiments on my iron compounds in his lab and especially, his student Dr. Jamie Neely who actually ran those experiments in Princeton University.

During my tenure of doctoral research, I had talented lab mates who are always being supportive. My special thanks to Dr. Tufan K. Mukhopadhyay and Dr. Raja Pal who taught me many experimental designs and helped me with new ideas. I really appreciate their constant effort to encourage me.

Importantly, I would like to thank my parents whose constant encouragement is always with me even though staying far away from them. Throughout my career, they always inspire me to fulfill my dreams and never stopped me whatever I wanted to do. Their love and guidance motivated me and directed me in this successful platform. I am also thankful to my husband Dr. Tufan K. Mukhopadhyay who is always beside me either being a lab mate or being a mentor in my personal life.

TABLE OF CONTENTS

	Page
LIST OF TABLES	xii
LIST OF FIGURES	xiv
Introduction	xxvi
CHAPTER	
1. SYNTHESIS OF A DIIMINE-BASED IRON DINITROGEN COMPLEX AND ITS REACTIVITY TOWARDS C-H & C-P BONDS	
1.1 Abstract	1
1.2 Introduction	1
1.3 Synthesis and Characterization	2
1.4 Plausible Mechanism for Dimer Formation.....	21
1.5 Reactivity Study of 2	22
1.6 Reactivity Study of 3	27
1.7 Conclusion	31
1.8 Experimental Procedure	31
1.8.1 General Considerations.....	31
1.8.2 X-ray Crystallography	32
1.8.3 DFT Calculation	32
1.8.4 Preparation of (^{Ph₂PPr} DI)FeBr ₂ (1)	33
1.8.5 Preparation of (^{Ph₂PPr} DI)Fe(N ₂) (2).....	33
1.8.6 Preparation of [(μ-PrPPh-κ ⁵ -P,N,N,C _γ ,P- ^{Ph₂PPr} DI ^{PrPPh})Fe] ₂ (3).....	35
1.9 References	39

CHAPTER	Page
2. SYNTHESIS OF REDOX ACTIVE LIGAND SUPPORTED IRON COMPLEXES	
2.1 Abstract	41
2.2 Introduction	42
2.3 Synthesis and Characterization	45
2.4 Conclusion	73
2.5 Experimental Section	74
2.5.1 Preparation of $^{\text{Ph}_2\text{PPr}}\text{DIFe}(\text{CO})_2$ (4).....	74
2.5.2 Preparation of $^{\text{Ph}_2\text{PPr}}\text{DIFe}(\text{CO})$ (5).....	75
2.5.3 Preparation of $(^{\text{tBu}_2\text{PPr}}\text{DI})\text{FeBr}_2$ (7)	76
2.5.4 Preparation of $(^{\text{tBu}_2\text{PPr}}\text{DI})\text{FeBr}$ (8)	76
2.5.5 Preparation of $(^{\text{tBu}_2\text{PPr}}\text{DI})\text{Fe}(\text{CO})_2$ (9).....	77
2.5.6 Preparation of $[(^{\text{Ph}_2\text{PPr}}\text{PDI})\text{Fe}(\text{Br})][\text{Br}]$ (10)	77
2.5.7 Preparation of $(^{\text{Ph}_2\text{PPr}}\text{PDI})\text{Fe}$ (11)	78
2.5.8 Preparation of $[(^{\text{Ph}_2\text{PPr}}\text{PDI})\text{Fe}(\text{H})][\text{BF}_4]$ (12)	79
2.5.9 Preparation of $(^{\text{Ph}_2\text{PEt}}\text{PDI})\text{Fe}$ (14)	79
2.6 References.....	80
3. DEVELOPMENT OF REDOX ACTIVE LIGAND BASED MANGANESE CATALYSTS FOR CARBONYL HYDROSILYLATION	
3.1 Abstract	83
3.2 Introduction.....	84
3.3 Synthesis and Characterization of 15 and 16	85
3.4 Synthesis and Characterization of 17 and 18	93

CHAPTER	Page
3.5 Catalytic Hydrosilylation Activity of 16	98
3.6 Catalytic Hydrosilylation Activity of 18	105
3.7 Conclusion	112
3.8 Experimental Section	113
3.8.1 General Considerations	113
3.8.2 X-ray Crystallography	114
3.8.3 Electron Paramagnetic Resonance Spectroscopy	115
3.8.4 Preparation of (^{PyEt} PDI)MnCl ₂ (15)	116
3.8.5 Preparation of (^{PyEt} PDEA)Mn (16)	117
3.8.6 Catalytic Trials Using Complex 16.....	118
3.8.7 Catalytic Trials Using Complex 18.....	162
3.9 References	202
4. A HIGHLY EFFICIENT COBALT CATALYST FOR NITRILE AND IMINE HYDROBORATION	
4.1 Abstract	207
4.2 Introduction	207
4.3 Synthesis and Characterization	210
4.4 Catalytic Dihydroboration of Nitriles	215
4.5 Catalytic Hydroboration of Imines	218
4.6 Mechanistic Study.....	222
4.7 Conclusion	229
4.8 Experimental Sections	229

CHAPTER	Page
4.8.1 Preparation of (^{PyEt} PDI)CoCl ₂ (19).....	229
4.8.2 Preparation of (^{PyEt} PDIH)Co (20).....	230
4.8.3 Catalytic Nitrile Dihydroboration Using Complex 20.....	231
4.8.4 Catalytic Imine Hydroboration Using Complex 20.....	275
4.9 References	295
BIBLIOGRAPHY.	299
APPENDIX A	
Copyright and Permissions	310
BIOGRAPHICAL SKETCH	315

LIST OF TABLES

Table	Page
1.1 Mössbauer fit parameters for 1, 2 and 3	4
1.2 Notable bond lengths (Å) and bond angles (°) determined for 1	5
1.3 Notable bond lengths (Å) and bond angles (°) determined for 2	11
1.4 Notable bond lengths (Å) and bond angles (°) determined for 3	19
2.1 Notable bond lengths (Å) and bond angles (°) determined for 4	48
2.2 Notable bond lengths (Å) and bond angles (°) determined for 5.	51
2.3 Notable bond lengths (Å) and bond angles (°) determined for 8.	62
3.1 Notable bond lengths (Å) and bond angles (°) determined for 15.	89
3.2 Notable bond lengths (Å) and bond angles (°) determined for 16.	93
3.3 Parameters used to fit the EPR spectrum of 18 at 9.40 GHz and T = 107 K.....	97
3.4 Notable bond lengths (Å) and bond angles (°) determined for 18.	98
3.5 Hydrosilylation of aldehydes using 16 as a pre-catalyst.....	100
3.6 Hydrosilylation of ketones using 16 as a pre-catalyst	102
3.7 Neat carbonyl hydrosilylation using 0.02 mol% 16 as a pre-catalyst.....	104
3.8 Control experiments using cyclohexanone as the substrate.....	105
3.9 Neat hydrosilylation of aldehydes using 0.05 mol% of 18 as a pre-catalyst	107
3.10 Neat hydrosilylation of formates using 0.01 mol% of 18 as a pre-catalyst	109
3.11 Comparison of carbonyl hydrosilylation activity of first row transition metal catalysts.....	112

Table	Page
4.1 Notable bond lengths (Å) and bond angles (°) determined for 20.	215
4.2 Dihydroboration of nitriles using 20 as pre-catalyst.....	218
4.3 Hydroboration of imines with varied nitrogen substituents using 20 as a pre-catalyst.....	220
4.4 Hydroboration of imines with variable substituents at carbon side using pre-catalyst 20.....	221

LIST OF FIGURES

Figure	Page
1.1 ^1H NMR spectrum of 1 in chloroform- <i>d</i> at 23 °C.....	3
1.2 Zero-field Mössbauer spectrum of 1.....	3
1.3 The solid-state Structure of 1.	5
1.4 Mulliken spin density plot for 1 using the UKS (S = 2) solution.....	6
1.5 Orbital representations for 1 using the UKS (S = 2) solution.....	7
1.6 Orbital representations and Mulliken spin density plot of 1.....	8
1.7 ^1H NMR spectrum of 2 in benzene- <i>d</i> ₆ at 25 °C.....	9
1.8 ^{31}P NMR spectrum of 2 in benzene- <i>d</i> ₆ at 25 °C.....	10
1.9 Solid-state infrared spectrum of 2 in KBr.....	10
1.10 The solid-state structure of 2.....	11
1.11 Orbital representations for 2 UKS (S = 0) solution	13
1.12 Orbital representations (a) and spin density plot (b) for 2 BS(1,1) solution.....	14
1.13 Zero-field ^{57}Fe Mossbauer spectra of 2	15
1.14 ^1H NMR spectrum showing a mixture of <i>cisoid</i> -3 and <i>transoid</i> -3 in benzene- <i>d</i> ₆	16
1.15 ^{31}P NMR spectra showing a mixture of <i>cisoid</i> -3 and <i>transoid</i> -3 in benzene- <i>d</i> ₆ after 3 h and 7 d at 25 °C.....	17
1.16 ^1H NMR spectrum of <i>cisoid</i> -3 in benzene- <i>d</i> ₆ at 25 °C.....	18
1.17. ^{31}P NMR spectrum of <i>cisoid</i> -3 in benzene- <i>d</i> ₆ at 25 °C	18
1.18 The solid-state structure of <i>cisoid</i> -3.....	19
1.19 Zero-field ^{57}Fe Mössbauer spectra of 3	21
1.20 Plausible mechanistic pathways for the formation of 3.....	22

Figure	Page
1.21 ^1H NMR spectrum of the reaction of 2 with 1 atmosphere of H_2 in benzene- d_6 at room temperature after 2 h.....	23
Figure	Page
1.22 ^{31}P NMR spectrum of the reaction of 2 with 1 atmosphere of H_2 in benzene- d_6 at room temperature after 2 h.....	23
1.23 ^1H NMR spectra of the progress of the reaction of 2 with 1 eq. of PhSiH_3 at room temperature over a period of time	24
1.24 ^{31}P NMR spectra of the progress of the reaction of 2 with 1 eq. of PhSiH_3 at room temperature over a period of time.....	25
1.25 ^1H NMR spectra of the progress of reaction of 2 with 1 eq. of HBPin at room temperature over a period of time.....	26
1.26 ^{31}P NMR spectra of the progress of reaction of 2 with 1 eq. of HBPin at room temperature over a period of time	26
1.27 ^{31}P NMR spectra of the progress of the reaction of <i>cisoid-3</i> with 1 atm. H_2 at different temperatures over a period of time.....	27
1.28 ^{31}P NMR spectra of the progress of the reaction of <i>cisoid-3</i> with 1 atm. CO at different temperatures over a period of time.....	28
1.29 ^{31}P NMR spectra of the progress of reaction of <i>cisoid-3</i> with 2 eq. PhCH_2OH at different temperatures over a period of time.....	29
1.30 ^1H NMR spectra of the reaction of mixture of the isomers of 3 with 2 eq. $\text{HBF}_4\cdot\text{OEt}_2$	30

Figure	Page
1.31 ^{31}P NMR spectrum of the reaction of mixture of the isomers of 3 with 2 eq. $\text{HBF}_4 \cdot \text{OEt}_2$	30
1.32 ^{13}C NMR spectrum of 2 in benzene- d_6 at 25 °C	35
1.33 ^{31}P NMR spectrum of 2 in benzene- d_6 after 5d at 25 °C	35
1.34 ^{13}C NMR spectrum showing a mixture of <i>cisoid</i> -3 and <i>transoid</i> -3 in benzene- d_6 at 25 °C	37
1.35 ^{13}C NMR spectrum of <i>cisoid</i> -3 in benzene- d_6 at 25 °C	37
1.36 gCOSY NMR spectrum of <i>cisoid</i> -3 in benzene- d_6 at 25 °C.	38
1.37 HSQCAD NMR spectrum of <i>cisoid</i> -3 in benzene- d_6 at 25 °C.	38
2.1 ^1H NMR spectrum of 4 in benzene- d_6 at 25 °C.....	46
2.2 ^{31}P NMR spectrum of 4 in benzene- d_6 at 25 °C	47
2.3 The solid-state structure of 4.....	48
2.4 ^1H NMR spectrum of 5 in benzene- d_6 at 25 °C	49
2.5 ^{31}P NMR spectrum of 5 in benzene- d_6 at 25 °C	50
2.6 The solid-state structure of 5.....	51
2.7 ^1H NMR spectrum of the reaction products of 5 and MeI in benzene- d_6 at 25 °C.....	52
2.8 ^{31}P NMR spectrum of the reaction products of 5 and MeI in benzene- d_6 at 25 °C.....	53
2.9 ^1H NMR spectrum of 6 in benzene- d_6 at 25 °C	54
2.10 ^{31}P NMR spectrum of 6 in benzene- d_6 at 25 °C	55
2.11 ^{31}P NMR spectrum of the reaction of 6 with NaBH_4	56
2.12 ^1H NMR and ^{31}P NMR spectrum (inset) of $^t\text{Bu}_2\text{PPrDI}$ ligand	58
2.13 ^1H NMR spectrum of 7 in chloroform- d at 25 °C	59

Figure	Page
2.14 ^1H NMR spectrum of crystals of 8 in benzene- d_6 at 25 °C.....	60
2.15 ^{31}P NMR spectrum of crystals of 8 in benzene- d_6 at 25 °C	61
2.16 Solid-state structure of 8	62
2.17 ^{31}P NMR spectrum of the reduction trial of 7 in benzene- d_6 at 25 °C	63
2.18 ^1H NMR spectrum of 9 in acetone- d_6 at 25 °C	64
2.19 ^{31}P NMR spectrum of 9 in acetone- d_6 at 25 °C	65
2.20 ^1H NMR spectrum of 10 in acetone- d_6 at 25 °C	66
2.21 ^{31}P NMR spectrum of 10 in acetone- d_6 at 25 °C	67
2.22 ^1H NMR spectrum of 11 in benzene- d_6 at 25 °C	68
2.23 ^{31}P NMR spectrum of 11 in benzene- d_6 at 25 °C	68
2.24 ^1H NMR spectrum of 12 in acetone- d_6 at 25 °C	70
2.25 ^{31}P NMR spectrum of 12 in acetone- d_6 at 25 °C	70
2.26 ^{31}P NMR spectrum of 13 in acetone- d_6 at 25 °C	71
2.27 ^1H NMR spectrum of 14 in benzene- d_6 at 25 °C	72
2.28 ^{31}P NMR spectrum of 14 in benzene- d_6 at 25 °C	73
3.1 ^1H NMR spectrum of 15 in chloroform- d at 25 °C.....	87
3.2 UV-visible spectrum of 15 in chloroform.....	87
3.3 The solid-state structure of 15.....	88
3.4 ^1H NMR spectrum of 16 in benzene- d_6 at 25 °C	90
3.5 EPR spectrum of 16 in toluene glass at 106 K.....	91
3.6 UV-visible spectrum of 16 in toluene.....	91
3.7 The solid-state structure of 16.....	92

Figure	Page
3.8 ^1H NMR spectrum of 18 in benzene- d_6 at 25 °C	94
3.9 ^{31}P NMR spectrum of 18 in benzene- d_6 at 25 °C	95
3.10 X-band EPR spectra of 18 in toluene at 107 K	96
3.11 The solid-state structure of 18	98
3.12 Plausible mechanism for 18-catalyzed carbonyl hydrosilylation	111
3.13 ^1H NMR spectrum of 16-catalyzed hydrosilylation of benzaldehyde	119
3.14 ^1H NMR spectrum of 16-catalyzed hydrosilylation of benzaldehyde	120
3.15 ^1H NMR spectrum of 16-catalyzed hydrosilylation of <i>p</i> -chlorobenzaldehyde	121
3.16 ^1H NMR spectrum of 16-catalyzed hydrosilylation of <i>p</i> -fluorobenzaldehyde	122
3.17 ^1H NMR spectrum of 16-catalyzed hydrosilylation of <i>p</i> -methylbenzaldehyde	123
3.18 ^1H NMR spectrum of 16-catalyzed hydrosilylation of <i>p</i> -methoxybenzaldehyde ...	124
3.19 ^1H NMR spectrum of 16-catalyzed hydrosilylation of <i>trans</i> -cinnamaldehyde	126
3.20 ^1H NMR spectrum of 16-catalyzed hydrosilylation of furfural	127
3.21 ^1H NMR spectrum of 16-catalyzed hydrosilylation of 3-cyclohexene-1- carboxaldehyde	128
3.22 ^1H NMR spectrum of 3-cyclohexene-1-methanol in benzene- d_6	129
3.23 ^{13}C NMR spectrum of 3-cyclohexene-1-methanol in benzene- d_6	130
3.24 ^1H NMR spectrum of 16-catalyzed hydrosilylation of cyclohexanecarboxaldehyde	131
3.25 ^1H NMR spectrum of 16-catalyzed hydrosilylation of acetophenone	132
3.26 ^1H NMR spectrum of 16-catalyzed hydrosilylation of <i>p</i> -fluoroacetophenone	133
3.27 ^1H NMR spectrum of 16-catalyzed hydrosilylation of <i>p</i> -methoxyacetophenone ...	134

Figure	Page
3.28 ¹ H NMR spectrum of 16-catalyzed hydrosilylation of <i>p</i> -dimethylaminoacetophenone	135
3.29 ¹ H NMR spectrum of 16-catalyzed hydrosilylation of benzophenone	136
3.30 ¹ H NMR spectrum of 16-catalyzed hydrosilylation of 2-hexanone.....	137
3.31 ¹ H NMR spectrum of 16-catalyzed hydrosilylation of cyclohexanone	138
3.32 ¹ H NMR spectrum of 16-catalyzed hydrosilylation of 2,4-dimethyl-3-pentanone.....	139
3.33 ¹ H NMR spectrum of 16-catalyzed hydrosilylation of 2',4',6'- trimethylacetophenone	140
3.34 ¹ H NMR spectrum of 16-catalyzed hydrosilylation of 2-hexanone.....	141
3.35 ¹ H NMR spectrum of isolated 2-hexanol in benzene- <i>d</i> ₆ solution	142
3.36 ¹³ C NMR spectrum of isolated 2-hexanol in benzene- <i>d</i> ₆ solution	143
3.37 ¹ H NMR spectrum of isolated PhSiH(OCH(Me)(ⁿ Bu)) ₂ in benzene- <i>d</i> ₆	144
3.38 ¹³ C NMR spectrum of isolated PhSiH(OCH(Me)(ⁿ Bu)) ₂ in benzene- <i>d</i> ₆	145
3.39 ¹ H NMR spectrum of 16-catalyzed hydrosilylation of cyclohexanone	146
3.40 ¹ H NMR spectrum of isolated cyclohexanol in benzene- <i>d</i> ₆ solution	147
3.41 ¹³ C NMR spectrum of isolated cyclohexanol in benzene- <i>d</i> ₆ solution.....	148
3.42 ¹ H NMR spectrum of isolated PhSiH(OCy) ₂ in benzene- <i>d</i> ₆	149
3.43 ¹³ C NMR spectrum of isolated PhSiH(OCy) ₂ in benzene- <i>d</i> ₆	150
3.44 ¹ H NMR spectrum of 16-catalyzed hydrosilylation of benzaldehyde	151
3.45 ¹ H NMR spectrum of isolated benzyl alcohol in benzene- <i>d</i> ₆ solution.....	152
3.46 ¹³ C NMR spectrum of isolated benzyl alcohol in benzene- <i>d</i> ₆ solution.....	153

Figure	Page
3.47 ¹ H NMR spectrum of 16-catalyzed hydrosilylation of <i>p</i> -fluorobenzaldehyde	154
3.48 ¹ H NMR spectrum of isolated <i>p</i> -fluorobenzyl alcohol in benzene- <i>d</i> ₆ solution.....	155
3.49 ¹³ C NMR spectrum of isolated <i>p</i> -fluorobenzyl alcohol in benzene- <i>d</i> ₆ solution	155
3.50 ¹ H NMR spectrum of 16-catalyzed hydrosilylation of benzaldehyde with PhSiH ₃ (30,000 eq. of substrate and silane)	156
3.51 ¹ H NMR spectrum of 16-catalyzed neat hydrosilylation of cyclohexanone with PhSiH ₃ in the presence of Hg ⁰	157
3.52 ¹ H NMR spectrum of unreacted PhSiH ₃ and cyclohexanone following exposure to Mn(0) powder.....	158
3.53 ¹ H NMR spectrum of unreacted PhSiH ₃ and cyclohexanone following exposure to (THF) ₂ MnCl ₂	159
3.54 ¹ H NMR spectrum of unreacted PhSiH ₃ and cyclohexanone following exposure to 15.....	160
3.55 ¹ H NMR spectrum of unreacted PhSiH ₃ and cyclohexanone following exposure to AIBN.....	161
3.56 ¹ H NMR spectrum of benzyl alcohol in benzene- <i>d</i> ₆	163
3.57 ¹³ C NMR spectrum of benzyl alcohol in benzene- <i>d</i> ₆	164
3.58 ¹ H NMR spectrum of 4-fluorobenzyl alcohol in benzene- <i>d</i> ₆	165
3.59 ¹³ C NMR spectrum of 4-fluorobenzyl alcohol in benzene- <i>d</i> ₆	166
3.60 ¹ H NMR spectrum of 4-chlorobenzyl alcohol in benzene- <i>d</i> ₆	167
3.61 ¹³ C NMR spectrum of 4-chlorobenzyl alcohol in benzene- <i>d</i> ₆	168
3.62 ¹ H NMR spectrum of 4-bromobenzyl alcohol in benzene- <i>d</i> ₆	169

Figure	Page
3.63 ^{13}C NMR spectrum of 4-bromobenzyl alcohol in benzene- d_6	170
3.64 ^1H NMR spectrum of 2-nitrobenzyl alcohol in benzene- d_6	171
3.65 ^{13}C NMR spectrum of 2-nitrobenzyl alcohol in benzene- d_6	172
3.66 ^1H NMR spectrum of 4-cyanobenzyl alcohol in benzene- d_6	173
3.67 ^{13}C NMR spectrum of 4-cyanobenzyl alcohol in benzene- d_6	174
3.68 ^1H NMR spectrum of 4-methoxybenzyl alcohol in benzene- d_6	175
3.69 ^{13}C NMR spectrum of 4-methoxybenzyl alcohol in benzene- d_6	176
3.70 ^1H NMR spectrum of 4-methylbenzyl alcohol in benzene- d_6	177
3.71 ^{13}C NMR spectrum of 4-methylbenzyl alcohol in benzene- d_6	178
3.72 ^1H NMR spectrum of 2-naphthalenemethanol in benzene- d_6	179
3.73 ^{13}C NMR spectrum of 2-naphthalenemethanol in benzene- d_6	180
3.74 ^1H NMR spectrum of silyl ethers observed prior to hydrolysis in benzene- d_6	181
3.75 ^1H NMR spectrum of isolated pyridine-3-carbinol in benzene- d_6	182
3.76 ^{13}C NMR spectrum of isolated pyridine-3-carbinol in benzene- d_6	183
3.77 ^1H NMR spectrum of furfuryl alcohol in benzene- d_6	184
3.78 ^{13}C spectrum of furfuryl alcohol in benzene- d_6	185
3.79 ^1H NMR spectrum showing partial 3-cyclohexene-1-carboxaldehyde hydrosilylation	186
3.80 ^1H NMR spectrum showing partial citral hydrosilylation in benzene- d_6	187
3.81 ^1H NMR spectrum showing the silyl ethers prepared from acetophenone using PhSiH ₃ and 18	188
3.82 ^1H NMR spectrum of PhSiH(OCy) ₂ and PhSiH ₃ in benzene- d_6	189

Figure	Page
3.83 ^1H NMR spectrum showing complete methyl formate hydrosilylation.....	192
3.84 ^1H NMR spectrum showing complete ethyl formate hydrosilylation.....	193
3.85 ^1H NMR spectrum of 1-octanol in benzene- d_6	194
3.86 ^{13}C NMR spectrum of 1-octanol in benzene- d_6	195
3.87 ^1H NMR spectrum of isoamyl alcohol in benzene- d_6	196
3.88 ^{13}C NMR spectrum of isoamyl alcohol in benzene- d_6	197
3.89 ^1H NMR spectrum of benzyl alcohol in benzene- d_6	198
3.90 ^{13}C NMR of benzyl alcohol in benzene- d_6	199
3.91 ^1H NMR spectrum of 4-methoxybenzyl alcohol in benzene- d_6	200
3.92 ^{13}C NMR spectrum of 4-methoxybenzyl alcohol in benzene- d_6	201
3.93 ^1H NMR spectrum of $\text{PhSi}(\text{OEt})_3$ and PhSiH_3 in benzene- d_6	202
4.1 ^1H NMR spectrum of 19 in chloroform- d at 25 °C.....	212
4.2 ^1H NMR spectrum of 20 in toluene- d_8 at 40 °C.....	213
4.3 The solid-state structure of 20.....	215
4.4 ^1H NMR spectrum of the reaction mixture of pre-catalyst 20 and HBPin in toluene- d_8 at 25 °C.....	223
4.5 ^{13}C NMR spectrum of the reaction mixture of pre-catalyst 20 and HBPin in toluene- d_8 at 25 °C.....	223
4.6 ^{11}B NMR spectrum of the reaction mixture of pre-catalyst 20 and HBPin in toluene- d_8 at 25 °C.....	224
4.7 Plausible mechanism for 20-mediated nitrile dihydroboration (Mechanism 1).....	225
4.8 Plausible mechanism for 20-mediated nitrile dihydroboration (Mechanism 2).....	228

Figure	Page
4.9 gCOSY spectrum of the reaction mixture of pre-catalyst 20 and HBPIn	228
4.10 HSQC spectrum of the reaction mixture of pre-catalyst 20 and HBPIn	229
4.11 gCOSY spectrum of 20 in toluene- <i>d</i> ₈ at 40 °C	231
4.12 Conversion of benzonitrile to diboryl amine using 1 mol% catalyst 20	232
4.13 ¹ H NMR spectrum of PhCH ₂ N(BPin) ₂ in benzene- <i>d</i> ₆	233
4.14 ¹³ C NMR spectrum of PhCH ₂ N(BPin) ₂ in benzene- <i>d</i> ₆	234
4.15 Conversion of 4-methylbenzonitrile to diboryl amine using 1 mol% catalyst 20 ..	235
4.16 ¹ H NMR spectrum of (4-MePh)CH ₂ N(BPin) ₂ in benzene- <i>d</i> ₆	236
4.17 ¹³ C NMR spectrum of (4-MePh)CH ₂ N(BPin) ₂ in benzene- <i>d</i> ₆	237
4.18 Conversion of 4-methoxybenzonitrile to diboryl amine using 1 mol% catalyst 20	238
4.19 ¹ H NMR spectrum of (4-OMePh)CH ₂ N(BPin) ₂ in benzene- <i>d</i> ₆	239
4.20 ¹³ C NMR spectrum of (4-OMePh)CH ₂ N(BPin) ₂ in benzene- <i>d</i> ₆	240
4.21 Conversion of 4-chlorobenzonitrile to diboryl amine using 1 mol% catalyst 20 ...	241
4.22 ¹ H NMR spectrum of (4-ClPh)CH ₂ N(BPin) ₂ in benzene- <i>d</i> ₆	242
4.23 ¹³ C NMR spectrum of (4-ClPh)CH ₂ N(BPin) ₂ in benzene- <i>d</i> ₆	243
4.24 Conversion of 4-fluorobenzonitrile using 1 mol% catalyst 20	244
4.25 ¹ H NMR spectrum of (4-FPh)CH ₂ N(BPin) ₂ in benzene- <i>d</i> ₆	245
4.26 ¹³ C NMR spectrum of (4-FPh)CH ₂ N(BPin) ₂ in benzene- <i>d</i> ₆	246
4.27 Conversion of 4-(trifluoromethyl)benzonitrile to diboryl amine using 1 mol% catalyst 20.	247
4.28 ¹ H NMR spectrum of (4-CF ₃ Ph)CH ₂ N(BPin) ₂ in benzene- <i>d</i> ₆	248

Figure	Page
4.29 ^{13}C NMR spectrum of $(4\text{-CF}_3\text{Ph})\text{CH}_2\text{N}(\text{BPin})_2$ in benzene- d_6	249
4.30 Conversion of 2-phenoxyacetonitrile to diboryl amine using 1 mol% catalyst 20	250
4.31 ^1H NMR spectrum of $(2\text{-OPh})\text{CH}_2\text{CH}_2\text{N}(\text{BPin})_2$ in benzene- d_6	251
4.32 ^{13}C NMR spectrum of $(2\text{-OPh})\text{CH}_2\text{CH}_2\text{N}(\text{BPin})_2$ in benzene- d_6	252
4.33 Conversion of 2-furonitrile to diboryl amine using 1 mol% catalyst 20	253
4.34 ^1H NMR spectrum of $(2\text{-furyl})\text{CH}_2\text{N}(\text{BPin})_2$ in benzene- d_6	254
4.35 ^{13}C NMR spectrum of $(2\text{-furyl})\text{CH}_2\text{N}(\text{BPin})_2$ in benzene- d_6	255
4.36 Conversion of 4-acetylbenzonitrile to diboryl amine using 1 mol% catalyst 20....	256
4.37 ^1H NMR spectrum of $(4\text{-C(H)(Me)OBPin})\text{PhCH}_2\text{N}(\text{BPin})_2$ in benzene- d_6	257
4.38 ^{13}C NMR spectrum of $(4\text{-C(H)(Me)OBPin})\text{PhCH}_2\text{N}(\text{BPin})_2$ in benzene- d_6	258
4.39 Conversion of acetonitrile to diboryl amine using 1 mol% catalyst 20	259
4.40 ^1H NMR spectrum of $\text{CH}_3\text{CH}_2\text{N}(\text{BPin})_2$ in benzene- d_6	260
4.41 ^{13}C NMR spectrum of $\text{CH}_3\text{CH}_2\text{N}(\text{BPin})_2$ in benzene- d_6	261
4.42 Conversion of propionitrile to diboryl amine using 1 mol% catalyst 20 in benzene- d_6 after 2 h	262
4.43 Conversion of propionitrile to diboryl amine using 1 mol% catalyst 20 in benzene- d_6 after 24 h	263
4.44 ^{13}C NMR spectrum for the conversion of propionitrile to diboryl amine using 1 mol% catalyst 20 in benzene- d_6 after 24 h.....	264
4.45 Conversion of isobutyronitrile to diboryl amine using 1 mol% catalyst 20 in benzene- d_6 after 2 h.....	265

Figure	Page
4.46 Conversion of isobutyronitrile to diboryl amine using 1 mol% catalyst 20 in benzene- <i>d</i> ₆ after 24 h.....	266
4.47 Conversion of isobutyronitrile to diboryl amine using 1 mol% catalyst 20 in benzene- <i>d</i> ₆ after 4 d.....	267
4.48 ¹³ C NMR spectrum for the conversion of isobutyronitrile to diboryl amine using 1 mol% catalyst 20 in benzene- <i>d</i> ₆ after 4 d.....	268
4.49 Conversion of (<i>N,N</i> -dimethylamino) propionitrile to diboryl amine using 1 mol% catalyst 20 in benzene- <i>d</i> ₆ after 2 h	269
4.50 Conversion of (<i>N,N</i> -dimethylamino) propionitrile to diboryl amine using 1 mol% catalyst 20 in benzene- <i>d</i> ₆ after 24 h	270
4.51 Conversion of (<i>N,N</i> -dimethylamino) propionitrile to diboryl amine using 1 mol% catalyst 20 in benzene- <i>d</i> ₆ after 4 d	271
4.52 ¹³ C NMR spectrum for the conversion of (<i>N,N</i> -dimethylamino) propionitrile to diboryl amine using 1 mol% catalyst 20 in benzene- <i>d</i> ₆ after 4 d.....	272
4.53 Conversion of (3-diphenylphosphino) propionitrile to diboryl amine using 1 mol% catalyst 20 in benzene- <i>d</i> ₆ after 2 h at 60 °C	273
4.54 ¹ H NMR spectrum of 3-PPh ₂ CH ₂ CH ₂ CH ₂ N(BPin) ₂ in benzene- <i>d</i> ₆ at 25 °C	274
4.55 ¹³ C NMR spectrum of 3-PPh ₂ CH ₂ CH ₂ CH ₂ N(BPin) ₂ in benzene- <i>d</i> ₆ at 25 °C.....	275
4.56 Hydroboration of <i>N</i> -benzylidenebenzylamine using 1 mol% catalyst 20	276
4.57 Hydroboration of 4-chloro- <i>N</i> -(phenylmethylene) benzenamine using 1 mol% catalyst 20	277

Figure	Page
4.58 Hydroboration of 2,6-difluoro- <i>N</i> -(phenylmethylene) benzenamine using 1 mol% catalyst 20	278
4.59 Hydroboration of 4-methyl- <i>N</i> -(phenylmethylene) benzenamine using 1 mol% catalyst 20	279
4.60 Partial hydroboration (85%) of 2,4,6-trimethyl- <i>N</i> -(phenylmethylene) benzenamine using 1 mol% catalyst 20 in benzene- <i>d</i> ₆ after 2 h	280
4.61 Hydroboration of 2,4,6-trimethyl- <i>N</i> -(phenylmethylene) benzenamine using 1 mol% catalyst 20 in benzene- <i>d</i> ₆ after 24 h	281
4.62 Partial hydroboration (34%) of <i>a</i> -methyl- <i>N</i> -(phenylmethylene) benzenemethanamine using 1 mol% catalyst 20 in benzene- <i>d</i> ₆ after 2 h	282
4.63 Hydroboration of <i>a</i> -methyl- <i>N</i> -(phenylmethylene) benzenemethanamine using 1 mol% catalyst 20 in benzene- <i>d</i> ₆ after 24 h	283
4.64 Partial hydroboration (72%) of <i>N</i> -(phenylmethylene)-2-propanamine using 1 mol% catalyst 20 in benzene- <i>d</i> ₆ after 2 h	284
4.65 Hydroboration of <i>N</i> -(phenylmethylene)-2-propanamine using 1 mol% catalyst 20 in benzene- <i>d</i> ₆ after 3 d	285
4.66 Partial hydroboration (86%) of <i>N</i> -(phenylmethylene)-1-butanamine using 1 mol% catalyst 20 in benzene- <i>d</i> ₆ after 2 h	286
4.67 Hydroboration of <i>N</i> -(phenylmethylene)-1-butanamine using 1 mol% catalyst 20 in benzene- <i>d</i> ₆ after 2 d	287
4.68 Hydroboration of <i>N</i> -[(4-fluorophenyl)methylene] benzenemethanamine using 1 mol% of catalyst 20	288

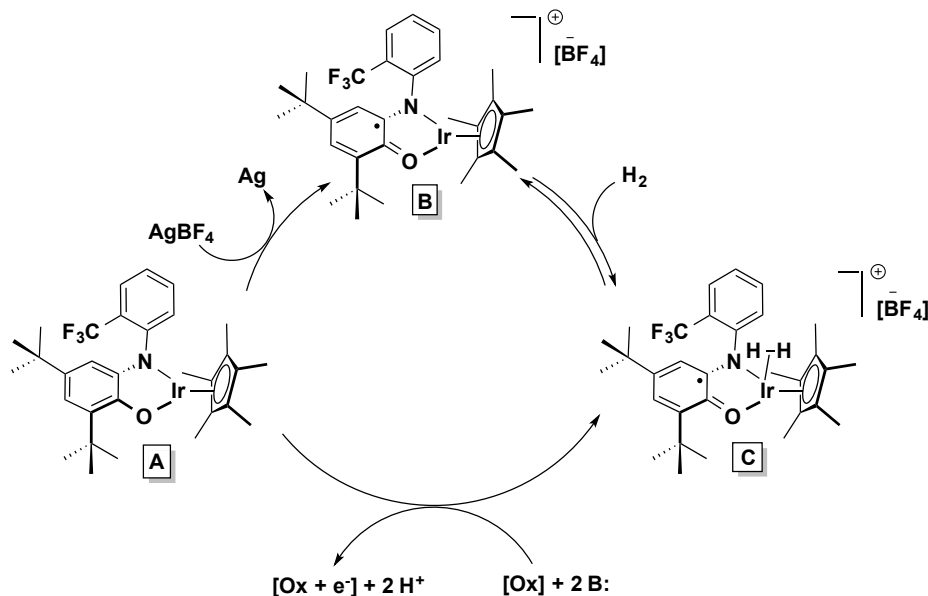
Figure	Page
4.69 Hydroboration of (<i>p</i> -methoxybenzylidene) benzylamine using 1 mol% catalyst 20	289
4.70 Hydroboration of <i>N</i> -(2-furanylmethylene) benzenemethanamine using 1 mol% catalyst 20	290
4.71 Partial hydroboration (55%) of <i>N</i> -(1-phenylethylidene) benzenemethanamine using 1 mol% catalyst 20 in benzene- <i>d</i> ₆ after 2 h.....	291
4.72 Partial hydroboration (88%) of <i>N</i> -(1-phenylethylidene) benzenemethanamine using 1 mol% of catalyst 20 in benzene- <i>d</i> ₆ after 24 h.....	292
4.73 Hydroboration of <i>N</i> -(1-phenylethylidene) benzenemethanamine using 1 mol% catalyst 20 in benzene- <i>d</i> ₆ after 48 h	293
4.74 Partial hydroboration (18%) of <i>N</i> -(diphenylmethylene) benzenemethanamine using 1 mol% catalyst 20.....	294

Introduction

Transition metal complexes have been immensely important in catalytic organic transformations for decades. Notably, precious metals (Ru, Rh, and Pt) have been extensively employed to address various challenges related to catalytic organic transformations such as hydrogenation, hydrosilylation of unsaturated functionalities, cross-coupling and cross metathesis reactions to make C-C bond. A few examples are worth mentioning here. Rh-based Wilkinson's catalyst $[(PPh_3)_3RhCl]$ is known for olefin hydrogenation.¹ Pt-based Karstedt's catalyst $[Pt_2(Me_2SiCH=CH_2)_2O]_3$ has been widely used in silicone coating industries for olefin hydrosilylation.² Additionally, Pd-catalyzed cross coupling reactions have been extensively employed to make C-C bond and for this invention, Prof. Heck, Negeshi and Suzuki received the Nobel prize in chemistry in 2010.³ Another breakthrough invention was Ru-based Grubbs' catalyst $[(Cl)Ru(=CHPh)(PCy_3)_2]$ ⁴ for cross metathesis and he received Nobel prize in chemistry in 2005 together with Prof. Schrock and Chauvin. These metal catalysts are highly efficient due to favorable two-electron redox changes, which are required for many organometallic pathways. Given their high efficiency, their high price and toxicity have driven researchers to hunt for inexpensive alternative substitutes. In this context, first row late transition metals would be suitable surrogates as they are highly earth abundant and non-toxic. However, first row metals are associated with a few disadvantages. Firstly, they are prone to make high spin paramagnetic complexes and therefore, are hard to characterize in some instances. Secondly, they have a propensity of participating in one-electron redox change processes, which are not favorable in organometallic transformations. These problems can be controlled by designing suitable ligands, which

can help to stabilize low spin metal complexes and aid in two-electron redox processes by accepting electrons. In this context, redox non-innocent ligand plays an important role. In traditional approaches, ligands play a spectator role (i.e. not directly involved in the bond activation processes), instead their electronic and steric effects are utilized to control the catalytic reaction rate. In the new approach of ligand design, ligands play more active role by participating in elementary bond activation process.^{5,6} In this case, both metal and ligand can work cooperatively in a synergistic manner to expedite the catalytic process. Therefore, these ligands are considered as “redox non-innocent”.⁷ These ligands participate in the redox processes during the catalytic reactions and modify the reactivity of transition metal complexes. There are mainly four strategies that redox non-innocent ligands can take part in, to facilitate the catalytic reactions.^{7b} First strategy involves modification of Lewis acidity of the metal via oxidation or reduction of the ligand, therefore influencing the substrate affinity and the reaction profile.^{8a,b} According to the second strategy, they can act as an “electron reservoir” by accepting the excess electrons from a metal center and again donating the electrons in the electron deficient elementary step, thereby maintaining the preferred oxidation state of the metal.^{9a-f} The third strategy engages the generation of a ligand radical that can actively participate in the bond breaking-making step of a catalytic process.^{5a-d} Therefore, the cooperative effort of metal and ligand allows reactions to occur which are difficult otherwise. A fourth approach involves radical-type activation of the substrate, where the substrate itself can play a role as a redox non-innocent ligand.^{6a-f}

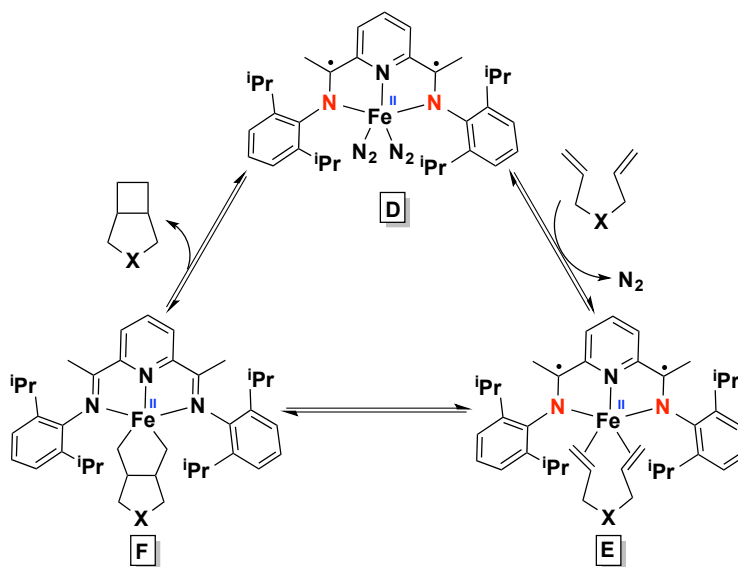
The first strategy (modification of Lewis acidity of the metal) can be demonstrated in the example of oxidation of dihydrogen by an iridium complex, reported by the Rauchfuss group (Scheme 1).^{8a}



Scheme 1: Iridium catalyzed oxidation of dihydrogen.

In this example, complex **A** is oxidized by silver tetrafluoroborate (AgBF_4) to generate a cationic complex **B**, which consists of a ligand centered radical. As a consequence, Lewis acidity of the metal center has been enhanced compared to its non-oxidized form **A**, which then form a H_2 -adduct **C** upon reaction with dihydrogen, followed by deprotonation by a non-coordinating base, 2,6-di-^tBu-pyridine (TBP). Furthermore, this entire process has been repeated one more time to complete the oxidation of dihydrogen. Electrons of dihydrogen reduce the oxidized form of the ligand back to its neutral form.

In the second strategy, redox non-innocent ligands can act as an “electron reservoir” and aid in multi-electron catalytic process, as found for Fe-catalyzed cyclization, reported by the Chirik group (Scheme 2).^{9a,b}

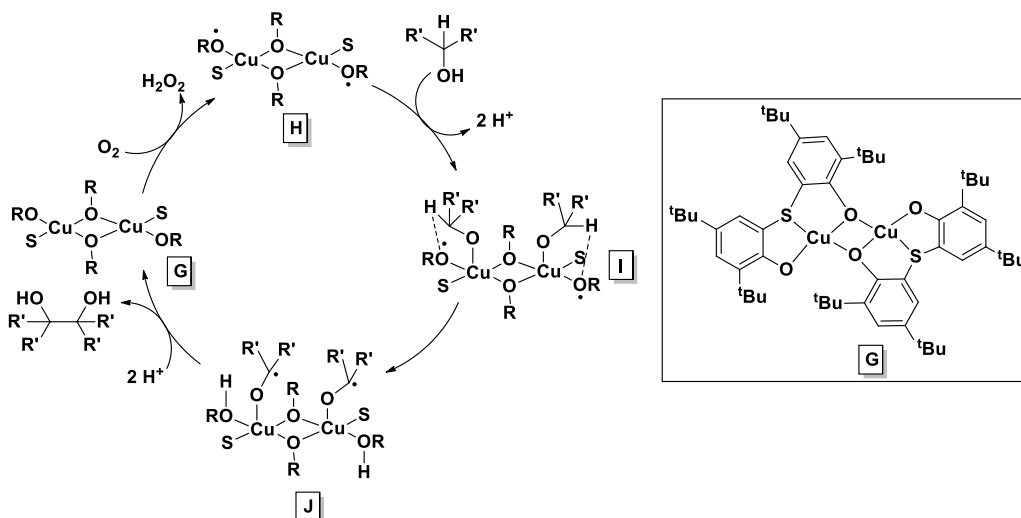


Scheme 2: Iron catalyzed cyclization of diene.

In this example, the iron catalyst **D** reacts with a diene substrate to generate a π complex **E** with concomitant loss of N_2 . Both complex **D** and **E** comprise of a dianionic tridentate pyridine diimine (PDI) ligand, which is formally two electron reduced form of the ligand and iron is in the +II oxidation state in these complexes. The next step of the catalytic cycle is the cyclization of the diene substrate, which is formally a two-electron oxidative addition process. For this process, required electrons originate from the ligand rather than the metal center, therefore the energetically preferred oxidation state (+II) of the iron is maintained rather than achieving energetically unfavorable (+IV) oxidation state. As a result, the ligand returns back to its neutral form (**F**) from the oxidized form. This example reflects the advantage of using a redox non-innocent ligand in multi-electron processes mediated by first row metals, avoiding the unfavorable oxidation states of the metal, and facilitating the entire catalytic process.

So far, the redox non-innocent ligands have been described in the aspect of redox change processes. However, according to the third strategy, the ligand can directly

participate in the elementary bond breaking-making steps of the catalytic cycle, which has been clearly demonstrated by the Wieghardt group in the example of Cu(II)-thiophenol catalyzed dimerization of secondary alcohols (Scheme 3).^{5a}

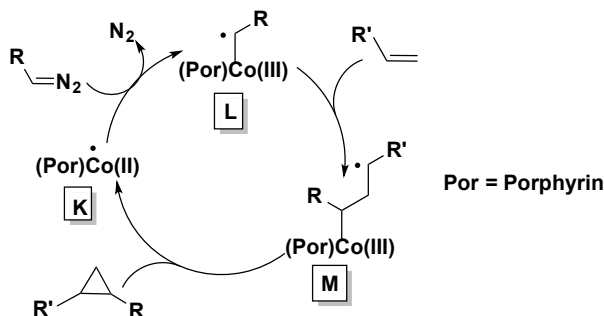


Scheme 3: Copper catalyzed dimerization of secondary alcohols.

The first step of the dimerization catalytic cycle is the oxidation of the Cu(II)-thiophenol catalyst **G** by oxygen to generate a biradical Cu intermediate species **H**. Coordination of two alcohol units to **H** furnishes the intermediate **I**, followed by the α -hydrogen abstraction of the alcohol moieties by oxygen-centered radicals of the thiophenol ligands to produce the intermediate **J**. Then the catalytic cycle ends with the dimerization of the radicals followed by elimination of the diol.

The fourth strategy is somewhat related to the previous one, where the incoming substrate (for e.g.- diazoalkanes and organic azides which produce carbenes and nitrenes intermediates, respectively, upon the loss of N_2 , which will then react with olefin to produce cyclopropane and aziridine, respectively, as a product) of a catalytic reaction itself acts as a redox non-innocent ligand. In this instance, electron transfer to or from the substrate generates a radical of the same substrate leading to radical-type reactivity,

useful for the catalytic transformation. This concept has been clearly illustrated in the example of Co(II)-porphyrin catalyzed carbene transfer reactions to olefin substrates (Scheme 4).^{6a-c}



Scheme 4: Cobalt catalyzed carbene insertion into olefin.

In this example, Co(II) catalyst **K** reacts with diazoalkane with concomitant loss of N_2 to produce a ligand centered radical species **L**. This step is the result of one electron transfer from Co(II) to the redox non-innocent carbene ligand. Then compound **L** reacts with olefin to generate intermediate species **M** followed by the cyclization and elimination of the cyclopropane to regenerate the catalyst **K**.

All of these aforementioned examples clearly show the influence of redox non-innocent ligands in catalytic transformations. Inspired by this, our group became interested in utilizing redox non-innocent ligands that can act as an “electron reservoir”. In this work, two types of redox non-innocent ligands (pyridine diimine or PDI and α -diimine or DI) have been studied. The electron acceptance property of the PDI ligands arises from their two energetically accessible π^* orbitals, which are the combination of two imine π^* orbitals with significant contribution from the pyridine ring.¹⁰ Similarly, DI ligand has one low lying π^* orbital that can accept electron.¹¹

As a result of electron transfer from a metal to one or both π^* orbitals of the PDI ligand, elongation of the imine bonds ($C=N$) and contraction of the corresponding $C_{im}-C_{ipso}$ bond are expected. These outcomes have been observed in the crystal structure parameters of many complexes containing a PDI ligand. These crystallographic results indicate that the PDI ligand can accept one electron^{12,13} to form a mono-radical anion or two electrons¹⁴ to form a dianion (Fig. 0.1). It can rarely also accept three electrons.¹⁵ The changes in bond lengths are listed in the Table 0.1. The extent of the electron transfer is very sensitive to small changes in the relative orbital energies of the metal and the ligand. These PDI ligands are remarkable due to their flexibility of storing and releasing electrons, which contributes to the stabilization of unusually low-valent oxidation states, which are actually the combination of a moderate oxidation state and ligand radical anions.

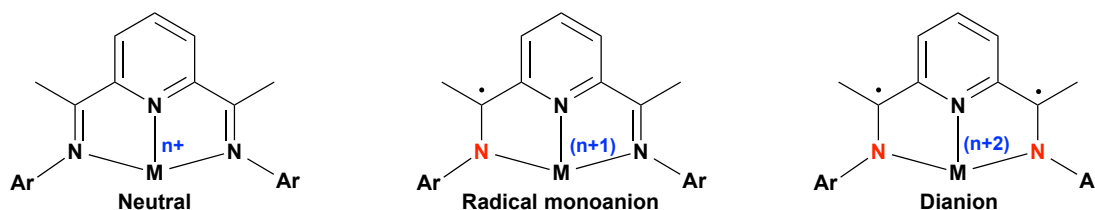


Figure 0.1: Different electronic forms of the PDI ligand.

Table 0.1: Changes of bond lengths as a result of electron transfer to the PDI ligand.

No. of electron reduction	$C_{im}-N_{im}$	$C_{im}-C_{ipso}$
0	1.28	1.50
1	1.32	1.44
2	1.36	1.40
3	1.40	1.37

Similarly, crystallographic data suggests that α -diimine or DI ligands can achieve three different oxidation levels, namely neutral, radical monoanion and dianion (Fig. 0.2) and their corresponding bond lengths are listed in table 0.2.¹¹

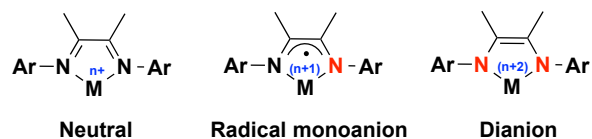


Figure 0.2: Different electronic forms of the DI ligand.

Table 0.2: Changes of bond lengths as a result of electron transfer to the DI ligand.

No. of electron reduction	$C_{im}-N_{im}$	$C_{im}-C_{ipso}$
0	1.29	1.47
1	1.34	1.38
2	1.40	1.36

PDI ligand supported first row metal complexes have been extensively studied by the Chirik group for catalytic organic transformations such as hydrogenation¹⁶, hydrosilylation of olefins¹⁷, hydroboration of alkynes¹⁸, polymerization¹⁹, cyclization.⁷ In a similar fashion, first row metal complexes containing DI ligands have also been explored as catalysts for organic transformations including polymerization²⁰, alkene hydrogenation²¹, alkene hydroboration.²² Encouraged by these seminal works, our group has designed a new version of the PDI or DI ligands by replacing the bulky aryl groups of the traditional PDI or DI ligands with modular arms tethered to donor atoms ($-PR_2$, $-NR_2$).²³ Along with the redox non-innocence property, these new types of ligands are also associated with coordination flexibility. These donor groups can protect the metal center from decomposition pathways and also dissociate to facilitate substrate coordination to the metal during catalytic process. At the end of the cycle, it can recombine to the metal

(Fig. 0.3). This concept has been recently observed in the mechanistic study of $(\text{Ph}_2\text{PPrPDI})\text{Mn}$ catalyzed carbonyl hydrosilylation.²⁴

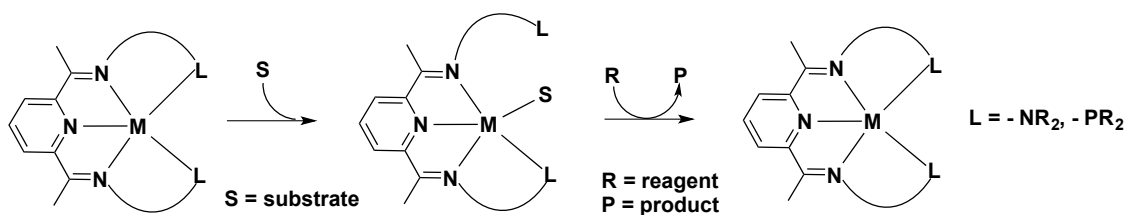


Figure 0.3: Depiction of the coordination flexibility of the ligand.

Considering all these criteria, this dissertation is focused on the utilization of redox non-innocent PDI and DI ligand supported inexpensive first row metal (Fe, Mn and Co) complexes in the bond activation and the catalytic hydrofunctionalization of unsaturated bonds. Each project commenced with synthesis of the ligand via Schiff base condensation of 2,6-diacetyl pyridine or diacetyl with the corresponding amines (2 equivalents) to generate PDI and DI ligands, respectively. After isolation of the ligand, metallation has been performed with the metal dibromide (FeBr_2) or metal dichlorides [$(\text{THF})_2\text{MnCl}_2$ or CoCl_2]. In order to obtain the low-valent metal complexes, these metal dichloride or dibromide complexes were reduced using excess Na-Hg. All of these compounds were characterized thoroughly with various spectroscopic techniques and single crystal X-ray diffraction analysis. Crystallographic parameters obtained for these low valent metal complexes indicate the single electron reduction of the ligands (PDI or DI radical monoanion) and deprotonation of the backbone methyl groups in one of the Mn complexes. Once characterized, these low-valent metal complexes have been investigated for bond activation or catalytic hydrofunctionalization of unsaturated functionalities. As expected, redox non-innocence nature of these ligands has been found

to play an important role in the catalytic cycles or bond activation processes to maintain the energetically favorable oxidation states of the metals.

References:

1. (a) Birch, A. J.; Williamson, D. H. *Org. React. (N.Y.)*, **1976**, *24*, 1. (b) James, B. R. (1973). *Homogeneous Hydrogenation*. New York, NY: John Wiley & Sons.
2. Stein, J.; Lewis, L. N.; Gao, Y.; Scott, R. A. *J. Am. Chem. Soc.* **1999**, *121*, 3693-3703.
3. (a) Heck, R. F.; Nolley, J. P. *J. Org. Chem.* **1972**, *37*, 2320-2322. (b) Dieck, H. A.; Heck, R. F. *J. Am. Chem. Soc.* **1974**, *96*, 1133-1136. (c) Miyaura, N.; Suzuki, A. *Chem. Rev.* **1995**, *95*, 2457-2483. (d) King, A. O.; Okukado, N.; Negishi, E.-i. *J. Chem. Soc., Chem. Commun.* **1977**, *0*, 683-684.
4. Chatterjee, A. K.; Choi, T.-L.; Sanders, D. P.; Grubbs, R. H. *J. Am. Chem. Soc.* **2003**, *125*, 11360-11370.
5. (a) Chaudhuri, P.; Hess, M.; Flörke, U.; Wieghardt, K. *Angew. Chem. Int. Ed.* **1998**, *37*, 2217-2220. (b) Que, L.; Tolman, W. B. *Nature* **2008**, *455*, 333-340. (c) Grapperhaus, C. A.; Ouch, K.; Mashuta, M. S. *J. Am. Chem. Soc.* **2009**, *131*, 64-65. (d) Wang, K.; Stiefel, E. I. *Science* **2001**, *291*, 106-109.
6. (a) Dzik, W. I.; Xu, X.; Zhang, X. P.; Reek, J. N. H.; de Bruin, B. *J. Am. Chem. Soc.* **2010**, *132*, 10891-10902. (b) Lu, H.; Dzik, W. I.; Xu, X.; Wojtas, L.; de Bruin, B.; Zhang, X. P. *J. Am. Chem. Soc.* **2011**, *133*, 8518-8521. (c) Zhu, S.; Xu, X.; Perman, J. A.; Zhang, X. P. *J. Am. Chem. Soc.* **2010**, *132*, 12796-12799. (d) Subbarayan, V.; Ruppel, J. V.; Zhu, S.; Perman, J. A.; Zhang, X. P. *Chem. Commun.* **2009**, 4266-4268. (e) Lu, H.; Subbarayan, V.; Tao, J.; Zhang, X. P. *Organometallics* **2010**, *29*, 389-393. (f) Caselli, A.; Gallo, E.; Fantauzzi, S.; Morlacchi, S.; Ragaini, F.; Cenini, S. *Eur. J. Inorg. Chem.* **2008**, 3009-3019.
7. (a) Luca, O. R.; Crabtree, R. H. *Chem. Soc. Rev.* **2013**, *42*, 1440-1459. (b) Lyaskovskyy, V.; de Bruin, B. *ACS Catal.* **2012**, *2*, 270-279.
8. (a) Ringenberg, M. R.; Kokatam, S. L.; Zachariah, M. H.; Rauchfuss, T. B. *J. Am. Chem. Soc.* **2008**, *130*, 788-789. (b) Ringenberg, M. R.; Rauchfuss, T. B. *Eur. J. Inorg. Chem.* **2012**, *3*, 490-495.
9. (a) Chirik, P. J.; Wieghardt, K. *Science* **2010**, *327*, 794-795. (b) Bouwkamp, M. W.; Bowman, A. C.; Lobkovsky, E.; Chirik, P. J. *J. Am. Chem. Soc.* **2006**, *128*, 13340-13341.

- (c) Luca, O. R.; Konezy, S. J.; Blakemore, J. D.; Saha, S.; Colosi, D. M.; Brudvig, G. W.; Barista, V. S.; Crabtree, R. H. *New J. Chem.* **2012**, *36*, 1149-1152. (d) Heyduk, A. F.; Zarkesh, R. A.; Nguyen, A. I. *Inorg. Chem.* **2011**, *50*, 9849-9863. (e) Smith, A. L.; Hardcastle, K. I.; Soper, J. D. *J. Am. Chem. Soc.* **2010**, *132*, 14358-14360. (f) Smith, A. L.; Clapp, L. A.; Hardcastle, K. I.; Soper, J. D. *Polyhedron* **2010**, *29*, 164-169.
10. Knijnenburg, Q.; Gambarotta, S.; Budzelaar, P. H. M. *Dalton Trans.* **2006**, 5442-5448.
11. Muresan, N.; Chlopek, K.; Weyhermüller, T.; Neese, F.; Wieghardt, K. *Inorg. Chem.* **2007**, *46*, 5327-5337.
12. de Bruin, B.; Bill, E.; Bothe, E.; Weyhermüller, T.; Wieghardt, K. *Inorg. Chem.* **2000**, *39*, 2936-2947.
13. Sugiyama, H.; Korobkov, I.; Gambarotta, S.; Möller, A.; Budzelaar, P. H. M. *Inorg. Chem.* **2004**, *43*, 5771.
14. Reardon, D.; Conan, F.; Gambarotta, S.; Yap, G. P. A.; Wang, Q. *J. Am. Chem. Soc.* **1999**, *121*, 9318.
15. Enright, D.; Gambarotta, S.; Yap, G. P. A.; Budzelaar, P. H. M. *Angew. Chem. Int. Ed.* **2002**, *41*, 3873.
16. (a) Trovitch, R.; Lobkovsky, E.; Bill, E.; Chirik, P. J. *Organometallics* **2008**, *27*, 1470-1478. (b) Bart, S. C.; Lobkovsky, E.; Chirik, P. J. *J. Am. Chem. Soc.* **2004**, *126*, 13794-13807. (c) Yu, R. P.; Darmon, J. M.; Hoyt, J. M.; Margulieux, G. W.; Turner, Z. R.; Chirik, P. J. *ACS Catal.* **2012**, *2*, 1760-1764. (d) Monfette, S.; Turner, Z. R.; Semproni, S. P.; Chirik, P. J. *J. Am. Chem. Soc.* **2012**, *134*, 4561-4564.
17. Schuster, C. H.; Diao, T.; Pappas, I.; Chirik, P. J. *ACS Catal.* **2016**, *6*, 2632-2636.
18. Obligacion, J. V.; Neely, J. M.; Yazdani, A. N.; Pappas, I.; Chirik, P. J. *J. Am. Chem. Soc.* **2015**, *137*, 5855-5858.
19. Schaefer, B. A.; Margulieux, G. W.; Tiedmann, M. A.; Small, B. L.; Chirik, P. J. *Organometallics* **2015**, *34*, 5615-5623.
20. Wang, H.; Yan, W.; Jiang, T.; Liu, B.; Xu, W.; Ma, J.; Hu, Y. *Chinese Science Bulletin* **2002**, *47*, 1616-1618.
21. Bart, S. C.; Hawrelak, E. J.; Lobkovsky, E.; Chirik, P. J. *Organometallics* **2005**, *24*, 5518-5527.
22. Palmer, W. N.; Diao, T.; Pappas, I.; Chirik, P. J. *ACS Catal.* **2015**, *5*, 622-626.

23. (a) Ben-Daat, H.; Hall, G. B.; Groy, T. L.; Trovitch, R. J. *Eur. J. Inorg. Chem.* **2013**, 4430-4442. (b) Porter, T. M.; Hall, G. B.; Groy, T. L.; Trovitch, R. J. *Dalton Trans.* **2013**, 42, 14689-14692.
24. Mukhopadhyay, T. K.; Rock, C. L.; Hong, M.; Ashley, D. C.; Groy, T. L.; Baik, M.-H.; Trovitch, R. J. *J. Am. Chem. Soc.* **2017**, *139*, 4901-4915.

CHAPTER 1

SYNTHESIS OF A DIIMINE-BASED IRON DINITROGEN COMPLEX AND ITS REACTIVITY TOWARDS C-H & C-P BONDS

1.1. Abstract:

Reduction of 6-coordinate ($^{\text{Ph}_2\text{PPrDI}}$)FeBr₂ under N₂ results in the formation of a terminal dinitrogen complex, ($^{\text{Ph}_2\text{PPrDI}}$)FeN₂. Heating this complex to 75 °C allows for the isolation of a dimeric complex, [(μ -PrPPh- κ^5 -P,N,N,C γ P- $^{\text{Ph}_2\text{PPrDI}^{\text{PrPPh}}}$)Fe]₂. Detailed NMR analysis and crystallographic characterization revealed the formation of *cisoid* and *transoid* isomers via C-H activation followed by C-P activation. Mechanistic possibilities for this transformation are discussed. Reactivity of the dimeric compound has also been examined.

1.2. Introduction:

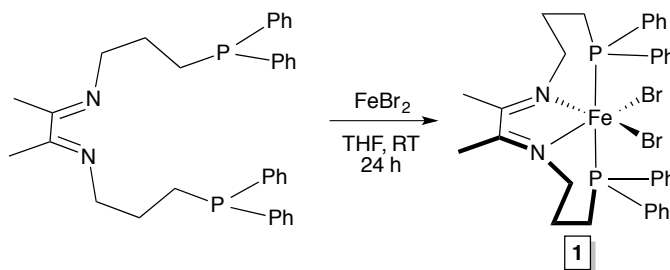
Bond activation is of fundamental interest to synthetic chemists since it allows for the preparation of value-added products from under-functionalized molecules.¹ While many C-H functionalization reactions rely on precious metal catalysts,² the utility of Fe precursors for this application has continued to expand,³ proving particularly useful in C-H bond oxidation⁴ and C-C bond forming reactions.⁵ The cleavage of C-P bonds by one or more Fe centers has also been well-established.⁶

Sequential C-H, C-P bond activation pathways by Group 8 metals are comparatively rare. Heating the tri(2-furyl)phosphine or tri(2-thienyl)phosphine adduct of [Ru₃(CO)₁₀(μ -dppm)] to 40 °C has been found to result in C-H and C-P bond cleavage to

yield a bridging furyl or thionyl moiety.⁷ Analogous reactivity has been described for $[\text{Os}_3(\text{CO})_{11}(\text{P}(2\text{-furyl})_3)]^8$ and simultaneous C-H, C-P activation has been observed while heating a diphenylphosphine-substituted fullerene adduct of $[\text{Os}_3(\text{CO})_{10}]$.⁹ Likewise, refluxing $\text{Fe}_2(\text{CO})_6(\mu\text{-PPh}_2)(\mu\text{-C}\equiv\text{C}^t\text{Bu})$ in the presence of PPh_3 results in a triiron product following C-H and C-P cleavage with concurrent C-P and C-C formation.¹⁰ Ruiz and co-workers have also suggested that the photochemical activation of $\text{Cp}_2\text{Fe}_2(\mu\text{-dppm})(\mu\text{-CO})$ induces a concerted C-H, C-P cleavage process to yield $[\text{Fe}_2\text{Cp}(\mu\text{-}\eta^5\text{:}\kappa^1\text{-C}_5\text{H}_4\text{CH}_2\text{PPh}_2)(\mu\text{-H})(\mu\text{-PPh}_2)(\text{CO})]$.¹¹

1.3. Synthesis and Characterization:

This project started with the metallation of $^{\text{Ph}_2\text{PPr}}\text{DI}$ ¹² using FeBr_2 at ambient temperature. The reaction mixture turned dark blue in color immediately upon addition of the DI ligand to the solution of FeBr_2 in THF, but was allowed to stir for 24 h to reach completion (Scheme 1). Following work-up, a high spin paramagnetic Fe(II) compound was isolated which showed a magnetic moment (μ_{eff}) of $5.0 \mu_{\text{B}}$ (Gouy balance method), suggesting four unpaired electrons, which was identified as $(^{\text{Ph}_2\text{PPr}}\text{DI})\text{FeBr}_2$ (Scheme 1.1, 1). The ^1H NMR spectrum of **1** exhibits resonances over a 200 ppm range (Fig 1.1).



Scheme 1.1: Synthesis of $(^{\text{Ph}_2\text{PPr}}\text{DI})\text{FeBr}_2$ (**1**).

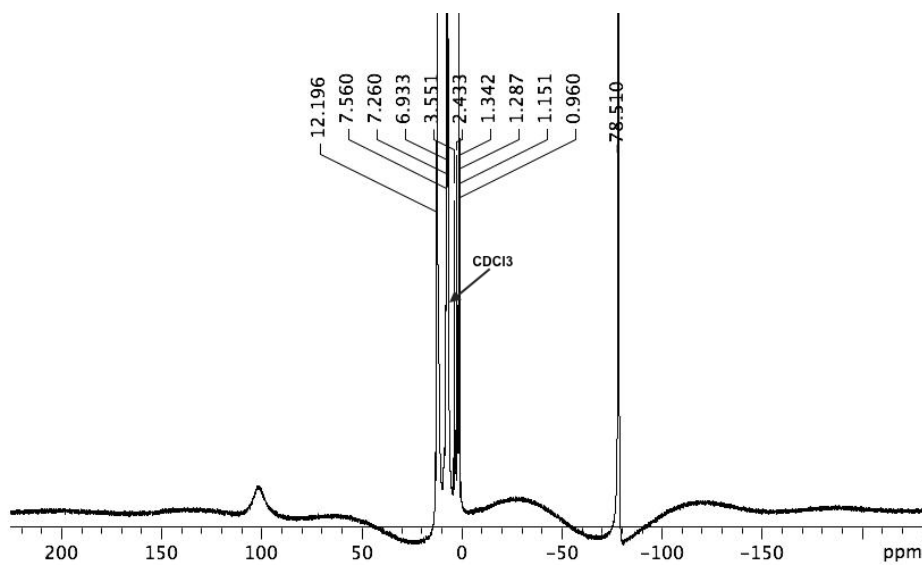


Figure 1.1: ^1H NMR spectrum of **1** in chloroform-*d* at 23 °C.

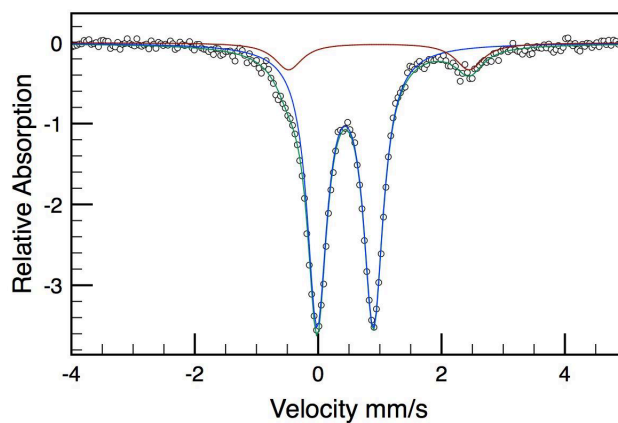


Figure 1.2: Zero-field Mössbauer spectrum of **1**. Sample contains approximately 12.2% of a high-spin impurity.

Table 1.1: Mössbauer fit parameters for **1**, **2** and **3**.

	1	2	<i>cisoid-3</i>
IS(1)	0.44 mm s ⁻¹	0.24 mm s ⁻¹	0.20 mm s ⁻¹
IS(2)	0.98 mm s ⁻¹	-	-
$\Delta E_Q(1)$	0.91 mm s ⁻¹	1.24 mm s ⁻¹	1.12 mm s ⁻¹
$\Delta E_Q(2)$	2.93 mm s ⁻¹	-	-
Fe(1)/Fe(2) relative abundance (%)	87.8/12.2	100	100

To confirm the denticity of the ligand and geometry, crystals of **1** were grown from a concentrated solution of chloroform layered with pentane at -35 °C. From single crystal X-ray diffraction (Fig 1.3), it was observed that iron(II) center possesses a distorted octahedral geometry having P(2)-Fe(1)-P(1), N(2)-Fe(1)-N(1), N(2)-Fe(1)-P(2) and N(2)-Fe(1)-Br(2) angles of 178.04(5)°, 79.60(15)°, 81.95(11)°, and 95.87(12)°, respectively (Table 1.2). As diimine ligands are known for their ability to be reduced,^{13,14} the bond distances of **1** were examined. Initially, ligand was thought to be singly reduced based on contraction of the C(2)-C(3) distance to 1.429(6) from 1.47 Å and elongation of the C-N distances to 1.312(6) Å and 1.314(6) Å from 1.29 Å (Table 2). Along with this data, Mössbauer spectroscopy revealed an isomer shift of 0.44 mm s⁻¹, which is more consistent with a high spin Fe(III) center rather than a Fe(II)¹⁵ center (Table 1.1).

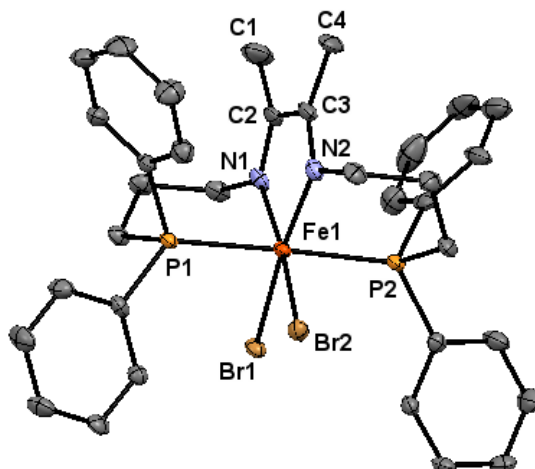


Figure 1.3: The solid-state structure of **1** at 30% probability ellipsoids. Hydrogen atoms and co-crystallized chloroform molecules are removed for clarity.

Table 1.2: Notable bond lengths (Å) and bond angles (°) determined for **1**.

Bond	Å	Angle	Degree
C(2)-C(3)	1.429(6)	N(1)-Fe(1)-N(2)	79.60(15)
C(2)-N(1)	1.312(6)	N(2)-Fe(1)-P(2)	81.95(11)
C(3)-N(2)	1.314(6)	N(1)-Fe(1)-P(2)	100.38(11)
Fe(1)-N(1)	1.939(4)	P(1)-Fe(1)-P(2)	178.04(5)
Fe(1)-N(2)	1.921(4)	N(2)-Fe(1)-Br(2)	95.87(12)
Fe(1)-P(1)	2.2792(12)	Br(1)-Fe(1)-Br(2)	90.42(2)
Fe(1)-P(2)	2.2775(13)		
Fe(1)-Br(1)	2.5044(7)		

To validate the ligand reduction and oxidation state of the iron center of **1**, DFT calculations were performed. Both unrestricted (UKS) and broken symmetry BS(5,1) calculations were carried out, however the BS(5,1) calculation converged to the UKS solution. The UKS solution indicates that **1** is a $S = 2$ compound with a high spin Fe(II) center and no reduction of the ligand (Fig 1.5). Moreover, the spin density plot shows a charge of +3.70 at the Fe(II) center (consistent with four unpaired electrons) and minimal

spin density on the DI ligand (Fig. 1.4). Since the bond distances and angles calculated for **1** did not match the experimentally determined metrical parameters, a single point UKS calculation was performed using the crystal structure geometry. This calculation converged to the BS(5,1) solution; however, the antiferromagnetically coupled electrons were both Fe-based, with an empty DI π^* orbital lying higher in energy than metal based orbitals. There was also a high overlap value ($S = 0.86$) between the coupled orbitals, and the spin density plot indicates little density on DI ligand due to backbonding (-0.21 , Fig. 1.6). Overall, the calculations suggest that the high spin Fe(II) is the most appropriate electronic structure description for **1**.

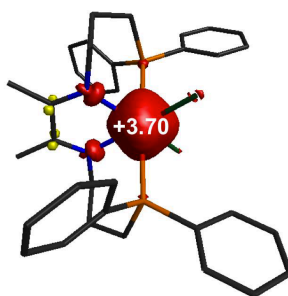


Figure 1.4: Mulliken spin density plot for **1** using the UKS ($S = 2$) solution.

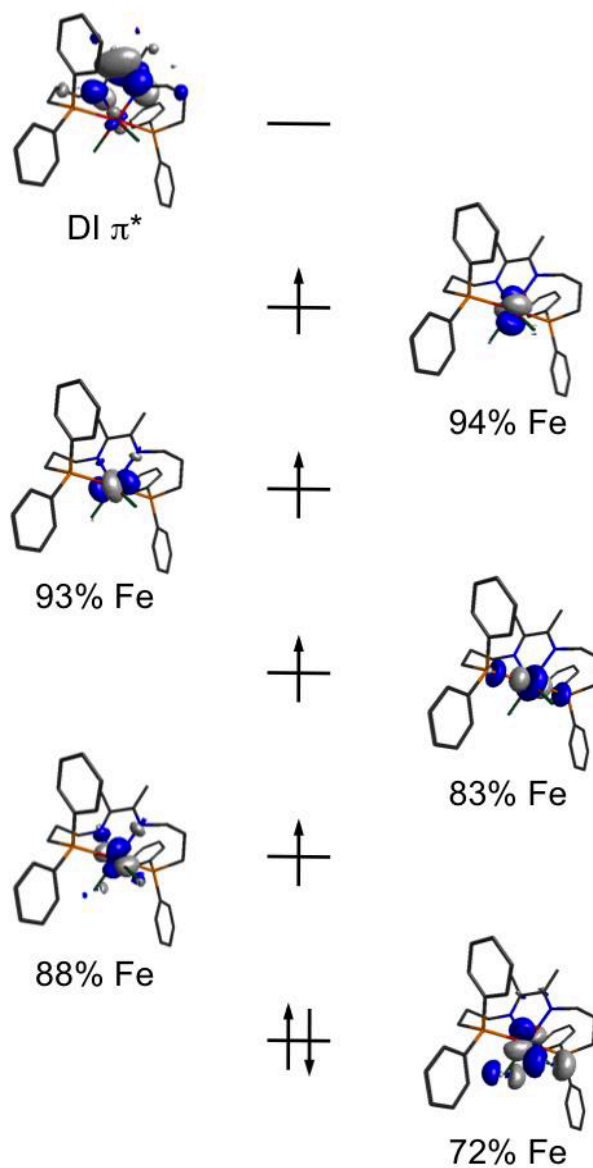


Figure 1.5: Orbital representations for **1** using the UKS ($S = 2$) solution.

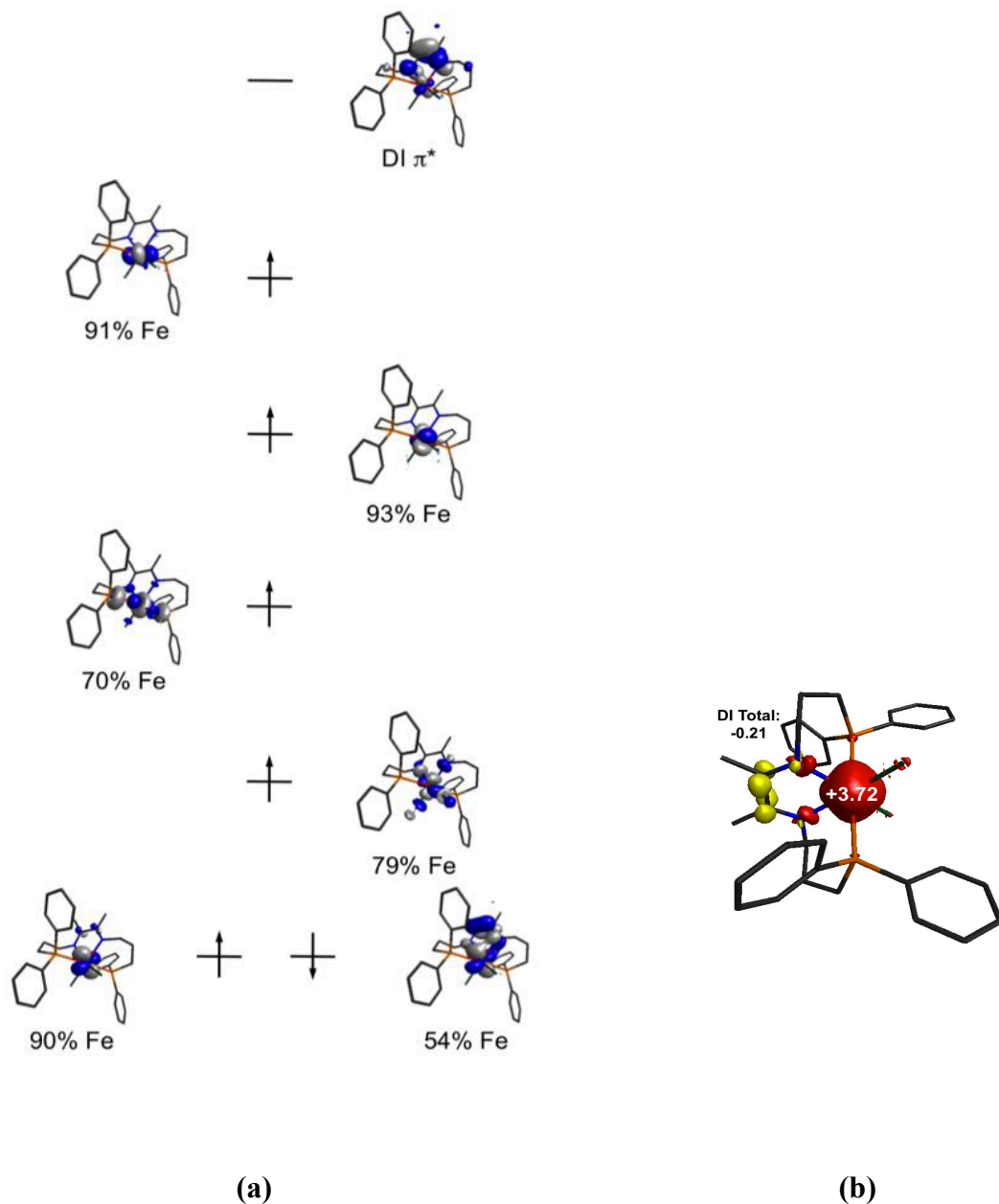
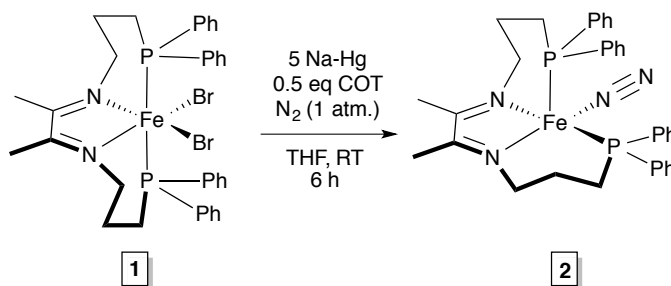


Figure 1.6: Orbital representations of **1** for the single point UKS ($S = 2$) solution (a) and Mulliken spin density plot for the single point **1** UKS ($S = 2$) solution (unoptimized solid state structure geometry) (b).

After isolating and characterizing the dibromide compound (**1**), it was reduced using excess Na-Hg. Over a period of 6 h, a greenish-brown diamagnetic compound was

obtained. A single resonance at 2.02 ppm for both backbone methyl groups was observed by ^1H NMR spectroscopy and a single resonance at 67.05 ppm (Fig. 1.8) was observed by ^{31}P NMR spectroscopy, suggesting C_2 -symmetry of the ligand environment around Fe in the solution phase. IR spectroscopy exhibited an N_2 stretching frequency at 2011 cm^{-1} (Fig. 1.9 b), which is consistent with a weakly activated N_2 ligand.¹⁶ Based on ^1H NMR, ^{31}P NMR and infrared spectroscopy, the compound was identified as $(^{\text{Ph}_2\text{PPrDI})\text{FeN}_2$ (Scheme 1.2, **2**).



Scheme 1.2: Synthesis of $(^{\text{Ph}_2\text{PPrDI})\text{FeN}_2$ (**2**).

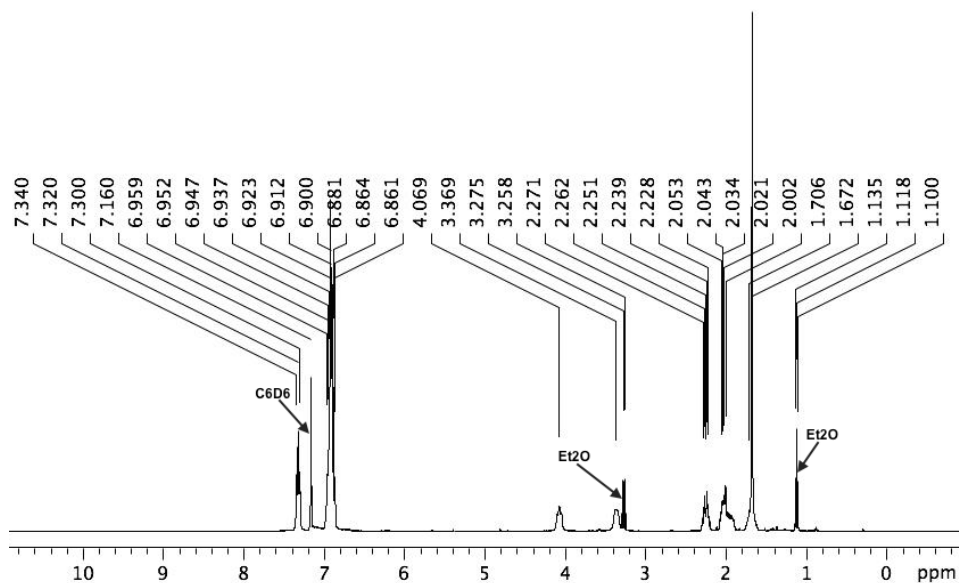


Figure 1.7: ^1H NMR spectrum of **2** in benzene- d_6 at 25 °C.

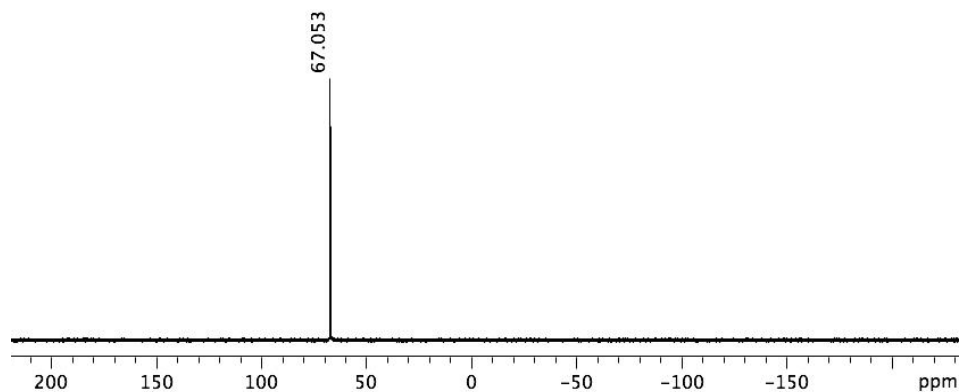


Figure 1.8: ^{31}P NMR spectrum of **2** in benzene- d_6 at 25 °C.

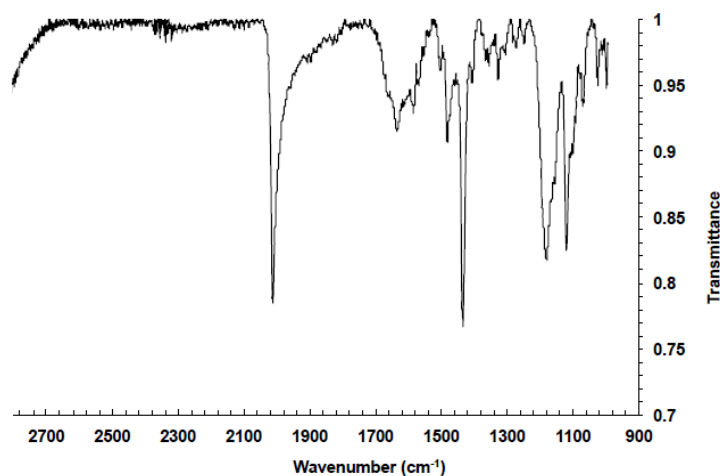


Figure 1.9: Solid-state infrared spectrum of **2** in KBr.

To obtain further structural information on **2**, crystals were grown from a concentrated diethyl ether solution at -35 °C. Single crystal XRD analysis displayed distorted square pyramidal geometry around the iron center (Fig. 1.10) with N(1)-Fe(1)-P(2), N(2)-Fe(1)-N(3) and N(2)-Fe(1)-N(1) angles of 162.70(5)°, 150.99(8)°, and

80.77(7)°, respectively (Table 1.3). Based on the Fe(1)-N(3) distance of 1.7945(19) Å and N(3)-N(4) distance of 1.117(3) Å, the N₂ ligand can be best described as unreduced compared to the literature, but accepting electrons from the Fe center via backbonding.¹⁶ Elongation of N(1)-C(2) and N(2)-C(3) distances from 1.28 Å (neutral ligand) to 1.354(3) Å and 1.371(3) Å, respectively, with concomitant shortening of the C(2)-C(3) distance from 1.47 Å (neutral ligand) to 1.390(3) Å indicates one electron reduction of the DI ligand to generate DI radical anion.¹⁴

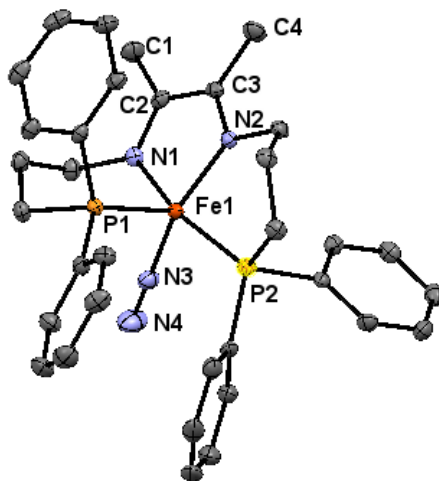


Figure 1.10: The solid-state structure of **2** at 30% probability ellipsoids.

Table 1.3: Notable bond lengths (Å) and bond angles (°) determined for **2**.

Bond	Å	Angle	Degree
C(2)-C(3)	1.390(3)	N(1)-Fe(1)-N(2)	80.77(7)
C(2)-N(1)	1.354(3)	N(2)-Fe(1)-P(2)	89.31(5)
C(3)-N(2)	1.371(3)	N(1)-Fe(1)-P(2)	162.70(5)
Fe(1)-N(1)	1.9196(17)	P(1)-Fe(1)-P(2)	105.76(2)
Fe(1)-N(2)	1.9009(17)	N(2)-Fe(1)-N(3)	150.99(8)
Fe(1)-P(1)	2.1845(6)		
Fe(1)-P(2)	2.1935(6)		
N(3)-N(4)	1.117(3)		

In a similar fashion, DFT calculations were conducted on **2**. The UKS calculation converged to a singlet featuring a doubly occupied DI-based HOMO with 26% Fe character (Fig. 1.11). A BS(1,1) calculation was also performed, revealing a low-spin Fe(I) center that is antiferromagnetically coupled to a DI-based electron ($S = 0.65$). The spin density plot shows a charge of +0.80 on Fe with an overall DI charge of -0.73 (Fig. 1.12 **b**), consistent with this formulation. Both the UKS and BS(1,1) solutions match with the experimental metrical parameters found for **2** and the BS(1,1) solution was determined to be 1.7 kcal mol⁻¹ lower in energy. Formulation of **2** having a DI radical anion is analogous to the electronic structure reported for 5-coordinate (Triphos)Fe(Bpy).¹⁷

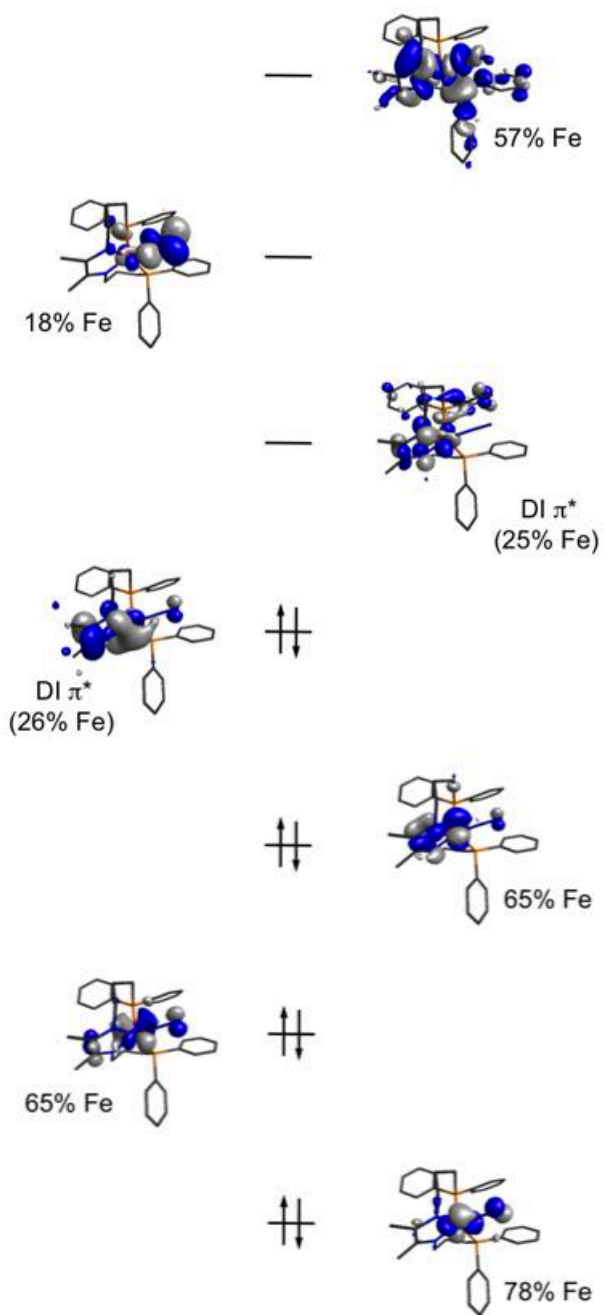


Figure 1.11: Orbital representations for 2 UKS ($S = 0$) solution.

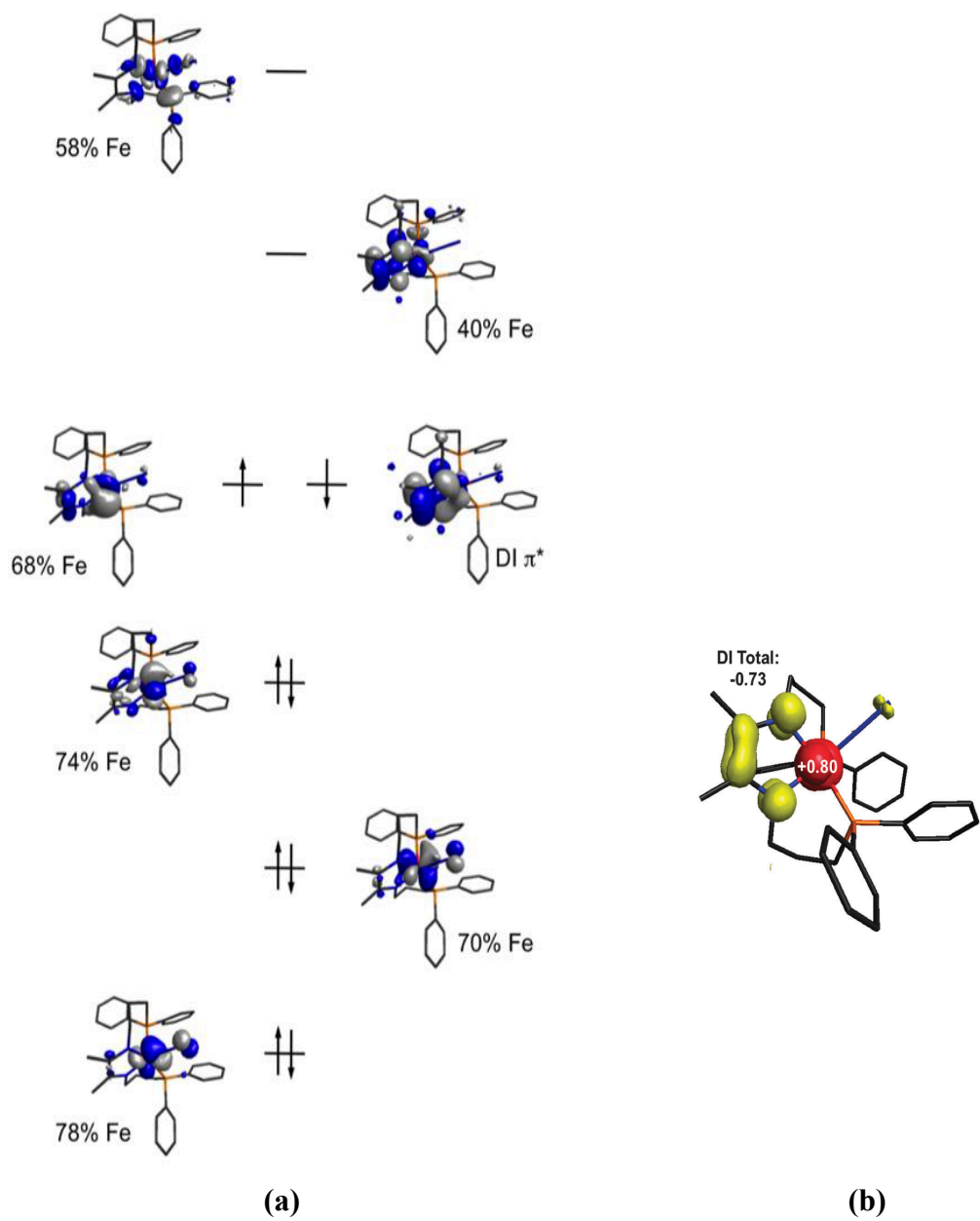


Figure 1.12: Orbital representations (a) and spin density plot (b) for 2 BS(1,1) solution.

Mössbauer spectroscopic data ($\delta = 0.24 \text{ mm s}^{-1}$, $\Delta E_Q = 1.24 \text{ mm s}^{-1}$) (Table 1.1) also corroborates the fact that the Fe center of **2** is low-spin Fe(I), antiferromagnetically coupled to a ligand radical anion.¹⁸

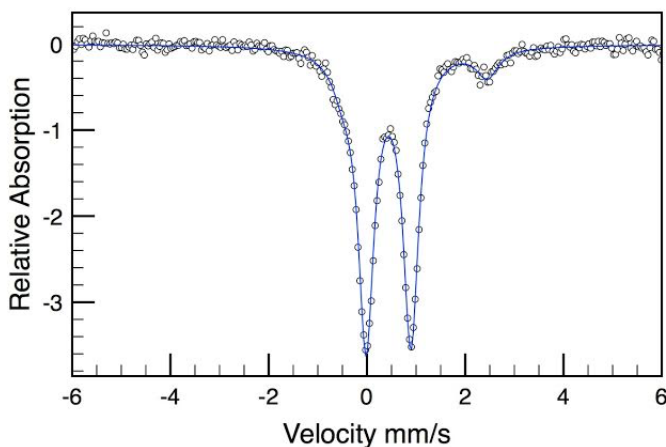
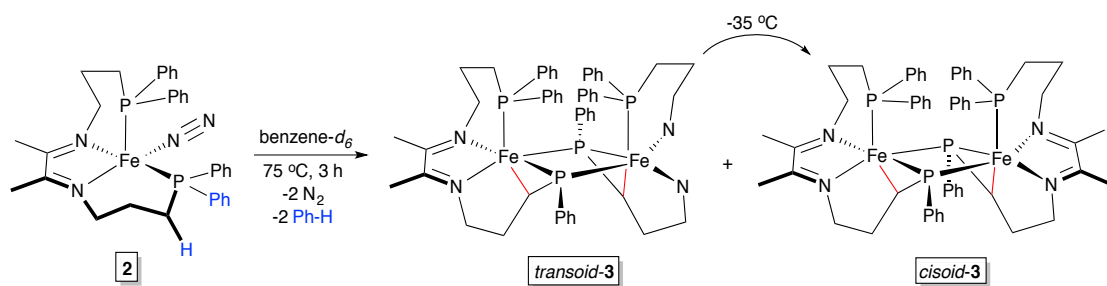


Figure 1.13: Zero-field ^{57}Fe Mossbauer spectra of **2**.

Notably, over extended period of time, a benzene- d_6 solution of **2** was slowly converted (11% conversion after 5 d) to two left-right equivalent compounds as evidenced from multinuclear NMR spectroscopy. This conversion was expedited by heating the solution of **2** in benzene- d_6 to 75 °C, which resulted in a reddish-brown compound within 30 minutes (Scheme 1.3). ^{31}P NMR spectroscopy displayed formation of major (68%) and minor (32%) isomers identified as *cisoid*- $[(\mu\text{-PrPPh-}\kappa^5\text{-P,N,N,C}_\gamma\text{,P-Ph}_2\text{PPrDI}^{\text{PrPPh}})\text{Fe}]_2$ (**3**) and *transoid*- $[(\mu\text{-PrPPh-}\kappa^5\text{-P,N,N,C}_\gamma\text{,P-Ph}_2\text{PPrDI}^{\text{PrPPh}})\text{Fe}]_2$ (**3**), having resonances at -90.26, 61.08 ppm and -61.45, 54.94 ppm, respectively (Fig. 1.15). Storing the solution at -35 °C led to complete conversion to the major *cisoid* isomer as reflected by ^{31}P NMR spectroscopy (Fig. 1.17).



Scheme 1.3: Synthesis of *cisoid*- $[(\mu\text{-PrPPh-}\kappa^5\text{-P,N,N,C}_\gamma\text{-P-Ph}_2\text{PPrDI}^{\text{PrPPh}})\text{Fe}]_2$ (**3**) and *transoid*- $[(\mu\text{-PrPPh-}\kappa^5\text{-P,N,N,C}_\gamma\text{-P-Ph}_2\text{PPrDI}^{\text{PrPPh}})\text{Fe}]_2$ (**3**).

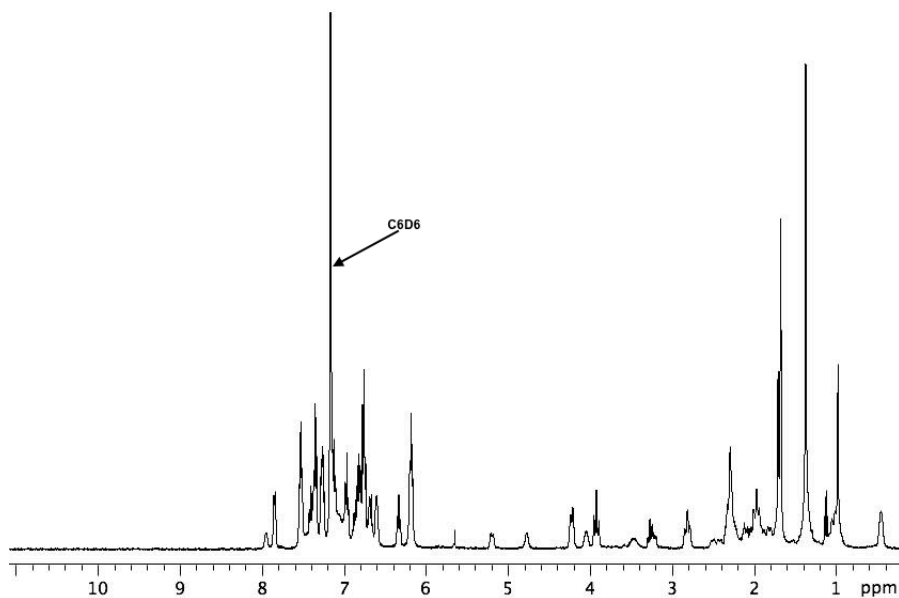


Figure 1.14: ^1H NMR spectrum showing a mixture of *cisoid*-**3** and *transoid*-**3** in benzene- d_6 .

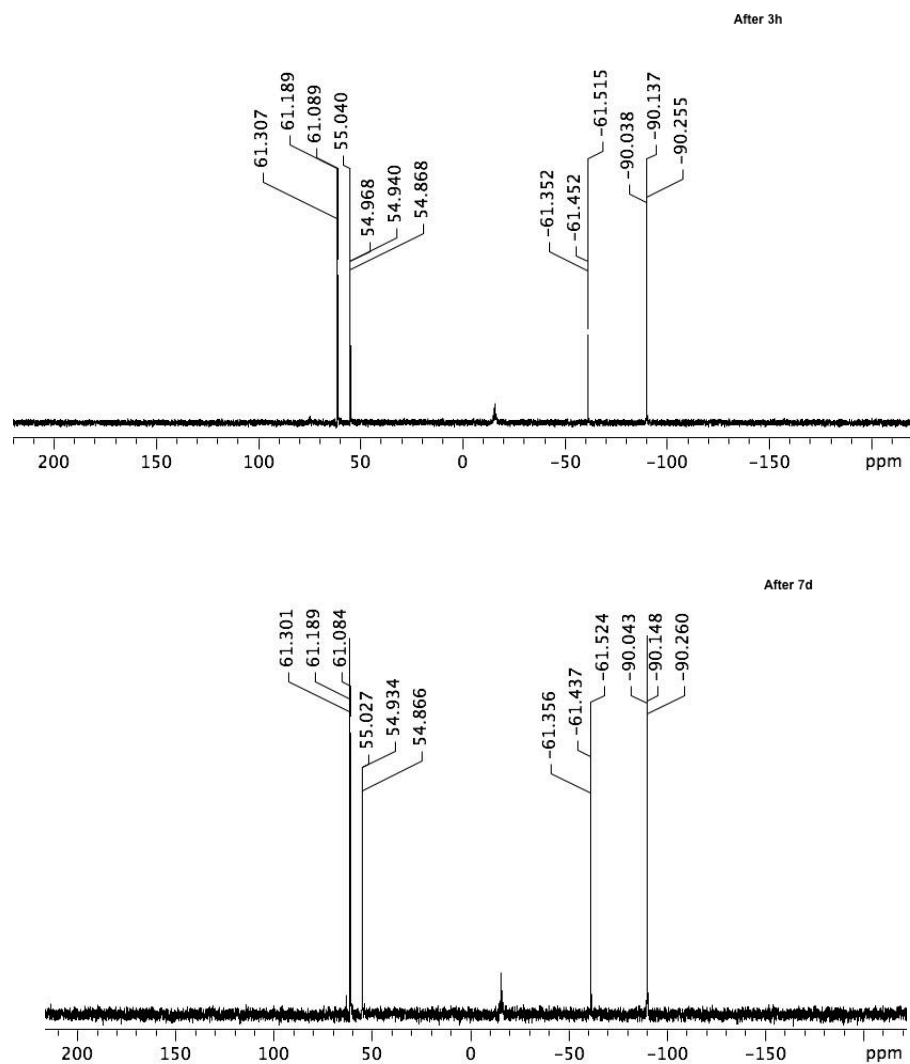


Figure 1.15: ^{31}P NMR spectra showing a mixture of *cisoid-3* and *transoid-3* in benzene- d_6 after 3 h and 7 d at 25 °C.

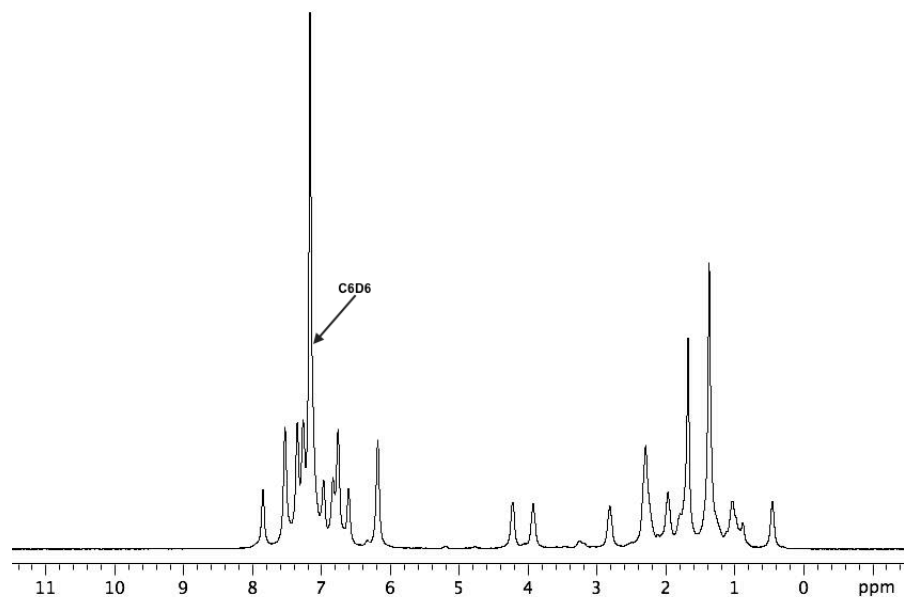


Figure 1.16: ^1H NMR spectrum of *cisoid-3* in benzene- d_6 at 25 °C.

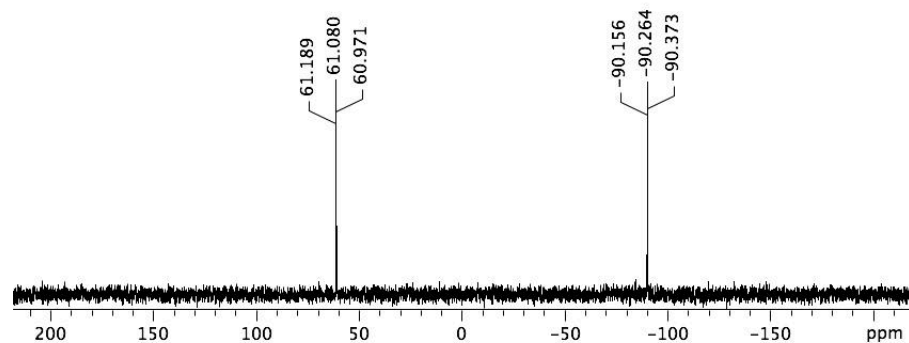


Figure 1.17: ^{31}P NMR spectrum of *cisoid-3* in benzene- d_6 at 25 °C.

To investigate the structure of **3**, recrystallization in benzene was attempted at 25 °C, which resulted in the isolation of the *cisoid-3* isomer (Two unique dimers per unit cell were observed, only one is shown in Fig. 1.18).

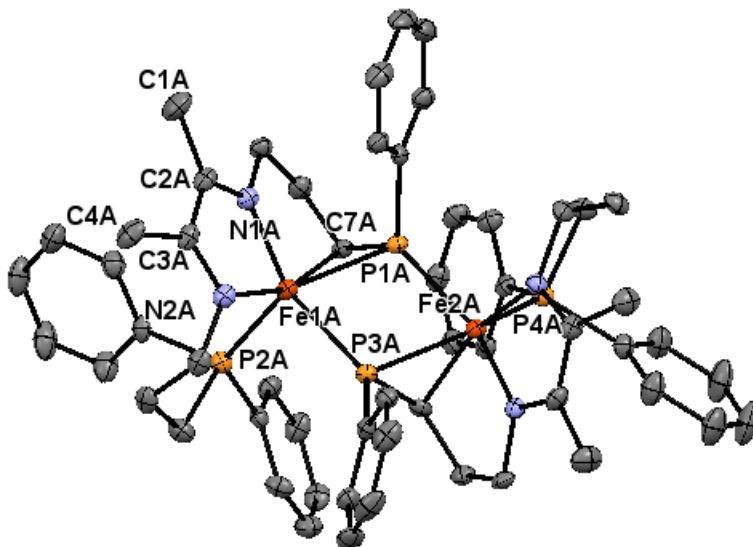


Figure 1.18: The solid-state structure of *cisoid-3* at 30% probability ellipsoids. Hydrogen atoms, co-crystallized solvent molecules, and second *cisoid-3* molecule removed for clarity.

Table 1.4: Notable bond lengths (Å) and bond angles (°) determined for **3**.

Bond	Å	Angle	Degree
C(2A)-C(3A)	1.407(4)	N(1A)-Fe(1A)-N(2A)	79.59(11)
C(2A)-N(1A)	1.337(4)	N(2)-Fe(1A)-P(2A)	91.02(8)
C(3A)-N(2A)	1.346(4)	N(1A)-Fe(1A)-P(2A)	110.65(8)
Fe(1A)-N(1A)	1.887(2)	P(1A)-Fe(1)-P(2)	134.98(3)
Fe(1A)-N(2A)	1.937(2)	N(2A)-Fe(1A)-C(7A)	161.44(11)
Fe(1A)-P(1A)	2.2648(9)	P(1A)-Fe(1A)-C(7A)	47.21(8)
Fe(1A)-P(2A)	2.1984(9)		
Fe(1A)-C(7A)	2.097(3)		
P(1A)-P(3A)	2.6163(11)		

Although, isolation of the *transoid* isomer failed, formation of this isomer was observed by NMR spectroscopy. Repeating this reaction in toluene- d_8 allowed for the detection of benzene as a byproduct, which is formed via sequential C-H, C-P bond activation from the chelate arm. The solid-state structure of *cisoid-3* revealed that each Fe

center of the dimer has pseudo octahedral geometry (Fig. 1.18), arising from γ -methylene C-H activation and the cleavage of one P-Ph bond per chelate. As an outcome of these sequential bond cleavages, a highly strained metallacyclopentane is formed having an average P-Fe-C angle of only 47.37° . The N-containing metallocyclopentane ring did not undergo β -hydrogen elimination even though alkyl complexes of Fe are well-known for β -H elimination.¹⁹ The rigidity of the chelate framework in *cisoid-3* is anticipated as an impediment for Fe to access the β -methylene group.²⁰ Even though Fe-phosphide bonds are formed, the distance of Fe-P bond (2.251 \AA) is longer than average Fe-phosphine bond (2.197 \AA), which suggests that they are weakly bonded. The average Fe-C distance of *cisoid-3* is determined to be 2.094 \AA , consistent with low spin Fe centers. In a similar fashion, the DI core can be considered as singly reduced radical anion, based on the elongation of the imine C-N distances and contraction of the C-C distances of the diimine moiety (Table 1.4).¹⁴ In the case of **3**, Mössbauer spectroscopic parameters ($\delta = 0.20 \text{ mm s}^{-1}$, $\Delta E_Q = 1.12 \text{ mm s}^{-1}$) (Table 1.1) failed to differentiate the Fe oxidation state as the Fe center is in low spin state. Based on an earlier report,²¹ terpyridine or pyridine diimine (PDI) supported Fe dialkyl complexes are known to have a Fe(III) center, antiferromagnetically coupled to a ligand radical anion. Although these complexes feature different spin states, it is likely that both Fe centers of *cisoid-3* are trivalent, and antiferromagnetically coupled to a DI radical anion.

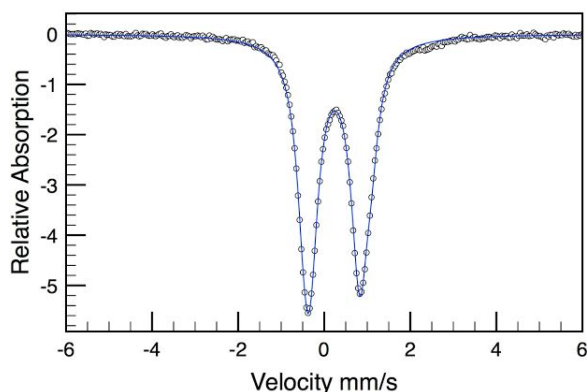


Figure 1.19: Zero-field ^{57}Fe Mössbauer spectra of **3**.

1.4. Plausible Mechanism For Dimer Formation:

There are two plausible intramolecular bond activation pathways that can lead to the formation of two isomers of **3**, *cisoid-3* and *transoid-3*. First, C-H bond activation of the γ -methylene group at one Ph_2PPrDI fragment, with concomitant N_2 loss, would result in the formation of one transient Fe-hydride species (Fig. 1.20, **A**). It is proposed that species **A** immediately reacts with a neighboring P-Ph bond to release a benzene molecule and generate a monomeric compound (Fig. 1.20, **B**). To achieve saturated coordination, iron phosphide complex (**B**) reacts with the Fe center of another molecule to form the isomers of **3**, involving the lone pairs of phosphorus. Rearrangement of kinetically favored product *transoid-3* to thermodynamically favored product *cisoid-3* has been observed while cooling to $-35\text{ }^\circ\text{C}$. It can be proposed that reversible dissociation of dimer to **B** occurs between $25\text{ }^\circ\text{C}$ and $-35\text{ }^\circ\text{C}$. An alternative intramolecular pathway

involving C-P activation is also possible, which can generate intermediate C (Fig. 1.20).

Dimer formation could also occur through intermolecular activation pathways.

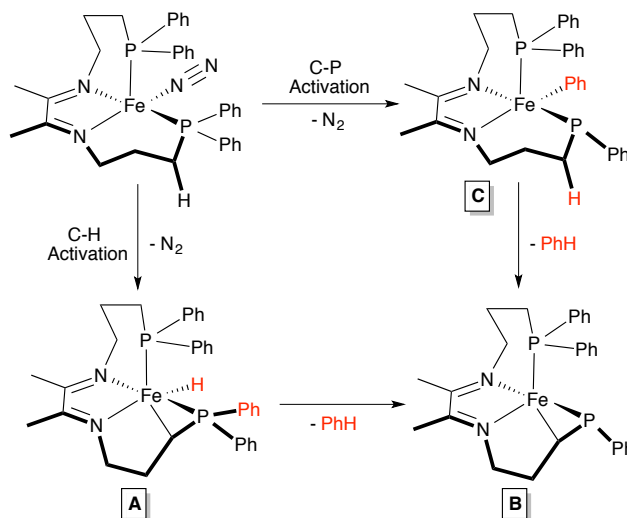


Figure 1.20: Plausible mechanistic pathways for the formation of **3**.

1.5. Reactivity Study of **2**:

The C-H bond activation of **2** inspired us to explore its reactivity towards other X-H (X = H, Si, B) bond activation processes. Upon addition of 1 atmosphere of H₂ gas to a benzene-*d*₆ solution of **2**, no color change was observed. However, a new diamagnetic compound was observed by the multinuclear NMR spectroscopy. The ¹H NMR spectrum of this compound featured a triplet peak at -15.82 ppm (*J*_{PH} = 84.9 Hz) (Fig. 1.21), indicating a hydride and ³¹P NMR spectroscopy showed a peak at 85.83 ppm (Fig. 1.22). These observations suggest that H-H bond activation of H₂ by **2** led to the formation of an iron dihydride compound. Attempts to isolate this new dihydride compound failed as it converted back to the starting iron dinitrogen compound **2**, upon exposure to the N₂ atmosphere of the glove box.

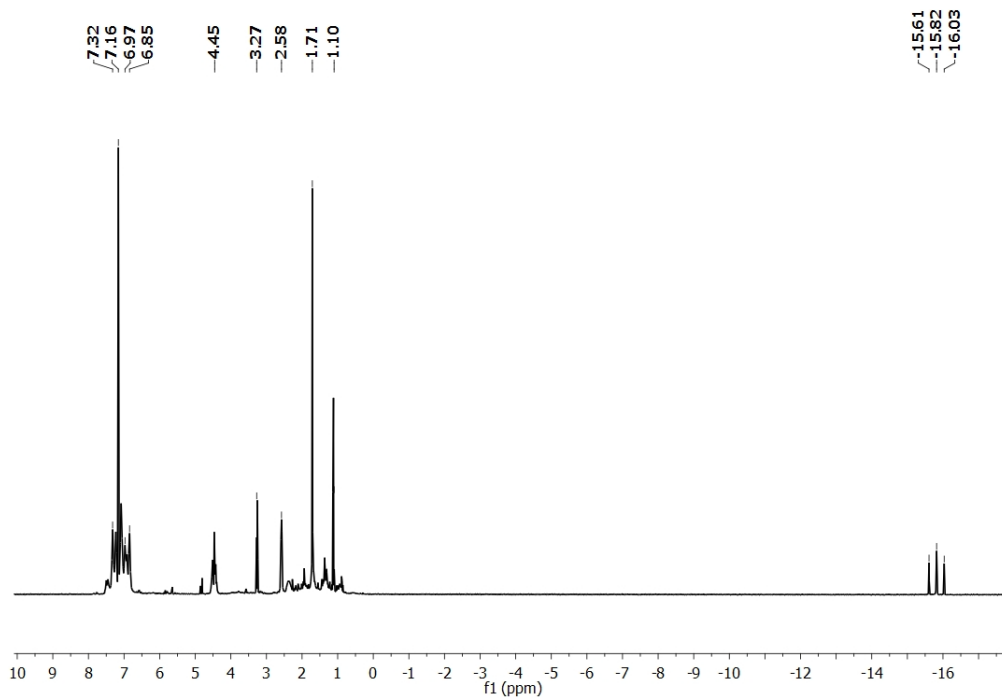


Figure 1.21: ^1H NMR spectrum of the reaction of **2** with 1 atmosphere of H_2 in benzene- d_6 at room temperature after 2 h.

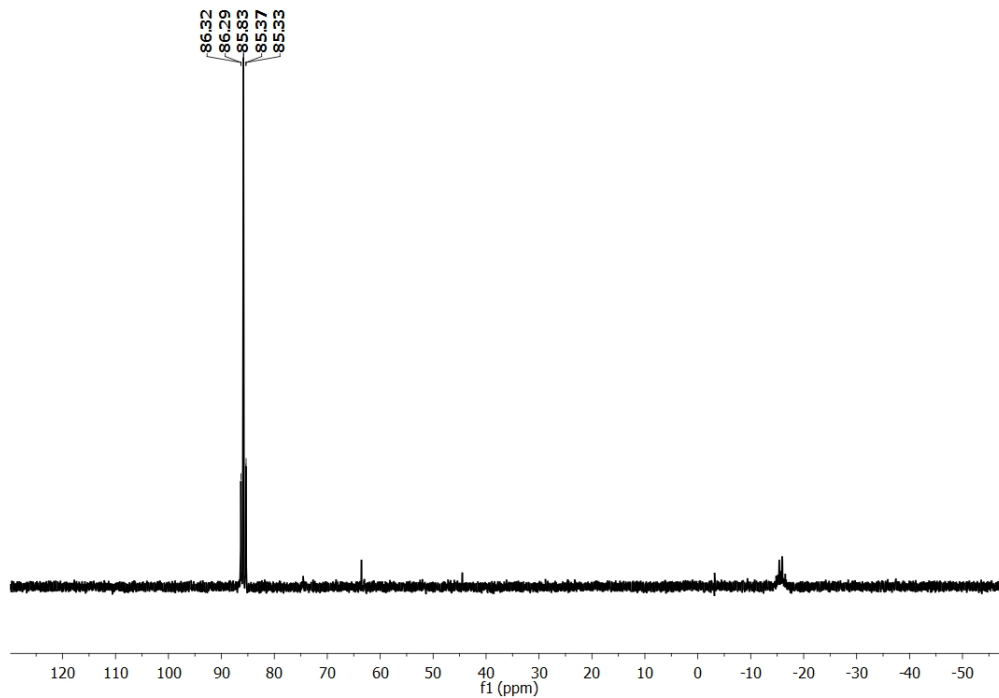


Figure 1.22: ^{31}P NMR spectrum of the reaction of **2** with 1 atmosphere of H_2 in benzene- d_6 at room temperature after 2 h.

Compound **2** was also reacted with 1 eq. of PhSiH₃ in benzene-*d*₆ at room temperature. The progress of the reaction was monitored by the NMR spectroscopy. After 2 h, a new diamagnetic compound with a resonance at -13.74 ppm (t, *J* = 42.4 Hz) in the ¹H NMR spectrum (Fig. 1.23) and two broad resonances at 63.59 and 68.78 ppm in the ³¹P NMR spectrum (Fig. 1.24) was observed. These observations indicate the formation of an *trans*-iron(II) silyl hydride compound following the Si-H bond activation of PhSiH₃ by **2**. Over a period of 3 days, another new hydride peak was found at -5.84 ppm (t, *J* = 55 Hz) with the existent hydride peak in the ¹H NMR spectrum (Fig. 1.24). Additionally, a new signal was also observed at 80.09 ppm in the ³¹P NMR spectrum (Fig. 1.25). This new compound can be anticipated as the *cis*-isomer of the iron(II) silyl hydride compound.

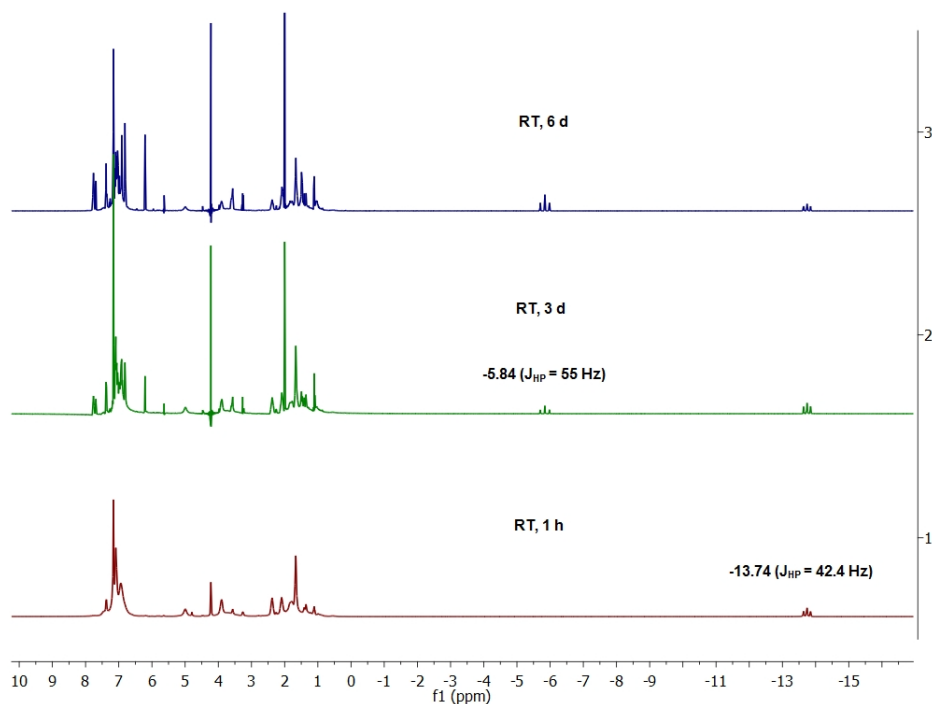


Figure 1.23: ¹H NMR spectra of the progress of the reaction of **2** with 1 eq. of PhSiH₃ at room temperature over a period of time.

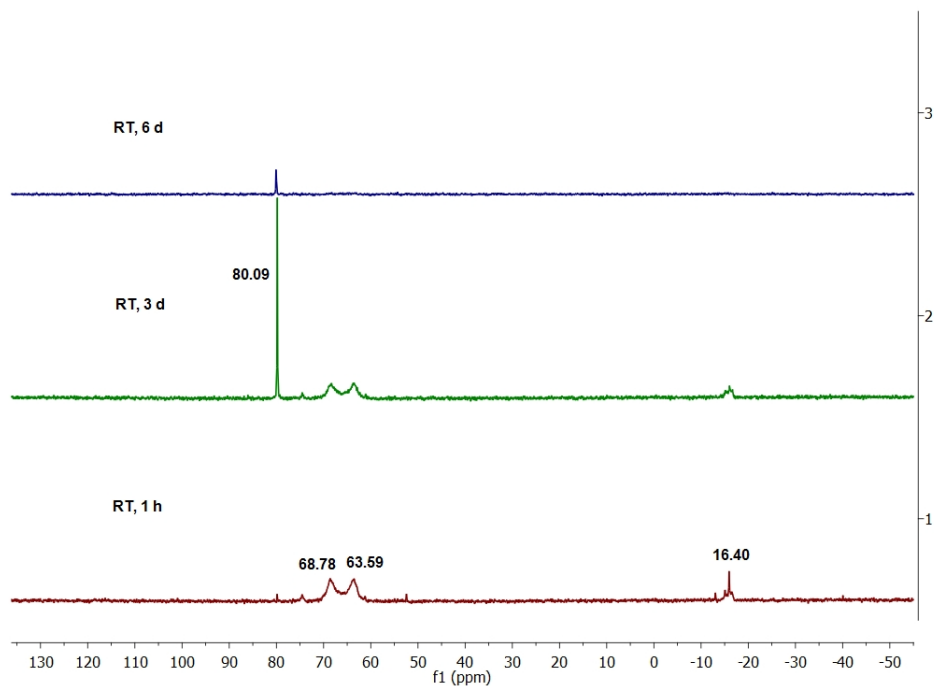


Figure 1.24: ^{31}P NMR spectra of the progress of the reaction of **2** with 1 eq. of PhSiH_3 at room temperature over a period of time.

In a similar fashion, one equivalent of pinacolborane (HBPin) was added to a benzene- d_6 solution of **2** at room temperature and the progress of the reaction was probed by the ^1H and ^{31}P NMR spectroscopy. A color change from green to orange was noticed. ^1H NMR spectroscopic analysis showed two signals at -5.29 ppm (t, $J = 63$ Hz) and -15.82 ppm (t, $J = 85.1$ Hz) (Fig. 1.25) and the ^{31}P NMR spectrum featured a resonance at 79.75 ppm (Fig. 1.26). No further change was detected by ^1H or ^{31}P NMR spectroscopy keeping the solution at room temperature over a period of time. This could be the result of B-H bond activation of HBPin by **2** to form a *trans*-iron(II) boryl hydride compound (hydride peak at -5.29 ppm and ^{31}P NMR: 79.75 ppm) and the other compound is probably the iron(II) dihydride compound (hydride peak at -15.82 ppm).

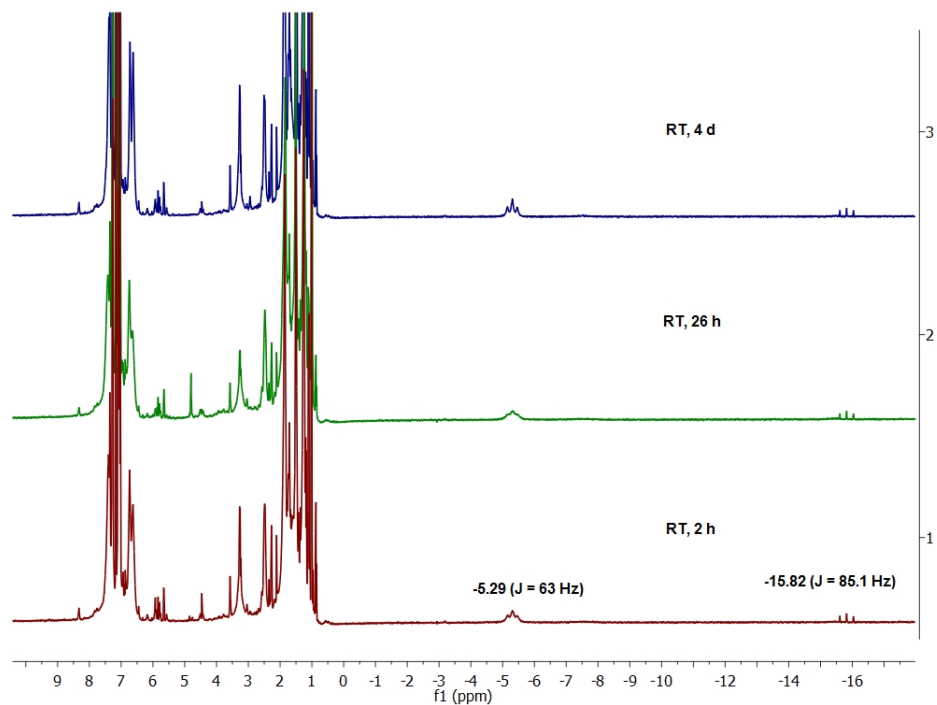


Figure 1.25: ^1H NMR spectra of the progress of reaction of **2** with 1 eq. of HBPin at room temperature over a period of time.

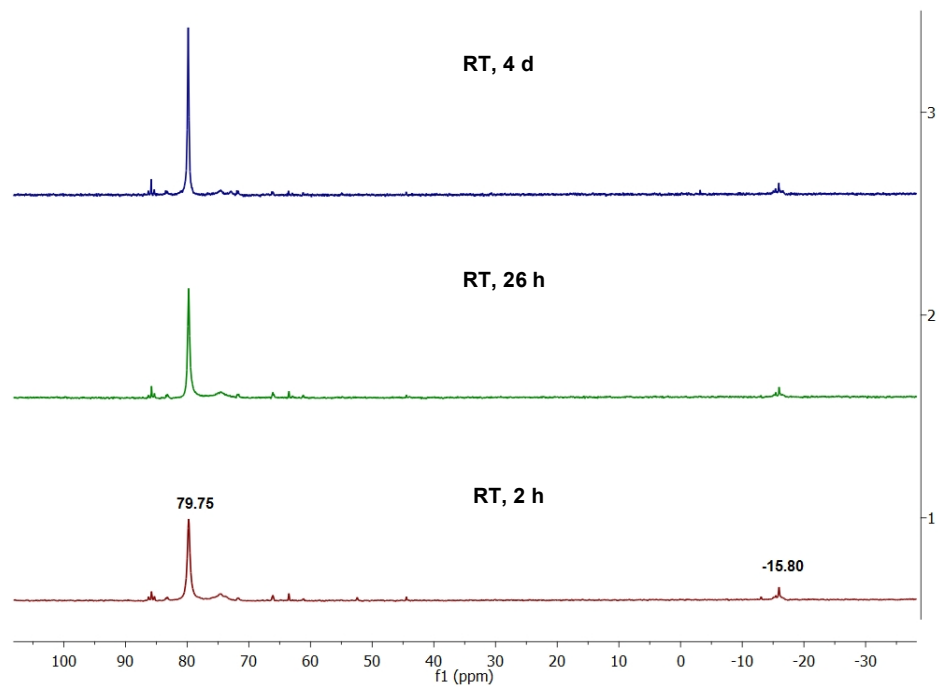


Figure 1.26: ^{31}P NMR spectra of the progress of reaction of **2** with 1 eq. of HBPin at room temperature over a period of time.

1.6. Reactivity Study of 3:

Having characterized the dimer, its reactivity was studied. To break the dimer into monomers, it was allowed to react with three neutral ligands (CO, H₂, and PMe₃). Upon reaction of *cisoid-3* with H₂ at ambient temperature in benzene-*d*₆, two new resonances were observed at 50.38 and -15.64 ppm in the ³¹P NMR spectrum. While heating to 95 °C, two more new ³¹P NMR signals were detected at 113.17 and 44.04 ppm after 24 h, which are doublets. The reaction mixture was then heated up to 120 °C for 24 h to allow complete consumption of the starting material, which finally afforded a mixture of complexes with the above four resonances in the ³¹P NMR spectrum (Fig. 1.27).

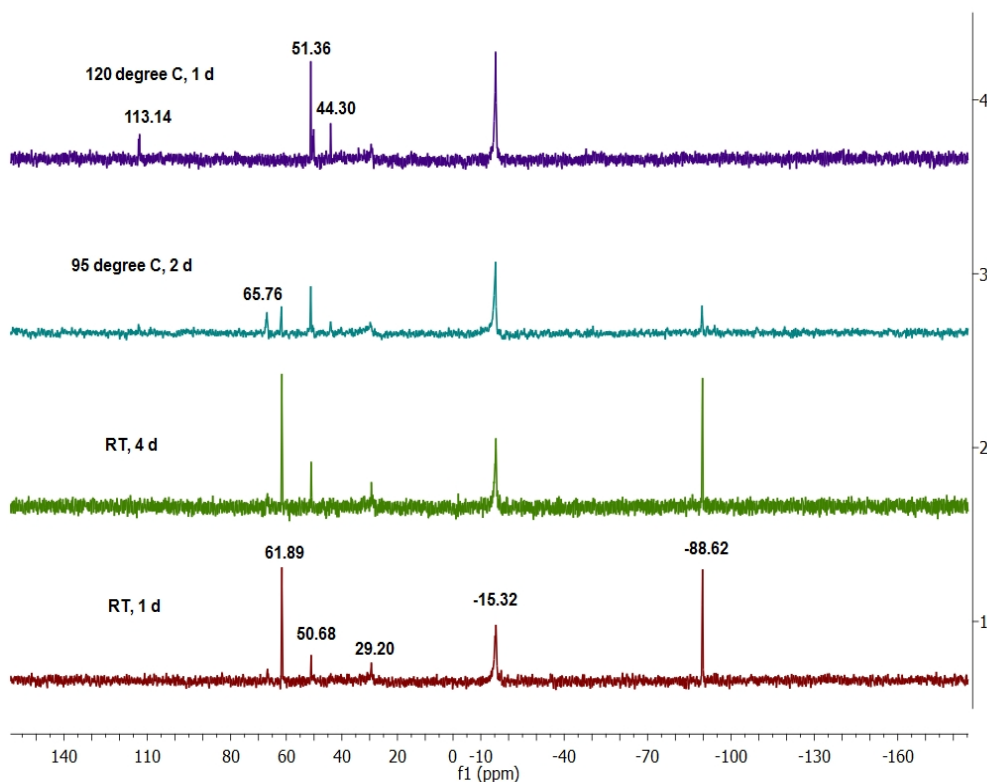


Figure 1.27: ³¹P NMR spectra of the progress of the reaction of *cisoid-3* with 1 atm. H₂ at different temperatures over a period of time.

Similarly, an NMR scale reaction of *cisoid-3* in benzene- d_6 with one atmosphere of CO was conducted and monitored by ^1H NMR and ^{31}P NMR spectroscopy. Two new ^{31}P NMR signals were detected at 69.92 (d, $J = 40$ Hz) and -74.54 ppm (d, $J = 40$ Hz) after 4 days at room temperature. These two peaks remain undisturbed upon heating to 120 °C after 24 h, and the starting material was not completely consumed (Fig. 1.28).

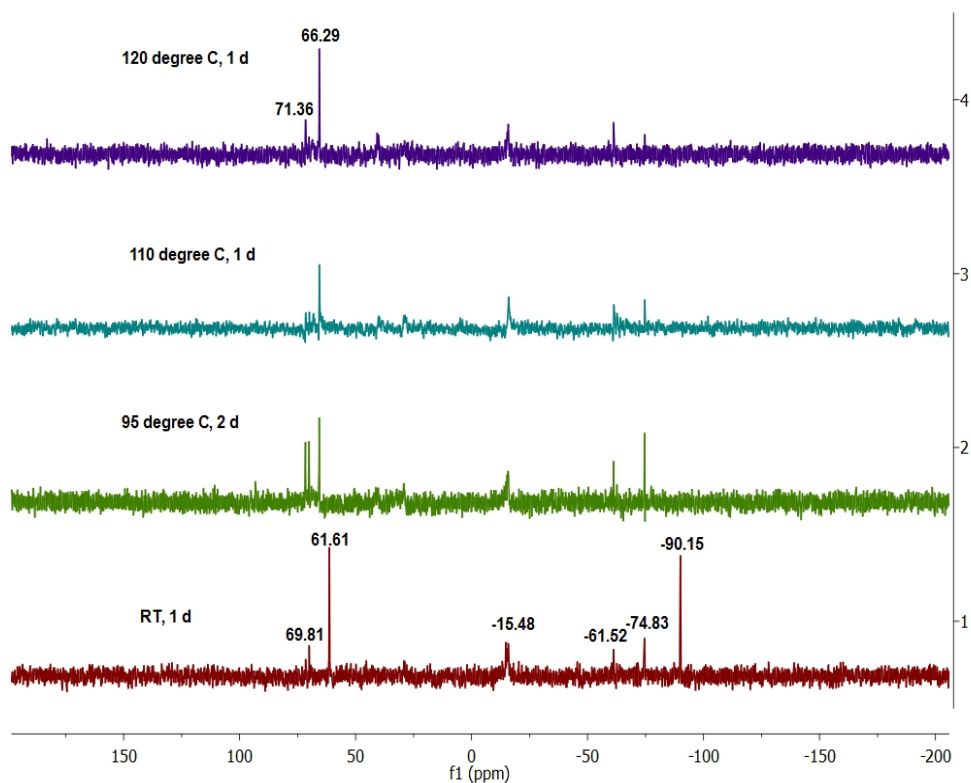


Figure 1.28: ^{31}P NMR spectra of the progress of the reaction of *cisoid-3* with 1 atm. CO at different temperatures over a period of time.

When a benzene- d_6 solution of *cisoid-3* was reacted with trimethylphosphine (PMe_3) and benzyl alcohol (PhCH_2OH), no reaction was observed at room temperature. Upon heating up to 100 °C, two new singlet resonances at 43.58 and 50.6 ppm were observed in the ^{31}P NMR spectrum as a result of the reaction between *cisoid-3* and benzyl

alcohol (Fig. 1.29), while PMe_3 did not react at all. The starting material was not completely consumed even after heating for 3 days at 100°C .

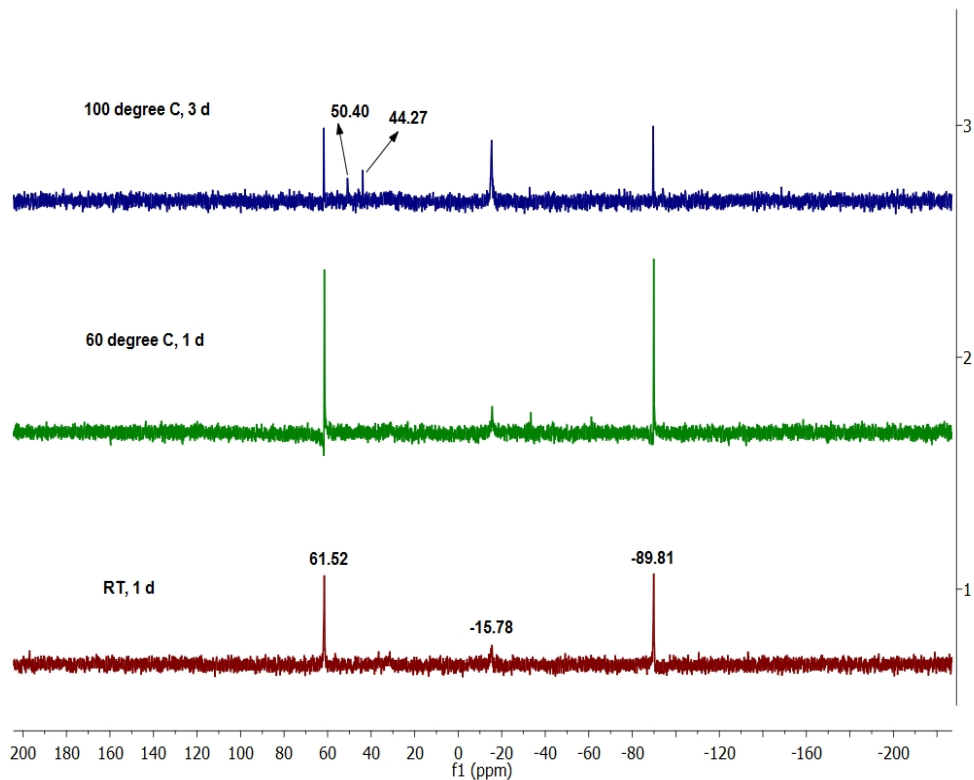


Figure 1.29: ^{31}P NMR spectra of the progress of reaction of *cisoid-3* with 2 eq. PhCH_2OH at different temperatures over a period of time.

Upon reaction with tetrafluoroboric acid ($\text{HBF}_4\cdot\text{OEt}_2$) in diethyl ether solvent, the color of the solution changed immediately from reddish brown to purple at ambient temperature. After stirring for 2 h, an insoluble purple compound was isolated having two distinguishable broad peaks at -15.17 and -16.14 ppm in the ^1H NMR spectroscopy (Fig 1.30) and two new resonances at 196.59 (d, $J = 375$ Hz) and 61.83 (d, $J = 345$ Hz) ppm (Fig 1.31) in ^{31}P NMR spectroscopy.

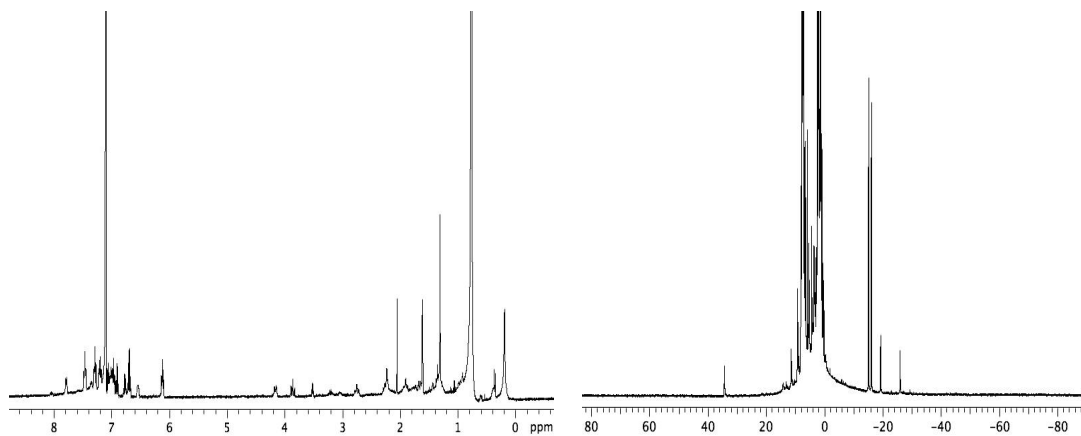


Figure 1.30: ¹H NMR spectra of the reaction of mixture of the isomers of **3** with 2 eq. HBF₄·OEt₂ (left: only diamagnetic region, right-full view).

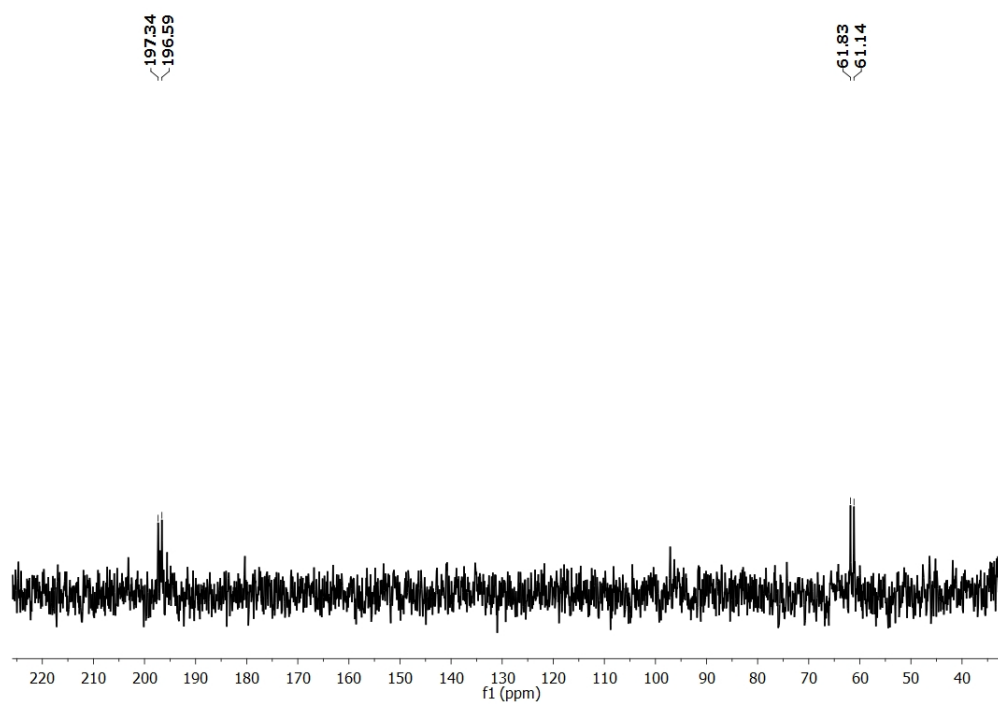


Figure 1.31: ³¹P NMR spectrum of the reaction of mixture of the isomers of **3** with 2 eq. HBF₄·OEt₂.

1.7. Conclusion:

In summary, a redox active α -diimine ligand-based iron dinitrogen compound has been isolated from reduction of the corresponding iron dibromide complex and thoroughly characterized via multinuclear spectroscopy, IR, Mössbauer, DFT and XRD. This compound undergoes sequential C-H, C-P activation upon heating which leads to the formation of a dimeric compound. To the best of our knowledge, this is a rare example of a two-bond activation processes at a single metal center. Presumably, it can be demonstrated that the redox non-innocence of α -diimine ligand paves the way for the C-H bond activation by removing an electron from Fe center, encouraging σ C-H coordination followed by scission.

1.8. Experimental Section:

1.8.1. General Considerations: All reactions were performed inside an MBraun glove box under an atmosphere of purified nitrogen. Toluene, tetrahydrofuran, pentane, and diethyl ether solvents were purchased from Sigma-Aldrich, purified using a Pure Process Technology solvent system, and stored in the glove box over activated 4Å molecular sieves and sodium before use. Benzene- d_6 , chloroform- d , and toluene- d_8 were purchased from Cambridge Isotope Laboratories and dried over 4Å molecular sieves prior to use. FeBr₂, 3-(diphenylphosphino)propylamine, and 1,3,5,7-cyclooctatetraene were used as received from Strem. Mercury was purchased from Sigma-Aldrich. ^{Ph₂PPr}DI was synthesized according to literature procedure.¹²

Solution ¹H nuclear magnetic resonance (NMR) spectra were recorded at room temperature on a Varian 400 MHz NMR spectrometer. All ¹H NMR and ¹³C NMR

chemical shifts (ppm) are reported relative to $\text{Si}(\text{CH}_3)_4$ using ^1H (residual) and ^{13}C chemical shifts of the solvent as a secondary standard. ^{31}P NMR data (ppm) is reported relative to H_3PO_4 . Elemental analyses were performed at the Goldwater Environmental Laboratory at Arizona State University. Solid state magnetic susceptibility was determined at 23 °C using a Johnson Matthey magnetic susceptibility balance calibrated with $\text{HgCo}(\text{SCN})_4$ and $\text{K}_3\text{Fe}(\text{CN})_6$. IR spectroscopy was conducted on a Bruker VERTEX spectrometer.

1.8.2. X-ray Crystallography: Single crystals suitable for X-ray diffraction were coated with polyisobutylene oil in the glove box and transferred to a glass fiber with Apiezon N grease, which was then mounted on the goniometer head of a Bruker APEX Diffractometer equipped with MoK_α radiation (Arizona State University). A hemisphere routine was used for data collection and determination of the lattice constants. The space group was identified and the data was processed using the Bruker SAINT+ program and corrected for absorption using SADABS. The structures were solved using direct method (SHELXS) completed by subsequent Fourier synthesis and refined by full-matrix, least square procedures on [F2] (SHELXL). The solid state structure of **1** was found to feature two co-crystallized chloroform molecules. The structure of *cisoid-3* features two unique dimers and two benzene sites, one of which has been modeled with pentane partial occupancy.

1.8.3. DFT Calculations: All DFT calculations were carried out using the ORCA program,²² and all compounds were optimized with the B3LYP functional.²³ Empirical

van der Waals corrections were included in the geometry optimization of all molecules.²⁴ The self-consistent field (SCF) calculations were tightly converged (1×10^{-8} Eh in energy, 1×10^{-7} Eh in density charge). Ahlrichs triple- ξ valence basis sets with one set of first polarization functions (def2-TZVP) were used for the iron and nitrogen atoms.²⁵ Ahlrichs split valence basis sets with one set of first polarization functions (def2-SVP) were used for the carbon and hydrogen atoms.⁵ Auxiliary basis sets were chosen to match the orbital basis sets used. Molecular orbitals were visualized using the Molekel program.²⁶

1.8.4. Preparation of (^{Ph₂PPr}DI)FeBr₂ (1): Under inert atmosphere, a 20 mL scintillation vial was charged with 0.155 g (0.719 mmol) of FeBr₂ followed by 0.386 g (0.719 mmol) of ^{Ph₂PPr}DI in approximately 15 mL of THF. The resulting solution turned dark blue in color immediately. The reaction mixture was stirred at ambient temperature for 24 h, and the resulting blue solution was filtered. The solvent was removed under vacuum and the resulting solid was washed with ether (4 X 5 mL) followed by toluene (1 X 4 mL) to remove residual free ligand. Upon drying, 0.489 g (90% yield) of a blue solid identified as **1** was collected. Crystals suitable for X-ray diffraction were obtained upon recrystallization from a concentrated chloroform solution layered with pentane at ambient temperature. Magnetic susceptibility (Gouy balance, 23 °C): $\mu_{\text{eff}} = 5.0 \mu_{\text{B}}$. Elemental Analysis: Calcd. C, 54.28%; H, 5.09%; N, 3.72%. Found: C, 54.81%; H, 5.07%; N, 3.57%. ¹H NMR (chloroform-*d*, 23 °C): 101.75 (peak width at half height = 2065 Hz), 12.20 (26 Hz), 6.94 (225 Hz), -78.58 (180 Hz).

1.8.5. Preparation of (^{Ph₂PPr}DI)Fe(N₂) (2): A 100 mL round bottom flask was charged with 2.65 g (13.253 mmol) of mercury and approximately 10 mL THF under inert

atmosphere. To this stirred solution, 0.015 g (0.663 mmol) of freshly cut Na was added and the solution turned cloudy and grey in color. The mixture was stirred at ambient temperature for approximately 20 min until it turned clear. After that, 7.5 μ L of cyclooctatetraene (0.0663 mmol) was added followed by a solution of 0.100 g (0.133 mmol) of **1** in approximately 20 mL of THF. The reaction mixture was stirred at ambient temperature for 6 h. The resulting green solution was filtered through Celite under vacuum and the solvent was removed. The residue was scraped off the sidewall of the flask with pentane (2 X 5 mL) and dried under vacuum. The residue was dissolved in toluene (~ 20 mL) and filtered through a Celite column to remove the remaining salt (NaCl) generated during reduction. This step was repeated twice and the solvent was removed under vacuum to obtain a greenish-brown solid identified as **2** (0.070 g, 85% yield). Crystals suitable for single crystal X-ray diffraction were obtained following recrystallization from a concentrated diethyl ether solution at -35 °C. Elemental Analysis: Calcd. C, 65.81%; H, 6.17%; N, 9.03%. Found: C, 65.81%; H, 5.91%; N, 7.14%. A lower than expected nitrogen content was observed in five separate elemental analysis trials, a consequence of facile N₂ loss in presence of O₂. ¹H NMR (benzene-*d*₆): 7.32 (m, 4H, *phenyl*), 6.92 (m, 16H, *phenyl*), 4.07 (m, 2H, CH₂), 3.37 (m, 2H, CH₂), 2.24 (m, 2H, CH₂), 2.00 (m, 6H, CH₂), 1.67 (s, 6H, CH₃). ¹³C NMR (benzene-*d*₆): 143.52 (*phenyl*), 141.28 (*phenyl*), 138.47 (*phenyl*), 133.76 (*phenyl*), 132.68 (*phenyl*), 53.33 (CH₂), 27.84 (CH₂), 27.57 (CH₂), 16.59 (CH₃). ³¹P NMR (benzene-*d*₆): 67.05 (s). IR (KBr): $\nu_{\text{NN}} = 2011 \text{ cm}^{-1}$.

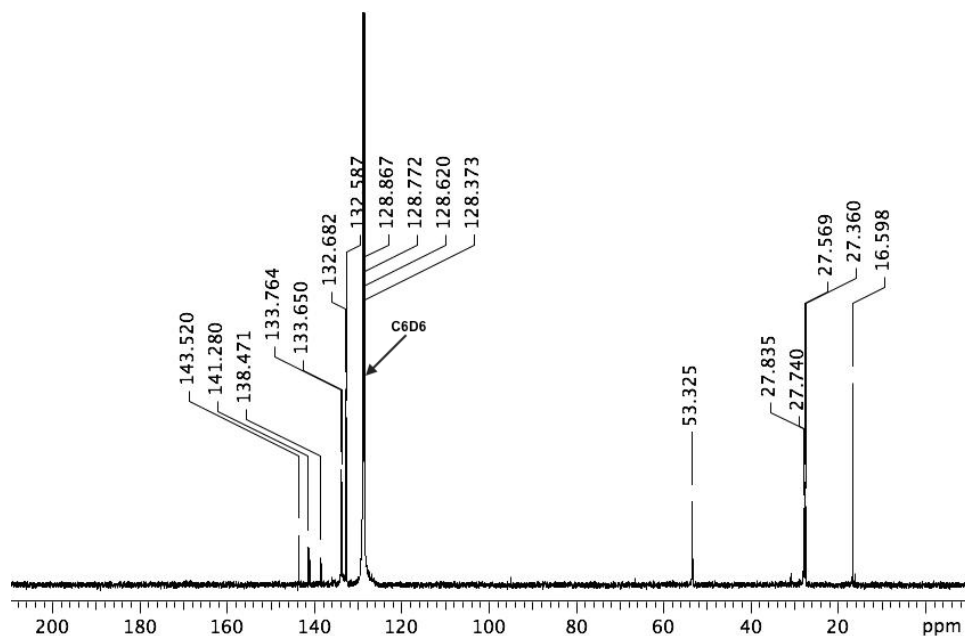


Figure 1.32: ^{13}C NMR spectrum of **2** in benzene- d_6 at 25 °C.

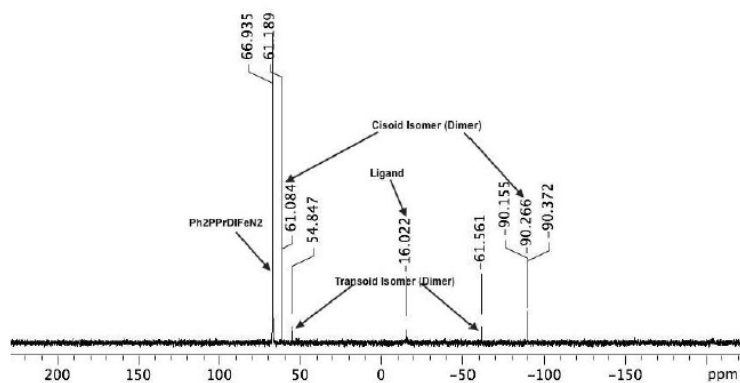


Figure 1.33: ^{31}P NMR spectrum of **2** in benzene- d_6 after 5d at 25 °C.

1.8.6. Preparation of $[(\mu\text{-PrPPh-}\kappa^5\text{-P,N,N,C}_\gamma\text{,P-Ph}_2\text{PPrDI}^{\text{PrPPh}})\text{Fe}]_2$ (3**):** Under inert atmosphere, a 20 mL scintillation vial was charged with 0.054 g (0.087 mmol) of **2** in approximately 1 mL of benzene- d_6 . This green solution was transferred into a J. Young NMR tube and sealed under N_2 . It was then heated to 75 °C in an oil bath. After 30 min, the color changed from green to reddish brown. The reaction mixture was heated for another 2.5 h to achieve the complete consumption of starting material, which was

confirmed by ^{31}P NMR. Then the mixture was filtered through Celite and the solvent was removed under vacuum to obtain a reddish brown solid identified as **3** (0.043 g, 47%). ^1H NMR and ^{31}P NMR spectroscopy revealed the *cisoid* and *transoid* isomers of this complex. Single crystals of *cisoid-3* were obtained following recrystallization of a concentrated benzene/pentane solution at 25 °C. Additionally, *cisoid-3* can be isolated upon storing solutions of mixture of *cisoid-3* and *transoid-3* at -35 °C. Elemental Analysis: Calcd. C, 65.26%; H, 6.45%; N, 5.44%. Found: C, 64.34%; H, 6.13%; N, 5.23%. *Cisoid* Isomer: ^1H NMR (benzene- d_6): 7.84 (m, 2H, *phenyl*), 7.52 (m, 4H, *phenyl*), 7.35 (m, 4H, *phenyl*), 7.26 (m, 4H, *phenyl*), 7.12 (m, 2H, *phenyl*), 6.96 (m, 2H, *phenyl*), 6.82 (m, 2H, *phenyl*), 6.75 (m, 4H, *phenyl*), 6.60 (m, 2H, *phenyl*), 6.18 (m, 4H, *phenyl*), 4.21 (m, 2H, CH_2), 3.93 (m, 2H, CH_2), 2.81 (m, 2H, CH_2), 2.29 (m, 6H, CH_2), 1.96 (m, 2H, CH_2), 1.67 (s, 6H, CH_3), 1.37 (s, 6H, CH_3), 1.36 (m, 4H, CH_2), 1.02 (m, 2H, CH_2), 0.45 (m, 2H, CH). ^{13}C NMR (benzene- d_6): 149.04 (*phenyl*), 147.93 (*phenyl*), 143.83 (*phenyl*), 142.84 (*phenyl*), 137.31 (*phenyl*), 133.41 (*phenyl*), 132.42 (*phenyl*), 129.16 (*phenyl*), 60.63 (CH), 53.50 (CH_2), 42.16 (CH_2), 36.64 (CH_2), 32.27 (CH_2), 30.79 (CH_2), 16.51 (CH_3), 16.09 (CH_3). ^{31}P NMR (benzene- d_6): 61.08 (t), -90.26 (t). *Transoid* Isomer: ^1H NMR (benzene- d_6): 7.95 m, *phenyl*), 7.41 (m, *phenyl*), 6.68 (m, *phenyl*), 6.34 (m, *phenyl*), 5.21 (m, CH_2), 4.77 (m, CH_2), 4.05 (m, CH_2), 1.71 (s, CH_3), 0.98 (s, CH_3), several resonances not located. ^{13}C NMR (benzene- d_6): 130.84 (*phenyl*), 66.48 (CH), 37.92 (CH_2), several resonances not located. ^{31}P NMR (benzene- d_6): 54.94 (t), -61.45 (t).

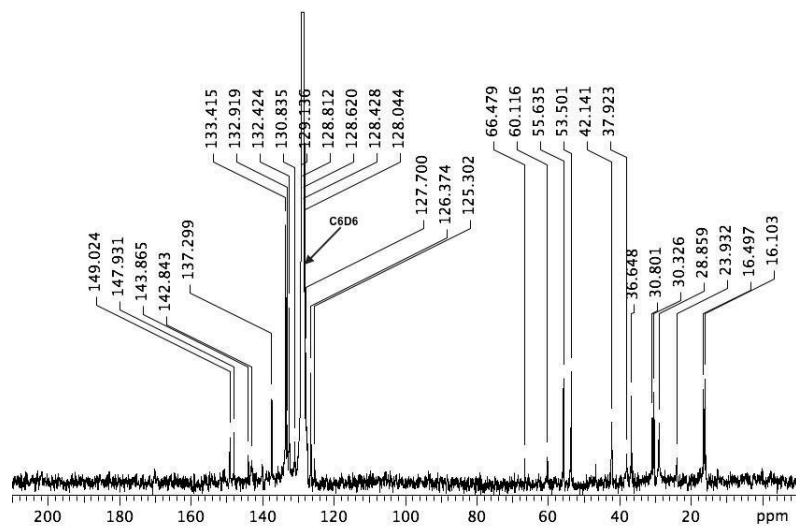


Figure 1.34: ^{13}C NMR spectrum showing a mixture of *cisoid-3* and *transoid-3* in benzene- d_6 at 25 °C.

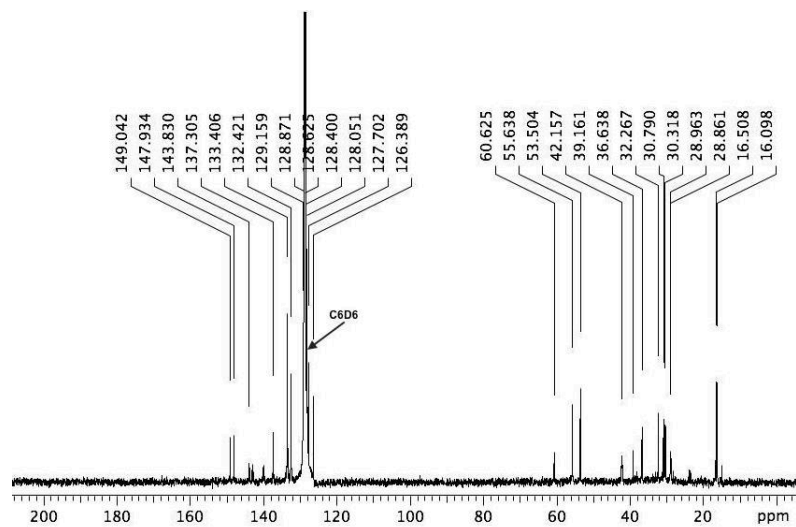


Figure 1.35: ^{13}C NMR spectrum of *cisoid-3* in benzene- d_6 at 25 °C.

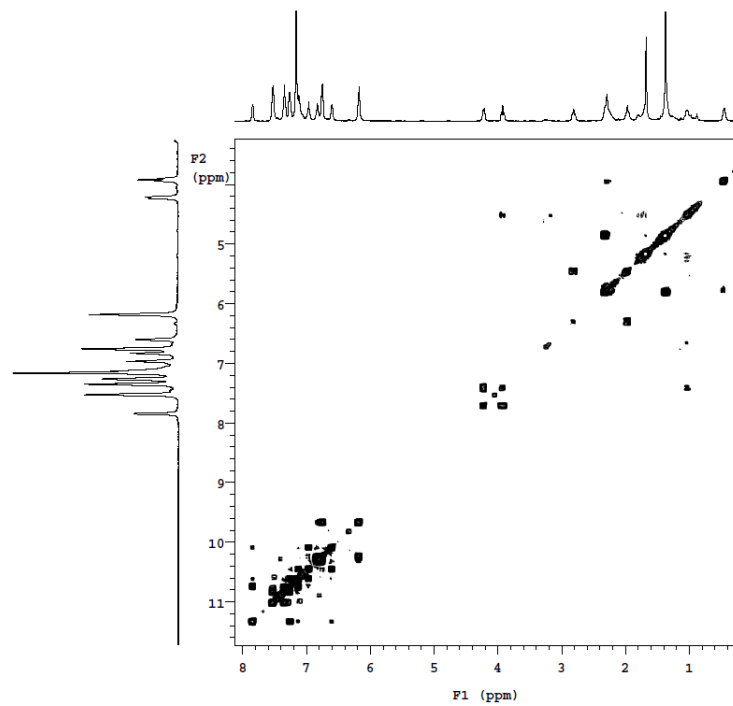


Figure 1.36: gCOSY NMR spectrum of *cisoid-3* in benzene- d_6 at 25 °C.

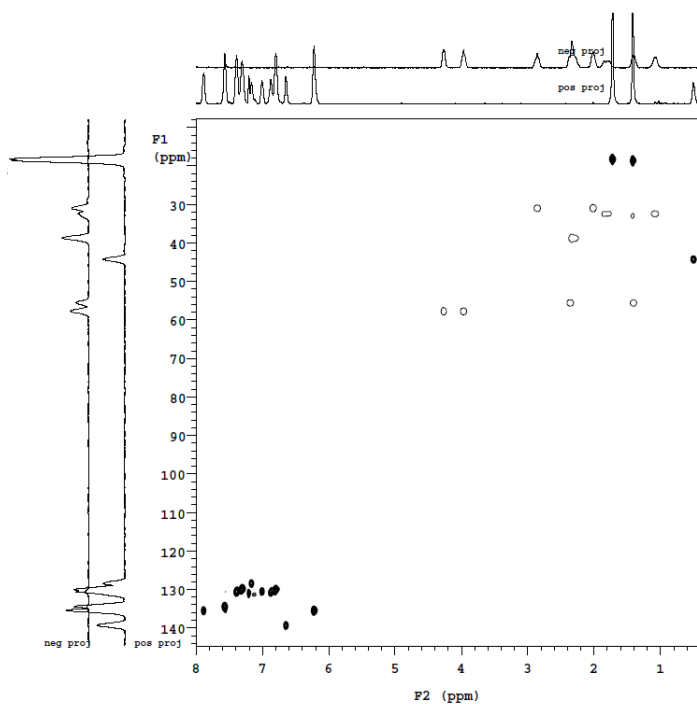


Figure 1.37: HSQCAD NMR spectrum of *cisoid-3* in benzene- d_6 at 25 °C.

1.9. References:

1. Labinger, J. A.; Bercaw, J. E. *Nature* **2002**, *417*, 507-514.
2. For leading examples see: (a) Jia, C.; Kitamura, T.; Fujiwara, Y. *Acc. Chem. Res.* **2001**, *34*, 633-639. (b) van der Boom, M. E.; Milstein, D. *Chem. Rev.* **2003**, *103*, 1759-1792. (c) Colby, D. A.; Bergman, R. G.; Ellman, J. A. *Chem. Rev.* **2010**, *110*, 624-655.
3. Sun, C.-L.; Li, B.-J.; Shi, Z.-J. *Chem. Rev.* **2011**, *111*, 1293-1314.
4. For leading examples see: (a) Chen, M. S.; White, M. C. *Science* **2007**, *318*, 783-787. (b) Chen, M. S.; White, M. C. *Science* **2010**, *327*, 566-571.
5. For leading examples see: (a) Sarhan, A. A. O.; Bolm, C. *Chem. Soc. Rev.* **2009**, *38*, 2730-2744, and references therein; (b) Baran, P. S.; Hafensteiner, B. D.; Ambhaikar, N. B.; Guerrero, C. A.; Gallagher, J. D. *J. Am. Chem. Soc.* **2006**, *128*, 8678-8693.
6. For leading examples see: (a) Vierling, P.; Riess, J. G. *J. Am. Chem. Soc.*, **1984**, *106*, 2432-2434. (b) Garrou, P. E. *Chem. Rev.* **1985**, *85*, 171-185. (c) Grohmann, A. *Dalton Trans.* **2010**, *39*, 1432-1440, and references therein.
7. Uddin, M. N.; Begum, N.; Hassan, M. R.; Hogarth, G.; Kabir, S. E.; Miah, M. A.; Nordlander, E.; Tocher, D. A. *Dalton Trans.* **2008**, 6219-6230.
8. Rahman, M. A.; Begum, N.; Ghosh, S.; Hossain, M. K.; Hogarth, G.; Tocher, D. A.; Nordlander, E.; Kabir, S. E. *J. Organomet. Chem.* **2011**, *696*, 607-612.
9. Yeh, W.-Y.; Tsai, K.-Y. *Organometallics* **2010**, *29*, 604-609.
10. Carty, A. J.; Hogarth, G.; Enright, G. D.; Steed, J. W.; Georganopoulou, D. *Chem. Commun.* **1999**, 1499-1500.
11. Alcaez, C. M.; Galán, B.; García, M. E.; Riera, V.; Ruiz, M. A.; Vaissermann, J. *Organometallics* **2003**, *22*, 5504-5512.
12. Porter, T. M.; Hall, G. B.; Groy, T. L.; Trovitch, R. J. *Dalton Trans.* **2013**, *42*, 14689-14692.
13. (a) Gardiner, M. G.; Hanson, G. R.; Henderson, M. J.; Lee, F. C.; Raston, C. L. *Inorg. Chem.* **1994**, *33*, 2456-2461. (b) Rijnberg, E.; Richter, B.; Thiele, K.-H.; Boersma, J.; Veldman, N.; Spek, A. L.; van Koten, G. *Inorg. Chem.* **1998**, *37*, 56-63.
14. (a) Khusniyarov, M. M.; Harms, K.; Burghaus, O.; Sundermeyer, J. *Eur. J. Inorg. Chem.* **2006**, 2985-2996. (b) Muresan, N.; Chlopek, K.; Weyhermüller, T.; Neese, F.; Wieghardt, K. *Inorg. Chem.*, **2007**, *46*, 5327-5337.

15. Accepted isomer shift ranges: high-spin Fe(III), 0.1 to 0.5 mm s⁻¹; high spin Fe(II), 0.6 to 1.7 mm s⁻¹; low-spin Fe(III), -0.1 to 0.5 mm s⁻¹; low-spin Fe(II), -0.2 to 0.5 mm s⁻¹. See: D. P. E. Dickson and F. J. Berry, *Mössbauer Spectroscopy*, Cambridge University Press, 1986, p. 22.
16. Crossland, J. L.; Tyler, D. R. *Coord. Chem. Rev.* **2010**, *254*, 1883-1894.
17. Mukhopadhyay, T. K.; Feller, R. K.; Rein, F. N.; Henson, N. J.; Smythe, N. C.; Trovitch, R. J.; Gordon, J. C. *Chem. Commun.* **2012**, *48*, 8670-8672.
18. Mukhopadhyay, T. K.; Flores, M.; Feller, R. K.; Scott, B. L.; Taylor, R. D.; Paz-Pasternak, M.; Henson, N. J.; Rein, F. N.; Smythe, N. C.; Trovitch, R. J.; Gordon, J. C. *Organometallics* **2014**, *33*, 7101-7112.
19. For examples see: Trovitch, R. J.; Lobkovsky, E.; Chirik, P. J. *J. Am. Chem. Soc.* **2008**, *130*, 11631-11640.
20. (a) Miller, T. M.; Whitesides, G. M. *Organometallics* **1986**, *5*, 1473-1480. (b) Chappell, S. D.; Cole-Hamilton, D. J. *Polyhedron* **1982**, *1*, 739-777.
21. Tondreau, A. M.; Atienza, C. C. H.; Darmon, J. M.; Milsmann, C.; Hoyt, H. M.; Weller, K. J.; Nye, S. A.; Lewis, K. M.; Boyer, J.; Delis, J. G. P.; Lobkovsky, E.; Chirik, P. J. *Organometallics* **2012**, *31*, 4886-4893.
22. Neese, F. Orca, an Ab Initio, Density Functional and Semiempirical Electronic Structure Program Package, version 2.9.1; Max Planck Institute for Bioinorganic Chemistry: Mülheim an der Ruhr, Germany, 2012.
23. (a) Becke, A. D. *J. Chem. Phys.* **1993**, *98*, 5648-5652. (b) Lee, C. T.; Yang, W. T.; Parr, R. G. *Phys. Rev.* **1988**, *37*, 785-789.
24. Grimme, S. *J. Comput. Chem.* **2006**, *27*, 1787-1799.
25. Pantazis, D. A.; Chen, X. Y.; Landis, C. R.; Neese, F. *J. Chem. Theory Comput.* **2008**, *4*, 908-919.
26. Molekel, Advanced Interactive 3D-Graphics for Molecular Sciences; Swiss National Supercomputing Center; [http:// www.cscs.ch/molekel](http://www.cscs.ch/molekel).

CHAPTER 2

SYNTHESIS OF REDOX ACTIVE LIGAND SUPPORTED IRON COMPLEXES

2.1. Abstract:

A series of redox non-innocent ligand supported low valent iron complexes have been synthesized. Reduction of ($^{\text{Ph}_2\text{PPr}}\text{DI}$)FeBr₂ (**1**) with excess Na-Hg in the presence of 1 atmosphere of CO gas afforded a red diamagnetic compound, having two CO stretching frequencies in the IR spectrum and $\kappa^3\text{-}N,N,P\text{-DI}$ coordination around Fe, identified as ($^{\text{Ph}_2\text{PPr}}\text{DI}$)Fe(CO)₂ (**4**). Upon heating for 10 days at 110 °C, **2** was observed to be converted to iron mono-carbonyl compound, ($^{\text{Ph}_2\text{PPr}}\text{DI}$)Fe(CO) (**5**). Both compounds have been characterized by multinuclear NMR spectroscopy, IR spectroscopy and X-ray diffraction analysis. Compound **3** was investigated for nucleophilic addition reactions at the carbonyl ligand. A six coordinate α -diimine ligand (DI) supported iron(II) compound was also synthesized by adding 1 atmosphere of CO gas to an acetone solution of **1** followed by heating at 55 °C for 24 h. Based on ¹H, ³¹P NMR and IR spectroscopy, the compound has been described as [($^{\text{Ph}_2\text{PPr}}\text{DI}$)Fe(CO)Br][Br] (**6**). Alkyl phosphine substituted DI ligands have also been explored. Metallation of $^{\text{tBu}_2\text{PPr}}\text{DI}$ with FeBr₂ in THF solvent at room temperature yielded a blue paramagnetic metal dibromide compound, ($^{\text{tBu}_2\text{PPr}}\text{DI}$)FeBr₂ (**7**) which produced the corresponding mono-bromide compound ($^{\text{tBu}_2\text{PPr}}\text{DI}$)FeBr (**8**) under reducing conditions. Like **4** and **5**, compound **8** has also been characterized by ¹H, ³¹P NMR spectroscopy and X-ray crystallography. After failed several attempts to isolate the completely reduced $^{\text{tBu}_2\text{PPr}}\text{DI}$ supported iron compound, **7** was reduced using Na-Hg in presence of 1 atmosphere of CO gas, which

furnished a diamagnetic orange compound, identified as (^tBu₂PPrDI)Fe(CO)₂ (**9**). Redox non-innocent pyridine diimine (PDI) based iron chemistry has also been investigated. Room temperature reaction of FeBr₂ with ^{Ph}₂PPrPDI or ^{Ph}₂PEtPDI in THF solvent yielded a purple diamagnetic compound and a purple mixture of diamagnetic and paramagnetic compounds, respectively. NMR analysis and a lack of solubility in common non-polar solvents identified those compounds as [(^{Ph}₂PPrPDI)FeBr][Br] (**10**) and [(^{Ph}₂PEtPDI)FeBr][Br] (**13**). Attempts to reduce **8** and **11** using Na-Hg in THF solvent furnished two diamagnetic C₂-symmetric compounds, [(^{Ph}₂PPrPDI)Fe] (**11**) and [(^{Ph}₂PEtPDI)Fe] (**14**), respectively. Furthermore, treatment of **11** with HBF₄·Et₂O solution produced a diamagnetic iron hydride compound, [(^{Ph}₂PPrPDI)FeH][BF₄] (**12**) with *cis*-phosphine ligands, as judged by ¹H and ³¹P NMR spectroscopy.

2.2. Introduction:

For decades, homogeneous catalysis mainly relied upon noble metal catalysts (Ru, Rh, Ir, Pt) due to their facile two electron redox processes, which are involved in most organometallic transformations. Although their catalytic efficiency and ease of mechanistic study due to formation of low spin diamagnetic intermediates makes them attractive, their high price, and toxicity render them less useful in real industrial applications and academic laboratories. On the other hand, first row transition metals, particularly iron could be utilized as an alternative due to its high abundance and intoxicity.¹ In fact, iron is considered as a “metal with minimum safety concern” by regulatory authorities.² Additionally, iron holds other advantages that have drawn the attention of researchers to design iron catalysts for organic transformation over the last

few years.³ Iron compounds can have formal oxidation states from –II to VI, therefore they can be used both in reductive and oxidative transformations. Depending on its oxidation state, Fe shows Lewis acidity from moderate to high, and this can be tuned with the choice of proper ligand system. Moreover, in nature iron is located in the active site of enzymes, for example nitrogenase and cytochrome P450, which also inspires mimics for their similar applications.⁴ In spite of all these advantages, the propensity towards single electron transfer (SET) process over two electron process, limits its application in catalysis. In order to imitate the chemical behavior of precious metal catalysts, this competitive SET mechanism needs to be excluded. To address this challenge, proper choice of ligand is important. Introduction of redox non-innocent ligands appears to be a significant contributor in this context. They act as an “electron reservoir”, therefore delocalizing the excess electron density of the metal center in their conjugated π -system and stabilizing the metal’s preferred oxidation state. By accepting electrons, they aid in the processes where two electrons can be distributed between the metal and ligand centers.⁵ It is worth to mention the catalytic transformations mediated by redox non-innocent ligand supported iron complexes. The Chirik group has developed a series of pyridine diimine (PDI) ligand supported iron complexes, which have shown versatile catalytic activities ranging from catalytic hydrogenation, and the hydrosilylation of unsaturated bonds to pericyclic reactions such as cycloaddition, cycloisomerization reactions, all of which are usually conducted by noble metal catalysts. In 2004, they reported that (^{Ar}PDI)Fe(N₂)₂ (where Ar = 2,6-di-isopropylbenzene) is capable of hydrogenating olefins with TOFs up to 1814 h⁻¹ and also hydrosilylating olefins with TOFs up to 364 h⁻¹ for 1-hexene substrate at 0.3 mol% catalyst loading.⁶ In 2006,

(^{Ar}PDI)Fe(N₂)₂ was found to be active for [2π + 2π] cycloaddition reactions at ambient temperature with TOFs up to 240 h⁻¹.^{7a} and in 2005, the catalytic cycloaddition of unactivated alkenes.^{7b} Along with PDI ligands, α-diimine ligand supported Fe complexes were found to be active for catalytic reactions such as olefin hydrogenation,^{8a} hydrovinylation of 1,3-dienes,^{8b} butadiene dimerization,^{8c} and ethylene oligomerization.^{8d} Besides the redox non-innocent ligands, pincer ligand supported iron complexes have occupied an enormous domain of catalytic research.⁹ Pyridine ring containing pincer complexes stabilize strong field ligands like hydride (H) and carbonyls (CO), which lead to the formation of low-spin complexes. Some of these compounds have shown metal ligand co-operativity through aromatization and dearomatization, therefore aiding in the two-electron process. They have been found to be active for catalytic hydrogenation of alkenes,^{10a} alkynes,^{10b} carbonyls,^{10c} nitriles,^{10d} transfer hydrogenation of carbonyls,^{10e} hydrosilylation of carbonyls,^{10f} and acceptorless dehydrogenation of alcohols,^{10g} and N-heterocycles.^{10h}

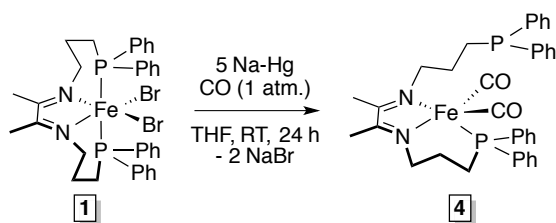
Inspired by this seminal work, we sought to develop redox non-innocent PDI and DI ligand based iron complexes and introduce strong field CO ligands in order to isolate low spin iron complexes. Our group has modified the traditional PDI or DI ligands by replacing the bulky aryl groups with a carbon chain tethered to a donor group (-PR₂ or -NR₂). Easy synthesis of the ligands, along with their coordination flexibility made them promising for potential catalytic activity, which will be investigated in the future.

2.3. Synthesis and Characterization:

Analogous to **2**, α -diimine ligand supported carbonyl compounds have been synthesized. Carbonyl compounds are considered to be the precursors of Fischer carbenes. The general approach for the synthesis of Fischer carbenes comprises two steps; the first step is the nucleophilic attack of alkyl lithium to the carbonyl group to followed by reaction with an alkylating agent.¹¹ Additionally, reductive coupling of CO to C₂₊-containing products remains an interesting research domain, which can allow for low-temperature Fischer-Tropsch reactions.¹² In this context, metal carbonyl compounds that can mediate reductive CO coupling remain attractive to researchers. In 2013, the Peters group reported a diphosphineborane supported iron dicarbonyl compound, which afforded a dicarbyne complex upon disilylation. This dicarbyne complex produced a CO-derived olefin compound upon hydrogenation with 1 atmosphere of H₂ at ambient temperature.^{13a} In 2016, the Agapie group reported the deoxygenative reductive coupling of CO to a C₂ fragment at molybdenum^{13b} and later on described the details of the mechanism.^{13c} With this in mind, we endeavored to develop iron carbonyl compounds on redox non-innocent ligand platforms.

Reduction of (^{Ph₂PPr}DI)FeBr₂¹⁴ with excess Na-Hg in the presence of 1 atmosphere of CO gas, followed by work up yielded a crimson red compound after 24 h at room temperature (Scheme 2.1, **4**). The compound was determined to be diamagnetic based on the multinuclear magnetic resonance spectroscopy. Analysis of the ¹H NMR spectrum revealed two different resonances (1.43 and 1.63 ppm) for the backbone methyl groups (Fig. 2.1) along with two different peaks in the ³¹P NMR spectrum, which is indicative of non-C₂ symmetric compound. Resonances at 67 ppm and -16 ppm, respectively, in the

^{31}P NMR spectrum (Fig. 2.2) suggest that one phosphine arm of the ligand is bound to the metal center while the other one is uncoordinated. Moreover, this is reflected in the single crystal X-ray diffraction analysis (discussed later). Two CO stretching frequencies are observed at 1945 and 1882 cm^{-1} in the infrared spectrum, indicating the coordination of two CO ligands. Incorporating both NMR spectroscopic data and IR results, compound **4** can be best described as $(^{\text{Ph}_2\text{PPr}}\text{DI})\text{Fe}(\text{CO})_2$.



Scheme 2.1: Synthesis of $(^{\text{Ph}_2\text{PPr}}\text{DI})\text{Fe}(\text{CO})_2$ (**4**).

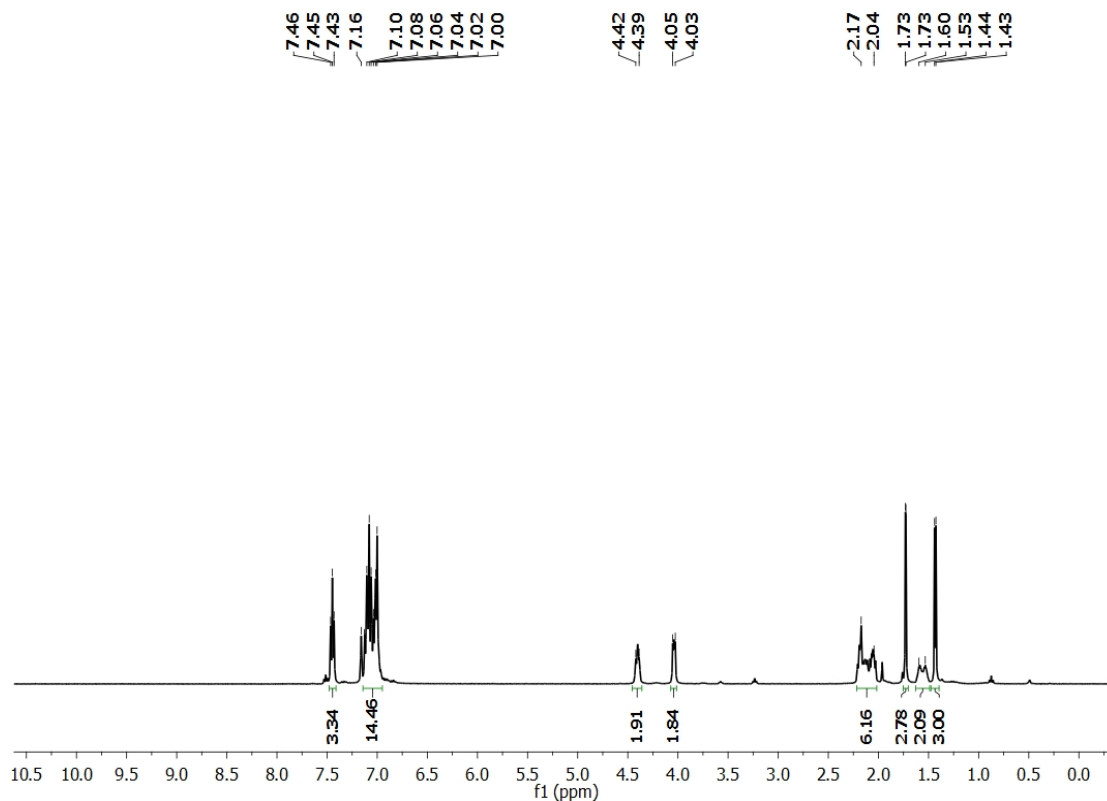


Figure 2.1: ^1H NMR spectrum of **4** in benzene- d_6 at $25\text{ }^\circ\text{C}$.

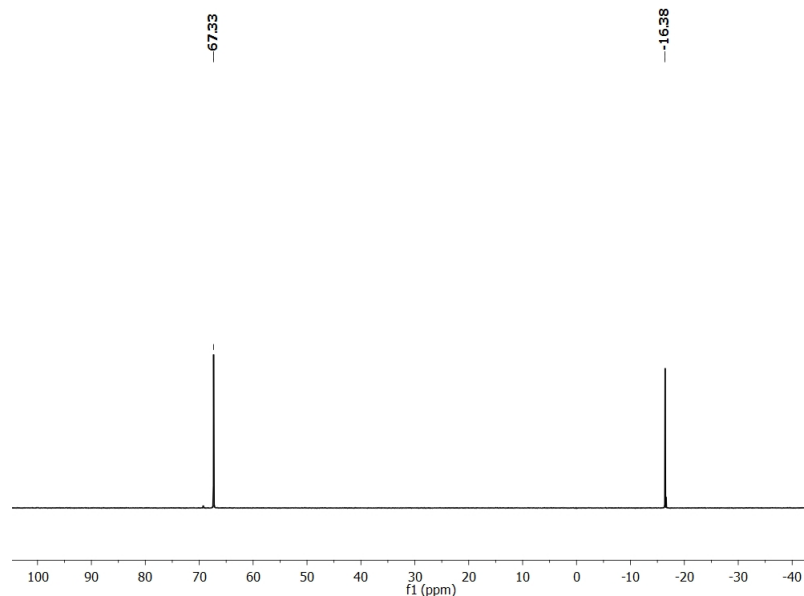


Figure 2.2: ^{31}P NMR spectrum of **4** in benzene- d_6 at 25 °C.

To confirm the geometry and coordination environment, crystals of **4** were grown from a concentrated diethyl ether solution at -35 °C. Refinement of the metrical parameters displayed a distorted trigonal bipyramidal geometry around Fe (Fig. 2.3) with N(1)-Fe(1)-N(2), N(1)-Fe(1)-P(1), N(2)-Fe(1)-P(1), N(1)-Fe(1)-C(35), and C(35)-Fe(1)-C(36) angles of 79.79 (12)°, 89.66 (9)°, 124.35 (9)°, 174.15 (17), and 90.92 (17)°, respectively (Table 2.1). Considering the redox non-innocent behavior of α -diimine (DI) ligands, the imine C-N distances and C(2)-C(3) distance have been examined. The C(2)-N(1) distance of 1.333 (4) Å and C(3)-N(2) contact of 1.344 (4) Å were determined to be elongated from the neutral ligand analog (1.29 Å),¹⁵ whereas the C(2)-C(3) distance of 1.408 (5) Å was found to be contracted from 1.47 Å (neutral ligand).¹⁵ This observation is consistent with mono-reduced DI ligand, modifying the oxidation state of the Fe center from formally zero valent to monovalent. As the complex has been found to be diamagnetic in its ground state, it is probably safe to propose that the unpaired electron on Fe(I) is antiferromagnetically coupled with the DI mono-radical anion. It is to be

noted here that single reduction of the DI ligand has also been found in the isoelectronic compound, **2**.¹⁴

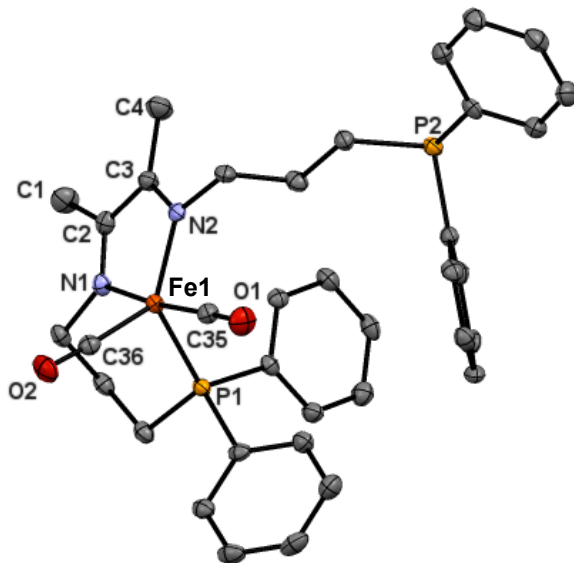


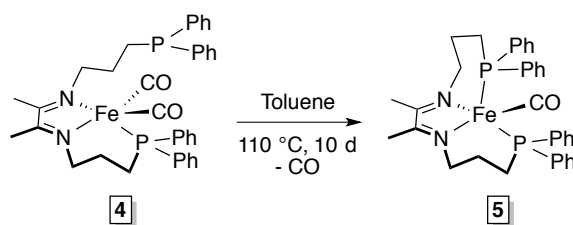
Figure 2.3: The solid-state structure of **4** shown with 30% probability ellipsoids. Hydrogen atoms have been omitted for clarity.

Table 2.1: Notable bond lengths (Å) and bond angles (°) determined for **4**.

Bond	Å	Angle	Degree
C(1)-C(2)	1.505(5)	N(1)-Fe(1)-N(2)	79.79(12)
C(2)-C(3)	1.408(5)	N(2)-Fe(1)-P(1)	124.35(9)
C(2)-N(1)	1.333(4)	N(1)-Fe(1)-P(1)	89.66(9)
C(3)-N(2)	1.344(4)	N(1)-Fe(1)-C(35)	174.15(17)
Fe(1)-N(1)	1.920(3)	C(35)-Fe(1)-C(36)	90.92(17)
Fe(1)-N(2)	1.903(3)		
Fe(1)-P(1)	2.1886(10)		
Fe(1)-C(35)	1.758(3)		

Heating **4** in toluene at 110 °C gradually changed the color from crimson red to burgundy, CO was removed in 2 day intervals, and the progress of the reaction was monitored by ¹H NMR and ³¹P NMR spectroscopy. After 10 days, two backbone methyl group resonances were found to merge into one resonance (1.76 ppm) and additionally

(Fig. 2.4), two resonances in the ^{31}P NMR spectrum changed to one resonance at 69 ppm (Fig. 2.5), indicating that both phosphine arms are coordinated to the metal center. These observations suggest the conversion of the non- C_2 symmetric compound, **4**, to a new C_2 -symmetric compound. IR spectroscopy showed one CO stretching frequency at 1858 cm^{-1} . Based on the NMR and IR results, the new compound can be best described as $(^{\text{Ph}_2\text{PPr}}\text{DI})\text{Fe}(\text{CO})$ (Scheme 2.2, **5**).



Scheme 2.2: Synthesis of $(^{\text{Ph}_2\text{PPr}}\text{DI})\text{Fe}(\text{CO})$ (**5**).

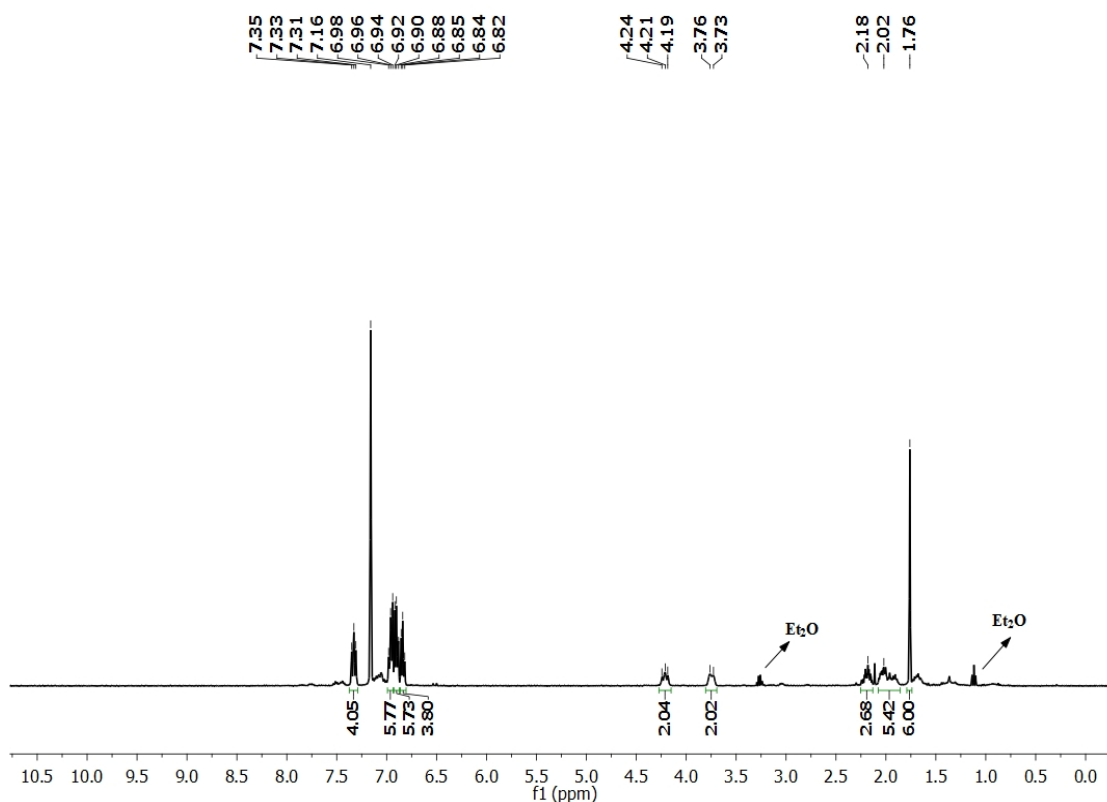


Figure 2.4: ^1H NMR spectrum of **5** in benzene- d_6 at $25\text{ }^\circ\text{C}$.

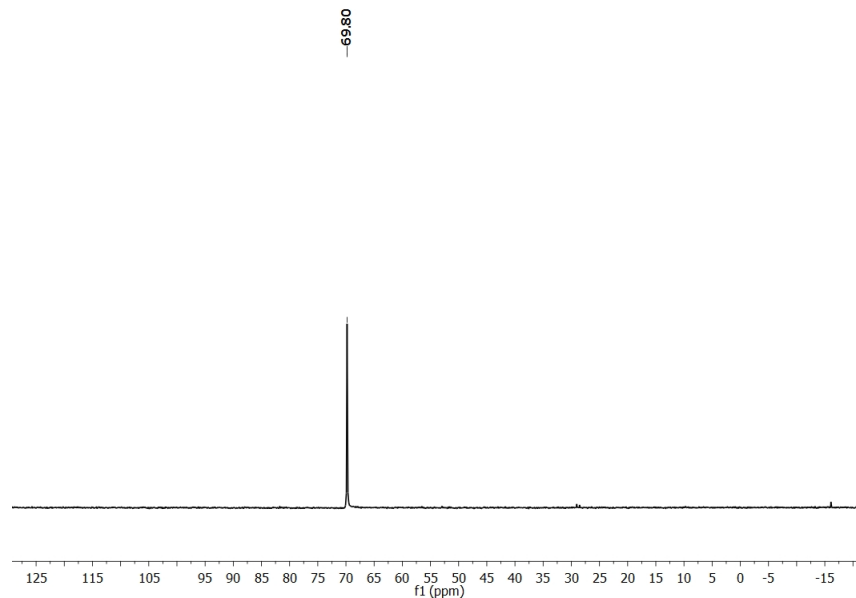


Figure 2.5: ^{31}P NMR spectrum of **5** in benzene- d_6 at 25 °C.

The structure was further confirmed by the X-ray diffraction analysis of a single crystal of **5**, grown from a concentrated diethyl ether solution at -35 °C (Fig. 2.6). Metrical parameters feature a distorted square pyramidal geometry around Fe with the angles of N(1)-Fe(1)-N(2), N(1)-Fe(1)-P(1), N(2)-Fe(1)-P(2), N(1)-Fe(1)-P(2), N(2)-Fe(1)-C(35) as 80.33 (9)°, 90.95 (7)°, 89.72 (7)°, 163.5 (7)°, and 148.98 (12)° respectively (Table 2.2). Similar to **4**, single electron reduction of the DI ligand is also observed in the case of **5**. The imine C-N distances were found to be elongated from 1.29 Å (neutral ligand) to 1.351(3) Å (C(2)-N(1)) and 1.360 (3) Å (C(3)-N(1)), whereas the C(2)-C(3) distance was determined to be contracted from its neutral ligand value (1.47 Å)¹⁵ to 1.396 (4) Å (Table 2.2).

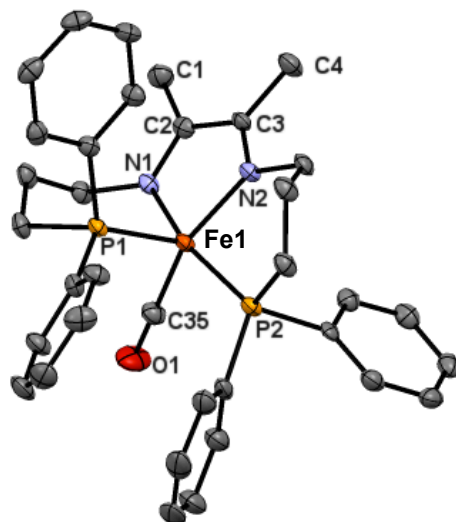


Figure 2.6: The solid-state structure of **5** shown with 30% probability ellipsoids. Hydrogen atoms have been omitted for clarity.

Table 2.2: Notable bond lengths (Å) and bond angles (°) determined for **5**.

Bond	Å	Angle	Degree
C(1)-C(2)	1.499(4)	N(1)-Fe(1)-N(2)	80.33(9)
C(2)-C(3)	1.396(4)	N(1)-Fe(1)-P(1)	90.95(7)
C(2)-N(1)	1.351(3)	N(1)-Fe(1)-P(2)	163.52(7)
C(3)-N(2)	1.360(3)	N(2)-Fe(1)-P(2)	89.72(7)
Fe(1)-N(1)	1.919(2)	P(1)-Fe(1)-P(2)	105.19(3)
Fe(1)-N(2)	1.921(2)	N(2)-Fe(1)-C(35)	148.98(12)
Fe(1)-P(1)	2.1770(9)		
Fe(1)-C(35)	1.740(3)		

To explore carbon monoxide fixation by generating formyl, hydroxymethyl or methyl complexes according to the literature,¹⁶ several attempts were made to react compound **5** with hydride reagents such as NaBH₄, NaEt₃BH, but neither the metal center nor the carbonyl group was affected. Addition of H₂ to **5** did not result in reaction. Additionally, **5** remained unreactive towards alkylating agents such as MeLi and PhLi, which is the general approach for Fischer carbene synthesis. However, a new compound

was observed upon reacting **5** with methyl iodide (MeI). An NMR scale reaction of **5** with one equivalent methyl iodide in benzene-*d*₆ produced a green compound that was completely soluble in acetone. The ³¹P NMR spectrum of the compound featured two doublets (*J*_{PP} = 261.6 and 113.6 Hz) (Fig. 2.8), indicating the presence of two different phosphorus environments. The ¹H NMR spectrum indicated the formation of two different compounds, one diamagnetic (major) and one paramagnetic (minor). Additionally, it showed a distinct feature of having three different methyl peak resonances at 1.36 (3H), 1.33 (9H), and 0.92 (br, 7H) ppm (Fig. 2.7). These observations, along with the solubility of the compound, indicate that plausible structures are (Ph₂PP^rDI)Fe^{II}(Me)(I) (diamagnetic) and [(Ph₂PP^rDI)Fe^{II}(Me)](I) or [(Ph₂PP^rDI)Fe^{II}(I)](I) (paramagnetic).

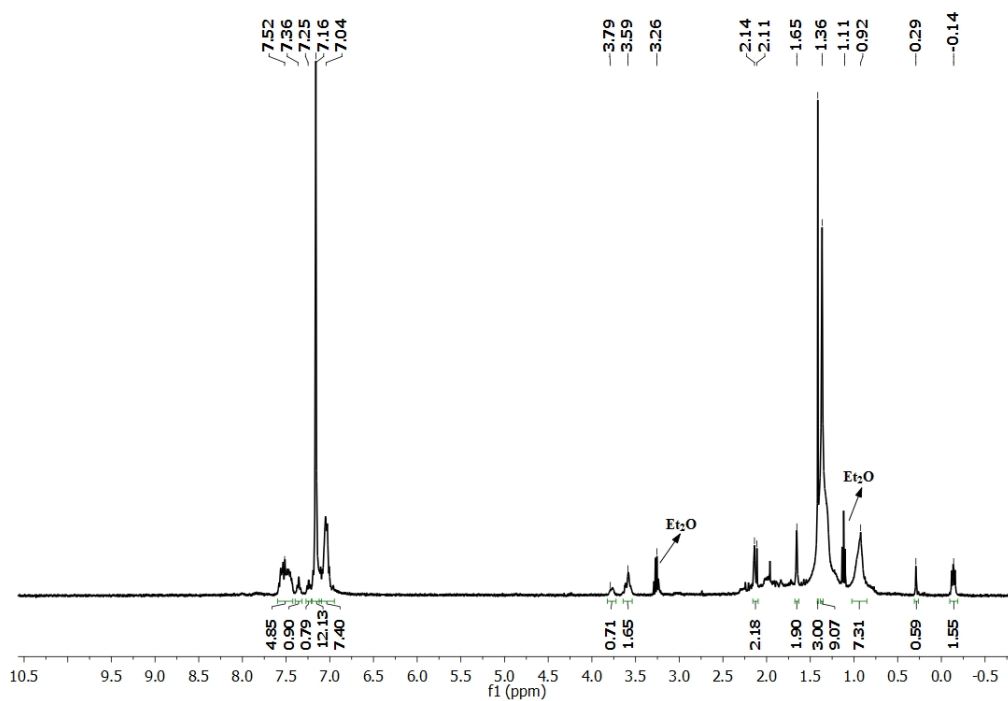


Figure 2.7: ¹H NMR spectrum of the reaction products of **5** and methyl iodide (MeI) in benzene-*d*₆ at 25 °C.

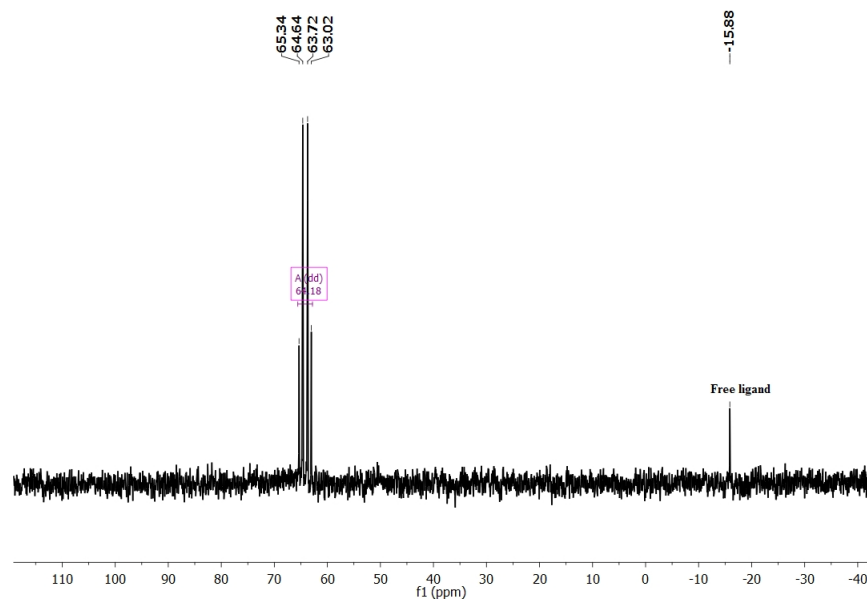
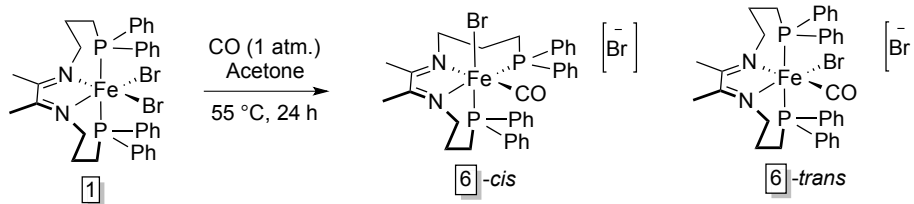


Figure 2.8: ^{31}P NMR spectrum of the reaction products of **5** and methyl iodide (MeI) in benzene- d_6 at 25 °C.

After these unsuccessful reactivity studies of **5**, it was anticipated that due to the electron rich formally zero-valent Fe center, the carbonyl group of **5** was not sufficiently electrophilic, which renders it to be unreactive towards nucleophilic substitution reactions. Then, a different approach was adopted. Instead of zero-valent iron mono carbonyl compounds, higher oxidation state metal compounds were targeted. To fulfill this requirement, $(\text{Ph}_2\text{PPrDI})\text{Fe}(\text{CO})\text{Br}_2$ (**6**) was synthesized by adding 1 atm. of CO gas to **1** in acetone (Scheme 2.3). A soluble red diamagnetic compound was isolated after heating at 55 °C for 24 h followed by work up and evaporation of the solvent. Infrared spectroscopy featured a single CO stretching frequency at 1970 cm^{-1} , indicating the presence of one carbonyl ligand in compound **6**. Due to the higher oxidation state (+II) of Fe in **6**, the extent of backbonding from metal to CO ligand is expected to be less compared to **5** (Fe is formally zero-valent), which is reflected in the higher CO stretching frequency compared to **5** ($\nu_{\text{CO}} = 1858\text{ cm}^{-1}$). The ^{31}P NMR spectrum of **6** revealed a doublet of

doublets at 53 ppm ($J = 120$ Hz) (Fig. 2.10) and ^1H NMR spectroscopy showed two different methyl group resonances at 1.11 and 1.95 ppm, suggesting two different phosphorus environments (Fig. 2.9).



Scheme 2.3: Synthesis of $[(\text{Ph}_2\text{PPrDI})\text{Fe}(\text{CO})\text{Br}][\text{Br}]$ (**6**).

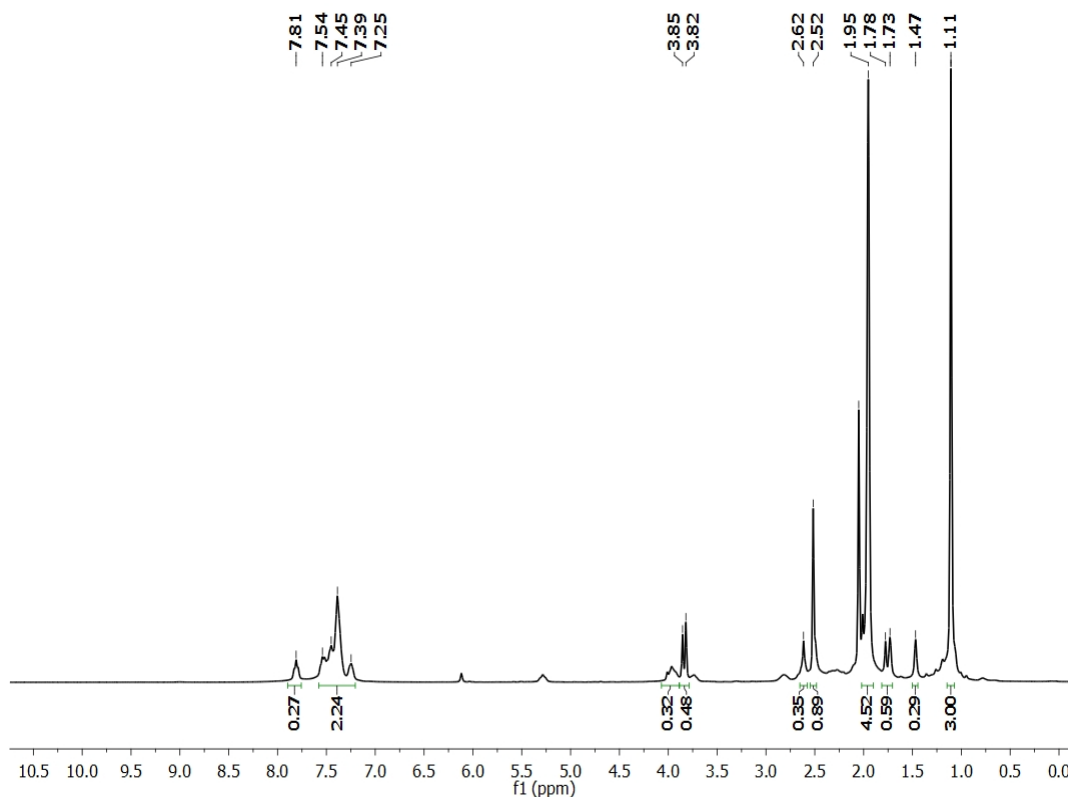


Figure 2.9: ^1H NMR spectrum of **6** in benzene- d_6 at 25 °C.

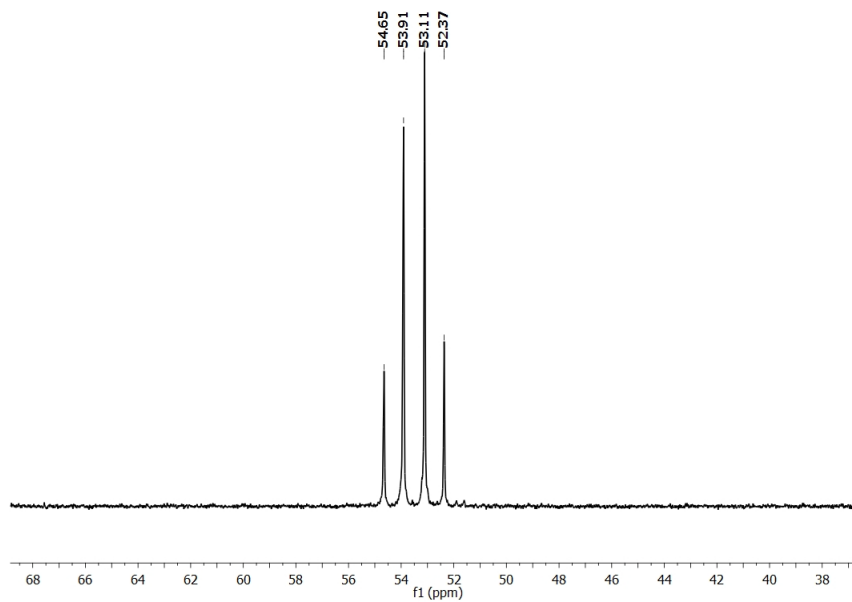


Figure 2.10: ^{31}P NMR spectrum of **6** in benzene- d_6 at 25 °C.

Targeting formyl complex synthesis, compound **6** was treated with excess (5 eq.) NaBH_4 in THF. After stirring for 24 h at room temperature, a red compound was obtained. ^{31}P NMR spectroscopic analysis revealed the formation of a mixture of two compounds, one with two different phosphorus resonances at 66 and 67 ppm while the second compound had a single resonance at 69 ppm, indicating a C_2 -symmetric ligand environment (Fig. 2.11A). To execute the reaction in a controlled fashion, 3 eq. of NaBH_4 was added, which yielded a burgundy compound after 4 days. ^{31}P NMR spectrum showed the compound with 69 ppm resonance (Fig. 2.11B) as the major compound, which turns out to be the previously synthesized **5**. It can be concluded that although formyl complex isolation remained unsuccessful, a time-saving new approach was discovered to synthesize iron mono-carbonyl compound, **5** rather than heating the dicarbonyl compound, **4** for 10 days. Alternatively, compound **5** can also be synthesized by adding $\text{Fe}(\text{CO})_5$ to compound **2** at room temperature.

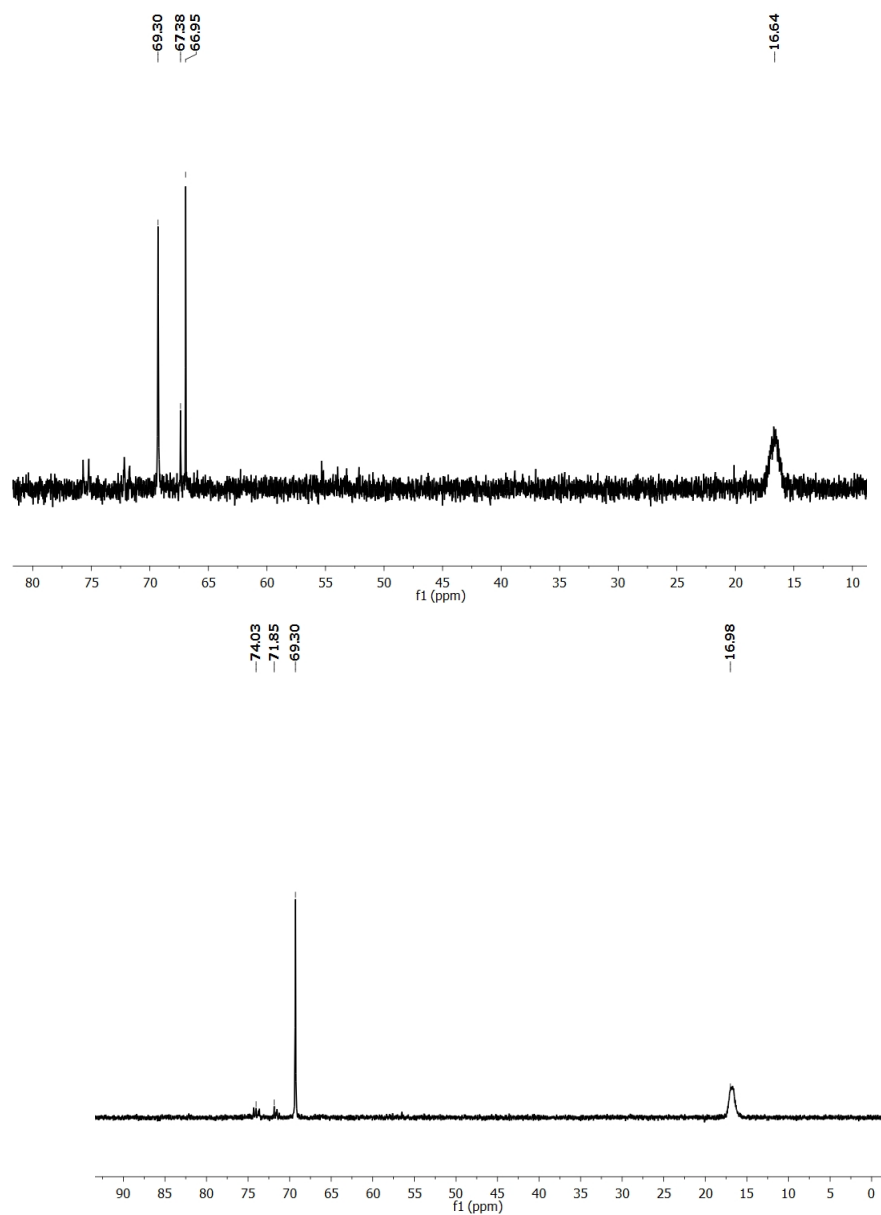
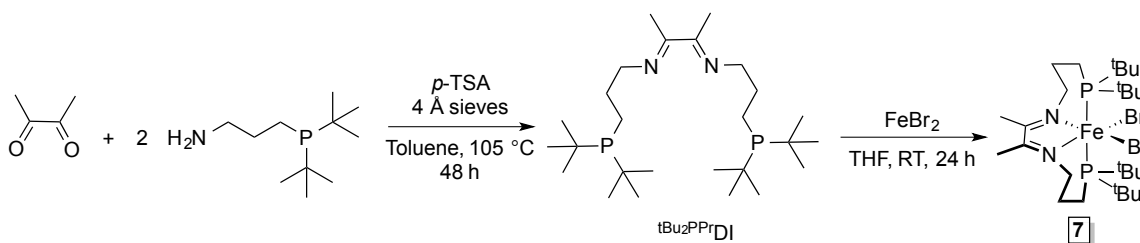


Figure 2.11: ^{31}P NMR spectrum of the reaction of **6** with 5 eq. NaBH_4 (top, A) and 3 eq. NaBH_4 (bottom, B) in benzene- d_6 at 25 °C.

Compound **6** was reacted with halide scavengers such as AgPF_6 and AgBF_4 in acetone solvent at room temperature. However, there was no indication that a reaction occurred based on ^1H and ^{31}P NMR spectroscopy and additionally no color change was

observed during the reaction period. This could be the result of exchange of the counterion bromide with PF_6^- or BF_4^- .

Besides the Ph_2PPrDI ligand, alkyl-substituted phosphine-tethered diimine ligand chemistry has also been investigated. In a similar fashion to other DI ligands, tBu_2PPrDI ¹⁷ was synthesized through Schiff base condensation between diacetyl and 3-(*t*-butylphosphino)propylamine at 105 °C for 48 h (Scheme 2.4), followed by purification via recrystallization from diethyl ether solvent at -35 °C. Double condensation was confirmed from ^1H NMR spectroscopic analysis, which showed only one backbone methyl resonance at 2.11 ppm and a single resonance was observed at 26.52 ppm in the ^{31}P NMR spectrum (Fig. 2.12).



Scheme 2.4: Synthesis of tBu_2PPrDI ligand and $(\text{tBu}_2\text{PPrDI})\text{FeBr}_2$ (**7**).

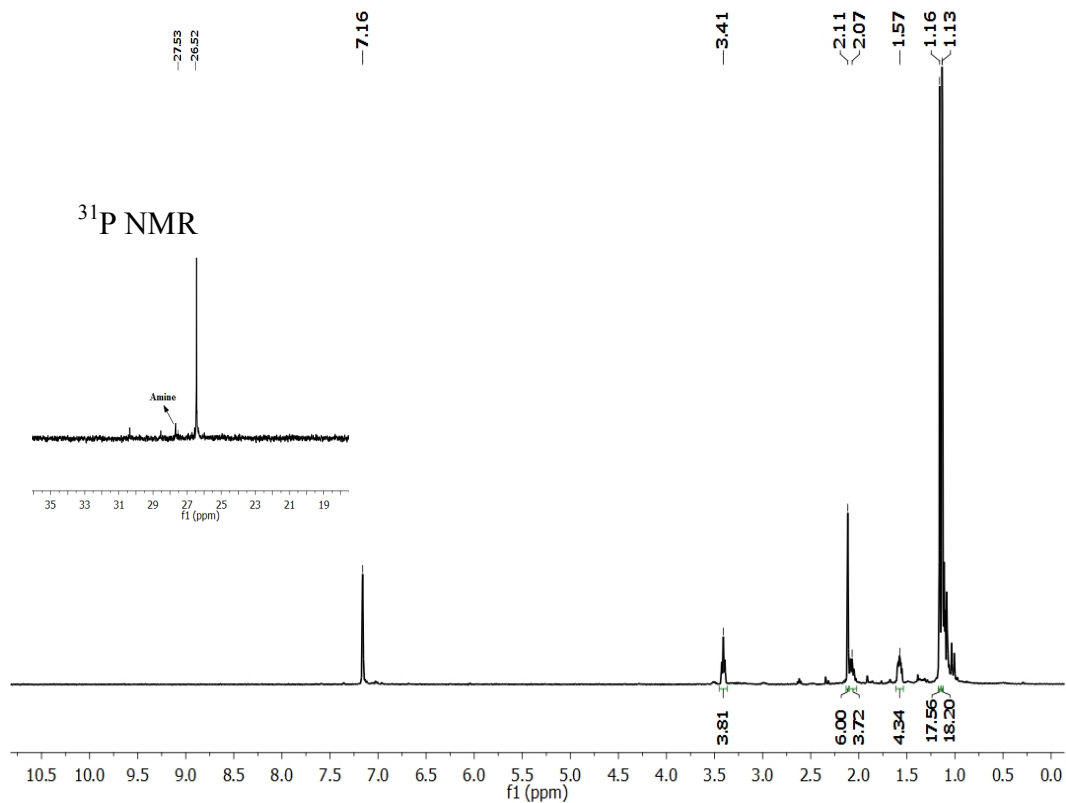


Figure 2.12: ^1H NMR and ^{31}P NMR spectrum (inset) of $t\text{Bu}_2\text{PPrDI}$ ligand in benzene- d_6 at 25 °C.

After isolation of the ligand, it was metallated with FeBr_2 in THF, which afforded a THF soluble blue paramagnetic compound (**7**) after 24 h. The ^1H NMR spectrum of this compound ranges over 200 ppm (Fig. 2.13). Based on the solubility and analogous compound **1**,¹⁴ **7** can be identified as $(\kappa^4\text{-}N,N,P,P\text{-}t\text{Bu}_2\text{PPrDI})\text{FeBr}_2$ (Scheme 2.4), having an Fe(II) center arranged in an octahedral geometry.

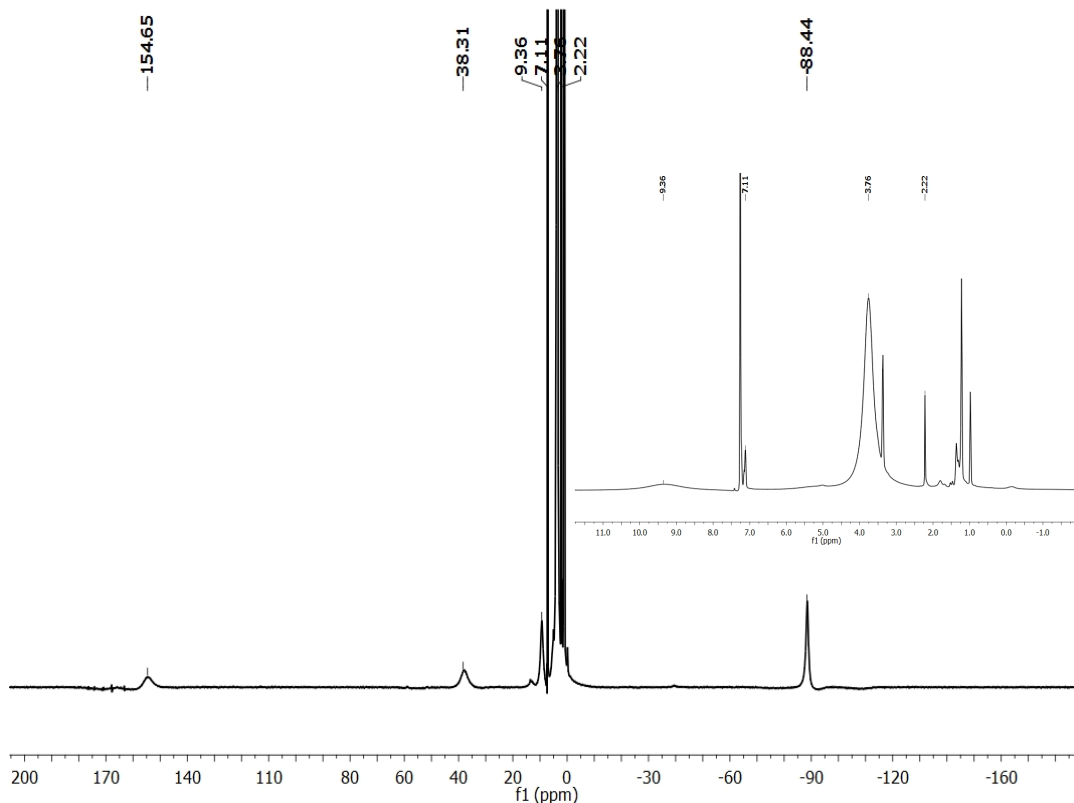
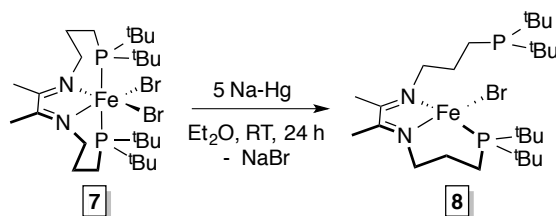


Figure 2.13: ¹H NMR spectrum of **7** in chloroform-*d* at 25 °C (inset- diamagnetic region of the same spectrum).

The sequential C-H, C-P bond activation of **2** encouraged us to develop an analogous Fe compound where C-P activation could be prevented. As a consequence, the proposed iron hydride intermediate would be isolated in order to bolster the mechanism of bond activation. It has been hypothesized that replacing the phenyl group of phosphine with bulky alkyl groups such as *tert*-butyl could lead us to our desired pathway. With this in mind, attempts were made to reduce compound **7** with excess Na-Hg in diethyl ether solvent (Scheme 2.5). A color change from blue to green was observed after 2 h and then a green color compound (**8**) was isolated after 24 h following work up. Analysis of the ¹H NMR spectrum confirmed the formation of a paramagnetic compound (Fig. 2.14), with one resonance at 4.27 ppm (singlet), one at 26.49 ppm (singlet) and several resonances

between 28-32 ppm were observed in the ^{31}P NMR spectrum. Purification of the reaction mixture via crystallization from diethyl ether at $-35\text{ }^\circ\text{C}$ allowed for the isolation of a single compound having two resonances (4.27 and 26.49 ppm) in the ^{31}P NMR spectrum (Fig. 2.15); resonance at 4.27 ppm is presumably due to the coordinated phosphine while the other one is uncoordinated phosphine.¹⁸ The structure is further confirmed from the crystallographic study.



Scheme 2.5: Synthesis of $(^t\text{Bu}_2\text{PPrDI})\text{FeBr}$ (**8**).

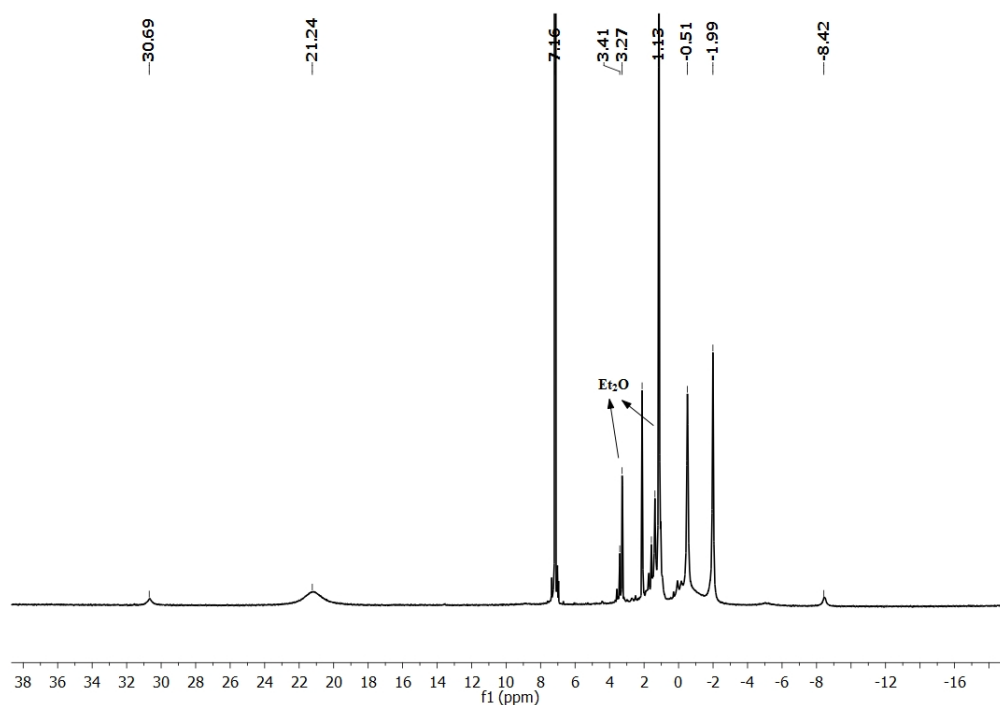


Figure 2.14: ^1H NMR spectrum of crystals of **8** in benzene- d_6 at $25\text{ }^\circ\text{C}$.

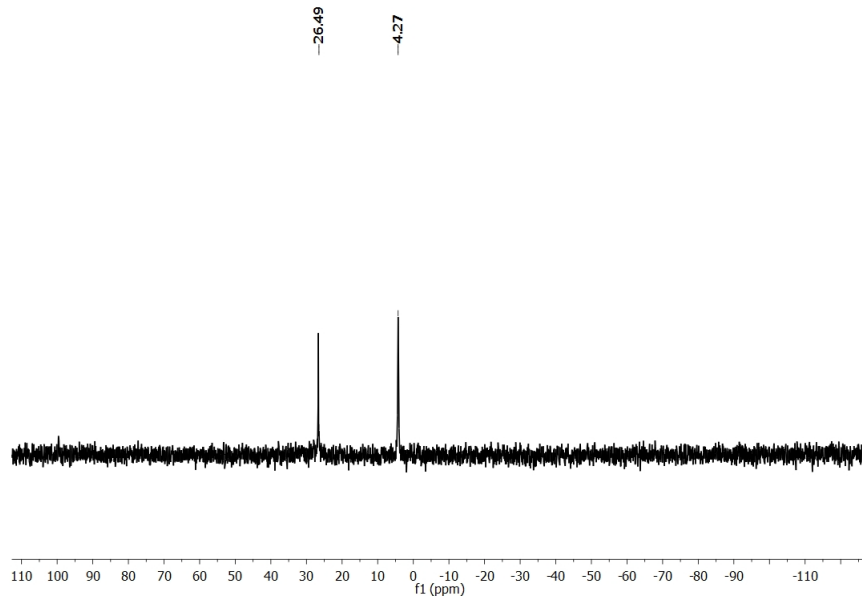


Figure 2.15: ^{31}P NMR spectrum of crystals of **8** in benzene- d_6 at 25 °C.

Single crystal X-ray diffraction analysis confirmed the identity of the compound as (κ^3 -*N,N,P*-^tBu₂PP^rDI)FeBr (**8**) (Fig. 2.16). Refinement of the metrical parameters revealed a distorted tetrahedral geometry around Fe(I) center with angles of N(1)-Fe(1)-N(2), N(1)-Fe(1)-P(1), N(2)-Fe(1)-P(1), N(1)-Fe(1)-Br(1), and P(1)-Fe(1)-Br(1) found to be 79.7 (2)°, 90.37 (15)°, 120.10 (16)°, 120.88 (15)°, and 116.46 (6)°, respectively (Table 2.3). Like the previously mentioned diimine ligand supported reduced iron compounds, single electron reduction of the ligand to mono-radical DI anion was also detected in the case of **8**. This is reflected in the elongation of imine C-N distances and contraction of C(2)-C(3) distance when compared to neutral ligand¹⁵ (Table 2.3).

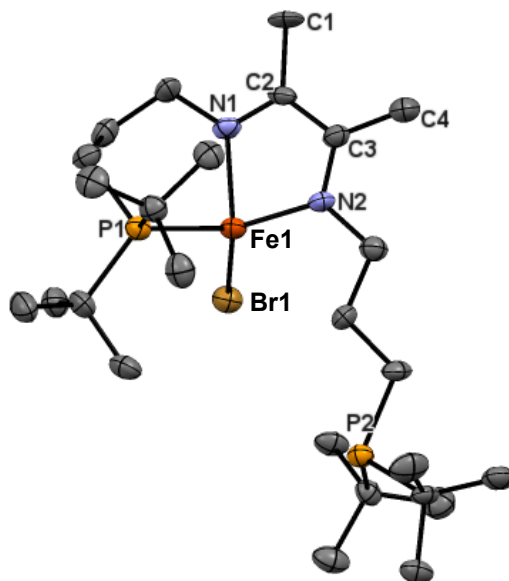


Figure 2.16: Solid-state structure of **8** shown with 30% probability ellipsoids. Hydrogen atoms have been omitted for clarity.

Table 2.3: Notable bond lengths (Å) and bond angles (°) determined for **8**.

Bond	Å	Angle	Degree
C(1)-C(2)	1.519(8)	N(1)-Fe(1)-N(2)	79.7(2)
C(2)-C(3)	1.424(8)	N(1)-Fe(1)-P(1)	90.37(15)
C(2)-N(1)	1.331(8)	N(2)-Fe(1)-P(1)	120.10(16)
C(3)-N(2)	1.344(7)	N(1)-Fe(1)-Br(1)	120.88(15)
Fe(1)-N(1)	2.015(5)	P(1)-Fe(1)-Br(1)	116.46(6)
Fe(1)-N(2)	1.972(5)		
Fe(1)-P(1)	2.3842(19)		
Fe(1)-Br(1)	2.3925(11)		

To obtain a fully reduced compound, different reduction conditions have been employed. Reduction with excess K-Hg after 2 days completely consumed the starting material and produced a mixture of compounds, as evidenced from ^{31}P NMR spectroscopy (Fig 2.17A). To accomplish the reduction in a controlled fashion, it was carried out in the presence of trapping agent 18-crown-6. However, it did not yield an

isolable compound. ^{31}P NMR showed a broad two doublet peaks at 32 ppm ($J = 453.8$ Hz, 247.5 Hz) (Fig. 2.17B). Additionally, using stronger reductant such as sodium naphthalenide also failed to furnish a single compound.

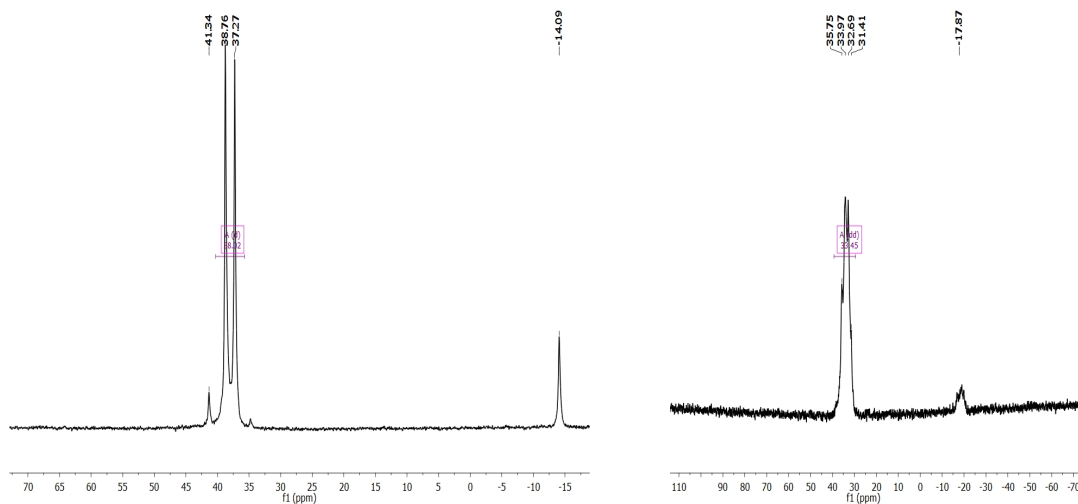
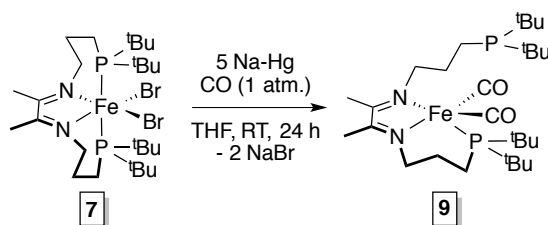


Figure 2.17: ^{31}P NMR spectrum of the reduction trial of **7** with K-Hg (left, A) and K/18-Crown-6 ether (right, B) in benzene- d_6 at 25 °C.

After all these unsuccessful reductions, a different strategy was followed. The hypothesis behind this strategy was to isolate the reduced iron compounds in presence of π -acceptor ligand, which can help to stabilize the iron center.^{8a,19} Following this strategy, reduction of **7** was carried out with excess Na-Hg in the presence of atmospheric CO gas (Scheme 2.6). After stirring for 24 h at room temperature followed by removal of excess CO gas and work up, an orange solid compound was isolated. ^1H NMR revealed two different resonances (1.60 and 2.31 ppm) for backbone methyl groups (Fig. 2.18) and two resonances at 91.7 ppm (coordinated phosphine arm) and 27.9 ppm (uncoordinated phosphine arm) were detected in ^{31}P NMR spectrum (Fig. 2.19). These observations resemble what was observed for previously synthesized **4** and therefore, the structure of

this new compound can be proposed as $(\kappa^3\text{-}N,N,P\text{-}^t\text{Bu}_2\text{PPrDI})\text{Fe}(\text{CO})_2$ (**9**) with one uncoordinated phosphine arm. However, unlike **4**, this new iron di-carbonyl compound (**9**) did not allow for the isolation of the corresponding mono-carbonyl compound upon heating for several days. This demonstrates that higher σ -donating ability of the $^t\text{Bu}_2\text{P}$ -groups compared to Ph_2P has increased the extent of backbonding from iron center to CO ligands, therefore diminishing the propensity for CO removal from the di-carbonyl compound to furnish the mono-carbonyl compound.



Scheme 2.6: Synthesis of $(^t\text{Bu}_2\text{PPrDI})\text{Fe}(\text{CO})_2$ (**9**).

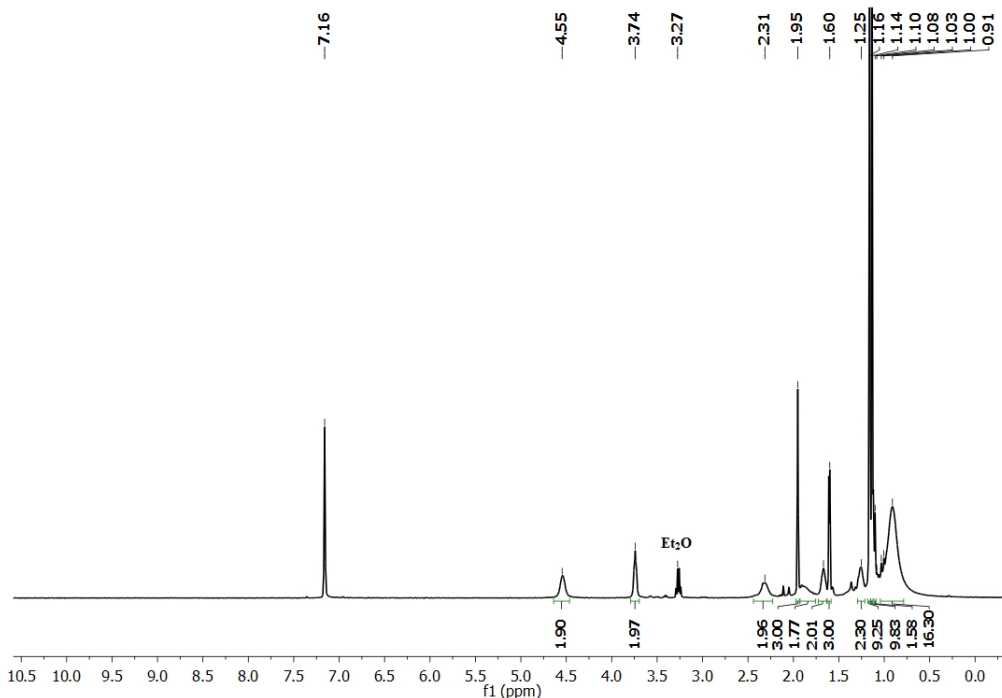


Figure 2.18: ^1H NMR spectrum of **9** in acetone- d_6 at 25 °C.

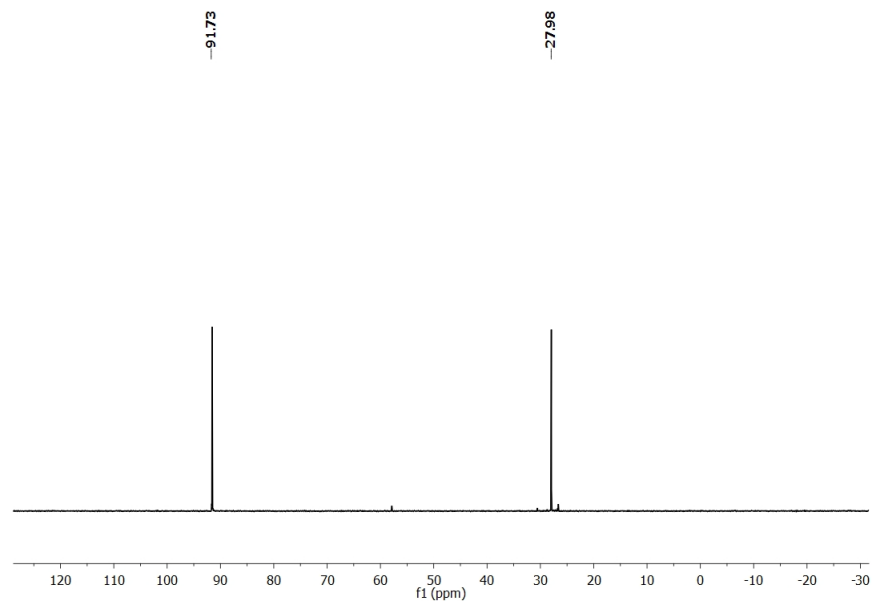
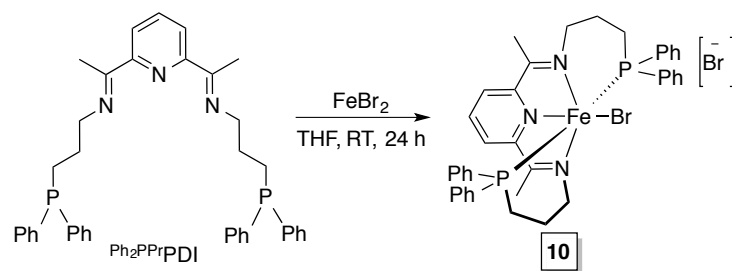


Figure 2.19: ^{31}P NMR spectrum of **9** in acetone- d_6 at 25 °C.

In addition to the diimine ligand, redox non-innocent pyridine diimine (PDI) ligand supported iron chemistry has also been explored. Here, instead of modifying the donor group, the number of carbons in the chain between the imine nitrogen and donor atom has been varied to study the effect of chain length on the electronics of the synthesized iron compounds. In a similar fashion, this project commenced with metallation of propyl bridged pyridine diimine ligand, $^{\text{Ph}_2\text{PPr}}\text{PDI}^{20,21}$ with FeBr_2 in THF, which afforded a purple, THF-insoluble compound after 24 h at room temperature (Scheme 2.7). Multinuclear NMR spectroscopy (^1H , ^{13}C , ^{31}P) determined the purple compound to be diamagnetic, having an Fe(II) center arranged in an octahedral environment. The ^{31}P NMR spectrum featured a single resonance for both phosphine arms at 31.46 ppm (Fig. 2.21), and in the ^1H NMR spectrum, one resonance was noticed for backbone methyl groups, indicating C_2 -symmetry of the compound (Fig. 2.20). Based on the spectroscopic data and solubility of the compound, it can best be identified as an ionic compound, $[(^{\text{Ph}_2\text{PPr}}\text{PDI})\text{FeBr}]\text{Br}$ (**10**).



Scheme 2.7: Synthesis of $[(\text{Ph}_2\text{PPr})\text{PDI}]\text{FeBr}]\text{Br}$ (**10**).

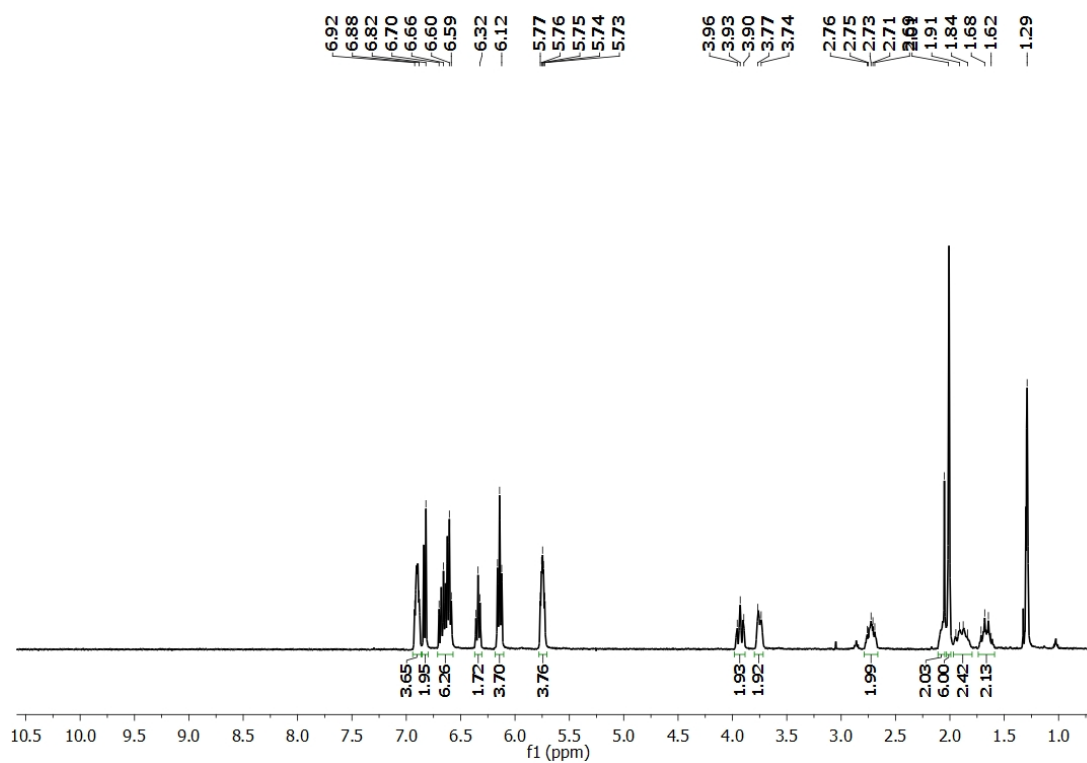


Figure 2.20: ^1H NMR spectrum of **10** in acetone- d_6 at 25 °C.

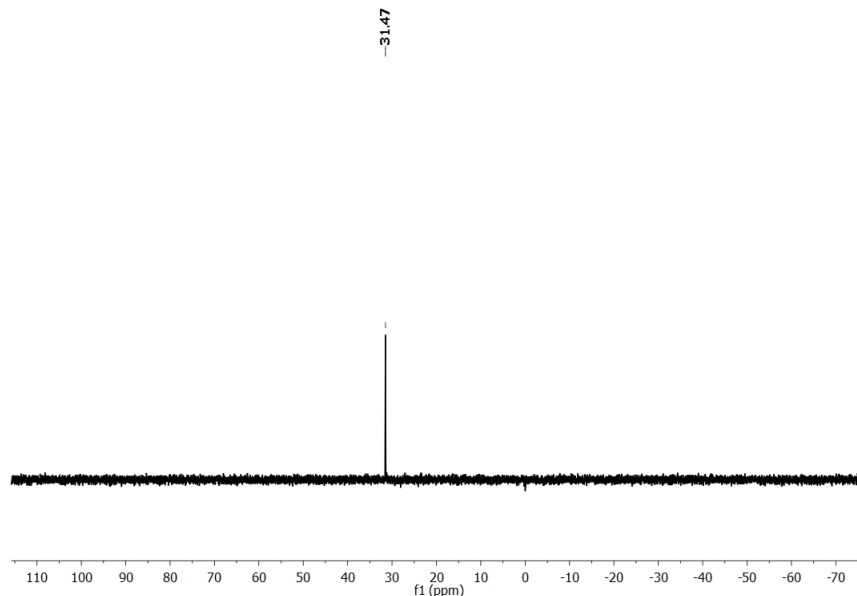
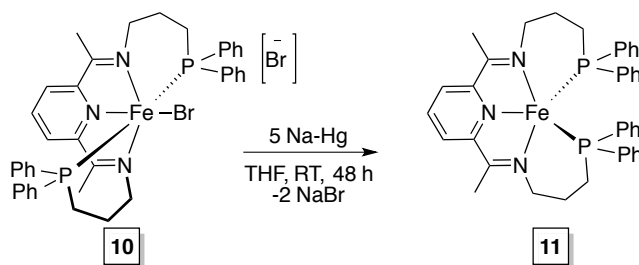


Figure 2.21: ^{31}P NMR spectrum of **10** in acetone- d_6 at 25 °C.

Reduction of **10** with excess Na-Hg followed by work up to remove byproduct NaBr, yielded a greenish brown compound after 48 h (Scheme 2.8). This compound has been characterized by multinuclear NMR spectroscopy. Like compound **10**, the reduced compound also showed a single resonance at 69.78 ppm in the ^{31}P NMR spectrum, indicating that both the phosphine arms are bound to the iron center (Fig. 2.23). Additionally, the C_2 -symmetry of the compound is reflected in the ^1H NMR spectrum, which showed a single resonance for both backbone methyl groups (Fig. 2.22). These observations led us to conclude the structure of the reduced compound as $(\kappa^5\text{-}N,N,N,P,P\text{-Ph}_2\text{PPrPDI})\text{Fe}$ (**11**).



Scheme 2.8: Synthesis of $(\text{Ph}_2\text{PPrPDI})\text{Fe}$ (**11**).

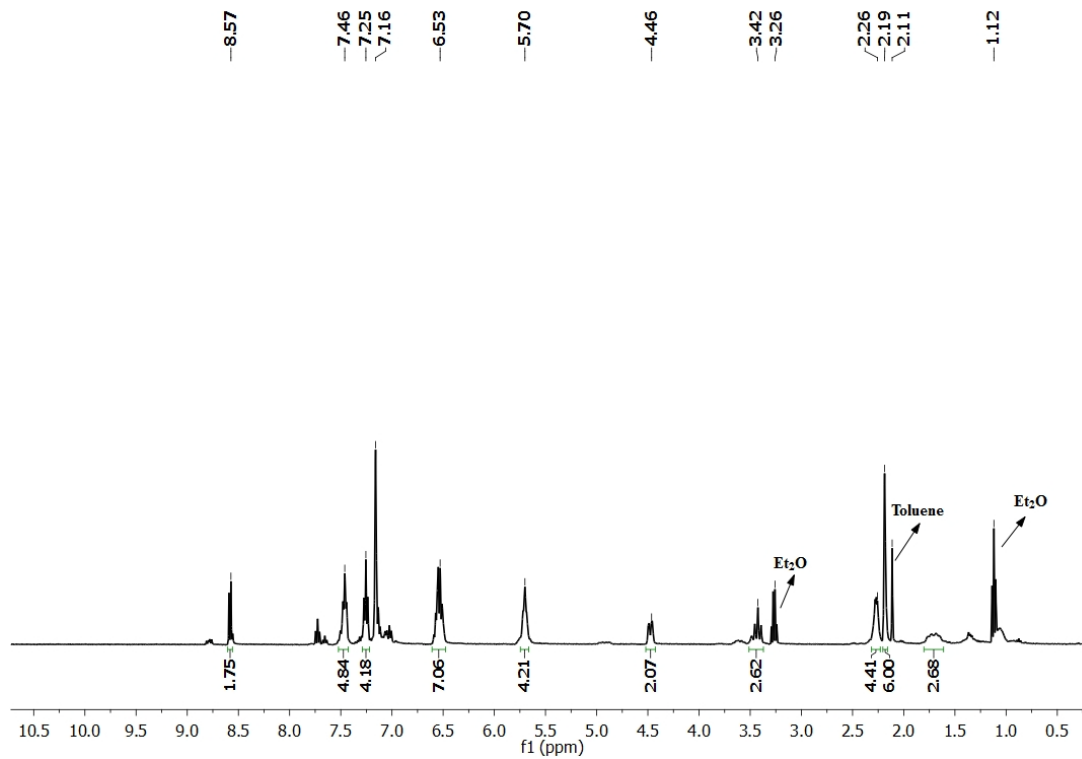


Figure 2.22: ^1H NMR spectrum of **11** in benzene- d_6 at 25 °C.

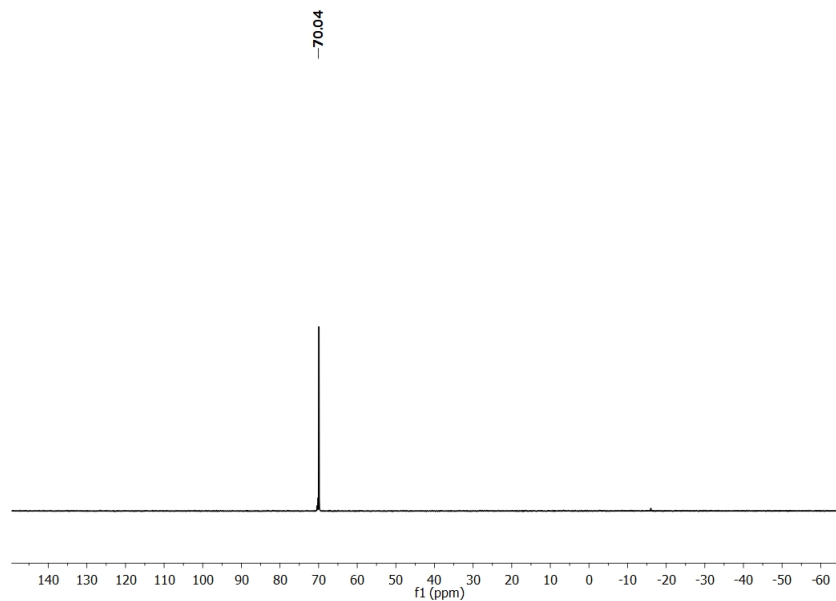
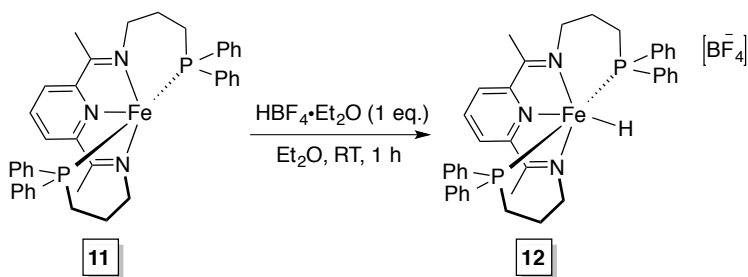


Figure 2.23: ^{31}P NMR spectrum of **11** in benzene- d_6 at 25 °C.

Formally zero valent iron compound **11** remained unreactive towards several oxidative addition reactions using neutral reagents, which could be the consequence of **11**

being an electronically (18 e⁻ system) and coordinatively saturated compound. However, treatment of **11** with tetrafluoroboric acid (HBF₄•Et₂O) resulted in a green diamagnetic ionic compound, **12** (Scheme 2.9), soluble in acetone. The distinct triplet peak at -4.98 ppm ($J_{\text{PH}} = 86.1$ Hz) in the ¹H NMR spectrum indicated the presence of a hydride in compound **12** (Fig. 2.24) and the P-H coupling constant is consistent with *cis*-conformation of hydride and phosphine.²² ³¹P NMR spectroscopic analysis showed a single resonance at 56.3 ppm (Fig. 2.25), suggesting the equivalence of both phosphines and their coordination to metal center. Taking all these observations together, **12** can be best described as [(κ⁵-*N,N,N,P,P*-Ph₂PPrPDI)Fe^{II}(H)][BF₄]. An analogous compound, [(κ⁵-*N,N,N,P,P*-Ph₂PPrPDI)Fe^{II}(H)][OTf] was also synthesized by treating **11** with trifluoromethanesulphonic acid (HOTf).



Scheme 2.9: Synthesis of [(κ⁵-Ph₂PPrPDI)Fe^{II}(H)][BF₄] (**12**).

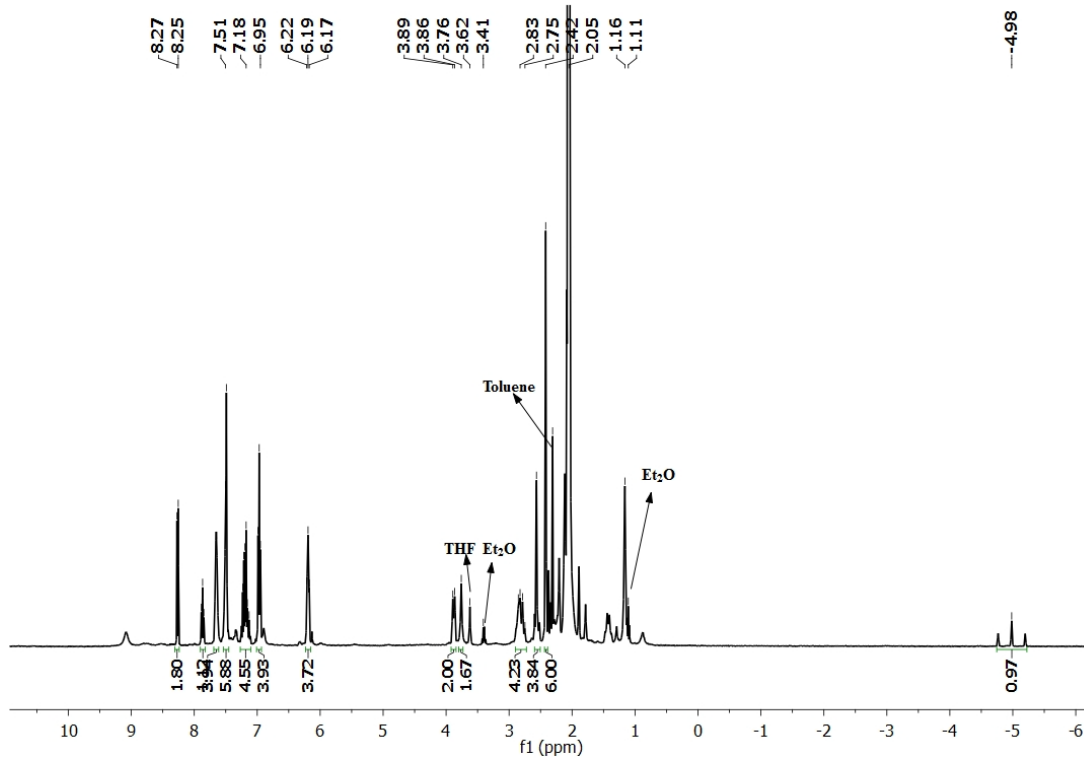


Figure 2.24: ^1H NMR spectrum of **12** in acetone- d_6 at 25 °C.

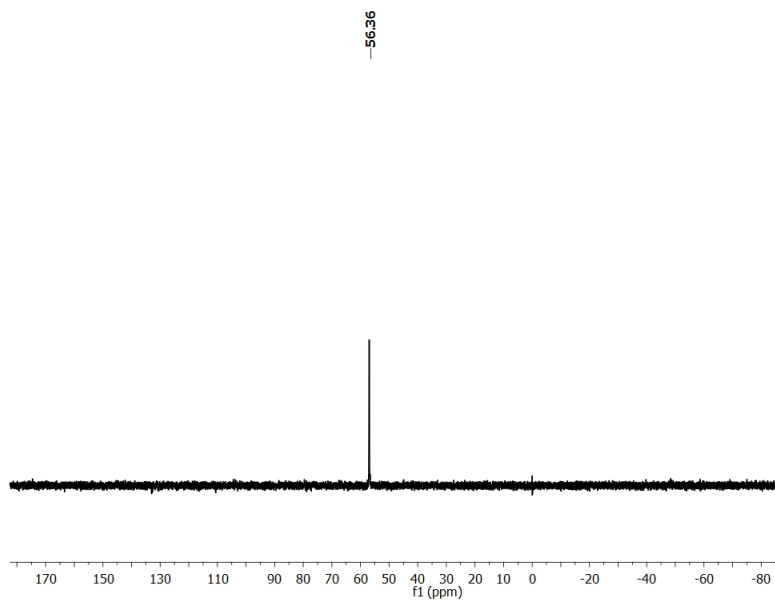
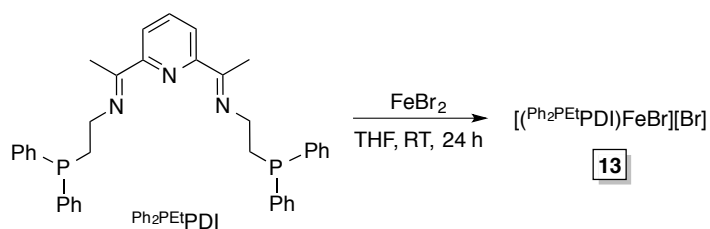


Figure 2.25: ^{31}P NMR spectrum of **12** in acetone- d_6 at 25 °C.

By truncating the chain length of the ligand from three to two, $^{\text{Ph}_2\text{PEt}}\text{PDI}^{19}$ ligand was synthesized. Like the $^{\text{Ph}_2\text{PPr}}\text{PDI}$ -supported iron dibromide compound **10**, metallation of $^{\text{Ph}_2\text{PEt}}\text{PDI}$ was accomplished by reacting it with FeBr_2 in THF at room temperature (Scheme 2.10). Unlike **8**, in this case, metallation led to the formation of a mixture of both paramagnetic and diamagnetic compounds (**13**), as judged by the ^1H NMR analysis. The ^{31}P NMR spectrum displayed two doublet resonances at 47.3 and 57.6 ppm ($J_{\text{PP}} = 59.1$ Hz) (Fig. 2.26), indicating that the phosphine groups exist in the *cis*-conformation of the octahedral arrangement of the ligand around iron center.



Scheme 2.10: Synthesis of $[(^{\text{Ph}_2\text{PEt}}\text{PDI})\text{FeBr}][\text{Br}]$ (**13**).

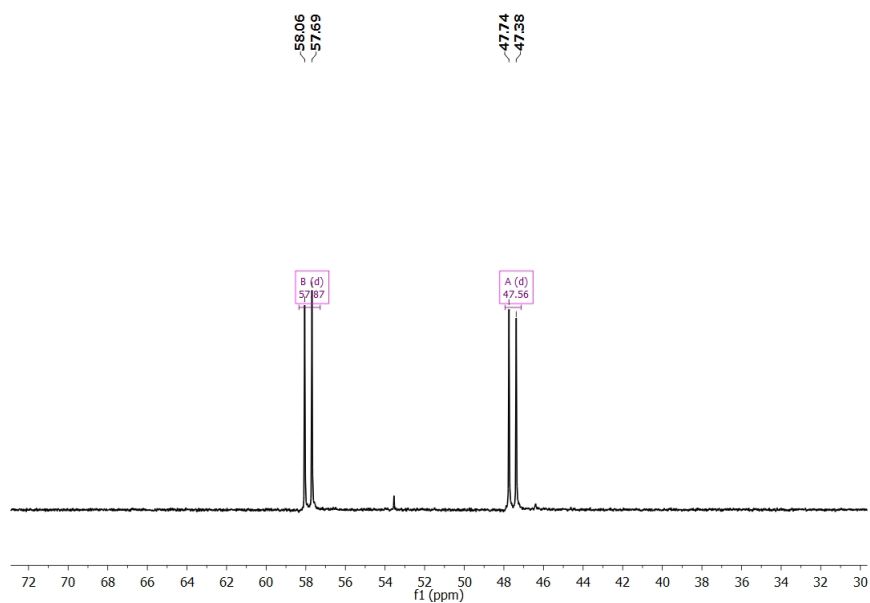
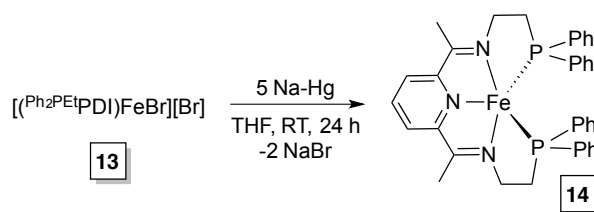


Figure 2.26: ^{31}P NMR spectrum of **13** in acetone- d_6 at 25 °C.

Reduction of the iron dibromide compound **13** with excess Na-Hg in THF solvent yielded a red diamagnetic compound after 48 h (Scheme 2.11, **14**). The presence of a single resonance for the backbone methyl groups (2.31 ppm) in the ^1H NMR spectrum (Fig. 2.27) and only one signal in the ^{31}P NMR spectrum (70.4 ppm) (Fig. 2.28) proved the C_2 -symmetry of the compound and therefore, **14** can be best identified as a formally zero-valent iron compound with $(^{\text{Ph}_2\text{PEt}}\text{PDI})\text{Fe}$ containing $\kappa^5\text{-N,N,N,P,P}$ coordination of the ligand around iron. Compound **14** has been found to be active for carbonyl (aldehyde and ketone) hydrosilylation.



Scheme 2.11: Synthesis of $(^{\text{Ph}_2\text{PEt}}\text{PDI})\text{Fe}$ (**14**).

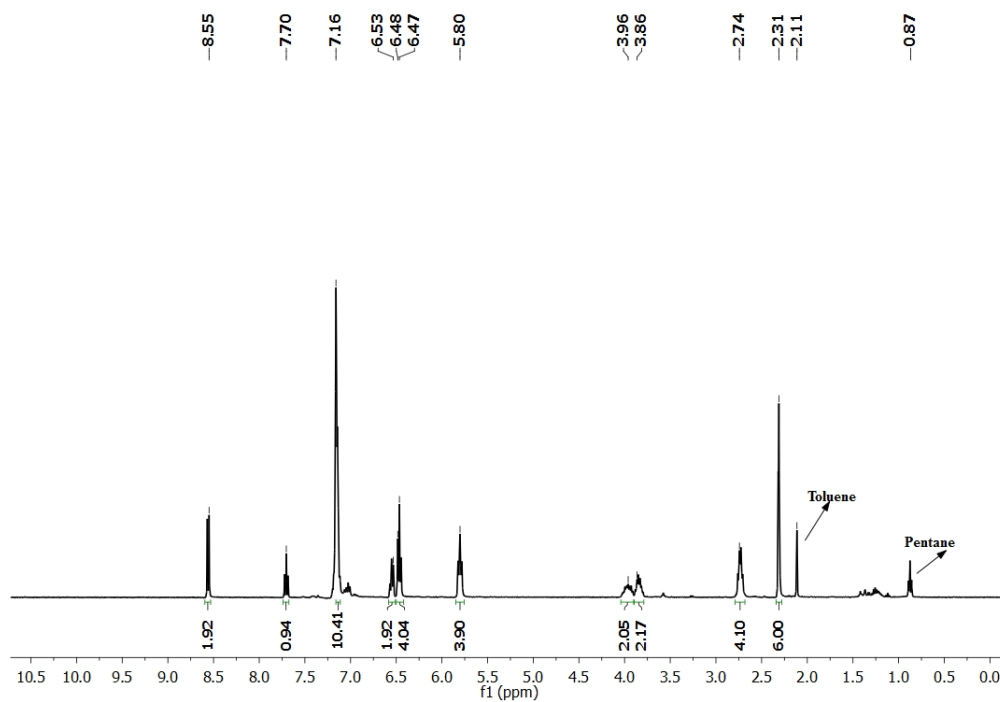


Figure 2.27: ^1H NMR spectrum of **14** in benzene- d_6 at 25 °C.

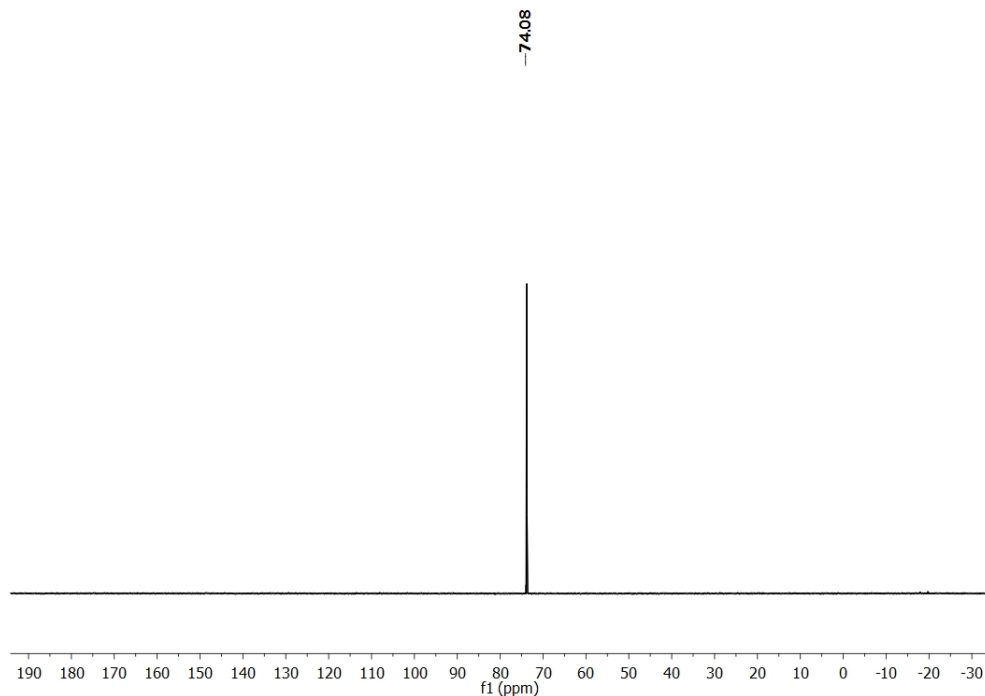


Figure 2.28: ^{31}P NMR spectrum of **14** in benzene- d_6 at 25 °C.

2.4. Conclusion:

In summary, the synthesis and reactivity of a series of low valent iron compounds has been described. One of the main goals of the reactivity study was to develop analogs of Fischer carbenes. To achieve this goal, attempts were made to design iron carbonyl compounds with phosphine-substituted redox non-innocent DI ligands. Our aims to isolate and characterize the di- and mono-carbonyl compounds, $(^{\text{Ph}_2\text{PPr}}\text{DI})\text{Fe}(\text{CO})_2$ (**4**) and $(^{\text{Ph}_2\text{PPr}}\text{DI})\text{Fe}(\text{CO})$ (**5**) were successfully accomplished. To effectuate the goal of carbene synthesis, nucleophilic attack on the CO ligands by alkyl lithium reagents was carried out, but these attempts failed. Other than alkyl lithium reagents, reaction of carbonyl compounds with hydride donor reagents (NaBH_4 , NaEt_3BH) was also conducted, but failed to produce any new compound. The iron mono-carbonyl compound **5** was only

observed to react with methyl iodide to produce a new diamagnetic compound. A different approach was then taken to make the nucleophilic attack on carbonyl ligands successful. Instead of using zero-valent iron carbonyl compounds, efforts were made to synthesize the carbonyl ligand containing Fe(II) compound, [^{Ph₂PPr}DIFe(CO)Br][Br] (**6**). However, compound **6** produced iron mono carbonyl compound (**5**) instead of making a formyl complex (which is the expected result of nucleophilic attack of hydride on CO ligand) upon reaction with hydride reagents. Alkyl phosphine substituted DI ligand chemistry has also been investigated. In this case, a mono-reduced compound, (^{tBu₂PPr}DI)FeBr and reduced di-carbonyl compound, (^{tBu₂PPr}DI)Fe(CO)₂ (**9**) have been successfully isolated and characterized. In similar fashion, low valent iron compounds containing redox non-innocent PDI ligands, identified as (^{Ph₂PPr}PDI)Fe (**11**) and (^{Ph₂PEt}PDI)Fe (**14**) have also been isolated and characterized. Between these two compounds, compound **14** was found to be active for carbonyl hydrosilylation.

2.5. Experimental Section:

2.5.1. Preparation of ^{Ph₂PPr}DIFe(CO)₂ (**4**):

In the nitrogen filled glove box, a 100 mL Schlenk tube was charged with 6.47 g of Hg⁰ (32.368 mmol) followed by freshly cut Na⁰ (37.2 mg, 1.618 mmol) in approximately 10 mL of THF solvent. The mixture was stirred for 20 minutes at room temperature until the cloudy grey suspension turned clear. To this Na-Hg mixture, the solution of **1** (243.5 mg, 0.324 mmol) in THF (~ 8 mL) was added. The Schlenk tube was then sealed, taken outside the box and thawed in liquid nitrogen and degassed. To this reaction mixture, one atmosphere of CO gas was introduced using the Schlenk line. After gas addition was

completed, it was warmed up to room temperature and stirred for another 24 h. Excess CO was removed using the Schlenk line and the red colored reaction mixture was filtered through Celite to remove the by-product NaBr inside the glove box. The solvent was removed under vacuum to obtain 186.3 mg of a red fluffy solid compound (yield = 88 %), identified as ($^{\text{Ph}_2\text{PPrDI}}\text{Fe}(\text{CO})_2$) (**4**). Single crystals of **4** were grown from a concentrated solution of diethyl ether at $-35\text{ }^\circ\text{C}$. ^1H NMR (400 MHz, benzene- d_6) δ 7.45 (t, $J = 6.8\text{ Hz}$, 4H, *phenyl*), 7.14 – 6.89 (m, 16H, *phenyl*), 4.40 (d, $J = 13.3\text{ Hz}$, 2H, $-\text{CH}_2$), 4.04 (d, $J = 10.2\text{ Hz}$, 2H, $-\text{CH}_2$), 2.04-2.17 (m, 6H, $-\text{CH}_2$), 1.73 (d, $J = 2.3\text{ Hz}$, 3H, $-\text{CH}_3$), 1.56 (d, $J = 25.1\text{ Hz}$, 2H, $-\text{CH}_2$), 1.43 (d, $J = 5.4\text{ Hz}$, 3H, $-\text{CH}_3$). ^{31}P NMR (400 MHz, benzene- d_6) δ 67.33, -16.58.

2.5.2. Preparation of ($^{\text{Ph}_2\text{PPrDI}}\text{Fe}(\text{CO})$) (**5**):

In the nitrogen filled glove box, a 100 mL Schlenk tube was filled with 60 mg (0.092 mmol) of ($^{\text{Ph}_2\text{PPrDI}}\text{Fe}(\text{CO})_2$) (**4**) in approximately 10 mL of toluene. The tube was sealed, taken outside the box and heated to $110\text{ }^\circ\text{C}$ in a pre-heated oil bath. In 2 day intervals, CO gas was removed on the Schlenk line to move the equilibrium of the reaction to the product side. After 10 days of heating and CO gas removal, the reaction mixture was filtered through Celite and the solvent was removed under vacuum to obtain 40.5 mg (yield = 71%) of a burgundy color solid compound, identified as ($^{\text{Ph}_2\text{PPrDI}}\text{Fe}(\text{CO})$) (**5**). Single crystals of **5** were grown from a concentrated solution of diethyl ether solvent at $-35\text{ }^\circ\text{C}$. ^1H NMR (400 MHz, benzene- d_6) δ 7.33 (t, $J = 8.3\text{ Hz}$, 4H, *phenyl*), 6.99 – 6.93 (m, 6H, *phenyl*), 6.93 – 6.87 (m, 6H, *phenyl*), 6.84 (t, $J = 7.2\text{ Hz}$, 4H, *phenyl*), 4.27 – 4.14 (m, 2H, $-\text{CH}_2$), 3.74 (d, $J = 14.0\text{ Hz}$, 2H, $-\text{CH}_2$), 2.18 (m, 3H, $-\text{CH}_2$), 2.02 (s, 5H, $-\text{CH}_2$), 1.76 (s, 3H, $-\text{CH}_3$). ^{31}P NMR (400 MHz, benzene- d_6) δ 69.80.

2.5.3. Preparation of (^tBu₂PPrDI)FeBr₂ (**7**):

In the nitrogen filled glove box, a 20 mL scintillation vial was charged with 28.5 mg (0.1321 mmol) of FeBr₂ in approximately 5 mL of THF solvent and stirred for 10 minutes until FeBr₂ was almost dissolved. To this, the solution of ^tBu₂PPrDI ligand (75.4 mg, 0.1651) in THF (~ 5 mL) was added and immediately the solution turned into blue color. The reaction was allowed to stir for 24 h at room temperature for completion, after which it was filtered. The solvent was removed under vacuum followed by washing with pentane (3 X 5 mL) and then dried to yield a blue THF soluble compound (78.5 mg, yield = 88 %), identified as (^tBu₂PPrDI)FeBr₂ (**7**). ¹H NMR (500 MHz, chloroform-*d*) δ 154.65 (2054.91 Hz), 38.31 (1571.15 Hz), 9.36 (631.58 Hz), 3.76 (146.86 Hz), -88.44 (520.84 Hz).

2.5.4. Preparation of (^tBu₂PPrDI)FeBr (**8**):

In the nitrogen filled glove box, a 20 mL scintillation vial was charged with 2.21 g of Hg⁰ (11.036 mmol) followed by freshly cut Na⁰ (12.7 mg, 0.552 mmol) in approximately 5 mL of Et₂O solvent. The mixture was stirred for 20 minutes at room temperature until the cloudy grey suspension turned clear. To this Na-Hg mixture, the solution of **7** (74.2 mg, 0.110 mmol) in Et₂O (~ 8 mL) was added. The color of the reaction mixture was changed from blue to green within 15 h. After stirring for 24 h at room temperature, the reaction mixture was filtered through Celite to remove the byproduct NaBr. The solvent was removed under vacuum to obtain 39.2 mg (yield = 60 %) of a green solid compound, identified as (^tBu₂PPrDI)FeBr (**8**). The compound was purified through crystallization from diethyl ether solvent. Single crystals of **8** were also grown from a concentrated solution

of diethyl ether solvent at -35 °C. ^1H NMR (400 MHz, benzene- d_6) δ 30.69, 21.24, 3.41, 1.58, 1.37, 1.16, -0.51, -1.99, -8.42. ^{31}P NMR (400 MHz, benzene- d_6) δ 26.49, 4.27.

2.5.5. Preparation of ($^t\text{Bu}_2\text{PPrDI}$)Fe(CO) $_2$ (**9**):

In the nitrogen filled glove box, a 100 mL Schlenk tube was charged with 1.76 g of Hg^0 (8.835 mmol) followed by freshly cut Na^0 (10.2 mg, 0.4117 mmol) in approximately 10 mL of THF solvent. The mixture was stirred for 20 minutes at room temperature until the cloudy grey suspension turned clear. To this Na-Hg mixture, a solution of **7** (59.4 mg, 0.088 mmol) in THF (~ 8 mL) was added. The Schlenk tube was then sealed, taken outside the box and thawed in liquid nitrogen and degassed. To this reaction mixture, one atmosphere of CO gas introduced on the Schlenk line. After gas addition was completed, it was warmed up to room temperature and stirred for another 24 h. Excess CO was removed on the Schlenk line and an orange colored reaction mixture was filtered through Celite to remove the byproduct NaBr inside the glove box. The solvent was removed under vacuum to obtain 30.2 mg of an orange fluffy solid compound (yield = 60%), identified as ($^t\text{Bu}_2\text{PPrDI}$)Fe(CO) $_2$ (**9**). ^1H NMR (400 MHz, benzene- d_6) δ 4.55 (m, 2H, - CH_2), 3.74 (m, 2H, - CH_2), 2.31 (m, 2H, - CH_2), 1.95 (m, 2H, - CH_2), 1.91 (s, 3H, - CH_3), 1.67 (m, 2H, - CH_2), 1.60 (s, 3H, - CH_3), 1.25 (m, 2H, - CH_2), 1.15 (d, $J = 10.6$ Hz, 9H, - $\text{C}(\text{CH}_3)_3$), 1.09 (d, $J = 7.5$ Hz, 9H, - $\text{C}(\text{CH}_3)_3$), 1.04 – 0.79 (m, 18H, - $\text{C}(\text{CH}_3)_3$). ^{31}P NMR (400 MHz, benzene- d_6) δ 91.73, 27.98.

2.5.6. Preparation of [$^{\text{Ph}_2\text{PPrPDI}}$ Fe(Br)][Br] (**10**):

In the nitrogen filled glove box, a 20 mL scintillation vial was charged with 123.4 mg (0.5724 mmol) of FeBr_2 in approximately 5 mL of THF solvent and stirred for 10 minutes until FeBr_2 was almost dissolved. To this, the solution of $^{\text{Ph}_2\text{PPrPDI}}$ ligand (350.9

mg, 0.5724 mmol) in THF (~ 5 mL) was added and immediately the solution turned purple in color. The reaction was allowed to stir for 24 h at room temperature for completion, after which it was filtered. An insoluble purple solid compound was collected from the top of the frit. The solid was washed with ether (3 X 5 mL) followed by pentane (3 X 5 mL) to obtain 397.6 mg of [$(^{\text{Ph}_2\text{PPr}}\text{PDI})\text{Fe}(\text{Br})][\text{Br}]$ (**10**) (yield = 84%). ^1H NMR (400 MHz, acetone- d_6) δ 6.90 (d, J = 16.6 Hz, 4H, *phenyl*), 6.82 (m, 2H, *phenyl*), 6.62-6.59 (m, 6H, *phenyl*), 6.34 (t, J = 7.3 Hz, 2H, *phenyl*), 6.14 (t, J = 7.6 Hz, 4H, *phenyl*), 5.78 – 5.71 (m, 4H, *phenyl*), 3.93 (t, J = 12.1 Hz, 2H, $-\text{CH}_2$), 3.75 (d, J = 12.2 Hz, 2H, $-\text{CH}_2$), 2.78 – 2.66 (m, 2H, $-\text{CH}_2$), 2.05 (m, 2H, $-\text{CH}_2$) 2.01 (s, 6H, $-\text{CH}_3$), 1.89 (dd, J = 28.3, 15.0 Hz, 2H, $-\text{CH}_2$), 1.74 – 1.59 (m, 2H, $-\text{CH}_2$).

2.5.7. Preparation of $(^{\text{Ph}_2\text{PPr}}\text{PDI})\text{Fe}$ (**11**):

In the nitrogen filled glove box, a 20 mL scintillation vial was charged with 3.81 g of Hg^0 (19.055 mmol) followed by freshly cut Na^0 (21.9 mg, 0.953 mmol) in approximately 5 mL of THF solvent. The mixture was stirred for 20 minutes at room temperature until the cloudy grey suspension turned clear. To this Na-Hg mixture, a solution of **10** (157.9 mg, 0.191 mmol) in THF (~ 8 mL) was added. The color of the reaction mixture was changed from purple to greenish brown within 15 h. After stirring for 48 h at room temperature, the reaction mixture was filtered through Celite to remove the byproduct NaBr. The solvent was removed under vacuum to obtain 104.5 mg (yield = 82%) of a greenish brown solid compound, identified as $(^{\text{Ph}_2\text{PPr}}\text{PDI})\text{Fe}$ (**11**). ^1H NMR (400 MHz, benzene- d_6) δ 8.58 (d, J = 7.6 Hz, 2H, *phenyl*), 7.46 (t, J = 7.2 Hz, 5H, *phenyl*), 7.25 (t, J = 7.4 Hz, 4H, *phenyl*), 6.54 (dd, J = 16.1, 8.7 Hz, 7H, *phenyl*), 5.70 (t, J = 7.1 Hz, 3H, *phenyl*), 4.48

(d, $J = 12.1$ Hz, 2H, $-CH_2$), 3.44 (dd, $J = 24.6, 12.5$ Hz, 2H, $-CH_2$), 2.27 (dd, $J = 9.1, 4.5$ Hz, 4H, $-CH_2$), 2.19 (s, 6H, $-CH_3$), 1.68 (m, 2H, $-CH_2$).

2.5.8. Preparation of $[(^{Ph_2PPr}PDI)Fe(H)][BF_4]$ (**12**):

In the nitrogen filled glove box, a 100 mL round bottom flask was charged with 126.1 mg of **11** (0.188 mmol) in an approximately 30 mL of Et_2O . To this stirred solution, 25.8 μ L (0.188 mmol) of $HBF_4 \cdot Et_2O$ solution was added dropwise. Within 10 minutes, a green compound precipitated out from the reaction mixture. After 1 h of stirring, the reaction mixture was filtered and green solid compound was collected from the top of the frit. The compound was re-dissolved in acetone, filtered through Celite and dried to obtain 92.7 mg of solid green compound, $[(^{Ph_2PPr}PDI)Fe(H)][BF_4]$ (**12**) (yield = 65%). 1H NMR (400 MHz, acetone- d_6) δ 9.1 (br, 2H, *phenyl*), 8.26 (d, $J = 7.9$ Hz, 2H, *phenyl*), 7.87 (t, $J = 7.9$ Hz, 1H, *phenyl*), 7.64 (m, 4H, *phenyl*), 7.50 (d, $J = 6.2$ Hz, 6H, *phenyl*), 6.97 (t, $J = 7.5$ Hz, 4H), 6.19 (t, $J = 8.4$ Hz, 4H), 3.88 (d, $J = 11.7$ Hz, 2H, $-CH_2$), 3.76 (m, 2H, $-CH_2$), 2.80 (dd, $J = 28.8, 13.4$ Hz, 4H, $-CH_2$), 2.56 (m, 4H, $-CH_2$), 2.42 (s, 6H, $-CH_3$), -4.98 (t, 1H, $J_{PH} = 86.7$ Hz, Fe- H).

2.5.9. Preparation of $(^{Ph_2PEt}PDI)Fe$ (**14**):

In the nitrogen filled glove box, a 20 mL scintillation vial was charged with 1.83 g of Hg^0 (9.155 mmol) followed by freshly cut Na^0 (10.5 mg, 0.458 mmol) in approximately 5 mL of THF. The mixture was stirred for 20 minutes at room temperature until the cloudy grey suspension turned into clear. To this Na-Hg mixture, the solution of $(^{Ph_2PEt}PDI)FeBr_2$ (73.3 mg, 0.092 mmol) in THF (~ 8 mL) was added. The color of the reaction mixture was changed from purple to red within 1 h. After stirring for 24 h at room temperature, the reaction mixture was filtered through Celite to remove the byproduct NaBr. The

solvent was removed under vacuum to obtain 49.3 mg (yield = 84%) of a red solid compound, identified as (^{Ph}₂PEtPDI)Fe(**14**). ¹H NMR (400 MHz, benzene-*d*₆) δ 8.56 (d, *J* = 7.6 Hz, 2H, *phenyl*), 7.70 (t, *J* = 7.6 Hz, 1H, *phenyl*), 7.14 (m, 10H, *phenyl*), 6.55 (t, *J* = 6.7 Hz, 2H, *phenyl*), 6.47 (t, *J* = 7.3 Hz, 4H, *phenyl*), 5.80 (t, *J* = 8.4 Hz, 4H, *phenyl*), 3.96 (dd, *J* = 16.8, 10.9 Hz, 2H, -CH₂), 3.88 – 3.78 (m, 2H, -CH₂), 2.73 (dd, *J* = 14.1, 7.4 Hz, 4H, -CH₂), 2.31 (s, 6H, -CH₃).

2.6. References:

1. Egorova, K. S.; Ananikov, V. P. *Angew. Chem., Int. Ed.* **2016**, *55*, 12150-12162.
2. European Medicines Agency, Guideline on the Specification Limits for Residues of Metal Catalysts or Metal Reagents, EMEA/CHMP/SWP/4446/2000, London, February 21, 2008.
3. Fürstner, A. *ACS Cent. Sci.* **2016**, *2*, 778-789.
4. Bertini, I.; Gray, H. B.; Lippard, S. J.; Valentine, J. S., Eds. *Bioinorganic Chemistry*; University Science Books: Mill Valley, CA, 1994.
5. (a) Lyaskovskyy, V.; Bruin, de; B. *ACS Catal.* **2012**, *2*, 270-279. (b) Luca, O.; R.; Crabtree, R.; H. *Chem. Soc. Rev.* **2013**, *42*, 1440-1459.
6. Bart, S. C.; Lobkovsky, E.; Chirik, P. J. *J. Am. Chem. Soc.* **2004**, *126*, 13794-13807.
7. (a) Bouwkamp, M. W.; Bowman, A. C.; Lobkovsky, E.; Chirik, P. J. *J. Am. Chem. Soc.* **2006**, *128*, 13340-13341. (b) Hoyt, O. M.; Schmidt, V. A.; Tondreau, A. M.; Chirik, P. J. *Science* **2015**, *349*, 960-963.
8. (a) Bart, S. C.; Hawrelak, E. J.; Lobkovsky, E.; Chirik, P., J. *Organometallics* **2005**, *24*, 5518-5527. (b) Schmidt, V. A.; Rose, K. C.; Bezdek, M.; Chirik, P. J. *J. Am. Chem. Soc.* **2018**, *140*, 3443-3453. (c) Lee, H.; Campbell, M. G.; Sánchez, R. H.; Börgel, J.; Raynaud, J.; Parker, S. E.; Ritter, T. *Organometallics* **2016**, *35*, 2923-2929. (d) Wang, H.; Yan, W.; Jiang, T.; Liu, B.; Xu, W.; Ma, J.; Hu, Y. *Chinese Science Bulletin* **2002**, *47*, 1616-1618.
9. Bauer, G.; Hu, X. *Inorg. Chem. Front.* **2016**, *3*, 741-765.

10. (a) Trovitch, R. J.; Lobkovsky, E.; Chirik, P. J. *Inorg. Chem* **2006**, *45*, 7252-7260. (b) Srimani, D.; Diskin-Posner, Y.; Ben-David, Y.; Milstein, D. *Angew. Chem. Int. Ed.* **2013**, *52*, 14131-14134. (c) (i) Langer, R.; Leitus, G.; Ben-David, Y.; Milstein, D. *Angew. Chem. Int. Ed.* **2011**, *50*, 2120-2124. (ii) Langer, R.; Iron, M. A.; Konstantinovski, L.; Diskin-Posner, Y.; Leitus, G.; Ben-David, Y.; Milstein, D. *Chem. – Eur. J.* **2012**, *18*, 7196-7209. (iii) Zell, T.; Ben-David, Y.; Milstein, D. *Catal. Sci. Technol.* **2015**, *5*, 822-826. (iv) Chakraborty, S.; Bhattacharya, P.; Dai, H.; Guan, H. *Acc. Chem. Res.* **2015**, *48*, 1995-2003. (v) Chakraborty, S.; Dai, H.; Bhattacharya, P.; Fairweather, N. T.; Gibson, M. S.; Krause, J. A.; Guan, H. *J. Am. Chem. Soc.* **2014**, *136*, 7869-7872. (vi) Werkmeister, S.; Junge, K.; Wendt, B.; Alberico, E.; Jiao, H.; Baumann, W.; Junge, H.; Gallou, F.; Beller, M. *Angew. Chem. Int. Ed.* **2014**, *53*, 8722-8726. (d) (i) Bornschein, C.; Werkmeister, S.; Wendt, B.; Jiao, H.; Alberico, E.; Baumann, W.; Junge, H.; Junge, K.; Beller, M. *Nat. Commun.* **2014**, *5*, 4111. (ii) Chakraborty, S.; Milstein, D. *ACS Catal.*, **2017**, *7*, 3968-3972. (e) Mazza, S.; Copelliti, R.; Hu, X. *Organometallics* **2015**, *34*, 1538-1545. (f) Bleith, T.; Wadepohl, H.; Gade, L. H. *J. Am. Chem. Soc.* **2015**, *137*, 2456-2459. (g) (i) Chakraborty, S.; Lagaditis, P. O.; Förster, M.; Bielinski, E. A.; Hazari, N.; Holthausen, M. C.; Jones, W. D.; Schneider, S. *ACS Catal.* **2014**, *4*, 3994-4003. (ii) Pena-Lopez, M.; Neumann, H.; Beller, M. *ChemCatChem* **2015**, *7*, 865-871. (h) Chakraborty, S.; Brennessel, W.; Jones, W. D.; *J. Am. Chem. Soc.* **2014**, *136*, 8564-8567.
11. Dötz, K. H.; Stendel, J. *Chem. Rev.* **2009**, *109*, 3227-3274.
12. West, N. M.; Miller, A. J. M.; Labinger, J. A.; Bercaw, J. E. *Coord. Chem. Rev.* **2011**, *255*, 881-898.
13. (a) Suess, D. L. M.; Peters, J. C. *J. Am. Chem. Soc.* **2013**, *135*, 12580-12583. (b) Buss, J. A.; Agapie, T. *Nature* **2016**, *529*, 72-75. (c) Buss, J. A.; Agapie, T. *J. Am. Chem. Soc.* **2016**, *138*, 16466-16477.
14. Ghosh, C.; Groy, T. L.; Bowman, A. C.; Trovitch, R. J. *Chem. Commun.* **2016**, *52*, 4553-4556.
15. Muresan, N.; Chlopek, K.; Weyhermüller, T.; Neese, F.; Wieghardt, K. *Inorg. Chem.* **2007**, *46*, 5327-5337.
16. (a) Cutler, A. R.; Hanna, P. K.; Vites, J. C. *Chem. Rev.* **1988**, *88*, 1363-1403. (b) Wolczanski, P. T.; Bercaw, J. E. *Acc. Chem. Res.* **1980**, *13*, 121-127. (c) Gladysz, J. A. *Adv. Organomet. Chem.* **1982**, *20*, 1-38.
17. Rock, C. L.; Groy, T. L.; Trovitch, R. J. *Dalton Trans.* **2018**, *47*, 8807-8816.
18. Mukhopadhyay, T. K.; Ghosh, C.; Flores, M.; Groy, T. L.; Trovitch, R. J. *Organometallics* **2017**, *36*, 3477-3483.

19. Bart, S. C.; Lobkovsky, E.; Chirik, P. J. *J. Am. Chem. Soc.* **2004**, *126*, 13794-13807.
20. Ben-Daat, H.; Hall, G. B.; Groy, T. L.; Trovitch, R. J. *Eur. J. Inorg. Chem.* **2013**, 4430-4442.
21. Mukhopadhyay, T. K.; Flores, M.; Groy, T. L.; Trovitch, R. J. *J. Am. Chem. Soc.* **2014**, *136*, 882-885.
22. (a) Bhattacharya, P.; Krause, J. A.; Guan, H. *J. Am. Chem. Soc.* **2014**, *136*, 11153-11161. (b) Zhao, H.; Sun, H.; Li, X. *Organometallics* **2014**, *33*, 3535-3539.

CHAPTER 3

DEVELOPMENT OF REDOX ACTIVE LIGAND BASED MANGANESE CATALYSTS FOR CARBONYL HYDROSILYLATION

3.1. Abstract:

Inspired by the excellent carbonyl hydrosilylation activity of our previously reported manganese catalyst, (^{Ph₂PPr}PDI)Mn an attempt was made to synthesize 2nd generation manganese catalysts with improved properties. Two catalysts have been designed; one modifying both donor groups and the number of carbons in the chain between the imine nitrogen and donor atom and the second one featuring only a truncated chain length. Refluxing the reaction mixture of (THF)₂MnCl₂ with the ligands ^{PyEt}PDI and ^{Ph₂PEt}PDI separately produces the corresponding dichloride complexes (^{PyEt}PDI)MnCl₂ (**15**) and (^{Ph₂PEt}PDI)MnCl₂ (**17**), respectively. Reduction of **15** with excess Na-Hg deprotonates the backbone methyl groups to generate the bis(enamide)tris(pyridine)-supported product, (κ⁵-*N,N,N,N,N*-^{PyEt}PDEA)Mn (**16**). On the other hand, reduction of **3** with excess Na-Hg allows for the isolation of a formally zero-valent dimeric compound, [(^{Ph₂PEt}PDI)Mn]₂ (**18**). Both **16** and **18** have been characterized by multinuclear NMR spectroscopy, EPR and single crystal XRD. After isolation and characterization, the carbonyl hydrosilylation activity of both the compounds **16** and **18** was evaluated. At ambient temperature, compound **16** has been found out to be an effective pre-catalyst for both aldehyde and ketone hydrosilylation, exhibiting turnover frequencies (TOF) of up to 2475 min⁻¹ under neat conditions. Similarly, it turns out that compound **18** is capable of catalyzing aldehyde hydrosilylation at a catalyst loading of 0.005 mol% (0.01 mol% relative to Mn) with a maximum

turnover frequency of $9,900 \text{ min}^{-1}$ ($4,950 \text{ min}^{-1}$ per Mn), while it is also an efficient catalyst for formate dihydrosilylation, exhibiting a highest TOF of 330 min^{-1} (165 min^{-1} relative to Mn).

3.2. Introduction:

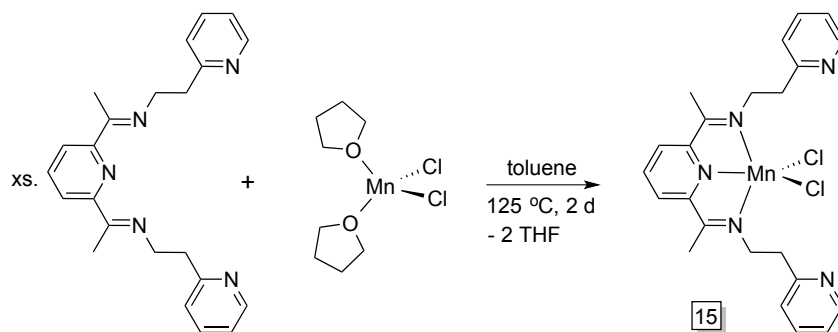
Over the past decade, the cost and toxicity of homogeneous precious metal catalysts have intensified the search for green alternatives that mediate organic transformations with competitive lifetimes, activities, and selectivities.¹ The development of late first-row transition metal catalysts has remained a specific area of interest because Fe, Co, and Ni are Earth-abundant² and significantly less expensive than their precious metal counterparts.³ For example, while Pt catalysts are typically used to prepare silicone coatings and elastomers via olefin hydrosilylation,⁴ recent progress has been made in the development of efficient first-row metal surrogates for this reaction.⁵ The formation of Si–O bonds by way of carbonyl hydrosilylation is considered a complementary technology for which several efficient Fe,⁶ Co,⁷ Ni,⁸ Cu,⁹ and Zn¹⁰ catalysts have been reported. Moreover, the hydrosilylation of ketones using chiral Fe catalysts has recently emerged as an efficient synthetic route to chiral alcohols.¹¹ For all the attention granted to the development of late first row metal hydrosilylation catalysts, Mn-based catalysts for this transformation have remained largely overlooked.¹² In 1983, it was reported that $(\text{CO})_5\text{Mn}^{\text{I}}\text{SiPh}_3$ catalyzes 1-pentene hydrosilylation upon irradiation or heating to $180 \text{ }^\circ\text{C}$.¹³ Similarly, $\text{Mn}_2(\text{CO})_{10}$ was found to mediate the hydrosilylation of 1-hexene with tertiary silanes under mild conditions ($40 \text{ }^\circ\text{C}$).¹⁴ Outside of these reports, Mn hydrosilylation catalysts have been used for the reduction of carbonyl-containing substrates. Cutler and co-workers demonstrated that $(\text{Ph}_3\text{P})(\text{CO})_4\text{Mn}^{\text{I}}\text{C}(\text{O})\text{CH}_3$ catalyzes

the dihydrosilylation of esters¹⁵ and hydrosilylation of ketones¹⁶ with turnover frequencies (TOFs) of up to 4 and 27 min⁻¹, respectively. A few years later, (η^5 -C₁₀H₉)Mn^I(CO)₃ was reported to mediate the hydrosilylation of ketones when Ph₂SiH₂ was used as a reductant.¹⁷ This effort was extended to the utilization of naphthalene-supported [(η^6 -C₁₀H₈)Mn^I(CO)₃][BF₄], which exhibited improved ketone reduction TOFs of up to 1.7 min⁻¹.¹⁸ The Mn⁰₂(CO)₁₀ catalyzed reduction of *N*-acetylpiperidine to *N*-ethylpiperidine¹⁹ and hydrosilylation of carboxylic acids into disilylacetals²⁰ have also been reported; however, modest TOFs were observed for both reactions. While (3,5-^tBu₂-salen)Mn^VN has been found to catalyze 4-nitrobenzaldehyde hydrosilylation with a TOF of 196 min⁻¹ at 80 °C, attempts to hydrosilylate benzaldehyde at ambient temperature using this complex (1 mol%) required 22 h for complete conversion.²¹ Recently, CpMn^I(CO)₂(^{Mes}NHC) has been found to mediate the hydrosilylation of aldehydes and ketones with modest TOFs upon being exposed to 350 nm light.²² In 2014, our group reported that the phosphine-substituted bis(imino)pyridine (or pyridine diimine, PDI) Mn(^{Ph₂PPr}PDI)Mn complex, exhibits ketone hydrosilylation TOFs of up to 1,280 min⁻¹ (76,800 h⁻¹) in the absence of solvent.²³ This catalyst yields either tertiary or quaternary silanes, depending on the reaction conditions, and also mediates the dihydrosilylation of esters to form a mixture of silyl ethers.^{12,23} With this in mind, truncating the carbon chain of the ligand inspired our search for second-generation (PDI)Mn hydrosilylation catalysts that exhibit improved catalytic properties.

3.3. Synthesis and Characterization of 15 and 16:

The search for new catalysts commenced with the synthesis of manganese

dichloride complexes. Heating a 1:1 mixture of $(\text{THF})_2\text{MnCl}_2$ and $^{\text{PyEt}}\text{PDI}^{24}$ in toluene at $95\text{ }^\circ\text{C}$ for 72 h, allows for partial conversion to a pale orange compound identified as $(^{\text{PyEt}}\text{PDI})\text{MnCl}_2$ (**15**) (Scheme 3.1). Upon optimization using excess ligand (1.9 eq.) and heating at $125\text{ }^\circ\text{C}$, the yield has been increased up to 93%. Compound **1** has been found to be paramagnetic based on the broad resonances at 62.76, 13.51 and -13.63 ppm observed in its ^1H NMR spectrum (Fig. 3.1). Magnetic susceptibility measurement of **15** by Guoy method produced a value of $6.3\ \mu_{\text{B}}$, which is consistent with five unpaired electrons. UV-visible spectra of **15** feature charge transfer bands at 306 nm ($\epsilon = 3844\ \text{M}^{-1}\text{cm}^{-1}$) and 318 nm ($\epsilon = 2601\ \text{M}^{-1}\text{cm}^{-1}$) with no observable d-d transition (Fig. 3.2). Incorporating all these observations, compound **15** can be best described as a high spin Mn(II) complex ($S_{\text{Mn}} = 5/2$), similar to the previously reported $(\text{PDI})\text{MnCl}_2$ complexes.^{23,25}



Scheme 3.1: Synthesis of $(^{\text{PyEt}}\text{PDI})\text{MnCl}_2$ (**15**).

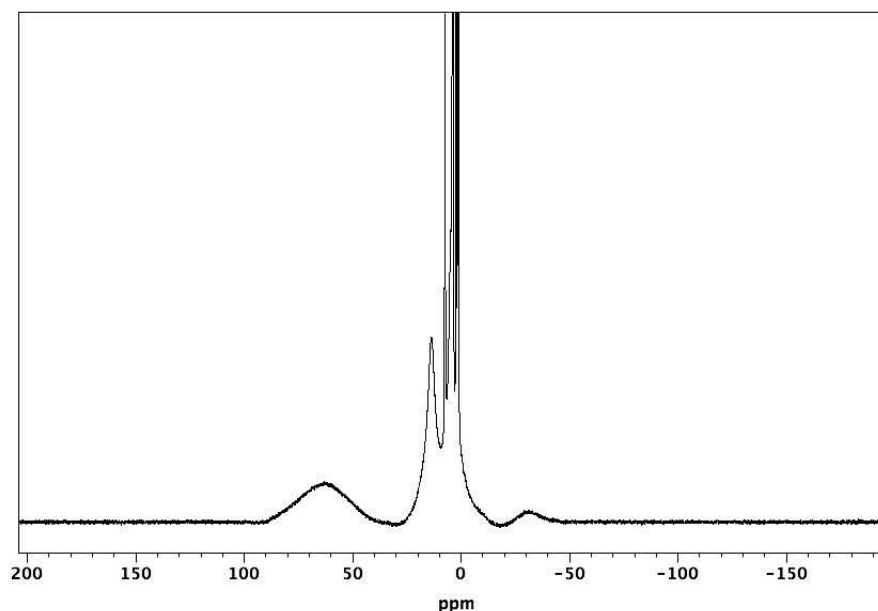


Figure 3.1: ^1H NMR spectrum of **15** in chloroform-*d* at 25 °C.

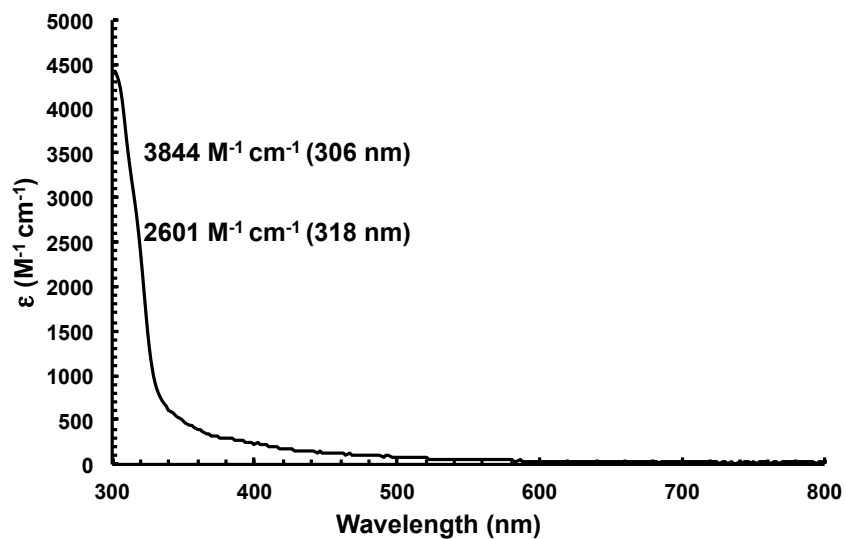


Figure 3.2: UV-visible spectrum of **15** in chloroform. Molar absorptivity values determined from absorbance vs. concentration plot for five independent concentrations.

To investigate the geometry and coordination, crystals of **15** were grown from dichloromethane at -35 °C. Single crystal X-ray diffraction displayed κ^3 -*N,N,N*

coordination of the PDI ligand around the Mn center (Fig. 3.3). The metrical parameters revealed N(1)-Mn(1)-N(1A), N(1)-Mn(1)-Cl(1), N(2)-Mn(1)-Cl(1), Cl(1)-Mn(1)-Cl(1A) and N(1)-Mn(1)-N(2) angles of $142.3(2)^\circ$, $102.16(12)^\circ$, $126.97(4)^\circ$, $106.06(8)^\circ$, $71.17(2)^\circ$, respectively (Table 3.1). Therefore, the geometry of **15** can be best described as distorted trigonal bipyramidal around Mn. Although the Mn-N imine distance of $2.264(4)$ Å determined for this complex is shorter than the same distances reported for ($i\text{Pr}_2\text{Ar}$ PDI)MnCl₂ [$2.333(5)$ and $2.318(5)$ Å]²³ and (Ph_2PPr PDI)MnCl₂ [$2.300(2)$ and $2.338(2)$ Å],²⁵ the Mn(1)-N(1) and Mn(1)-Cl(1) contacts observed for **15** are indicative of high-spin Mn. The N(1)-C(2) and C(2)-C(3) distances were determined to be $1.291(7)$ and $1.505(7)$ Å, respectively (Table 3.1), which indicate an unreduced PDI ligand with minimal backbonding.²⁶

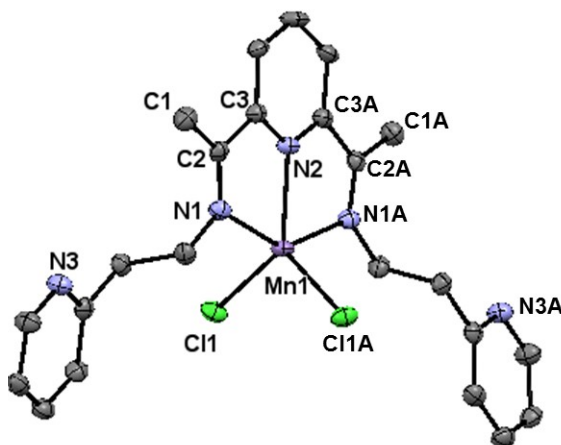
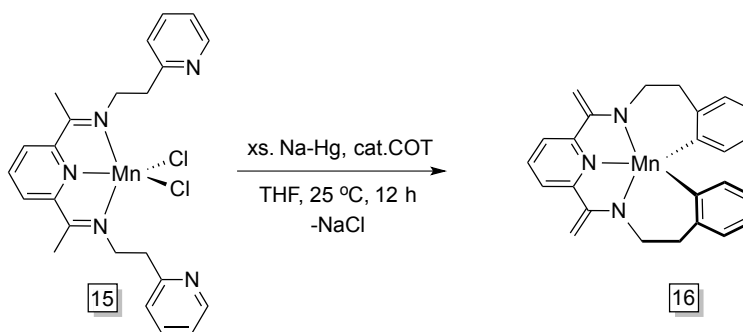


Figure 3.3: The solid-state structure of **15** shown at 30% probability ellipsoids. Labelled atoms ending with ‘A’ have been generated by symmetry. Hydrogen atoms and co-crystallized dichloromethane molecules are omitted for clarity.

Table 3.1: Notable bond lengths (Å) and bond angles (°) determined for **15**.

Bond	Å	Angle	Degree
C(1)-C(2)	1.505(7)	N(1)-Mn(1)-N(2)	71.17(12)
C(2)-C(3)	1.505(7)	N(1A)-Mn(1)-N(1)	142.3(2)
C(2)-N(1)	1.291(7)	N(2)-Mn(1)-Cl(1)	126.97(4)
Mn(1)-N(1)	2.264(4)	N(1)-Mn(1)-Cl(1)	100.23(11)
Mn(1)-N(2)	2.224(6)	N(1A)-Mn(1)-Cl(1)	102.16(12)
Mn(1)-N(1A)	2.264(4)	Cl(1)-Mn(1)-Cl(1A)	106.06(8)
Mn(1)-Cl(1)	2.3740(15)		

After isolating the manganese dichloride complex **15**, its reduction was performed using excess Na-Hg and a catalytic amount of 1,3,5,7-cyclooctatetraene (COT), which helped to expedite the reduction (Scheme 3.2). A greenish-brown doubly deprotonated Mn(II) compound, identified as (^{PyEt}PDEA)Mn (**16**), was isolated after stirring for 12 h at ambient temperature followed by work up to remove the byproduct, NaCl. Compound **16** features broadened ¹H NMR resonances over a 100 ppm range (Fig. 3.4). The magnetic susceptibility of **16** (by Evans method) was found to be 3.8 μ_B at ambient temperature, which is consistent with two unpaired electrons.



Scheme 3.2: Synthesis of (^{PyEt}PDEA)Mn (**16**).

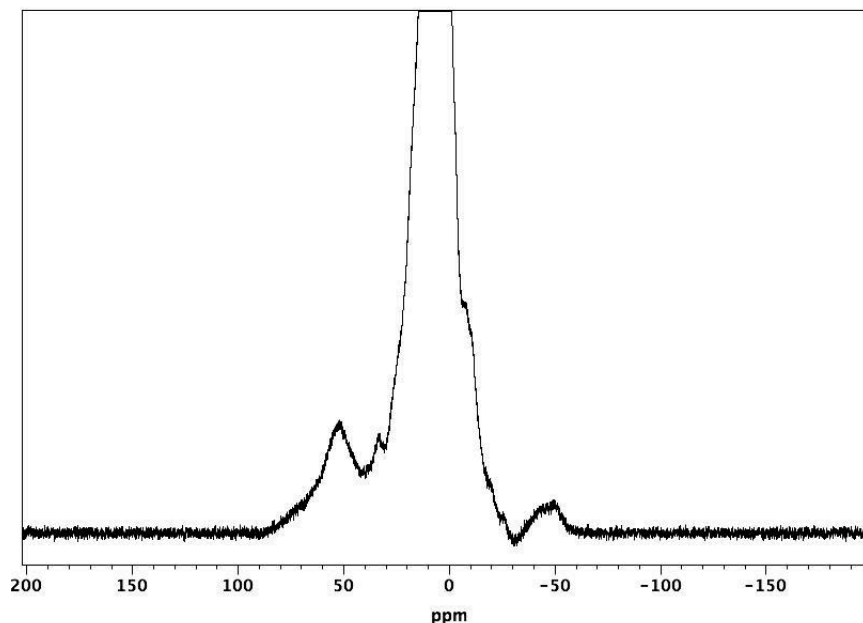


Figure 3.4: ^1H NMR spectrum of **16** in benzene- d_6 at 25 °C.

To further investigate the electronic structure and spin state of Mn, an X-band EPR spectrum was collected in toluene glass at 106 K. The spectrum showed multiline signals typical of Mn(II) around 330 mT ($g_{\text{eff}} = 2.0$) and 150 mT ($g_{\text{eff}} = 4.3$) (Fig. 3.5, which features a broad $S = 5/2$ impurity). These spectral features are consistent with an intermediate-spin ^{55}Mn center ($S = 3/2$; $I = 5/2$) and correspond to resonances within both Kramer's doublets of a $3/2$ spin system with large and rhombic zero-field splitting (i.e., $D \gg g\beta_e B_0/h$, and $E/D = 0.333$).²⁷ The UV-visible spectrum of **16** revealed d-d transitions at 512 nm ($\epsilon = 524 \text{ M}^{-1}\text{cm}^{-1}$) and 624 nm ($\epsilon = 504 \text{ M}^{-1}\text{cm}^{-1}$) (Fig. 3.6), which also corroborates the spin-state of the Mn center of **16** as intermediate.

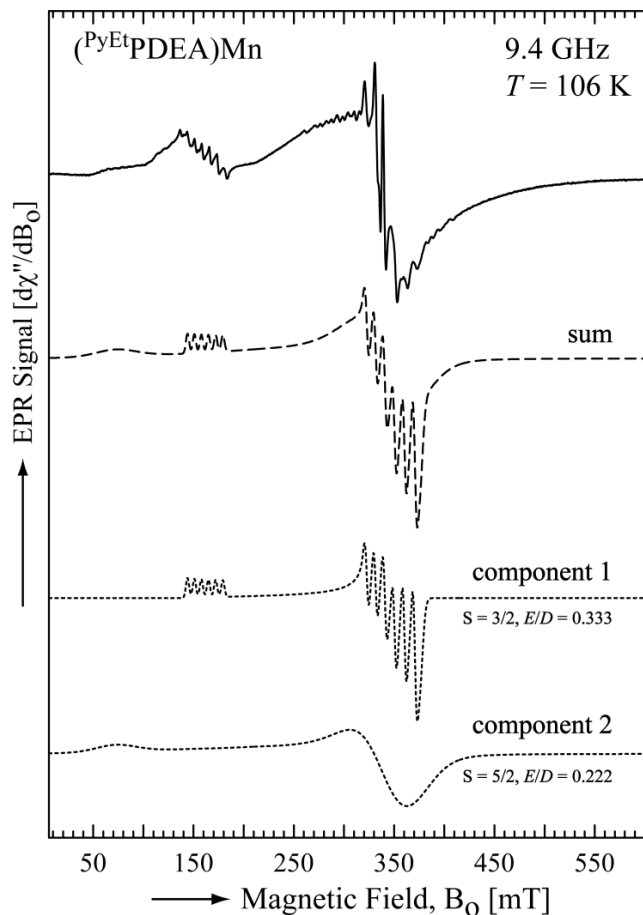


Figure 3.5: EPR spectrum of **16** in toluene glass at 106 K.

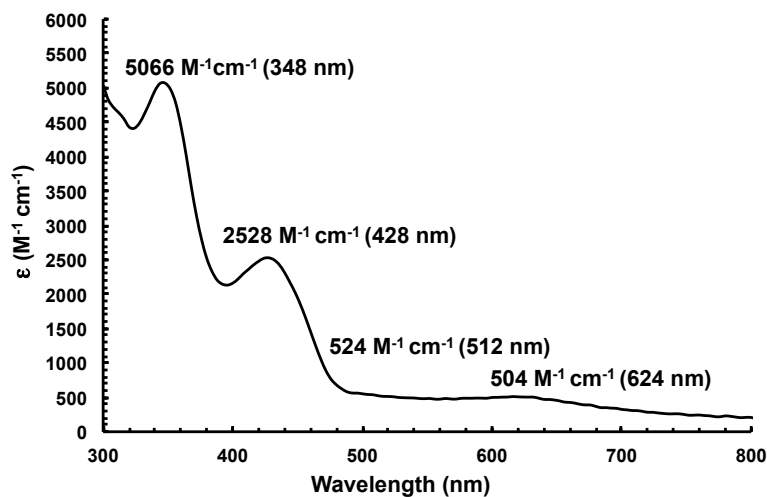


Figure 3.6: UV-visible spectrum of **16** in toluene. Molar absorptivity values determined from absorbance vs. concentration plot for five independent concentrations.

To gather further structural information, single crystals of **16** were grown from a concentrated solution of toluene layered with diethyl ether at $-35\text{ }^{\circ}\text{C}$ (Fig. 3.7). Chelate deprotonation was determined based on the C(1)-C(2) distance of $1.363(3)\text{ \AA}$, which is consistent with a C-C double bond (Table 3.2). Furthermore, the C-N distances of $1.369(3)\text{ \AA}$ of the ligand are indicative of a C-N single bond rather than an imine C-N double bond, which converts the neutral PDI ligand to dianionic ligand, PDEA^{2-} . The Mn(1)-N(1) and Mn(1)-N(2) contacts observed for **16** of $2.1123(18)\text{ \AA}$ and $2.158(3)\text{ \AA}$, respectively (Table 3.2), are shorter than **15** and hence, also supports PDEA^{2-} coordination and a different spin state of Mn in **16**. Similar to **15**, complex **16** also possess C_2 -symmetry along the Mn(1)-N(2) axis and the geometry around Mn can be best described as distorted trigonal bipyramidal (Fig. 3.7).

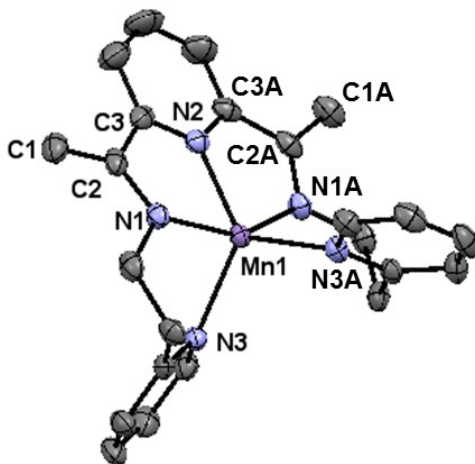


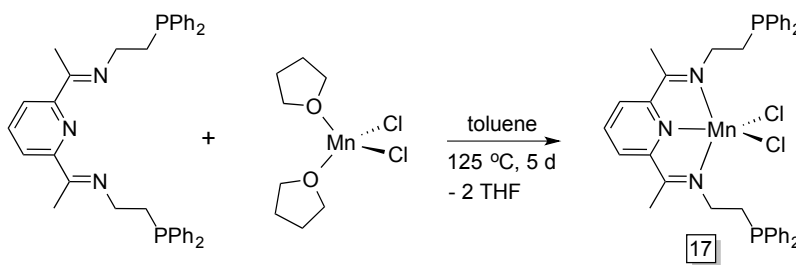
Figure 3.7: The solid-state structure of **16** shown with 30% probability ellipsoids. Labeled atoms ending with A have been generated by symmetry. Hydrogen atoms and a cocrystallized toluene molecule have been omitted for the sake of clarity.

Table 3.2: Notable bond lengths (Å) and bond angles (°) determined for **16**.

Bond	Å	Angle	Degree
C(1)-C(2)	1.363(3)	N(1)-Mn(1)-N(2)	74.33(5)
C(2)-C(3)	1.491(3)	N(2)-Mn(1)-N(1A)	74.34(5)
C(2)-N(1)	1.369(3)	N(1)-Mn(1)-N(1A)	148.67(10)
Mn(1)-N(1)	2.1123(18)	N(2)-Mn(1)-N(3)	126.59(5)
Mn(1)-N(2)	2.158(3)	N(3)-Mn(1)-N(3A)	106.81(9)
Mn(1)-N(3)	2.2178(17)		

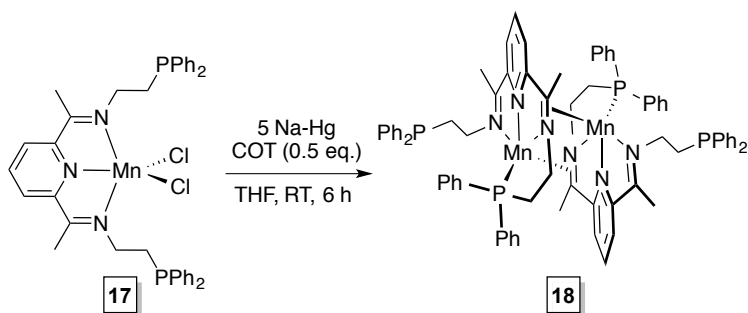
3.4. Synthesis and Characterization of **17** and **18**:

Similar to the synthesis of **15**, (^{Ph₂PEt}PDI)MnCl₂ (**17**) has also been isolated by heating a 1:1 mixture of ^{Ph₂PEt}PDI²⁸ and (THF)₂MnCl₂ at 125 °C in toluene for 5 days (Scheme 3.3). Compound **3** was found to be NMR silent. Magnetic susceptibility measurement by Guoy balance showed a value of 6.0 μ_B at room temperature, consistent with five unpaired electrons, which supports a high spin Mn(II) center (*S* = 5/2). Based on these observations, and prior structural characterization of (^{Ph₂PPr}PDI)MnCl₂²³ and (^{PyEt}PDI)MnCl₂, it can be proposed that **17** possesses a κ³-*N,N,N*-^{Ph₂PEt}PDI chelate.

**Scheme 3.3:** Synthesis of (^{Ph₂PEt}PDI)MnCl₂ (**17**).

Reduction of **17** was carried out with excess Na-Hg in the presence of 1,3,5,7-cyclooctatetraene (COT), to accelerate the reduction²³ (Scheme 3.4). A red paramagnetic dimeric complex, identified as [(^{Ph₂PEt}PDI)Mn]₂ (**18**) was obtained after stirring for 6 h at ambient temperature followed by work up to remove the byproduct, NaCl. Analysis of

the ^1H NMR spectrum revealed broadened resonances at 32.26 and 26.23 ppm (Fig. 3.8). A single broad resonance at -58.49 ppm was also observed in the ^{31}P NMR spectrum, which is presumably due to an uncoordinated phosphine arm of the dimeric compound (Fig. 3.9). To examine the number of unpaired electrons, solution state magnetic susceptibility was performed using Evans method and a magnetic moment value of 3.3 μ_{B} at room temperature was observed, indicating two unpaired electrons in the ground state.



Scheme 3.4: Synthesis of $[(^{\text{Ph}_2\text{PEt}}\text{PDI})\text{Mn}]_2$ (**18**).

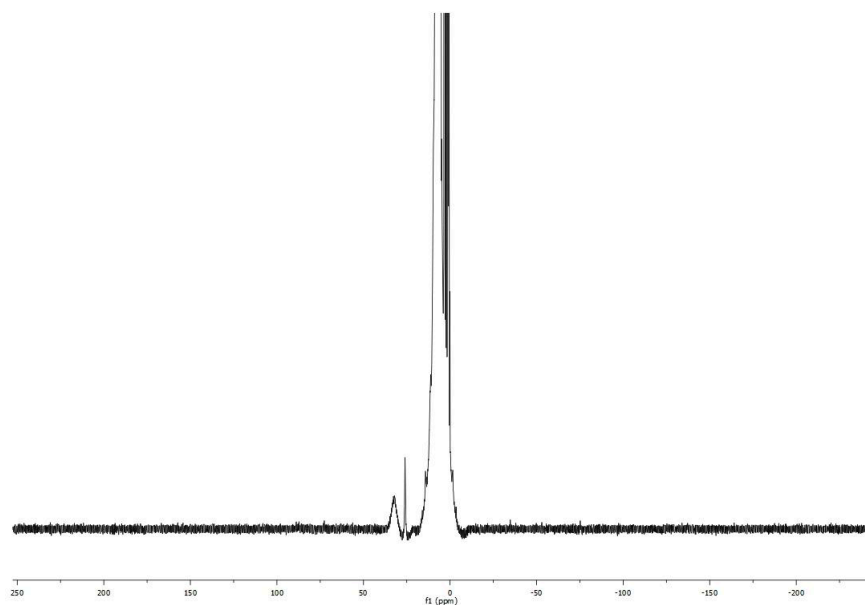


Figure 3.8: ^1H NMR spectrum of **18** in benzene- d_6 at 25 $^\circ\text{C}$.

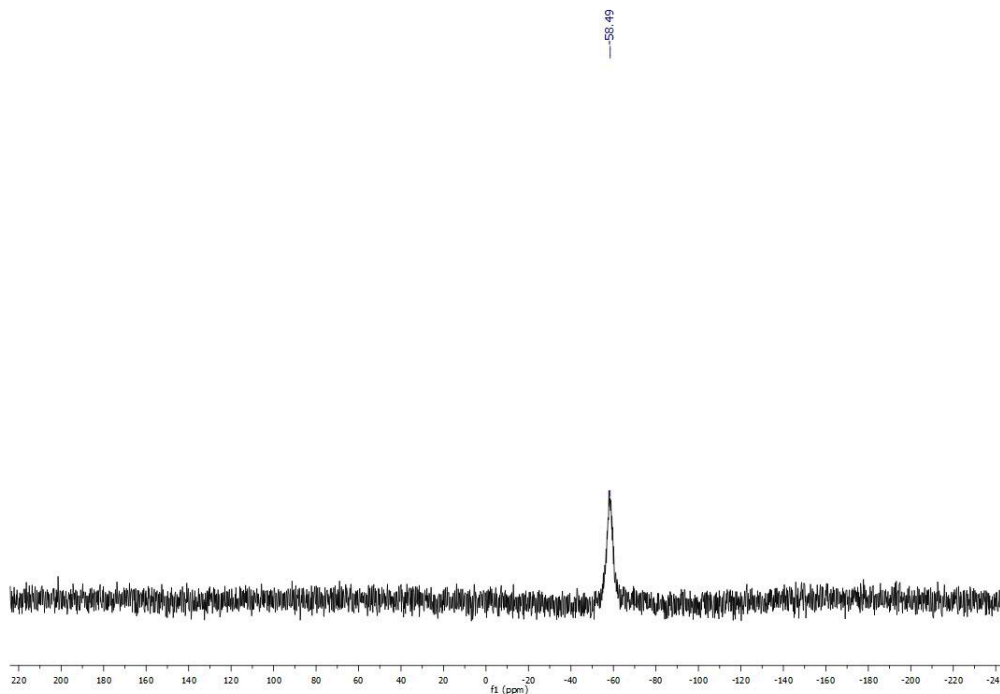


Figure 3.9: ^{31}P NMR spectrum of **18** in benzene- d_6 at 25 °C.

To further investigate the electronic state of **18**, an X-band (9.40 GHz) EPR spectroscopic measurement was performed in toluene at 107 K. The observed spectral features are consistent with the presence of two manganese centers, i.e., a broad signal showing a multiline pattern due to hyperfine coupling (hfc) interactions between the magnetic moment of an unpaired electron system (Fig. 3.10) and the magnetic moment of a neighboring ^{55}Mn ($I = 5/2$) nuclei. On the basis of the electronic structure model proposed above, each Mn center was assumed to carry one net unpaired electron that results in an electronic configuration with two unpaired electrons present in **18**. Thus, the best fit of the EPR spectrum, corresponding to **18**, was obtained considering a triplet state ($S = 1$) as the ground state of the electron spin system. The parameters that were obtained from the fit are summarized in Table 3.3. The g values are anisotropic and reflect a large

electron spin delocalization, which is consistent with the crystallographically determined molecular structure of **18** (discussed later). The zero-field splitting (ZFS) parameters are relatively small and show a nearly axial ZFS (i.e., $D \ll g\beta_e B_0/h$, and $E/D \approx 0$). This finding indicates weak electron-electron repulsion between the two unpaired electrons present in **18**.

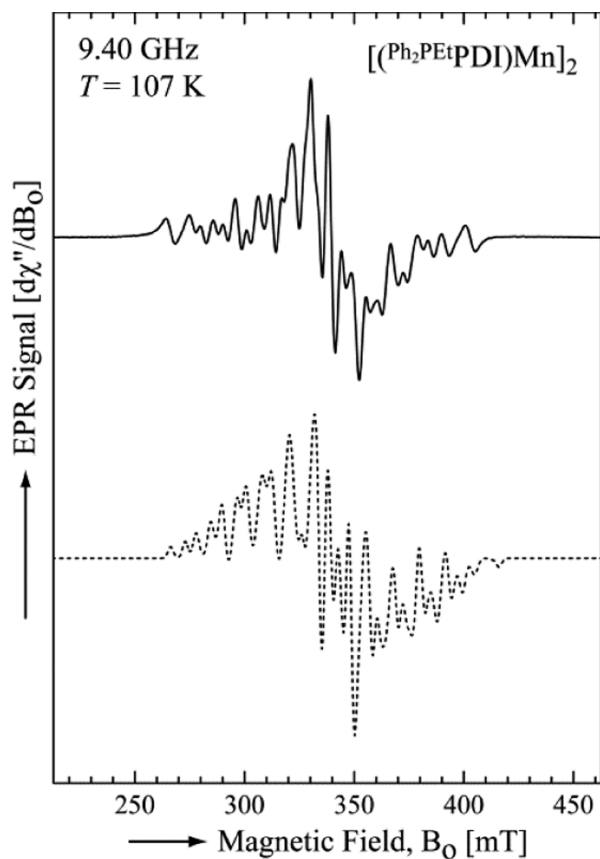


Figure 3.10: Experimental (solid line) and simulated (dashed line) X-band EPR spectra of **18** in toluene at 107 K. These spectra showed small discrepancies for the magnetic field resonances above 390 mT. Such discrepancies, as well the differences in line intensities, might be due to inhomogeneities present in the frozen solution (powder) sample.

Table 3.3: Parameters used to fit the EPR spectrum of **18** at 9.40 GHz and T = 107 K.

Parameters	18
g_x	2.037
g_y	1.980
g_z	1.893
$ D $	$77.7 \times 10^{-4} \text{ cm}^{-1}$
$ E $	$2.0 \times 10^{-4} \text{ cm}^{-1}$
$ A_x^{\text{Mn}_i} $	$114.1 \times 10^{-4} \text{ cm}^{-1}$
$ A_y^{\text{Mn}_i} $	$43.7 \times 10^{-4} \text{ cm}^{-1}$
$ A_z^{\text{Mn}_i} $	$94.7 \times 10^{-4} \text{ cm}^{-1}$

To probe the geometry and coordination, single crystals of **18** were collected from a concentrated solution of diethyl ether at -35 °C. Single crystal X-ray diffraction analysis displayed a dimeric compound, where each Mn center is surrounded by a κ^4 -*N,N,N,P*-PDI chelate (Fig. 3.10). Each Mn center is also coordinated to the imine bond of the neighboring Mn-PDI moiety in η^2 fashion [Mn(1)-C(8A) and Mn(1)-N(3A) are 2.233(6) and 1.977(4) Å, respectively]. This interaction results in significant backbonding into the imine bond, which is reflected in the elongation of the C(8)-N(3) imine bond to 1.395(6) Å, compared to the average uncoordinated C=N bond length of 1.271(17) Å.²⁹ The geometry around each Mn center can be best described as distorted trigonal bipyramidal based on the angles of N(1)-Mn(1)-N(3), N(2)-Mn(1)-P(1), N(2)-Mn(1)-N(3A), and N(2)-Mn(1)-N(1) as 150.85(16)°, 129.25(12)°, 100.30(15)° and 77.00(16)°, respectively (Table 3.4). The unbridged portion of each PDI chelate exhibits elongation of the C(2)-N(1) bond and contraction of the C(2)-C(3) distance, suggesting single electron reduction of an α -diimine (DI) ligand.³⁰ The Mn(1)-N(1), Mn(1)-N(2) and Mn(1)-N(3) distances were found to be 2.022(4), 1.947(4), and 2.092(4) Å, respectively, and the two Mn centers are 2.7889(14) Å apart (Table 3.4). Accumulating all these observations and the

obtained magnetic moment, it can be proposed that **18** consists of two intermediate Mn(I) centers, which are antiferromagnetically coupled to their respective singly reduced supporting DI fragment.

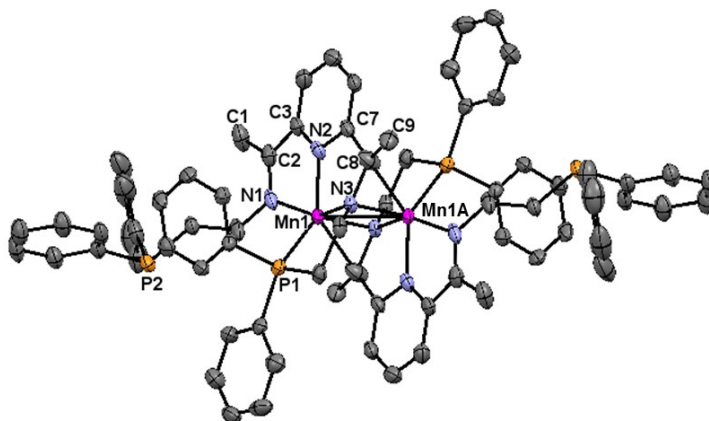


Figure 3.11: The molecular structure of **18** shown at 30% probability ellipsoids. Hydrogen atoms and co-crystallized toluene molecules (4 per dimer) are omitted for clarity.

Table 3.4: Notable bond lengths (Å) and bond angles (°) determined for **18**.

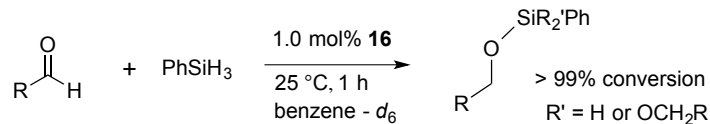
Bond	Å	Angle	Degree
C(2)-C(3)	1.425(7)	N(1)-Mn(1)-N(3)	150.85(16)
C(2)-N(1)	1.338(6)	N(2)-Mn(1)-P(1)	129.25(12)
C(8)-N(3)	1.395(6)	N(2)-Mn(1)-N(3A)	100.30(15)
Mn(1)-N(1)	2.022(4)	N(2)-Mn(1)-N(1)	77.00(16)
Mn(1)-N(2)	1.947(4)		
Mn(1)-N(3)	2.092(4)		
Mn(1)-N(3A)	1.977(4)		
Mn(1)-C(8A)	2.233(6)		
Mn(1)-Mn(1A)	2.7889(14)		

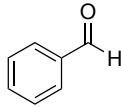
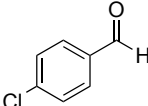
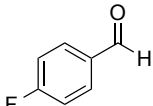
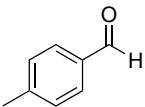
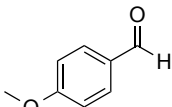
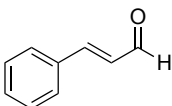
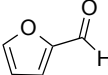
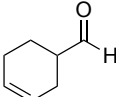
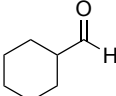
3.5. Catalytic Hydrosilylation Activity of **16**:

Inspired by our previous report,²³ compound **16** was screened for catalytic carbonyl hydrosilylation although it lacks redox non-innocence. As PhSiH₃ has been found to be suitable reductant for carbonyl hydrosilylation in our previous work,²³ an

equimolar mixture of an aldehyde and PhSiH_3 were added to a 1 mol% benzene- d_6 solution of compound **16** at 25 °C. Nine aldehydes have been chosen for this transformation and regardless of functional groups, aromatic and aliphatic aldehydes exhibited >99% conversion to a mixture of silyl ethers over a period of 1 h (Table 3.5). All the products and conversions were determined based on integration of the ^1H NMR spectrum and turnover frequencies (TOF) were measured to be 1.7 min^{-1} with 1 mol% catalyst loading. Hydrosilylation of benzaldehyde yielded an approximate 13:1 ratio of $\text{PhSi}(\text{OCH}_2(\text{Ph}))_3$ to $\text{PhSiH}(\text{OCH}_2(\text{Ph}))_2$ and a significant amount of unreacted PhSiH_3 was observed based on the ^1H NMR spectrum collected after catalysis. These observations indicate that in-situ generated $\text{PhSiH}(\text{OCH}_2(\text{Ph}))_2$ is more reactive towards **16**-mediated carbonyl hydrosilylation than PhSiH_3 . When this experiment was repeated with 0.33 equivalents of PhSiH_3 , complete conversion of benzaldehyde to $\text{PhSi}(\text{OCH}_2(\text{Ph}))_3$ was observed in 1 h and 88% yield was obtained based on integration of the ^1H NMR spectrum using anisole as an internal standard. A similar conversion and product ratio trend was followed for other substituted benzaldehydes as well, which indicates that the peripheral electron donating or electron withdrawing groups do not hinder conversion or interfere with selectivity. Chemoselective hydrosilylation of carbonyl over alkene functionalities was noticed when *trans*-cinnamaldehyde (entry 6) and 3-cyclohexene-1-carboxaldehyde (entry 8) were used as substrates. This observation is also corroborated with the fact that hydrosilylation of 1-hexene and cyclooctene remained unsuccessful using **16**. A higher proportion of tertiary silanes were produced in the case of aliphatic substrates such as 3-cyclohexene-1-carboxaldehyde (entry 8) and cyclohexanecarboxaldehyde (entry 9).

Table 3.5: Hydrosilylation of aldehydes using **16** as a pre-catalyst.

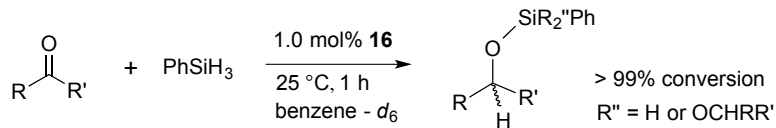


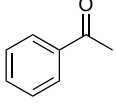
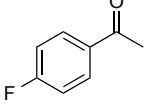
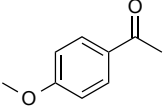
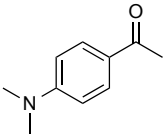
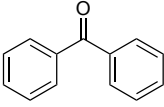
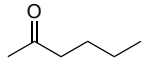
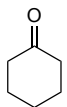
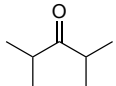
Entry	Substrate	Product ^a
1.		PhSi(OCH ₂ (Ph)) ₃ (93%) ^b PhSiH(OCH ₂ (Ph)) ₂ (7%)
2.		PhSi(OCH ₂ (<i>p</i> -Cl-Ph)) ₃ (92%) PhSiH(OCH ₂ (<i>p</i> -Cl-Ph)) ₂ (8%)
3.		PhSi(OCH ₂ (<i>p</i> -F-Ph)) ₃ (93%) PhSiH(OCH ₂ (<i>p</i> -F-Ph)) ₂ (7%)
4.		PhSi(OCH ₂ (<i>p</i> -Me-Ph)) ₃ (92%) PhSiH(OCH ₂ (<i>p</i> -Me-Ph)) ₂ (8%)
5.		PhSi(OCH ₂ (<i>p</i> -OMe-Ph)) ₃ (93%) PhSiH(OCH ₂ (<i>p</i> -OMe-Ph)) ₂ (7%)
6.		PhSi(OCH ₂ CH=CH(Ph)) ₃ (73%) PhSiH(OCH ₂ CH=CH(Ph)) ₂ (27%)
7.		PhSi(OCH ₂ (C ₄ H ₃ O)) ₃ (93%) PhSiH(OCH ₂ (C ₄ H ₃ O)) ₂ (7%)
8.		PhSi(OCH ₂ (C ₆ H ₉)) ₃ (52%) ^c PhSiH(OCH ₂ (C ₆ H ₉)) ₂ (48%)
9.		PhSi(OCH ₂ (Cy)) ₃ (67%) PhSiH(OCH ₂ (Cy)) ₂ (33%)

^aProduct ratios and percent conversion determined by ¹H NMR spectroscopy. ^bOverall silyl ether yield of 96% determined by ¹H NMR integration vs. anisole internal standard. ^cOverall silyl ether yield of 91% determined by ¹H NMR integration vs. anisole internal standard.

After investigating aldehyde hydrosilylation, ketone reduction was targeted using catalyst **16** under similar conditions. Eight different ketone substrates were screened for hydrosilylation using PhSiH_3 as the reductant and all of them were successfully transformed to their respective silyl ethers over a period of 1 h at room temperature (Table 3.6). The hydrosilylation of acetophenone using 1 mol% **16** resulted in the formation of $\text{PhSiH}(\text{OCH}(\text{Me})(\text{Ph}))_2$ and $\text{PhSi}(\text{OCH}(\text{Me})(\text{Ph}))_3$ in an approximate 3:1 ratio (entry 1). The electron-donating groups of *p*-acetanisole (entry 3) and *p*-dimethylaminoacetophenone (entry 4) appear to assist in the formation of the tertiary silane products. Catalyst **16** was found to be more efficient for the hydrosilylation of *p*-fluoroacetophenone (entry 2) and *p*-dimethylaminoacetophenone (entry 4), compared to our previously reported Mn catalyst,²³ which required 4 and 6 h to complete conversion of these substrates, respectively. When aliphatic ketones were hydrosilylated, tertiary silanes were found to be the major product along with small quantities of mono-silylated products. To study the effect of steric hindrance of the substrate on hydrosilylation, 2,4,6-trimethylacetophenone was added to PhSiH_3 and **16**; however, only 2% conversion was observed after 1 h and after 5 days, 67% conversion was noticed, which is slightly lower than our previous work (80%).²³

Table 3.6: Hydrosilylation of ketones using **16** as a pre-catalyst.

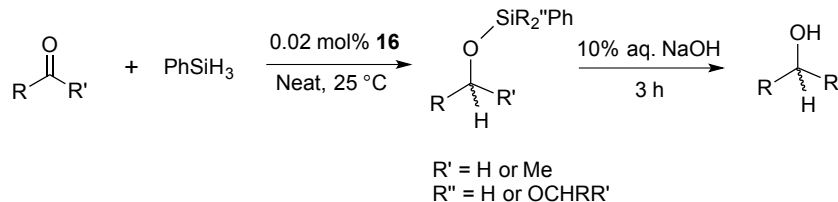


Entry	Substrate	Product ^a
1.		PhSiH(OCH(Me)(Ph)) ₂ (73%) PhSi(OCH(Me)(Ph)) ₃ (27%)
2.		PhSiH(OCH(Me)(<i>p</i> -F-Ph)) ₂ (50%) PhSi(OCH(Me)(<i>p</i> -F-Ph)) ₃ (50%)
3.		PhSiH(OCH(Me)(<i>p</i> -OMe-Ph)) ₂ (78%) PhSi(OCH ₂ (<i>p</i> -OMe-Ph)) ₃ (22%)
4.		PhSiH(OCH(Me)(<i>p</i> -NMe ₂ -Ph)) ₂
5.		PhSiH(OCH(Ph) ₂) ₂ (55%) PhSi(OCH(Ph) ₃) ₃ (45%)
6.		PhSiH(OCH(Me)(ⁿ Bu)) ₂ (96%) PhSiH ₂ (OCH(Me)(ⁿ Bu)) (4%)
7.		PhSiH(OCy) ₂ (97%) PhSiH ₂ (OCy) (3%)
8.		PhSiH(OCH(ⁱ Pr) ₂) ₂ (70%) PhSiH ₂ (OCH(ⁱ Pr) ₂) (30%)

^aProduct ratios and percent conversion determined by ¹H NMR spectroscopy.

To investigate the synthetic utility of **16**, hydrosilylation experiments were targeted that feature reduced catalyst loadings and no solvent (Table 3.7). When the hydrosilylation of 2-hexanone was conducted using 0.02 mol% of **16** in the absence of solvent, heat was generated and complete conversion to silyl ethers was observed after 5

minutes, as judged by ^1H NMR integration. The turnover number (TON) and turnover frequency for this experiment were determined to be 4950 and 990 min^{-1} , respectively (entry 1). The resulting silyl ethers were hydrolyzed by treatment with NaOH, followed by extraction with ether and silica gel filtration to isolate 2-hexanol in 72% yield. Repeating the analogous procedure for cyclohexanone hydrosilylation and hydrolysis resulted in the isolation of cyclohexanol in 99% yield (entry 2). Additionally, tertiary silyl ethers, $\text{PhSiH}(\text{OCH}(\text{Me})(^n\text{Bu}))_2$ and $\text{PhSiH}(\text{OCy})_2$, were isolated from these transformations in 63% and 55% yield, respectively. Considering aldehydes are easier to reduce than ketones,²⁴ this treatment was then also employed on aldehyde substrates (Entry 3 and 4). As expected, complete reduction of benzaldehyde and *p*-fluorobenzaldehyde turned out to be faster than ketones (2 minutes only), equating to a hydrosilylation TOF of $2,475\text{ min}^{-1}$ (TON = 4950) for aldehyde. To determine the highest TON for **16**-mediated aldehyde hydrosilylation, the previous steps were repeated by adding 5,000 equivalents of benzaldehyde and PhSiH_3 every 10 min over 1 h (5 additions, total of 30,000 total eq. of benzaldehyde). Based on ^1H NMR analysis 47% conversion of benzaldehyde was observed, which was equating to a TON of 14,170. The TOFs observed for **16**-mediated hydrosilylation are twice those reported for our previous ketone hydrosilylation catalyst ($1240\text{-}1280\text{ min}^{-1}$)²³ and two orders of magnitude greater than the TOFs reported for $(\text{Ph}_3\text{P})(\text{CO})_4\text{MnC}(\text{O})\text{CH}_3$ (27 min^{-1}).¹⁶

Table 3.7: Neat carbonyl hydrosilylation using 0.02 mol% **16** as a pre-catalyst.

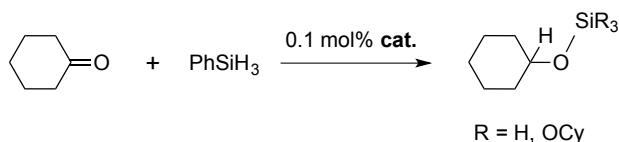
Entry	Substrate	Product	Time (min) ^a	Yield (%) ^b	TOF (min ⁻¹) ^c
1.			5	72	990
2.			5	99	990
3.			2	99	2,475
4.			2	71	2,475

^aTime of hydrosilylation reaction prior to catalyst quench. ^bIsolated yields based on substrate added. All hydrosilylation reactions had reached >99% conversion as judged by ¹H NMR spectroscopy. ^cTOF values are based on substrate conversion.

A series of control experiments were performed in order to prove that carbonyl hydrosilylation is mediated by catalyst **16** or a homogeneous derivative (Table 3.8). To investigate the homogeneity of **16**, the neat hydrosilylation of cyclohexanone was conducted using PhSiH₃ and 0.1 mol% **16** in the presence of 50,000 equivalents of Hg⁰ (entry 1). Conversion was not hindered, and complete conversion was observed in 5 minutes, indicating the homogeneity of catalyst **16**. The same reaction was repeated using the Mn⁰ powder (entry 2) and no conversion was observed suggesting that presence of heterogeneous species is unlikely to be responsible for catalysis. The Mn-containing precursors (THF)₂MnCl₂ and **15** remained unsuccessful under these conditions (entry 3 and 4). To probe the possibility of **16** acting as a radical initiator, 2,2'-azobis-(2-methylpropionitrile) (AIBN) was screened as a pre-catalyst and it remained unreactive

after 5 min at room temperature and even after heating to 90 °C for 7 min. These observations signify that carbonyl hydrosilylation doesn't proceed through a radical chain mechanism, but at the Mn center.

Table 3.8: Control experiments using cyclohexanone as the substrate.



Entry	Catalyst	Time (min)	Temp (°C)	Conversion ^a
1.	2 + 50,000 eq. Hg ⁰	5	25	> 99
2.	Mn ⁰	5	25	0
3.	(THF) ₂ MnCl ₂	5	25	0
4.	16	5	25	0
5.	AIBN	5	25	0
6.	AIBN	7	90	0

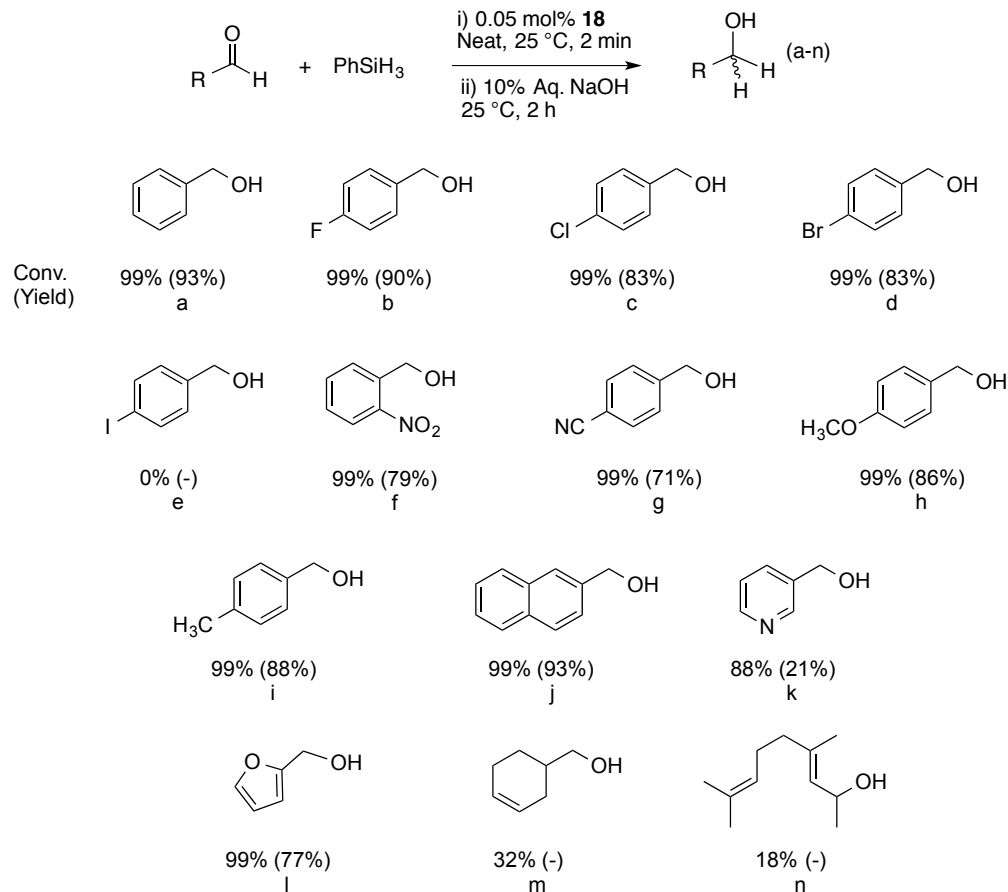
^aDetermined by ¹H NMR spectroscopy.

3.6. Catalytic Hydrosilylation Activity of **18**:

In a similar fashion, compound **18** was also screened for the catalytic hydrosilylation of carbonyls. To obtain better turnover numbers (TONs) and turnover frequencies (TOFs) for carbonyl hydrosilylation compared to our previous catalyst, (^{Ph}₂PP^rPDI)Mn,²³ efforts were made to lower the catalyst loading in absence of solvent (i.e. neat conditions). When a neat mixture of benzaldehyde and PhSiH₃ were added to 0.05 mol% of **18** (0.1 mol% relative to Mn) at room temperature, an exothermic reaction occurred, which led to complete conversion of benzaldehyde to a mixture of silyl ethers after 2 min. Treatment of these silyl ethers with 10% aq. NaOH followed by extraction with diethyl ether produced the hydrolyzed product, benzyl alcohol in 93% yield (Table

3.9, entry a). Thirteen additional aldehydes were assayed under similar reaction conditions (Table 3.9). Pre-catalyst **18** was found to tolerate various functional groups including fluoro, chloro, bromo (entry b-d), but not the iodo-functionality of 4-iodobenzaldehyde. Unlike the other substrates, this substrate did not undergo exothermic reaction with PhSiH₃ and **18** due to catalyst decomposition (entry e). This catalyst also exhibits tolerance of nitro- and cyano-functionalities as the reduction of these groups was not observed during hydrosilylation of the substrates, 2-nitrobenzaldehyde and 4-cyanobenzaldehyde, respectively (entry f, g). Catalytic efficiency was not affected by the electron donating groups, such as methoxy and methyl groups of *p*-anisaldehyde and *p*-tolualdehyde (entry h, i). Heteroatomic aldehydes were also successfully hydrosilylated although 88% conversion of pyridine-3-carboxaldehyde was noticed within 2 min reaction conditions (entry k, l). Moreover, the hydrosilylation of 3-cyclohexene-1-carboxaldehyde and citral revealed only 32% (entry m) and 18% (entry n) conversion within the 2 min frame of the experiments. Under similar conditions, our previous catalyst, (^{Ph₂PPr}PDI)Mn was found to reach complete conversion,³¹ indicating that catalysis by **18** was inhibited due to olefin coordination. It should be noted that olefin hydrosilylation was not observed for these substrates although olefin coordination was assumed to be deleterious to the aldehyde hydrosilylation pathway. Additionally, pre-catalyst **18** failed to reduce 1-hexene using PhSiH₃ as a reductant, even at 120 °C.

Table 3.9: Neat hydrosilylation of aldehydes using 0.05 mol% of **18** as a pre-catalyst.



Two ketone substrates were also targeted to compare the catalytic efficiency of **18** with our previously reported Mn-catalyst. The neat hydrosilylation of acetophenone and cyclohexanone using 0.05 mol% of **18** (0.1 mol% relative to Mn) led to complete conversion to their corresponding silyl ethers within the 4 min frame of the experiment. TOFs of 495 and 248 min⁻¹ (relative to Mn) were obtained based on the isolated yields of the corresponding alcohols of acetophenone and cyclohexanone, respectively. It was noticed that **18** mediated hydrosilylation took several seconds longer to initiate an exothermic reaction compared to (^{Ph}₂PP_rPDI)Mn.

An attempt was also made to lower the catalyst loading to 0.005 mol% (0.01 mol% Mn) for aldehyde hydrosilylation. This effort proved to be successful, leading to

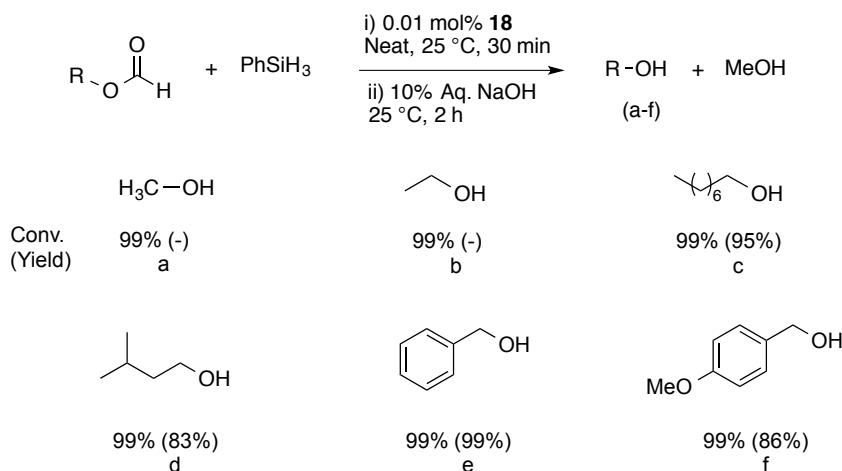
the complete conversion of benzaldehyde after 2 min under neat conditions, and a TOF of 9,900 min⁻¹ (4,950 min⁻¹ per Mn) was achieved. The highest TON obtained per Mn matched with the one achieved by (Ph₂PPr)Mn,³¹ for benzaldehyde hydrosilylation. However, this result was not attained for the other aldehydes mentioned in Table 3.9. For example, repeating this procedure with 4-fluorobenzaldehyde resulted in only 18% conversion after 2 min, equating to a TOF of 1,800 min⁻¹ (900 min⁻¹ per Mn).

Similar to **16**-mediated hydrosilylation, control experiments using AIBN (radical initiator), Mn powder, (THF)₂MnCl₂ and (Ph₂PEt)PDI)MnCl₂ as catalyst did not show any conversion. Moreover, the conversion of **18**-mediated benzaldehyde hydrosilylation in the presence of excess Hg⁰ was not hindered, suggesting homogeneity of **18** during the process of catalysis. To prove that phosphine arm dissociation does not require light, the experiment was carried out in dark, and no influence on the percentage conversion was detected. This result is in opposition with the work showing that CpMn carbonyl catalysts require³² photolytic loss of two CO ligands prior to the carbonyl substrate coordination. Adding 2 equiv. of NaEt₃BH to **17** did not allow for the observation or isolation of a catalytically relevant hydride complex.

Compound **18**-catalyzed formate hydrosilylation activity was also evaluated. Six different formates were screened (Table 3.10). When a neat equimolar mixture of methyl formate or ethyl formate and PhSiH₃ was added to 0.01 mol% **18** (0.02 mol% relative to Mn), an exothermic reaction ensued along with complete conversion to a mixture of silyl ethers within 30 min (entry a, b). Hydrolysis of the silyl ethers was carried out with aq. NaOH, however, isolation of the corresponding products, MeOH and EtOH failed through evaporation due to their low boiling points. Furthermore, the reaction scale was

not large enough to separate these products by short path distillation. To address this problem, the dihydrosilylation of higher molecular weight formate substrates was investigated. Compound **18** was found to successfully catalyze octyl (Entry c), isoamyl (entry d), benzyl (entry e) and *p*-anisyl formate (entry f) dihydrosilylation, leading to greater than 99% conversion of formates to silyl ethers. Alkaline hydrolysis followed by extraction with ether and evaporation to remove the solvent and byproduct MeOH, afforded the corresponding alcohols in good yield (Table 3.10). The TOFs of 330 min⁻¹ (165 min⁻¹ relative to Mn) obtained for **18**-mediated formate dihydrosilylation was lower than those observed for (^{Ph₂PPr}PDI)Mn on a per Mn basis³¹, but still higher compared to other transition metal complexes. After investigating formates, efforts were made to reduce one acetate substrate and it turned out that the complete reduction of ethyl acetate to PhSi(OEt)₃ required 7.2 h at 25 °C (TOF = 14 h⁻¹) using 1.0 mol % **18** and equimolar PhSiH₃ in benzene-*d*₆. This is again slower than the 5.5 h needed to complete ethyl acetate dihydrosilylation using (^{Ph₂PPr}PDI)Mn.²³

Table 3.10: Neat hydrosilylation of formates using 0.01 mol% of **18** as a pre-catalyst.



Incorporating insights from the mechanistic investigation of (^{Ph₂PPr}PDI)Mn catalyzed hydrosilylation and the observations made in the control experiments for **18**-

mediated catalysis, it can be proposed that hydrosilylation occurs through a modified Ojima mechanism (Fig. 3.12). The first step of the cycle must be the dissociation of the dimer into monomeric units, which will then oxidatively add the Si-H bond of PhSiH₃ to afford a manganese silyl hydride intermediate (**A**, Fig. 3.11). After silane bond activation, the carbonyl substrate will coordinate to Mn (**B**) and C=O bond insertion into the Mn-H bond will generate the manganese silyl alkoxide intermediate (**C**). At the end of the catalytic cycle, intermediate **C** will undergo reductive elimination to produce the silyl ether and the pre-catalyst. In the case of carboxylate hydrosilylation, the silyl alkoxide is believed to undergo fast β-alkoxide elimination to yield the silyl ether product and an equivalent of formaldehyde, as described for (^{Ph₂PPr}PDI)Mn.³¹ Then, formaldehyde will reenter the catalytic cycle and quickly be reduced by PhSiH₃ to yield methoxysilane equivalents. Considering the delayed catalytic onset and slower ethyl acetate dihydrosilylation, dimer **18** can be proposed as the catalytic resting state. Our inability to observe a Mn hydride complex upon adding 2 equiv. of NaEt₃BH to **17** also suggests that catalysis is unlikely to proceed through a straightforward insertion mechanism analogous to the one described for (^{Ph₂PPr}PDI)MnH.³¹

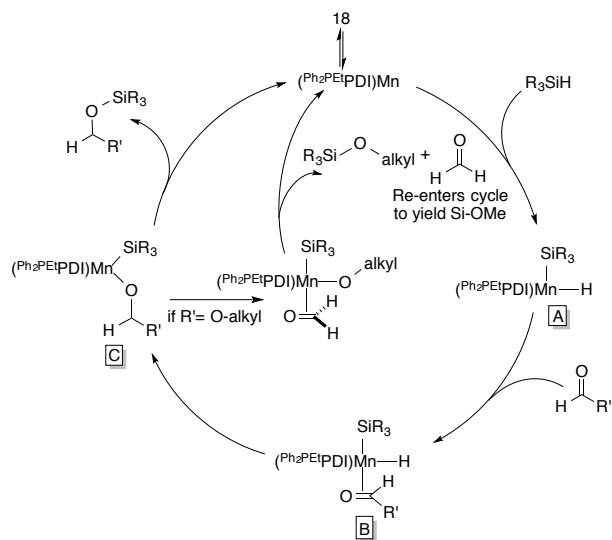


Figure 3.12: Plausible mechanism for **18**-catalyzed carbonyl hydrosilylation.

Although our previous Mn catalyst, (Ph_2PPrPDI)Mn proved to be the best catalyst for carbonyl hydrosilylation, **16** and **18** showed better activities compared to all other first row transition metal catalysts. In order to strengthen this statement, a comparative study is provided in Table 3.11. Relative to late transition metals, only a handful of examples of early transition metal catalysts for carbonyl hydrosilylation have been reported. Among the reported ones, the most effective Sc, Ti, and Cr catalysts show maximal TOFs of less than 1 min^{-1} (entries 1, 2 & 4).^{33,34,35} Late transition metals have been well investigated for this transformation. In 2014, Sydora, Turculet and Stradiotto reported the best Fe catalyst, which exhibited TOFs of up to 393 min^{-1} for acetophenone hydrosilylation (entry 6).^{6b} The most efficient Co,^{7f} Ni,^{8c,36} and Zn^{10m} catalysts for this transformation (entries 7, 8, and 10, respectively) showed maximal TOFs which are lower than those determined for **16** and **18**. The TOF comparison to leading Cu catalysts is more difficult. The maximum TOF obtained is 660 min^{-1} (entry 9),^{9k} however, this is calculated based on ligand instead of Cu in order to minimize the use of expensive reagent, (S)-Xyl-P-Phos. In 2013, using a similar methodology, Lipshutz and co-workers reported an asymmetric

acetophenone hydrosilylation TOF of 77 min⁻¹ at -50 °C, suggesting greater TOFs might have been achieved at or near ambient temperature. A number of well-defined Cu hydride catalysts have also been reported, but they were used for low temperature asymmetric ketone hydrosilylation and were not investigated for highest TOF.

Table 3.11: Comparison of carbonyl hydrosilylation activity of first row transition metal catalysts.

Entry	Metal	Catalyst	Silane	Substrate	Temp (°C)	TOF (min ⁻¹)
1.	Sc	(κ ⁴ N ₃ O)Sc(O ₂ CCH ₂ SiMe ₂ Ph) ·(BC ₆ F ₅) ₃	Et ₃ SiH	carbon dioxide	65	0.2
2.	Ti	(Cp) ₂ TiCl ₂ + 2 ⁿ BuLi	(EtO) ₃ SiH	methyl benzoate	25	0.7
3.	V	-	-	-	-	-
4.	Cr	(η ⁶ -C ₆ H ₆) ₂ Cr	Ph ₂ SiH ₂	<i>p</i> -anisaldehyde	70	0.1
5.	Mn	16 18	PhSiH ₃	benzaldehyde	25	2,475 4,950
6.	Fe	(κ ² -PN)Fe(N(SiMe ₃) ₂)	PhSiH ₃	acetophenone	25	393
7.	Co	(DPB)Co(N ₂)	Ph ₂ SiH ₂	propanal	25	49.5
8.	Ni	(Cp [*] -NHC ^{Me})Ni(O ^t Bu)	PhSiH ₃	<i>p</i> -CF ₃ - benzaldehyde	25	38.4
9.	Cu	CuF ₂ + (S)-Xyl-P-Phos	PhSiH ₃	<i>p</i> -NO ₂ - acetophenone	25	660
10.	Zn	(κ ³ -Tptm)ZnH	PhSiH ₃	acetaldehyde	25	20

3.7. Conclusion:

The synthesis and characterization of manganese pre-catalyst, (Py^{Et}PDEA)Mn have been described. Although, it lacks ligand redox-noninnocence due to deprotonation of the PDI backbone methyl groups, this compound exhibits TOFs of up to 2,475 min⁻¹ and TONs of up to 14,170 for carbonyl hydrosilylation under mild conditions, which is still higher than most reported first row metal transition catalysts. In a similar fashion, the

synthesis, electronic structure and hydrosilylation activity of the other manganese pre-catalyst, $[(^{\text{Ph}_2\text{PEt}}\text{PDI})\text{Mn}]_2$ have been investigated. Unlike, the other PDI containing manganese complexes, the ethyl bridged complex revealed κ^4 -PDI coordination and to complete the coordination sphere around Mn, it was found to bind to the neighboring imine bond in η^2 -fashion. Although dimer formation was found not to be detrimental for carbonyl hydrosilylation, it resulted in slower transformation of the aldehydes containing pyridine or olefin functionalities and delayed onset compare to the previously reported Mn catalyst, $(^{\text{Ph}_2\text{PPr}}\text{PDI})\text{Mn}$. Our dimeric Mn pre-catalyst revealed TOFs of up to 4,950 min^{-1} and 165 min^{-1} per Mn basis for benzaldehyde and formates, respectively. Both the pre-catalysts have been found to tolerate a range of functional groups. Based on the propyl-bridged Mn catalyst mechanistic study, control experiments for **18**-mediated catalysis, and our inability to isolate a $(^{\text{Ph}_2\text{PEt}}\text{PDI})\text{Mn}$ hydride complex, it is believed that the catalytic transformation initiates through the dissociation of dimer into monomeric units which then follows a modified Ojima mechanism.

3.8. Experimental Section:

3.8.1. General Considerations: All reactions were performed inside an MBraun glove box under an atmosphere of purified nitrogen. Toluene, tetrahydrofuran, pentane, and diethyl ether were purchased from Sigma-Aldrich, purified using a Pure Process Technology solvent system, and stored in the glove box over activated 4 Å molecular sieves and sodium before use. Benzene- d_6 and chloroform- d were purchased from Cambridge Isotope Laboratories and dried over 4 Å molecular sieves. 1,3,5,7-Cyclooctatetraene was purchased from Strem, while Mn^0 powder and Hg^0 were used as

received from Sigma-Aldrich. 2,6-Diacetylpyridine, 2-(2-aminoethyl)pyridine, acetophenone, *p*-methoxyacetophenone, *p*-dimethylaminoacetophenone, *p*-chlorobenzaldehyde, 3-cyclohexene-1-carbaldehyde, and *trans*-cinnamaldehyde were obtained from TCI America. Cyclohexanone, 2-hexanone, 2,4-dimethyl-3-pentanone, cyclohexanecarboxaldehyde, *p*-tolualdehyde, furfural, benzaldehyde, and *p*-anisaldehyde were purchased from Sigma-Aldrich. *p*-fluoroacetophenone and phenylsilane were obtained from Oakwood. Celite, sodium hydroxide, anhydrous sodium sulfate, (THF)₂MnCl₂, and *p*-fluorobenzaldehyde were purchased from Acros. Ketones, aldehydes, and phenylsilane were scrupulously dried over 4 Å molecular sieves, and solid substrates were recrystallized from ether before use. Cyclohexanone, 2-hexanone, *p*-fluorobenzaldehyde, and furfural were distilled prior to use. ^{PyEt}PDI was synthesized according to a literature procedure.²⁴ Solution ¹H NMR spectra were recorded at room temperature on a Varian 400-MR (400 MHz) NMR spectrometer. All ¹H NMR and ¹³C NMR chemical shifts are reported in parts per million relative to Si(CH₃)₄ using ¹H (residual) and ¹³C chemical shifts of the solvent as secondary standards. Elemental analyses were performed at Robertson Microlit Laboratories Inc. (Ledgewood, NJ). Solid state magnetic susceptibilities were determined at 23 °C using a Johnson Matthey magnetic susceptibility balance calibrated with HgCo(SCN)₄ and K₃Fe(CN)₆. Solution state magnetic susceptibility was determined via the Evans method on the Varian 400 MHz NMR spectrometer. UV-visible spectra were recorded on an Agilent model 8453 spectrophotometer.

3.8.2. X-ray Crystallography: Single crystals suitable for X-ray diffraction were coated with polyisobutylene oil in the glove box and transferred to a glass fiber with Apiezon N

grease, which was then mounted on the goniometer head of a Bruker APEX diffractometer equipped with Mo K α radiation. A hemisphere routine was used for data collection and determination of the lattice constants. The space group was identified, and the data were processed using the Bruker SAINT+ program and corrected for absorption using SADABS. The structures were determined using direct methods (SHELXS) completed by subsequent Fourier synthesis and refined by full-matrix, least-squares procedures on [F²].

3.8.3. Electron Paramagnetic Resonance Spectroscopy. Instrumentation: Studies were performed at the EPR Facility of Arizona State University. Continuous wave EPR spectra were recorded at 106 K using a Bruker ELEXSYS E580 continuous wave X-band spectrometer (Bruker, Rheinstetten, Germany) equipped with a liquid nitrogen temperature control system (ER 4131VT). The magnetic field modulation frequency was 100 kHz with a field modulation of 1 mT from peak to peak. The microwave power was 1 mW, the microwave frequency 9.40 GHz, and the sweep time 168 s.

Spin Hamiltonian: The EPR spectrum of **16** was interpreted using a spin Hamiltonian, H, containing the electron Zeeman interaction with the applied magnetic field B₀, the zero-field interaction, and the the hyperfine coupling (hfc) term.³⁷

$$H = \beta_e S \cdot g \cdot B_0 + h S \cdot D \cdot S + h S \cdot A \cdot I$$

where S is the electron spin operator, I is the nuclear spin operator of ⁵⁵Mn, D and A are the zero-field interaction and hfc tensors, respectively, both in frequency units, g is the electronic g tensor, β_e is the electron magneton, and h is Planck's constant. The so-called zero-field interaction occurs in the absence of an applied magnetic field because of electron-electron repulsion. For d⁵ systems [e.g., Fe(III) and Mn(II)], the zero-field

interaction partially breaks the degeneracy of the Kramer's doublets causing the energy of these levels to shift by the term Dm_S^2 , where D is the axial zero-field splitting (ZFS) parameter and m_S is the magnetic quantum number corresponding to the d^5 system. Additional shifting of the energy of the Kramer's doublet is induced by the rhombic zero-field splitting term, which is characterized by the parameter E . The electron Zeeman interaction contributes to the Hamiltonian when an external magnetic field is applied. This interaction is anisotropic and depends on the relative orientation between the magnetic field and the molecular axes of the Mn(II) ion. The Zeeman interaction breaks the remaining degeneracy of the Kramer's doublets causing an additional shift given by the term $g\beta_e B_0 m_S / h$ in the energy of these levels, where g is the g value. A further energetic consideration is the contribution of the hfc interaction, which represents the interaction between the magnetic moment of the unpaired electron system and the magnetic moment of the ^{55}Mn nucleus. The hyperfine interaction is described to first order by the expression $A m_S m_I$, where A is the hfc interaction along an arbitrary magnetic field direction and m_I is the magnetic quantum number of the nucleus.

3.8.4. Preparation of $(^{\text{PyEt}}\text{PDI})\text{MnCl}_2$ (15): A 100 mL thick-walled glass bomb was charged with 0.275 g (1.018 mmol) of $(\text{THF})_2\text{MnCl}_2$, 0.728 g (1.962 mmol) of $^{\text{PyEt}}\text{PDI}$, and approximately 20 mL of toluene under an inert atmosphere. The bomb was then sealed under N_2 , taken out of the glove box, and heated to 125 °C in an oil bath for 48 h while its contents were being stirred. Upon cooling, the reaction vessel was brought back into the glove box; the resulting light orange suspension was vacuum filtered, and the insoluble solid was washed with toluene (4 X 5 mL) and diethyl ether (3 X 5 mL) to remove the excess ligand. The remaining solid material was dried under vacuum to afford

0.473 g of **15** (93% yield) as a light orange solid. Single crystals suitable for X-ray diffraction were obtained following recrystallization from dichloromethane. Anal. Calcd for $C_{23}H_{25}N_5Cl_2Mn$: C, 55.55%; H, 5.07%; N, 14.08%. Found: C, 55.27%; H, 4.90%; N, 13.79%. Magnetic susceptibility (Guoy balance, 23 °C): $\mu_{\text{eff}} = 6.3 \mu_B$. ^1H NMR spectroscopy (benzene- d_6 , 23 °C): δ 62.76 (peak width at half-height of 9830 Hz), 13.51 (2020 Hz), -31.63 (3000 Hz). UV-vis (from five independent concentrations in CHCl_3): $\lambda_{\text{max}} = 306$ ($\epsilon = 3844 \text{ M}^{-1} \text{ cm}^{-1}$), 318 nm ($\epsilon = 2601 \text{ M}^{-1} \text{ cm}^{-1}$).

3.8.5. Preparation of ($\text{PyEt}^{\text{PDEA}}\text{Mn}$) (16**):** In the glove box, a 20 mL scintillation vial was charged with 8.12 g (40.62 mmol) of Hg^0 in approximately 6 mL of dry THF. To this, was added 0.047 g (2.030 mmol) of freshly cut Na^0 , and the resulting amalgam was stirred for 25 min. After this, 0.017 g (0.162 mmol) of 1,3,5,7-cyclooctatetraene was added and the mixture stirred for 5 min while it turned yellow in color. Then a 10 mL THF slurry of **15** (0.202 g, 0.406 mmol) was added. An instant color change to a greenish-brown solution was observed. The reaction mixture was stirred at ambient temperature for 12 h, after which time it was filtered through Celite under vacuum and the THF was evacuated. The resulting residue was washed with pentane (2 X 5 mL) and dried. The residue was dissolved in toluene (~15 mL) and filtered through a Celite column. This was repeated once again, and the filtrate was dried under vacuum to afford **16** (0.084 g, 49% yield). Single crystals suitable for X-ray diffraction were grown from a concentrated toluene solution layered with diethyl ether (1:1). Anal. Calcd for $C_{23}H_{23}N_5Mn \cdot C_7H_8$: C, 69.76%; H, 6.05%; N, 13.56%. Found: C, 68.39%; H, 5.78%; N, 13.10%. Complex **16** quickly decomposes in the presence of air or water. Magnetic susceptibility (Evans method, 23 °C): $\mu_{\text{eff}} = 3.8 \mu_B$. ^1H NMR spectroscopy (benzene- d_6 ,

23 °C): δ 52.85 (7,320 Hz), 33.10 (31,850 Hz), -8.08 (16,000 Hz, shoulder), -48.20 (3,600 Hz). UV-vis (from five independent concentrations in toluene): $\lambda_{\text{max}} = 348$ ($\epsilon = 5066 \text{ M}^{-1} \text{ cm}^{-1}$), 428 ($\epsilon = 2,528 \text{ M}^{-1} \text{ cm}^{-1}$), 512 ($\epsilon = 524 \text{ M}^{-1} \text{ cm}^{-1}$), 624 nm ($\epsilon = 504 \text{ M}^{-1} \text{ cm}^{-1}$).

3.8.6. Catalytic Trials Using Complex 16:

NMR scale hydrosilylation of benzaldehyde (1 mol% 16):

In the glove box, a benzene- d_6 solution of PhSiH₃ (66.9 μL , 0.542 mmol), benzaldehyde (55.2 μL , 0.542 mmol), and anisole (internal standard, 11.8 μL , 0.11 mmol) was added to a vial containing 2.3 mg (0.0054 mmol) of **16**. The resulting solution turned brown in color and was then transferred into a J. Young tube, where it remained at ambient temperature. The progress of the reaction was monitored by ¹H NMR spectroscopy. The resonances observed at 4.85 and 4.74 ppm after 1 h confirmed conversion of benzaldehyde to PhSi(OCH₂(Ph))₃ (93%) and PhSiH(OCH₂(Ph))₂ (7%) in 96% overall yield. Resonances observed at 7.38, 7.07, and 4.22 ppm indicated the presence of unreacted phenylsilane.

PhSi(OCH₂(Ph))₃: ¹H NMR (benzene- d_6): 7.85 (2H, d, $J_{\text{HH}} = 6.3 \text{ Hz}$, *phenyl*), 7.28 (6H, d, $J_{\text{HH}} = 7.1 \text{ Hz}$, *phenyl*), 7.13 (12H, m, *phenyl*), 4.85 (6H, s, *CH*₂). PhSiH(OCH₂(Ph))₂: ¹H NMR (benzene- d_6 , selected resonances): 5.33 (1H, s, *SiH*), 4.74 (4H, s, *CH*₂).

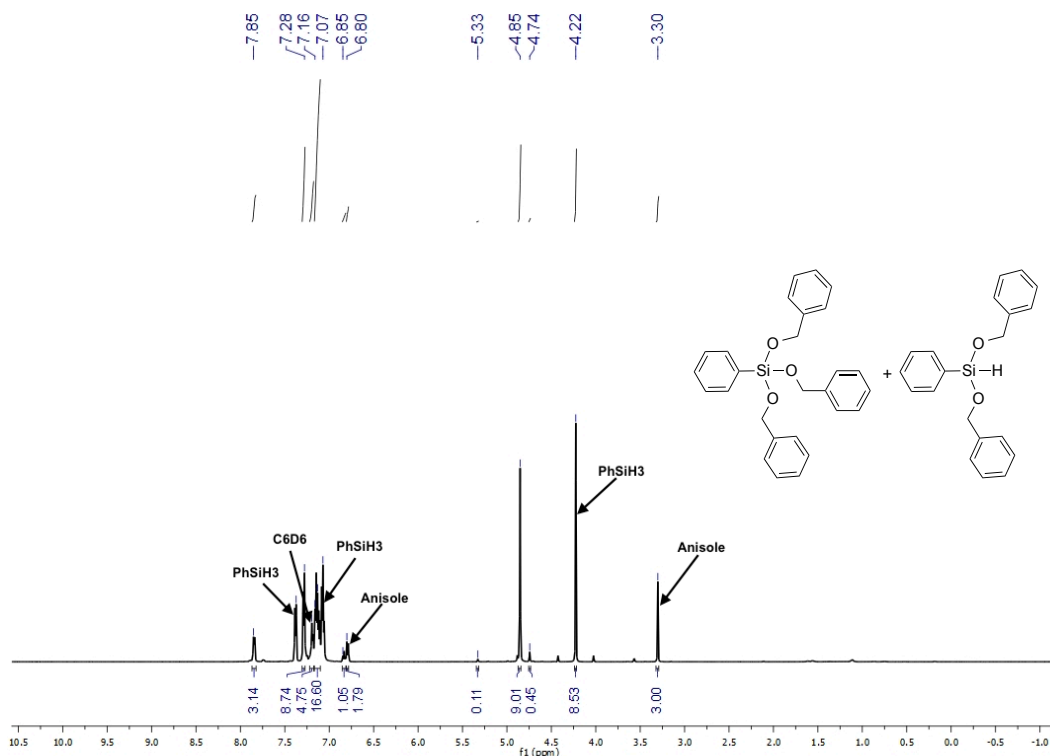


Figure 3.13: ^1H NMR spectrum of **16**-catalyzed (1 mol%) hydrosilylation of benzaldehyde with PhSiH_3 in benzene- d_6 solution.

Atom-efficient hydrosilylation of benzaldehyde (1 mol% **16**):

In the glove box, a benzene- d_6 solution of PhSiH_3 (22.3 μL , 0.181 mmol), benzaldehyde (55.2 μL , 0.542 mmol) and anisole (internal standard, 11.8 μL , 0.11 mmol) was added to a vial containing 2.3 mg (0.0054 mmol) of **16**. The resulting solution turned brown in color and was then transferred into a J. Young tube, where it remained at ambient temperature. The progress of the reaction was monitored by ^1H NMR spectroscopy. The resonances observed at 4.85 ppm after 1 h confirmed greater than 99% conversion of benzaldehyde to $\text{PhSi}(\text{OCH}_2(\text{Ph}))_3$ in 88% yield (as judged by integration against anisole). Resonances observed at 7.07 and 4.23 ppm indicate the presence of unreacted PhSiH_3 .

PhSi(OCH₂(Ph))₃: ¹H NMR (benzene-*d*₆): 7.86 (2H, d, *J*_{HH} = 6.3 Hz, *phenyl*), 7.28 (6H, d, *J*_{HH} = 7.1 Hz, *phenyl*), 7.13 (12H, m, *phenyl*), 4.85 (6H, s, CH₂).

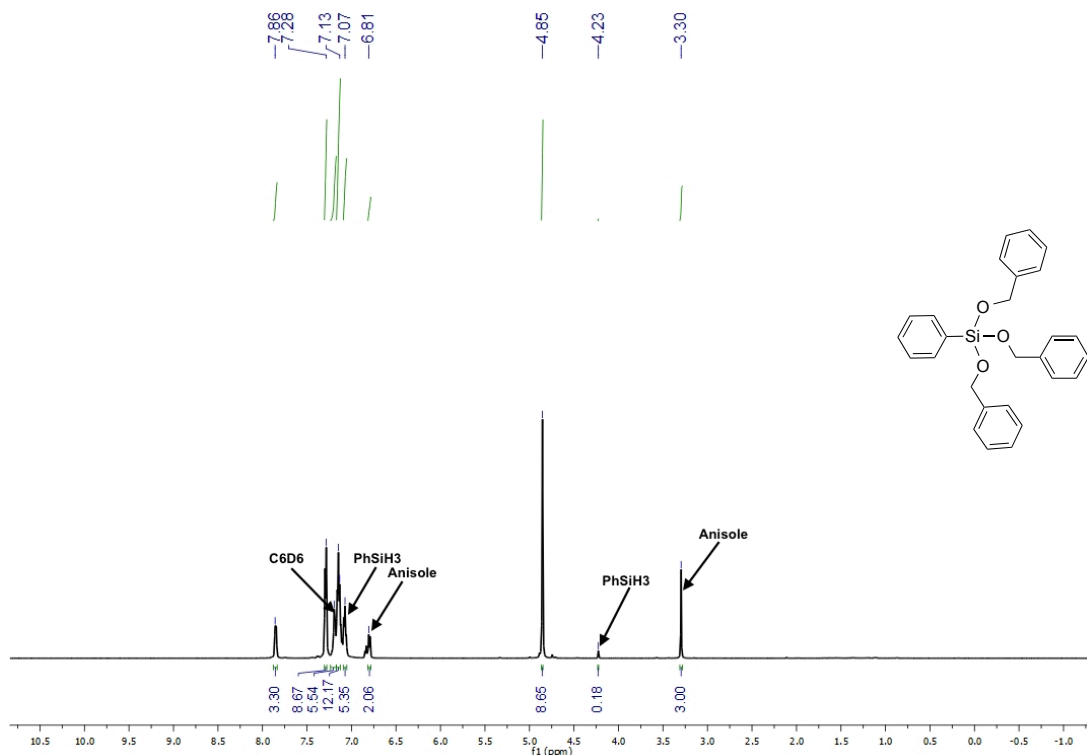


Figure 3.14: ¹H NMR spectrum of **16**-catalyzed (1 mol%) hydrosilylation of benzaldehyde using 1/3 PhSiH₃ in benzene-*d*₆ solution.

NMR scale hydrosilylation of *p*-chlorobenzaldehyde (1 mol% **16**):

In the glove box, a benzene-*d*₆ solution of PhSiH₃ (63.9 μL, 0.518 mmol) and *p*-chlorobenzaldehyde (72.9 mg, 0.518 mmol) was added to a vial containing 2.2 mg (0.00518 mmol) of **16**. The resulting solution turned brown in color and was then transferred into a J. Young tube, where it remained at ambient temperature. The progress of the reaction was monitored by ¹H NMR spectroscopy. The resonances observed at 4.63 and 4.54 ppm after 1 h confirmed greater than 99% conversion of *p*-chlorobenzaldehyde to PhSi(OCH₂(*p*-Cl-Ph))₃ (92%) and PhSiH(OCH₂(*p*-Cl-Ph))₂ (8%). Unreacted phenylsilane resonances were observed at 7.38, 7.07, and 4.23 ppm.

PhSi(OCH₂(*p*-Cl-Ph))₃: ¹H NMR (benzene-*d*₆): 7.75 (2H, m, *phenyl*), 7.23 (2H, m, *phenyl*), 7.11 (8H, m, *phenyl*), 6.96 (5H, m, *phenyl*), 4.63 (6H, s, CH₂). PhSiH(OCH₂(*p*-Cl-Ph))₂: ¹H NMR (benzene-*d*₆, selected resonances): 5.22 (1H, s, SiH), 4.54 (4H, s, CH₂).

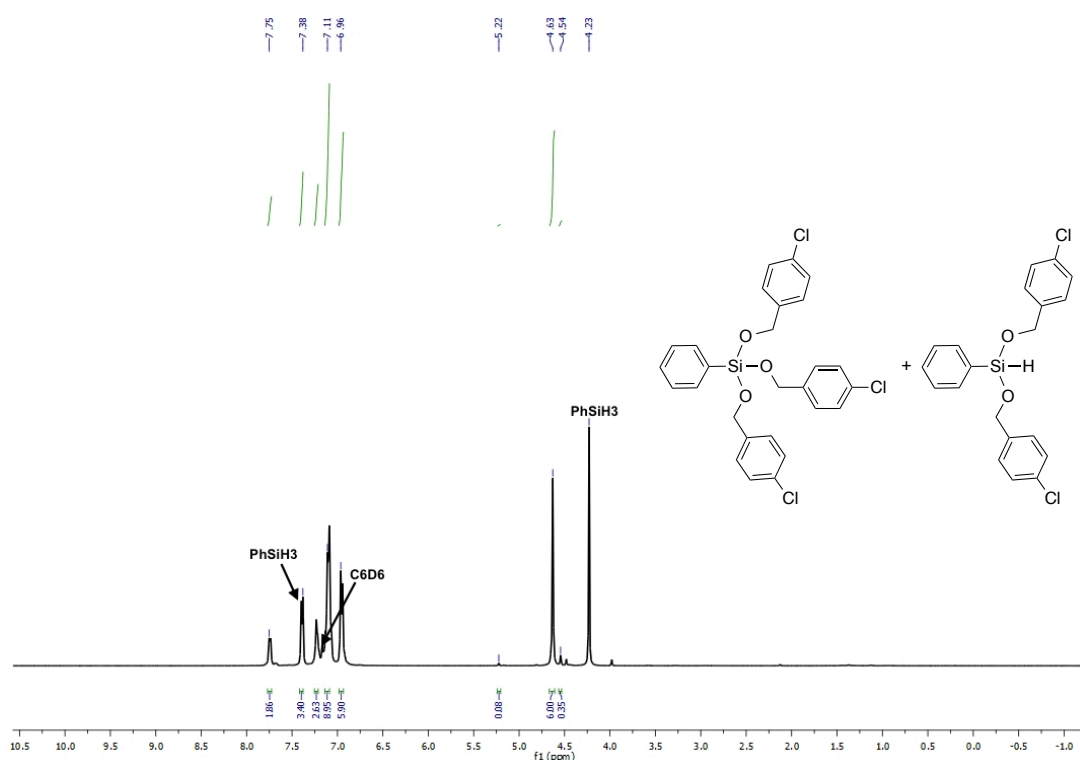


Figure 3.15: ¹H NMR spectrum of **16**-catalyzed (1 mol%) hydrosilylation of *p*-chlorobenzaldehyde with PhSiH₃ in benzene-*d*₆ solution.

NMR scale hydrosilylation of *p*-fluorobenzaldehyde (1 mol% **16**):

In the glove box, a benzene-*d*₆ solution of PhSiH₃ (69.8 μL, 0.566 mmol) and *p*-fluorobenzaldehyde (60.6 μL, 0.566 mmol) was added to a vial containing 2.4 mg (0.00566 mmol) of complex **16**. The resulting solution turned brown in color and was then transferred into a J. Young tube, where it remained at ambient temperature. The progress of the reaction was monitored by ¹H NMR spectroscopy. The resonances observed at 4.68 and 4.59 ppm after 1 h confirmed greater than 99% conversion of *p*-

fluorobenzaldehyde to $\text{PhSi}(\text{OCH}_2(p\text{-F-Ph}))_3$ (93%) and $\text{PhSiH}(\text{OCH}_2(p\text{-F-Ph}))_2$ (7%).

$\text{PhSi}(\text{OCH}_2(p\text{-F-Ph}))_3$: ^1H NMR (benzene- d_6): 7.78 (2H, m, *phenyl*), 7.23 (3H, m, *phenyl*), 7.03 (6H, m, *phenyl*), 6.80 (6H, m, *phenyl*), 4.68 (6H, s, CH_2). $\text{PhSiH}(\text{OCH}_2(p\text{-F-Ph}))_2$: ^1H NMR (benzene- d_6 , selected resonances): 5.25 (1H, s, SiH), 4.59 (4H, s, CH_2).

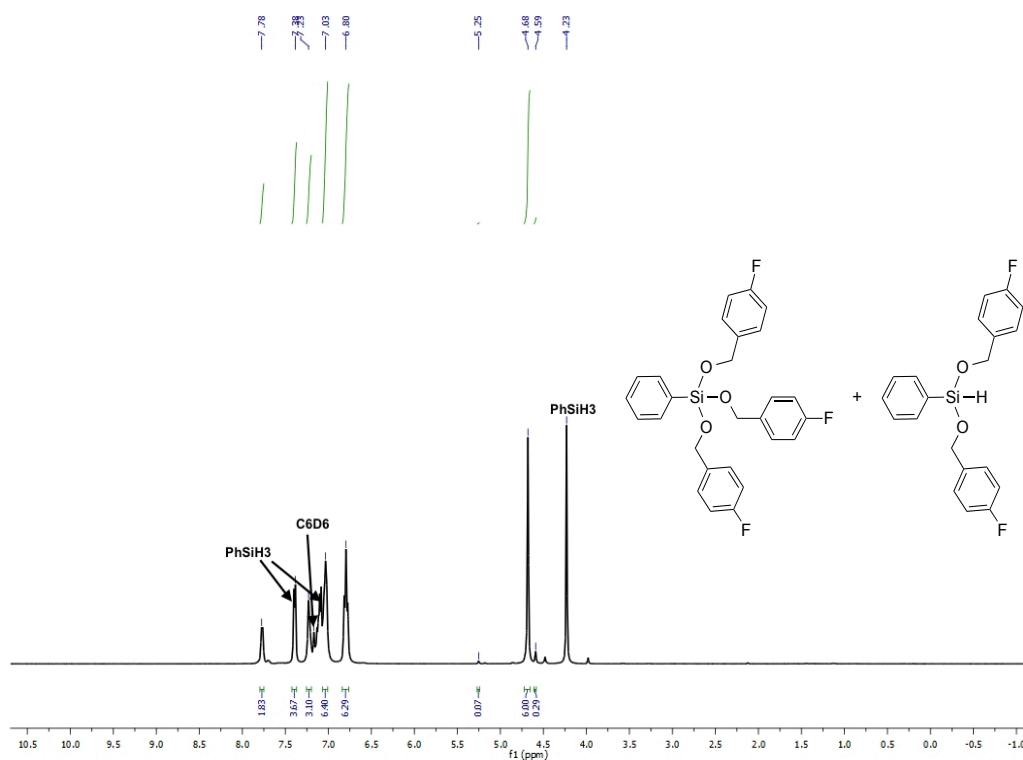


Figure 3.16: ^1H NMR spectrum of **16**-catalyzed (1 mol%) hydrosilylation of *p*-fluorobenzaldehyde with PhSiH_3 in benzene- d_6 solution.

NMR scale hydrosilylation of *p*-methylbenzaldehyde (1 mol% **16**):

In the glove box, a benzene- d_6 solution of PhSiH_3 (66.9 μL , 0.542 mmol) and *p*-methylbenzaldehyde (63.9 μL , 0.542 mmol) was added to a vial containing 2.3 mg (0.00542 mmol) of complex **16**. The resulting solution turned brown in color and was transferred into a J. Young tube, which was allowed to stand at ambient temperature. The progress of the reaction was monitored by ^1H NMR spectroscopy. The resonances observed at 4.90 and 4.78 ppm after 1 h confirmed greater than 99% conversion of *p*-

methylbenzaldehyde to $\text{PhSi}(\text{OCH}_2(p\text{-Me-Ph}))_3$ (92%) and $\text{PhSiH}(\text{OCH}_2(p\text{-Me-Ph}))_2$ (8%). Resonances observed at 7.37, 7.07 and 4.23 ppm indicated the presence of unreacted phenylsilane.

$\text{PhSi}(\text{OCH}_2(p\text{-Me-Ph}))_3$: ^1H NMR (benzene- d_6): 7.89 (2H, m, *phenyl*), 7.26 (10H, m, *phenyl*), 7.00 (5H, m, *phenyl*), 4.90 (6H, s, CH_2), 2.11 (9H, s, $p\text{-CH}_3\text{-Ph}$).

$\text{PhSiH}(\text{OCH}_2(p\text{-Me-Ph}))_2$: ^1H NMR (benzene- d_6 , selected resonances): 5.36 (1H, s, SiH), 4.78 (4H, s, CH_2).

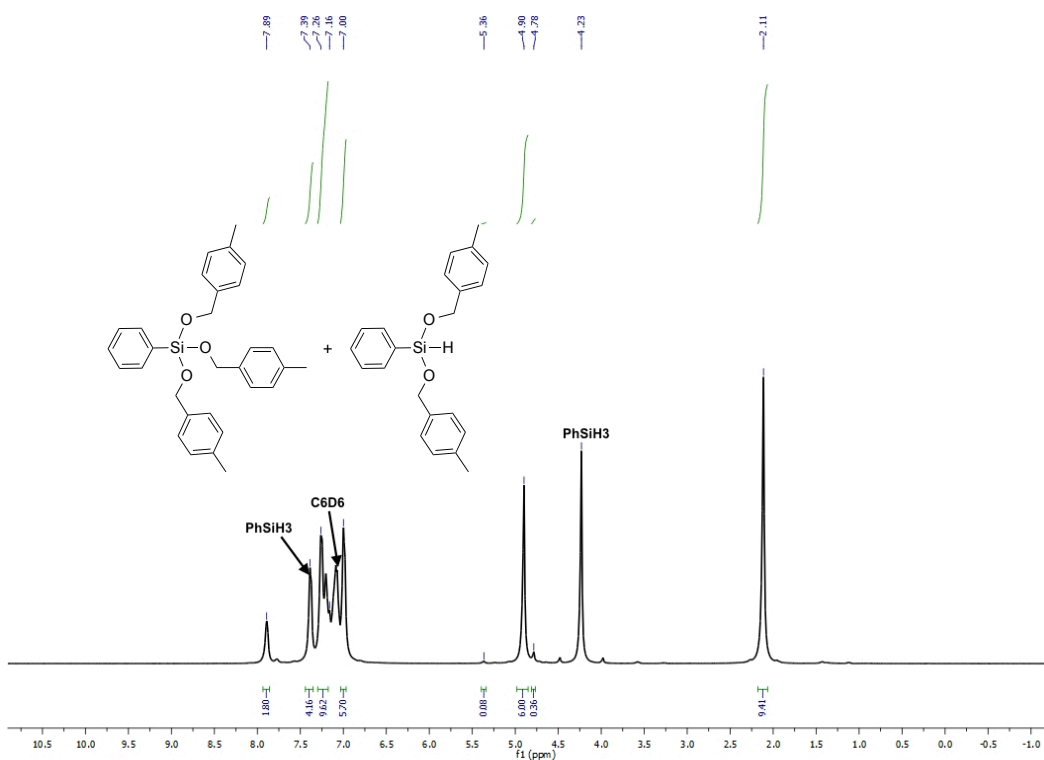


Figure 3.17: ^1H NMR spectrum of **16**-catalyzed (1 mol%) hydroxylation of *p*-methylbenzaldehyde with PhSiH_3 in benzene- d_6 solution.

NMR scale hydroxylation of *p*-methoxybenzaldehyde (1 mol% **16**):

In the glove box, a benzene- d_6 solution of PhSiH_3 (81.4 μL , 0.660 mmol) and *p*-methoxybenzaldehyde (80.3 μL , 0.660 mmol) was added to a vial containing 2.8 mg (0.00660 mmol) of complex **16**. The resulting solution turned brown in color and was

then transferred into a J. Young tube, where it was allowed to stand at ambient temperature. The progress of the reaction was monitored by ^1H NMR spectroscopy. The resonances observed at 4.89 and 4.78 ppm after 1 h confirmed greater than 99% conversion of *p*-methoxybenzaldehyde to $\text{PhSi}(\text{OCH}_2(p\text{-OMe-Ph}))_3$ (93%) and $\text{PhSiH}(\text{OCH}_2(p\text{-OMe-Ph}))_2$ (7%).

$\text{PhSi}(\text{OCH}_2(p\text{-OMe-Ph}))_3$: ^1H NMR (benzene- d_6): 7.90 (2H, m, *phenyl*), 7.25 (9H, m, *phenyl*), 6.80 (6H, m, *phenyl*), 4.89 (6H, s, CH_2), 3.33 (9H, s, $p\text{-OCH}_3\text{-Ph}$).

$\text{PhSiH}(\text{OCH}_2(p\text{-OMe-Ph}))_2$: ^1H NMR (benzene- d_6 , selected resonances): 5.37 (1H, s, SiH), 4.78 (4H, s, CH_2).

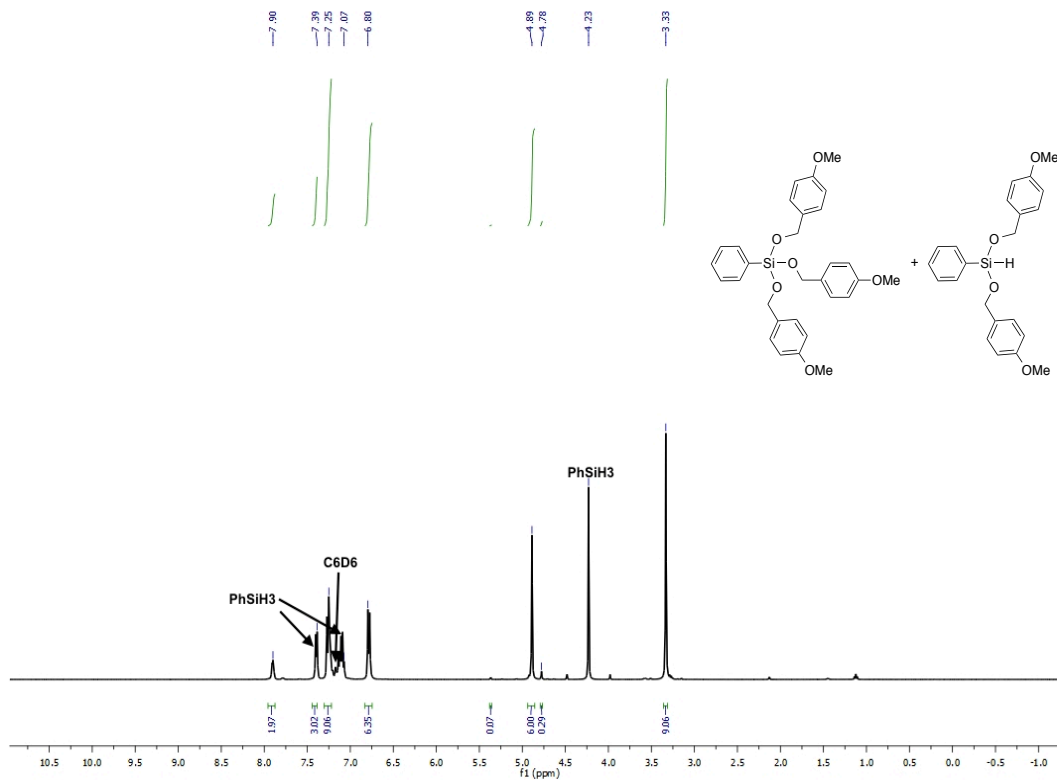


Figure 3.18: ^1H NMR spectrum of **16**-catalyzed (1 mol%) hydroxylation of *p*-methoxybenzaldehyde with PhSiH_3 in benzene- d_6 solution.

NMR scale hydrosilylation of *trans*-cinnamaldehyde (1 mol% **16):**

In the glove box, a benzene-*d*₆ solution of PhSiH₃ (69.8 μL, 0.566 mmol) and *trans*-cinnamaldehyde (71.2 μL, 0.566 mmol) was added to the vial containing 2.4 mg (0.00566 mmol) of complex **16**. The resulting solution turned brown in color and was then transferred into a J. Young tube, where it was allowed to stand at ambient temperature. The progress of the reaction was monitored by ¹H NMR spectroscopy. The resonances observed at 4.58 and 4.43 ppm after 1 h confirmed greater than 99% conversion of *trans*-cinnamaldehyde to PhSi(OCH₂CH=CH(Ph))₃ (73%) and PhSiH(OCH₂CH=CH(Ph))₂ (27%).

PhSi(OCH₂CH=CH(Ph))₃: ¹H NMR (benzene-*d*₆): 7.98 (2H, m, *phenyl*), 7.08 (18H, m, *phenyl*), 6.69 (3H, m, CH=CH), 6.26 (3H, m, CH=CH), 4.58 (6H, s, CH₂).

PhSiH(OCH₂CH=CH(Ph))₂: ¹H NMR (benzene-*d*₆, selected resonances): 7.83 (m, *phenyl*), 7.21 (m, *phenyl*), 5.37 (1H, s, SiH), 4.43 (4H, s, CH₂).

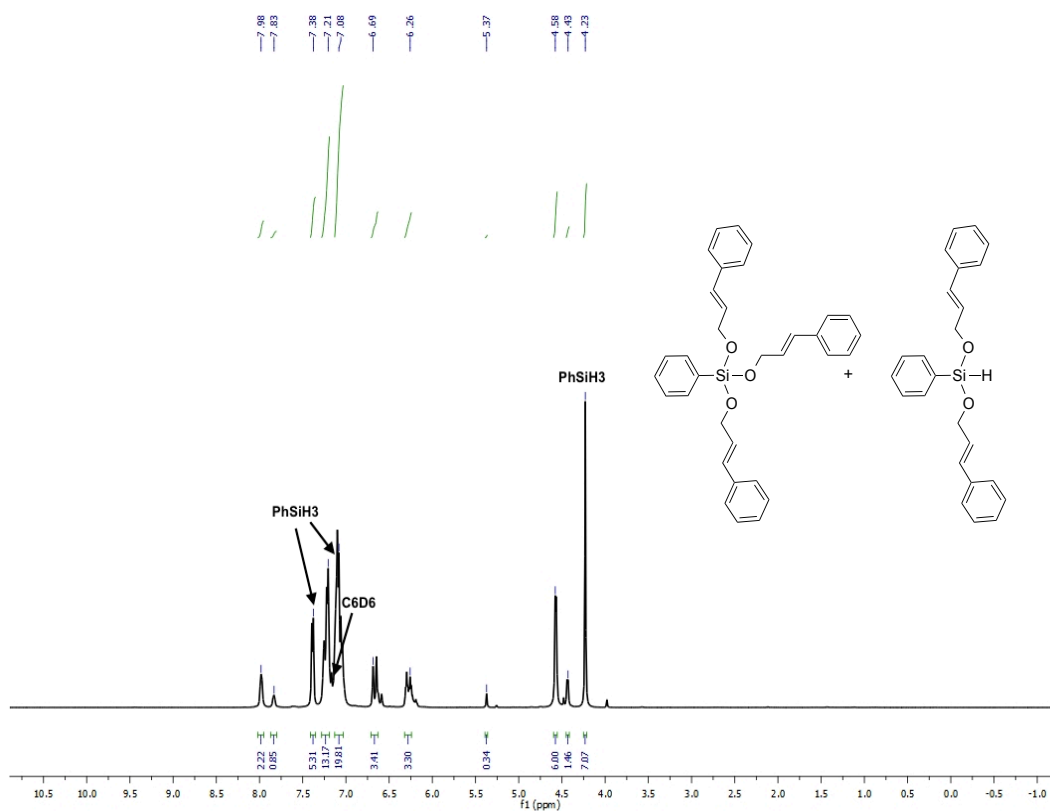


Figure 3.19: ¹H NMR spectrum of **16**-catalyzed (1 mol%) hydrosilylation of *trans*-cinnamaldehyde with PhSiH₃ in benzene-*d*₆ solution.

NMR scale hydrosilylation of furfural (1 mol% **16**):

In the glove box, a benzene-*d*₆ solution of PhSiH₃ (63.9 μL, 0.519 mmol) and furfural (42.9 μL, 0.519 mmol) was added to the vial containing 2.2 mg (0.00519 mmol) of complex **16**. The resulting solution turned brown in color and was then transferred into a J. Young tube, where it was allowed to stand at ambient temperature. The progress of the reaction was monitored by ¹H NMR spectroscopy. The resonances observed at 4.76 and 4.67 ppm after 1 h confirmed greater than 99% conversion of furfural to PhSi(OCH₂(C₄H₃O))₃ (93%) and PhSiH(OCH₂(C₄H₃O))₂ (7%).

PhSi(OCH₂(C₄H₃O))₃: ¹H NMR (benzene-*d*₆): 7.78 (2H, m, *phenyl*), 7.29-7.22 (5H, m),

6.03 (7H, m, *furan*), 4.76 (6H, s, OCH₂). PhSiH(OCH₂(C₄H₃O))₂: ¹H NMR (benzene-*d*₆, selected resonances): 5.25 (1H, s, SiH), 4.67 (4H, s, OCH₂).

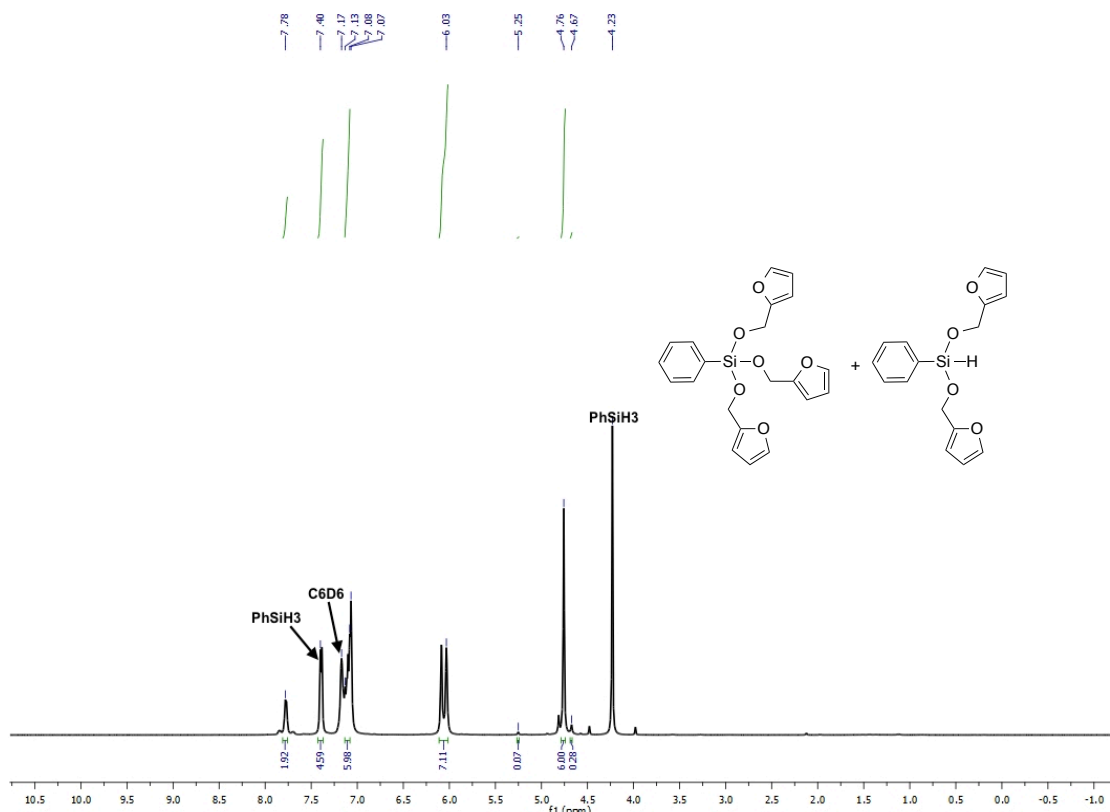


Figure 3.20: ¹H NMR spectrum of **16**-catalyzed (1 mol%) hydrosilylation of furfural with PhSiH₃ in benzene-*d*₆ solution.

NMR scale hydrosilylation of 3-cyclohexene-1-carboxaldehyde (1 mol% **16**):

In the glove box, a benzene-*d*₆ solution of PhSiH₃ (75.6 μL, 0.613 mmol), 3-cyclohexene-1-carboxaldehyde (69.6 μL, 0.613 mmol), and anisole (internal standard, 13.3 μL, 0.12 mmol) was added to a vial containing 2.6 mg (0.0061 mmol) of complex **16**. The resulting solution turned brown in color and was then transferred into a J. Young tube, where it was allowed to stand at ambient temperature. The progress of the reaction was monitored by ¹H NMR spectroscopy. The resonances observed at 3.77 and 3.66 ppm

after 1 h confirmed greater than 99% conversion of 3-cyclohexene-1-carboxaldehyde to a mixture of $\text{PhSi}(\text{OCH}_2(\text{C}_6\text{H}_9))_3$ (67%) and $\text{PhSiH}(\text{OCH}_2(\text{C}_6\text{H}_9))_2$ (33%) in 91% overall yield.

^1H NMR (benzene- d_6): 7.86 (2H, m, *phenyl*), 7.76 (2H, m, *phenyl*), 7.24 (6H, m, *phenyl*), 5.65 (10H, m, $\text{CH}=\text{CH}$), 5.20 (1H, s, *SiH*), 3.77 (6H, d, $J_{\text{HH}} = 5.3$ Hz, OCH_2), 3.66 (4H, d, $J_{\text{HH}} = 5.3$ Hz, OCH_2), 2.09 (5H, m, CH), 1.96 (14H, m, CH_2), 1.78 (12H, m, CH_2), 1.32 (4H, m, CH_2).

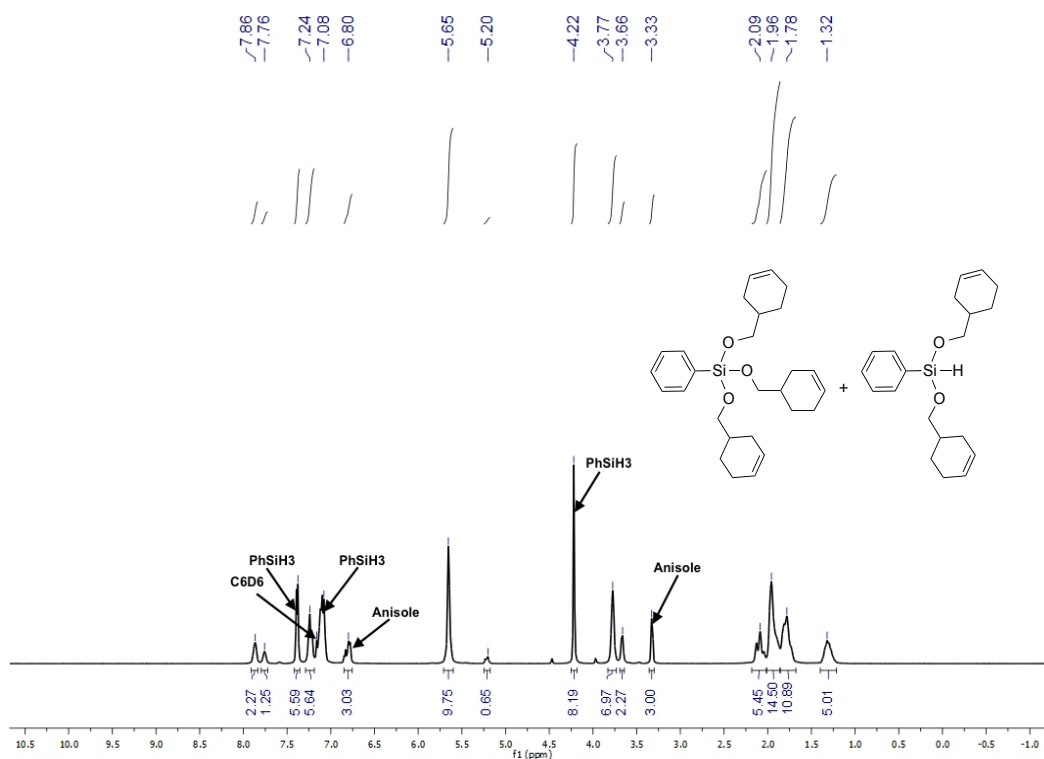


Figure 3.21: ^1H NMR spectrum of **16**-catalyzed (1 mol%) hydrosilylation of 3-cyclohexene-1-carboxaldehyde with PhSiH_3 in benzene- d_6 solution.

After 1 h, the reaction mixture was exposed to air to deactivate the catalyst. The resulting pale-yellow solution was immediately filtered through Celite and the solvent was removed under vacuum. The hydrosilylation products were then hydrolyzed by 10%

NaOH solution (1 mL) upon stirring for 3 h. Then the organic products were extracted with diethyl ether (3 x 4 mL), dried over Na₂SO₄, and decanted off. Finally, the solution was run through a pipet column filled with silica gel and the solvent was removed under pressure to obtain a thick colorless liquid. The product was identified as 3-cyclohexene-1-methanol by ¹H NMR and ¹³C NMR spectroscopy.

¹H NMR (benzene-*d*₆): C₇H₁₂O: 5.66 (2H, m, CH=CH), 3.78 (2H, d, OCH₂), 2.10 (1H, m, CH), 1.96 (3H, m, CH₂), 1.82 (2H, m, CH₂), 1.61 (1H, m, OH), 1.33 (1H, m, CH₂).

¹³C NMR (benzene-*d*₆): C₇H₁₂O: 127.88, 126.95, 68.62, 37.16, 29.09, 26.24, 25.61.

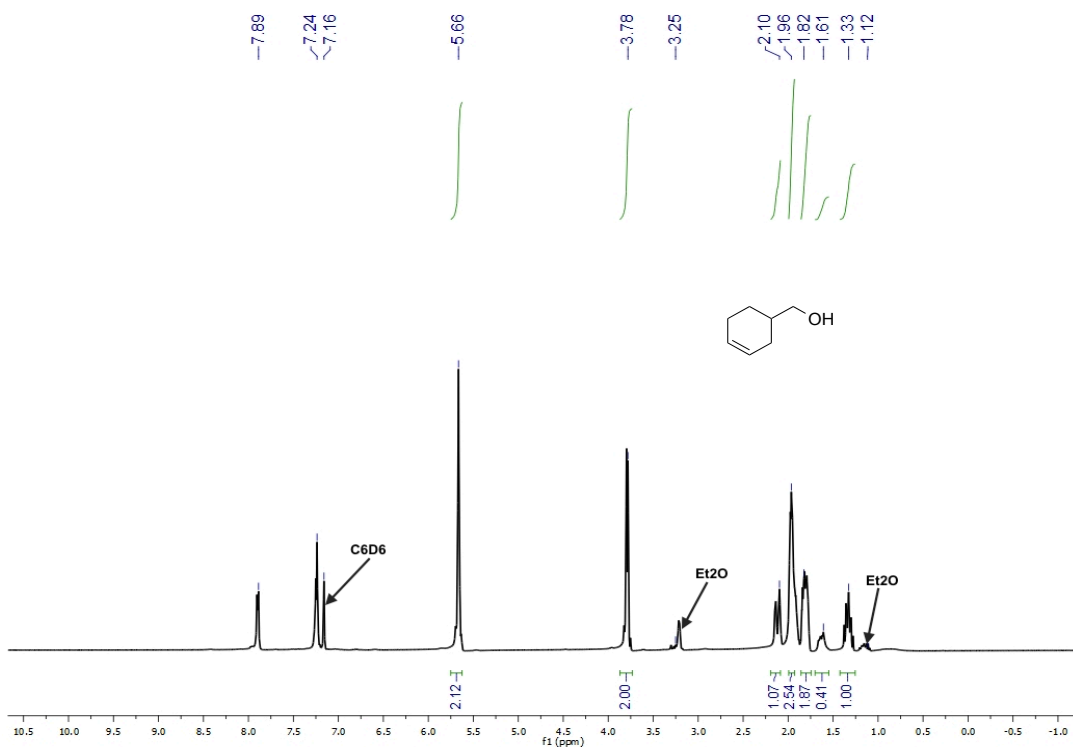


Figure 3.22: ¹H NMR spectrum of 3-cyclohexene-1-methanol in benzene-*d*₆.

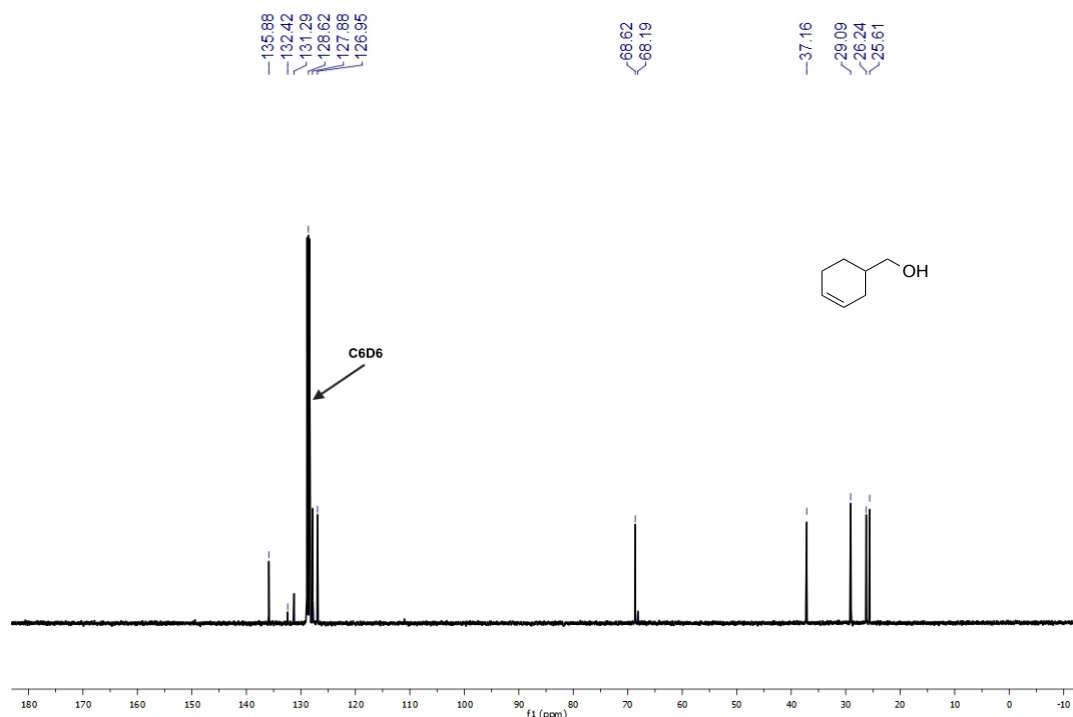


Figure 3.23: ^{13}C NMR spectrum of 3-cyclohexene-1-methanol in benzene- d_6 .

NMR scale hydrosilylation of cyclohexanecarboxaldehyde (1 mol% **16):**

In the glove box, a benzene- d_6 solution of PhSiH_3 (69.8 μL , 0.566 mmol) and cyclohexanecarboxaldehyde (68.5 μL , 0.566 mmol) was added to a vial containing 2.4 mg (0.00566 mmol) of complex **16**. The resulting solution turned brown in color and was then transferred into a J. Young tube, where it was allowed to stand at ambient temperature. The progress of the reaction was monitored by ^1H NMR spectroscopy. The resonances observed at 3.77 and 3.65 ppm after 1 h confirmed greater than 99% conversion of cyclohexanecarboxaldehyde to $\text{PhSi}(\text{OCH}_2\text{Cy})_3$ (52%) and $\text{PhSiH}(\text{OCH}_2\text{Cy})_2$ (48%).

^1H NMR (benzene- d_6): 7.92 (2H, m, *phenyl*), 7.80 (2H, m, *phenyl*), 7.23 (6H, m, *phenyl*), 5.26 (1H, s, SiH), 3.77 (6H, d, $J_{\text{HH}} = 6.2$ Hz, OCH_2), 3.65 (4H, d, $J_{\text{HH}} = 5.8$ Hz, OCH_2), 1.83 (10H, m, CH_2), 1.67 (20H, m, CH_2), 1.19 (15H, m), 0.98 (10H, m, CH_2).

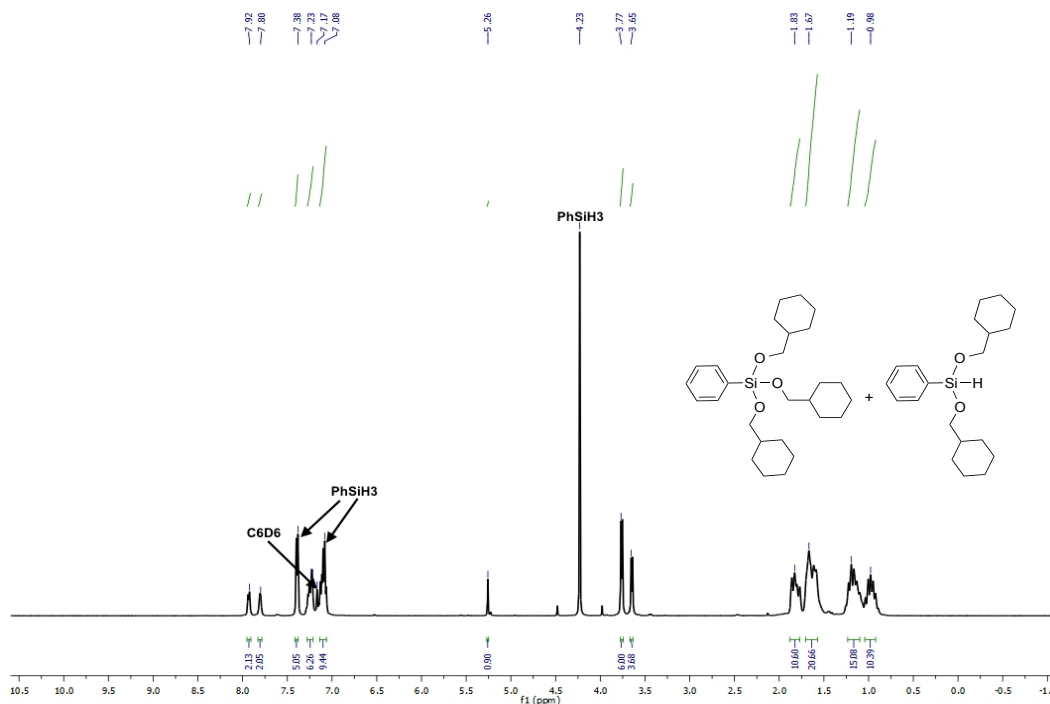


Figure 3.24: ¹H NMR spectrum of **16**-catalyzed (1 mol%) hydrosilylation of cyclohexanecarboxaldehyde with PhSiH₃ in benzene-*d*₆ solution.

NMR scale hydrosilylation of acetophenone (1 mol% catalyst **16**):

In the glove box, a benzene-*d*₆ solution of PhSiH₃ (95.9 μL, 0.778 mmol) and acetophenone (90.8 μL, 0.778 mmol) was added to a vial containing 3.3 mg (0.00778 mmol) of complex **16**. The resulting solution turned brown in color and was then transferred into a J. Young tube, where it was allowed to stand at ambient temperature. The progress of the reaction was monitored by ¹H NMR spectroscopy. The resonances observed at 5.18 and 5.00 ppm after 1 h confirmed greater than 99% conversion of acetophenone to a mixture of PhSiH(OCH(Me)(Ph))₂ (73%) and PhSi(OCH(Me)(Ph))₃ (27%). PhSiH(OCH(Me)(Ph))₂: ¹H NMR (benzene-*d*₆): 7.74 (4H, m, *phenyl*), 7.25 (11H, m, *phenyl*), 5.30 (1H, s, SiH), 5.00 (2H, m, OCH), 1.37 (m, CH₃). PhSi(OCH(Me)(Ph))₃: ¹H NMR (benzene-*d*₆): 7.79 (2H, m, *phenyl*), 7.29 (8H, m, *phenyl*), 7.14 (10H, m, *phenyl*), 5.18 (3H, m, CH), 1.42 (m, CH₃).

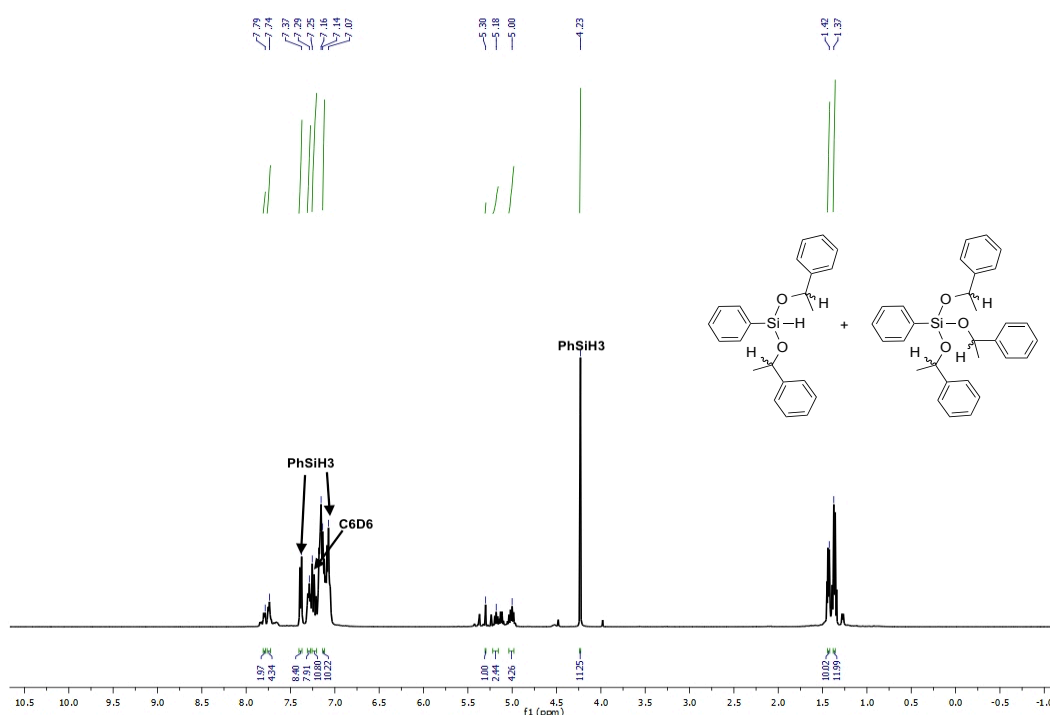


Figure 3.25: ¹H NMR spectrum of **16**-catalyzed (1 mol%) hydrosilylation of acetophenone with PhSiH₃ in benzene-*d*₆ solution.

NMR scale hydrosilylation of *p*-fluoroacetophenone (1 mol% **16**):

In the glove box, a benzene-*d*₆ solution of PhSiH₃ (98.8 μL, 0.801 mmol) and *p*-fluoroacetophenone (97.2 μL, 0.801 mmol) was added to a vial containing 3.4 mg (0.00801 mmol) of complex **16**. The resulting solution turned brown in color and was then transferred into a J. Young tube, where it was allowed to stand at ambient temperature. The progress of the reaction was monitored by ¹H NMR spectroscopy. The resonances observed at 5.03 and 4.85 ppm after 1 h confirmed greater than 99% conversion of *p*-fluoroacetophenone to a mixture of PhSi(OCH(Me)*p*-F-Ph)₃ (50%) and PhSiH(OCH(Me)*p*-F-Ph)₂ (50%) respectively.

^1H NMR (benzene- d_6): 7.69 (4H, m, *phenyl*), 7.21 (7H, m, *phenyl*), 7.05-6.95 (9H, m, *phenyl*), 6.78 (10H, m, *phenyl*), 5.22 (1H, s, SiH), 5.03 (3H, m, OCH), 4.85 (2H, m, OCH), 1.35 (6H, m, CH₃), 1.29 (9H, m, CH₃).

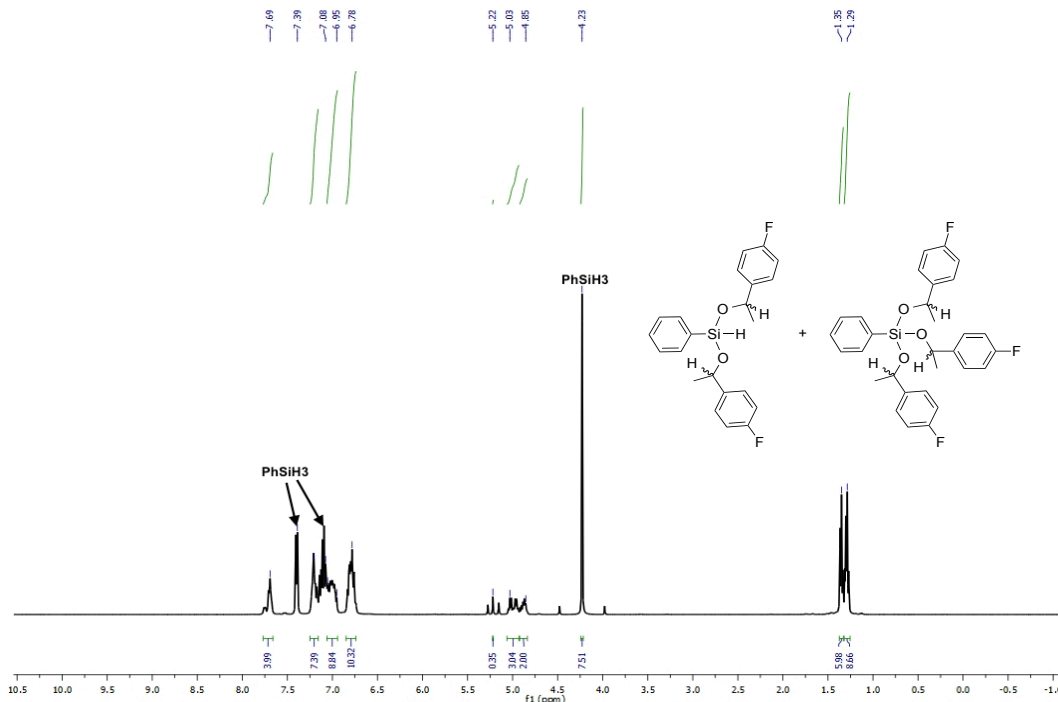


Figure 3.26: ^1H NMR spectrum of **16**-catalyzed (1 mol%) hydroxylation of *p*-fluoroacetophenone with PhSiH₃ in benzene- d_6 solution.

NMR scale hydroxylation of *p*-methoxyacetophenone (1 mol% **16**):

In the glove box, a benzene- d_6 solution of PhSiH₃ (72.7 μL , 0.589 mmol) and *p*-methoxyacetophenone (88.5 mg, 0.589 mmol) was added to a vial containing 2.5 mg (0.00589 mmol) of complex **16**. The resulting solution turned brown in color and was then transferred into a J. Young tube, where it was allowed to stand at ambient temperature. The progress of the reaction was monitored by ^1H NMR spectroscopy. The resonances observed at 5.21 and 5.04 ppm after 1 h confirmed greater than 99% conversion of *p*-methoxyacetophenone to a mixture of PhSiH(OCH(Me)(*p*-OMe-Ph))₂ (78%) and PhSi(OCH(Me)(*p*-OMe-Ph))₃ (22%).

PhSiH(OCH(Me)(*p*-OMe-Ph))₂: ^1H NMR (benzene- d_6): 7.78 (2H, m, *phenyl*), 7.21 (6H,

m, *phenyl*), 6.78 (5H, m, *phenyl*), 5.33 (1H, s, SiH), 5.04 (2H, m, OCH), 3.34 (6H, s, OCH₃), 1.50 (6H, m, CH₃). PhSi(OCH(Me)(*p*-OMe-Ph))₃: ¹H NMR (benzene-*d*₆, selected resonances): 7.85 (m, *phenyl*), 5.21 (3H, m, OCH), 1.44 (9H, m, CH₃).

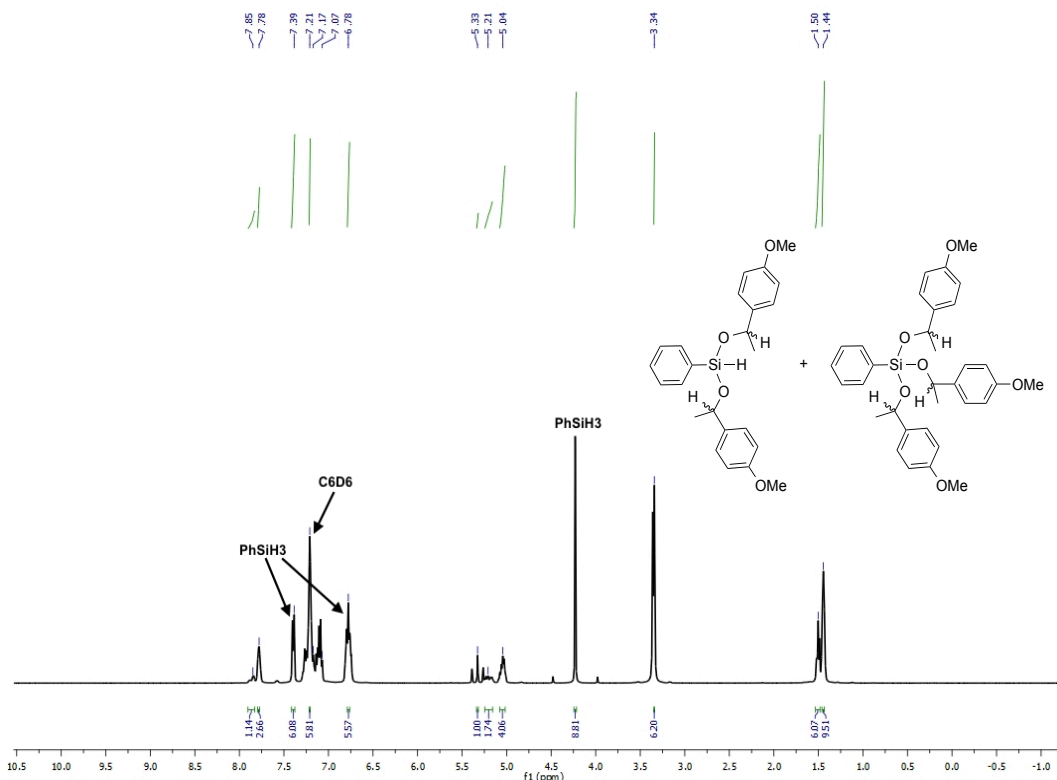


Figure 3.27: ¹H NMR spectrum of **16**-catalyzed (1 mol%) hydroxylation of *p*-methoxyacetophenone with PhSiH₃ in benzene-*d*₆ solution.

NMR scale hydroxylation of *p*-dimethylaminoacetophenone (1 mol% **16**):

In the glove box, a benzene-*d*₆ solution of PhSiH₃ (93.0 μL, 0.754 mmol) and *p*-dimethylaminoacetophenone (123.1 mg, 0.754 mmol) was added to a vial containing 3.2 mg (0.00754 mmol) of complex **16**. The resulting solution turned brown in color and was then transferred into a J. Young tube, where it was allowed to stand at ambient temperature. The progress of the reaction was monitored by ¹H NMR spectroscopy. The resonance observed at 5.14 ppm after 1 h confirmed greater than 99% conversion of *p*-dimethylaminoacetophenone to PhSiH(OCH(Me)(*p*-NMe₂-Ph))₂.

PhSiH(OCH(Me)(*p*-NMe₂-Ph))₂: ¹H NMR (benzene-*d*₆): 7.84 (2H, m, *phenyl*), 7.35-7.29 (3H, m, *phenyl*), 7.20 (4H, m, *phenyl*), 6.61 (4H, m, *phenyl*), 5.40 (1H, s, SiH), 5.14 (2H, m, OCH), 2.53 (12H, s, N(CH₃)₂), 1.54 (6H, m, CH₃).

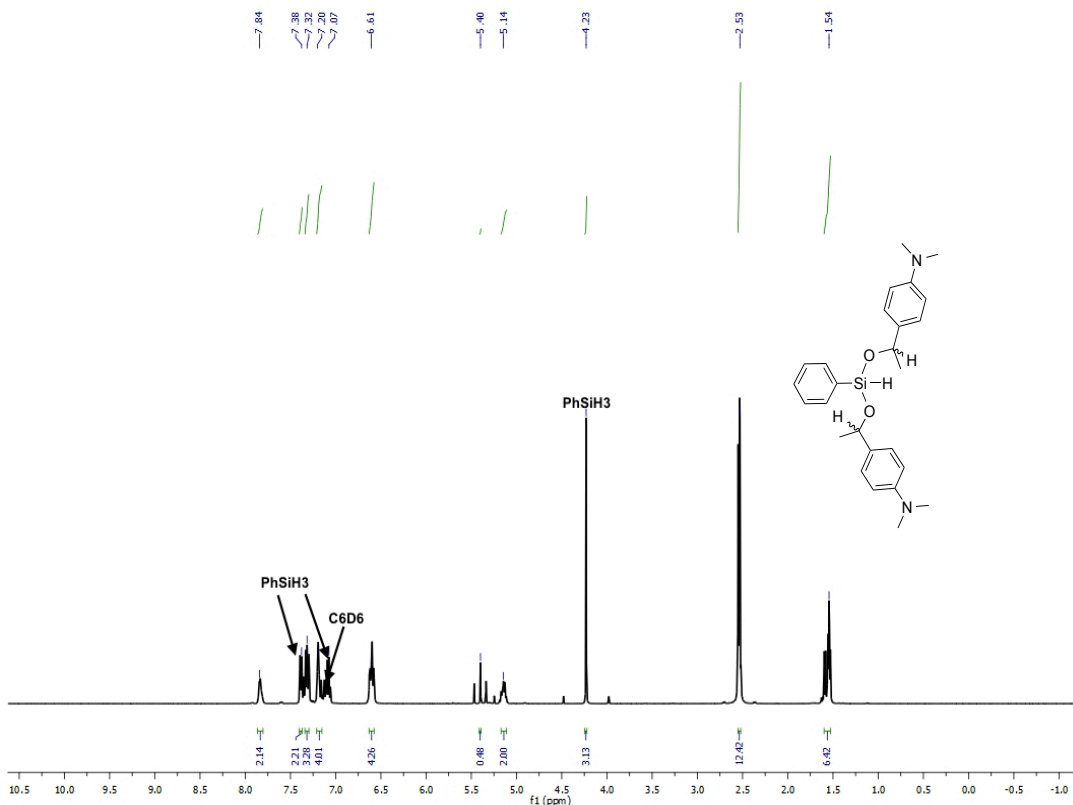


Figure 3.28: ¹H NMR spectrum of **16**-catalyzed (1 mol%) hydroxylation of *p*-dimethylaminoacetophenone with PhSiH₃ in benzene-*d*₆ solution.

NMR scale hydroxylation of benzophenone (1 mol% **16**):

In the glove box, a benzene-*d*₆ solution of PhSiH₃ (66.9 μL, 0.542 mmol) and benzophenone (98.7 mg, 0.542 mmol) was added to a vial containing 2.3 mg (0.00542 mmol) of complex **16**. The resulting solution turned brown in color and was then transferred into a J. Young tube, where it was allowed to stand at ambient temperature. The progress of the reaction was monitored by ¹H NMR spectroscopy. The resonances observed at 6.06 and 5.94 ppm after 1 h confirmed greater than 99% conversion of

benzophenone to a mixture of $\text{PhSiH}(\text{OCH}(\text{Ph})_2)_2$ (55%) and $\text{PhSi}(\text{OCH}(\text{Ph})_2)_3$ (45%).

^1H NMR (benzene- d_6): 7.66 (5H, m, *phenyl*), 7.29 (11H, m, *phenyl*), 7.23 (9H, m, *phenyl*), 7.05-7.00 (35H, m, *phenyl*), 6.06 (2H, s, OCH), 5.94 (3H, s, OCH), 5.36 (1H, s, SiH).

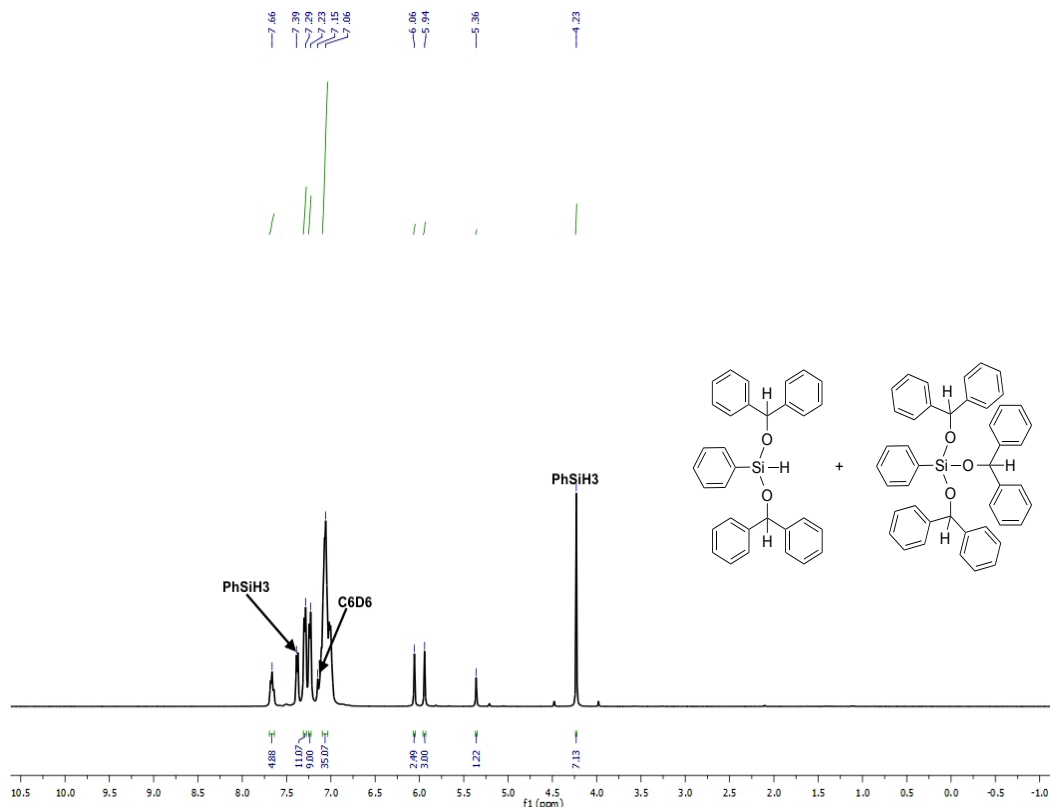


Figure 3.29: ^1H NMR spectrum of **16**-catalyzed (1 mol%) hydrosilylation of benzophenone with PhSiH_3 in benzene- d_6 solution.

NMR scale hydrosilylation of 2-hexanone (1 mol% **16**):

In the glove box, a benzene- d_6 solution of PhSiH_3 (84.3 μL , 0.683 mmol) and 2-hexanone (84.4 μL , 0.683 mmol) was added to a vial containing 2.9 mg (0.00683 mmol) of complex **16**. The resulting solution turned brown in color and was then transferred into a J. Young tube, where it was allowed to stand at ambient temperature. The progress of

the reaction was monitored by ^1H NMR spectroscopy. The resonances observed at 4.08 and 3.80 ppm after 1 h confirmed greater than 99% conversion of 2-hexanone to $\text{PhSiH}(\text{OCH}(\text{Me})(^n\text{Bu}))_2$ (96%) and $\text{PhSiH}_2(\text{OCH}(\text{Me})(^n\text{Bu}))$ (4%). $\text{PhSiH}(\text{OCH}(\text{Me})(^n\text{Bu}))_2$: ^1H NMR (benzene- d_6): 7.81 (2H, m, *phenyl*), 7.22 (3H, m, *phenyl*), 5.31 (1H, s, SiH), 4.08 (2H, m, OCH), 1.60 (2H, m, CH_2), 1.40 (4H, m, CH_2), 1.23 (12H, m, CH_3), 0.86 (6H, m, CH_2). $\text{PhSiH}_2(\text{OCH}(\text{Me})(^n\text{Bu}))$: ^1H NMR (benzene- d_6 , selected resonances): 5.25 (2H, s, SiH), 3.80 (1H, m, CH).

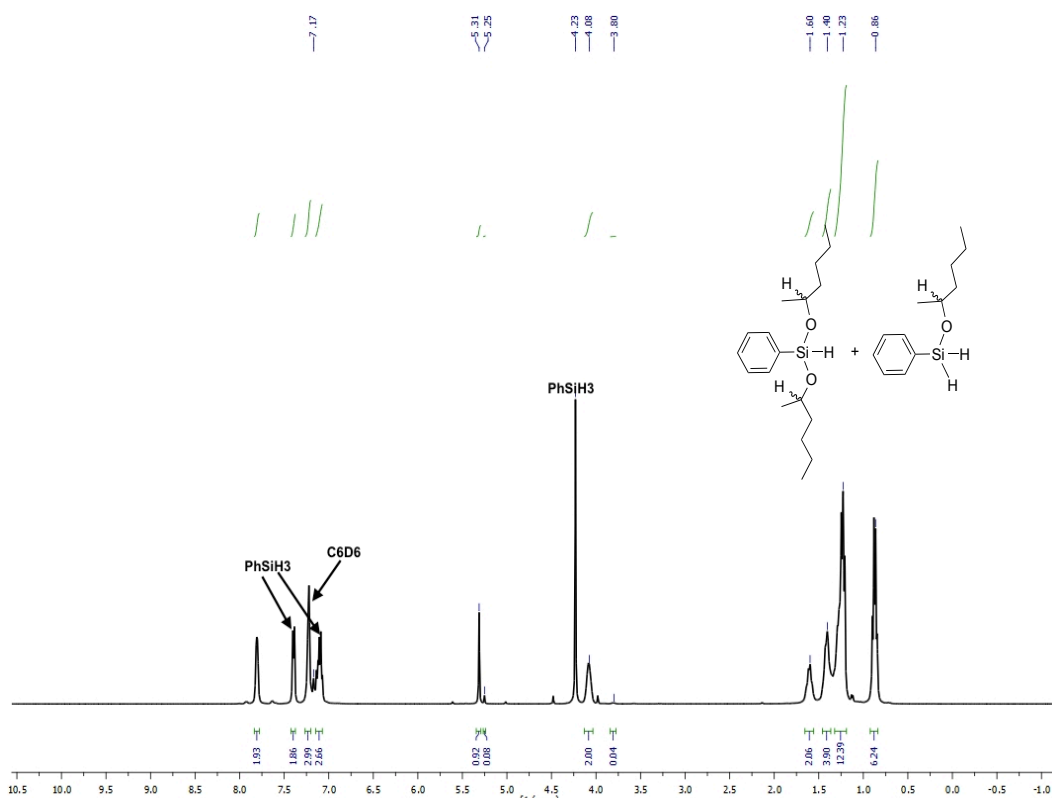


Figure 3.30: ^1H NMR spectrum of **16**-catalyzed (1 mol%) hydrosilylation of 2-hexanone with PhSiH_3 in benzene- d_6 solution.

NMR scale hydrosilylation of cyclohexanone (1 mol% **16**):

In the glove box, a benzene- d_6 solution of PhSiH_3 (81.4 μL , 0.660 mmol) and cyclohexanone (68.3 μL , 0.660 mmol) was added to a vial containing 2.8 mg (0.00660 mmol) of complex **16**. The resulting solution turned brown in color and was then

transferred into a J. Young tube, where it was allowed to stand at ambient temperature. The progress of the reaction was monitored by ^1H NMR spectroscopy. The resonances observed at 3.98 and 3.69 ppm after 1 h confirmed greater than 99% conversion of cyclohexanone to $\text{PhSiH}(\text{OCy})_2$ (97%) and $\text{PhSiH}_2(\text{OCy})$ (3%).

$\text{PhSiH}(\text{OCy})_2$: ^1H NMR (benzene- d_6): 7.84 (2H, m, *phenyl*), 7.23 (3H, m, *phenyl*), 5.34 (1H, s, SiH), 3.98 (2H, m, CH), 1.88 (4H, m, CH_2), 1.65 (4H, m, CH_2), 1.51 (4H, m, CH_2), 1.34 (2H, m, CH_2), 1.13 (6H, m, CH_2). $\text{PhSiH}_2(\text{OCy})$: ^1H NMR (benzene- d_6 , selected resonances): 5.27 (2H, s, SiH), 3.69 (1H, m, CH).

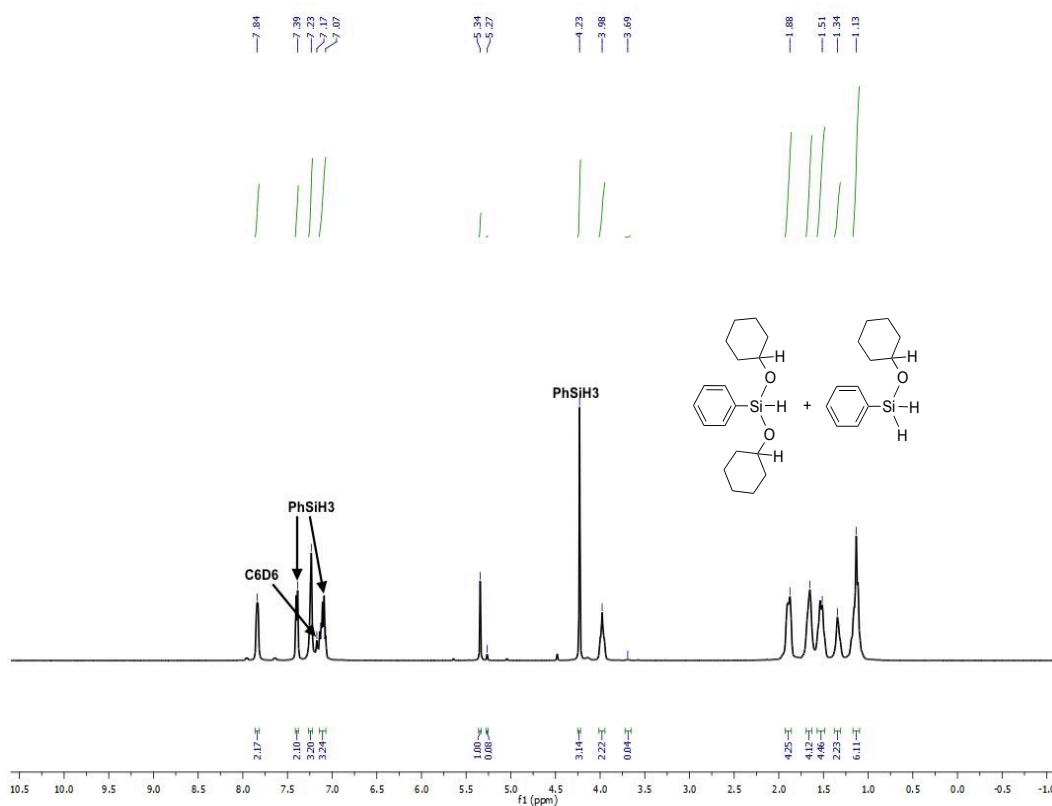


Figure 3.31: ^1H NMR spectrum of **16**-catalyzed (1 mol%) hydrosilylation of cyclohexanone with PhSiH_3 in benzene- d_6 solution.

NMR scale hydrosilylation of 2,4-dimethyl-3-pentanone (1 mol% **16**):

In the glove box, a benzene- d_6 solution of PhSiH_3 (93.0 μL , 0.754 mmol) and 2,4-dimethyl-3-pentanone (106.8 μL , 0.754 mmol) was added to the vial containing 3.2 mg

(0.00754 mmol) of complex **16**. The resulting solution turned brown in color and was then transferred into a J. Young tube, where it was allowed to stand at ambient temperature. The progress of the reaction was monitored by ^1H NMR spectroscopy. The resonances observed at 3.36 and 3.15 ppm after 1 h confirmed greater than 99% conversion of 2,4-dimethyl-3-pentanone to a mixture of $\text{PhSiH}(\text{OCH}(\text{}^i\text{Pr})_2)_2$ (70%) and $\text{PhSiH}_2(\text{OCH}(\text{}^i\text{Pr})_2)$ (30%). $\text{PhSiH}(\text{OCH}(\text{}^i\text{Pr})_2)_2$: ^1H NMR ($\text{benzene-}d_6$): 7.75 (2H, m, *phenyl*), 7.21 (3H, m, *phenyl*), 5.33 (1H, s, SiH), 3.36 (2H, m, OCH), 1.74 (4H, m, CH), 1.08 (6H, d, $J_{\text{HH}} = 6.3$ Hz, CH_3), 0.95 (12H, d, $J_{\text{HH}} = 6.3$ Hz, CH_3), 0.80 (6H, m, CH_3). $\text{PhSiH}_2(\text{OCH}(\text{}^i\text{Pr})_2)$: ^1H NMR ($\text{benzene-}d_6$, selected resonances): 7.66 (2H, m, *phenyl*), 5.31 (2H, s, SiH), 3.15 (1H, m, CH).

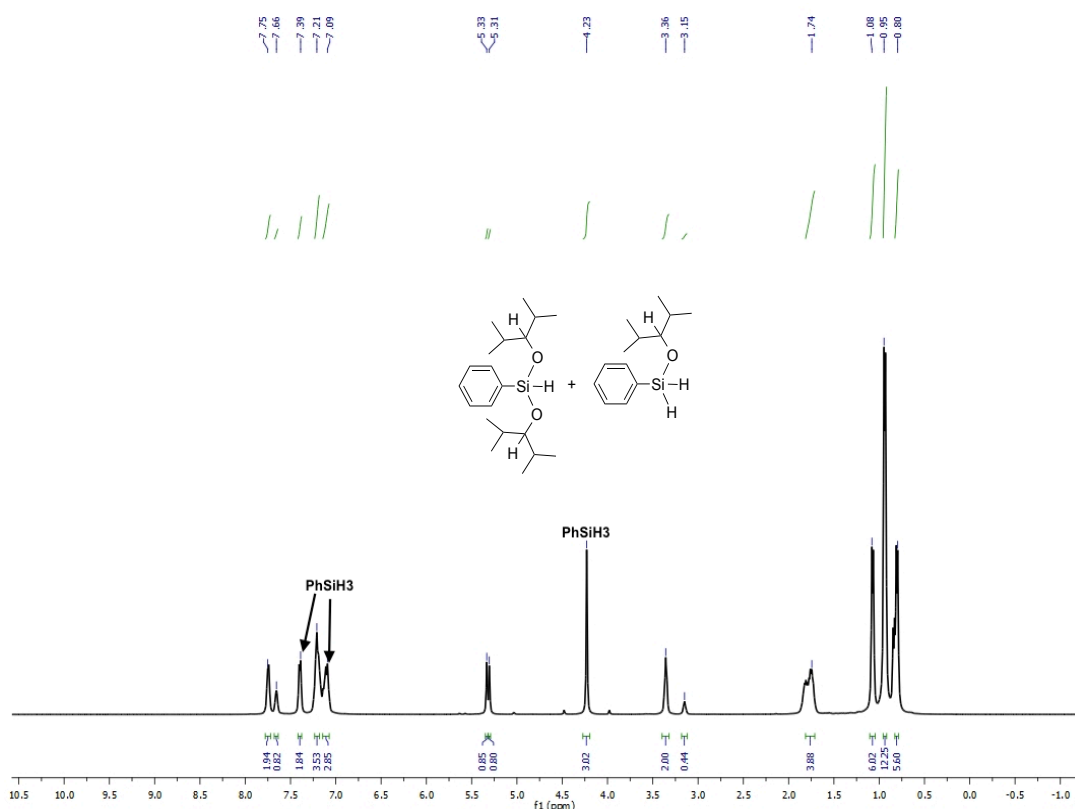


Figure 3.32: ^1H NMR spectrum of **16**-catalyzed (1 mol%) hydrosilylation of 2,4-dimethyl-3-pentanone with PhSiH_3 in $\text{benzene-}d_6$ solution.

NMR scale hydrosilylation of 2',4',6'-trimethylacetophenone (1 mol% **16**):

In the glove box, a benzene- d_6 solution of PhSiH₃ (58.4 μ L, 0.471 mmol) and 2',4',6'-trimethylacetophenone (78.4 μ L, 0.471 mmol) was added to a vial containing 2.0 mg (0.00471 mmol) of **16** at ambient temperature. The resulting solution turned brown in color and was then transferred into a J. Young tube. The progress of the reaction was monitored by ¹H NMR spectroscopy. After 1 h, 2% substrate conversion was observed. Based on methyl group integration, 67% conversion was observed after 5 d at ambient temperature.

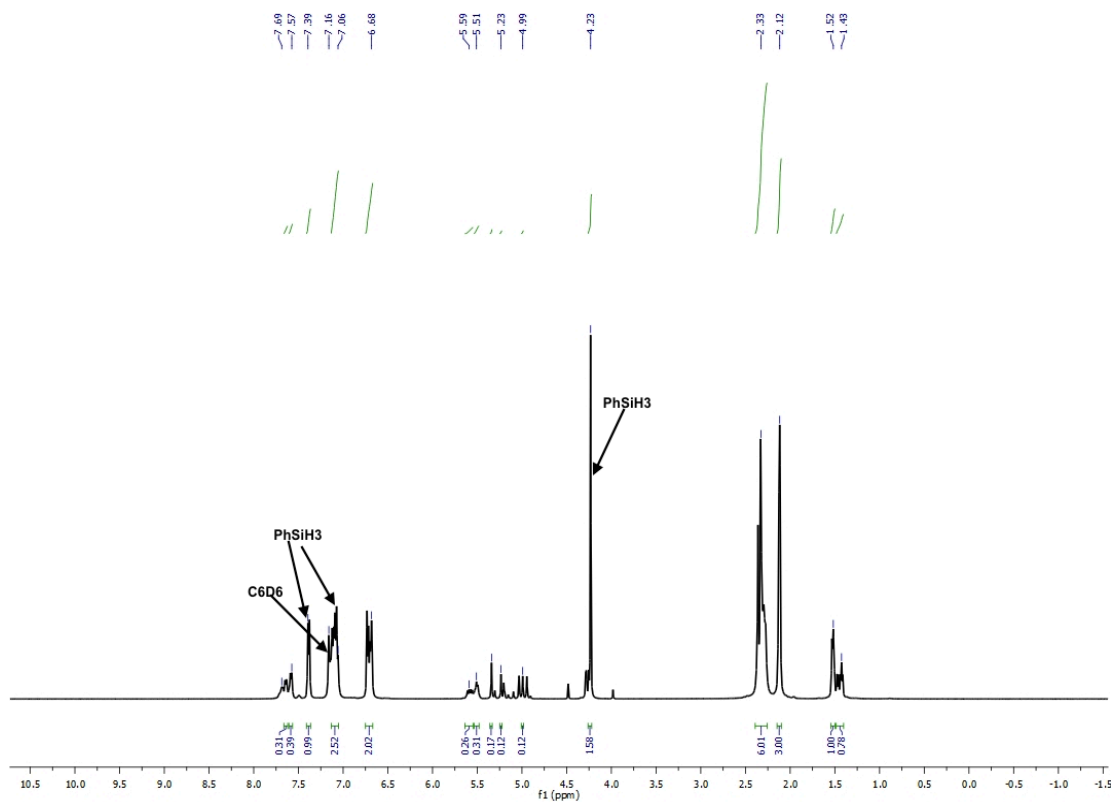


Figure 3.33: ¹H NMR spectrum of **16**-catalyzed (1 mol%) hydrosilylation of 2',4',6'-trimethylacetophenone with PhSiH₃ after 5 d in benzene- d_6 solution.

Neat hydrosilylation of 2-hexanone (0.02 mol% **16**):

In the glove box, a solution of 2-hexanone (1.2 mL, 9.42 mmol) and PhSiH₃ (1.2 mL, 9.42 mmol) was added to a 100 mL round-bottom flask containing 0.8 mg (0.00188 mmol) of complex **16**. The solution color turned brown and heat was generated. The reaction mixture was stirred for 5 min inside the glove box and then exposed to air to deactivate the catalyst. The resulting pale-yellow solution was immediately filtered through Celite. ¹H NMR data was recorded after dissolving 3 drops of the resulting solution in benzene-*d*₆ and greater than 99% conversion was observed along with the formation of PhSiH(OCH(Me)(ⁿBu))₂ (95%) and PhSiH₂(OCH(Me)(ⁿBu)) (5%).

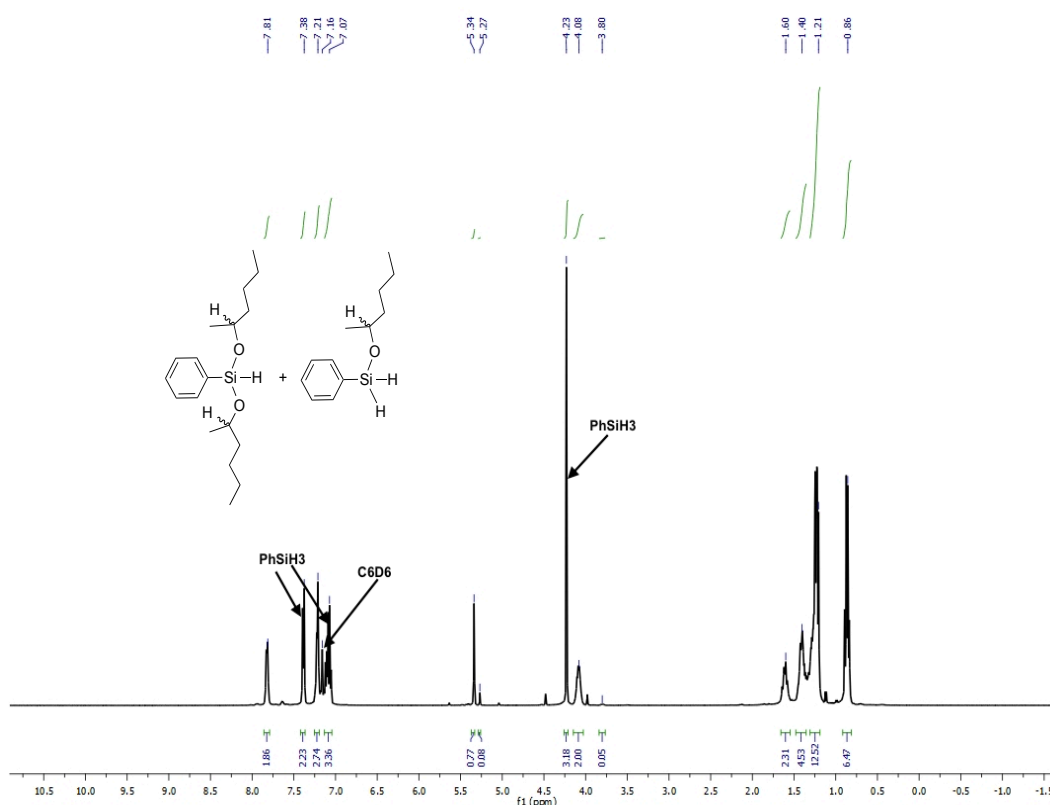


Figure 3.34: ¹H NMR spectrum of **16**-catalyzed (0.02 mol%) hydrosilylation of 2-hexanone with PhSiH₃ following benzene-*d*₆ dilution.

The hydrosilylation products were then hydrolyzed in 10% NaOH solution (4 mL) upon stirring for 3 h. The organic products were extracted with diethyl ether (3 x 5 mL) and dried over Na₂SO₄. After being decanted, the solution was run through a silica gel pipet column and the solvent was removed under pressure to obtain a colorless thick liquid (0.71 g, 72% yield). The product was identified as 2-hexanol by ¹H NMR and ¹³C NMR spectroscopy.

C₆H₁₄O: ¹H NMR (benzene-*d*₆): 3.58 (1H, s, OCH), 1.23 (7H, m), 1.04 (3H, m, CH₃), 0.87 (3H, m, CH₃). ¹³C NMR (benzene-*d*₆): 68.23, 40.00, 30.78, 28.91, 23.69, 14.90.

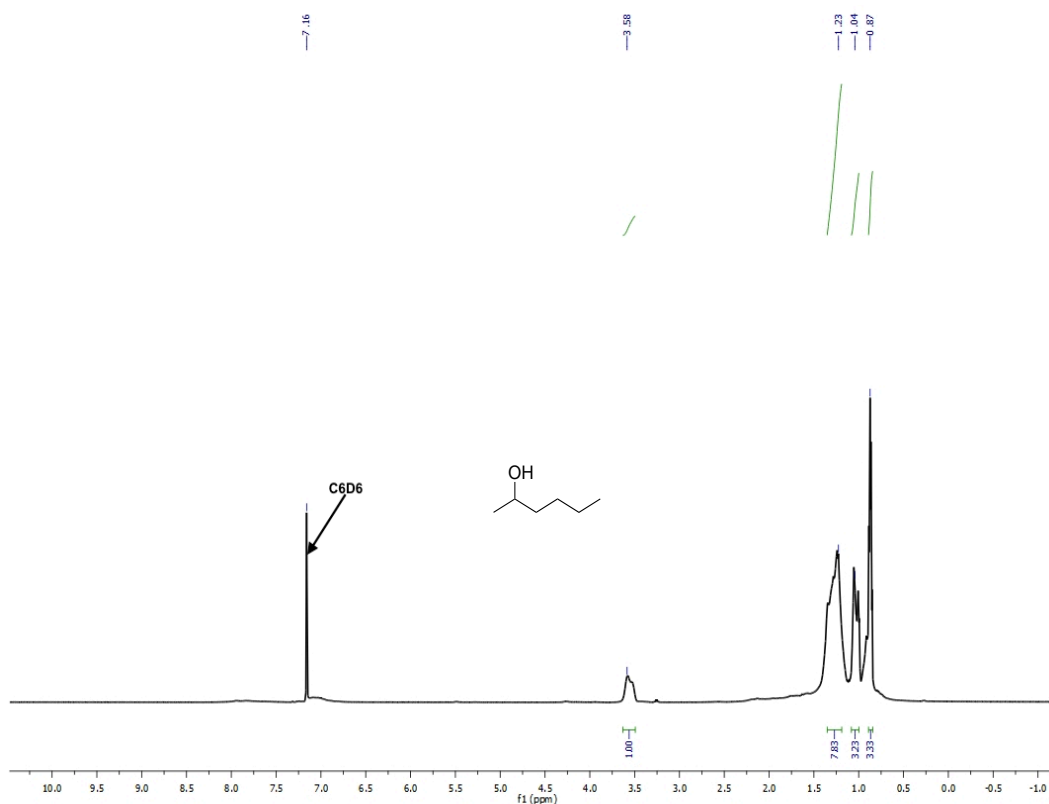


Figure 3.35: ¹H NMR spectrum of isolated 2-hexanol in benzene-*d*₆ solution.

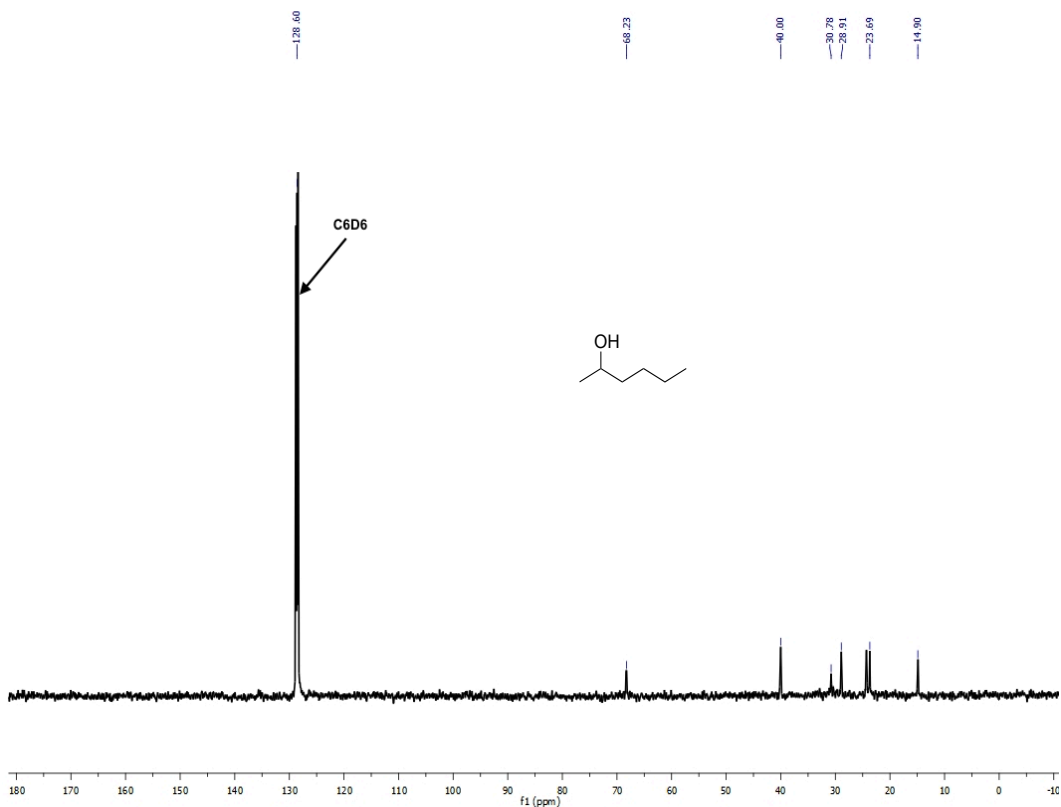


Figure 3.36: ^{13}C NMR spectrum of isolated 2-hexanol in benzene- d_6 solution.

Isolation of $\text{PhSiH}(\text{OCH}(\text{Me})(^n\text{Bu}))_2$ following 2-hexanone hydrosilylation (0.02 mol% **16):**

In the glove box, a solution of 2-hexanone (1.45 mL, 11.78 mmol) and PhSiH_3 (1.45 mL, 11.78 mmol) was added to a 100 mL round-bottom flask containing 1.0 mg (0.00235 mmol) of complex **16**. The solution color turned brown and heat was generated. The reaction mixture was stirred for 5 min inside the glove box and then exposed to air to deactivate the catalyst. The resulting pale-yellow solution was immediately filtered through Celite. ^1H NMR data was recorded by dissolving 3 drops of the resulting yellow mixture in benzene- d_6 and greater than 99% conversion was observed with the formation of $\text{PhSiH}(\text{OCH}(\text{Me})(^n\text{Bu}))_2$ (96%) and $\text{PhSiH}_2(\text{OCH}(\text{Me})(^n\text{Bu}))$ (4%). Evaporation of the reaction mixture for 7 h yielded only the tertiary silane product, $\text{PhSiH}(\text{OCH}(\text{Me})(^n\text{Bu}))_2$

(2.29 g, 63%).

PhSiH(OCH(Me)ⁿBu)₂: ¹H NMR (benzene-*d*₆): 7.85 (2H, m, *phenyl*), 7.21 (3H, m, *phenyl*), 5.36 (1H, s, SiH), 4.10 (2H, m, OCH), 1.63 (2H, m, CH₂), 1.40 (4H, m, CH₂), 1.24 (12H, m, CH₃), 0.86 (6H, m, CH₂). PhSiH(OCH(Me)ⁿBu)₂: ¹³C NMR (benzene-*d*₆): 135.22, 131.21, 71.03, 40.30, 28.83, 24.50, 23.55, 14.90.

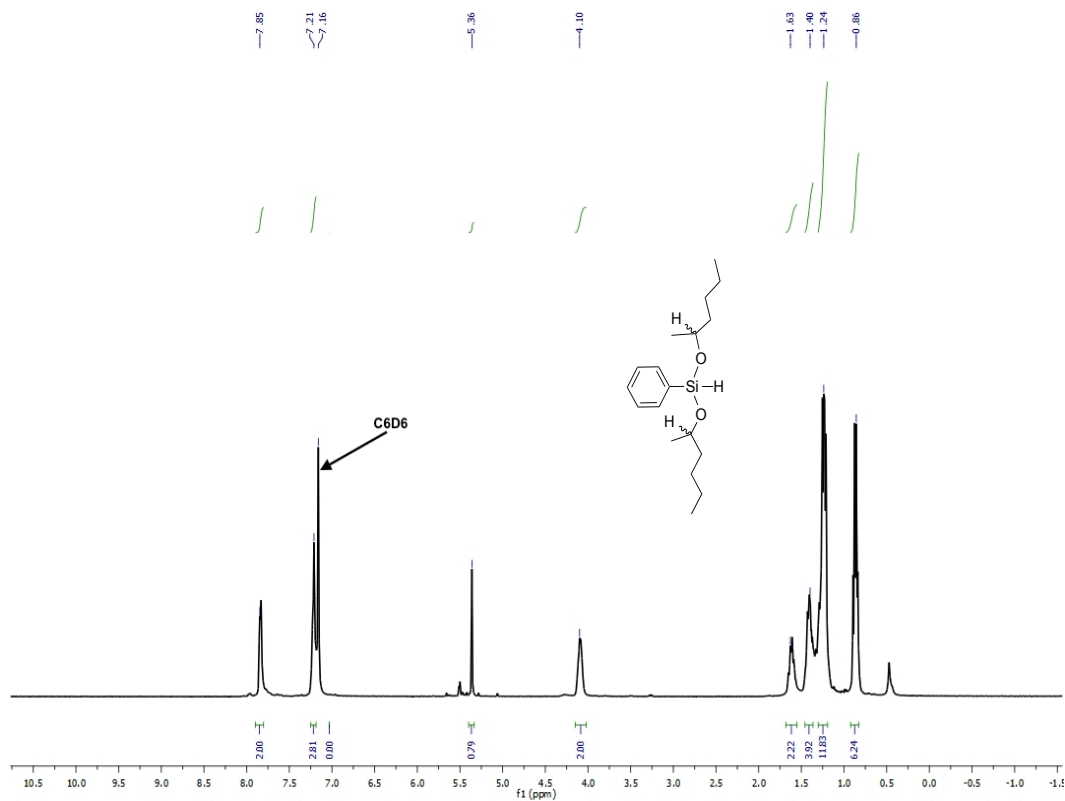


Figure 3.37: ¹H NMR spectrum of isolated PhSiH(OCH(Me)ⁿBu)₂ in benzene-*d*₆.

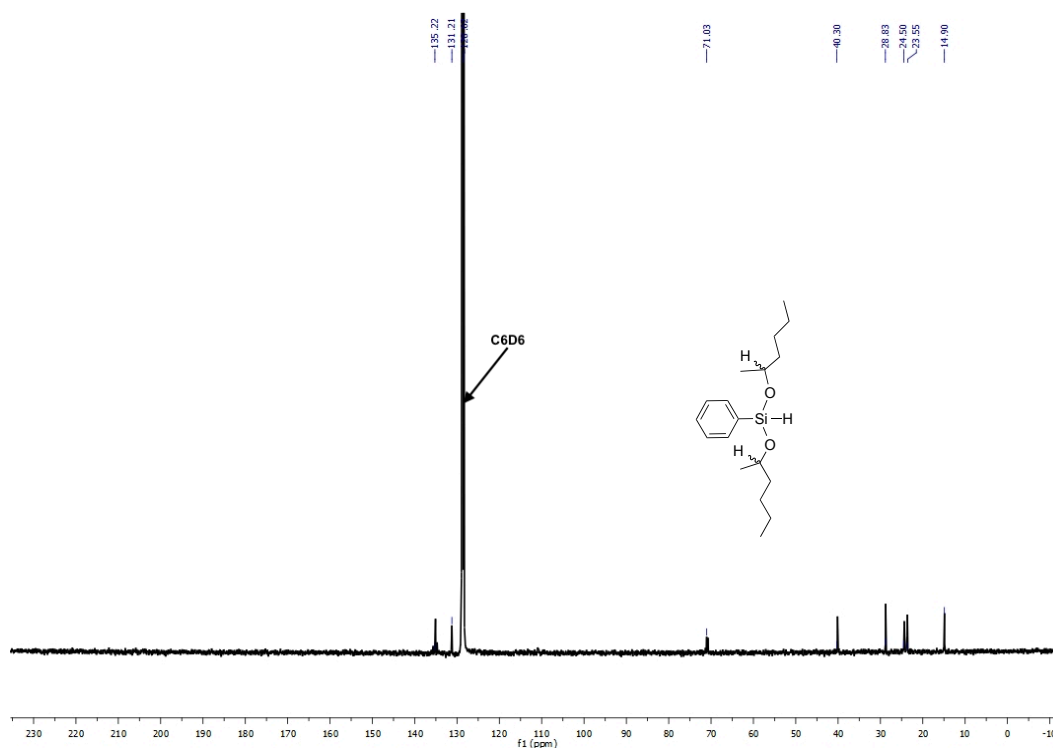


Figure 3.38: ^{13}C NMR spectrum of isolated $\text{PhSiH}(\text{OCH}(\text{Me})(n\text{Bu}))_2$ in benzene- d_6 .

Neat hydrosilylation of cyclohexanone (0.02 mol% **16**):

In the glove box, a solution of cyclohexanone (2.1 mL, 20.03 mmol) and PhSiH_3 (2.5 mL, 20.03 mmol) was added to a 100 mL round-bottom flask containing 1.7 mg (0.0040 mmol) of complex **16**. The solution color turned brown and heat was generated. The reaction mixture was stirred for 5 min inside the glove box and then exposed to air to deactivate the catalyst. The resulting pale-yellow solution was immediately filtered through Celite. ^1H NMR data was recorded upon dissolving 3 drops of the resulting yellow solution in benzene- d_6 and greater than 99% conversion was observed along with the formation of $\text{PhSiH}(\text{OCy})_2$ (96%) and $\text{PhSiH}_2(\text{OCy})$ (4%).

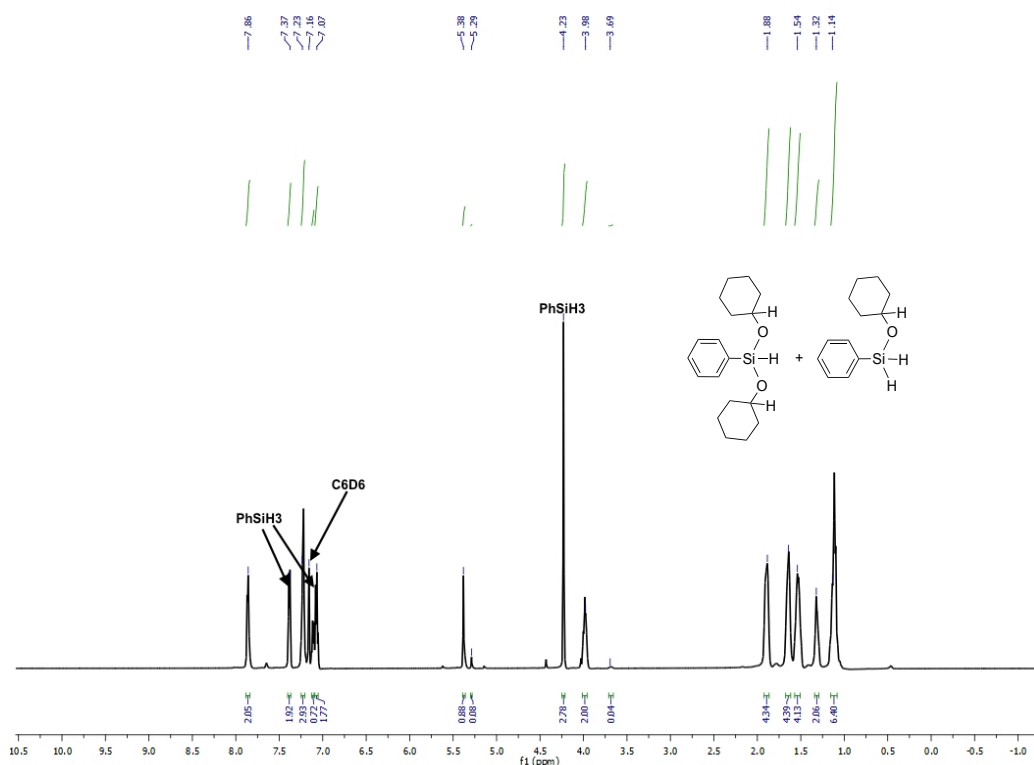


Figure 3.39: ^1H NMR spectrum of **16**-catalyzed (0.02 mol%) hydrosilylation of cyclohexanone following benzene- d_6 solution.

The hydrosilylation products were then hydrolyzed in 10% NaOH solution (4 mL) upon stirring for 3 h. The organic products were extracted with diethyl ether (3 x 5 mL), dried over Na_2SO_4 . After being decanted, the solution was run through a silica gel pipet column and the solvent was removed under pressure to obtain a colorless thick liquid (1.92 g, 99% yield). The product was identified as cyclohexanol by ^1H NMR and ^{13}C NMR spectroscopy.

$\text{C}_6\text{H}_{12}\text{O}$: ^1H NMR (benzene- d_6): 3.35 (1H, s, OCH), 1.67 (2H, m, CH_2), 1.58 (2H, m, CH_2), 1.35 (1H, s, OH), 1.10 (5H, m, CH_2), 0.85 (1H, m, CH_2). $\text{C}_6\text{H}_{12}\text{O}$: ^{13}C NMR (benzene- d_6): 70.36, 36.56, 26.37, 24.81.

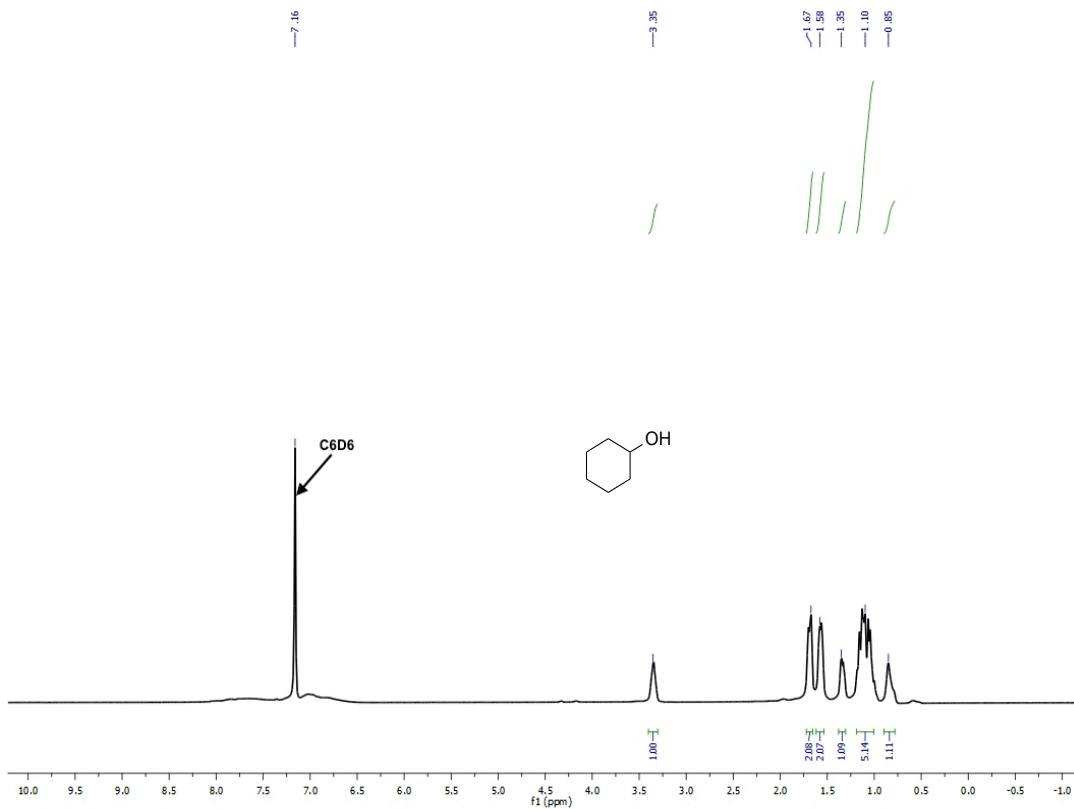


Figure 3.40: ^1H NMR spectrum of isolated cyclohexanol in benzene- d_6 solution.

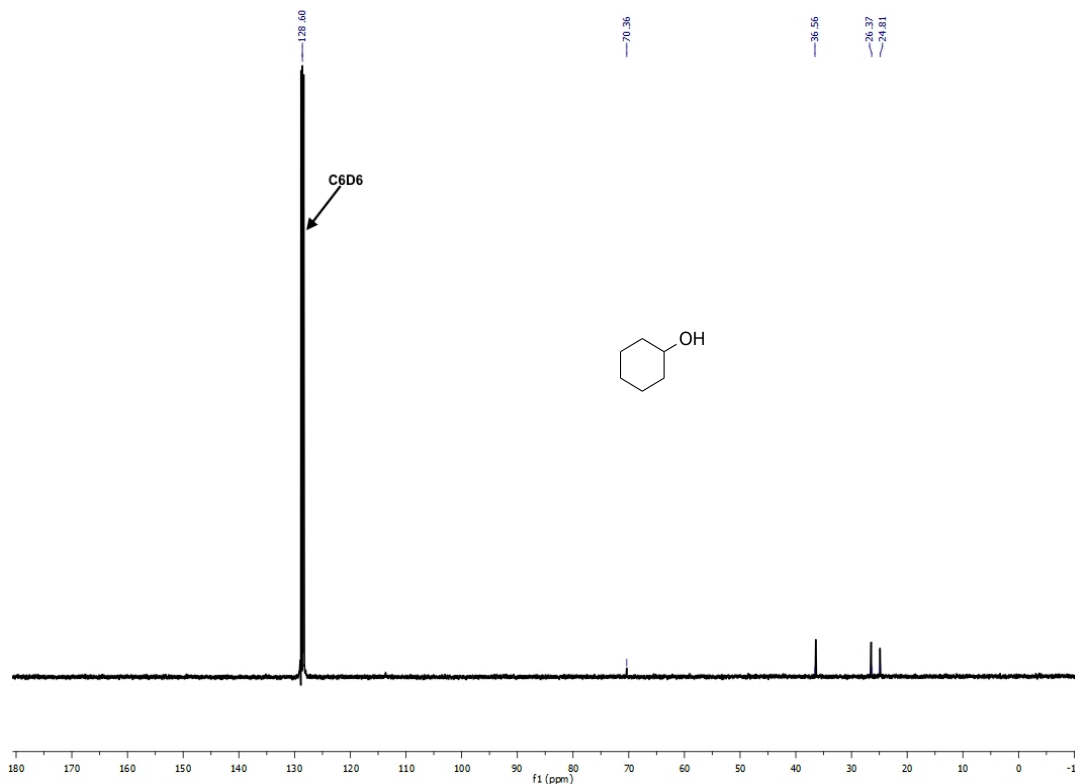


Figure 3.41: ^{13}C NMR spectrum of isolated cyclohexanol in benzene- d_6 solution.

Isolation of $\text{PhSiH}(\text{OCy})_2$ following cyclohexanone hydrosilylation (0.02 mol% **16):**

In the glove box, at ambient temperature a benzene- d_6 solution of cyclohexanone (1.34 mL, 12.96 mmol) and PhSiH_3 (1.59 mL, 12.96 mmol) was added to a vial containing 1.1 mg (0.00259 mmol) of complex **16**. The solution color turned brown and heat was generated. The reaction mixture was stirred for 5 min inside the glove box and then exposed to air to deactivate the catalyst. The resulting pale-yellow solution was immediately filtered through Celite. ^1H NMR data was recorded upon dissolving 3 drops of the resulting yellow mixture in benzene- d_6 and greater than 99% conversion was observed along with the formation of $\text{PhSiH}(\text{OCy})_2$ (97%) and $\text{PhSiH}_2(\text{OCy})$ (3%). Evaporation of the reaction mixture for 7 h yielded only the tertiary silane product, $\text{PhSiH}(\text{OCy})_2$ (2.15 g, 55%).

PhSiH(OCy)₂: ¹H NMR (benzene-*d*₆): 7.87 (2H, m, *phenyl*), 7.22 (3H, m, *phenyl*), 5.39 (1H, s, SiH), 3.98 (2H, m, CH), 1.89 (4H, m, CH₂), 1.66 (4H, m, CH₂), 1.55 (4H, m, CH₂), 1.32 (2H, m, CH₂), 1.14 (6H, m, CH₂). PhSiH(OCy)₂: ¹³C NMR (benzene-*d*₆): 134.93, 131.22, 72.61, 36.48, 26.38, 24.83.

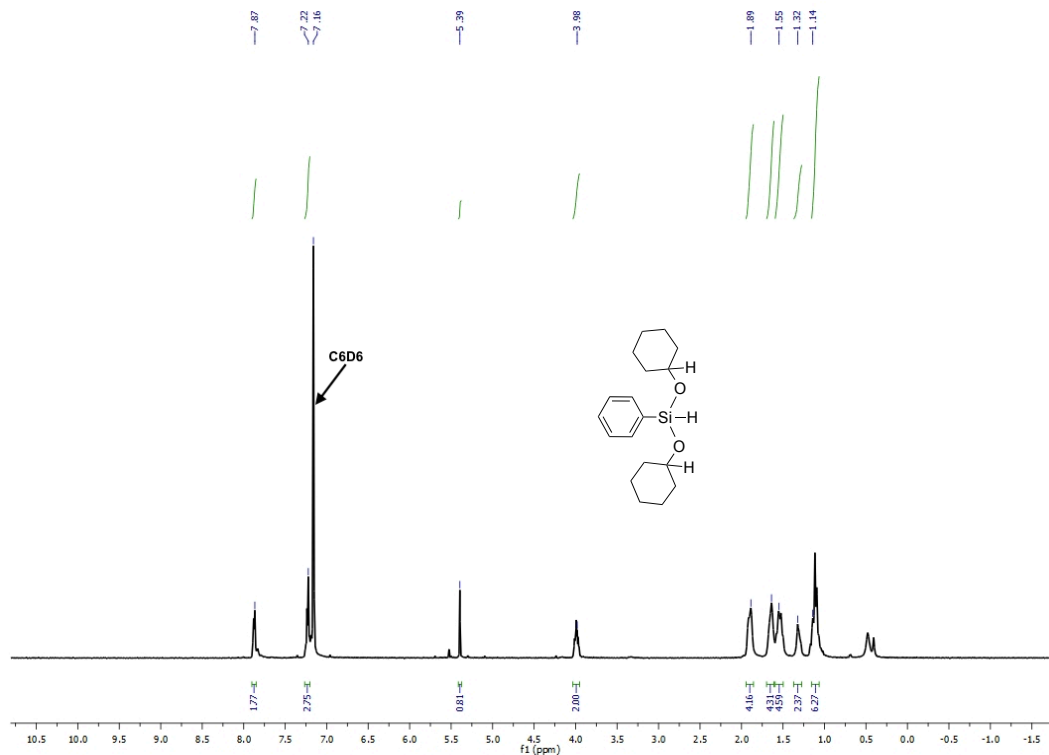


Figure 3.42: ¹H NMR spectrum of isolated PhSiH(OCy)₂ in benzene-*d*₆.

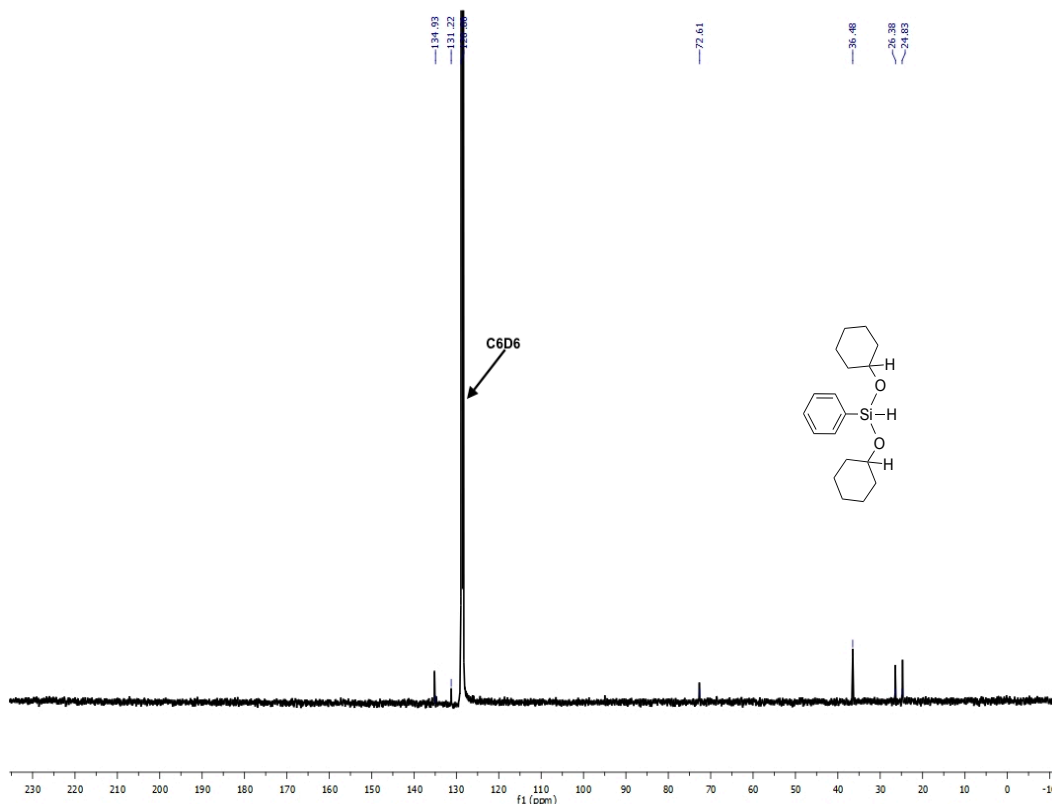


Figure 3.43: ^{13}C NMR spectrum of isolated $\text{PhSiH}(\text{OCy})_2$ in benzene- d_6 .

Neat hydrosilylation of benzaldehyde (0.02 mol% **16**):

In the glove box, a solution of benzaldehyde (1.3 mL, 12.95 mmol) and PhSiH_3 (1.6 mL, 12.95 mmol) was added to a 100 mL round-bottom flask containing 1.1 mg (0.00259 mmol) of complex **16**. The solution color turned brown and heat was generated. The reaction mixture was stirred for 2 min inside the glove box and then exposed to air to deactivate the catalyst. The resulting pale-yellow solution was immediately filtered through Celite. ^1H NMR data was recorded upon dissolving 3 drops of the resulting yellow mixture in benzene- d_6 and greater than 99% conversion was observed along with the formation of $\text{PhSi}(\text{OCH}_2\text{Ph})_3$ (81%) and $\text{PhSiH}(\text{OCH}_2\text{Ph})_2$ (19%).

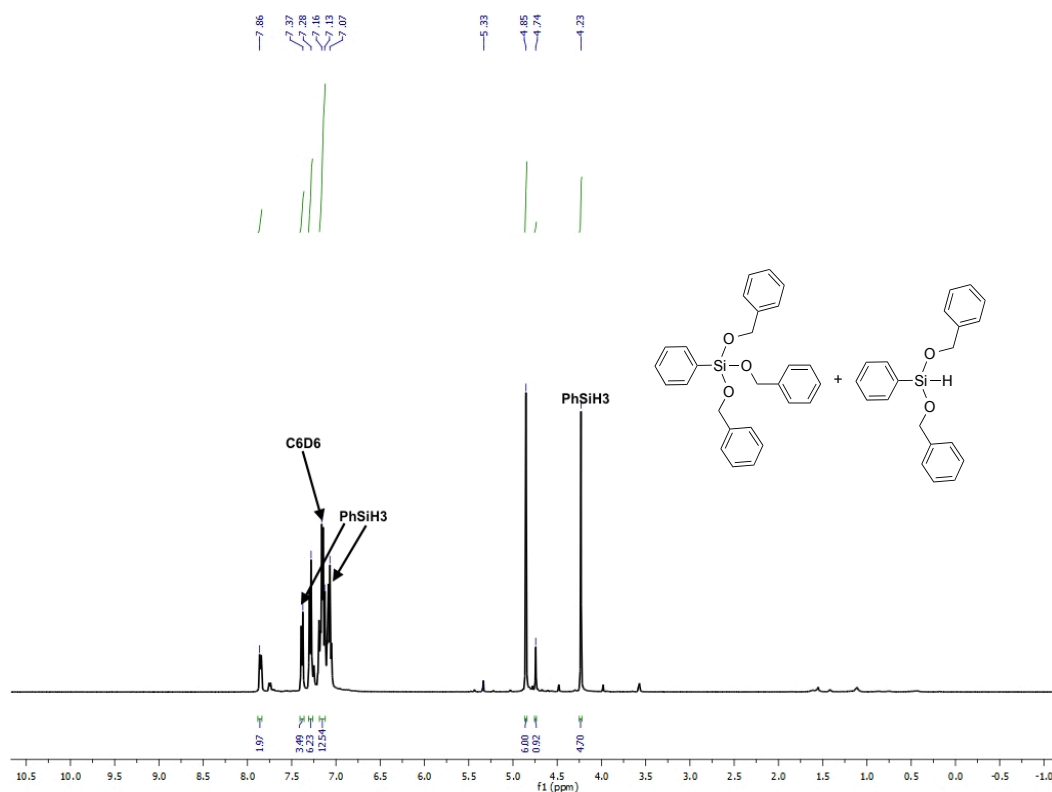


Figure 3.44: ^1H NMR spectrum of **16**-catalyzed (0.02 mol%) hydrosilylation of benzaldehyde with PhSiH_3 following benzene- d_6 dilution.

The hydrosilylation products were then hydrolyzed in 10% NaOH solution (4 mL) upon stirring for 3 h. The organic products were extracted with diethyl ether (3 x 5 ml), dried over Na_2SO_4 . After being decanted, the solution was run through a silica gel pipet column and the solvent was removed under pressure to obtain a colorless thick liquid (1.37 g, 99% yield). The product was identified as benzyl alcohol by ^1H NMR and ^{13}C NMR spectroscopy.

$\text{C}_7\text{H}_8\text{O}$: ^1H NMR (benzene- d_6): 7.13 (4H, m, *phenyl*), 7.06 (1H, m, *phenyl*), 4.33 (2H, s, OCH_2), 2.87 (1H, s, OH). $\text{C}_7\text{H}_8\text{O}$: ^{13}C NMR (benzene- d_6): 142.30, 135.10, 129.13, 127.67, 65.40.

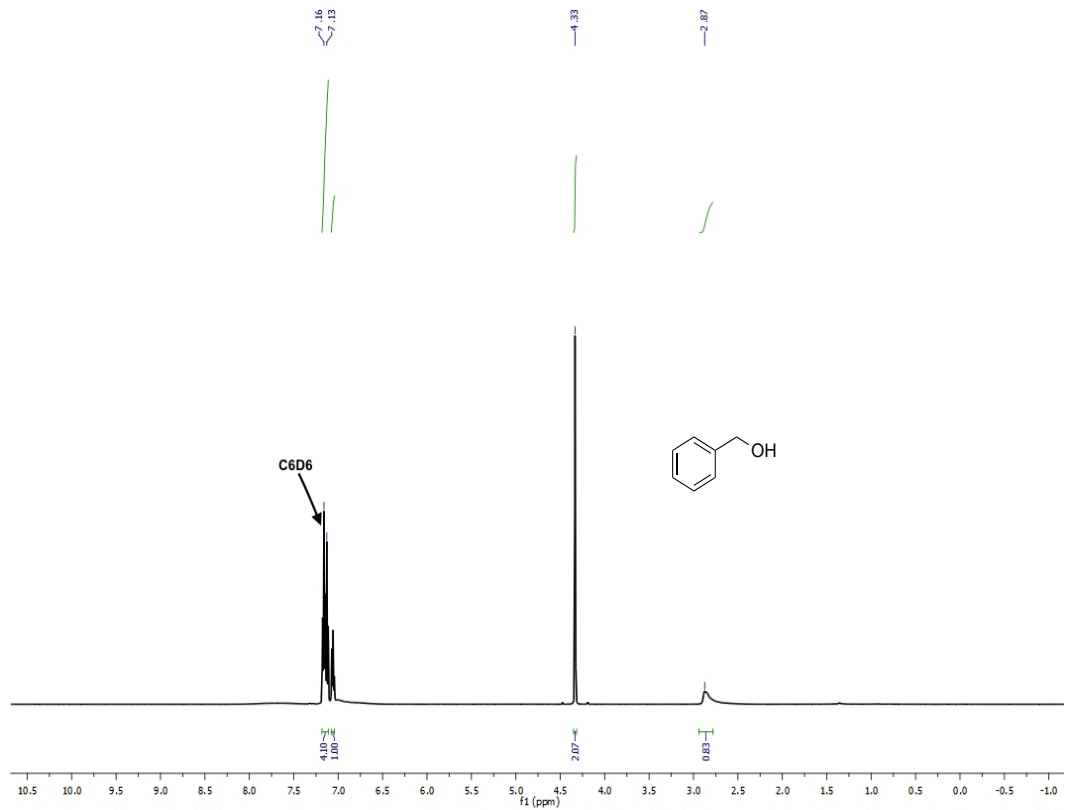


Figure 3.45: ^1H NMR spectrum of isolated benzyl alcohol in benzene- d_6 solution.

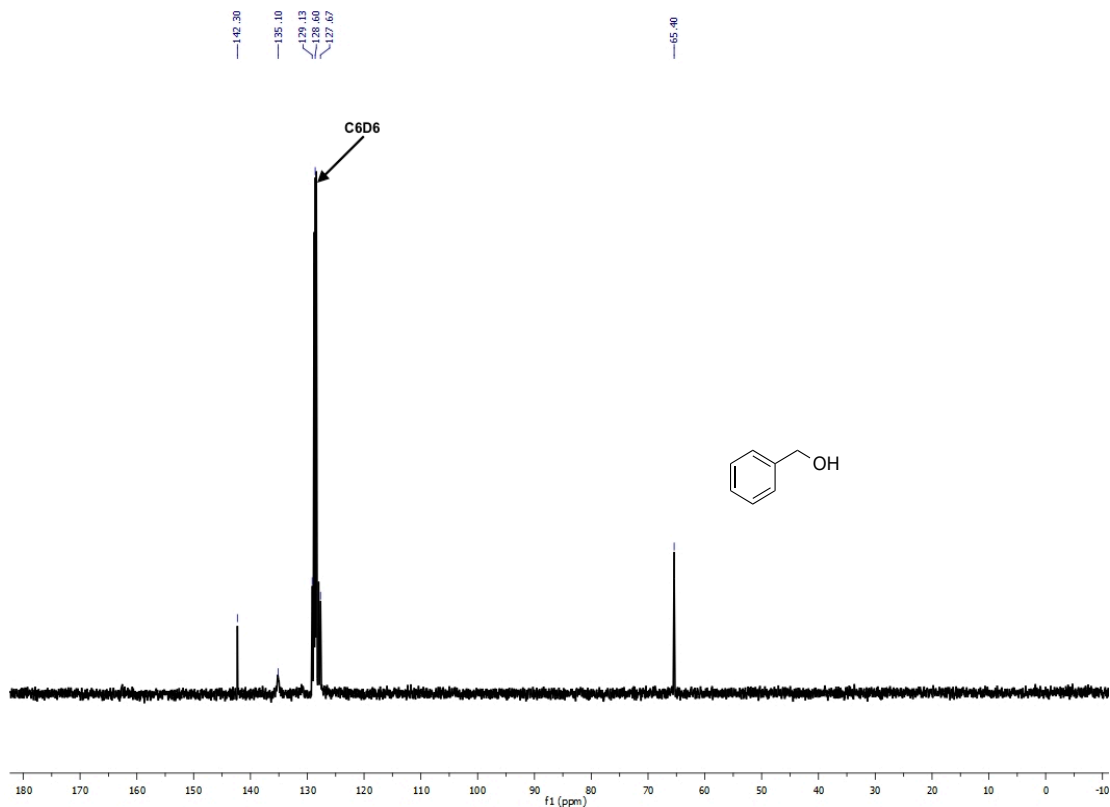


Figure 3.46: ^{13}C NMR spectrum of isolated benzyl alcohol in benzene- d_6 solution.

Neat hydrosilylation of *p*-fluorobenzaldehyde (0.02 mol% **16**):

In the glove box, a solution of *p*-fluorobenzaldehyde (2.92 mL, 27.10 mmol) and PhSiH_3 (3.34 mL, 27.10 mmol) was added to a 100 mL round-bottom flask containing 2.3 mg (0.00542 mmol) of complex **16**. The solution color turned brown and heat was generated. The reaction mixture was stirred for 2 min inside the glove box and then exposed to air to deactivate the catalyst. The resulting pale-yellow solution was immediately filtered through Celite. ^1H NMR data was recorded upon dissolving 3 drops of the resulting solution in benzene- d_6 and greater than 99% conversion was observed along with the formation of $\text{PhSiH}(\text{OCH}_2(p\text{-F}(\text{C}_6\text{H}_4))_2)$ (52%) and $\text{PhSi}(\text{OCH}_2(p\text{-F}(\text{C}_6\text{H}_4)))_3$ (48%).

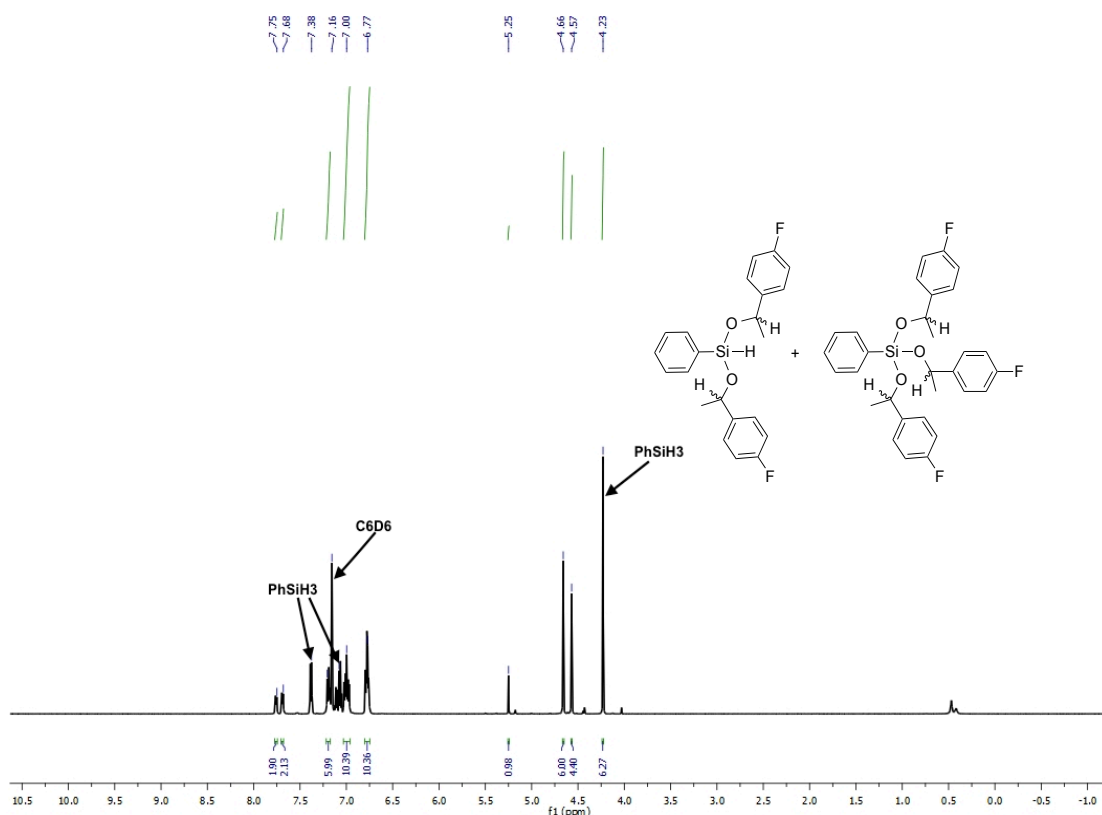


Figure 3.47: ^1H NMR spectrum of **16**-catalyzed (0.02 mol%) hydroxylation of *p*-fluorobenzaldehyde with PhSiH_3 following benzene- d_6 dilution.

The hydroxylation products were then hydrolyzed in 10% NaOH solution (3 mL) upon stirring for 3 h. The organic products were extracted with diethyl ether (3 x 5 mL), dried over Na_2SO_4 . After being decanted, the solution was run through a silica gel pipet column and the solvent was removed under pressure to obtain a colorless thick liquid (3.40 g, 71% yield). The product was identified as *p*-fluorobenzyl alcohol by ^1H and ^{13}C NMR spectroscopy.

$\text{C}_7\text{H}_7\text{OF}$: ^1H NMR (benzene- d_6): 6.92 (2H, m, *phenyl*), 6.78 (2H, m, *phenyl*), 4.14 (2H, s, OCH_2). $\text{C}_7\text{H}_7\text{OF}$: ^{13}C NMR (benzene- d_6): 164.40, 161.94, 129.24, 115.97, 64.75.

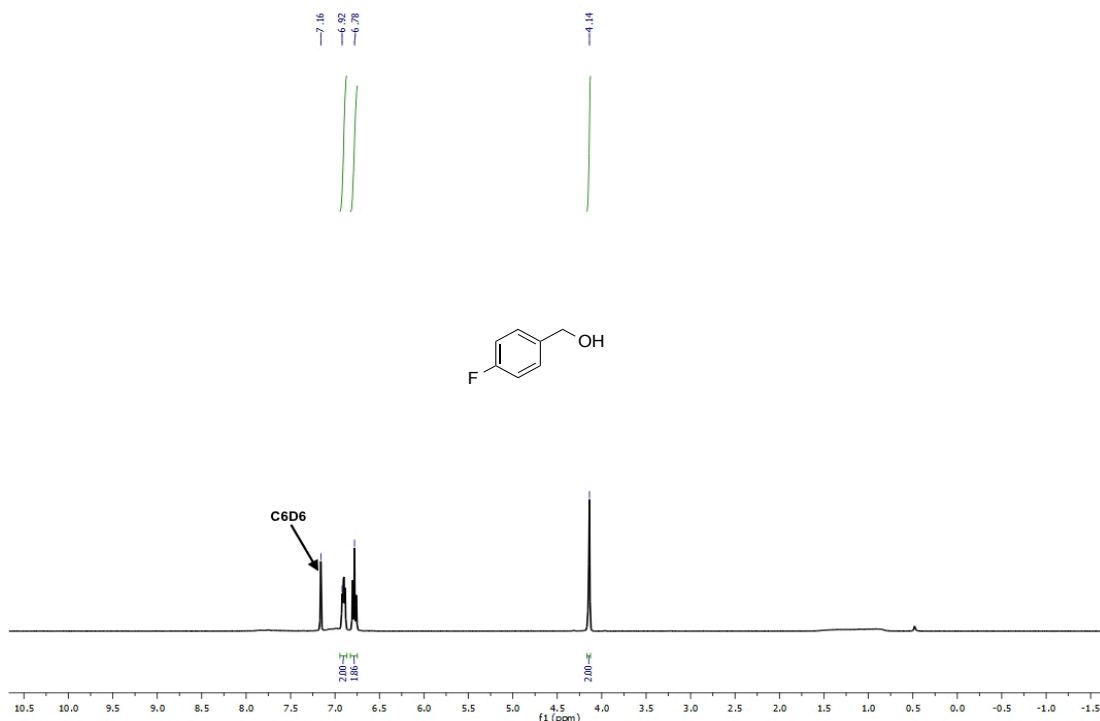


Figure 3.48: ^1H NMR spectrum of isolated *p*-fluorobenzyl alcohol in benzene- d_6 solution.

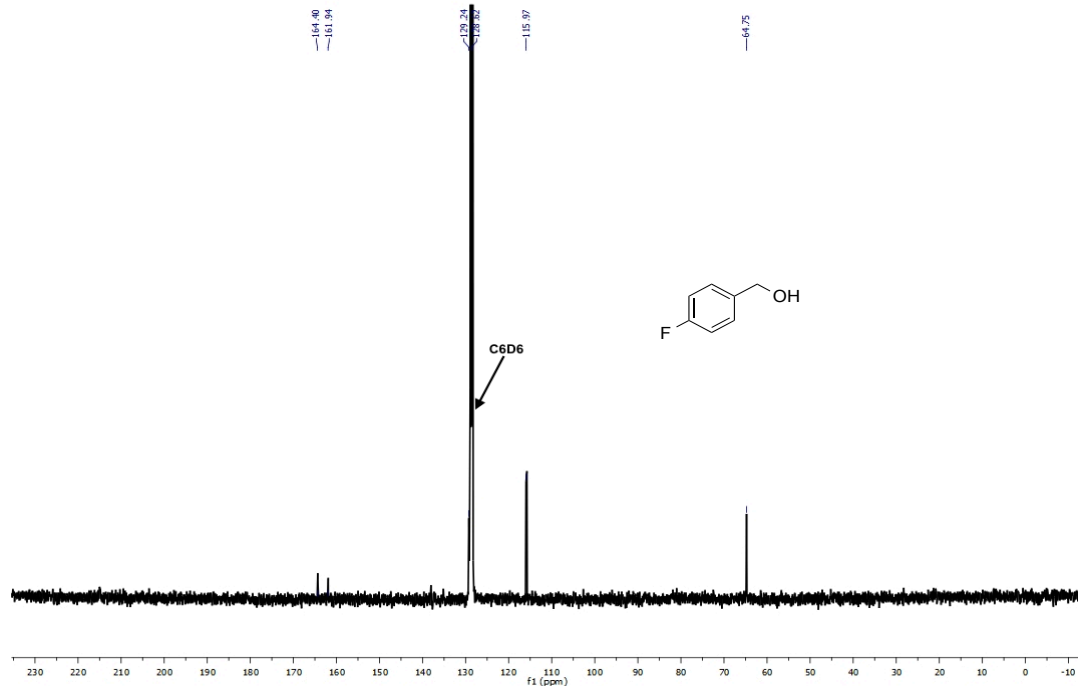


Figure 3.49: ^{13}C NMR spectrum of isolated *p*-fluorobenzyl alcohol in benzene- d_6 solution.

Determination of maximum benzaldehyde hydrosilylation TON:

In the glove box, a solution of benzaldehyde (2.5 mL, 24.74 mmol) and PhSiH₃ (3.1 mL, 24.74 mmol) was added to a 100 mL round-bottom flask containing 2.1 mg (0.00495 mmol) of **16**. The solution turned brown in color and heat was generated. The reaction mixture was stirred for 2 min and was allowed to cool for an additional 8 min. At that time, a second solution containing benzaldehyde (2.5 mL, 24.74 mmol) and PhSiH₃ (3.1 mL, 24.74 mmol) was added. After waiting 10 min, this step was repeated four additional times until a total of 15 mL of benzaldehyde and 18.6 mL of PhSiH₃ was added. After 40 min, a portion of the mixture was transferred into a vial, dissolved in benzene-*d*₆, and a ¹H NMR spectrum was recorded. ¹H NMR of this solution revealed 47.2% benzaldehyde hydrosilylation (of 30,000 eq.), equating to a TON of 14,170.

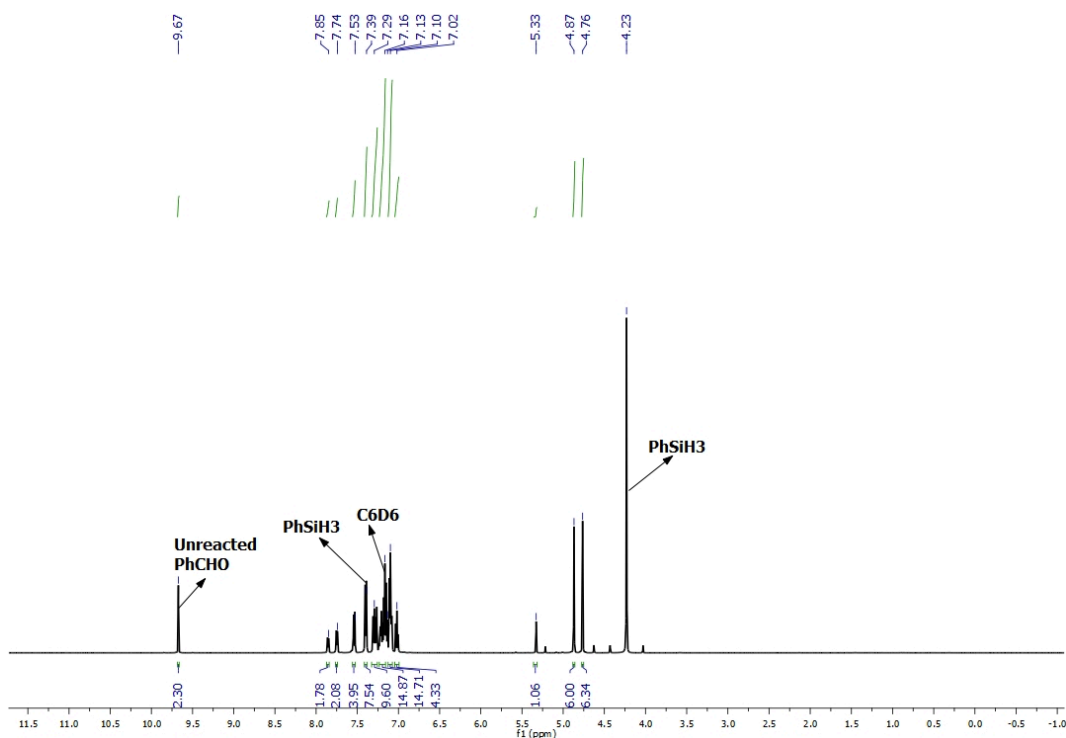


Figure 3.50: ¹H NMR spectrum (benzene-*d*₆) of **16**-catalyzed hydrosilylation of benzaldehyde with PhSiH₃ (30,000 eq. of substrate and silane).

Test for Catalyst Homogeneity:

In the glove box, a mixture of cyclohexanone (0.29 mL, 2.83 mmol) and PhSiH₃ (0.35 mL, 2.83 mmol) was added to a 100 mL round bottom flask containing Hg⁰ (28.27 g, 141.37 mmol). To this mixture, 1.2 mg (0.00283 mmol) of complex **16** was added and the resulting brown-colored mixture was stirred for 5 min. Then it was exposed to air to deactivate the catalyst. The resulting colorless mixture was pipetted out (leaving behind Hg⁰) and filtered through Celite. The resulting colorless organic fraction was pipetted out (leaving behind Hg⁰) and filtered through Celite. The ¹H NMR spectrum of the colorless liquid in benzene-*d*₆ revealed greater than 99% conversion of cyclohexanone to a mixture of PhSiH(OCy)₂ (96%) and PhSiH₂(OCy) (4%).

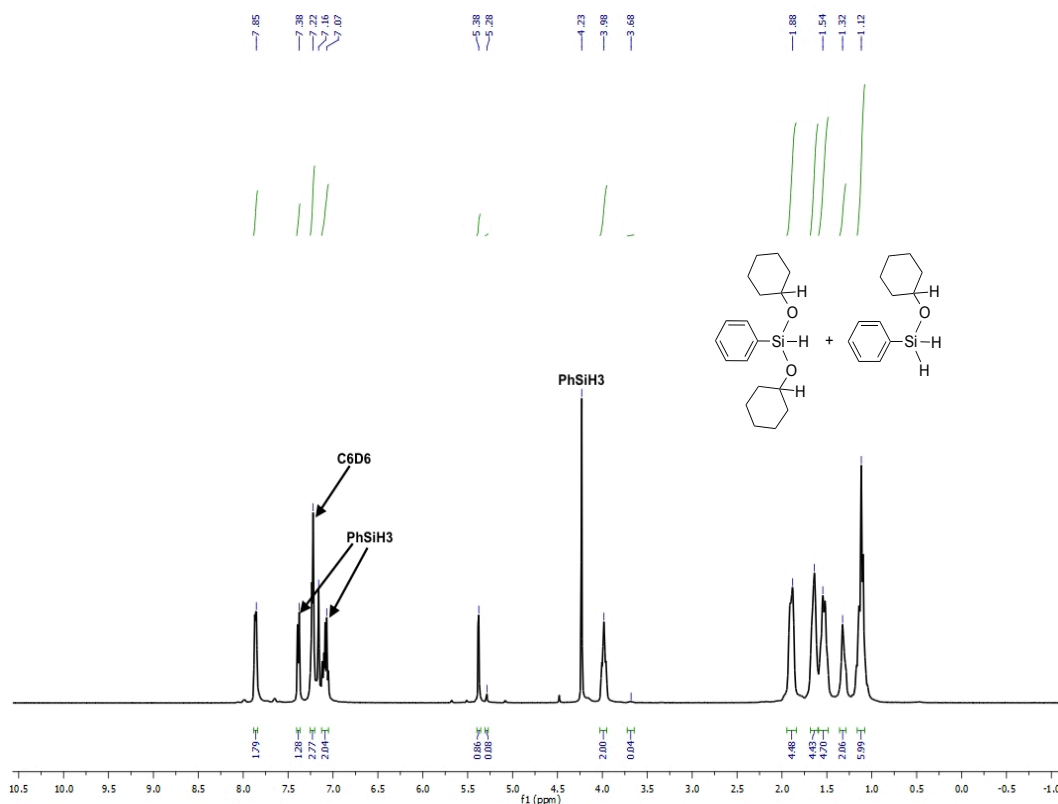


Figure 3.51: ¹H NMR spectrum (benzene-*d*₆) of **16**-catalyzed (0.1 mol%, neat) hydrosilylation of cyclohexanone with PhSiH₃ in the presence of Hg⁰.

Trial for neat hydrosilylation of cyclohexanone with Mn^0 powder (0.1 mol%):

In the glove box, a solution of cyclohexanone (5.84 mL, 56.43 mmol) and PhSiH_3 (6.96 mL, 56.43 mmol) was added to a 20 mL vial containing 3.1 mg (0.05643 mmol) of $\text{Mn}(0)$ powder. The solution remained clear with $\text{Mn}(0)$ powder sitting at the bottom of the vial; no generation of heat was observed. The reaction mixture was stirred for 5 min in the glove box and then exposed to air. The resulting clear solution was filtered through Celite immediately. ^1H NMR data was recorded upon dissolving 3-4 drops of the clear solution in benzene- d_6 and no conversion of cyclohexanone to hydrosilylated products was observed.

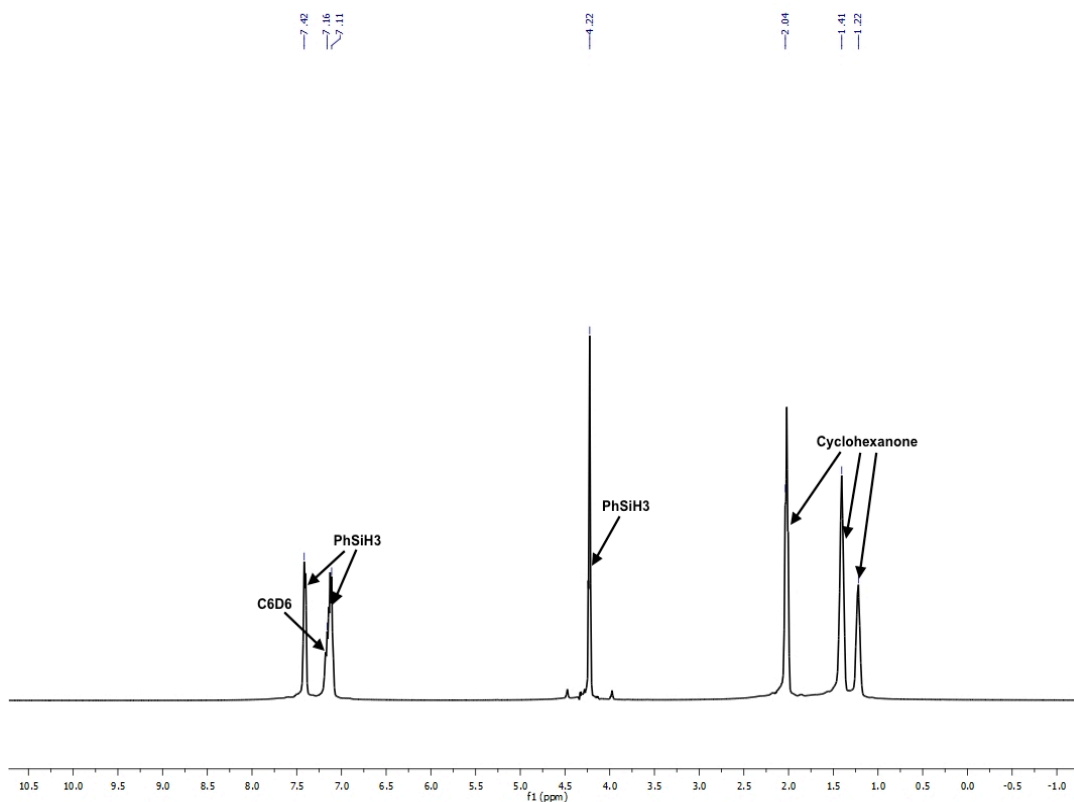


Figure 3.52: ^1H NMR spectrum of unreacted PhSiH_3 and cyclohexanone following exposure to $\text{Mn}(0)$ powder (benzene- d_6).

Trial for neat hydrosilylation of cyclohexanone with (THF)₂MnCl₂ (0.1 mol%):

In the glove box, a solution of cyclohexanone (0.42 mL, 4.07 mmol) and PhSiH₃ (0.50 mL, 4.07 mmol) was added to a 20 mL vial containing 1.1 mg (0.004073 mmol) of (THF)₂MnCl₂. The solution remained clear with (THF)₂MnCl₂ sitting at the bottom of the vial, no generation of heat was observed. The reaction mixture was stirred for 5 min in the glove box and then exposed to air. The resulting clear solution was filtered through Celite immediately. ¹H NMR data was recorded upon dissolving 3-4 drops of the clear solution in benzene-*d*₆ and no conversion of cyclohexanone to hydrosilylated products was observed.

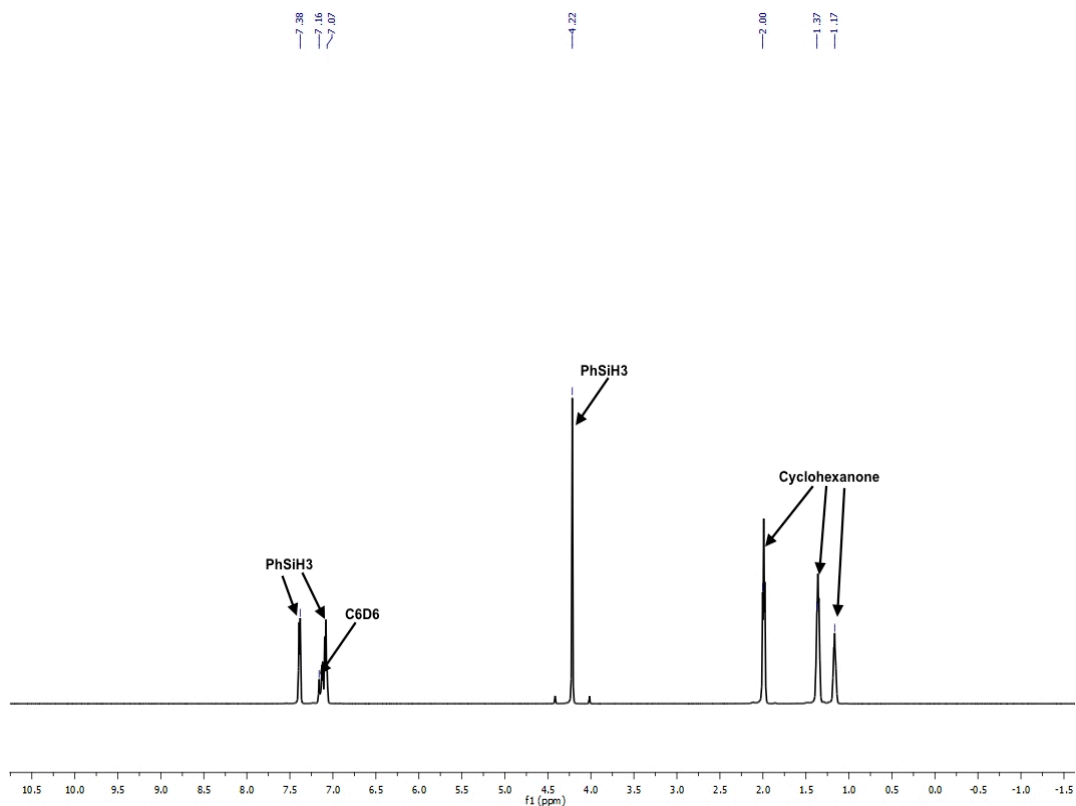


Figure 3.53: ¹H NMR spectrum of unreacted PhSiH₃ and cyclohexanone following exposure to (THF)₂MnCl₂ (benzene-*d*₆).

Trial for neat hydrosilylation of cyclohexanone with (^{PyEt}PDI)MnCl₂ (0.1 mol% **15):**

In the glove box, a solution of cyclohexanone (0.39 mL, 3.82 mmol) and PhSiH₃ (0.47 mL, 3.82 mmol) was added to a 20 mL vial containing 1.9 mg (0.00382 mmol) of **1**. The solution turned into pale orange in color, but no generation of heat was observed. The reaction mixture was stirred for 5 min in the glove box and then exposed to air. The resulting clear solution was filtered through Celite immediately. ¹H NMR data was recorded upon dissolving 3-4 drops of the clear solution in benzene-*d*₆ and no conversion of cyclohexanone to hydrosilylated products was observed.

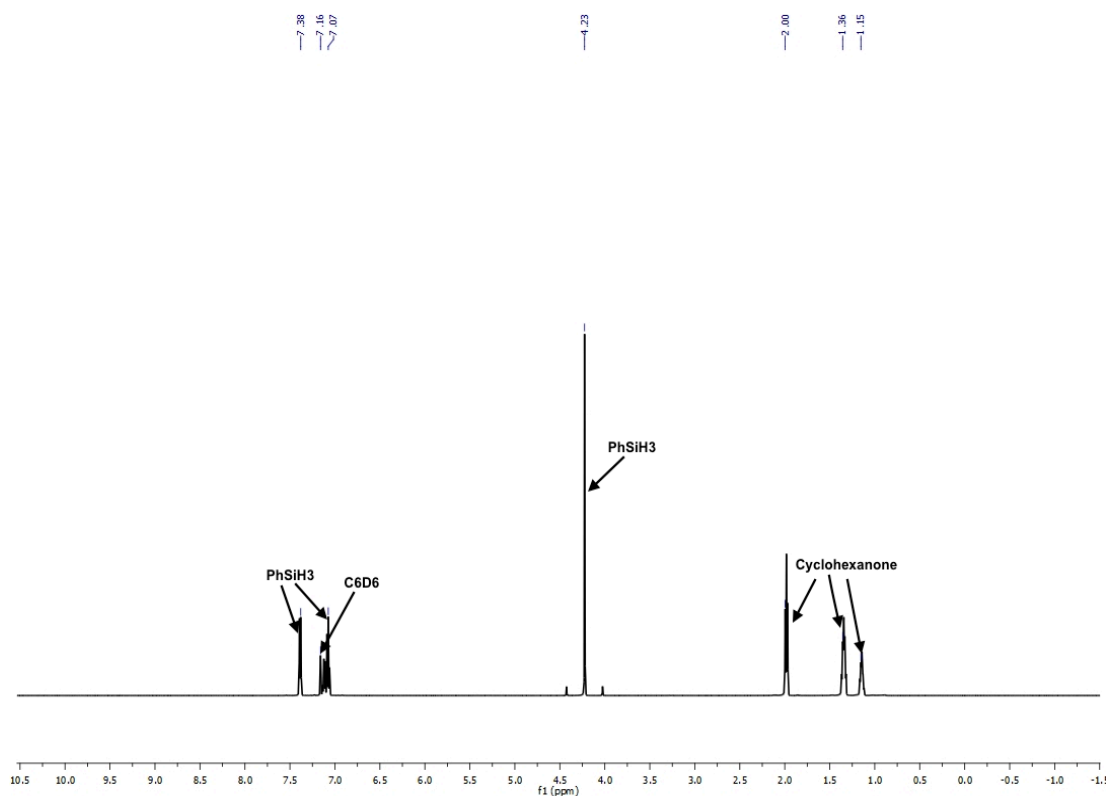


Figure 3.54: ¹H NMR spectrum of unreacted PhSiH₃ and cyclohexanone following exposure to **15** (benzene-*d*₆).

Trial for neat hydrosilylation of cyclohexanone with 2,2'-azobis(2-methylpropionitrile) (0.1 mol%):

In the glove box, a solution of cyclohexanone (1.07 mL, 10.35 mmol) and PhSiH_3 (1.27 mL, 10.35 mmol) was added to a 20 mL vial containing 1.7 mg (0.01035 mmol) of 2,2'-azobis(2-methylpropionitrile). No generation of heat was observed. The reaction mixture was stirred for 5 min in the glovebox and then exposed to air. The resulting clear solution was filtered through Celite immediately. ^1H NMR data was recorded by dissolving 3-4 drops of the clear solution in benzene- d_6 and no conversion of cyclohexanone to hydrosilylated products was observed. This experiment was then modified such that the reagents were heated to 90 °C for 7 min. No conversion was observed by ^1H NMR spectroscopy.

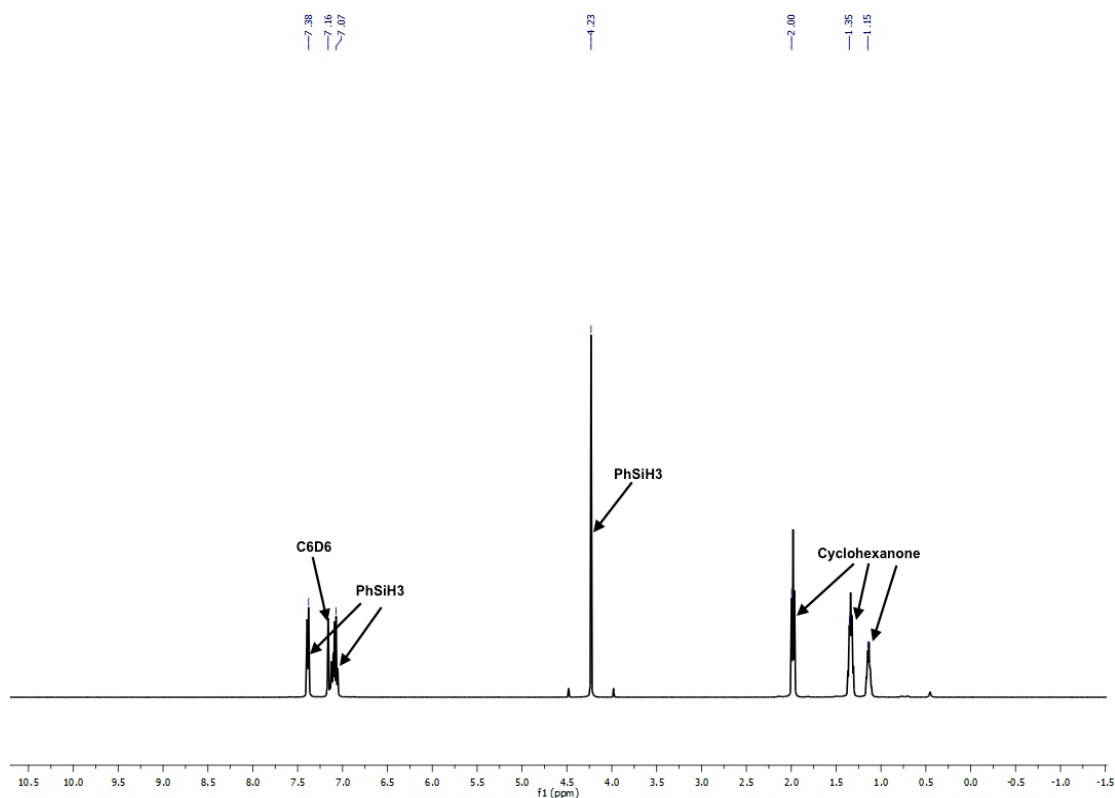


Figure 3.55: ^1H NMR spectrum of unreacted PhSiH_3 and cyclohexanone following exposure to AIBN (5 min at 25 °C, benzene- d_6).

3.8.7. Catalytic Trials Using Complex 18:

Hydrosilylation of benzaldehyde catalyzed by 0.05 mol% 18 (0.1 mol% relative to Mn): This trial was conducted by Tufan K. Mukhopadhyay.

In the glove box, a neat mixture of PhSiH₃ (0.347 mL, 2.81 mmol) and benzaldehyde (0.286 mL, 2.81 mmol) was added to 0.0018 g (0.0014 mmol) of **18** pre-weighed into a 20 mL vial. The resulting red solution vigorously bubbled and became hot. It was stirred for 2 min and then exposed to air to deactivate the catalyst. The colorless solution was filtered through Celite and a ¹H NMR spectrum was recorded to determine the percent conversion. The products were hydrolyzed with 2 mL aqueous 10% NaOH at room temperature for 2 h. The organic fraction was extracted with diethyl ether (3 x 4 mL) and the organic layer was dried over anhydrous Na₂SO₄. Removal of the solvent on a rotavap afforded a colorless oil identified as benzyl alcohol (0.281 g, 2.61 mmol, yield = 93%). ¹H NMR (benzene-*d*₆): 7.08-7.15 (5H, m, *phenyl*), 4.32 (2H, s, CH₂OH). ¹³C NMR (benzene-*d*₆): 142.14, 128.91, 127.80, 127.42, 65.26.

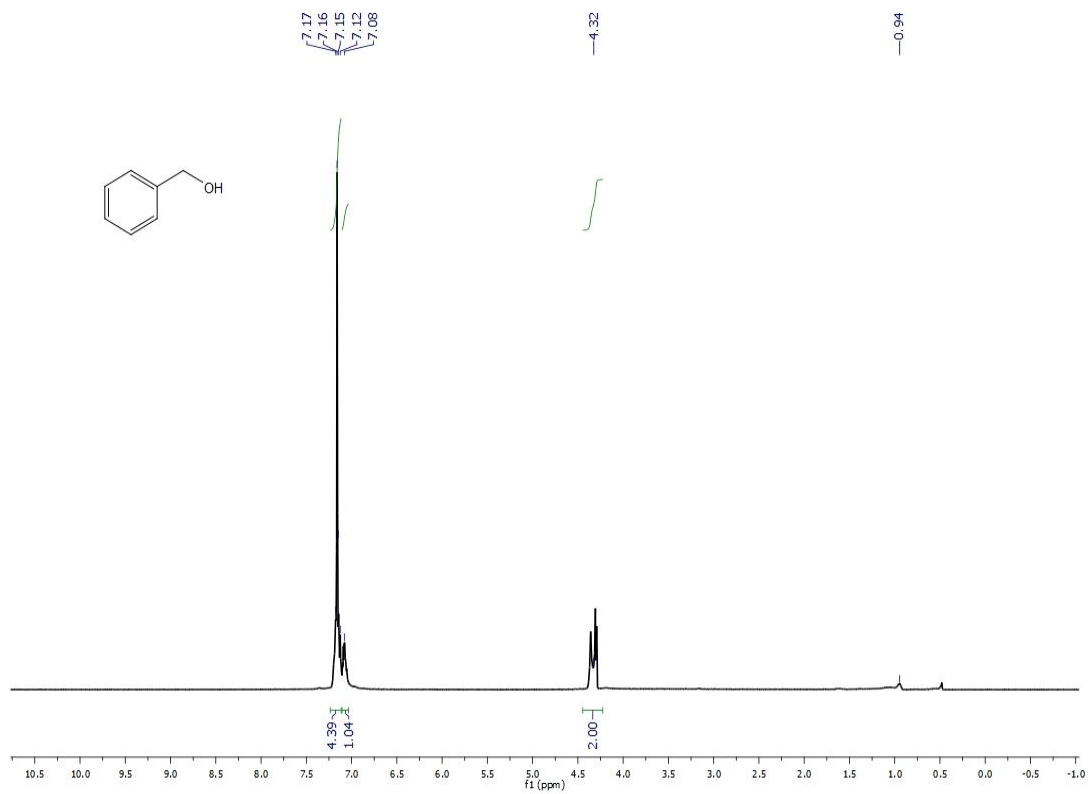


Figure 3.56: ^1H NMR spectrum of benzyl alcohol in benzene- d_6 .

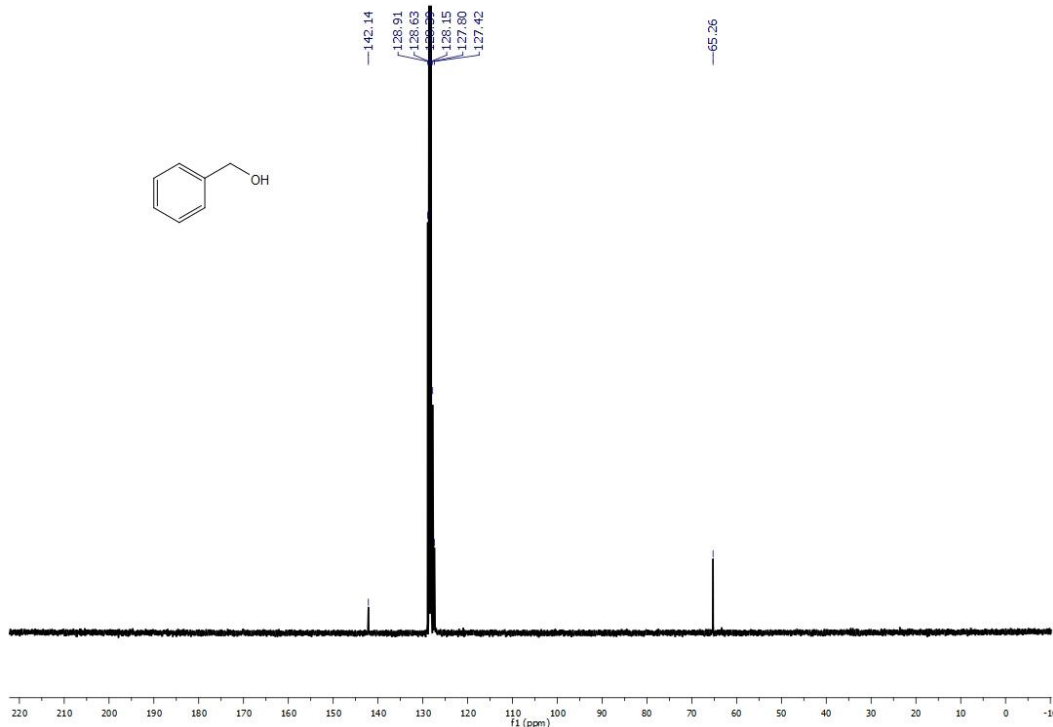


Figure 3.57: ^{13}C NMR spectrum of benzyl alcohol in benzene- d_6 .

Hydrosilylation of 4-fluorobenzaldehyde catalyzed by 0.05 mol% **18 (0.1 mol% relative to Mn):** This trial was conducted by Tufan K. Mukhopadhyay.

In the glove box, a neat mixture of PhSiH_3 (0.365 mL, 2.96 mmol) and 4-fluorobenzaldehyde (0.319 mL, 2.96 mmol) was added to 0.0019 g (0.0015 mmol) of **18** pre-weighed in a 20 mL vial. The resulting brown solution vigorously bubbled and became hot. It was stirred for 2 min and then exposed to air to deactivate the catalyst. The colorless solution was filtered through Celite and a ^1H NMR spectrum was recorded to determine the percent conversion. The products were hydrolyzed with 2 mL aqueous 10% NaOH at room temperature for 2 h. The organic fraction was extracted with diethyl ether (3 x 4 mL) and the organic layer was dried over anhydrous Na_2SO_4 . Removal of the solvent on a rotavap afforded a colorless oil identified as 4-fluorobenzyl alcohol (0.334 g, 2.64 mmol, yield = 90%). ^1H NMR (benzene- d_6): 6.95 (2H, d, *phenyl*), 6.79 (2H, d,

phenyl), 4.21 (2H, s, CH₂OH). ¹³C NMR (benzene-*d*₆): 162.91 (d, ¹J_{CF} = 244 Hz), 137.57, 129.16 (d, ³J_{CF} = 8 Hz), 115.68 (d, ²J_{CF} = 21 Hz), 64.34.

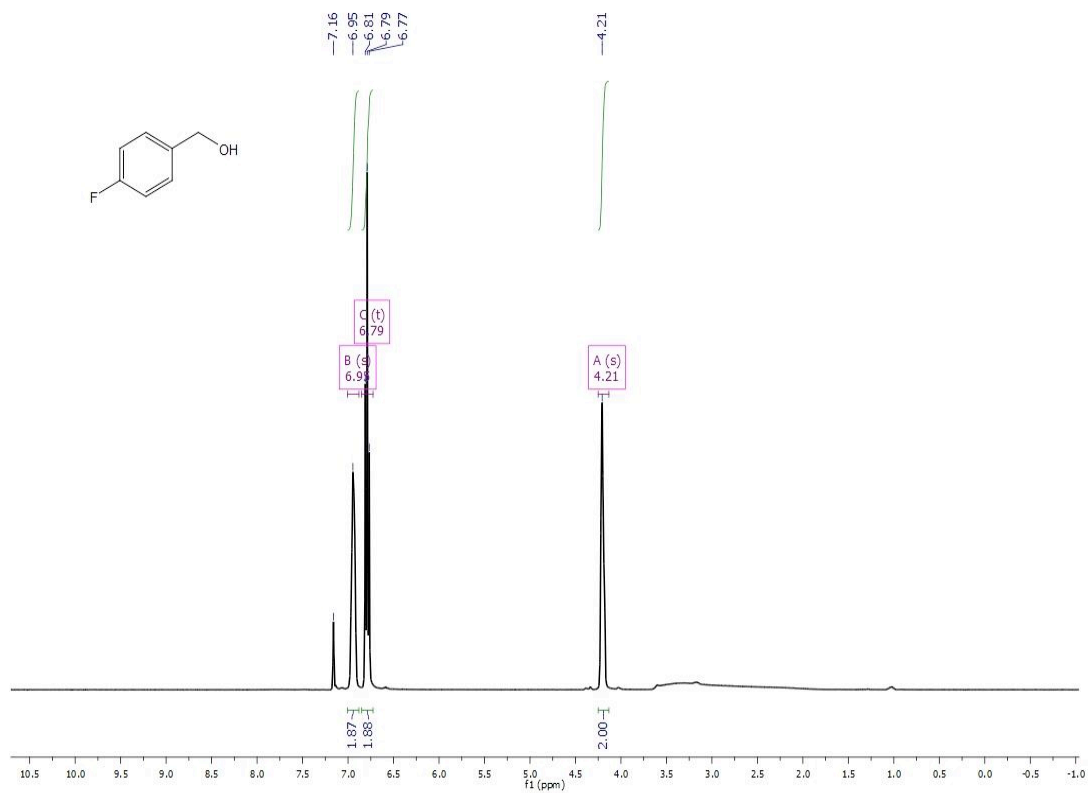


Figure 3.58: ¹H NMR spectrum of 4-fluorobenzyl alcohol in benzene-*d*₆.

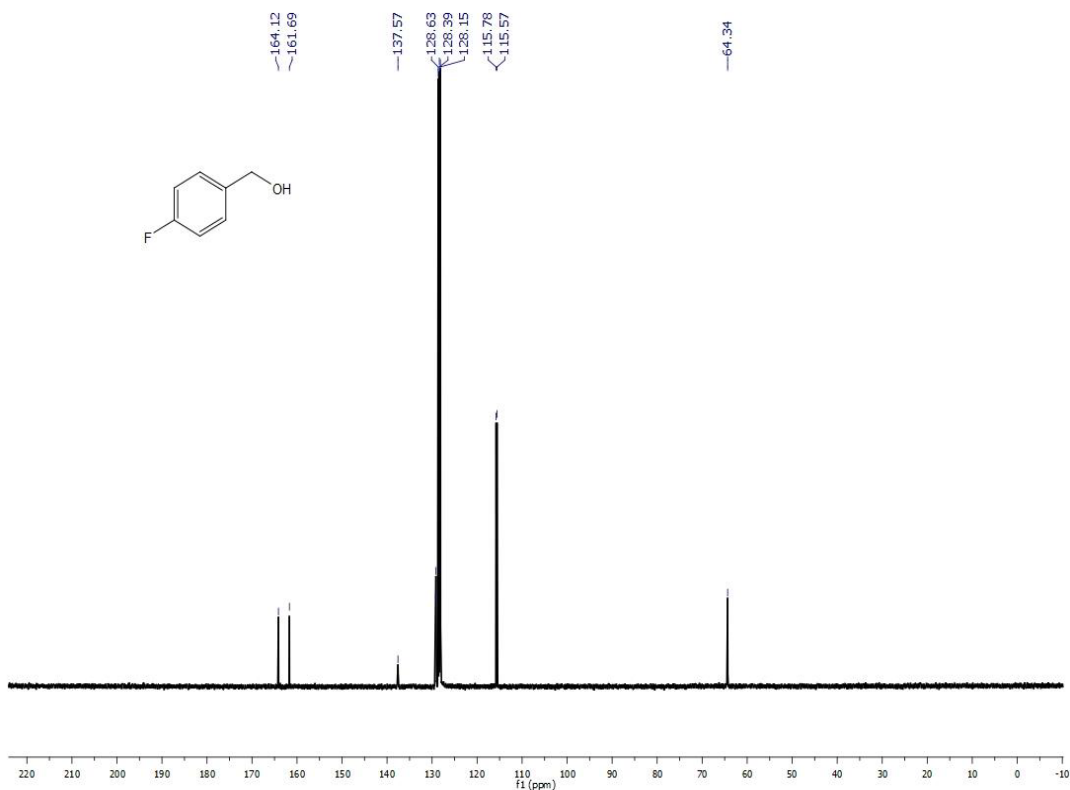


Figure 3.59: ^{13}C NMR spectrum of 4-fluorobenzyl alcohol in benzene- d_6 .

Hydrosilylation of 4-chlorobenzaldehyde catalyzed by 0.05 mol% **18 (0.1 mol% relative to Mn):** This trial was conducted by Tufan K. Mukhopadhyay.

In the glove box, a mixture of PhSiH_3 (0.424 mL, 3.43 mmol) and 4-chlorobenzaldehyde (0.483 g, 3.43 mmol) in 0.5 mL of diethyl ether was added to 0.0022 g (0.0017 mmol) of **18** pre-weighed into a 20 mL vial. The resulting red solution vigorously bubbled and became hot. It was stirred for 2 min and then exposed to air to deactivate the catalyst. The colorless solution was filtered through Celite and a ^1H NMR spectrum was recorded to determine the percent conversion. It was followed by a hydrolytic work up whereby the mixture was stirred with 2 mL aqueous 10% NaOH solution at room temperature for 2 h. The organic fraction was extracted with diethyl ether (3 x 4 mL) and the organic layer was dried over anhydrous Na_2SO_4 . Removal of the solvent on a rotavap afforded a white solid identified as 4-chlorobenzyl alcohol (0.405 g,

2.83 mmol, yield = 83%). ^1H NMR (benzene- d_6): 7.08 (2H, d, *phenyl*), 6.83 (2H, d, *phenyl*), 4.10 (2H, s, CH_2OH). $\{^1\text{H}\}^{13}\text{C}$ NMR (benzene- d_6): 140.50, 133.60, 129.02, 128.63, 64.41. Melting Point: 71.1-72.3 °C (colorless crystalline solid).

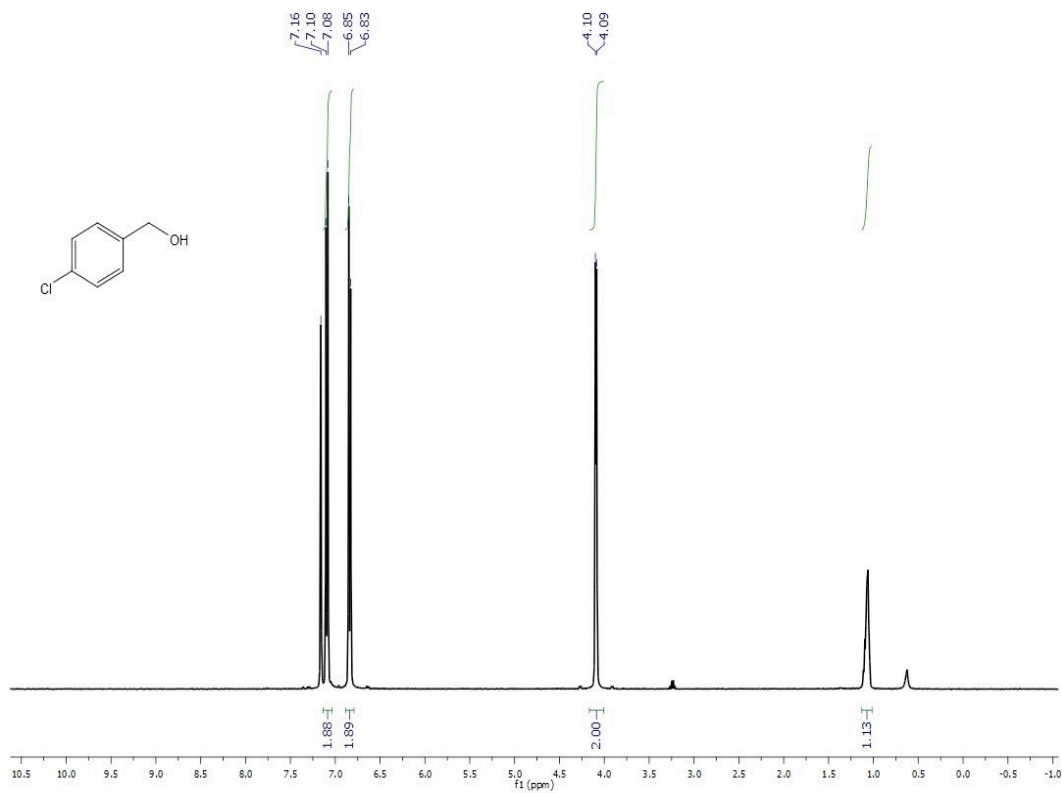


Figure 3.60: ^1H NMR spectrum of 4-chlorobenzyl alcohol in benzene- d_6 .

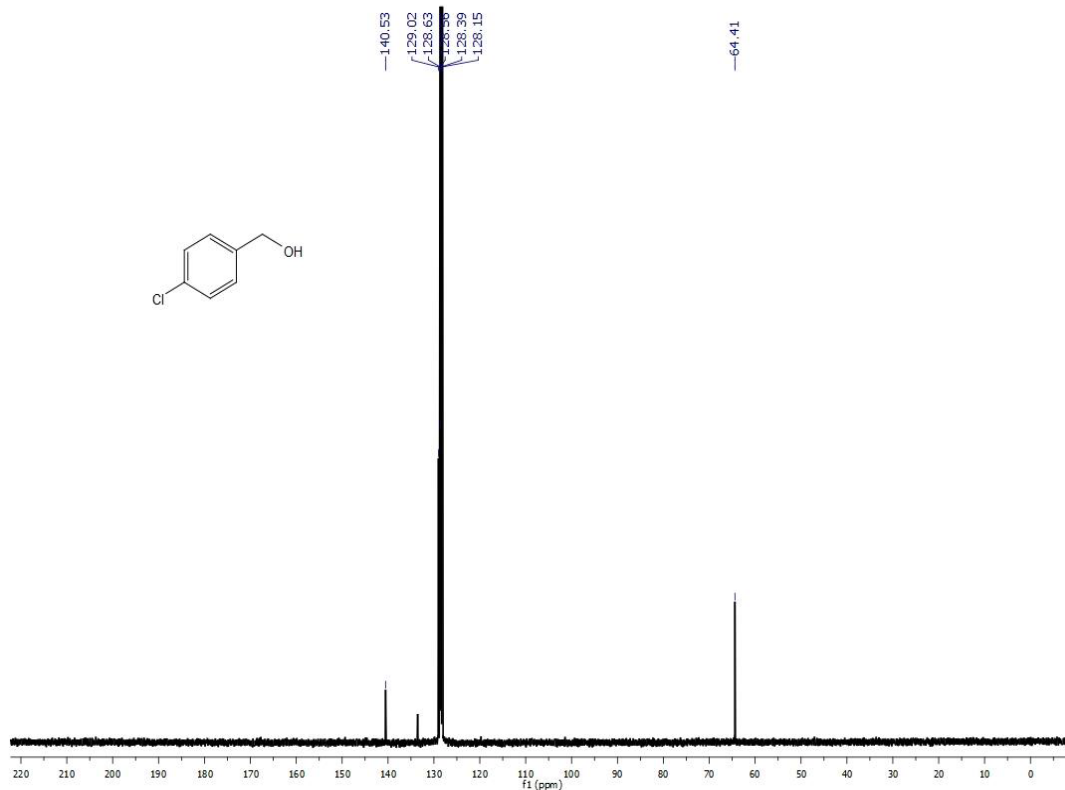


Figure 3.61: ^{13}C NMR spectrum of 4-chlorobenzyl alcohol in benzene- d_6 .

Hydrosilylation of 4-bromobenzaldehyde catalyzed by 0.05 mol% **18 (0.1 mol% relative to Mn):** This trial was conducted by Tufan K. Mukhopadhyay.

In the glove box, a mixture of PhSiH_3 (0.424 mL, 3.43 mmol) and 4-bromobenzaldehyde (0.635 g, 3.43 mmol) in 0.5 mL diethyl ether was added to 0.0022 g (0.0017 mmol) of **18** pre-weighed into a 20 mL vial. The resulting brown solution vigorously bubbled and became hot. It was stirred for 2 min and then exposed to air to deactivate the catalyst. The colorless solution was filtered through Celite and a ^1H NMR spectrum was recorded to determine the percent conversion. It was followed by a hydrolytic work up whereby the mixture was stirred with 2 mL aqueous 10% NaOH solution at room temperature for 2 h. The organic fraction was extracted with diethyl ether (3 x 4 mL) and the organic layer was dried over anhydrous Na_2SO_4 . Removal of the solvent on a rotavap afforded a white solid identified as 4-bromobenzyl alcohol (0.536 g,

2.87 mmol, yield = 83%). ^1H NMR (benzene- d_6): 7.23 (2H, d, *phenyl*), 6.76 (2H, d, *phenyl*), 4.07 (2H, s, CH_2OH), 1.36 (1H, s, CH_2OH). ^{13}C NMR (benzene- d_6): 140.94, 131.50, 121.66, 64.41, one resonance not located. Melting Point: 77.1-78.4 °C (colorless crystalline solid).

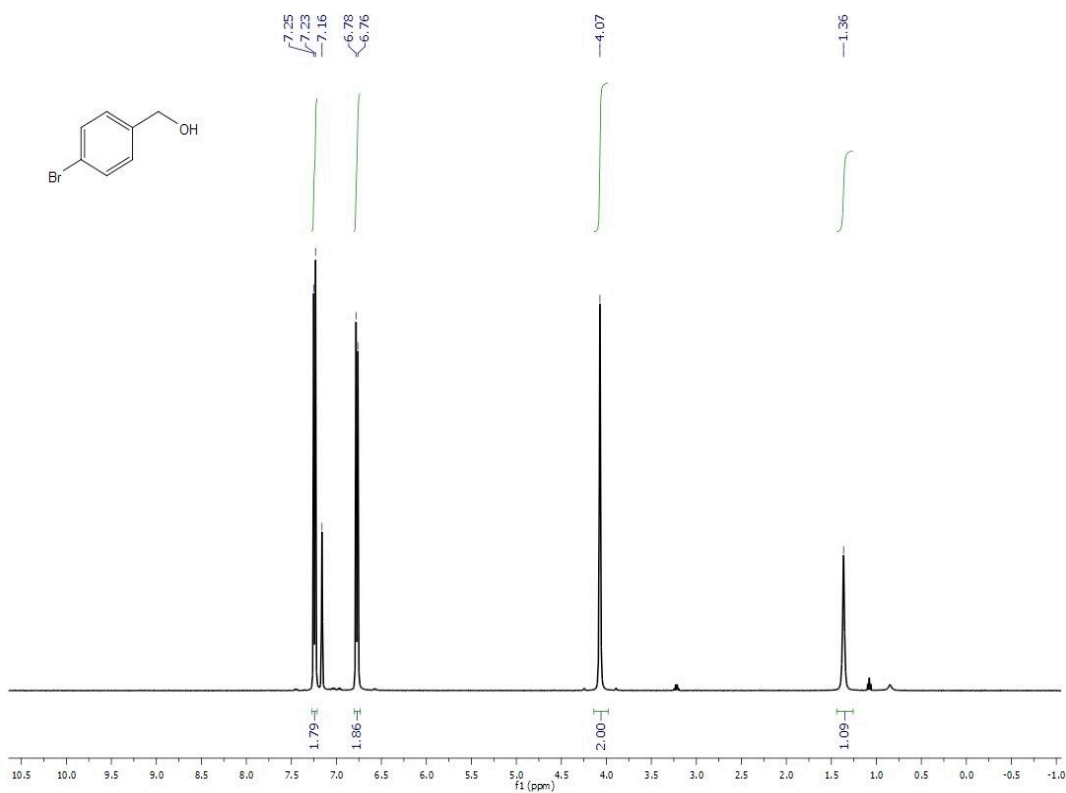


Figure 3.62: ^1H NMR spectrum of 4-bromobenzyl alcohol in benzene- d_6 .

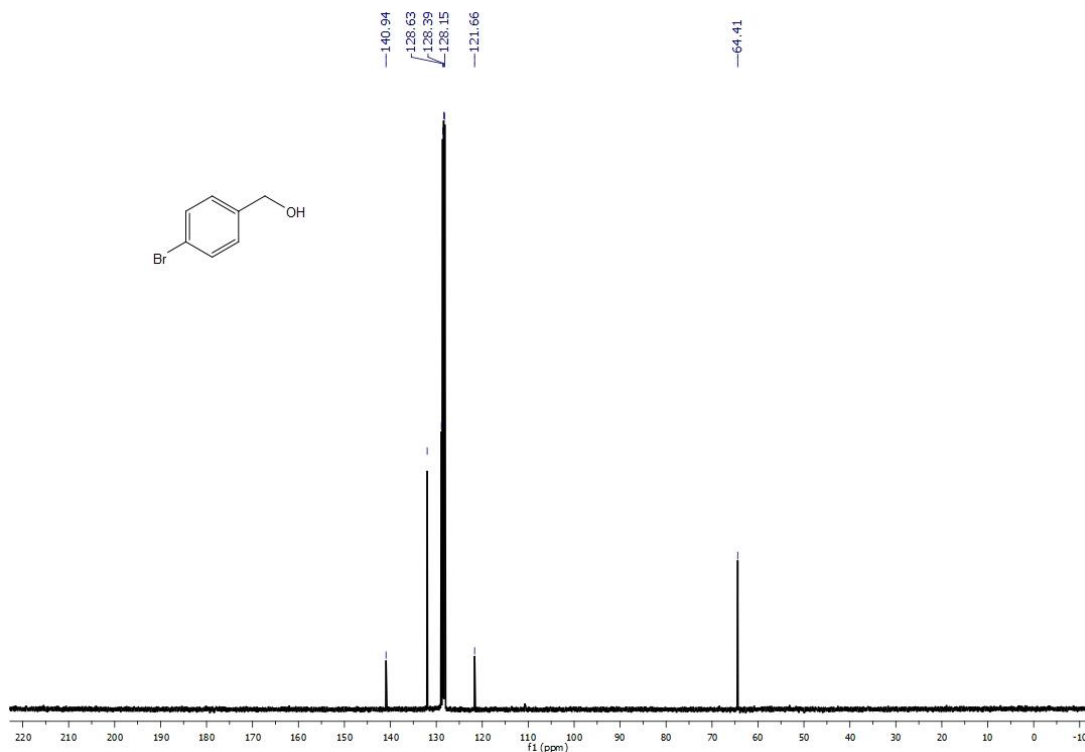


Figure 3.63: ¹³C NMR spectrum of 4-bromobenzyl alcohol in benzene-*d*₆.

Attempt to hydrosilylate 4-iodobenzaldehyde using 0.05 mol% **18 (0.1 mol% relative to Mn):** This trial was conducted by Tufan K. Mukhopadhyay.

In the glove box, a mixture of PhSiH₃ (0.385 mL, 3.12 mmol) and 4-iodobenzaldehyde (0.724 g, 3.12 mmol) in 0.5 mL toluene was added to 0.002 g (0.0016 mmol) of **18** pre-weighed into a 20 mL vial. The resulting solution was stirred for 2 min and then exposed to air to deactivate the catalyst. The solution was then filtered through Celite and ¹H NMR spectroscopy revealed no conversion.

Hydrosilylation of 2-nitrobenzaldehyde catalyzed by 0.05 mol% **18 (0.1 mol% relative to Mn):** This trial was conducted by Tufan K. Mukhopadhyay.

In the glove box, a neat mixture of PhSiH₃ (0.327 mL, 2.65 mmol) and 2-nitrobenzaldehyde (0.400 g, 2.65 mmol) was added to 0.0017 g (0.0013 mmol) of **18** pre-weighed into a 20 mL vial. The resulting brown solution vigorously bubbled and became hot. It was stirred for 2 min and then exposed to air to deactivate the catalyst. The

colorless solution was filtered through Celite and a ^1H NMR spectrum was recorded to determine the percent conversion. It was followed by a hydrolytic work up whereby the mixture was stirred with 2 mL aqueous 10% NaOH solution at room temperature for 2 h. The organic fraction was extracted with diethyl ether (3 x 4 mL) and the organic layer was dried over anhydrous Na_2SO_4 . Removal of the diethyl ether on a rotavap afforded a pale-yellow solid identified as 2-nitrobenzyl alcohol (0.322 g, 2.17 mmol, yield = 79%). ^1H NMR (benzene- d_6): 7.62 (1H, d, *phenyl*), 7.35 (1H, d, *phenyl*), 6.91 (1H, d, *phenyl*), 6.64 (1H, d, *phenyl*), 4.54 (2H, s, CH_2OH), 1.52 (1H, s, CH_2OH). ^{13}C NMR (benzene- d_6): 137.98, 133.68, 129.20, 127.99, 124.95, 62.27. Melting Point: 70.3-72.1 $^\circ\text{C}$ (orange crystalline solid).

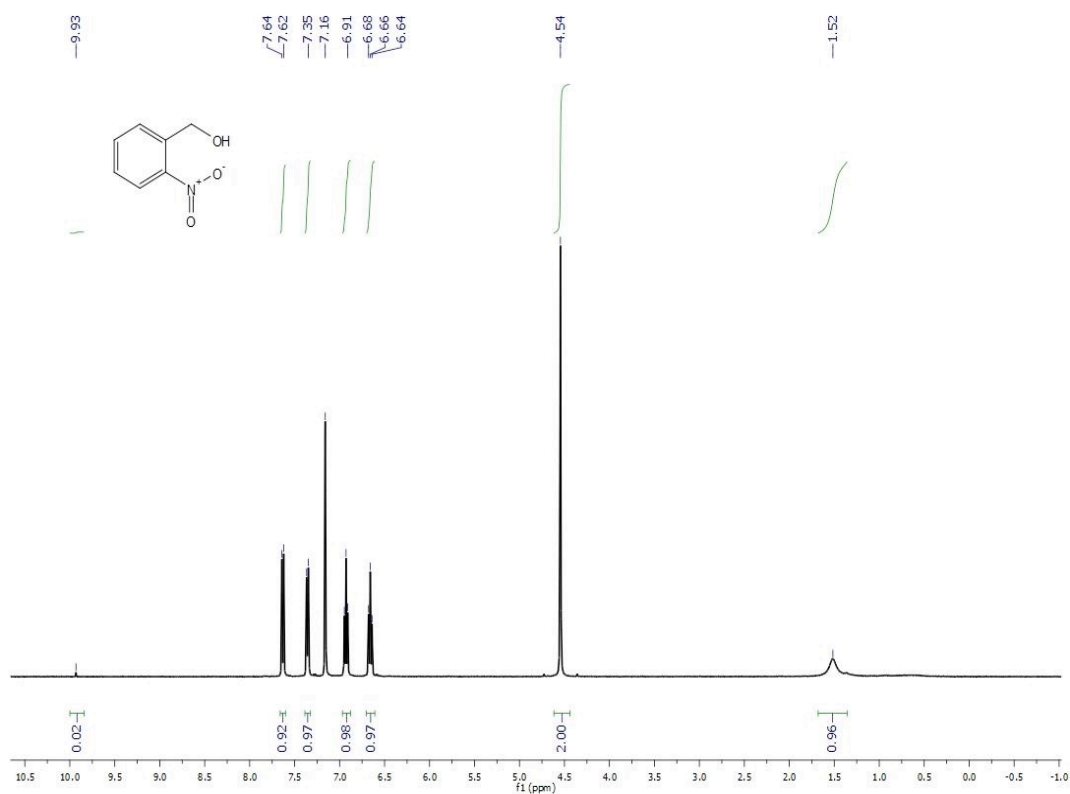


Figure 3.64: ^1H NMR spectrum of 2-nitrobenzyl alcohol in benzene- d_6 .

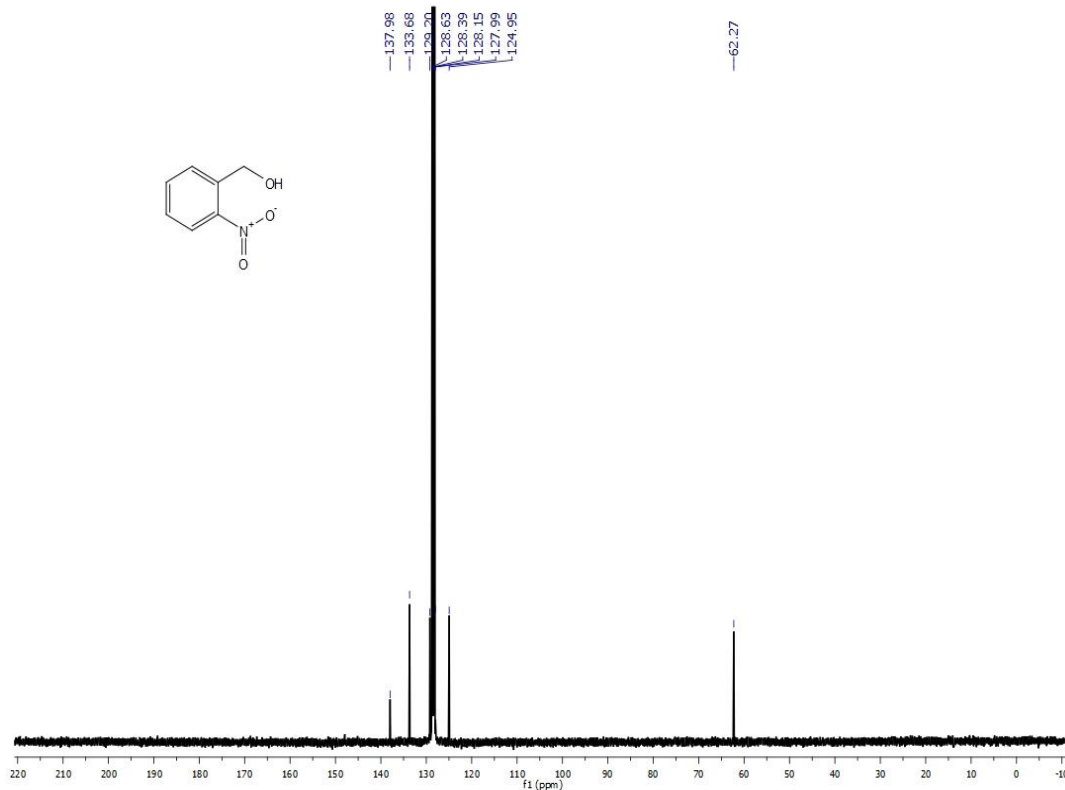


Figure 3.65: ¹³C NMR spectrum of 2-nitrobenzyl alcohol in benzene-*d*₆.

Hydrosilylation of 4-cyanobenzaldehyde catalyzed by 0.05 mol% **18 (0.1 mol% relative to Mn):** This trial was conducted by Tufan K. Mukhopadhyay.

In the glove box, a mixture of PhSiH₃ (0.347 mL, 2.81 mmol) and 4-cyanobenzaldehyde (0.368 g, 2.81 mmol) was added to 0.0018 g (0.0014 mmol) of **18** pre-weighed into a 20 mL vial. The resulting brown solution vigorously bubbled and became hot. It was stirred for 2 min and then exposed to air to deactivate the catalyst. The colorless solution was filtered through Celite and a ¹H NMR spectrum was recorded to determine the percent conversion. It was followed by a hydrolytic work up whereby the mixture was stirred with 2 mL aqueous 10% NaOH solution at room temperature for 2 h. The organic fraction was extracted with diethyl ether (3 x 4 mL) and the organic layer was dried over anhydrous Na₂SO₄. Removal of the diethyl ether on a rotavap afforded a white solid identified as 4-cyanobenzyl alcohol (0.266 g, 1.997 mmol, yield = 71%).

^1H NMR (benzene- d_6): 7.00 (2H, d, *phenyl*), 6.77 (2H, d, *phenyl*), 4.03 (2H, s, CH_2OH), 1.23 (1H, s, CH_2OH). ^{13}C NMR (benzene- d_6): 146.84, 132.37, 127.02, 119.32, 111.65, 110.69, 63.96. Melting Point: 34.1-37.4 °C (yellow crystalline solid).

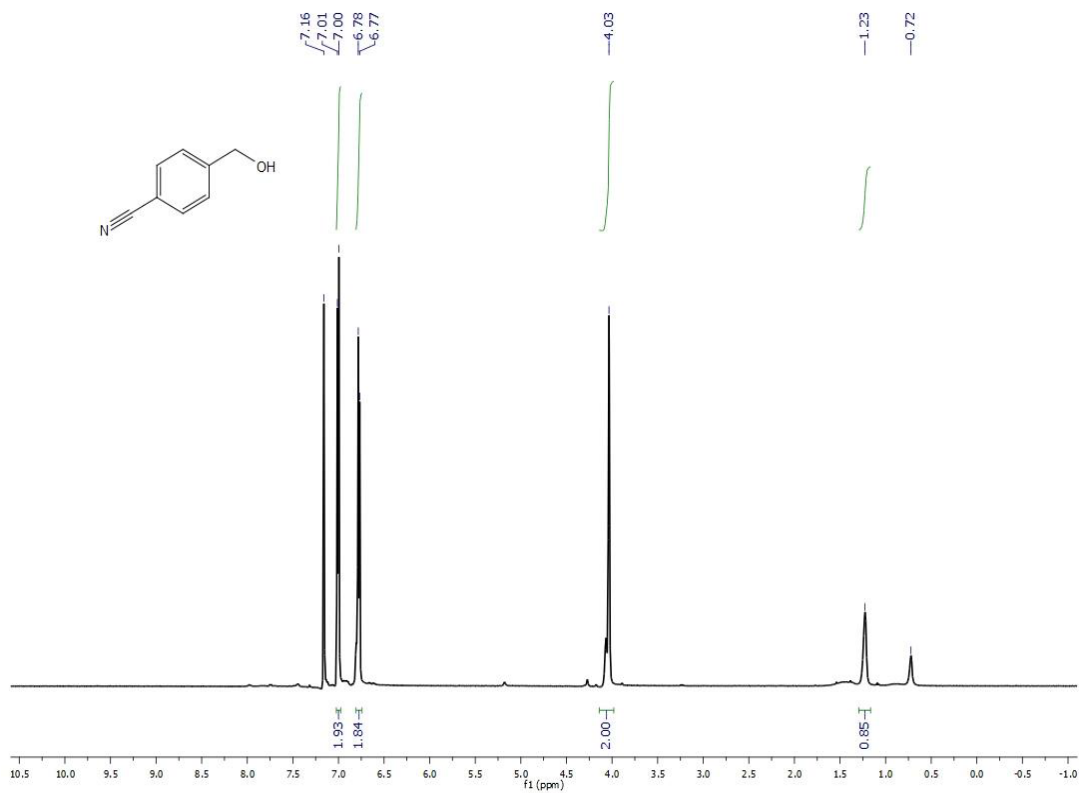


Figure 3.66: ^1H NMR spectrum of 4-cyanobenzyl alcohol in benzene- d_6 .

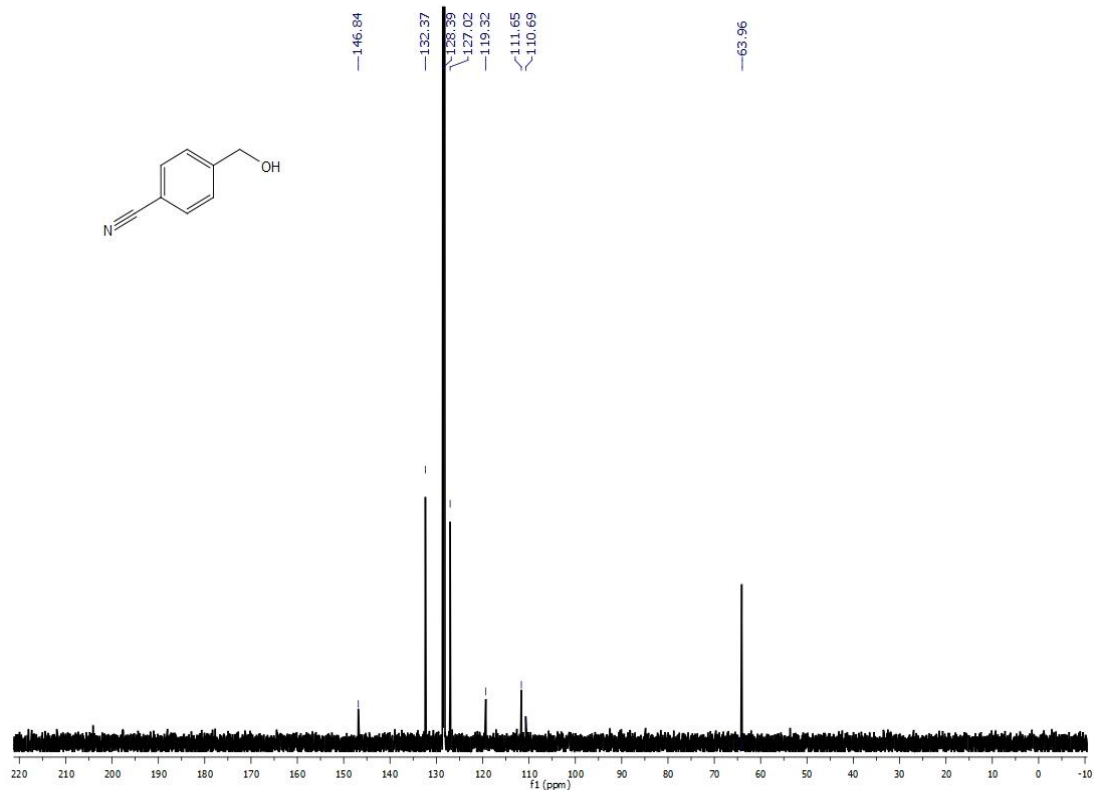


Figure 3.67: ¹³C NMR spectrum of 4-cyanobenzyl alcohol in benzene-*d*₆.

Hydrosilylation of *p*-anisaldehyde catalyzed by 0.05 mol% **18 (0.1 mol% relative to **Mn**):** This trial was conducted by Tufan K. Mukhopadhyay.

In the glove box, a neat mixture of PhSiH₃ (0.424 mL, 3.43 mmol) and *p*-anisaldehyde (0.393 mL, 3.43 mmol) was added to 0.0022 g (0.0017 mmol) of **18** pre-weighed in a 20 mL vial. The resulting brown solution vigorously bubbled and became hot. It was stirred for 2 min and then exposed to air to deactivate the catalyst. The colorless solution was filtered through Celite and a ¹H NMR spectrum was recorded to determine the percent conversion. It was followed by a hydrolytic work up whereby the mixture was stirred with 2 mL aqueous 10% NaOH solution at room temperature for 2 h. The organic fraction was extracted with diethyl ether (3 x 4 mL) and the organic layer was dried over anhydrous Na₂SO₄. Removal of the diethyl ether on a rotavap afforded colorless oil identified as 4-methoxybenzyl alcohol (0.406 g, 2.94 mmol, yield = 86%).

^1H NMR (benzene- d_6): 7.13 (2H, d, *phenyl*), 6.76 (2H, d, *phenyl*), 4.38 (2H, s, CH_2OH), 3.31 (3H, s, OCH_3), 2.56 (1H, s, CH_2OH). ^{13}C NMR (benzene- d_6): 159.85, 134.35, 114.44, 65.01, 55.15.

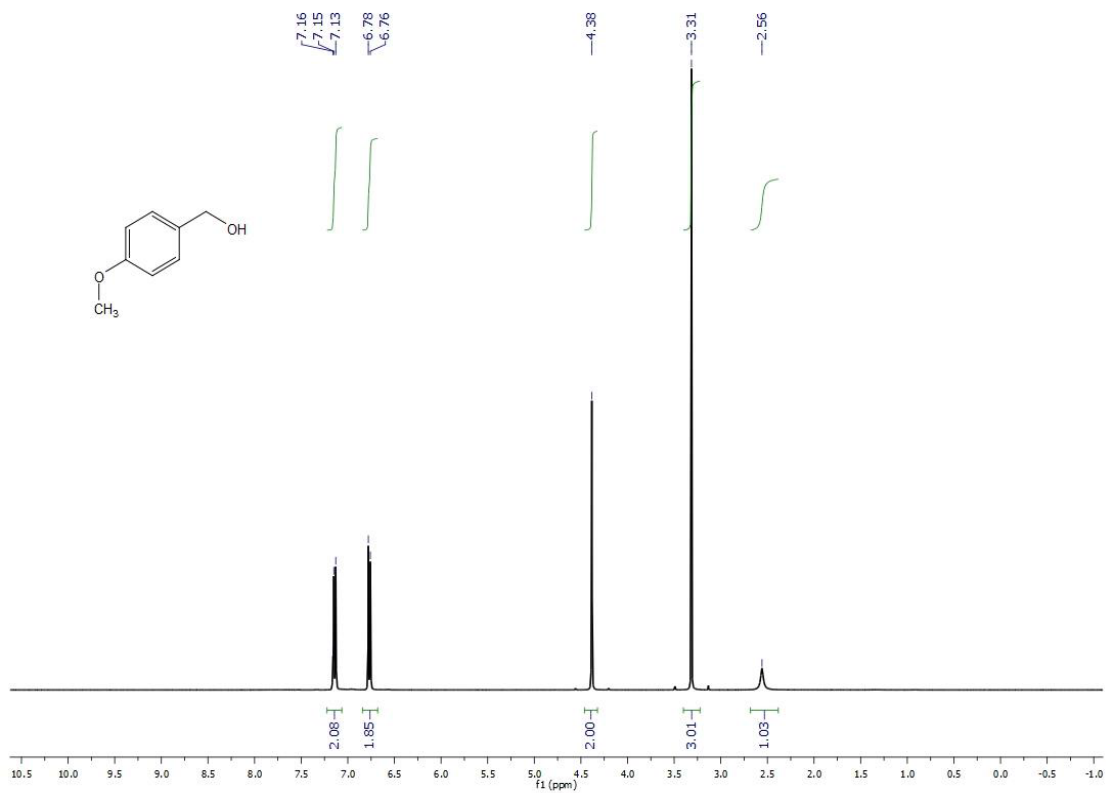


Figure 3.68: ^1H NMR spectrum of 4-methoxybenzyl alcohol in benzene- d_6 .

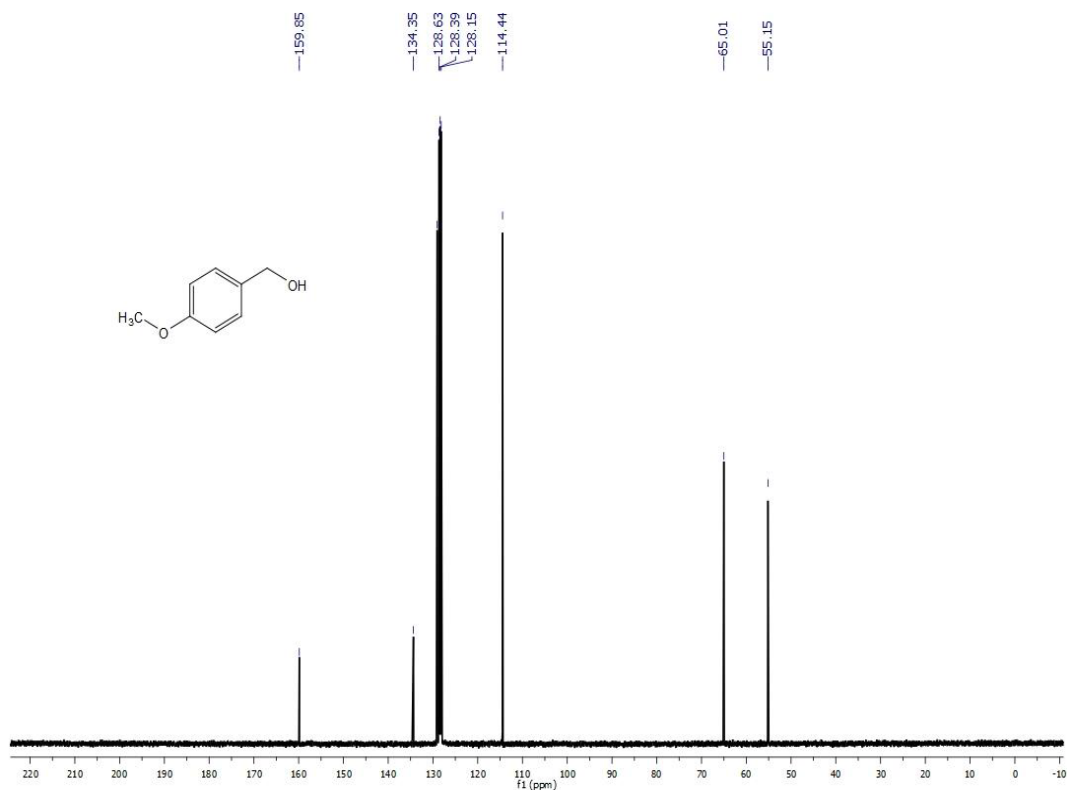


Figure 3.69: ^{13}C NMR spectrum of 4-methoxybenzyl alcohol in benzene- d_6 .

Hydrosilylation of *p*-tolualdehyde catalyzed by 0.05 mol% **18 (0.1 mol% relative to **Mn**):** This trial was conducted by Tufan K. Mukhopadhyay.

In the glove box, a neat mixture of PhSiH_3 (0.347 mL, 2.81 mmol) and *p*-tolualdehyde (0.331 mL, 2.81 mmol) was added to 0.0018 g (0.0014 mmol) of **18** pre-weighed into a 20 mL vial. The resulting brown solution vigorously bubbled and became hot. It was stirred for 2 min and then exposed to air to deactivate the catalyst. The colorless solution was filtered through Celite and a ^1H NMR spectrum was recorded to determine the percent conversion. It was followed by a hydrolytic work up whereby the mixture was stirred with 2 mL aqueous 10% NaOH solution at room temperature for 2 h. The organic fraction was extracted with diethyl ether (3 x 4 mL) and the organic layer was dried over anhydrous Na_2SO_4 . Removal of the diethyl ether on a rotavap afforded a white solid identified as 4-methylbenzyl alcohol (0.303 g, 2.48 mmol, yield = 88%).

^1H NMR (benzene- d_6): 7.11 (2H, d, *phenyl*), 6.98 (2H, d, *phenyl*), 4.35 (2H, s, CH_2OH), 2.12 (3H, s, CH_3), 1.48 (1H, s, CH_2OH). ^{13}C NMR (benzene- d_6): 139.35, 137.20, 129.62, 127.52, 65.29, 21.46. Melting Point: 59.9-61.2 $^\circ\text{C}$ (colorless crystalline solid).

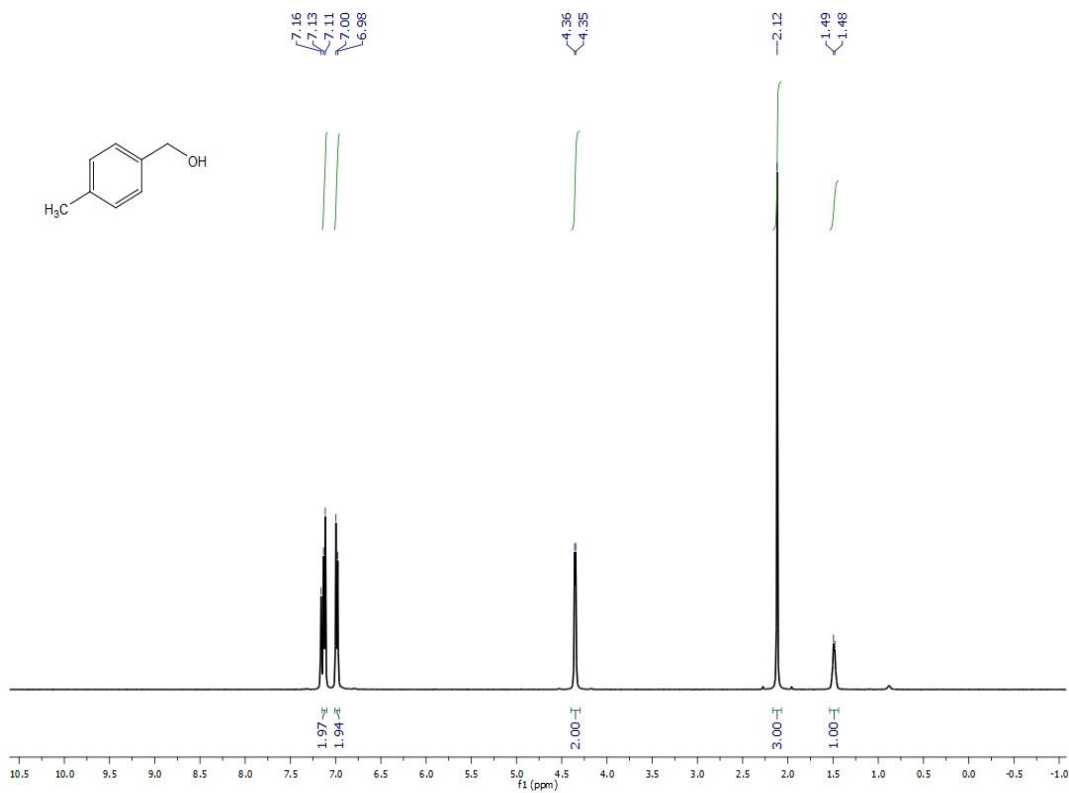


Figure 3.70: ^1H NMR spectrum of 4-methylbenzyl alcohol in benzene- d_6 .

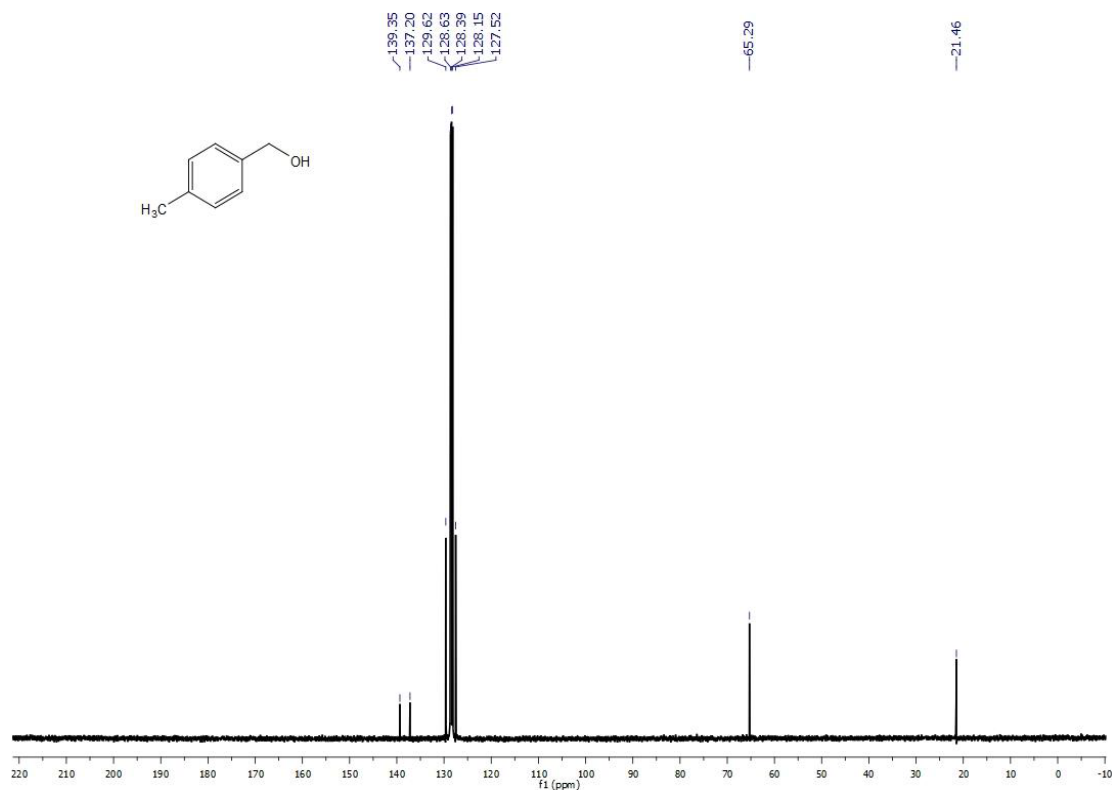


Figure 3.71: ¹³C NMR spectrum of 4-methylbenzyl alcohol in benzene-*d*₆.

Hydrosilylation of 2-naphthaldehyde catalyzed by 0.05 mol% **18 (0.1 mol% relative to Mn):** This trial was conducted by Tufan K. Mukhopadhyay.

In the glove box, a mixture of PhSiH₃ (0.289 mL, 2.34 mmol) and 2-naphthaldehyde (0.365 g, 2.34 mmol) in 0.5 mL toluene was added to 0.0015 g (0.0012 mmol) of **18** pre-weighed into a 20 mL vial. The resulting brown solution vigorously bubbled and became hot. It was stirred for 2 min and then exposed to air to deactivate the catalyst. The colorless solution was filtered through Celite and a ¹H NMR spectrum was recorded to determine the percent conversion. It was followed by a hydrolytic work up whereby the mixture was stirred with 2 mL aqueous 10% NaOH solution at room temperature for 2 h. The organic fraction was extracted with diethyl ether (3 x 4 mL) and the organic layer was dried over anhydrous Na₂SO₄. Removal of the diethyl ether on a rotavap afforded a white solid identified as 2-naphthalenemethanol (0.344 g, 2.18 mmol,

yield = 93%). ^1H NMR (benzene- d_6): 8.01-7.96 (1H, m, *phenyl*), 7.68 (1H, s, *phenyl*), 7.52-7.47 (1H, m, *phenyl*), 7.38 (1H, m, *phenyl*), 7.26 (1H, d, *phenyl*), 7.20 (2H, m, *phenyl*), 5.04 (2H, s, CH_2OH), 4.45 (1H, s, CH_2OH). ^{13}C NMR (benzene- d_6): 138.37, 135.86, 134.27, 133.78, 131.46, 131.10, 126.61, 126.31, 126.08, 125.75, 66.03. Melting Point: 79.5-80.6 $^\circ\text{C}$ (colorless crystalline solid).

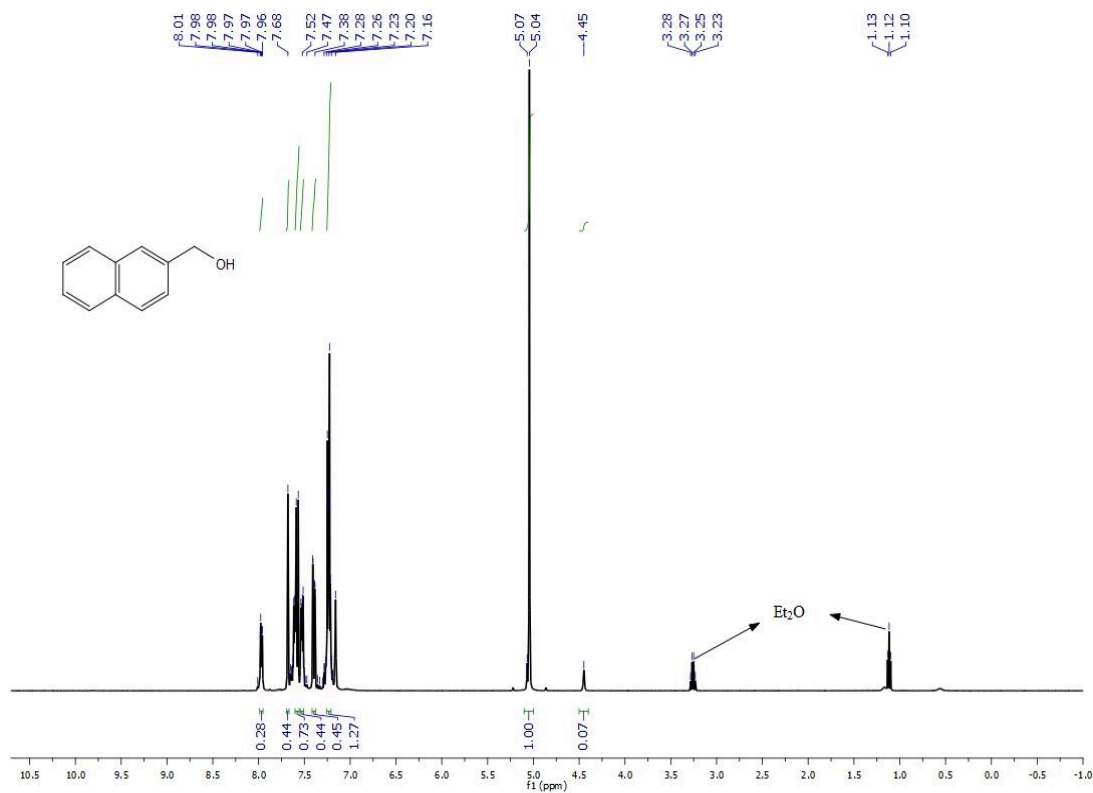


Figure 3.72: ^1H NMR spectrum of 2-naphthalenemethanol in benzene- d_6 .

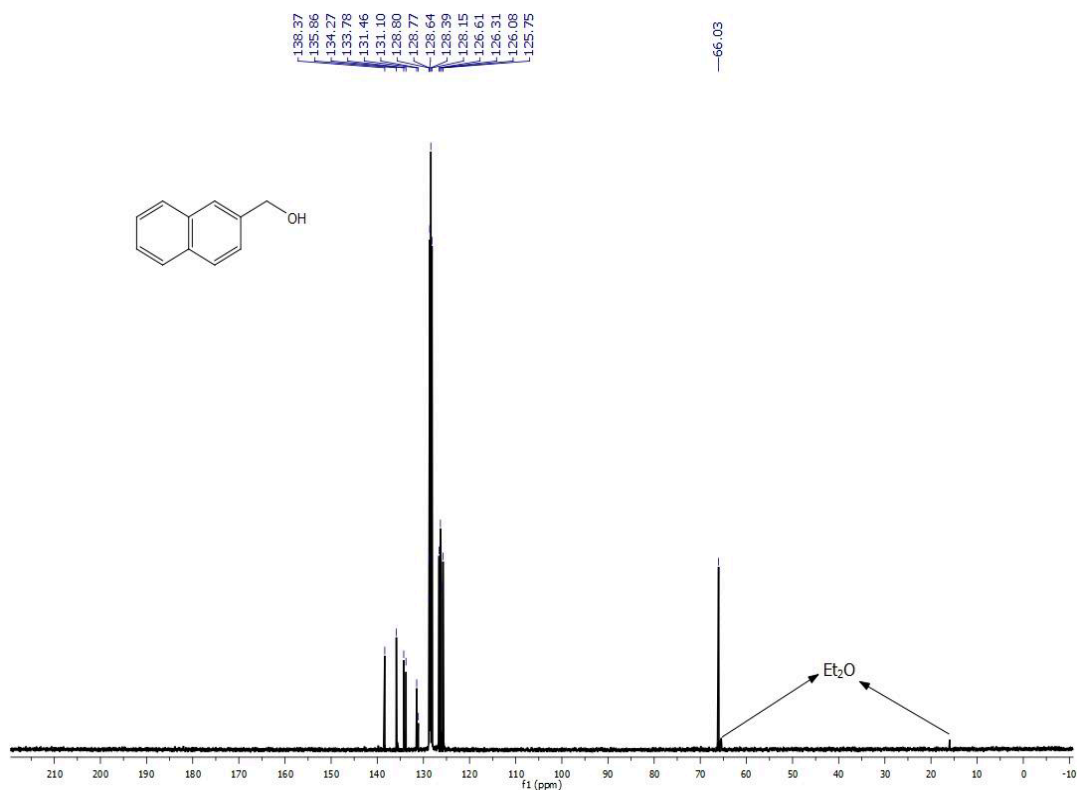


Figure 3.73: ^{13}C NMR spectrum of 2-naphthalenemethanol in benzene- d_6 .

Hydrosilylation of pyridine-3-carboxaldehyde catalyzed by 0.05 mol% **18 (0.1 mol% relative to Mn):** This trial was conducted by Tufan K. Mukhopadhyay.

In the glove box, a neat mixture of PhSiH_3 (0.424 mL, 3.43 mmol) and pyridine-3-carboxaldehyde (0.322 mL, 3.43 mmol) was added to 0.0022 g (0.0017 mmol) of **18** pre-weighed in a 20 mL vial. The resulting brown solution became warm. It was stirred for 2 min and then exposed to air to deactivate the catalyst. The colorless solution was filtered through Celite and a ^1H NMR spectrum was recorded to determine the percent conversion, which revealed 88% substrate conversion to mono-, di-, and trihydrosilylated products in a 1:1:1 ratio. It was followed by a hydrolytic work up whereby the mixture was stirred with 2 mL aqueous 10% NaOH solution at room temperature for 2 h. The organic fraction was extracted with diethyl ether (3 x 4 mL) and the organic layer was

dried over anhydrous Na_2SO_4 . Removal of the diethyl ether on a rotavap afforded a white solid identified as pyridine-3-carbinol (0.03 g, 0.275 mmol, yield = 21%). ^1H NMR (benzene- d_6): 8.47 (1H, d, *phenyl*), 8.21 (1H, d, *phenyl*), 7.35 (1H, d, *phenyl*), 6.73-6.70 (1H, m, *phenyl*), 5.27 (1H, br, CH_2OH), 4.41 (2H, s, CH_2OH). ^{13}C NMR (benzene- d_6): 148.70, 138.35, 135.29, 123.94, 62.29.

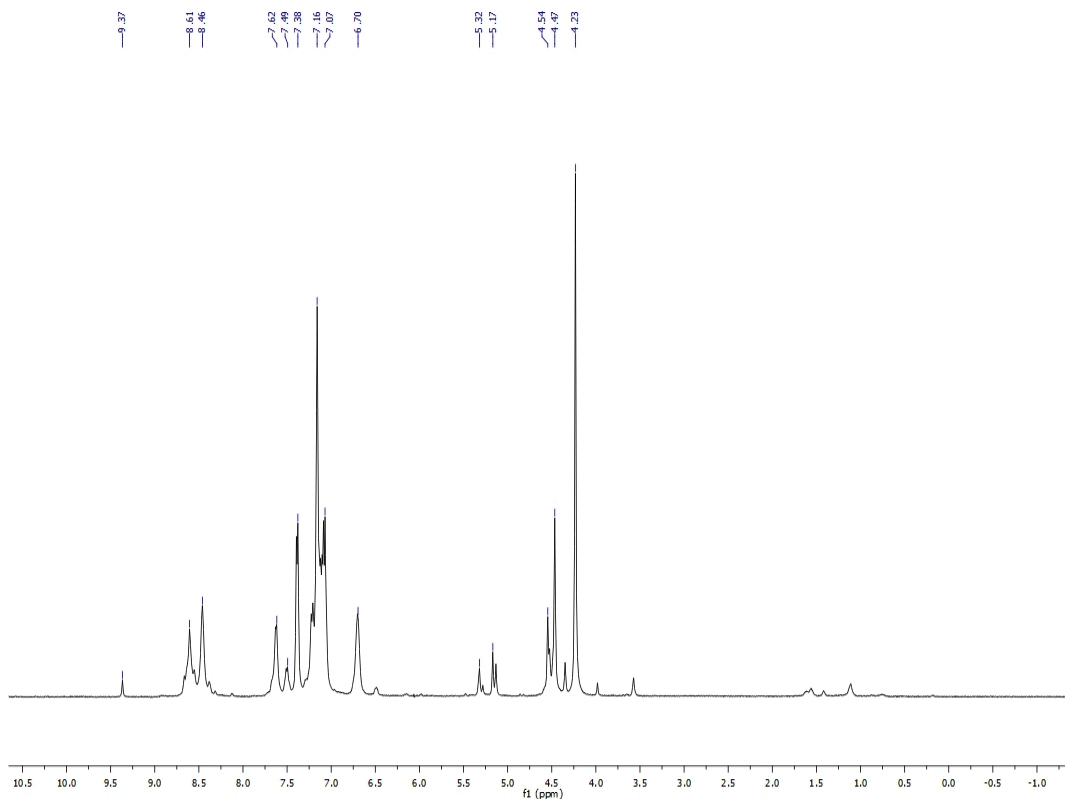


Figure 3.74: ^1H NMR spectrum of silyl ethers observed prior to hydrolysis in benzene- d_6 .

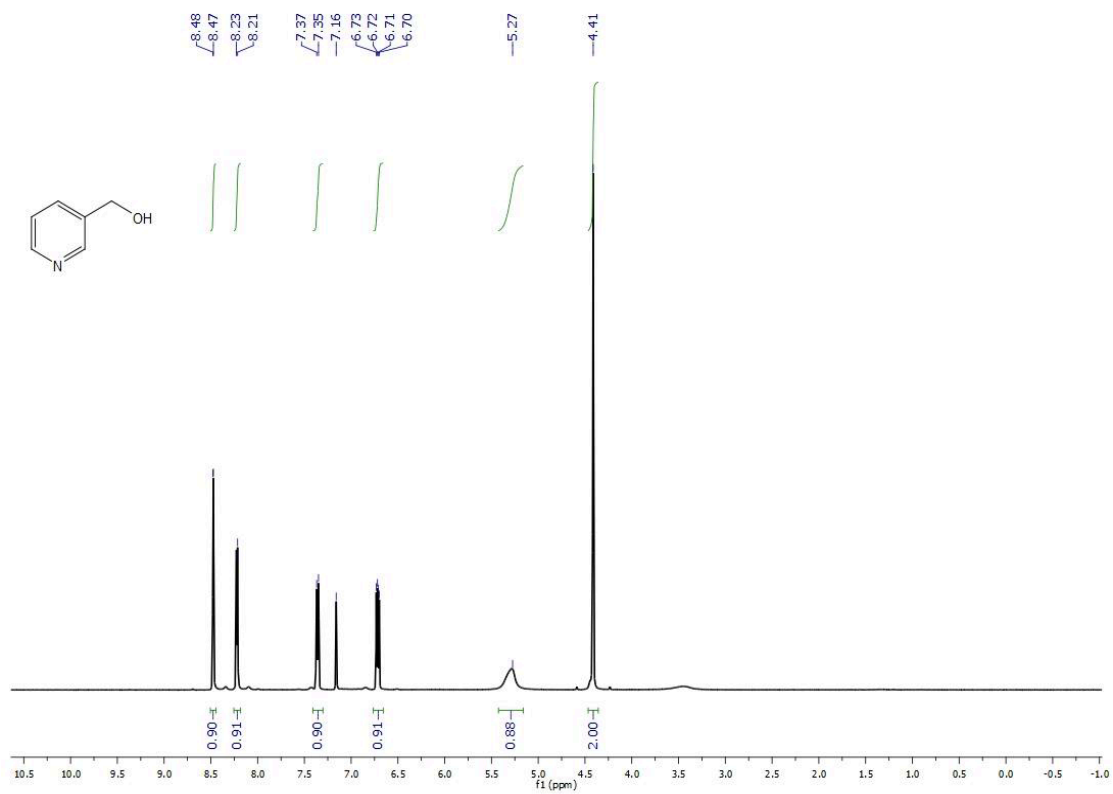


Figure 3.75: ^1H NMR spectrum of isolated pyridine-3-carbinol in benzene- d_6 .

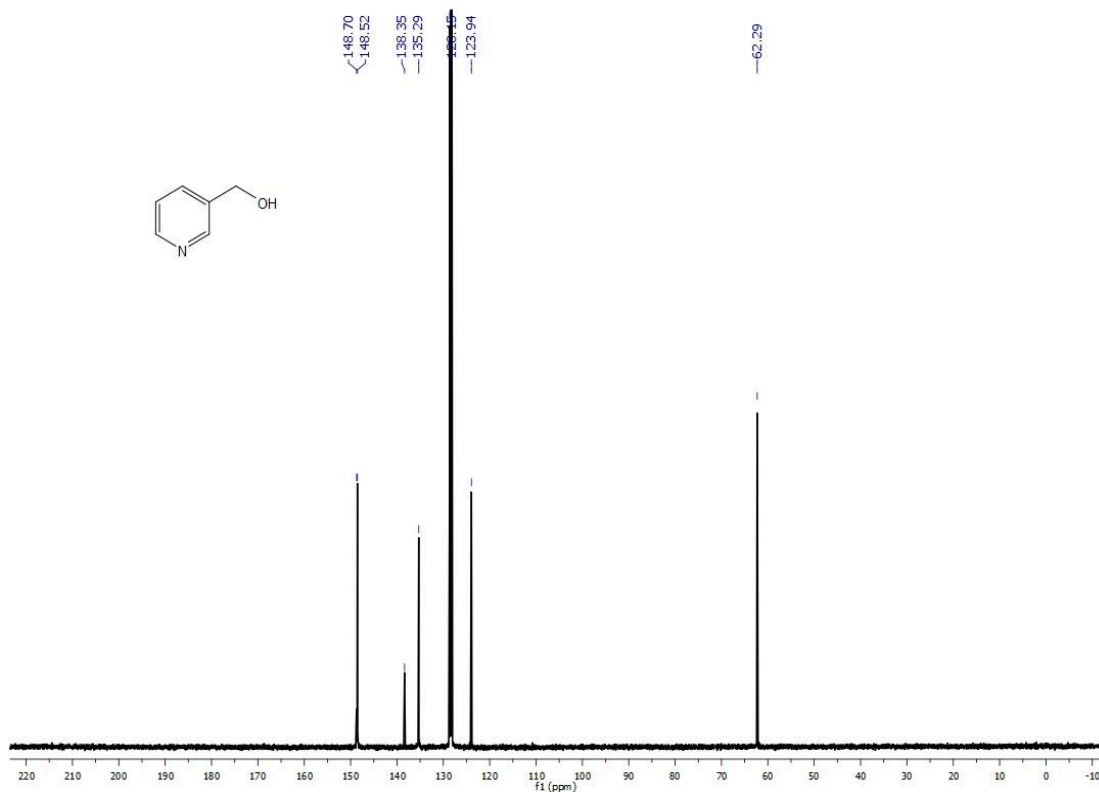


Figure 3.76: ¹³C NMR spectrum of isolated pyridine-3-carbinol in benzene-*d*₆.

Hydrosilylation of furfural catalyzed by 0.05 mol% **18 (0.1 mol% relative to Mn):**
This trial was conducted by Tufan K. Mukhopadhyay.

In the glove box, a neat mixture of PhSiH₃ (0.327 mL, 2.65 mmol) and furfural (0.219 mL, 2.65 mmol) was added to 0.0017 g (0.0013 mmol) of **18** pre-weighed into a 20 mL vial. The resulting brown solution vigorously bubbled and became hot. It was stirred for 2 min and then exposed to air to deactivate the catalyst. The colorless solution was filtered through Celite and a ¹H NMR spectrum was recorded to determine the percent conversion. It was followed by a hydrolytic work up whereby the mixture was stirred with 2 mL aqueous 10% NaOH at room temperature for 2 h. The organic fraction was extracted with diethyl ether (3 x 4 mL) and the organic layer was dried over anhydrous Na₂SO₄. Removal of the diethyl ether on a rotavap afforded a yellow oil

identified as furfuryl alcohol (0.1998 g, 2.04 mmol, yield = 77%). ^1H NMR (benzene- d_6): 7.06 (1H, d, *furfuryl*), 6.02 (1H, m, *furfuryl*), 5.95 (1H, d, *furfuryl*), 4.22 (2H, s, CH_2OH), 1.28 (1H, br, CH_2OH). ^{13}C NMR (benzene- d_6): 154.81, 142.64, 110.84, 108.01, 57.78.

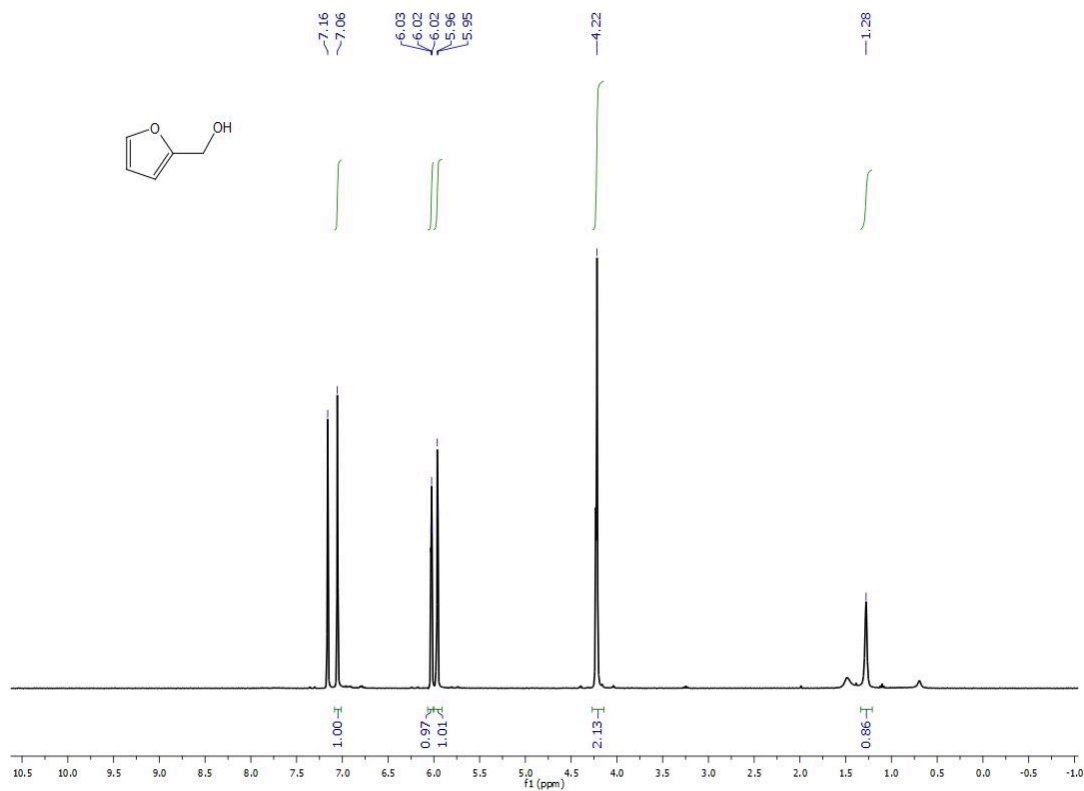


Figure 3.77: ^1H NMR spectrum of furfuryl alcohol in benzene- d_6 .

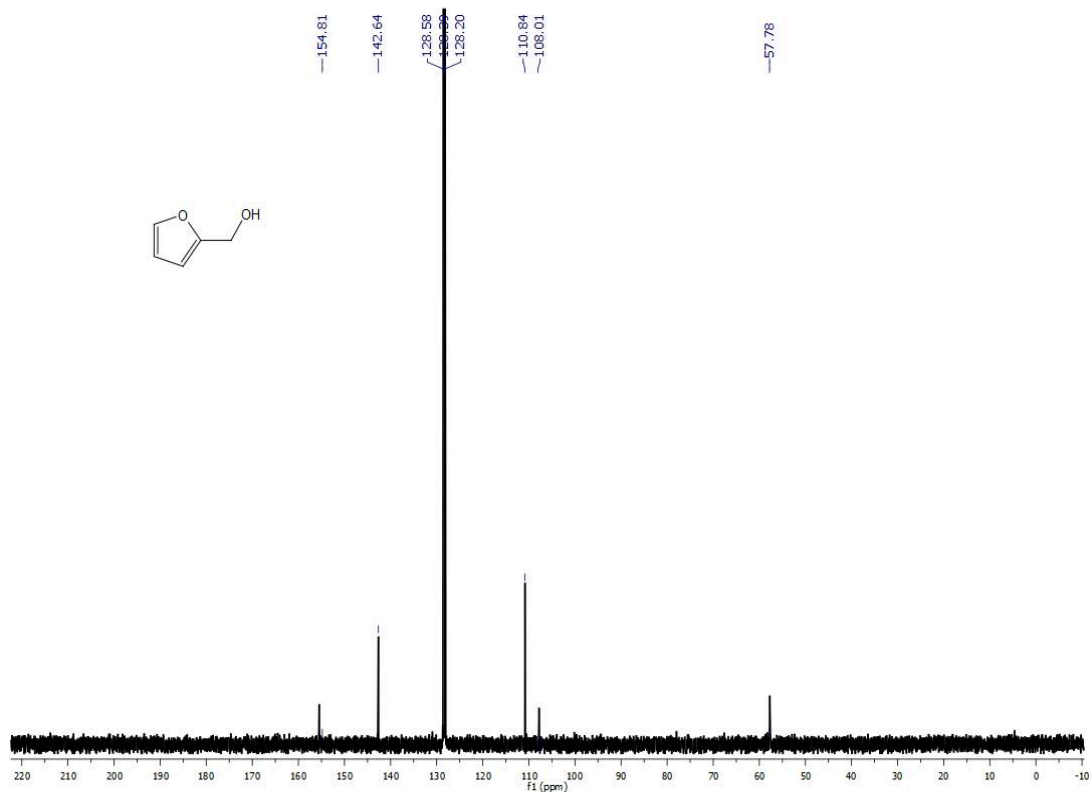


Figure 3.78: ^{13}C spectrum of furfuryl alcohol in benzene- d_6 .

Hydrosilylation of 3-cyclohexene-1-carboxaldehyde using 0.05 mol% **18 (0.1 mol% relative to Mn):** This trial was conducted by Tufan K. Mukhopadhyay.

In the glove box, a neat mixture of PhSiH_3 (0.424 mL, 3.43 mmol) and 3-cyclohexene-1-carboxaldehyde (0.389 mL, 3.43 mmol) was added to 0.0022 g (0.0017 mmol) of **18** pre-weighed in a 20 mL vial. The resulting brown solution became warm. It was stirred for 2 min and then exposed to air to deactivate the catalyst. The colorless solution was filtered through Celite and a ^1H NMR spectrum was recorded, which revealed 32% conversion to the quaternary silane product.

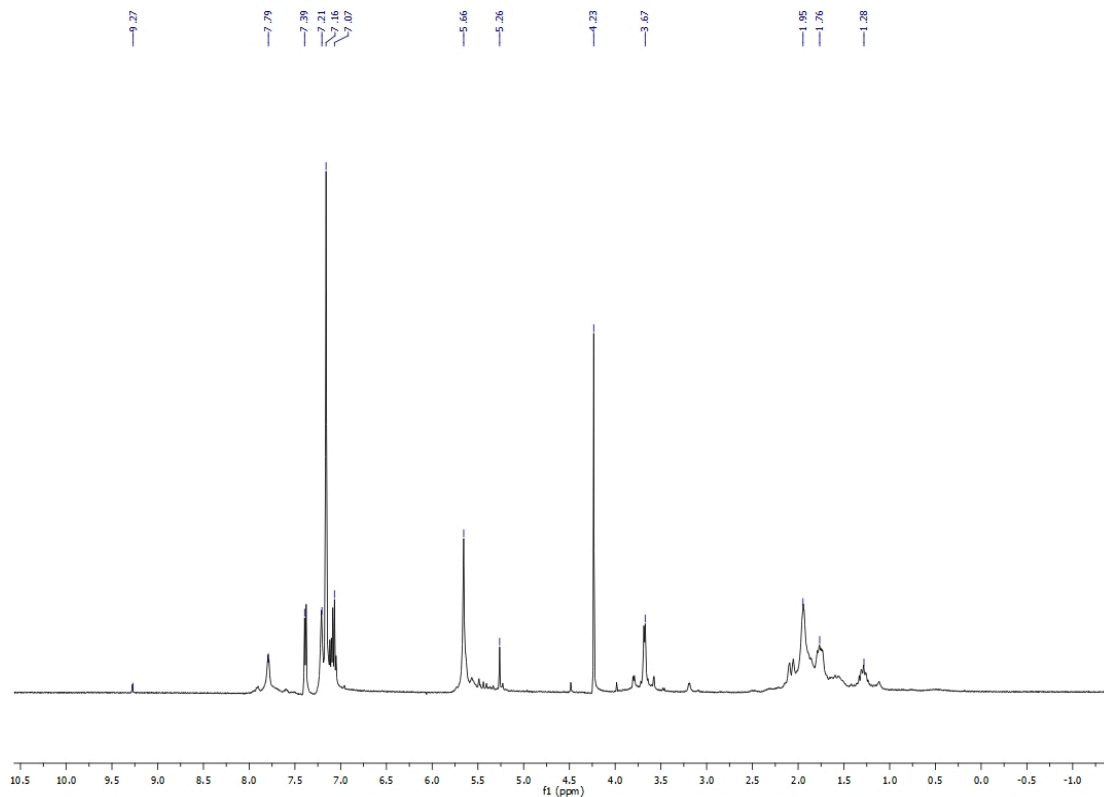


Figure 3.79: ^1H NMR spectrum showing partial 3-cyclohexene-1-carboxaldehyde hydrosilylation in benzene- d_6 .

Hydrosilylation of citral using 0.05 mol% **18 (0.1 mol% relative to Mn):** This trial was conducted by Tufan K. Mukhopadhyay.

In the glove box, a mixture of PhSiH_3 (0.347 mL, 2.81 mmol) and citral (0.480 mL, 2.81 mmol) was added to 0.0018 g (0.0014 mmol) of **18** pre-weighed into a 20 mL vial. The resulting brown solution became warm. It was stirred for 2 min and then exposed to air to deactivate the catalyst. The colorless solution was filtered through Celite and a ^1H NMR spectrum was recorded, which showed only 18% conversion made up of 84% quaternary silane and 16% tertiary silane.

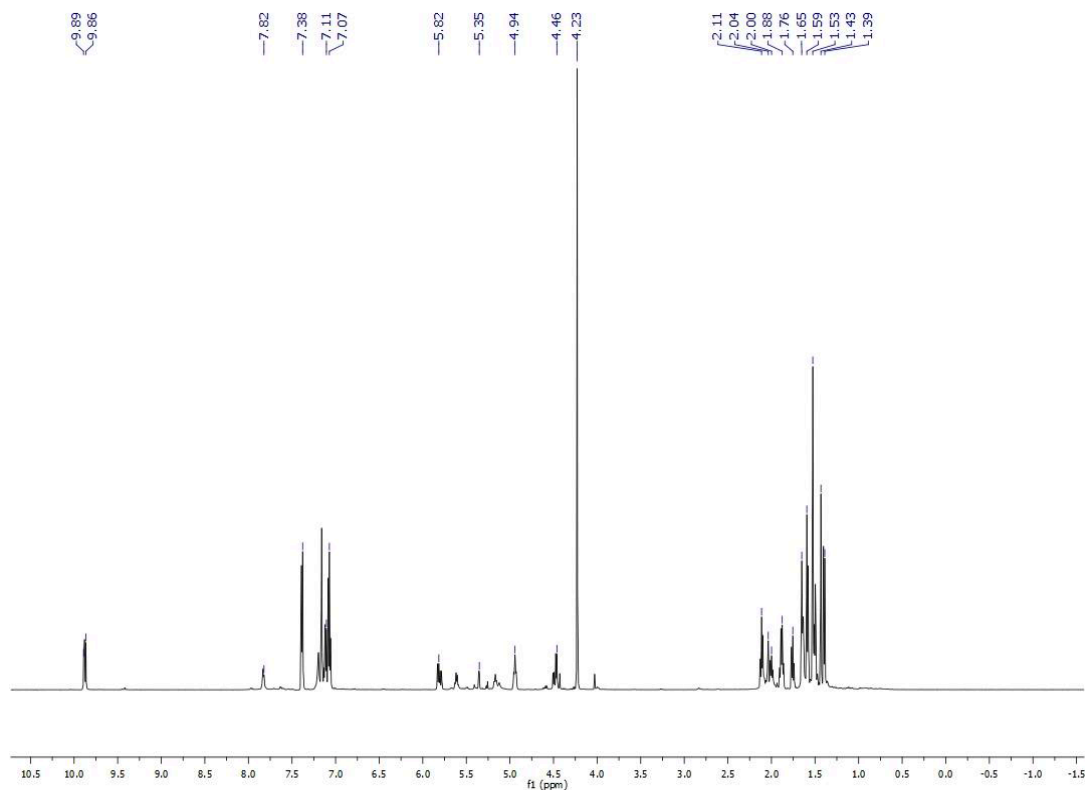


Figure 3.80: ^1H NMR spectrum showing partial citral hydrosilylation in benzene- d_6 .

Hydrosilylation of acetophenone using 0.05 mol% of **18 (0.1 mol% relative to Mn):**
This trial was conducted by Tufan K. Mukhopadhyay.

In the glove box, a neat mixture of PhSiH_3 (0.233 mL, 1.873 mmol) and acetophenone (0.218 mL, 1.873 mmol) was added to **18** (0.0012 g, 0.00094 mmol) pre-weighed into a 20 mL vial. The resulting red solution became hot and started to bubble. It was stirred for 4 min and then exposed to air to deactivate the catalyst. The colorless solution was filtered and a ^1H NMR spectrum was recorded. Greater than 99% conversion to $\text{PhSiH}[\text{OCH}(\text{Me})(\text{Ph})]_2$ (55%) and $\text{PhSi}[\text{OCH}(\text{Me})(\text{Ph})]_3$ (45%) was detected. Excess PhSiH_3 was also observed. These percentages were obtained by integrating the peaks at 4.99 ppm $\text{PhSiH}[\text{OCH}(\text{Me})(\text{Ph})]_2$ and 5.10-5.17 ppm $\text{PhSi}[\text{OCH}(\text{Me})(\text{Ph})]_3$.

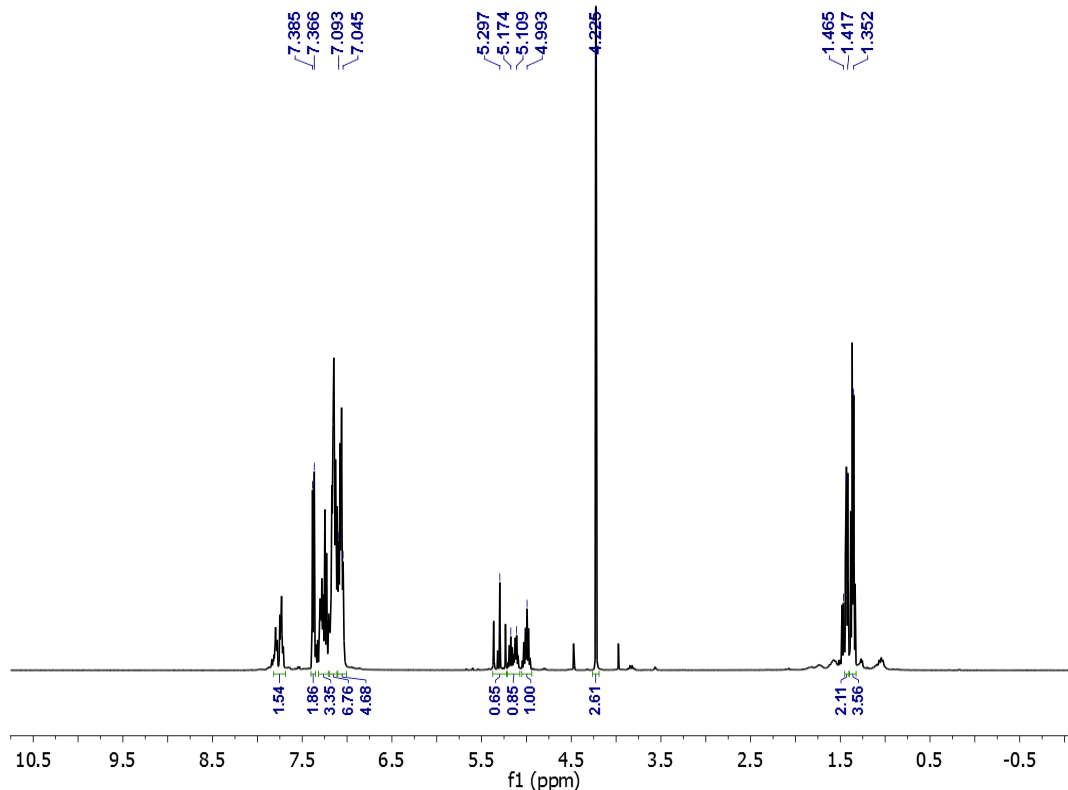


Figure 3.81: ¹H NMR spectrum showing the silyl ethers prepared from acetophenone using PhSiH₃ and 0.05 mol% of **18** in benzene-*d*₆.

Hydrosilylation of cyclohexanone using 0.05 mol% of **18 (0.1 mol% relative to Mn):**
This trial was conducted by Tufan K. Mukhopadhyay.

In the glove box, a neat mixture of PhSiH₃ (0.233 mL, 1.873 mmol) and cyclohexanone (0.193 mL, 1.873 mmol) was added to **18** (0.0012 g, 0.00094 mmol) pre-weighed in a 20 mL vial. The resulting red solution became hot and started to bubble. It was stirred for 4 min and then exposed to air to deactivate the catalyst. The colorless solution was filtered and a ¹H NMR spectrum was recorded, revealing 99% conversion to PhSiH(OCy)₂ and the presence of excess PhSiH₃. ¹H NMR (400 MHz, benzene-*d*₆): 7.84 (m, 2H), 7.38 (m, 2H, excess PhSiH₃), 7.22 (s, 3H), 7.13-7.06 (m, 3H, excess PhSiH₃), 5.34 (s, 1H, SiH), 4.22 (s, 3H, excess PhSiH₃), 3.97 (s, 2H, OCH), 1.87 (s, 4H, Cy), 1.65 (s, 4H, Cy), 1.53 (s, 4H, Cy), 1.33 (s, 2H, Cy), 1.15 (s, 6H, Cy).

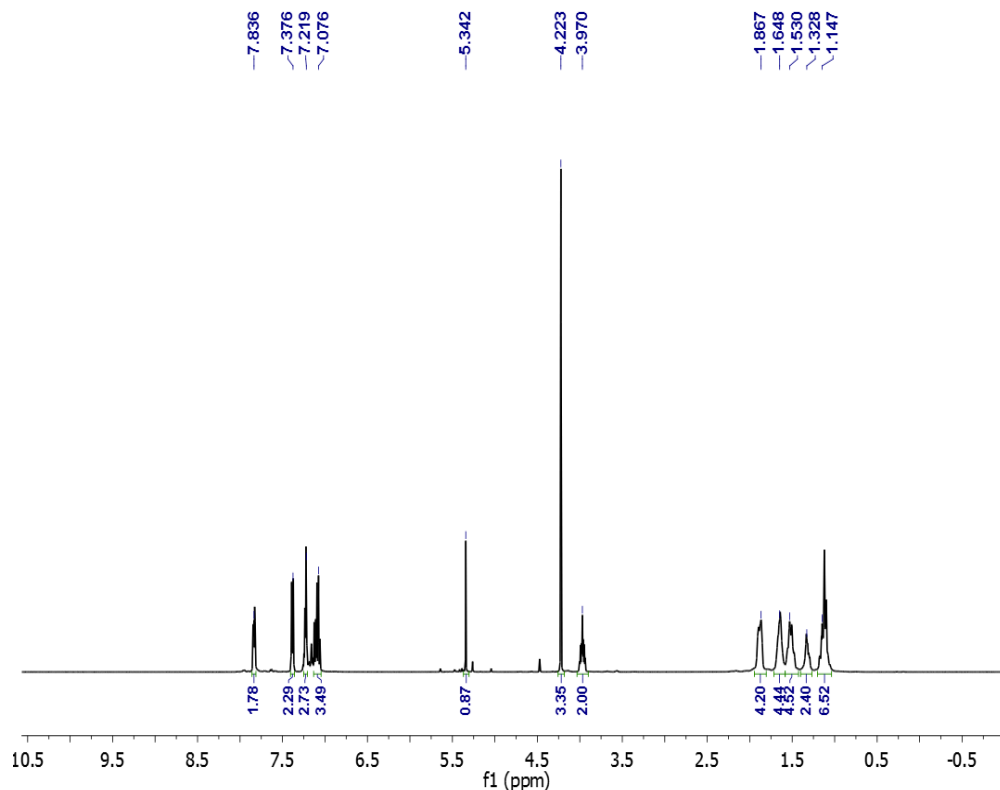


Figure 3.82: ^1H NMR spectrum of $\text{PhSiH}(\text{OCy})_2$ and PhSiH_3 in benzene- d_6 .

Hydrosilylation of benzaldehyde catalyzed by 0.005 mol% of **18 (0.01 mol% relative to Mn):** This trial was conducted by Tufan K. Mukhopadhyay.

In the glove box, a mixture of PhSiH_3 (3.08 mL, 24.98 mmol) and benzaldehyde (2.54 mL, 24.98 mmol) was added to 0.0016 g (0.0013 mmol) of **18** pre-weighed in a 20 mL vial. The resulting red solution vigorously bubbled and became hot. It was stirred for 2 min and then exposed to air to deactivate the catalyst. The colorless solution was filtered through Celite and a ^1H NMR spectrum was recorded to determine the percent conversion. It was followed by a hydrolytic work up whereby the mixture was stirred with 2 mL aqueous 10% NaOH solution at room temperature for 2 h. The organic fraction was extracted with diethyl ether (3 x 4 mL) and the organic layer was dried over anhydrous Na_2SO_4 . Removal of the solvent on a rotavap afforded a colorless oil identified as benzyl alcohol (2.477 g, 22.89 mmol, yield = 92%).

Hydrosilylation of 4-fluorobenzaldehyde catalyzed by 0.005 mol% of 18 (0.01 mol% relative to Mn): This trial was conducted by Tufan K. Mukhopadhyay.

In the glove box, a mixture of PhSiH₃ (2.50 mL, 20.29 mmol) and 4-fluorobenzaldehyde (2.19 mL, 20.29 mmol) was added to 0.0013 g (0.0010 mmol) of **18** pre-weighed into a 100 mL round bottom flask. The resulting brown solution vigorously bubbled and became hot. It was stirred for 2 min and then exposed to air to deactivate the catalyst. The resulting colorless solution was filtered through Celite and a ¹H NMR spectrum was recorded, which showed only 18% conversion (equating to a TOF of 900 min⁻¹ per Mn).

Attempt at benzaldehyde hydrosilylation using 0.2 mol% of Mn(0): This trial was conducted by Tufan K. Mukhopadhyay.

In the glove box, a mixture of PhSiH₃ (2.2 mL, 18.2 mmol) and benzaldehyde (1.85 mL, 18.2 mmol) was added to 0.002 g (0.036 mmol) of Mn(0) powder pre-weighed into a 20 mL vial. The resulting solution was stirred for 2 min (no heat or bubbling was noticed) and then exposed to air to deactivate the catalyst. The colorless solution was filtered through Celite and a ¹H NMR spectrum was recorded, which revealed no conversion.

Attempt at benzaldehyde hydrosilylation using 0.1 mol% of (THF)₂MnCl₂: This trial was conducted by Tufan K. Mukhopadhyay.

In the glove box, a mixture of PhSiH₃ (0.900 mL, 7.41 mmol) and benzaldehyde (0.750 mL, 7.41 mmol) was added to 0.002 g (0.0074 mmol) of (THF)₂MnCl₂ pre-weighed into a 20 mL vial. The resulting solution was stirred for 2 min (no heat or bubbling was noticed) and then exposed to air to deactivate the catalyst. The colorless solution was filtered through Celite and a ¹H NMR spectrum was recorded, which revealed no conversion.

Attempt at benzaldehyde hydrosilylation using 0.1 mol% 17: This trial was conducted by Tufan K. Mukhopadhyay.

In the glove box, a mixture of PhSiH₃ (0.350 mL, 2.81 mmol) and benzaldehyde (0.285 mL, 2.81 mmol) was added to 0.002 g (0.0028 mmol) of **17** pre-weighed in a 20 mL vial. The resulting solution was stirred for 2 min (no heat or bubbling was noticed) and then exposed to air to deactivate the catalyst. The colorless solution was filtered through Celite and a ¹H NMR spectrum was recorded, which revealed no conversion.

Test for catalyst homogeneity: This trial was conducted by Tufan K. Mukhopadhyay.

A 20 mL scintillation vial was charged with 15.61 g of Hg⁰ (78.05 mmol) and 0.31 mL benzaldehyde (3.12 mmol) was added to it. A solution of **18** (0.002 g, 0.0016 mmol) in 0.38 mL PhSiH₃ (3.12 mmol) was added to the vial and stirred for 2 min, while heat and bubble formation was noticed. Then it was exposed to air to deactivate the catalyst. The mixture was filtered through Celite and a ¹H NMR spectrum was collected, which showed greater than 99% conversion.

Hydrosilylation of benzaldehyde catalyzed by 0.05 mol% of 18 in absence of light: This trial was conducted by Tufan K. Mukhopadhyay.

In the glove box, a mixture of PhSiH₃ (0.40 mL, 3.28 mmol) and benzaldehyde (0.33 mL, 3.28 mmol) was prepared in an electrical tape-wrapped 20 mL scintillation vial under dark conditions. Another wrapped vial was charged with 0.0021 g (0.0016 mmol) of **18**. The mixture was added to the catalyst in absence of light. The solution vigorously bubbled and became hot. It was stirred for 2 min and then exposed to air to deactivate the catalyst. The colorless solution was filtered through Celite and a ¹H NMR spectrum was recorded, which revealed greater than 99% conversion.

Hydrosilylation of methyl formate catalyzed by 0.01 mol% of **18 (0.02 mol% relative to Mn):**

In the glove box, a neat mixture of PhSiH₃ (1.5 mL, 12.49 mmol) and methyl formate (0.76 mL, 12.49 mmol) was added to 0.0016 g (0.0013 mmol) of **18** pre-weighed into a 20 mL vial. The resulting brown solution vigorously bubbled and became hot. It was stirred for 30 min and then exposed to air to deactivate the catalyst. The colorless solution was filtered through Celite and a ¹H NMR spectrum was recorded to determine the percent conversion (>99 %).

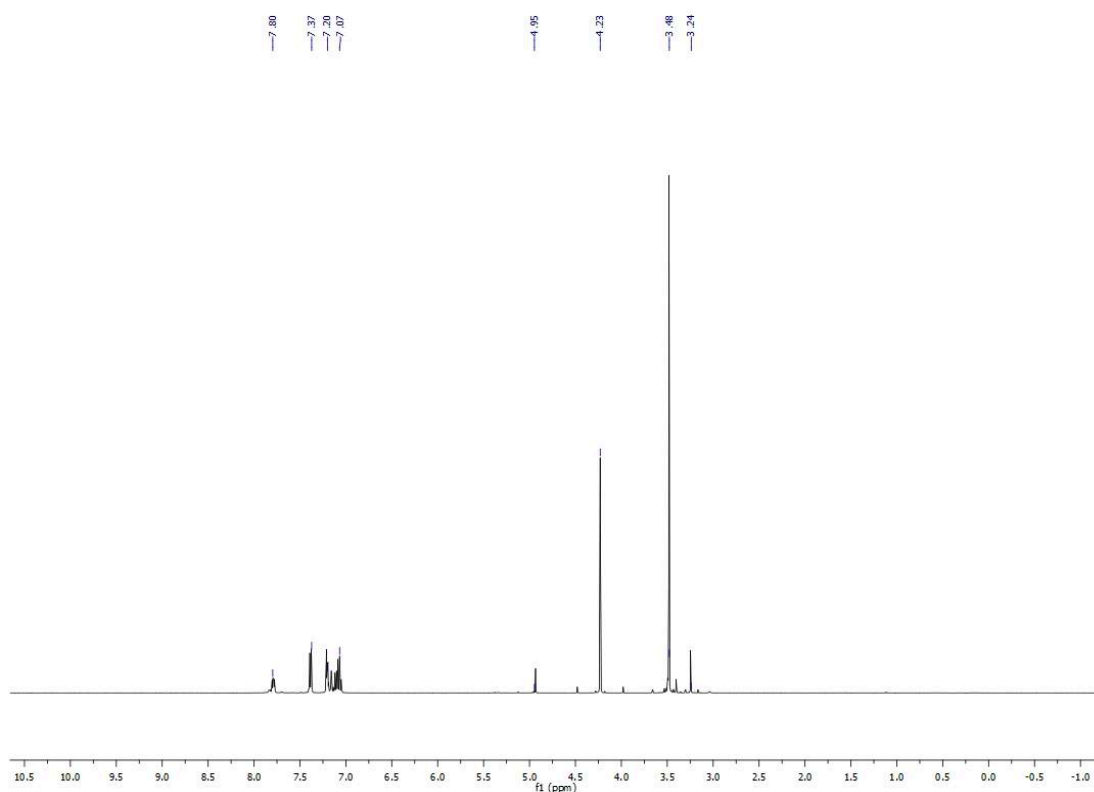


Figure 3.83: ¹H NMR spectrum showing complete methyl formate hydrosilylation in benzene-*d*₆.

Hydrosilylation of ethyl formate catalyzed by 0.01 mol% of **18 (0.02 mol% relative to Mn):**

In the glove box, a neat mixture of PhSiH₃ (1.9 mL, 15.6 mmol) and ethyl formate (1.3 mL, 15.6 mmol) was added to 0.002 g (0.0016 mmol) of **18** pre-weighed into a 20 mL vial. The resulting brown solution vigorously bubbled and became hot. It was stirred for 30 min and then exposed to air to deactivate the catalyst. The colorless solution was filtered through Celite and a ¹H NMR spectrum was recorded to determine the percent conversion (>99 %).

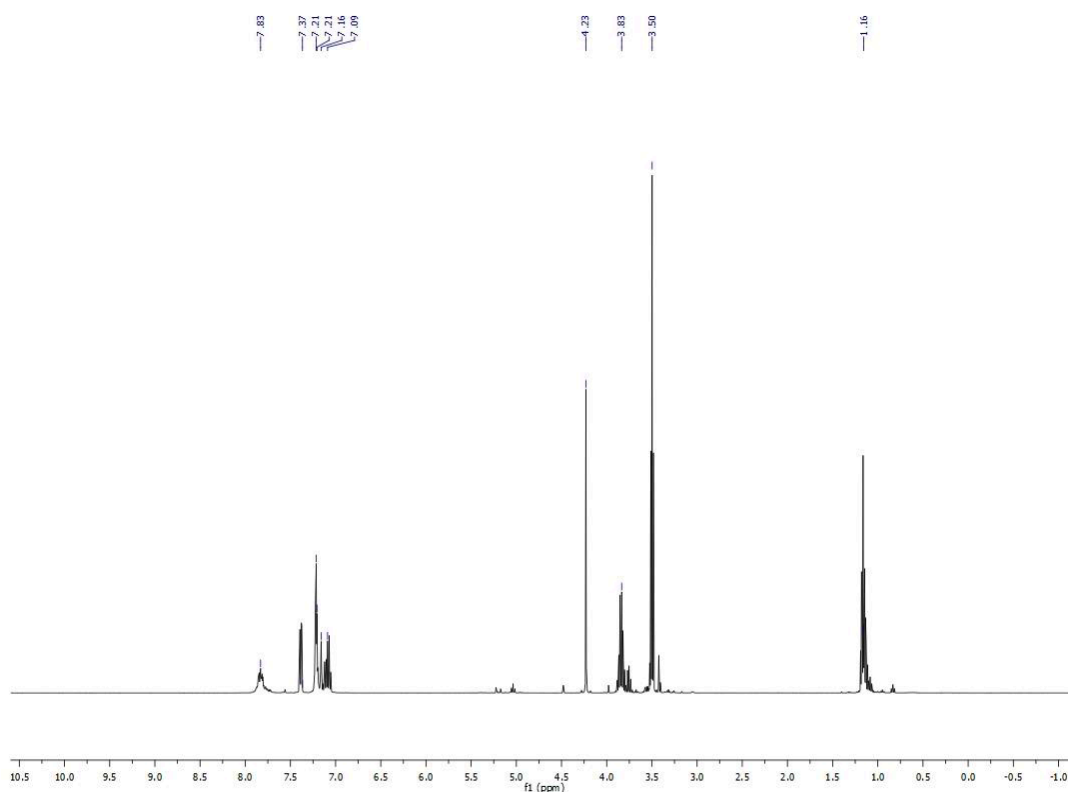


Figure 3.84: ¹H NMR spectrum showing complete ethyl formate hydrosilylation in benzene-*d*₆.

Hydrosilylation of octyl formate catalyzed by 0.01 mol% of **18 (0.02 mol% relative to Mn):**

In the glove box, a neat mixture of PhSiH₃ (1.6 mL, 13.2 mmol) and octyl formate (2.4 mL, 13.2 mmol) was added to 0.0021 g (0.0016 mmol) of **18** pre-weighed into a 20

mL vial. The resulting brown solution vigorously bubbled and became hot. It was stirred for 30 min and then exposed to air to deactivate the catalyst. The colorless solution was filtered through Celite and a ^1H NMR spectrum was recorded to determine the percent conversion (>99 %). Then the reaction mixture was hydrolyzed with 2 mL 10% aqueous NaOH solution upon stirring for 2 h at room temperature. The organic fraction was extracted with diethyl ether (3 x 4 mL) and the organic layer was dried over anhydrous Na_2SO_4 . Removal of the solvent on a rotavap afforded a colorless oil identified as 1-octanol (1.64 g, yield = 95 %). ^1H NMR (benzene- d_6): 3.40 (2H, t, CH_2), 1.40 (2H, m, CH_2), 1.23 (10H, m, CH_2), 0.90 (3H, t, CH_3). ^{13}C NMR (benzene- d_6): 63.09, 33.57, 32.58, 30.20, 30.09, 26.54, 23.42 14.68.

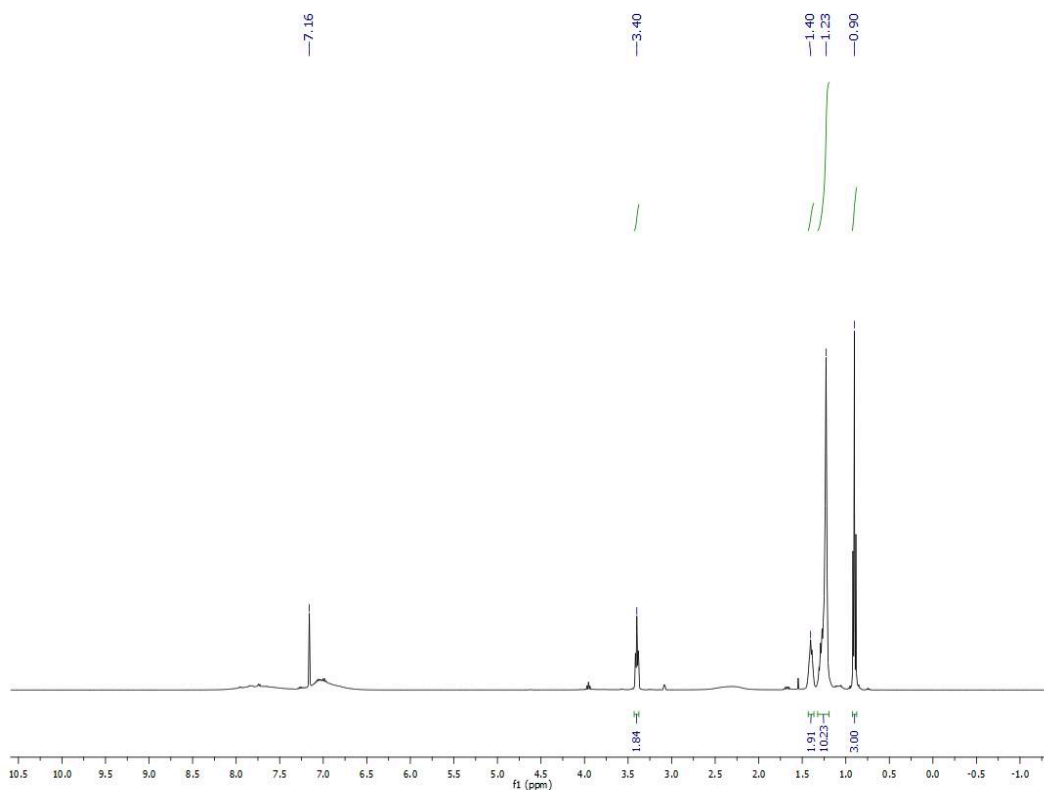


Figure 3.85: ^1H NMR spectrum of 1-octanol in benzene- d_6 .

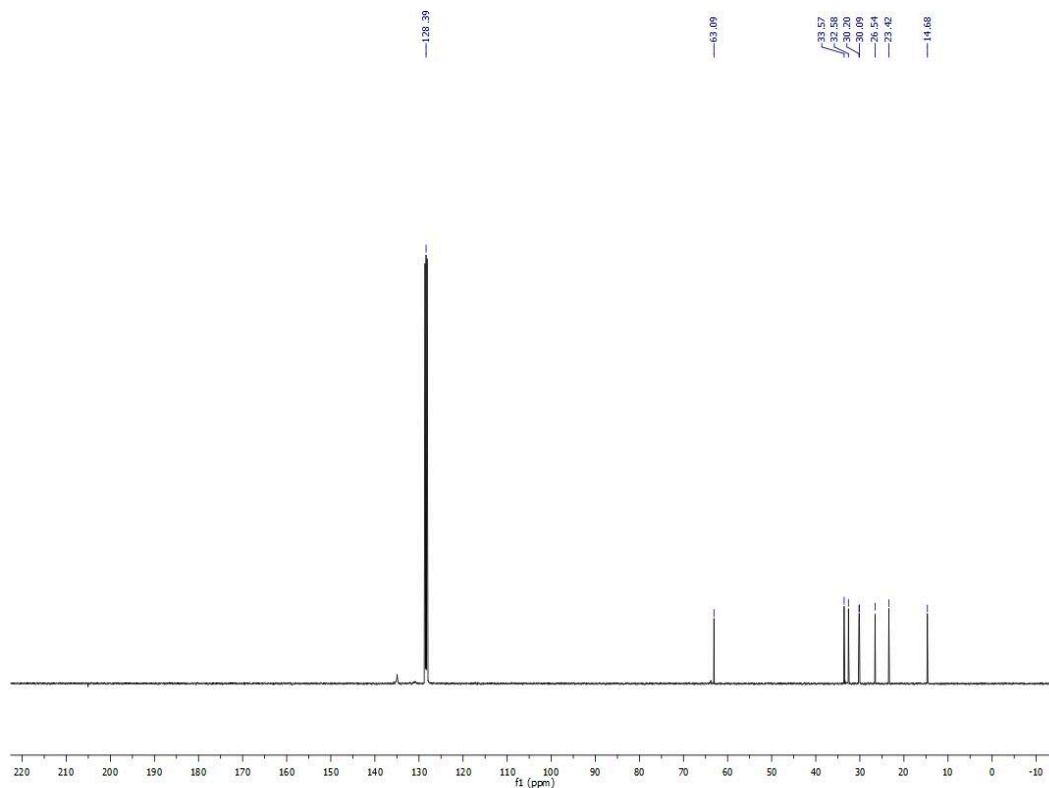


Figure 3.86: ^{13}C NMR spectrum of 1-octanol in benzene- d_6 .

Hydrosilylation of isoamyl formate catalyzed by 0.01 mol% of **18 (0.02 mol% relative to Mn):**

In the glove box, a neat mixture of PhSiH_3 (2.4 mL, 19.5 mmol) and isoamyl formate (2.6 mL, 19.5 mmol) was added to 0.0026 g (0.0019 mmol) of **18** pre-weighed in a 20 mL vial. The resulting brown solution vigorously bubbled and became hot. It was stirred for 30 min and then exposed to air to deactivate the catalyst. The colorless solution was filtered through Celite and a ^1H NMR spectrum was recorded to determine the percent conversion. Then the reaction mixture was hydrolyzed with 2 mL 10% aqueous NaOH solution upon stirring for 2 h at room temperature. The organic fraction was extracted with diethyl ether (3 x 4 mL) and the organic layer was dried over anhydrous Na_2SO_4 . Removal of the solvent on a rotavap afforded a pale-yellow oil identified as isoamyl alcohol (1.4 g, 15.88 mmol, yield = 83 %). ^1H NMR (benzene- d_6): 3.34 (2H, t,

CH_2), 1.57 (1H, m, CH), 1.25 (2H, m, CH_2), 0.81 (6H, d, CH_3). ^{13}C NMR (benzene- d_6): 61.33, 42.30, 25.28, 23.09.

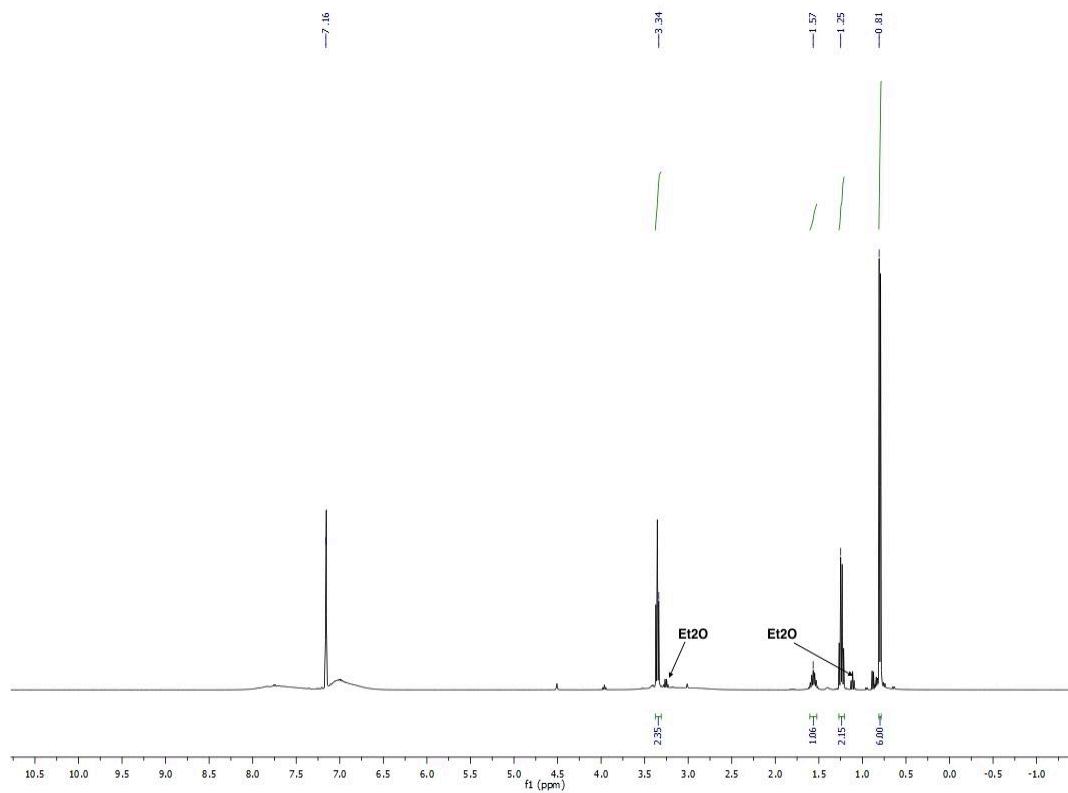


Figure 3.87: 1H NMR spectrum of isoamyl alcohol in benzene- d_6 .

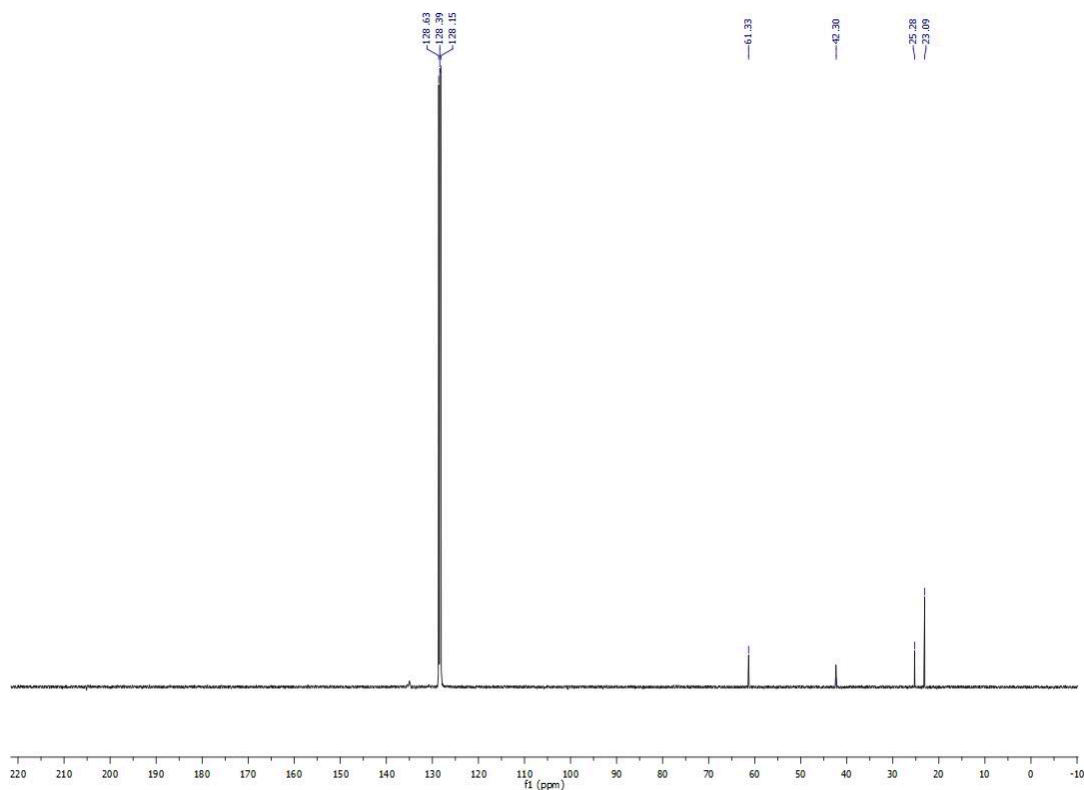


Figure 3.88: ^{13}C NMR spectrum of isoamyl alcohol in benzene- d_6 .

Hydrosilylation of benzyl formate catalyzed by 0.01 mol% of **18 (0.02 mol% relative to Mn):**

In the glove box, a neat mixture of PhSiH_3 (2.4 mL, 19.51 mmol) and benzyl formate (2.4 mL, 19.51 mmol) was added to 0.0025 g (0.0019 mmol) of **18** pre-weighed into a 20 mL vial. The resulting brown solution vigorously bubbled and became hot. It was stirred for 30 min and then exposed to air to deactivate the catalyst. The colorless solution was filtered through Celite and a ^1H NMR spectrum was recorded to determine the percent conversion. Then the reaction mixture was hydrolyzed with 2 mL 10% aqueous NaOH solution upon stirring for 2 h at room temperature. The organic fraction was extracted with diethyl ether (3 x 4 mL) and the organic layer was dried over anhydrous Na_2SO_4 . Removal of the solvent on a rotavap afforded a pale-yellow oil identified as benzyl alcohol (2.06 g, 19.05 mmol, yield = 99%). ^1H NMR (benzene- d_6):

7.09-7.14 (5H, m, *phenyl*), 4.30 (2H, s, CH_2OH), 1.42 (1H, br, *OH*). ^{13}C NMR (benzene- d_6): 142.11, 128.91, 127.80, 127.32, 65.20.

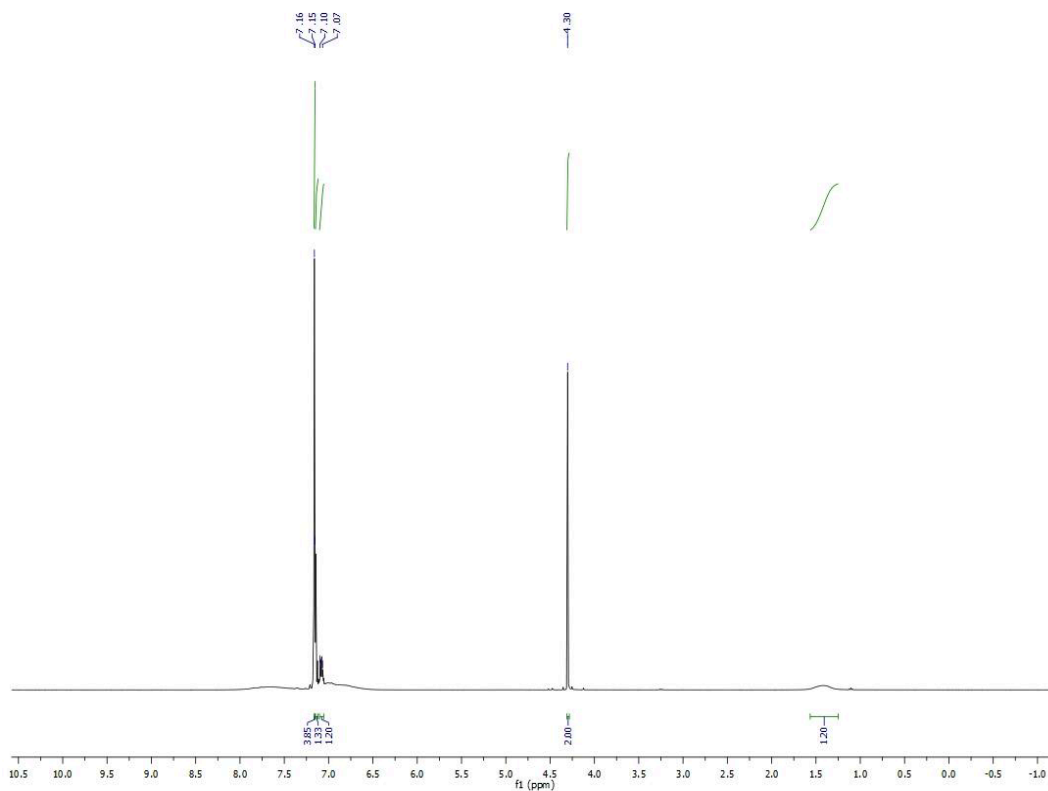


Figure 3.89: ^1H NMR spectrum of benzyl alcohol in benzene- d_6 .

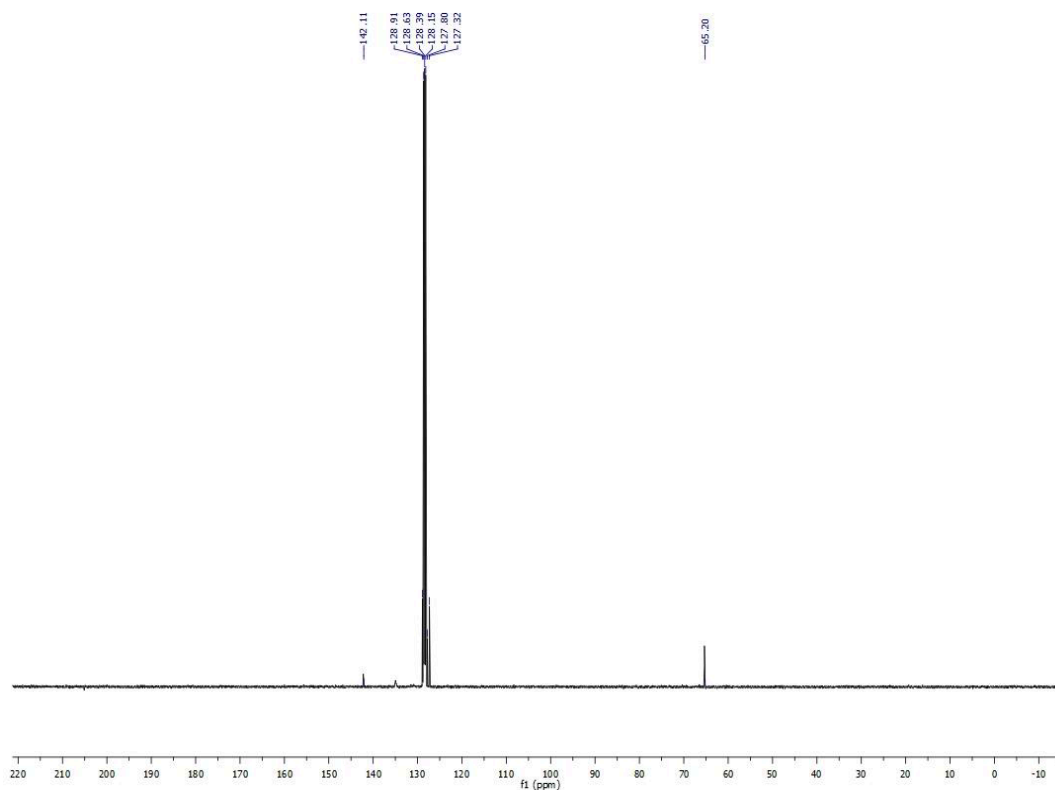


Figure 3.90: ^{13}C NMR of benzyl alcohol in benzene- d_6 .

Hydrosilylation of *p*-anisyl formate catalyzed by 0.01 mol% of **18 (0.02 mol% relative to Mn):**

In the glove box, a neat mixture of PhSiH_3 (2.7 mL, 21.8 mmol) and *p*-anisyl formate (3.5 mL, 21.8 mmol) was added to 0.0028 g (0.0022 mmol) of **18** pre-weighed into a 20 mL vial. The resulting brown solution vigorously bubbled and became hot. It was stirred for 30 min and then exposed to air to deactivate the catalyst. The colorless solution was filtered through Celite and a ^1H NMR spectrum was recorded to determine the percent conversion. Then the reaction mixture was hydrolyzed with 2 mL 10% aqueous NaOH solution upon stirring for 2 h at room temperature. The organic fraction was extracted with diethyl ether (3 x 4 mL) and the organic layer was dried over anhydrous Na_2SO_4 . Removal of the solvent on a rotavap afforded a pale-yellow oil identified as 4-methoxybenzyl alcohol (2.9 g, 20.99 mmol, yield = 86%). ^1H NMR

(benzene- d_6): 7.09 (2H, d, *phenyl*), 6.75 (2H, d, *phenyl*), 4.34 (2H, s, CH_2OH), 3.31 (3H, s, OCH_3). ^{13}C NMR (benzene- d_6): 159.76, 134.37, 114.46, 65.06, 55.14.

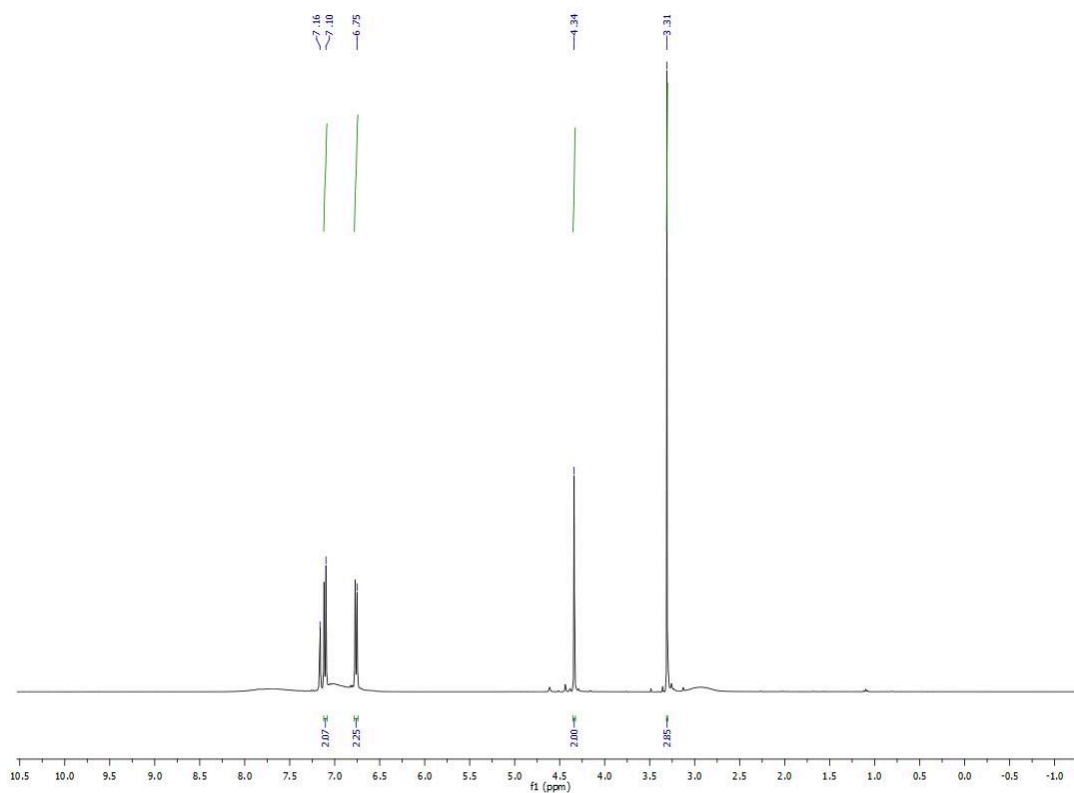


Figure 3.91: 1H NMR spectrum of 4-methoxybenzyl alcohol in benzene- d_6 .

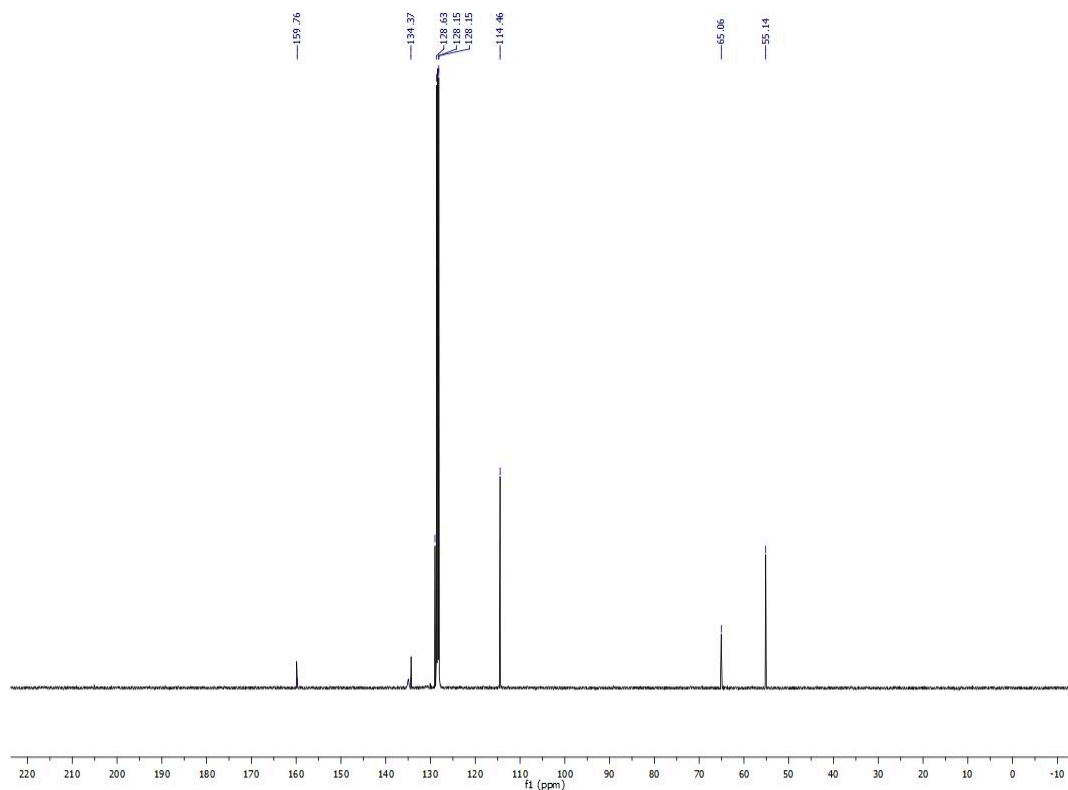


Figure 3.92: ^{13}C NMR spectrum of 4-methoxybenzyl alcohol in benzene- d_6 .

Hydrosilylation of ethyl acetate using 0.5 mol% of **18 (1 mol% relative to Mn):** This trial was conducted by Tufan K. Mukhopadhyay.

In the glove box, a solution of PhSiH_3 (53.9 mL, 0.437 mmol) and ethyl acetate (42.9 mL, 0.437 mmol) in 0.7 mL of benzene- d_6 was added to **18** (0.0028 g, 0.00219 mmol) pre-weighed in a 20 mL vial. The resulting red solution was transferred into a J. Young tube and sealed under N_2 atmosphere. The progress of the reaction was monitored by ^1H NMR spectroscopy, which revealed greater than 99% conversion after 7.2 h to $\text{PhSi}(\text{OEt})_3$. Excess PhSiH_3 was also observed. ^1H NMR (400 MHz, benzene- d_6): 7.85 (m, 2H), 7.38 (excess PhSiH_3), 7.22 (m, 3H), 7.13-7.06 (m, 2H, excess PhSiH_3), 4.22 (s, excess PhSiH_3), 3.85 (qd, $J = 7.0, 0.9$ Hz, 6H), 1.17 (td, $J = 7.0, 0.9$ Hz, 9H).

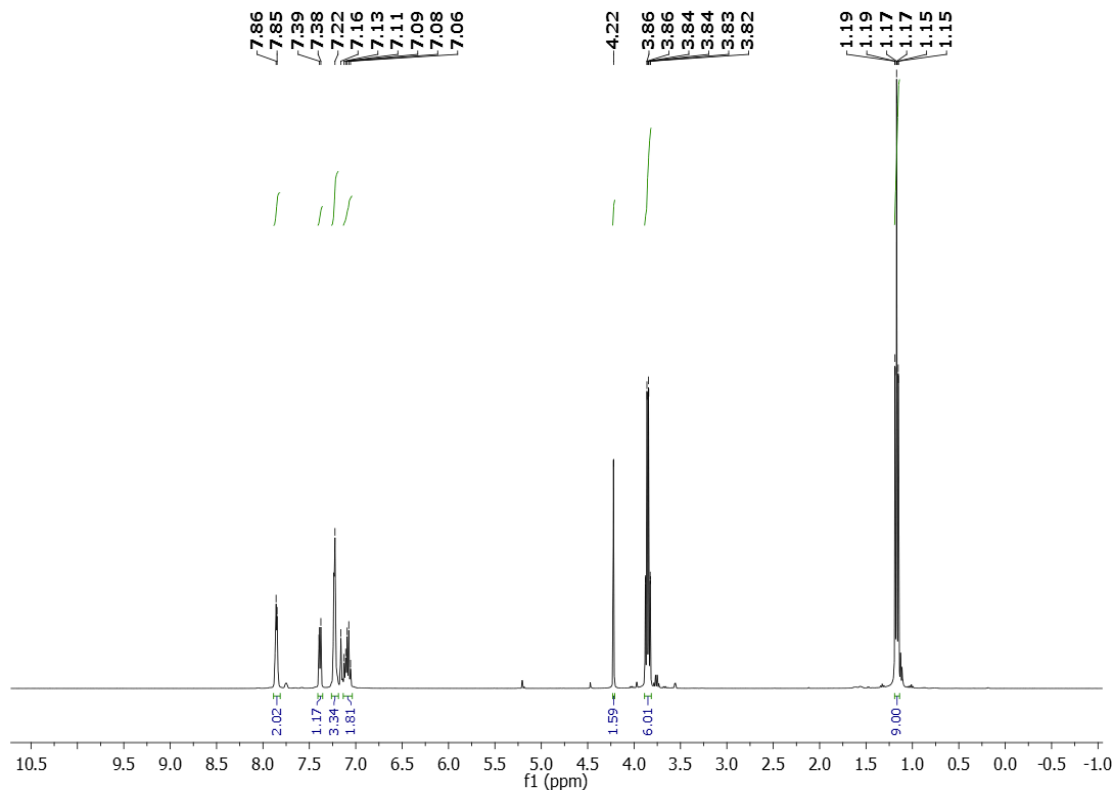


Figure 3.93: ^1H NMR spectrum of $\text{PhSi}(\text{OEt})_3$ and PhSiH_3 in benzene- d_6 .

3.9. References:

1. (a) Junge, K.; Schröder, K.; Beller, M. *Chem. Commun.* **2011**, 47, 4849-4859. (b) Le Bailly, B. A. F.; Thomas, S. P. *RSC Adv.* **2011**, 1, 1435. (c) Bullock, R. M. *Catalysis without Precious Metals*; Wiley-VCH: Weinheim, Germany, 2010. (d) Gosmini, C.; Bégouin, J.-M.; Moncomble, A. *Chem. Commun.* **2008**, 3221-3233. (e) Gaillard, S.; Renaud, J.-L. *ChemSusChem* **2008**, 1, 505-509.
2. Haynes, W. M. *CRC Handbook of Chemistry and Physics: A Ready reference Book of Chemical and Physical Data*, 94th ed.; Taylor & Francis: Boca Raton, FL, 2013-2014.
3. (a) Enthaler, S.; Junge, K.; Beller, M. *Angew. Chem. Int. Ed.* **2008**, 47, 3317-3321. (b) Plietker, B. *Iron Catalysis in Organic Chemistry*; Wiley-VCH: Weinheim, Germany, 2008.
4. (a) Hitchcock, P. B.; Lappert, M. F.; Warhurst, N. J. W. *Angew. Chem., Int. Ed. Engl.* **1991**, 30, 438-440. (b) Speier, J. L.; Webster, J. A.; Barnes, G. H. *J. Am. Chem. Soc.* **1957**, 79, 974-979.

5. (a) Srinivas, V.; Nakajima, Y.; Ando, W.; Sato, K.; Shimada, S. *Catal. Sci. Technol.* **2015**, *5*, 2081-2084. (b) Peng, D.; Zhang, Y.; Du, X.; Zhang, L.; Leng, X.; Walter, M. D.; Huang, Z. *J. Am. Chem. Soc.* **2013**, *135*, 19154–19166. (c) Tondreau, A. M.; Atienza, C. C. H.; Darmon, J. M.; Milsmann, C.; Hoyt, H. M.; Weller, K. J.; Nye, S. A.; Lewis, K. M.; Boyer, J.; Delis, J. G. P.; Lobkovsky, E.; Chirik, P. J. *Organometallics* **2012**, *31*, 4886-4893. (d) Hojilla Atienza, C. C.; Tondreau, A. M.; Weller, K. J.; Lewis, K. M.; Cruse, R. W.; Nye, S. A.; Boyer, J. L.; Delis, J. G. P.; Chirik, P. J. *ACS Catal.* **2012**, *2*, 2169-2172. (e) Tondreau, A. M.; Atienza, C. C. H.; Weller, K. J.; Nye, S. A.; Lewis, K. M.; Delis, J. G. P.; Chirik, P. J. *Science* **2012**, *335*, 567-570. (f) Troegel, D.; Stohrer, J. *Coord. Chem. Rev.* **2011**, *255*, 1440-1459.

6. For leading Fe examples, see: (a) Blom, B.; Enthaler, S.; Inoue, S.; Irran, E.; Driess, M. *J. Am. Chem. Soc.* **2013**, *135*, 6703-6713. (b) Ruddy, A. J.; Kelly, C. M.; Crawford, S. M.; Wheaton, C. A.; Sydora, O. L.; Small, B. L.; Stradiotto, M.; Turculet, L. *Organometallics* **2013**, *32*, 5581-5588. (c) Bhattacharya, P.; Krause, J. A.; Guan, H. *Organometallics* **2011**, *30*, 4720-4729. (d) Yang, J.; Tilley, T. D. *Angew. Chem. Int. Ed.* **2010**, *49*, 10186-10188. (e) Kandepi, V. V. K. M.; Cardoso, J. M. S.; Peris, E.; Royo, B. *Organometallics* **2010**, *29*, 2777-2782. (f) Tondreau, A. M.; Darmon, J. M.; Wile, B. M.; Floyd, S. K.; Lobkovsky, E.; Chirik, P. J. *Organometallics* **2009**, *28*, 3928-3940. (g) Tondreau, A. M.; Lobkovsky, E.; Chirik, P. J. *Org. Lett.* **2008**, *10*, 2789-2792.

7. For leading Co examples, see: (a) Zhou, H.; Sun, H.; Zhang, S.; Li, X. *Organometallics* **2015**, *34*, 1479-1486. (b) Niu, Q.; Sun, H.; Li, X.; Klein, H.-F.; Flörke, U. *Organometallics* **2013**, *32*, 5235–5238. (c) Sauer, D. C.; Wadehohl, H.; Gade, L. H. *Inorg. Chem.* **2012**, *51*, 12948-12958. (d) Yu, F.; Zhang, X.-C.; Wu, F.-F.; Zhou, J.-N.; Fang, W.; Wu, J.; Chan, A. S. C. *Org. Biomol. Chem.* **2011**, *9*, 5652. (e) Brunner, H.; Amberger, K. *J. Organomet. Chem.* **1991**, *417*, C63–C65. (f) Nesbit, M. A.; Suess, D. L. M.; Peters, J. C. *Organometallics* **2015**, *34*, 4741.

8. For leading Ni examples, see: (a) Porter, T. M.; Hall, G. B.; Groy, T. L.; Trovitch, R. J. *Dalton Trans.* **2013**, *42*, 14689-14692. (b) Bheeter, L. P.; Henrion, M.; Brelot, L.; Darcel, C.; Chetcuti, M. J.; Sortais, J.-B.; Ritleng, V. *Adv. Synth. Catal.* **2012**, *354*, 2619-2624. (c) Postigo, L.; Royo, B. *Adv. Synth. Catal.* **2012**, *354*, 2613-2618. (d) Tran, B. L.; Pink, M.; Mindiola, D. J. *Organometallics* **2009**, *28*, 2234-2243. (e) Chakraborty, S.; Krause, J. A.; Guan, H. *Organometallics* **2009**, *28*, 582-586 and references cited therein. (f) MacMillan, S. N.; Harman, H. W.; Peters, J. C. *Chem. Sci.* **2014**, *5*, 590-597. (g) Steiman, T. J.; Uyeda, C. *J. Am. Chem. Soc.* **2015**, *137*, 6104-6110.

9. For leading Cu examples, see: (a) Roy, S. R.; Sau, S. C.; Mandal, S. K. *J. Org. Chem.* **2014**, *79*, 9150-9160. (b) Albright, A.; Gawley, R. E. *J. Am. Chem. Soc.* **2011**, *133*, 19680-19683. (c) Yu, F.; Zhou, J.-N.; Zhang, X.-C.; Sui, Y.-Z.; Wu, F.-F.; Xie, L.-J.; Chan, A. S. C.; Wu, J. *Chem. - Eur. J.* **2011**, *17*, 14234-14240. (d) Zhang, X.-C.; Wu, F.-F.; Li, S.; Zhou, J.-N.; Wu, J.; Li, N.; Fang, W.; Lam, K. H.; Chan, A. S. C. *Adv. Synth. Catal.* **2011**, *353*, 1457-1462. (e) Diez-González, S.; Escudero-Adán, E.; Benet-Buchholz, J.; Stevens, E. D.; Slawin, A. M. Z.; Nolan, S. P. *Dalton Trans.* **2010**, *39*, 7595-7606. (f) Fujihara, T.; Semba, K.; Terao, J.; Tsuji, Y. *Angew. Chem. Int. Ed.* **2010**,

49, 1472-1476. (g) Mostefaï, N.; Sirol, S.; Courmarcel, J.; Riant, O. *Synthesis* **2007**, *2007*, 1265-1271. (h) Díez-González, S.; Scott, N. M.; Nolan, S. P. *Organometallics* **2006**, *25*, 2355-2358. (i) Lipshutz, B. H.; Lower, A.; Kucejko, R. J.; Noson, K. *Org. Lett.* **2006**, *8*, 2969-2972. (j) Díez-González, S.; Kaur, H.; Zinn, F. K.; Stevens, E. D.; Nolan, S. P. *J. Org. Chem.* **2005**, *70*, 4784-4796. (k) Wu, J.; Ji, J.-X.; Chan, A. S. C. *Proc. Natl. Acad. Sci. U. S. A.* **2005**, *102*, 3570-3575. (l) Lee, D.; Yun, J. *Tetrahedron Lett.* **2004**, *45*, 5415-5417. (m) Kaur, H.; Zinn, F. K.; Stevens, E. D.; Nolan, S. P. *Organometallics* **2004**, *23*, 1157-1160. (n) Lipshutz, B. H.; Noson, K.; Chrisman, W.; Lower, A. *J. Am. Chem. Soc.* **2003**, *125*, 8779-8789. (o) Lipshutz, B. H.; Noson, K.; Chrisman, W. *J. Am. Chem. Soc.* **2001**, *123*, 12917-12918. (p) Sirol, S.; Courmarcel, J.; Mostefaï, N.; Riant, O. *Org. Lett.* **2001**, *3*, 4111-4113. (q) Brunner, H.; Miehl, W. *J. Organomet. Chem.* **1984**, *275*, C17-C21.

10. For leading Zn examples, see: (a) Rit, A.; Zanardi, A.; Spaniol, T. P.; Maron, L.; Okuda, J. *Angew. Chem. Int. Ed.* **2014**, *53*, 13273-13277. (b) Lummis, P. A.; Momemi, M. R.; Lui, M. W.; McDonald, R.; Ferguson, M. J.; Miskolzie, M.; Brown, A.; Rivard, E. *Angew. Chem, Int. Ed.* **2014**, *53*, 9347-9351. (c) Łowicki, D.; Bezlada, A.; Mlynarski, J. *Adv. Synth. Catal.* **2014**, *356*, 591-595. (d) Boone, C.; Korobkov, I.; Nikonov, G. I. *ACS Catal.* **2013**, *3*, 2336-2340. (e) Pang, S.; Peng, J.; Li, J.; Bai, Y.; Xiao, W.; Lai, G. *Chirality* **2013**, *25*, 275-280. (f) Enthaler, S.; Schröder, K.; Inoue, S.; Eckhardt, B.; Junge, K.; Beller, M.; Drieß, M. *Eur. J. Org. Chem.* **2010**, *2010*, 4893-4901. (g) Gajewy, J.; Kwit, M.; Gawroński, J. *Adv. Synth. Catal.* **2009**, *351*, 1055-1063. (h) Gérard, S.; Pressel, Y.; Riant, O. *Tetrahedron: Asymmetry* **2005**, *16*, 1889-1891. (i) Bette, V.; Mortreux, A.; Savoia, D.; Carpentier, J.-F. *Adv. Synth. Catal.* **2005**, *347*, 289-302. (j) Bette, V.; Mortreux, A.; Savoia, D.; Carpentier, J.-F. *Tetrahedron* **2004**, *60*, 2837-2842. (k) Mastranzo, V. M.; Quintero, L.; Anaya de Parrodi, C. A.; Juaristi, E.; Walsh, P. J. *Tetrahedron* **2004**, *60*, 1781-1789. (l) Mimoun, H. *J. Org. Chem.* **1999**, *64*, 2582-2589. (m) Sattler, W.; Ruccolo, S.; Rostami Chaijan, M.; Nasr Allah, T.; Parkin, G. *Organometallics* **2015**, *34*, 4717.

11. For leading examples, see: (a) Bleith, T.; Wadepohl, H.; Gade, L. H. *J. Am. Chem. Soc.* **2015**, *137*, 2456-2459. (b) Darwish, M.; Wills, M. *Catal. Sci. Technol.* **2012**, *2*, 243-255. (c) Inagaki, T.; Ito, A.; Ito, J.; Nishiyama, H. *Angew. Chem. Int. Ed.* **2010**, *49*, 9384-9387. (d) Inagaki, T.; Phong, L. T.; Furuta, A.; Ito, J.; Nishiyama, H. *Chem. - Eur. J.* **2010**, *16*, 3090-3096. (e) Morris, R. H. *Chem. Soc. Rev.* **2009**, *38*, 2282-2291. (f) Langlotz, B. K.; Wadepohl, H.; Gade, L. H. *Angew. Chem. Int. Ed.* **2008**, *47*, 4670-4674. (g) Shaikh, N. S.; Enthaler, S.; Junge, K.; Beller, M. *Angew. Chem, Int. Ed.* **2008**, *47*, 2497-2501. (h) Nishiyama, H.; Furuta, A. *Chem. Commun.* **2007**, 760-762.

12. (a) Valyaev, D. A.; Lavigne, G.; Lugan, N. *Coord. Chem. Rev.* **2015**. (b) Trovitch, R. *J. Synlett* **2014**, *25*, 1638-1642.

13. Pratt, S. L.; Faltynek, R. A. *J. Organomet. Chem.* **1983**, *258*, C5-C8.

14. Hilal, H. S.; Abu-Eid, M.; Al-Subu, M.; Khalaf, S. *J. Mol. Catal.* **1987**, *39*, 1-11.

15. Mao, Z.; Gregg, B. T.; Cutler, A. R. *J. Am. Chem. Soc.* **1995**, *117*, 10139-10140.
16. DiBiase Cavanaugh, M.; Gregg, B. T.; Cutler, A. R. *Organometallics* **1996**, *15*, 2764-2769.
17. Son, S. U.; Paik, S.-J.; Lee, I. S.; Lee, Y.-A.; Chung, Y. K.; Seok, W. K.; Lee, H. N. *Organometallics* **1999**, *18*, 4114-4118.
18. Son, S. U.; Paik, S.-J.; Chung, Y. K. *J. Mol. Catal. A: Chem.* **2000**, *151*, 87-90.
19. Igarashi, M.; Fuchikami, T. *Tetrahedron Lett.* **2001**, *42*, 1945-1947.
20. Zheng, J.; Chevance, S.; Darcel, C.; Sortais, J.-B. *Chem. Commun.* **2013**, *49*, 10010-10012.
21. Chidara, V. K.; Du, G. *Organometallics* **2013**, *32*, 5034-5037.
22. Zheng, J.; Elangovan, S.; Valyaev, D. A.; Brousses, R.; César, V.; Sortais, J.-B.; Darcel, C.; Lugan, N.; Lavigne, G. *Adv. Synth. Catal.* **2014**, *356*, 1093-1097.
23. Mukhopadhyay, T. K.; Flores, M.; Groy, T. L.; Trovitch, R. J. *J. Am. Chem. Soc.* **2014**, *136*, 882-885.
24. Pal, R.; Groy, T. L.; Bowman, A. C.; Trovitch, R. J. *Inorg. Chem.* **2014**, *53*, 9357-9365.
25. Reardon, D.; Aharonian, G.; Gambarotta, S.; Yap, G. P. A. *Organometallics* **2002**, *21*, 786-788.
26. Knijnenburg, Q.; Gambarotta, S.; Budzelaar, P. H. M. *Dalton-Trans.* **2006**, 5442-5448.
27. Palmer, G. In *Physical Methods in Bioinorganic Chemistry. Spectroscopy and Magnetism*; Que, L. J., Ed.; University Science Books: Sausalito, CA, **2000**; pp 145-153.
28. Ben-Daat, H.; Hall, G. B.; Groy, T. L.; Trovitch, R. J. *Eur. J. Inorg. Chem.* **2013**, *2013*, 4430-4442.
29. Bart, S. C.; Chlopek, K.; Bill, E.; Bouwkamp, M. W.; Lobkovsky, E.; Neese, F.; Wiegardt, K.; Chirik, P. J. *J. Am. Chem. Soc.* **2006**, *128*, 13901-13912.
30. (a) Khusniyarov, M. M.; Harms, K.; Burghaus, O.; Sundermeyer, J. *Eur. J. Inorg. Chem.* **2006**, *2006*, 2985-2996. (b) Muresan, N.; Chlopek, K.; Weyhermüller, T.; Neese, F.; Wiegardt, K. *Inorg. Chem.* **2007**, *46*, 5327-5337.
31. Mukhopadhyay, T. K.; Rock, C. L.; Ashley, D. C.; Hong, M.; Groy, T. L.; Baik, M. H.; Trovitch, R. J. *J. Am. Chem. Soc.* **2017**, *139*, 4901-4915.

32. Valyaev, D. A.; Wei, D.; Elangovan, S.; Cavailles, M.; Dorcet, V.; Sortais, J.-B.; Darcel, C.; Lukan, N. *Organometallics* **2016**, *35*, 4090-4098.
33. LeBlanc, F. A.; Piers, W.; Parvez, M. *Angew. Chem. Int. Ed.* **2014**, *53*, 789-792.
34. Berk, S. C.; Kreutzer, K. A.; Buchwald, S. L. *J. Am. Chem. Soc.* **1991**, *113*, 5093-5095.
35. Le Bideau, F.; Henique, J.; Samuel, E.; Elschenbroich, C. *Chem. Commun.* **1999**, 1397-1398.
36. In a prior assessment of Ni-mediated carbonyl hydrosilylation, catalysts in refs 8e (ref 23) and 8b (ref 12b) were cited as the most active for this transformation. However, TOFs of up to 2,304 h⁻¹ have been reported in ref 8c.
37. Weil, J. A.; Bolton, J. R. *Electron paramagnetic resonance: Elementary theory and practical applications*; Wiley: Hoboken, NJ, **2007**.

CHAPTER 4

A HIGHLY EFFICIENT COBALT CATALYST FOR NITRILE AND IMINE HYDROBORATION

4.1. Abstract:

Heating a mixture of excess pyridine-substituted bis(imino)pyridine ligand, ^{PyEt}PDI and CoCl₂ at 95 °C in toluene for 4 days afforded a green compound identified as (^{PyEt}PDI)CoCl₂. This compound was determined to be paramagnetic based on ¹H NMR analysis and room temperature magnetic susceptibility experiment ($\mu_{\text{eff}} = 3.8 \mu_{\text{B}}$). Treatment of the metal halide with 2 equivalents of NaEt₃BH allowed for the isolation of a forest green compound after 7 h at room temperature. Detailed 1D and 2D NMR analysis and X-ray diffraction analysis confirmed the structure of the compound to be κ^4 -*N,N,N,N*-(^{PyEt}PDIH)Co, which features a protonated ligand. X-ray diffraction also confirmed a distorted square planar geometry around cobalt and a mono-reduced DI ligand center which is antiferromagnetically coupled with cobalt (II). This compound was determined to successfully catalyze nitriles to their corresponding diboryl amines within 2 h at room temperature at 1 mol% catalyst loading. Along with nitriles, it also reduces imines to their corresponding mono-boryl amines under the same conditions. Broad substrate scopes for both nitriles and imines have been investigated. The mechanistic pathway of nitrile dihydroboration has been studied with a series of stoichiometric reactions.

4.2. Introduction:

The double reduction of nitriles is a powerful technique as it produces primary amines and its derivatives, which are useful in the pharmaceutical and agrochemical

industries and also serves as precursors for fine chemicals, polymers, and dyes.¹ The catalytic hydrogenation of nitriles is a well-known method, however this process lacks product selectivity, leading to the formation of a mixture of primary and secondary amines,² sometimes requiring high temperature and pressure. In addition, this method mostly relies upon the use of precious metal catalysts³ and there are limited examples of earth abundant metal catalyzed nitrile hydrogenation.⁴ Recently, amino borane reagents have been used in metal-catalyzed nitrile hydrogenation.⁵ Nitrile reduction can also be achieved by using stoichiometric amounts of reducing agents such as LiAlH_4 and NaBH_4 , but the flammable nature of these reagents and production of large amounts of inorganic waste by-products make this method fruitless. As an alternative strategy, catalytic hydroboration can be considered as a benign and atom-efficient route to selectively produce primary amine derivatives. Hydroboration of nitriles generates diboryl amines, a protected version of primary amines, which can further be utilized in the synthesis of imines upon reacting with aldehydes, without the need for water removal and the use of dehydrating agents.⁶ Boryl amines also have importance as iminium generators, which can participate in a nucleophilic addition reaction with enolates and cyanides.⁷ Recently, intramolecular nitrile hydroboration has been employed in the application of BN heterocycle synthesis.⁸ Although nitrile hydroboration has been found to be an efficient and selective method, the high bond dissociation energy of nitrile C-N bonds has resulted in few reported metal catalysts. In 2012, Nikonov reported a molybdenum-imido hydride complex, $(\text{ArN})\text{Mo}(\text{H})(\text{Cl})(\text{PMe}_3)_3$, that catalyzes nitrile hydroboration, however the substrate scope was limited to only benzonitrile and acetonitrile.⁶ In 2015, the Szymczak group showed that a proton switchable bifunctional Ru complex is capable of nitrile

hydroboration at 5 mol% catalyst loading at room temperature, with a good substrate scope.⁹ Following these works, the Gunanathan group published nitrile and imine hydroboration achieved by $[\text{Ru}(p\text{-cymene})\text{Cl}_2]_2$ ¹⁰ and Hill and co-workers developed a β -diketiminato n-butylmagnesium complex,¹¹ however both catalysts require 60 °C for successful catalytic transformation. In 2017, Shimada and co-workers described nitrile hydroboration with HBcat in the presence of nickel salts including bis(acetylacetonato)nickel(II) and their derivatives at room temperature.¹² Meanwhile, Nakazawa reported an iron-iridium complex, $[\text{Fe}(\text{CH}_3\text{CN})_6][\text{cis-Fe}(\text{CO})_4(\text{InCl}_3)_2]$, which successfully converted both aromatic and aliphatic nitriles to their corresponding diboryl amines in the presence of HBPin at 10 mol% catalyst loading under heated conditions (80 °C).¹³ Cobalt has been extensively explored for catalytic transformations, such as the hydrogenation, hydrosilylation and hydroboration of unsaturated bonds.¹⁴ Recently, efforts also have been made to develop cobalt catalysts for nitrile hydroboration. In this context, Fout's work is notable to mention as they have shown that $(^{\text{DIPPr}}\text{CCC})\text{CoN}_2$ can catalyze nitrile reduction in the presence of HBPin at 2.5 mol% catalyst loading at 70 °C.¹⁵ At the same time, our group reported a cobalt hydride complex, $(^{\text{Ph}_2\text{PPr}}\text{DI})\text{CoH}$ that can perform nitrile hydroboration with HBpin at a better catalyst loading (1 mol%) at 70 °C.¹⁶

Similarly, imine reduction can be accomplished through hydrogenation¹⁷ or the use of alkali metal hydrides (LiAlH_4 , NaBH_4).¹⁸ Like nitrile reductions, imine reductions achieved by these processes are also associated with poor yield and product selectivity. Unlike metal catalyzed hydrogenation,¹⁹ hydroboration has been scarcely investigated. In 2009, the Clark group reported imine hydroboration catalyzed by a boron-substituted Ru

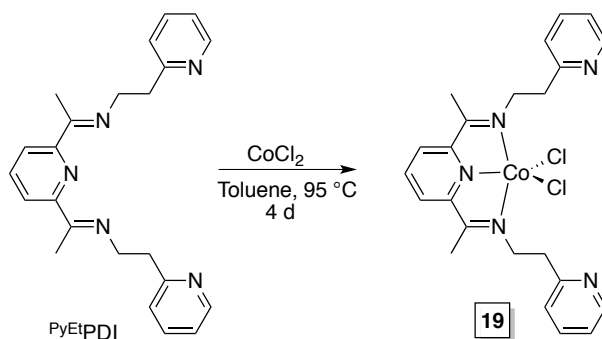
catalyst in presence of HBPin at 2.0 mol% catalyst loading at 70 °C.²⁰ In 2013, the Hill group presented a β -diketiminato magnesium alkyl complex, capable of imine hydroboration and in 2016,²¹ Gordon and co-workers explored the activity of redox non-innocent bipyridine ligand supported Ni-catalyst in this domain of research.²² In addition to transition metals, BAr_3^{F} ^{23a} and borenium salts have also contributed to this catalytic transformation.^{23b} Recently, the Radosevich group has shown P-N bond co-operativity of the phosphorus triamide ligand in B-H bond activation and further extended this methodology to imine hydroboration.²⁴ Additionally, Zhang group reported cobalt(II) coordination polymer mediated catalytic imine hydroboration at 0.1 mol% catalyst loading at 70 °C.²⁵

The scarcity of earth abundant metal application in the field of nitrile and imine hydroboration and the reactivity of our previous cobalt catalyst¹⁶ has led us towards the development of second-generation cobalt catalysts that can perform the same transformations under mild conditions. So herein, we report a protonated pyridine diimine (PDIH) supported cobalt (I) complex capable of nitrile hydroboration at ambient temperature.

4.3. Synthesis and Characterization:

Anticipating that strong phosphine coordination to the metal center may have hindered substrate coordination to $(^{\text{Ph}_2\text{PPr}}\text{DI})\text{CoH}$, therefore requiring heating to 60 °C, we have incorporated a different ligand system that substitutes the phosphine substituents with weakly coordinating pyridine donor arms. This ligand system on Mn has been already been explored in the successful catalytic hydrosilylation of carbonyl groups.²⁶

Keeping this in mind, the pyridine substituted ethyl-bridged pyridine diimine ligand, $\text{Py}^{\text{Et}}\text{PDI}$ (1.05 eq.), was metallated with the cobalt precursor, CoCl_2 in THF at room temperature, but only partial conversion was noticed. To optimize the yield, the mixture was heated at $95\text{ }^\circ\text{C}$ in toluene and the complete consumption of CoCl_2 was observed, resulting in the formation of an insoluble light green compound (Scheme 4.1, **19**). ^1H NMR analysis of the compound revealed resonances over a 150 ppm range (Fig. 4.1) and indicated C_2 symmetry of the compound. Magnetic susceptibility measurement by Evans method at ambient temperature showed a value of $3.8\ \mu_{\text{B}}$, suggesting three unpaired electrons in the ground state although this value is slightly lower than those reported for similar compounds.²⁷ Considering the NMR data and magnetic moment, **19** can be best described as the high spin $\text{Co}(\text{II})$ (d^7 , $S = 3/2$) complex, $(\text{Py}^{\text{Et}}\text{PDI})\text{CoCl}_2$.



Scheme 4.1: Synthesis of $(\text{Py}^{\text{Et}}\text{PDI})\text{CoCl}_2$ (**19**).

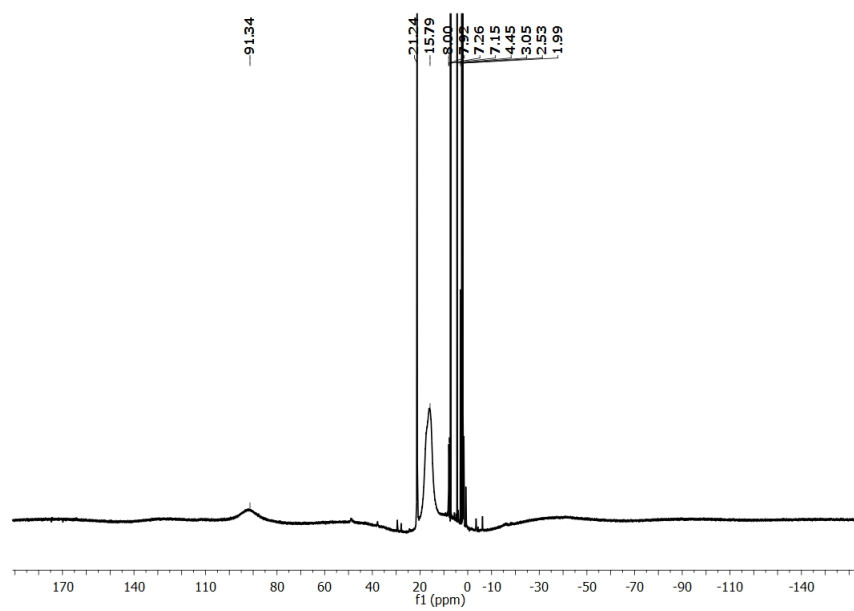
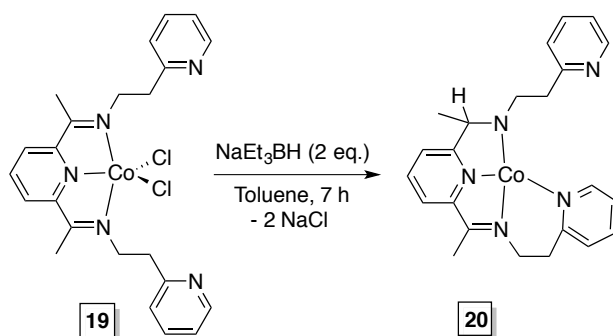


Figure 4.1: ^1H NMR spectrum of **19** in chloroform-*d* at 25 °C.

In order to isolate a hydride complex similar to our previous catalyst, **19** was treated with two equivalents of NaEt_3BH in toluene, which afforded a forest green compound (Scheme 4.2, **20**) after stirring for 7 h at room temperature. Compound **20** was determined to be diamagnetic based on multinuclear NMR (^1H and ^{13}C) spectroscopic analysis. Two distinguishable resonances for backbone methyl groups were detected; one doublet at 1.89 ppm and one singlet at -1.75 ppm. Along with this observation, the existence of four different resonances for the $-\text{CH}_2$ groups suggested a lack of C_2 symmetry (Fig. 4.2). Although **20** was anticipated to be a cobalt hydride complex, no resonance for a metal-hydride bond was detected in the ^1H NMR spectrum.



Scheme 4.2: Synthesis of $(^{\text{PyEt}}\text{PDIH})\text{Co}$ (**20**).

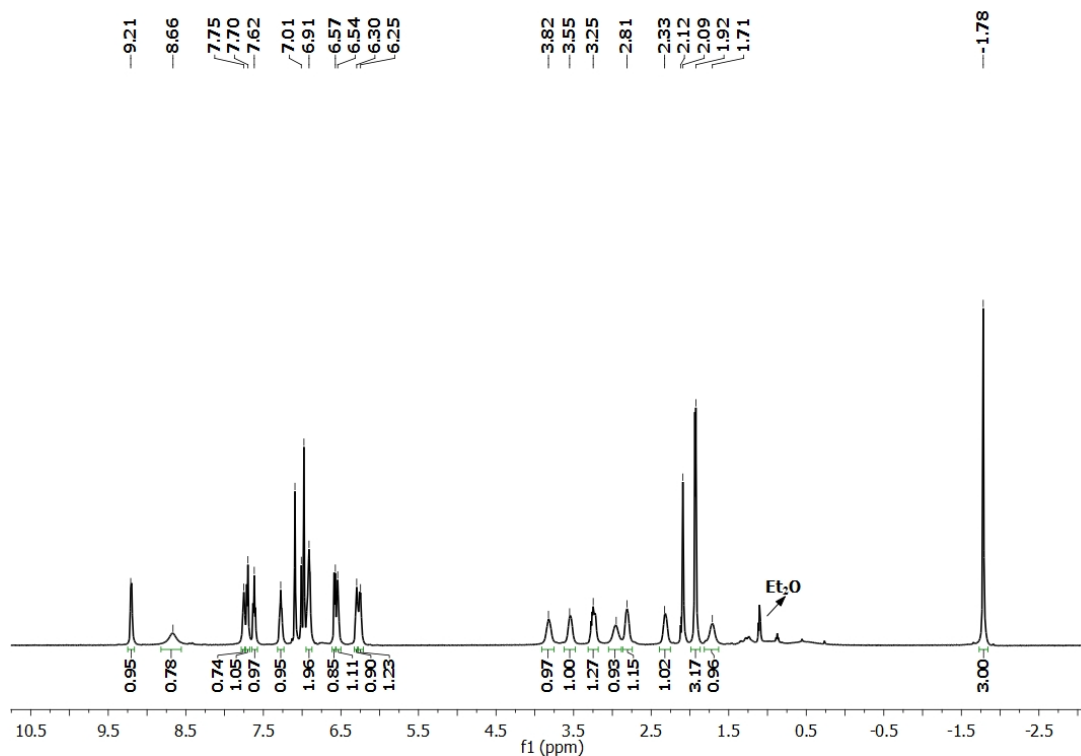


Figure 4.2: ^1H NMR spectrum of **20** in toluene- d_8 at 40 °C.

Single crystals of **20** obtained from a concentrated ether solution at -35 °C were analyzed by X-ray diffraction. The hydrogen atom was not found to be coordinated to the cobalt center, instead it migrated to one of the imine C-N bond, turning the imine nitrogen into an amide nitrogen that is bound to the cobalt center (Fig. 4.3). In the

literature, plenty examples of such metal ligand co-operativity have been found, which plays an important role in homogeneous catalysis.²⁸ It should be noted here that ligand hydride incorporation is responsible for the doublet splitting pattern of the methyl group attached to the same carbon atom. Refinement of the crystal structure revealed κ^4 -*N,N,N,N*-PDI coordination around Co center (Fig. 4.3), with one uncoordinated pyridine arm. Considering the redox non-innocent nature of the DI ligand, attention was drawn to the metrical parameters (Table 4.1). The C_{im} - N_{im} distance was determined to be elongated ($C(2)$ - $N(1) = 1.355(4) \text{ \AA}$), whereas contraction of $C(2)$ - $C(3)$ distance was also observed (1.409 \AA) compared to its neutral ligand analog.^{29a} These distances are more consistent with mono-reduced DI radical anion,^{29b} therefore the Co center of compound **20** can be best described as low spin Co(II) (d^7 , $S = 1/2$) with one unpaired electron that is antiferromagnetically coupled to a DI radical anion. Preliminary DFT results have further corroborated this observation. Additionally, the Co(II)- N_{amide} contact of $1.914(2) \text{ \AA}$ appears to be comparable with the reported Co(II)- N_{amide} distances of TMEDA supported Co(II) complexes, $[(CoL_2)_2(TMEDA)]$ ($L = N(Si^tBuMe_2)(2-C_5H_3N-6-Me)$) and $CoL(Cl)(TMEDA)$ ($L = [N(C_6F_5)(C_6H_3^iPr_2-2,6)]$) respectively by the Lee group.³⁰ The bond angles of $N(1)$ -Co(1)- $N(2)$, $N(1)$ -Co(1)- $N(3)$, $N(2)$ -Co(1)- $N(3)$ and $N(2)$ -Co(1)- $N(4)$ were determined to be $82.11(11)^\circ$, $164.65(11)^\circ$, $84.12(11)^\circ$ and $169.30(11)^\circ$, respectively, giving rise to a distorted square planar geometry around the Co(II) center. It should be mentioned that both chelate mono-reduction and square planar geometry have been found for low spin Co(II) analogues in the literature.³¹

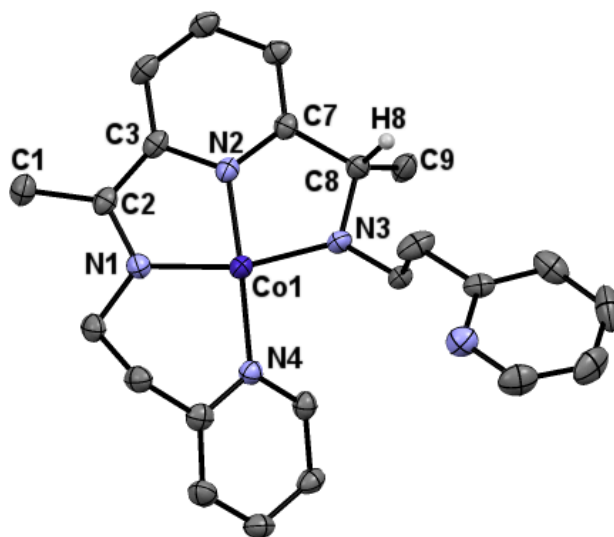


Figure 4.3: The solid-state structure of **20** shown with 30% probability ellipsoids. Hydrogen atoms (except H8) have been omitted for clarity.

Table 4.1: Notable bond lengths (Å) and bond angles (°) determined for **20**.

Bond	Å	Angle	Degree
C(1)-C(2)	1.501(4)	N(1)-Co(1)-N(2)	82.11(11)
C(2)-C(3)	1.409(5)	N(2)-Co(1)-N(3)	84.12(11)
C(7)-C(8)	1.508(4)	N(1)-Co(1)-N(4)	95.77(11)
C(2)-N(1)	1.355(4)	N(2)-Co(1)-N(4)	169.30(11)
C(8)-N(3)	1.473(4)	N(1)-Co(1)-N(3)	164.65(11)
Co(1)-N(1)	1.858(3)		
Co(1)-N(2)	1.825(3)		
Co(1)-N(3)	1.849(3)		

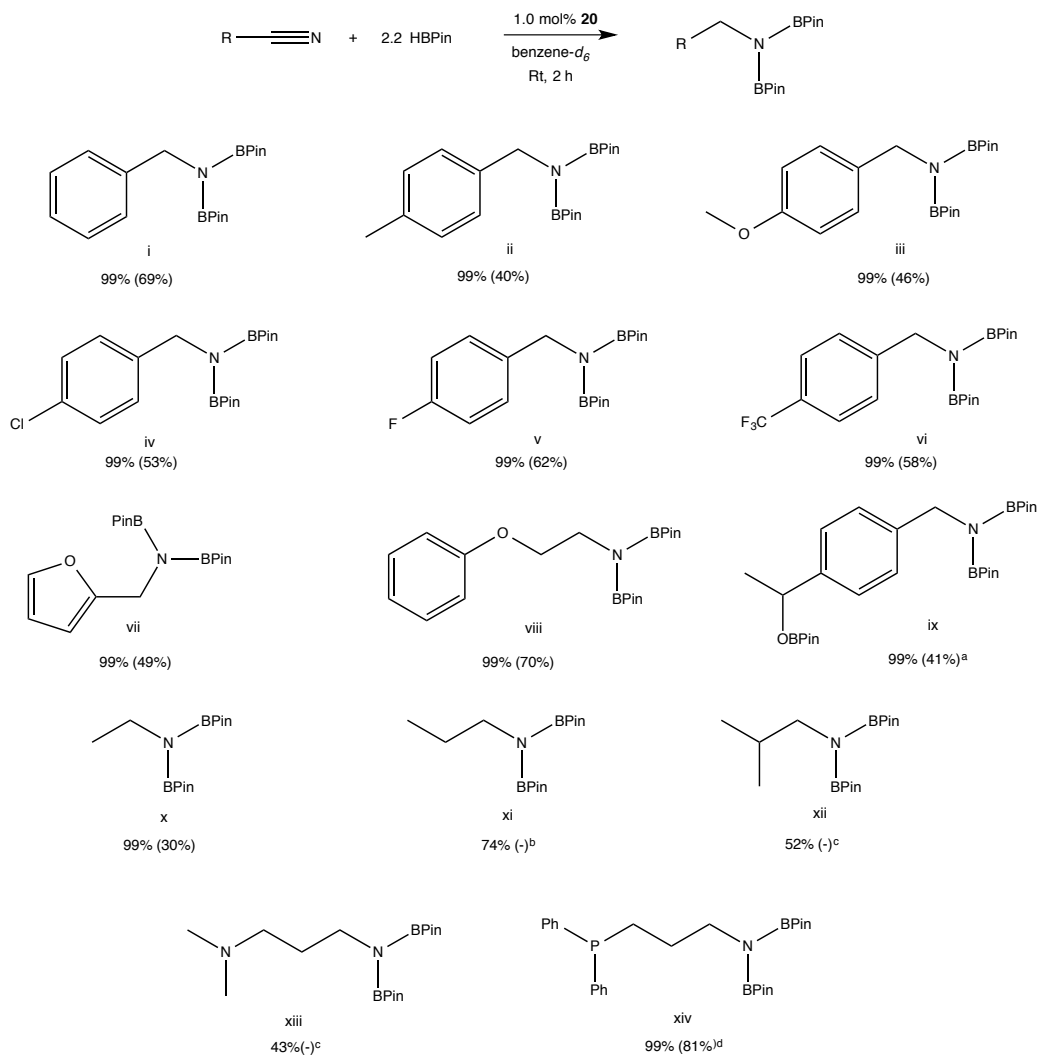
4.4. Catalytic Dihydroboration of Nitriles:

Having isolated and characterized **20**, this pre-catalyst was screened for nitrile dihydroboration activity. In our previous study, HBPin was found to be a suitable borylating reagent and an excess amount (2.2 eq.) was determined to be essential for complete conversion. Following these criteria, a benzene-*d*₆ solution of benzonitrile and

HBPin was added to 1 mol% of **20**. The progress of the reaction was monitored by NMR spectroscopy and >99% conversion of the starting material to diboryl amine was observed after 2 h at room temperature. Inspired by this result, an additional 14 nitrile substrates were screened (Table 4.2) and products were isolated via recrystallization from ether with decent yield. Pre-catalyst **20** was found to be efficient in converting both electron-donating (Entry ii and iii) and electron-withdrawing group containing nitriles (Entry iv, v and vi) to their corresponding diboryl amines within the 2 h reaction time frame. It should be noted that 1 mol% catalytic reactions of 2-phenoxy acetonitrile, 4-(trifluoromethyl) benzonitrile and 4-fluoronitrile became exothermic, suggesting electron withdrawing groups facilitate dihydroboration reactions compared to electron-donating groups. Pre-catalyst **20** was also determined to be tolerant towards various functional groups including halides (Entry iv, v), ethers (Entry iii, viii), and heterocycles (Entry vii). However, olefin functionalities (acrylonitrile did not show any conversion) and phosphine groups (Entry xiv) were found to hinder the catalytic process. Upon addition of the mixture of HBPin and 2-(diphenylphosphino) propionitrile to pre-catalyst **20**, a color change from forest green to red (a brown color was observed for other nitrile substrates) was noticed immediately, which could be due to the coordination of phosphine to the metal center, therefore deterring the substrate coordination and eventually the entire catalytic process. This observation seems to be reasonable, as our previous phosphine-substituted (DI)Co¹⁶ catalyst required heating. However, heating this catalytic mixture to 60 °C allowed for the complete conversion of starting material to its corresponding diboryl amine within 2 h. Knowing that **20** might be active for carbonyl hydroboration, 3.3 eq. of HBPin was added for the reduction of 4-acetyl benzonitrile, and

after 2 h, it was found that both the acetyl and nitrile groups were converted to their respective borylated analog. Along with aromatic nitriles, aliphatic nitriles were also studied and it was found that acetonitrile revealed complete conversion while propionitrile and isobutyronitrile showed 74% and 52% conversion, respectively, after 2 h at room temperature. Moreover, *N,N*-dimethyl propionitrile was determined to be only 43% converted to its corresponding diboryl amine within 2 h and took 3 days for complete conversion. This might be due to coordination of the NMe_2 group of the substrate, which can be the product or starting material that coordinates slows down the catalytic cycle.

Table 4.2: Dihydroboration of nitriles using **20** as pre-catalyst.



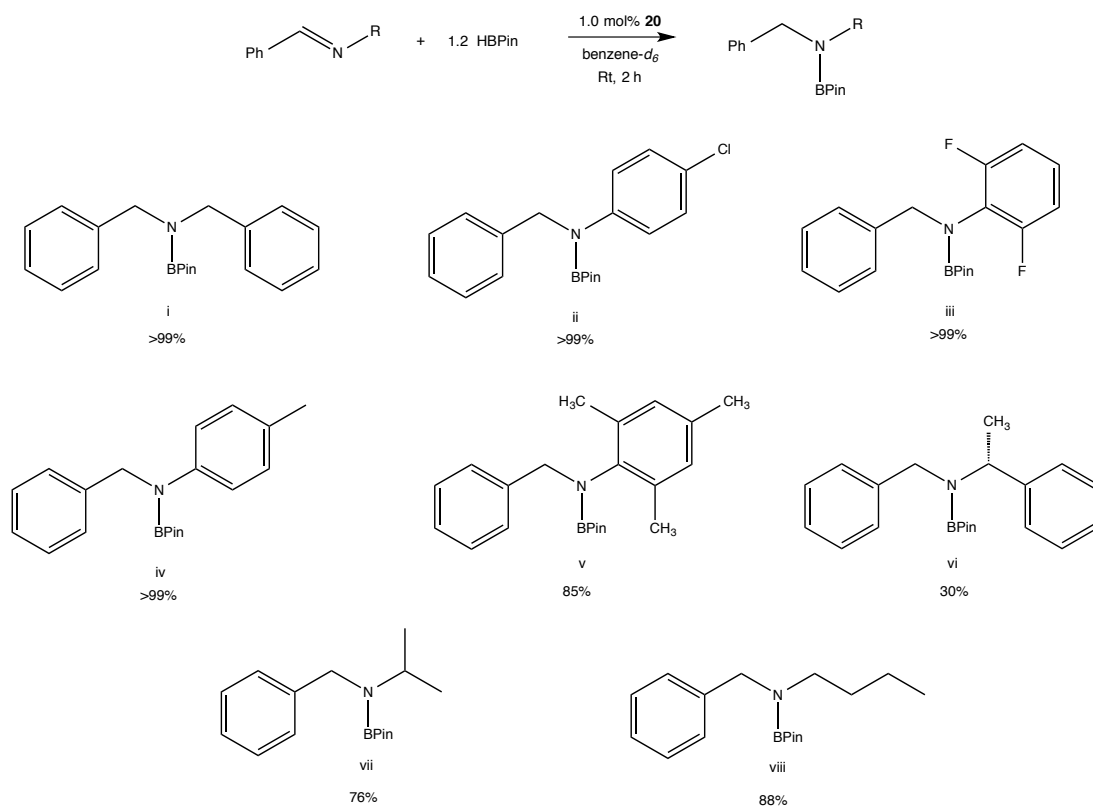
Isolated yields are in parenthesis. a. 3.3 eq. of HBPi was used. b. Conversion reported for 2 h and required 24 h for complete conversion. c. Conversion reported for 2 h and required 72 h for complete conversion. d. Conversion reported at 60 °C.

4.5. Catalytic Hydroboration of Imines:

Expecting imines to be the intermediate of nitrile dihydroboration, **20** was employed as a pre-catalyst for imine hydroboration. A total of 14 imine substrates were synthesized³⁶ through Schiff-base condensation of aldehydes with amines and screened for the study. Anticipating that imines coordinate to the metal center prior to insertion during the catalytic cycle, the steric and electronic effects of the groups attached to the

imine carbon atom have been probed by using phenyl group derivatives. Like the nitriles, a benzene- d_6 solution of the imine and HBPIn (1.2 eq.) was added to 1 mol% of the pre-catalyst **20** at room temperature. Eight imine substrates were studied that feature different nitrogen substitution while keeping phenyl substitution at carbon (Table 4.3). It has been found that **20** successfully hydroborylated imines containing both electron-donating (Entry iv) and electron-withdrawing (Entry ii, iii) nitrogen substituents. All of these substrates were completely (>99%) converted to their corresponding mono-boryl amines, suggesting that electronics of the functional groups present on the nitrogen side have no impact on the catalytic rate. However, the steric effects of the groups present on the nitrogen atom appear to be influencing the catalytic rate. Comparing entries iii and v, it has been found that v having methyl groups on the *ortho* position resulted in 85% conversion after 2 h while ii showed complete conversion. This can be attributed to the smaller size of fluorine compared to a methyl group. Additionally, 30% conversion was determined for entry vi containing a methyl group at α -carbon of the N-substituent whereas complete conversion was observed for entry i, having only hydrogens at the α -carbon. For entries vii and viii, 76% and 88% conversion was found, respectively, which could be the result of trace water present in the imine substrates after synthesis. Due to this reason, complete conversion required 3 days and 2 days for entries vii and viii, respectively.

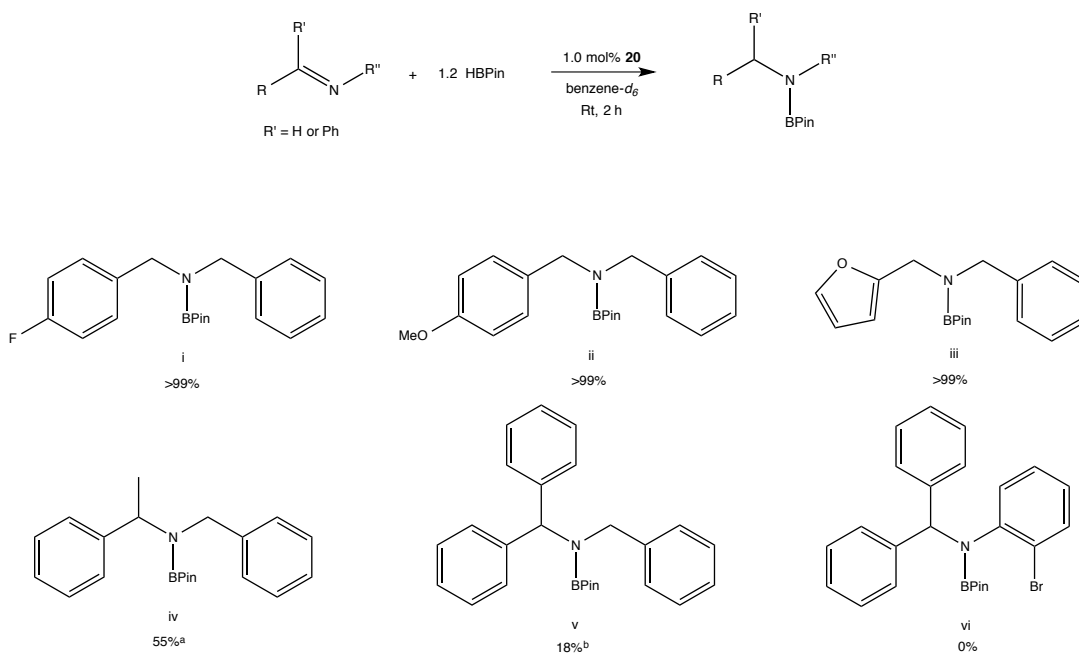
Table 4.3: Hydroboration of imines with varied nitrogen substituents using **20** as a pre-catalyst.



Imine substrates featuring substituted phenyl rings, heterocycles and di-substituted carbon atoms have also been screened (Table 4.4). Like nitrogen substitution, imine carbon atoms containing electron donating (Entry ii) and electron withdrawing phenyl substituents (Entry i) were successfully hydroborated with 1 mol% catalyst loading within 2 h at room temperature. A heterocyclic furan ring (Entry iii) did not hinder the percentage conversion of the imine to its corresponding mono-boryl amine. Replacing the hydrogen atom attached to the imine carbon with a methyl group or phenyl ring drastically slowed down the conversion rate. The percent conversion for entries iv and v was determined to be 55% and 18%, respectively, under similar catalytic conditions. The steric effects of methyl and phenyl substitution can be considered as the

contributor for this diminished rate. In fact, entry v, containing two phenyl groups did not show complete conversion even after 7 days. Although **20** has been found to tolerate halide substitution at the *para*-position of the phenyl ring, it seems likely to participate in an oxidative addition reaction with the C-Br bond of 2-bromo-N-(diphenylmethylene) benzenamine (Entry vi). Upon addition of this substrate to the benzene-*d*₆ solution of **20**, the solution turned green in color and the ¹H NMR spectrum of the mixture indicated formation of a paramagnetic compound. Unlike the nitriles, attempts to isolate the mono-boryl amines via crystallization failed due to hydrolysis of the N-B bond. Although, the reason for hydrolysis remains elusive, a -CH₂ new signal was detected over time along with more ¹H NMR resonances in the aromatic region.

Table 4.4: Hydroboration of imines with variable substituents at carbon side using pre-catalyst **20**.



a. Required 24 h for complete conversion. b. Not completed even after 7 days.

4.6. Mechanistic Study:

To investigate the operative mechanism of **20**-mediated catalytic nitrile dihydroboration, a series of stoichiometric reactions have been executed. Upon addition of one equivalent of benzonitrile or *p*-tolunitrile to a benzene-*d*₆ solution of pre-catalyst **20**, no color change was noticed and ¹H NMR spectroscopy did not indicate the generation of any new compound. This observation led us to preclude nitrile addition as the activation step of the catalytic cycle. Then, the impact of stoichiometric addition of pinacolborane to the pre-catalyst was investigated. Reaction of pre-catalyst (**20**) with pinacolborane (HBPin) furnished a new compound as evidenced from ¹H NMR spectroscopy (Fig. 4.4) and the ¹¹B NMR spectrum featured one sharp and one broad peak (Fig. 4.6), indicating the formation of a new boryl compound. However, it should be noted that the complete consumption of starting material required 2.2 equivalents of HBPin and no excess HBPin has been detected at the end of the reaction. In the case of alkene,³² alkyne³³ or nitrile^{15,21,22} hydroboration, oxidative addition of borane to generate a metal hydride complex has been proposed to be the catalyst activation step. However, no hydride peak was detected by ¹H NMR spectroscopy for the reaction mixture of the pre-catalyst and HBPin at room temperature after 2 h. Based on this observation, it has been hypothesized that a transient cobalt hydride may have been formed, which immediately reacted with HBPin to yield a new compound. Integration of methyl resonances between 0.88-1.22 ppm (which is consistent with Co-BPin complexes^{34,45}) accounted for 24 H (Fig. 4.4) and additionally, ¹³C NMR spectroscopy showed the presence of two HBPin quaternary carbons (82.2 and 83.2 ppm) (Fig. 4.5). These spectroscopic observations opened up two plausible mechanisms.

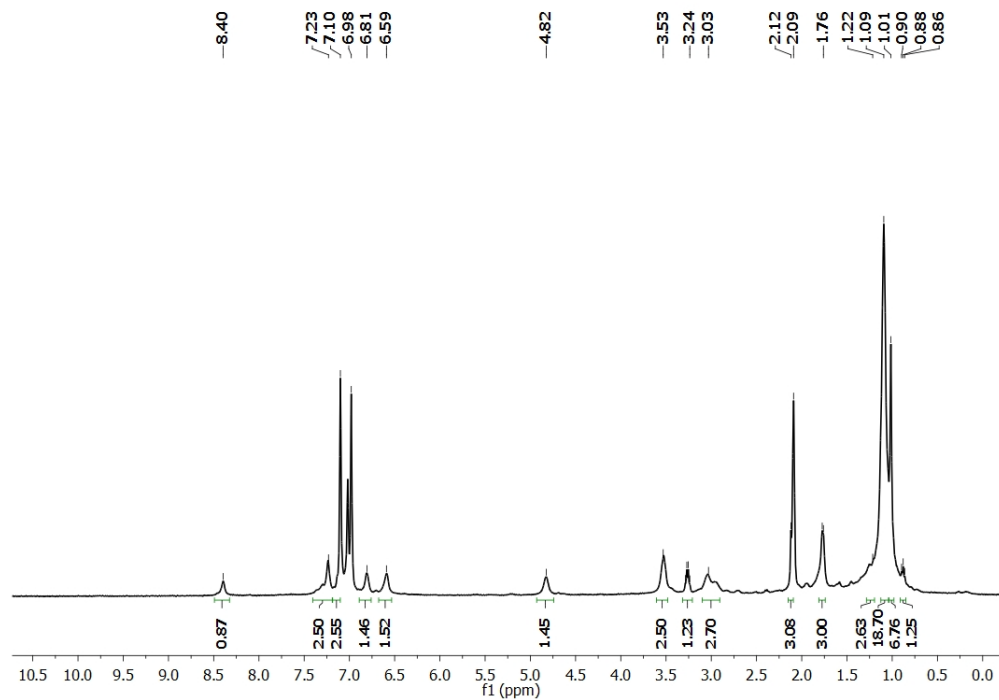


Figure 4.4: ^1H NMR spectrum of the reaction mixture of pre-catalyst **20** and HBPin (2.2 eq.) in toluene- d_8 at 25 °C.

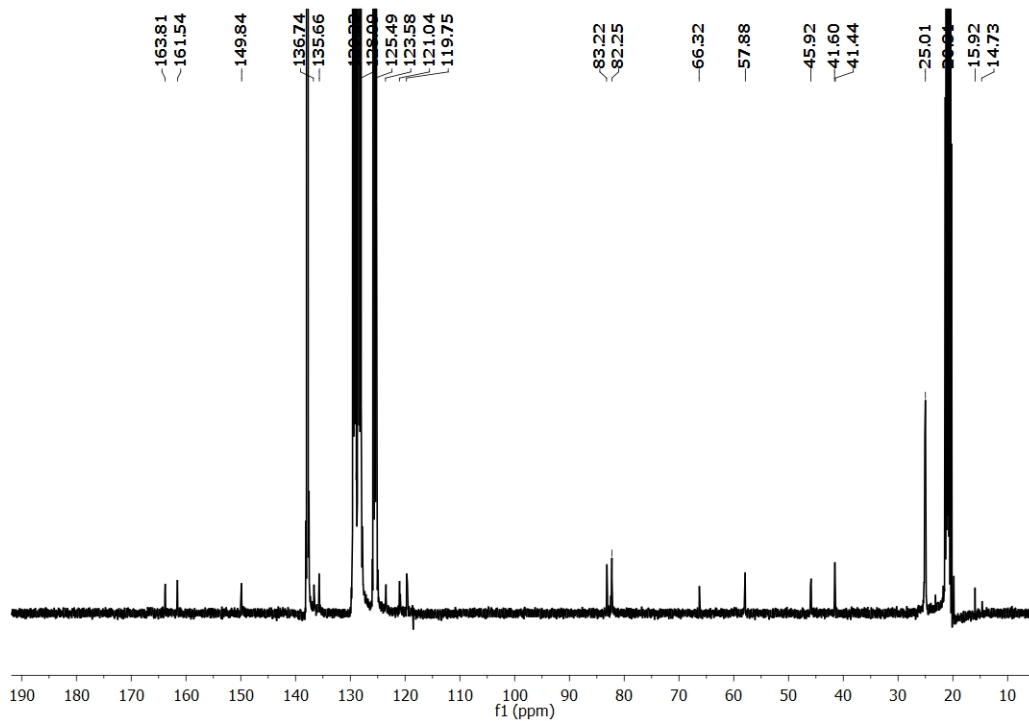


Figure 4.5: ^{13}C NMR spectrum of the reaction mixture of pre-catalyst **20** and HBPin (2.2 eq.) in toluene- d_8 at 25 °C.

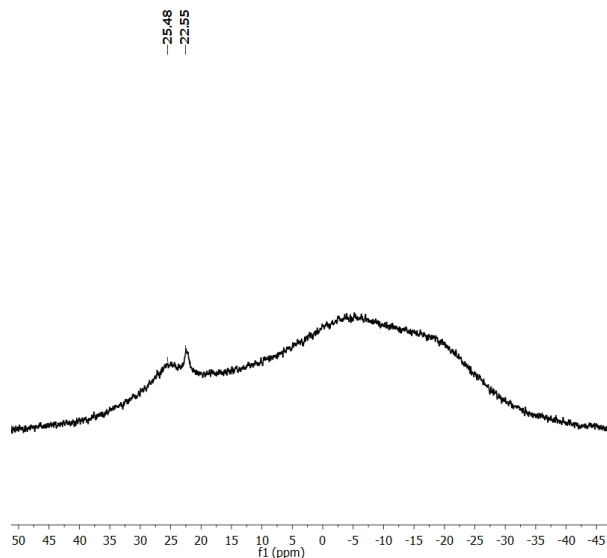


Figure 4.6: ^{11}B NMR spectrum of the reaction mixture of pre-catalyst **20** and HBPIn (2.2 eq.) in toluene- d_8 at 25 °C.

According to pathway 1 (Fig. 4.7), a cobalt(III) diboryl complex (**A**) can be formed upon oxidative addition of HBPIn to **20** to generate a cobalt(III) hydrido boryl intermediate, which can then undergo σ -bond metathesis with another HBPIn releasing H_2 . Incoming nitrile can insert into the cobalt-boron bond of **A** to yield a borylated imine intermediate **B**, which can then participate in σ -bond metathesis with incoming HBPIn to release the imine intermediate and regenerate the catalyst. Then, this intermediate can re-enter the catalytic cycle following insertion into the cobalt-boron bond (**C**) and another σ -bond metathesis reaction will finally release the desired diboryl amine product. According to pathway 2, the first step could be the σ -bond metathesis of HBPIn across the cobalt-nitrogen (amide) bond to afford an N-borylated cobalt(I) hydride intermediate, which will then undergo σ -bond metathesis with the B-H bond of incoming HBPIn to furnish an N-borylated cobalt(I) boryl intermediate **D** (Fig. 4.8). Following the generation of **D**, a similar mechanism can operate in order to produce the diboryl amine product.

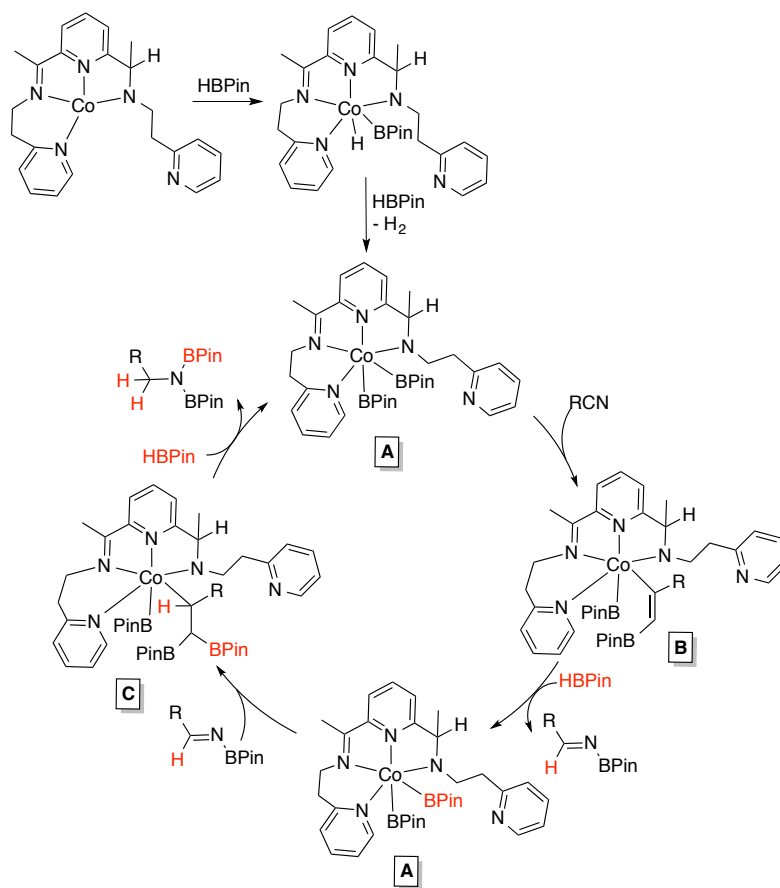


Figure 4.7: Plausible mechanism for **20**-mediated nitrile dihydroboration (Mechanism 1).

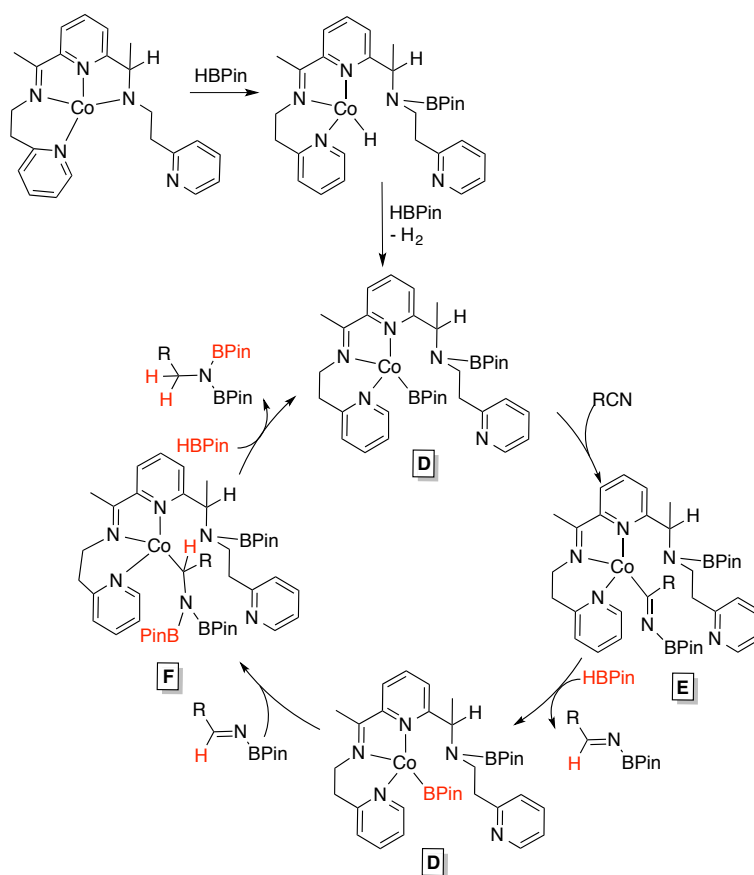


Figure 4.8: Plausible mechanism for **20**-mediated nitrile dihydroboration (Mechanism 2).

To find out the resting state of the catalytic cycle, the HBPin addition product has been probed through 1D, 2D (Fig. 4.9, 4.10), ^{13}C and ^{11}B NMR spectroscopy. ^1H NMR spectroscopy revealed the presence of two backbone methyl groups, one singlet resonance at 2.12 ppm (20.99 ppm in ^{13}C NMR) and one doublet resonance at 1.76 ppm (19.47 ppm in ^{13}C NMR), arising from hydrogen coupling. Moreover, the coupled hydrogen appeared as a multiplet at 4.82 ppm (57.88 ppm in ^{13}C NMR). These results suggest that the intermediate does not possess C_2 symmetry, which is reflected in the presence of 4 different $-\text{CH}_2$ groups. Based on examination of the 1D and 2D spectra, $-\text{CH}_2$ groups have been located at 3.52 ppm (45.92 ppm in ^{13}C NMR), 3.25 ppm (66.32 ppm in ^{13}C NMR), 3.03 ppm (41.44 ppm in ^{13}C NMR) and 1.09 ppm (24.02 ppm in ^{13}C

NMR). Additionally, resonances for two different boryl groups have been observed in the region of 0.88-1.09 ppm, the corresponding methyl group carbon atoms have been found in the region of 25 ppm (^{13}C NMR), and the quaternary carbons have been located at 83.2 and 82.2 ppm (^{13}C NMR). However, all these spectroscopic observations are consistent with the structure assignment of both **A** and **D**. On the other hand, ^{11}B NMR spectroscopy showed a sharp peak at 22.5 ppm along with a broad peak at 25.55 ppm. The ^{11}B resonance for cobalt boryl complexes are known to be broad as reported by the Chirik group^{34,35} and the sharp peak is expected to be a non-metal bound boryl functionality. These observations have strengthened the preference for intermediate **C** over **A**. Additionally, the study of C-H borylation mediated by different cobalt complexes reported by the Chirik group indicated the formation of a Co(I) resting state is preferred for insertion chemistry over a Co(III),³⁴ which has been proven in their alkene hydroboration study.^{32b}

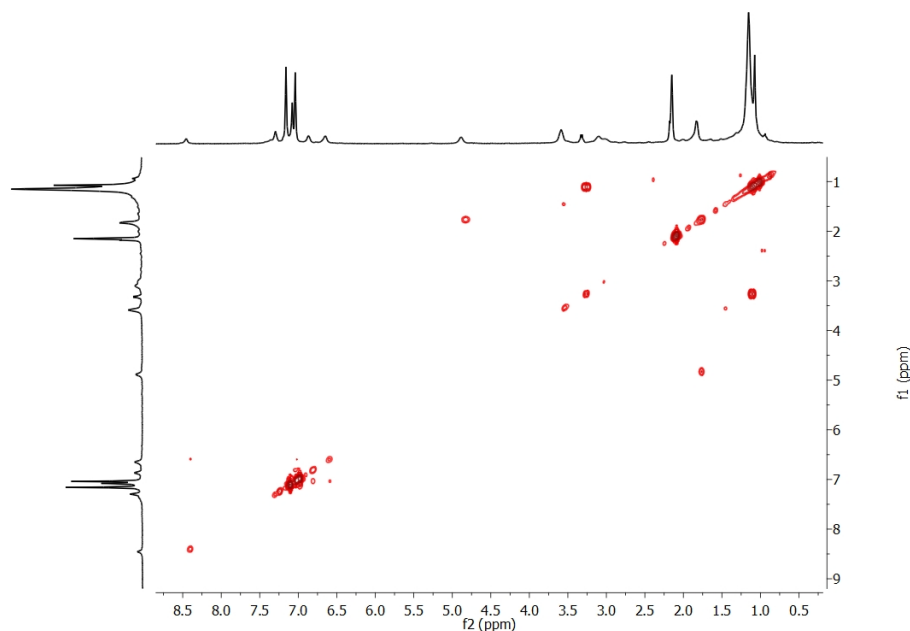


Figure 4.9: gCOSY spectrum of the reaction mixture of pre-catalyst **20** and HBPin (2.2 eq.) in toluene- d_8 at 25 °C.

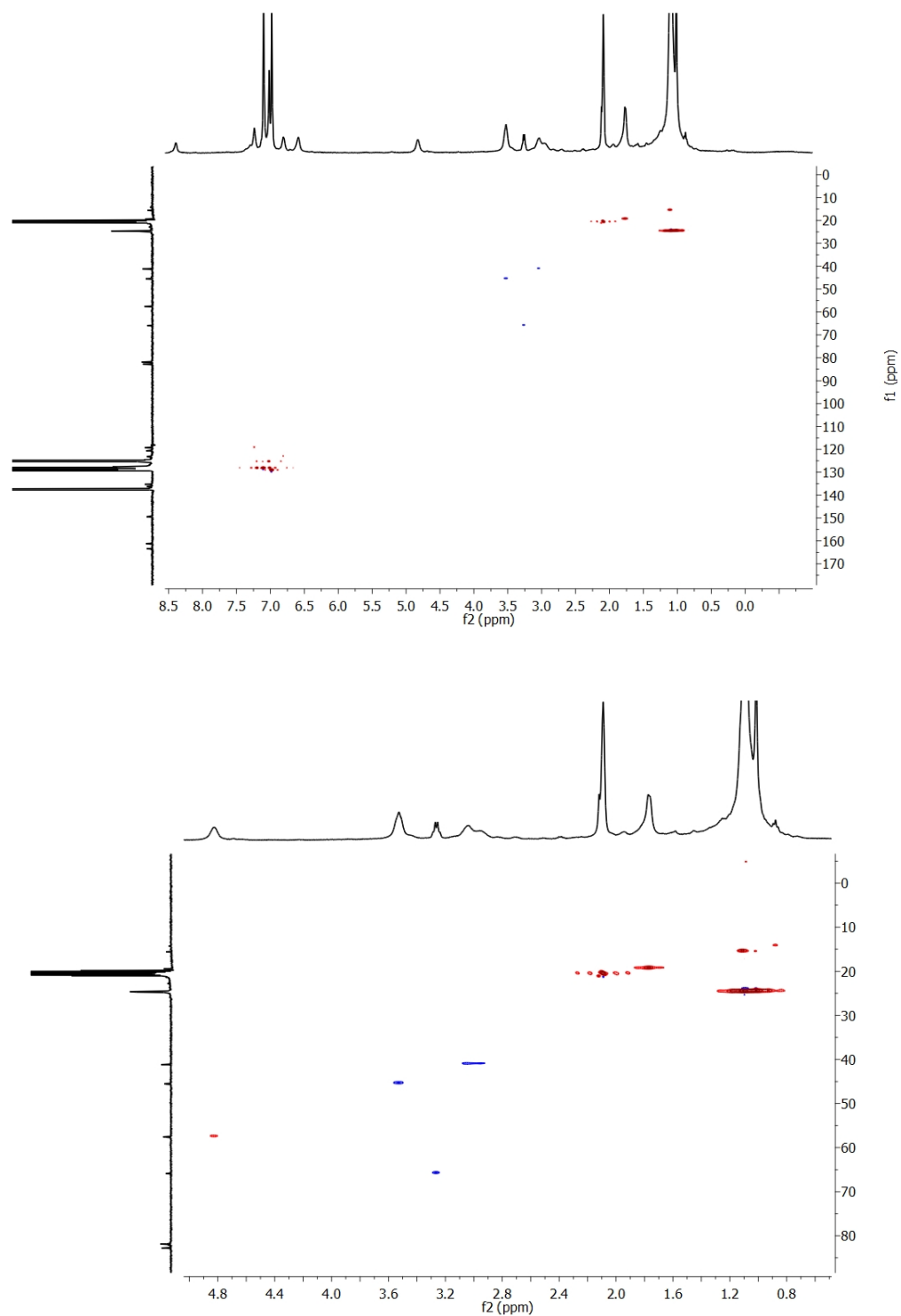


Figure 4.10: HSQC spectrum of the reaction mixture of pre-catalyst **20** and HBPIn (2.2 eq.) in toluene- d_8 at 25 °C (top, entire region and bottom, selected aliphatic region).

4.7. Conclusion:

In summary, the synthesis of a protonated pyridine-substituted pyridine diimine Co(I) complex has been synthesized and characterized through multinuclear spectroscopy and X-ray diffraction analysis. Upon adding NaEt₃BH to cobalt dichloride complex, the hydrogen atom has been found to migrate from the metal center to one of the imine bonds of PDI, which has been confirmed by NMR spectroscopy and XRD structural analysis. The catalytic nitrile and imine hydroboration activity of **20** has been documented with a broad substrate scope for both nitriles and imines. It has been determined that electronic effects of the substituent at the *para*-position of the phenyl ring of nitriles or imines has no impact on the catalytic rate. The cobalt pre-catalyst is tolerant to various functional groups including halides, ethers and heterocycles. However, the steric effects of bulky substituents at the carbon atom or in close proximity to the nitrogen atom have been found to diminish the catalytic rate. The mechanism for nitrile dihydroboration has been investigated with detailed 1D and 2D NMR spectroscopy. To the best of our knowledge, **20** is the first known cobalt catalyst capable of catalyzing nitrile hydroboration at room temperature with a low catalyst (1 mol%) loading.

4.8. Experimental Section:

4.8.1. Preparation of (P^{PyEt}PDI)CoCl₂ (**19**) :

In a nitrogen filled glove box, a 100 mL bomb apparatus was charged with CoCl₂ (83.9 mg, 0.6460 mmol) followed by P^{PyEt}PDI (252 mg, 0.6783 mmol) in approximately 10 mL of toluene. The apparatus was sealed, taken outside the box and heated at 95 °C in a pre-heated oil bath. After stirring for 4 days, the reaction mixture was filtered and a light

green insoluble compound was collected from the top of the frit with an orange colored liquid as the filtrate. The residue was washed with ether (3 X 5 mL) and pentane (3 X 5 mL) to remove excess ligand and dried under vacuum to yield 0.250 g of a light green solid compound (77 %) identified as (^{PyEt}PDI)CoCl₂ (**19**). Anal. Calcd for C₂₃H₂₅N₅Cl₂Co: C, 55.10%; H, 5.03%; N, 13.97%. Found: C, 44.92%; H, 4.28%; N, 11.23%. Magnetic susceptibility (Evans method in acetonitrile-*d*₃ solvent, 25 °C): $\mu_{\text{eff}} = 3.8 \mu_{\text{B}}$. ¹H NMR (chloroform-*d*, 25 °C): δ 91.34 (3315.93 Hz), 16.28 (2094.64 Hz).

4.8.2. Preparation of (^{PyEt}PDIH)Co (**20**) :

In a nitrogen filled glove box, a 100 mL round bottom flask was filled with (^{PyEt}PDI)CoCl₂ (**19**) (99.9 mg, 0.1993 mmol) in an approximately 20 mL of toluene and cooled in cold well for 20 minutes. A 20 mL scintillation vial containing a solution of NaEt₃BH (0.4 mL, 0.3985 mmol) in toluene was also cooled in the cold well for 20 minutes. Then the NaEt₃BH was added drop wise to the round bottom flask containing the suspension of **19** in toluene. Initially, the color changed from light green to red and then to forest green color. After stirring for 7 h, the reaction mixture was filtered through Celite to remove the byproduct NaCl and then the solvent was removed under vacuum. The residue was washed with pentane (2 X 3 mL) and then dried to obtain 64.5 g (75%) of a forest green solid compound, identified as (^{PyEt}PDIH)Co (**20**). Anal. Calcd for C₂₃H₂₆N₅Co: C, 64.03%; H, 6.07%; N, 16.23%. Found: C, 63.62%; H, 6.28%; N, 15.86%. ¹H NMR (500 MHz, toluene-*d*₈) δ 9.20 (d, *J* = 6.4 Hz, 1H, *phenyl*), 8.66 (br, 1H, *phenyl*), 7.75 (m, 1H, *phenyl*), 7.71 (d, *J* = 8.2 Hz, 1H, *phenyl*), 7.62 (t, *J* = 7.5 Hz, 1H, *phenyl*), 7.28 (t, *J* = 6.3 Hz, 1H, *phenyl*), 6.91 (m, 2H, *phenyl*), 6.58 (d, *J* = 7.6 Hz, 1H, *phenyl*), 6.54 (m, 1H, *phenyl*), 6.30 (m, 1H, *phenyl*), 6.25 (m, 1H, -CH), 3.82 (br, 1H, -

CH_2), 3.55 (br, 1H, $-CH_2$), 3.25 (br, 1H, $-CH_2$), 2.95 (br, 1H, $-CH_2$), 2.81 (br, 1H, $-CH_2$), 2.33 (br, 1H, $-CH_2$), 1.93 (d, $J = 6.4$ Hz, 3H, $-CH_3$), 1.71 (br, 1H, $-CH_2$), -1.78 (s, 3H, $-CH_3$).

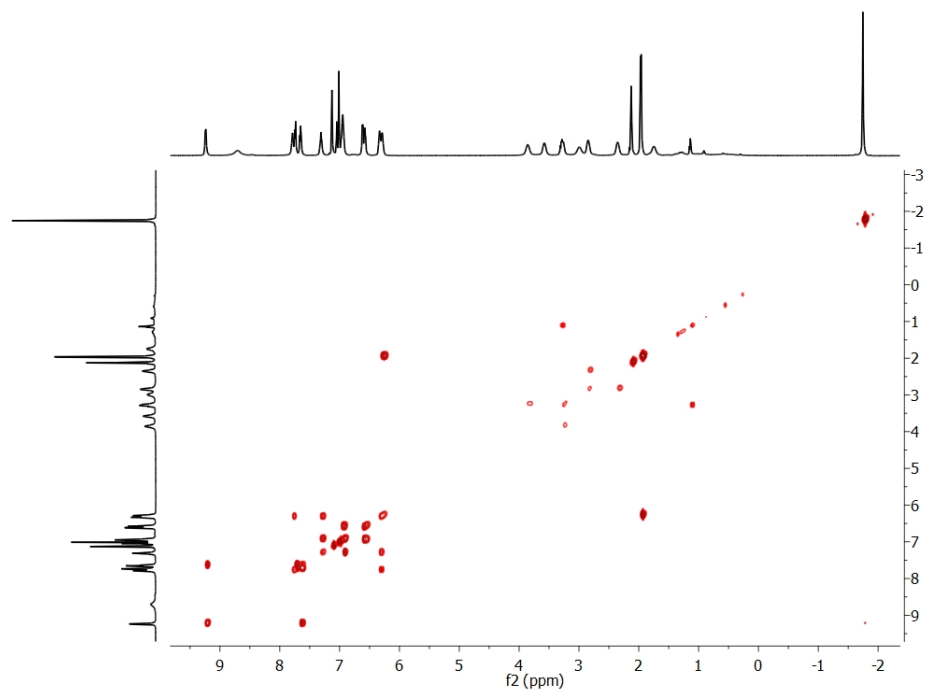


Figure 4.11: gCOSY spectrum of **20** in toluene- d_8 at 40 °C.

4.8.3. Catalytic Nitrile Dihydroboration Using Complex **20**:

NMR scale dihydroboration of benzonitrile (1 mol% **20**):

In the nitrogen filled glove box, a benzene- d_6 solution of benzonitrile (62.1 μ L, 0.603 mmol) and pinacolborane (0.19 mL, 1.326 mmol) was added to a vial containing 2.6 mg (0.0060 mmol) of **20**. The resulting solution immediately changed color from green to dark purple, which was transferred to a J. Young tube and remained at ambient temperature for 2 h. Both 1H NMR and ^{13}C NMR spectroscopy confirmed >99% conversion of the starting nitrile compound to diboryl amine, $PhCH_2N(BPin)_2$ after 2 h at

room temperature. After removal of the solvent under vacuum, the product was recrystallized from pentane at $-35\text{ }^{\circ}\text{C}$ to obtain a white solid compound (0.150 g, yield = 69 %). ^1H NMR (500 MHz, benzene- d_6) δ 7.60 (d, $J = 7.2$ Hz, 2H, *phenyl*), 7.26 (t, $J = 7.7$ Hz, 2H, *phenyl*), 7.12 (t, $J = 7.4$ Hz, 1H, *phenyl*), 4.63 (s, 2H, $-\text{CH}_2-$), 1.04 (s, 24H, $\text{C}(\text{CH}_3)_2$). ^{13}C NMR (126 MHz, benzene- d_6) δ 144.44 (*phenyl*), 128.93 (*phenyl*), 127.23 (*phenyl*), 83.17 ($-\text{CH}_2\text{N}$), 48.52 ($-\text{C}(\text{CH}_3)_2$), 25.23 ($-\text{C}(\text{CH}_3)_2$).

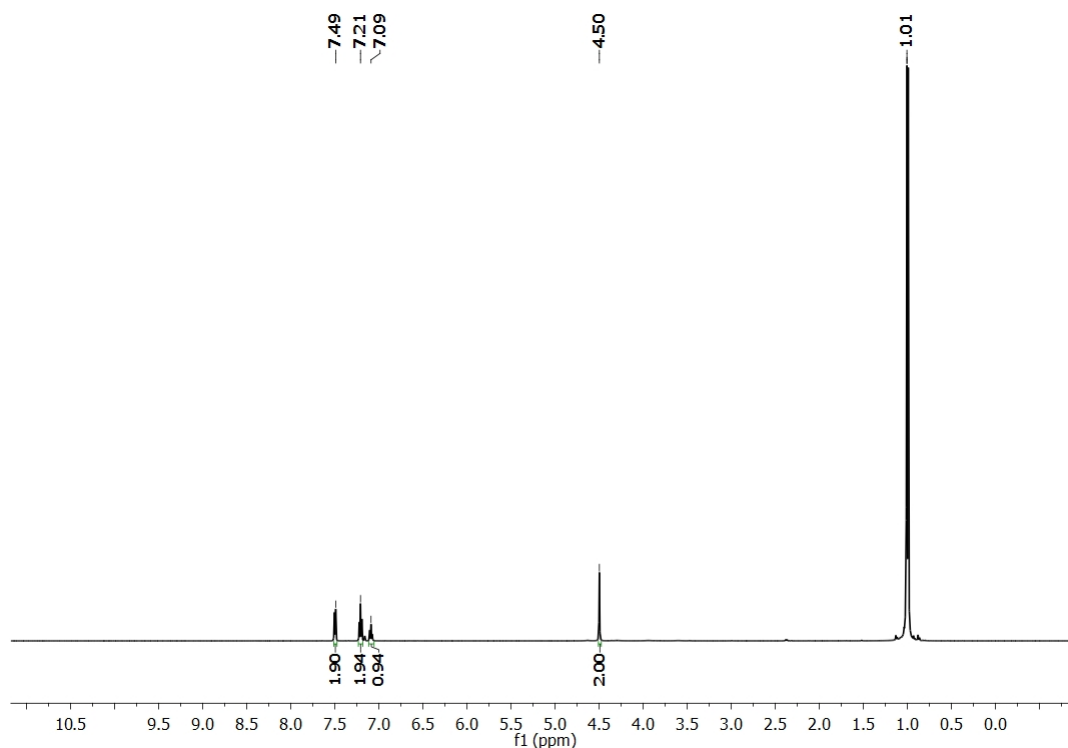


Figure 4.12: Conversion of benzonitrile to diboryl amine using 1 mol% catalyst **20** in benzene- d_6 .

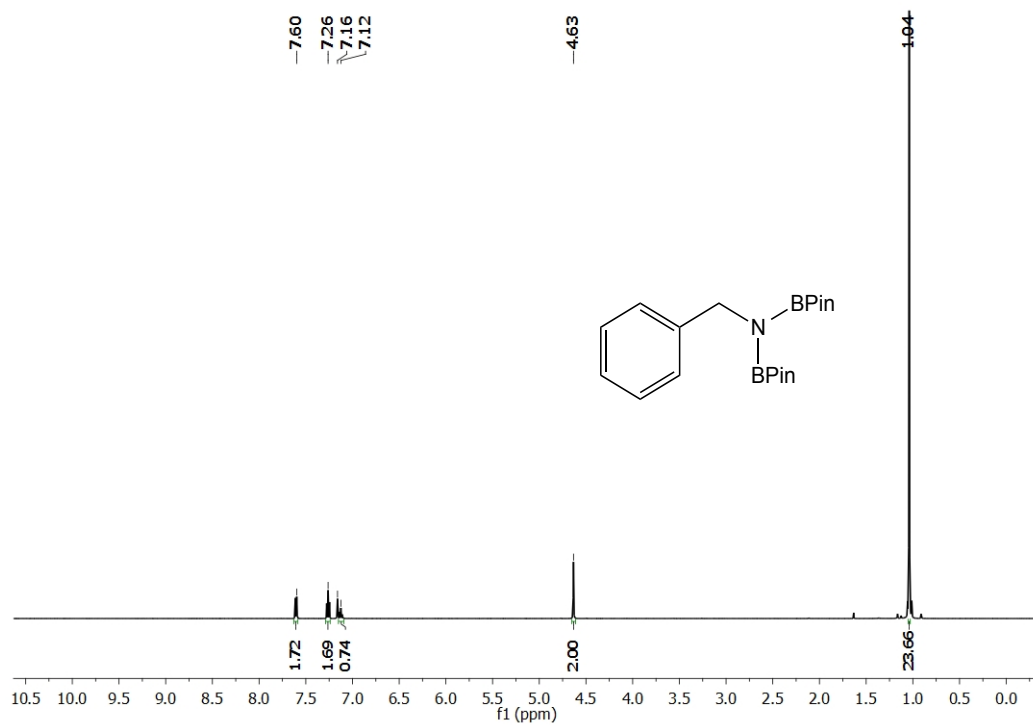


Figure 4.13: ^1H NMR spectrum of $\text{PhCH}_2\text{N}(\text{BPin})_2$ in $\text{benzene-}d_6$.

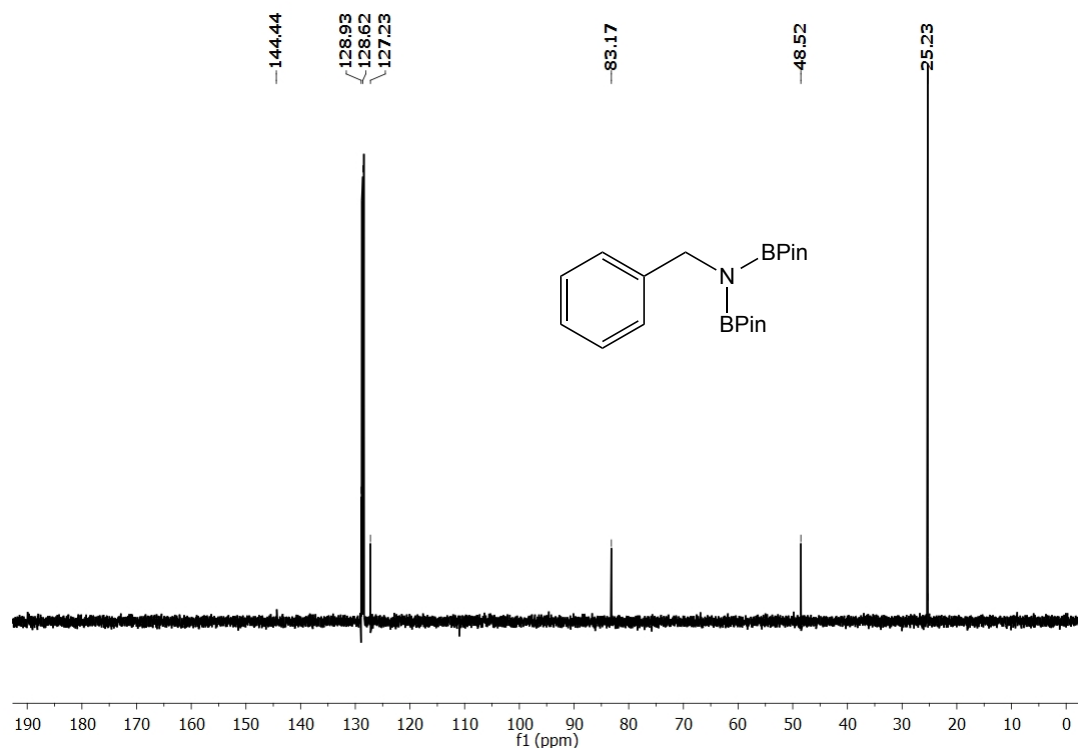


Figure 4.14: ^{13}C NMR spectrum of $\text{PhCH}_2\text{N}(\text{BPin})_2$ in $\text{benzene-}d_6$.

NMR scale dihydroboration of 4-methylbenzotrile (1 mol% **20**):

In the nitrogen filled glove box, a $\text{benzene-}d_6$ solution of 4-methylbenzotrile (70.6 mg, 0.603 mmol) and pinacolborane (0.19 ml, 1.326 mmol) was added to a vial containing 2.6 mg (0.0060 mmol) of **20**. The resulting solution immediately changed color from green to dark purple, which was transferred to a J. Young tube and remained at ambient temperature for 2 h. Both ^1H NMR and ^{13}C NMR spectra confirmed >99% conversion of the starting nitrile compound to diboryl amine, $(4\text{-MePh})\text{CH}_2\text{N}(\text{BPin})_2$ after 2 h at room temperature. After removal of the solvent under vacuum, the product was recrystallized from ether at $-35\text{ }^\circ\text{C}$ to obtain a white solid compound (0.091 g, yield = 40%). ^1H NMR (500 MHz, $\text{benzene-}d_6$) δ 7.02 (d, $J = 7.8$ Hz, 2H, *phenyl*), 6.97 (d, $J = 7.9$ Hz, 2H, *phenyl*), 3.55 (s, 2H, $\text{N}(\text{CH}_2)$), 2.12 (s, 3H, $-\text{CH}_3$), 1.05 (s, 24H, $-\text{C}(\text{CH}_3)_2$).

^{13}C NMR (126 MHz, benzene- d_6) δ 141.38 (*phenyl*), 136.20 (*phenyl*), 129.56 (*phenyl*), 82.96 (-NCH $_2$), 48.07 (-C(CH $_3$) $_2$), 25.64 (-C(CH $_3$) $_2$), 21.65 (-CH $_3$).

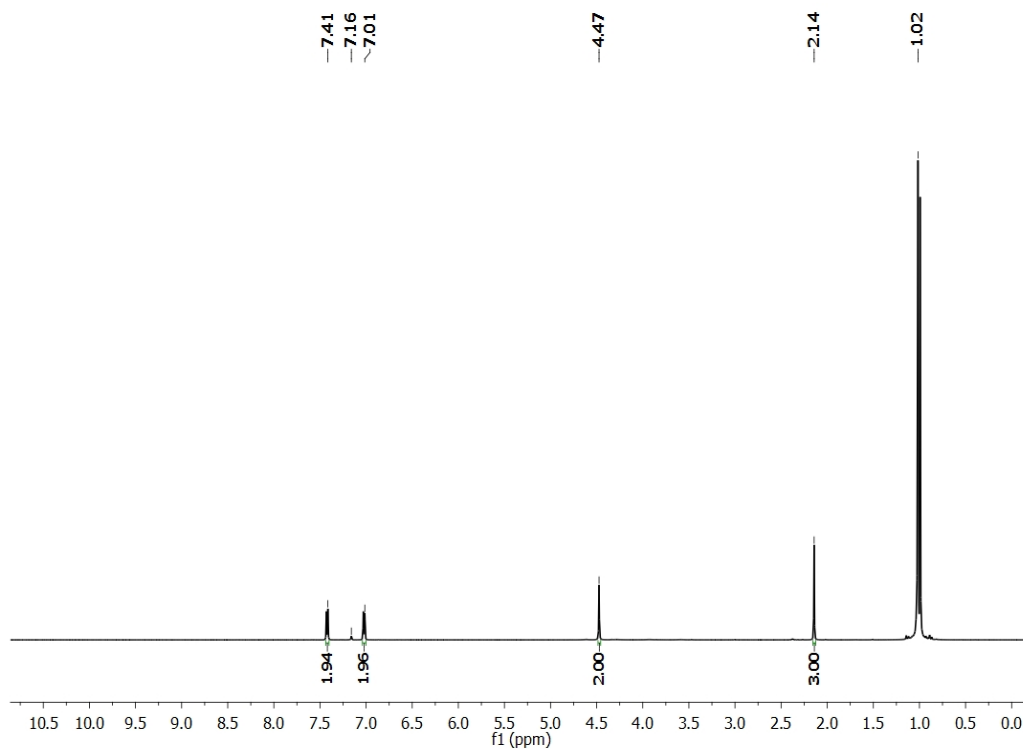


Figure 4.15: Conversion of 4-methylbenzamide to diboryl amine using 1 mol% catalyst **20** in benzene- d_6 after 2 h.

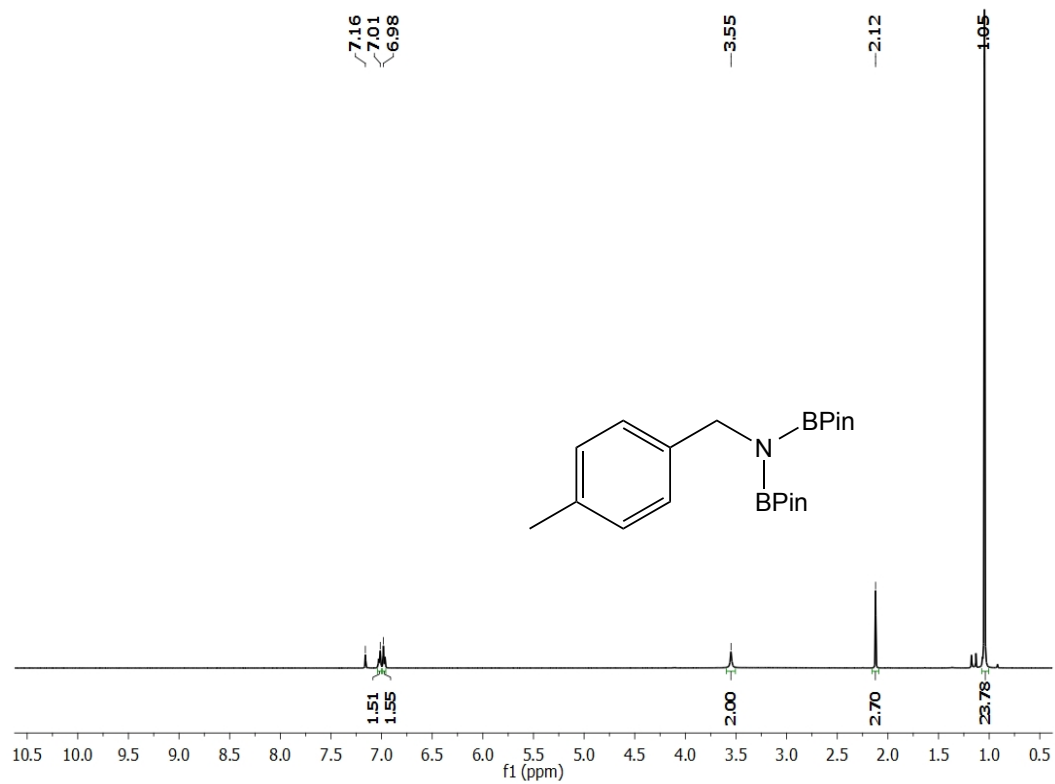


Figure 4.16: ^1H NMR spectrum of (4-MePh) $\text{CH}_2\text{N}(\text{BPin})_2$ in benzene- d_6 .

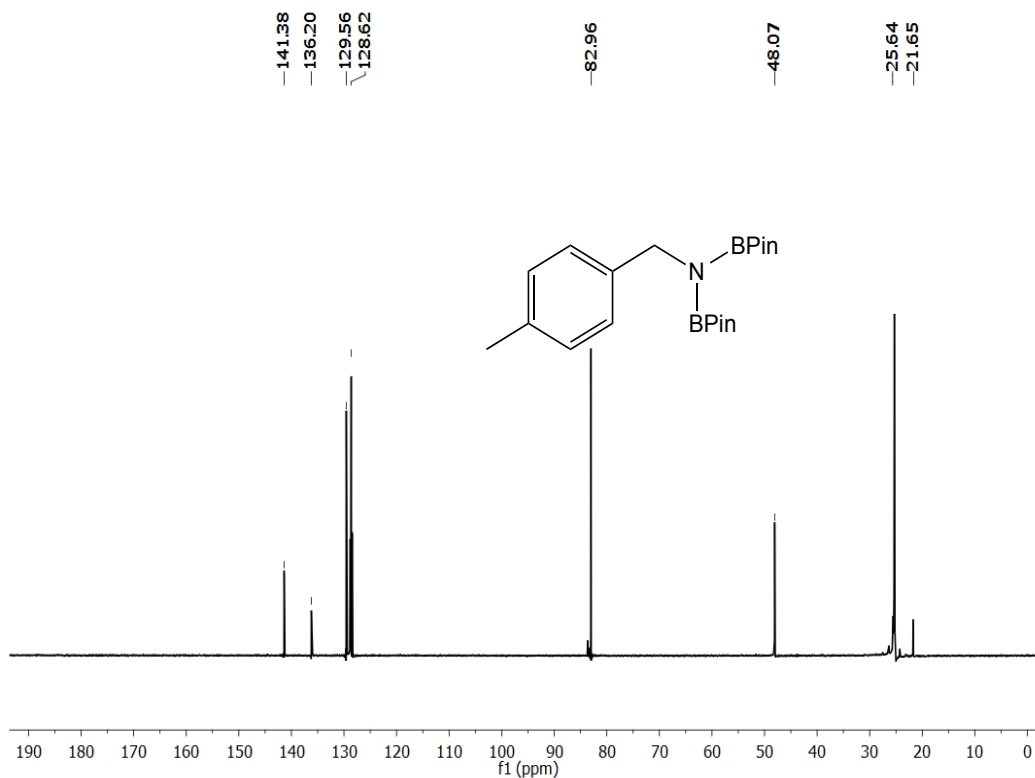


Figure 4.17: ^{13}C NMR spectrum of (4-MePh) $\text{CH}_2\text{N}(\text{BPin})_2$ in benzene- d_6 .

NMR scale dihydroboration of 4-methoxybenzotrile (1 mol% **20**):

In the nitrogen filled glove box, a benzene- d_6 solution of 4-methoxybenzotrile (74.1 mg, 0.556 mmol) and pinacolborane (0.18 mL, 1.224 mmol) was added to a vial containing 2.4 mg (0.0056 mmol) of **20**. The resulting solution immediately changed color from green to dark purple, which was transferred to a J. Young tube and remained at ambient temperature for 2 h. Both ^1H NMR and ^{13}C NMR spectroscopy confirmed >99% conversion of the starting nitrile compound to diboryl amine, (4-OMePh) $\text{CH}_2\text{N}(\text{BPin})_2$ after 2 h at room temperature. After removal of the solvent under vacuum, the product was recrystallized from ether at $-35\text{ }^\circ\text{C}$ to obtain a white solid compound (0.100 g, yield = 46 %). ^1H NMR (500 MHz, benzene- d_6) δ 7.59 (d, $J = 8.7$ Hz, 2H, *phenyl*), 6.89 (d, $J = 8.7$ Hz, 2H, *phenyl*), 4.61 (s, 2H, $-\text{NCH}_2$), 3.35 (s, 3H, -

OCH₃), 1.06 (s, 24H, -C(CH₃)₂). ¹³C NMR (126 MHz, benzene-*d*₆) δ 159.37 (*phenyl*), 136.54 (*phenyl*), 129.96 (*phenyl*), 114.34 (*phenyl*), 82.97 (-NCH₂), 55.36 (-C(CH₃)₂), 47.77 (-C(CH₃)₂), 25.21 (-OCH₃).

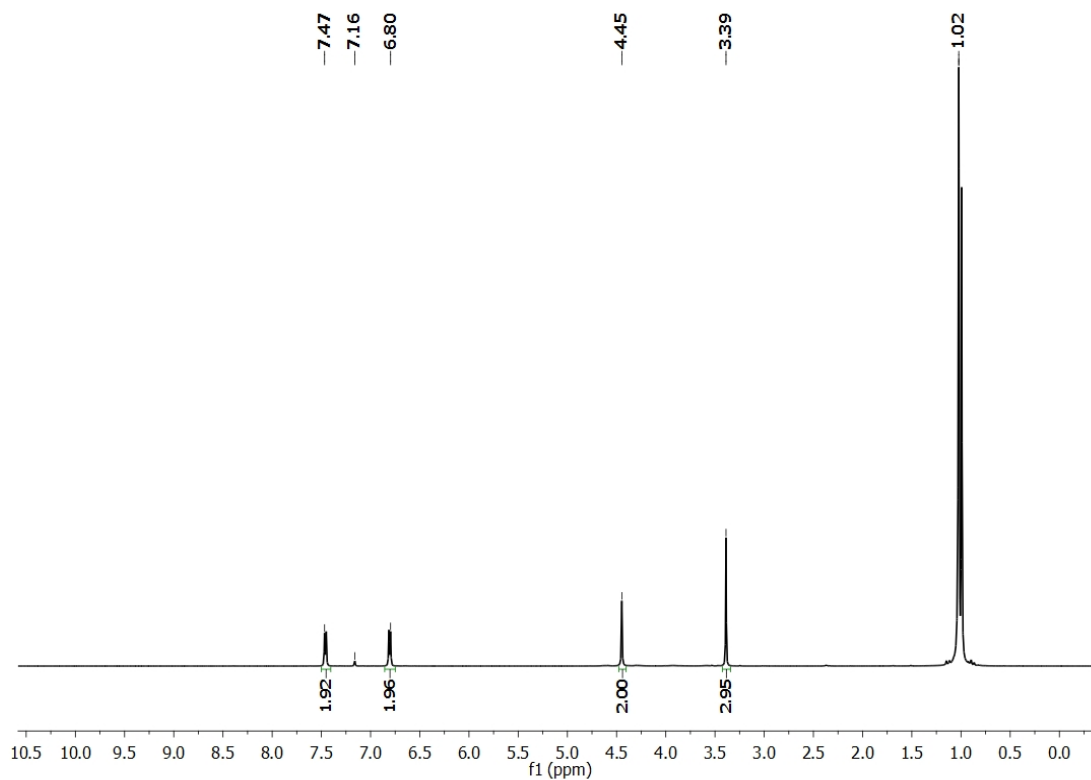


Figure 4.18: Conversion of 4-methoxybenzotrile to diboryl amine using 1 mol% catalyst **20** in benzene-*d*₆ after 2 h.

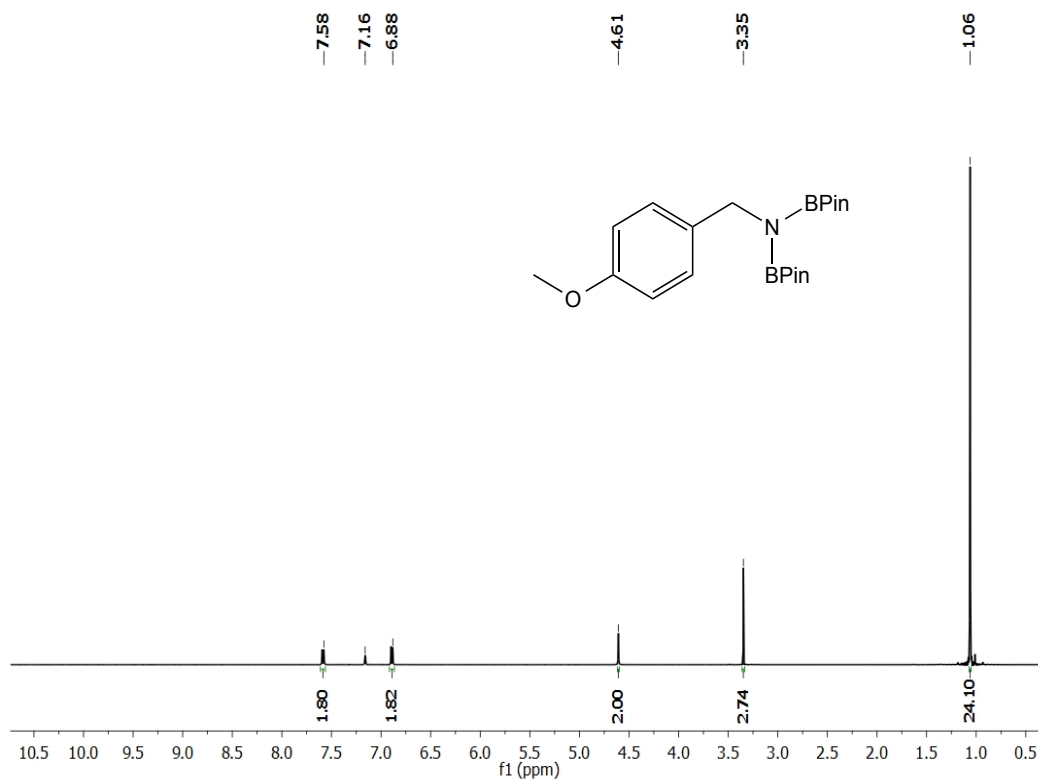


Figure 4.19: ^1H NMR spectrum of (4-OMePh) $\text{CH}_2\text{N}(\text{BPin})_2$ in benzene- d_6 .

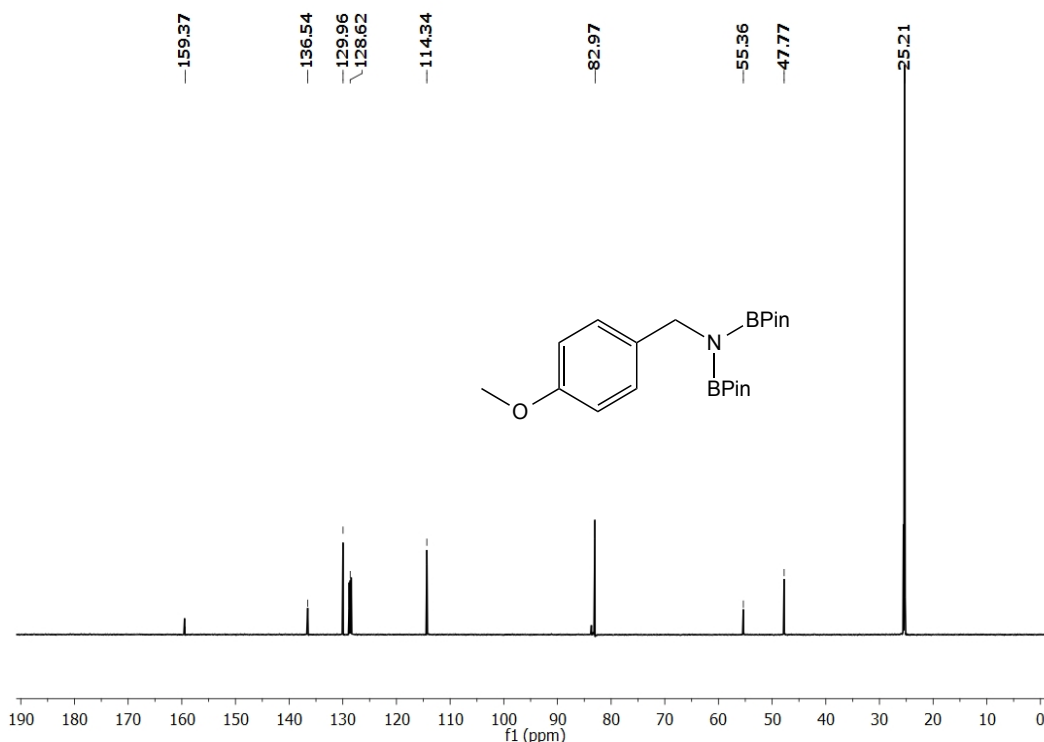


Figure 4.20. ¹³C NMR spectrum of (4-OMePh)CH₂N(BPin)₂ in benzene-*d*₆.

NMR scale dihydroboration of 4-chlorobenzonitrile (1 mol% **20):**

In the nitrogen filled glove box, a benzene-*d*₆ solution of 4-chlorobenzonitrile (79.7 mg, 0.579 mmol) and pinacolborane (0.18 ml, 1.274 mmol) was added to a vial containing 2.5 mg (0.0058 mmol) of **20**. The resulting solution immediately changed color from green to dark purple, which was transferred to a J. Young tube and remained at ambient temperature for 2 h. Both ¹H NMR and ¹³C NMR spectroscopy confirmed >99% conversion of the starting nitrile compound to diboryl amine, (4-ClPh)CH₂N(BPin)₂ after 2 h at room temperature. After removal of the solvent under vacuum, the product was recrystallized from ether at -35 °C to obtain a white solid compound (0.120 g, yield = 53 %). ¹H NMR (400 MHz, benzene-*d*₆) δ 7.36 (d, *J* = 8.0 Hz, 2H, *phenyl*), 7.20 (d, *J* = 8.1 Hz, 2H, *phenyl*), 4.46 (s, 2H, -NCH₂), 1.02 (s, 24H, -

$C(CH_3)_2$. ^{13}C NMR (126 MHz, benzene- d_6) δ 142.82 (*phenyl*), 130.13 (*phenyl*), 129.08 (*phenyl*), 83.20 (-NCH $_2$), 47.69 (-C(CH $_3$) $_2$), 25.28 (-C(CH $_3$) $_2$).

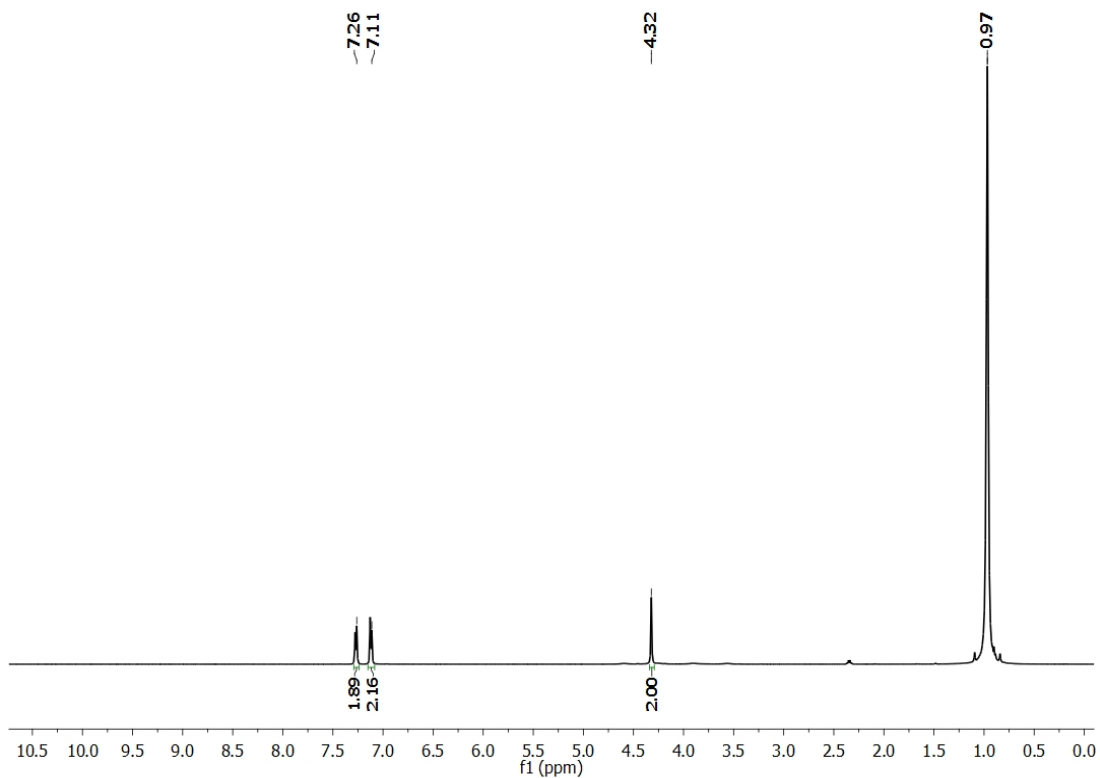


Figure 4.21: Conversion of 4-chlorobenzonitrile to diboryl amine using 1 mol% catalyst **20** in benzene- d_6 after 2 h.

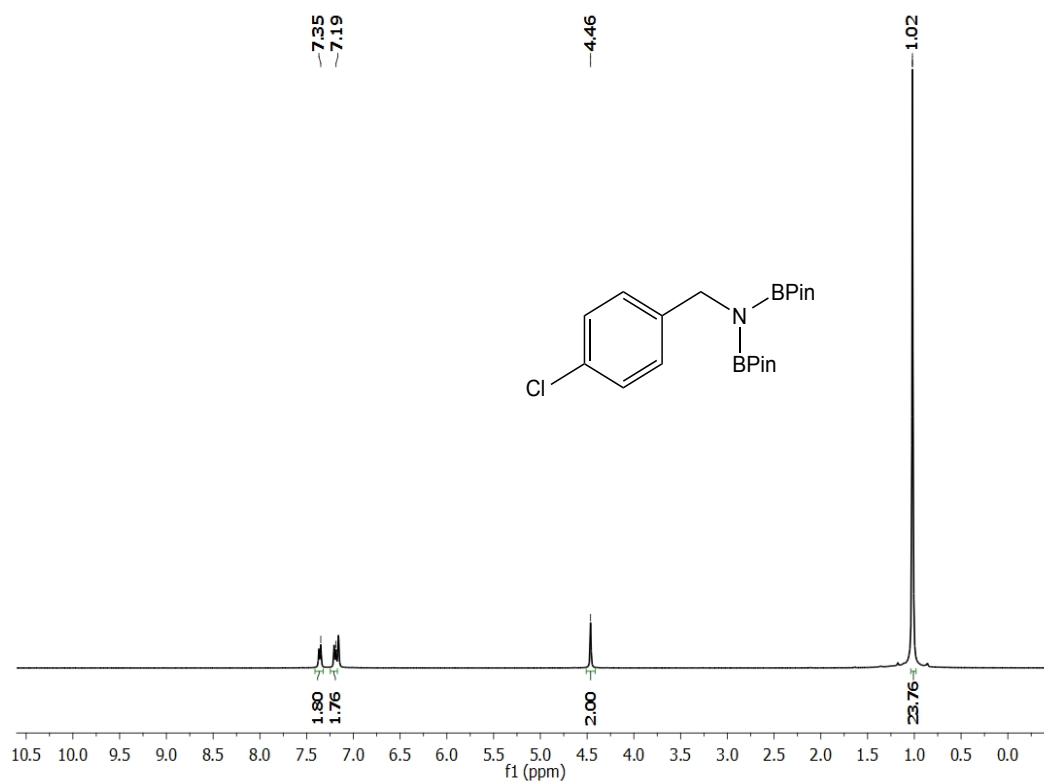


Figure 4.22: ^1H NMR spectrum of (4-ClPh) $\text{CH}_2\text{N}(\text{BPin})_2$ in benzene- d_6 .

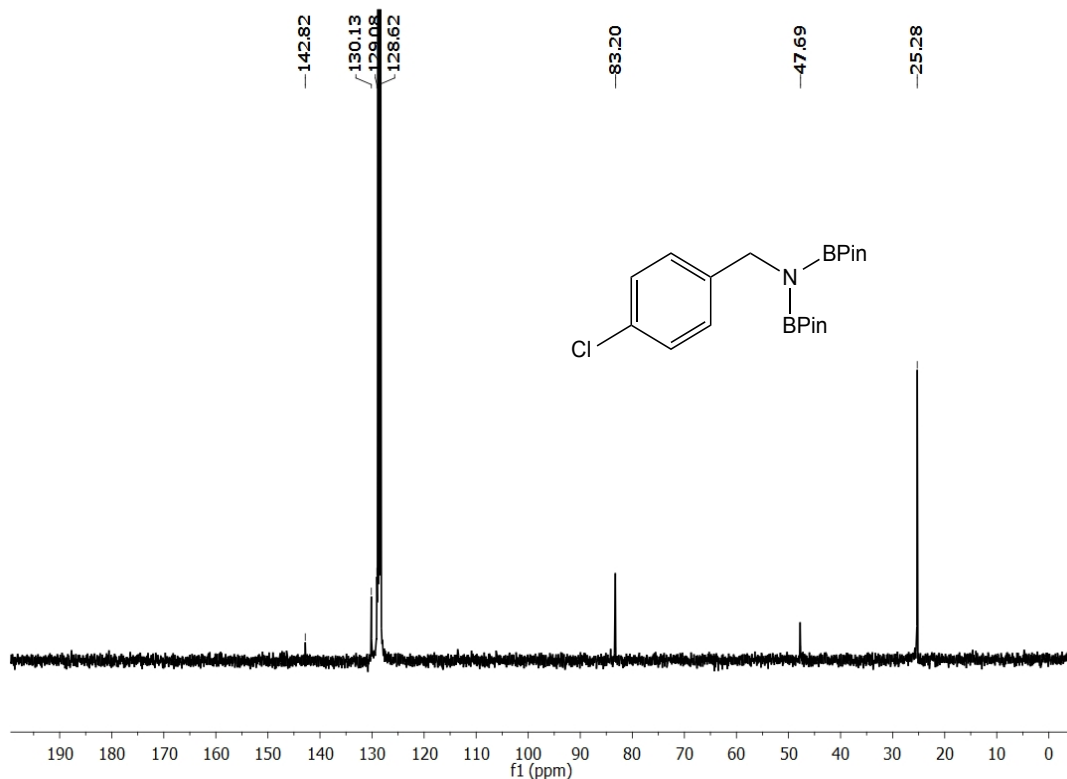


Figure 4.23: ^{13}C NMR spectrum of (4-ClPh)CH₂N(BPin)₂ in benzene-*d*₆.

NMR scale dihydroboration of 4-fluorobenzonitrile (1 mol% **20):**

In the nitrogen filled glove box, a benzene-*d*₆ solution of 4-fluorobenzonitrile (67.4 mg, 0.556 mmol) and pinacolborane (0.18 mL, 1.224 mmol) was added to a vial containing 2.4 mg (0.0056 mmol) of **20**. The resulting solution immediately changed color from green to dark purple, which was transferred to a J. Young tube and remained at ambient temperature for 2 h. Both ^1H NMR and ^{13}C NMR spectroscopy confirmed >99% conversion of the starting nitrile compound to diboryl amine, (4-FPh)CH₂N(BPin)₂ after 2 h at room temperature. After removal of the solvent under vacuum, the product was recrystallized from ether at -35 °C to obtain a white solid compound (0.130 g, yield

= 62 %). ^1H NMR (500 MHz, benzene- d_6) δ 7.46 – 7.40 (m, 2H, *phenyl*), 6.90 (t, $J = 8.8$ Hz, 2H, *phenyl*), 4.50 (s, 2H, $-\text{NCH}_2$), 1.03 (s, 24H, $-\text{C}(\text{CH}_3)_2$). ^{13}C NMR (126 MHz, benzene- d_6) δ 130.37 (d, $J = 7.5$ Hz, *phenyl*), 115.60 (d, $J = 19.5$ Hz, *phenyl*), 83.27 ($-\text{NCH}_2$), 47.74 ($-\text{C}(\text{CH}_3)_2$), 25.44 ($-\text{C}(\text{CH}_3)_2$).

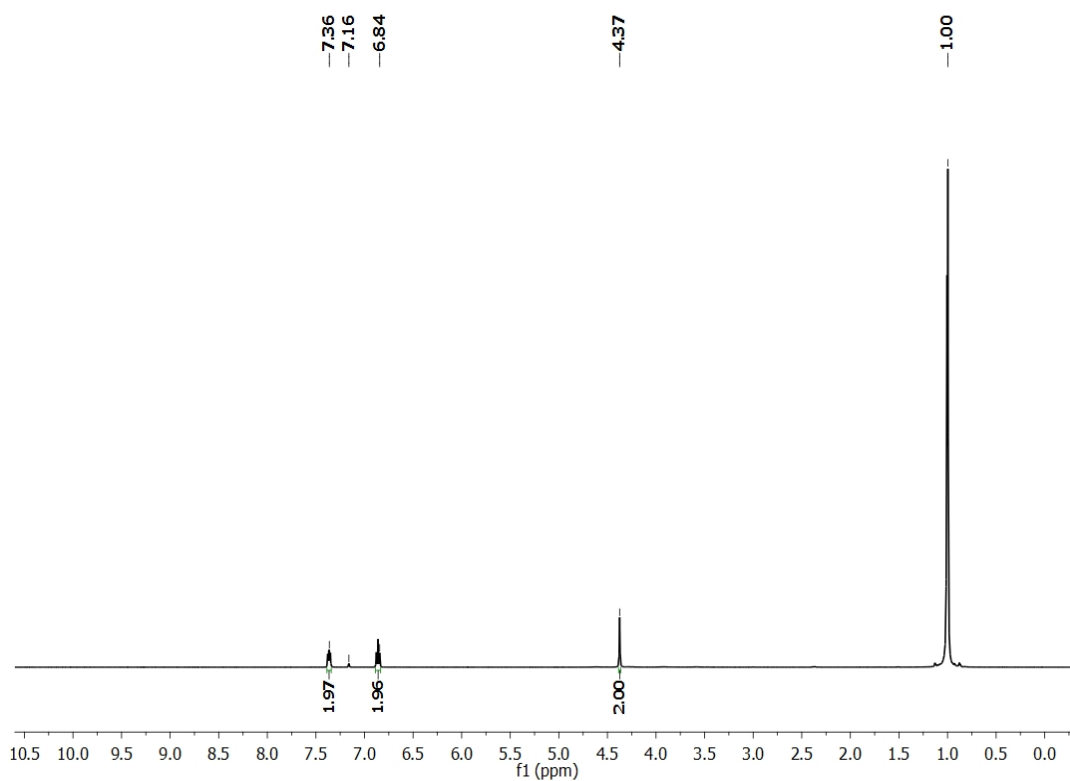


Figure 4.24: Conversion of 4-fluorobenzonitrile using 1 mol% catalyst **20** in benzene- d_6 after 2 h.

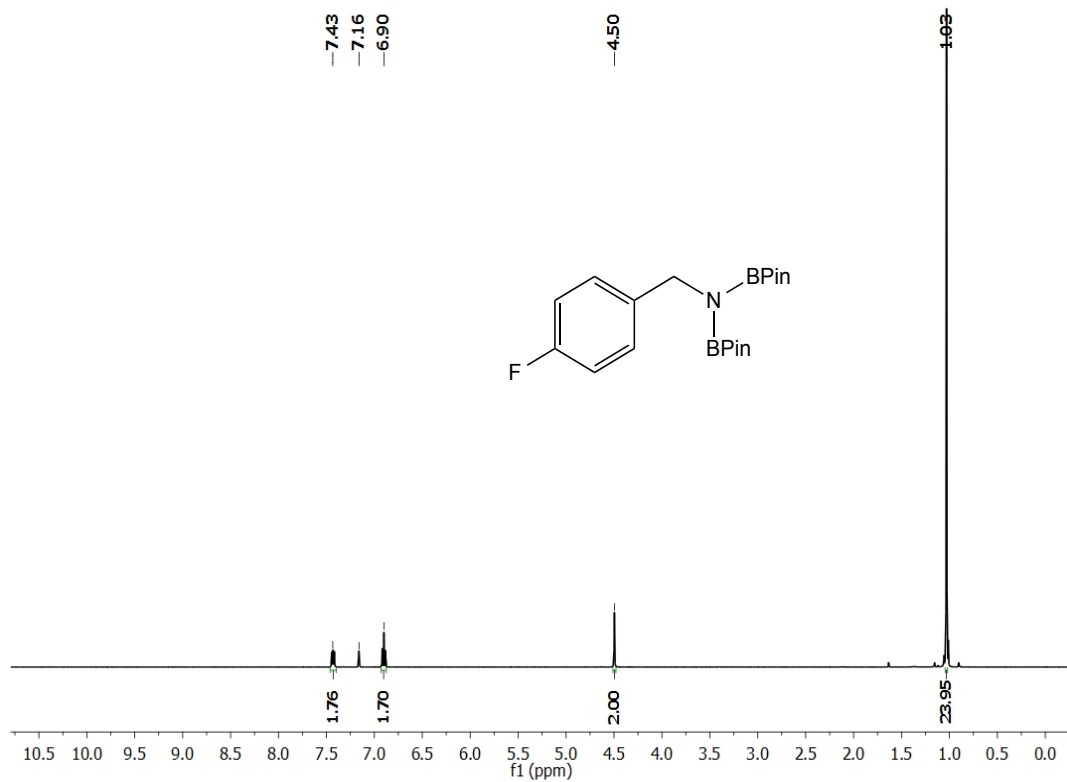


Figure 4.25. ^1H NMR spectrum of (4-FPh)CH₂N(BPin)₂ in benzene-*d*₆.

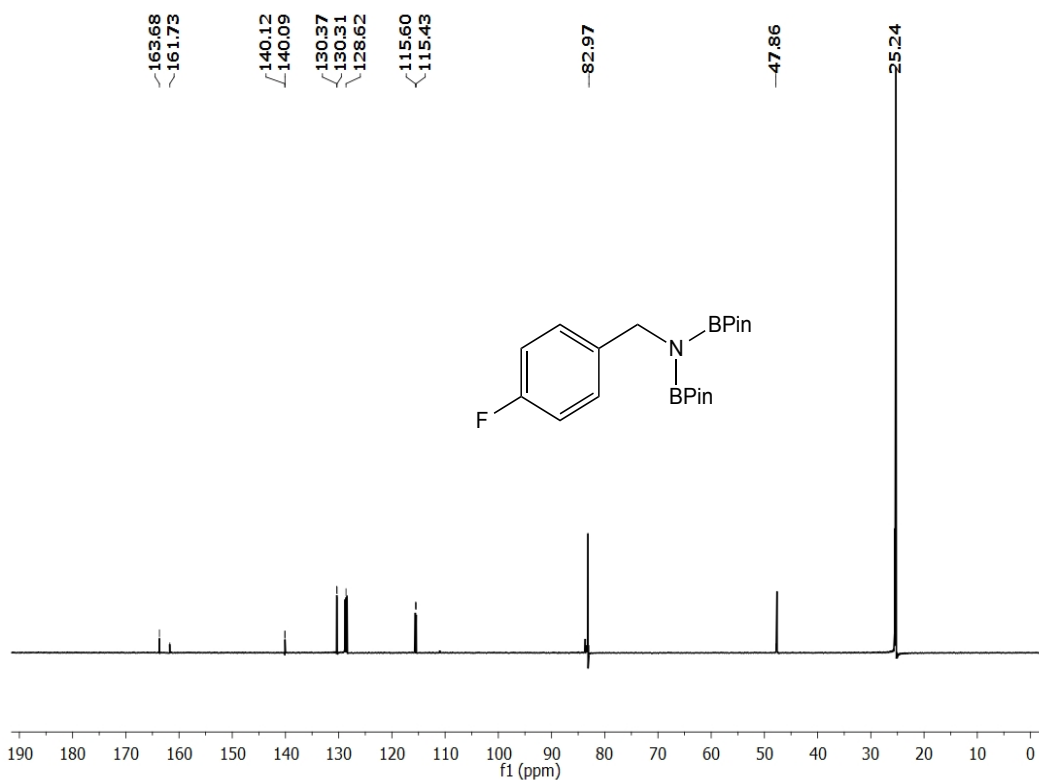


Figure 4.26: ^{13}C NMR spectrum of (4-FPh)CH₂N(BPin)₂ in benzene-*d*₆.

NMR scale dihydroboration of 4-(trifluoromethyl)benzotrile (1 mol% **20):**

In the nitrogen filled glove box, a benzene-*d*₆ solution of 4-methyl benzotrile (87.2 mg, 0.509 mmol) and pinacolborane (0.16 mL, 1.122 mmol) was added to a vial containing 2.2 mg (0.0051 mmol) of **20**. The resulting solution immediately changed color from green to dark purple, which was transferred to a J. Young tube and remained at ambient temperature for 2 h. Both ^1H NMR and ^{13}C NMR spectroscopy confirmed >99% conversion of the starting nitrile compound to diboryl amine, (4-CF₃Ph)CH₂N(BPin)₂ after 2 h at room temperature. After removal of the solvent under vacuum, the product was recrystallized from ether -35 °C to obtain a white solid compound (0.126 g, yield = 58 %). ^1H NMR (400 MHz, benzene-*d*₆) δ 7.42 (d, J = 1.4 Hz, 4H, *phenyl*), 4.50 (s, 2H, -NCH₂), 1.02 (s, 24H, -C(CH₃)₂). ^{13}C NMR (126 MHz,

benzene- d_6) δ 147.83 (*phenyl*), 128.73 (*phenyl*), 125.81(*phenyl*), 83.36 (-NCH₂), 47.96 (-C(CH₃)₂), 25.25 (-C(CH₃)₂).

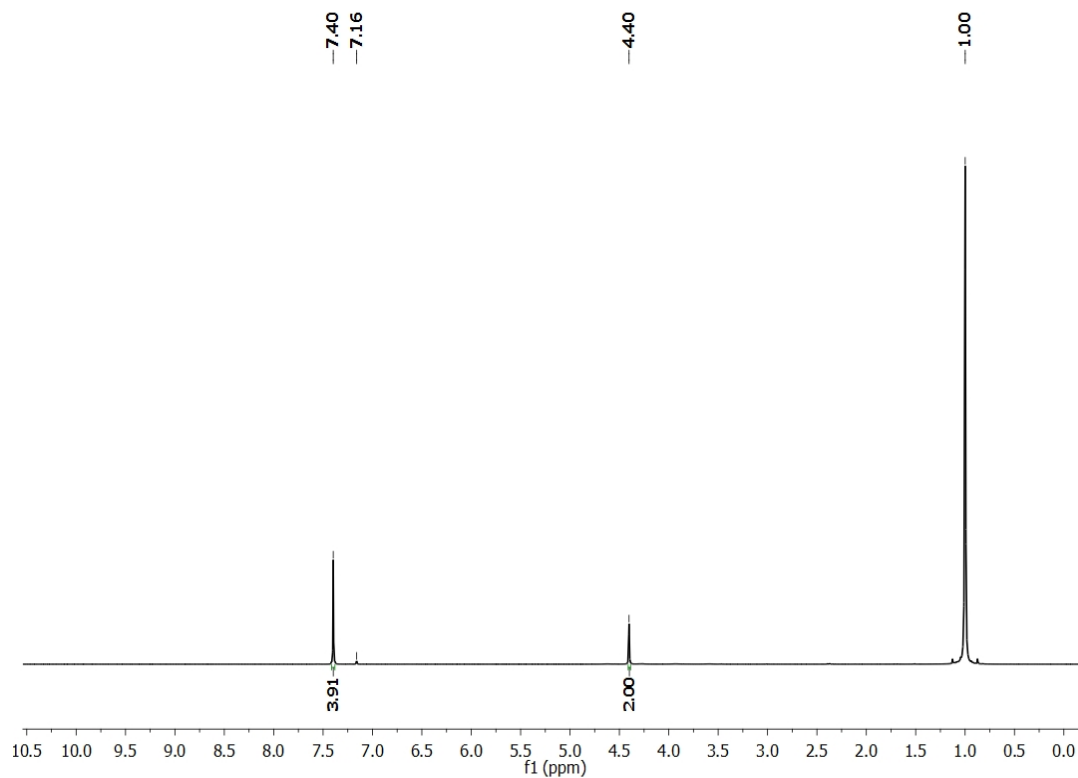


Figure 4.27: Conversion of 4-(trifluoromethyl)benzylamine to diboryl amine using 1 mol% catalyst **20** in benzene- d_6 after 2 h.

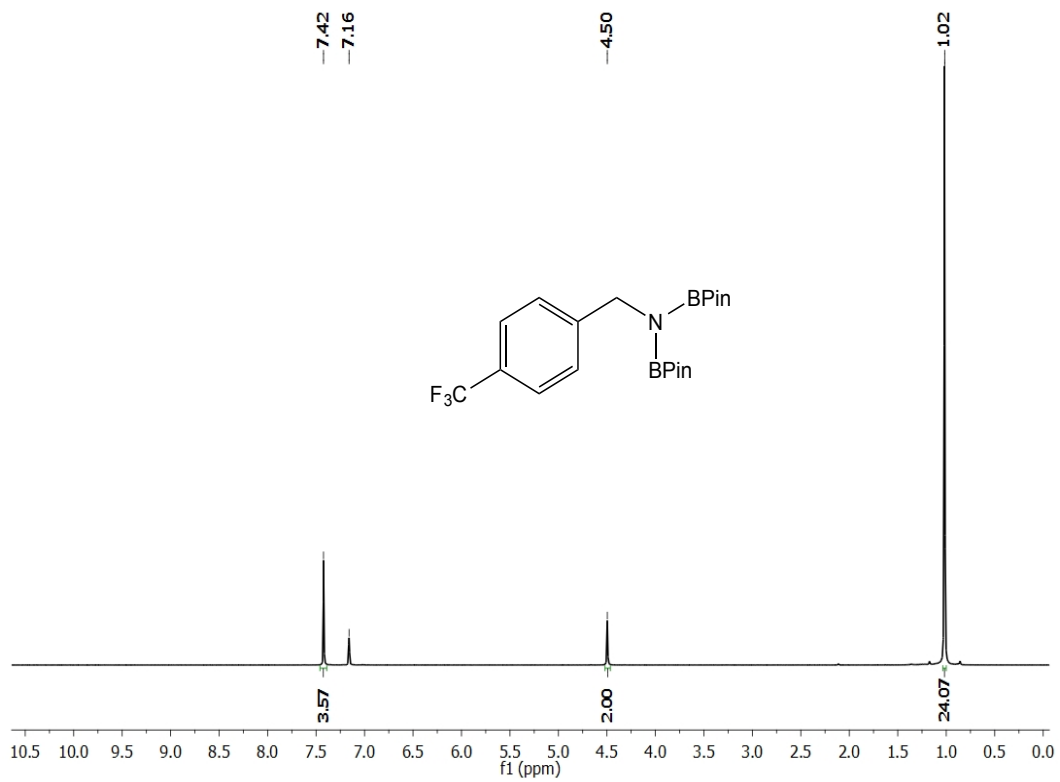


Figure 4.28: ^1H NMR spectrum of $(4\text{-CF}_3\text{Ph})\text{CH}_2\text{N}(\text{BPin})_2$ in $\text{benzene-}d_6$.

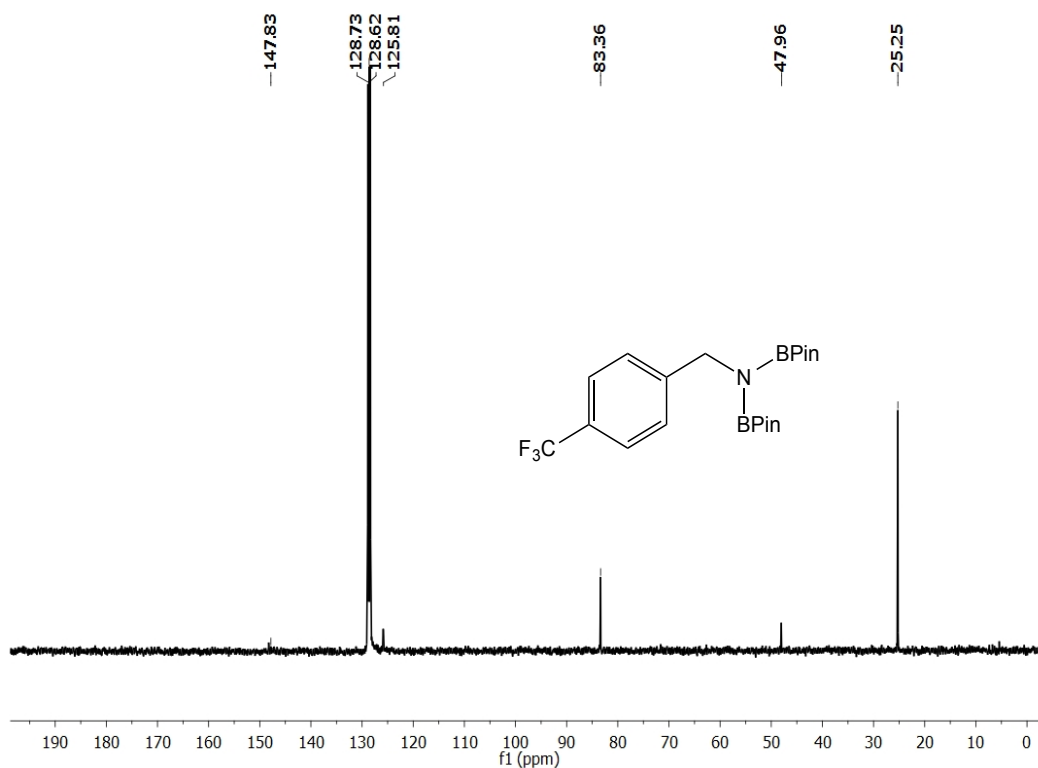


Figure 4.29: ^{13}C NMR spectrum of $(4\text{-CF}_3\text{Ph})\text{CH}_2\text{N}(\text{BPin})_2$ in benzene- d_6 .

NMR scale dihydroboration of 2-phenoxyacetonitrile (1 mol% **20**):

In the nitrogen filled glove box, a benzene- d_6 solution of 2-phenoxyacetonitrile (70.7 μL , 0.579 mmol) and pinacolborane (0.18 mL, 1.275 mmol) was added to a vial containing 2.5 mg (0.0058 mmol) of **20**. The resulting solution immediately changed color from green to dark purple, which was transferred to a J. Young tube and remained at ambient temperature for 2 h. Both ^1H NMR and ^{13}C NMR spectroscopy confirmed >99% conversion of the starting nitrile compound to diboryl amine, $(2\text{-OPh})\text{CH}_2\text{CH}_2\text{N}(\text{BPin})_2$ after 2 h at room temperature. After removal of the solvent under vacuum, the product was recrystallized from pentane at $-35\text{ }^\circ\text{C}$ to obtain a white solid compound (0.165 g, yield = 70 %). ^1H NMR (400 MHz, benzene- d_6) δ 7.03 (d, $J = 7.7$ Hz, 2H, *phenyl*), 6.85 (t, $J = 6.3$ Hz, 3H, *phenyl*), 4.13 (t, $J = 6.0$ Hz, 2H, $-\text{NCH}_2$), 3.82 (t, $J = 5.9$ Hz, 2H, $-\text{OCH}_2$), 1.06 (s, 24H, $-(\text{CH}_3)_2$). ^{13}C NMR (126 MHz, benzene- d_6) δ

160.66 (*phenyl*), 130.18 (*phenyl*), 121.23 (*phenyl*), 115.56 (*phenyl*), 82.73 (-NCH₂),
69.72 (-NCH₂CH₂), 43.77 (C(CH₃)₂), 25.30 (C(CH₃)₂).

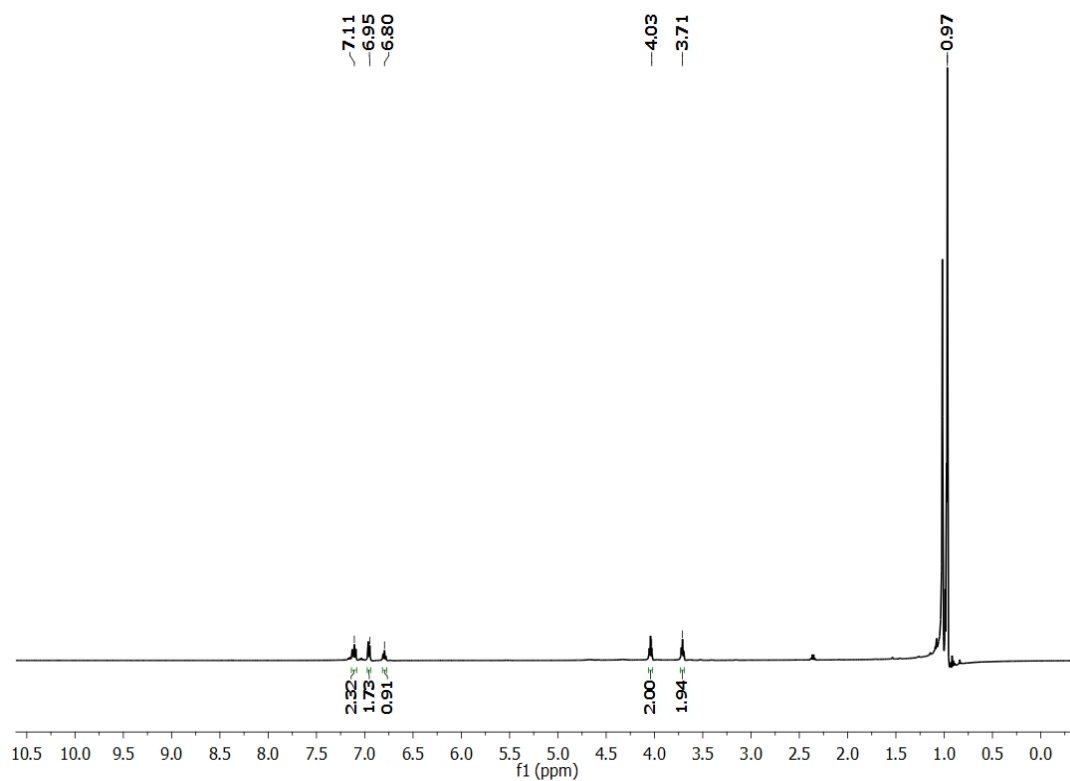


Figure 4.30: Conversion of 2-phenoxyacetonitrile to diboryl amine using 1 mol% catalyst **20** in benzene-*d*₆ after 2 h.

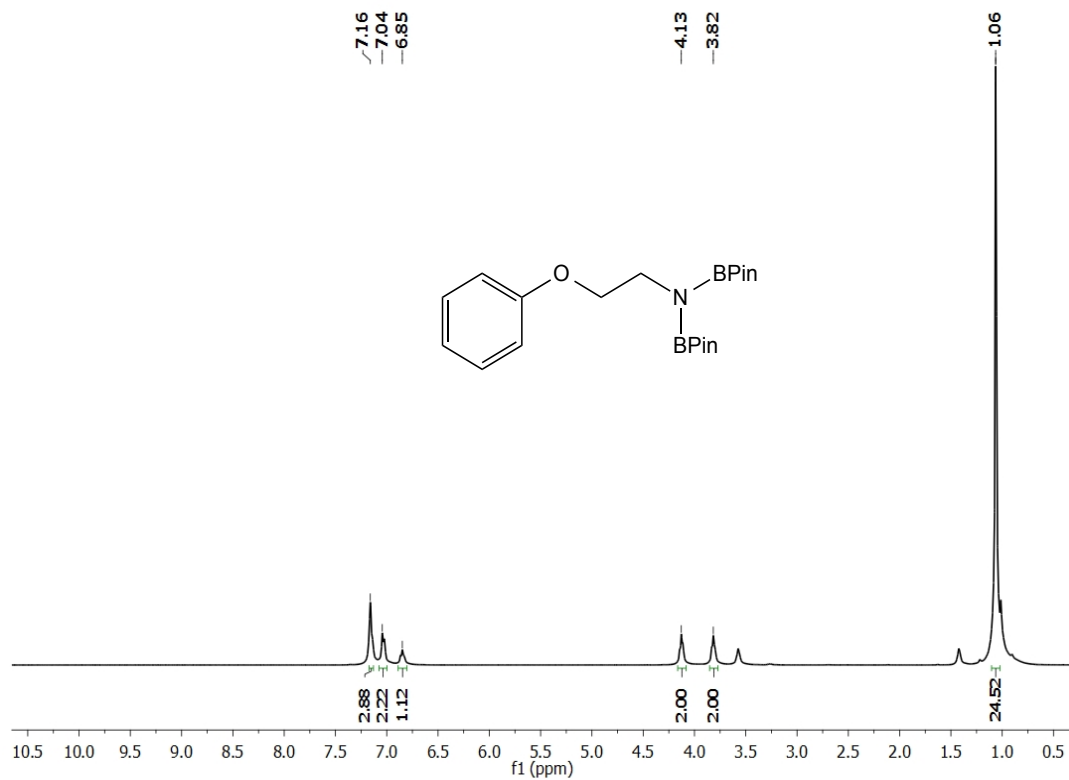


Figure 4.31: ^1H NMR spectrum of $(2\text{-OPh})\text{CH}_2\text{CH}_2\text{N}(\text{BPin})_2$ in benzene- d_6 .

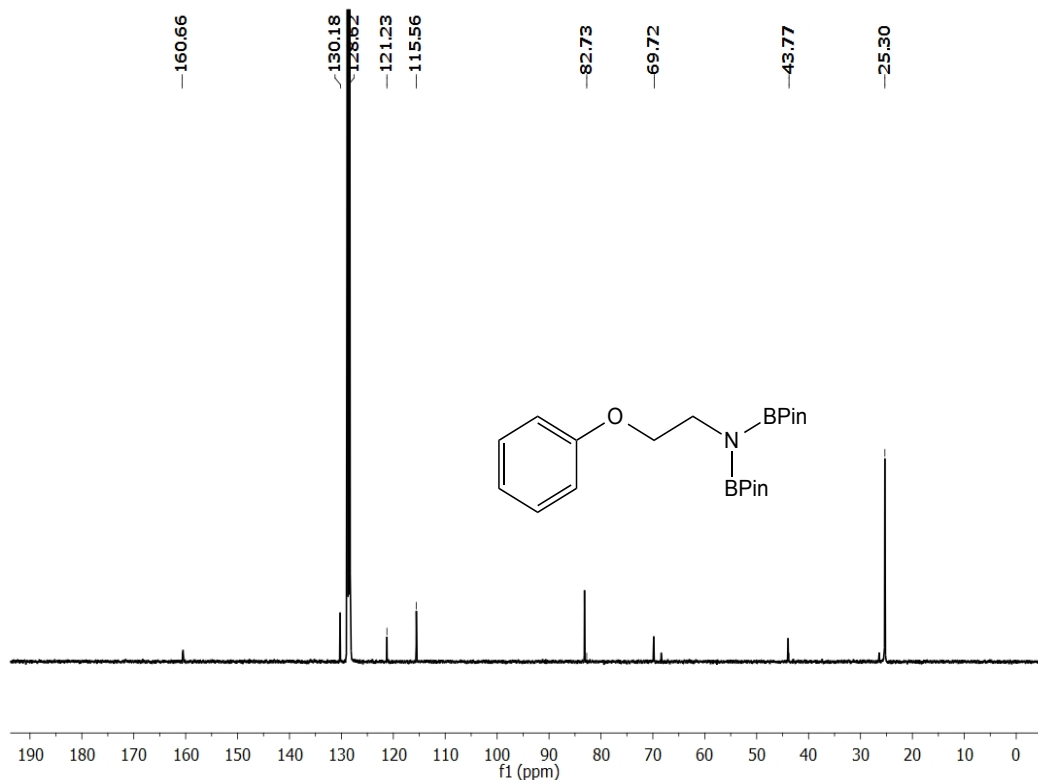


Figure 4.32: ^{13}C NMR spectrum of $(2\text{-OPh})\text{CH}_2\text{CH}_2\text{N}(\text{BPin})_2$ in benzene- d_6 .

NMR scale dihydroboration of 2-furonitrile (1 mol% **20):**

In the nitrogen filled glove box, a benzene- d_6 solution of 2-furonitrile (56.7 μL , 0.649 mmol) and pinacolborane (0.21 mL, 1.428 mmol) was added to a vial containing 2.8 mg (0.0065 mmol) of **20**. The resulting solution immediately changed color from green to dark purple, which was transferred to a J. Young tube and remained at ambient temperature for 2 h. Both ^1H NMR and ^{13}C NMR spectroscopy confirmed >99% conversion of the starting nitrile compound to diboryl amine, $(2\text{-furyl})\text{CH}_2\text{N}(\text{BPin})_2$ after 2 h at room temperature. After removal of the solvent under vacuum, the product was recrystallized from pentane at $-35\text{ }^\circ\text{C}$ to obtain a white solid compound (0.110 g, yield = 49%). ^1H NMR (400 MHz, benzene- d_6) δ 7.13 (d, $J = 0.8$ Hz, 1H, *furan*), 6.29 (d, $J = 3.7$ Hz, 1H, *furan*), 6.16 (dd, $J = 3.0$ Hz, 1.9 Hz, 1H, *furan*), 4.61 (s, 2H, $-\text{NCH}_2$), 1.06 (s,

24H, C(CH₃)₂). ¹³C NMR (126 MHz, benzene-*d*₆) δ 157.84 (*furan*), 141.67 (*furan*), 111.03 (*furan*), 106.34 (*furan*), 83.05 (-NCH₂), 41.98 (-C(CH₃)₂), 25.28 (-C(CH₃)₂).

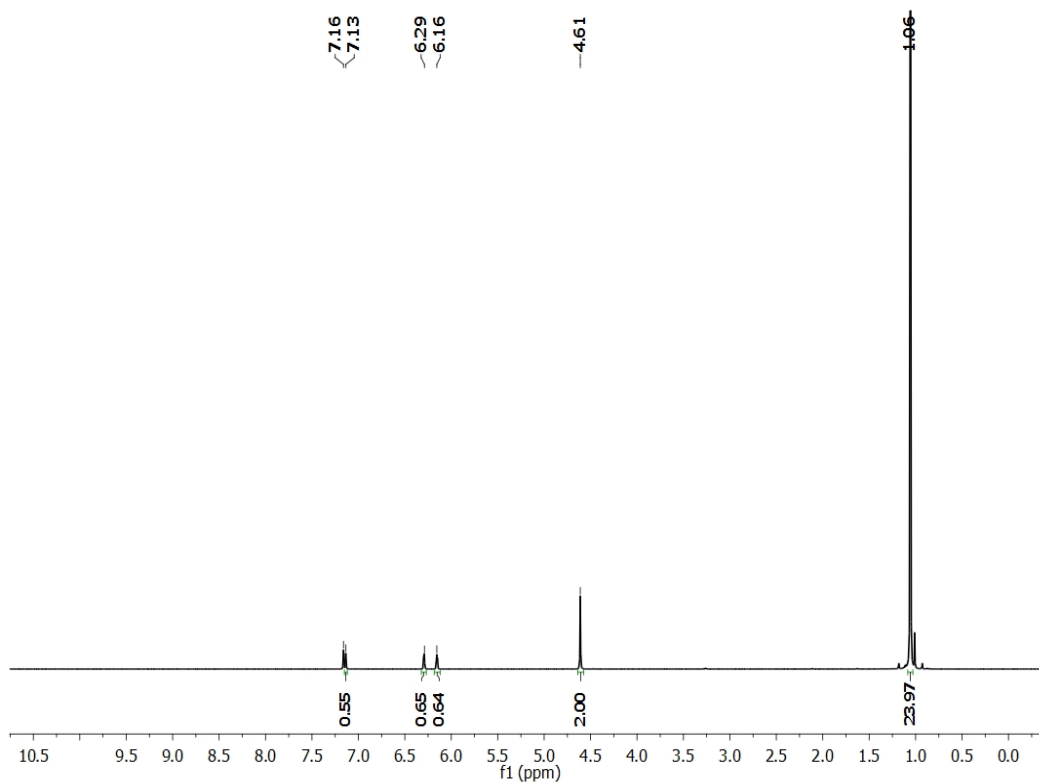


Figure 4.33: Conversion of 2-furonitrile to diboryl amine using 1 mol% catalyst **20** in benzene-*d*₆ after 2 h.

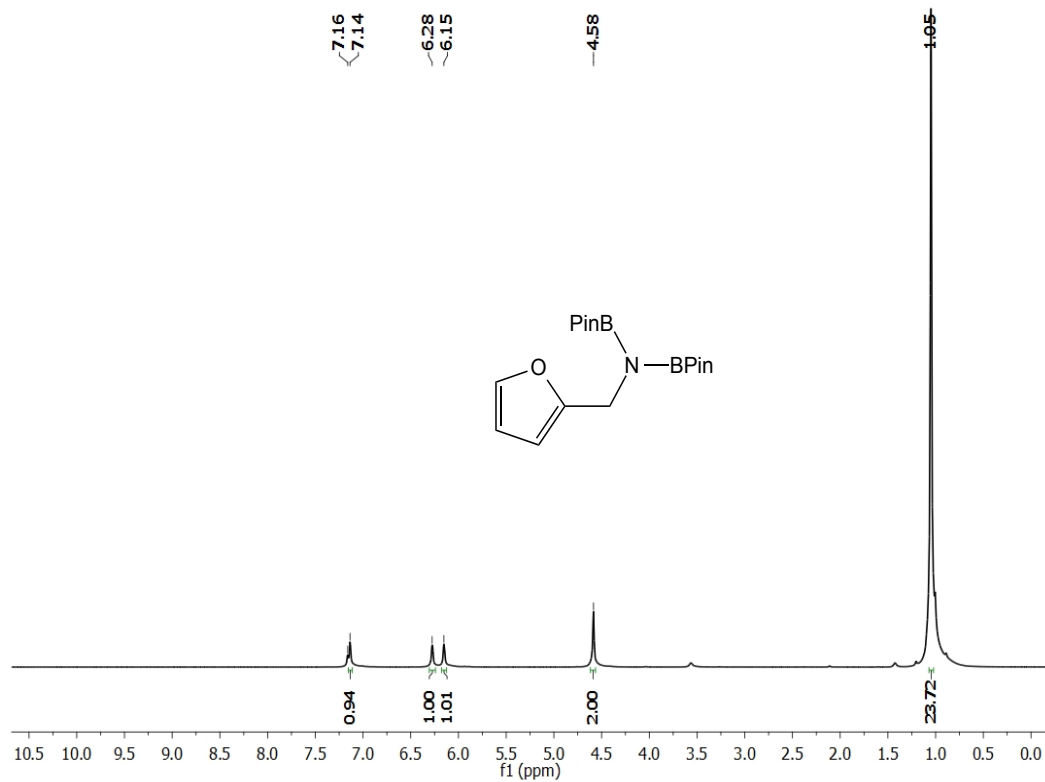


Figure 4.34: ^1H NMR spectrum of (2-furyl)CH₂N(BPin)₂ in benzene-*d*₆.

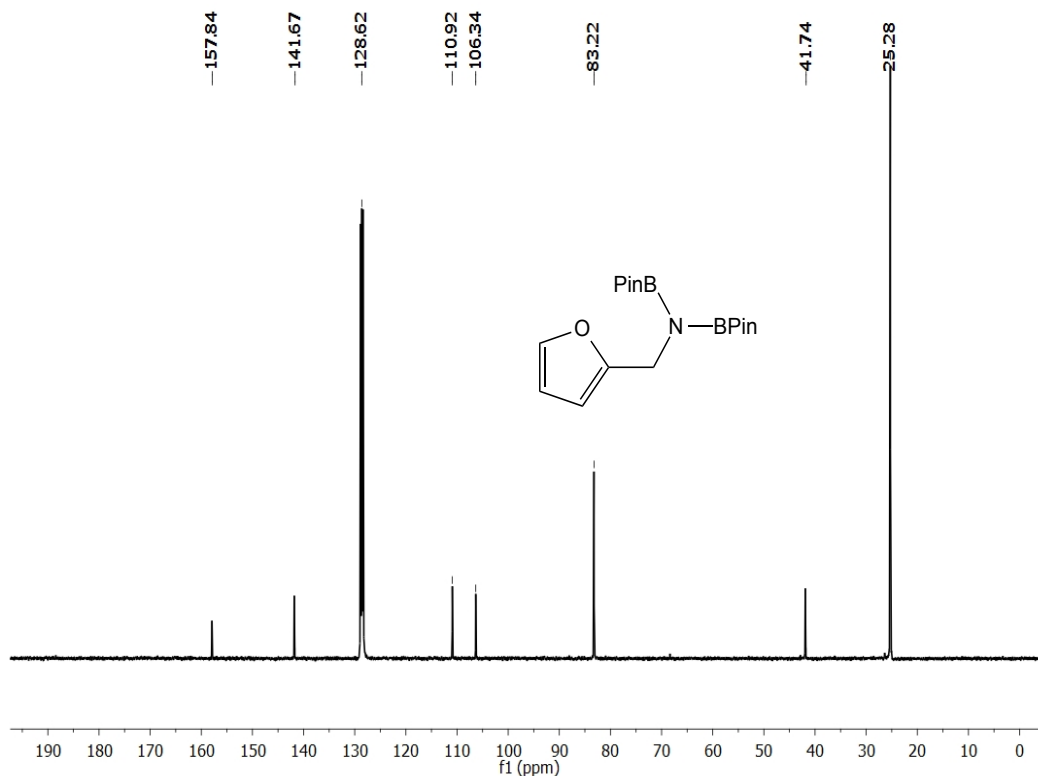


Figure 4.35: ^{13}C NMR spectrum of (2-furyl) $\text{CH}_2\text{N}(\text{BPin})_2$ in benzene- d_6 .

NMR scale dihydroboration of 4-acetylbenzotrile (1 mol% **20):**

In the nitrogen filled glove box, a benzene- d_6 solution of 4-acetylbenzotrile (80.7 mg, 0.556 mmol) and pinacolborane (0.26 mL, 1.836 mmol) was added to a vial containing 2.4 mg (0.0055 mmol) of **20**. The resulting solution immediately changed color from green to dark purple, which was transferred to a J. Young tube and remained at ambient temperature for 2 h. Both ^1H NMR and ^{13}C NMR spectroscopy confirmed >99% conversion of the starting nitrile compound to diboryl amine, (4-COMePh) $\text{CH}_2\text{N}(\text{BPin})_2$ after 2 h at room temperature. After removal of the solvent under vacuum, the product was recrystallized from ether at $-35\text{ }^\circ\text{C}$ to obtain a white solid compound (0.120 g, yield = 41 %). ^1H NMR (400 MHz, benzene- d_6) δ 7.54 (d, $J = 7.9$ Hz, 2H, *phenyl*), 7.40 (d, $J = 7.9$ Hz, 2H, *phenyl*), 5.43 (dd, $J = 12.5, 6.2$ Hz, 1H, -

OCH(CH₃), 4.57 (s, 2H), 1.48 (d, *J* = 6.4 Hz, 3H, -OCH(CH₃), 1.03 (s, 24H, -NB(CH₃)₂), 1.01 (s, 12H, -OB(CH₃)₂). ¹³C NMR (126 MHz, benzene-*d*₆) δ 205.34 (-OCH(Me)B), 143.95 (*phenyl*), 143.19 (*phenyl*), 126.08 (*phenyl*), 83.12 (-NCH₂), 73.50 (-OCH(CH₃)), 48.20 (-C(CH₃)₂), 26.24 (-OBC(CH₃)₂), 25.17 (-NBC(CH₃)₂).

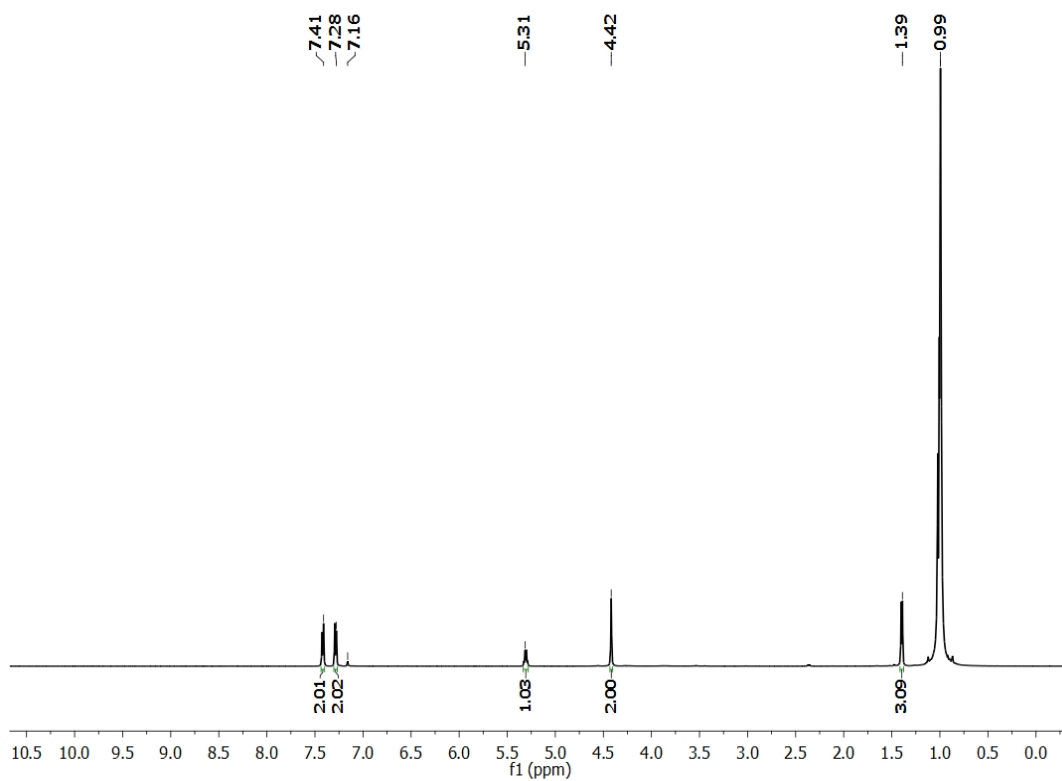


Figure 4.36: Conversion of 4-acetylbenzointrile to diboryl amine using 1 mol% catalyst **20** in benzene-*d*₆ after 2 h.

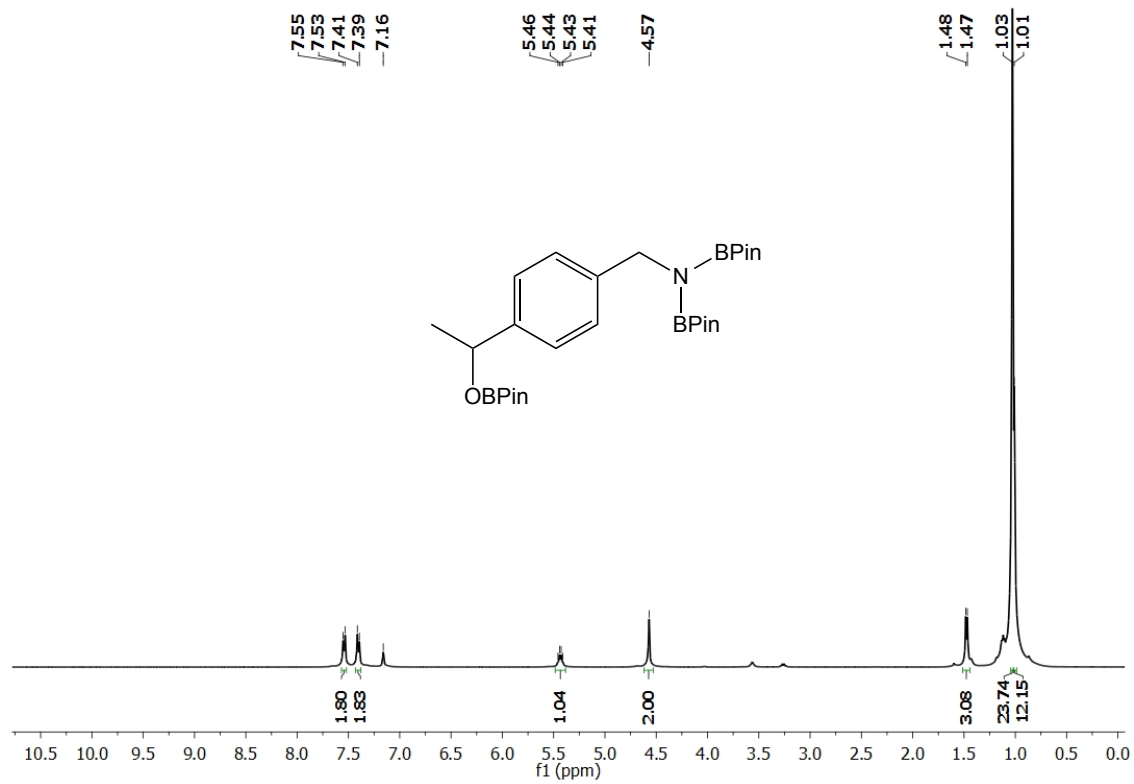


Figure 4.37: ^1H NMR spectrum of $(4\text{-C(H)(Me)OBPin)PhCH}_2\text{N(BPin)}_2$ in benzene- d_6 .

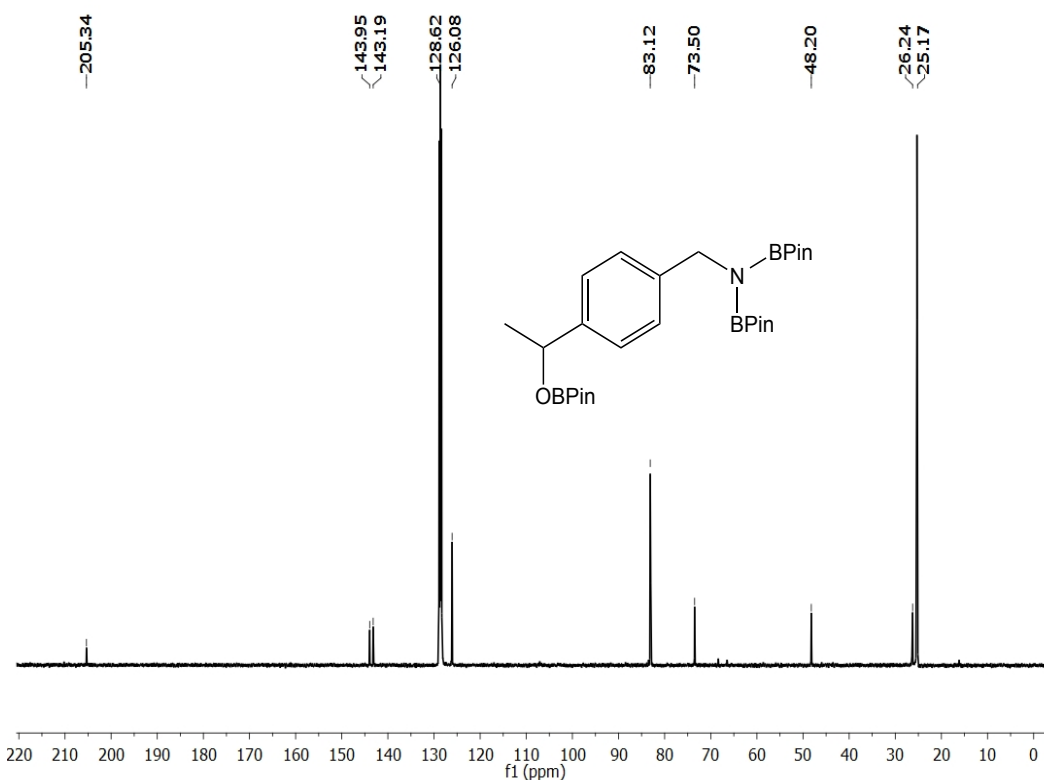


Figure 4.38: ¹³C NMR spectrum of (4-C(H)(Me)OBPin)PhCH₂N(BPin)₂ in benzene-*d*₆.

NMR scale dihydroboration of acetonitrile (1 mol% **20**):

In the nitrogen filled glove box, a benzene-*d*₆ solution of acetonitrile (42.5 μL, 0.811 mmol) and pinacolborane (0.25 mL, 1.785 mmol) was added to a vial containing 3.5 mg (0.0081 mmol) of **20**. The resulting solution immediately changed color from green to dark purple, which was transferred to a J. Young tube and remained at ambient temperature for 2 h. Both ¹H NMR and ¹³C NMR spectroscopy confirmed >99% conversion of the starting nitrile compound to diboryl amine, CH₃CH₂N(BPin)₂ after 2 h at room temperature. After removal of the solvent under vacuum, the product was recrystallized from pentane at -35 °C to obtain a white solid compound (0.073 g, yield = 30 %). ¹H NMR (500 MHz, benzene-*d*₆) δ 3.48 (q, *J* = 6.7 Hz, 2H, -NCH₂), 1.32 (t, *J* =

6.9 Hz, 3H, -CH₃), 1.06 (s, 24H, C(CH₃)₂). ¹³C NMR (126 MHz, benzene-*d*₆) δ 82.54 (-NCH₂), 39.73 (-C(CH₃)₂), 25.47 (C(CH₃)₂), 19.89 (-CH₃).

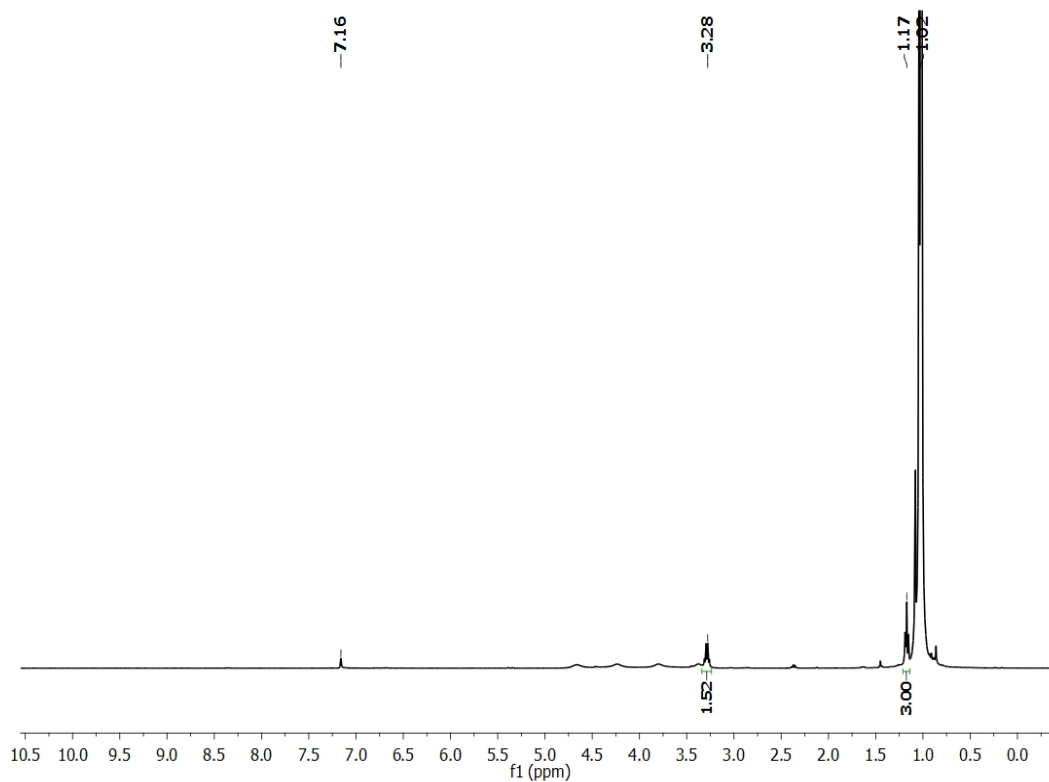


Figure 4.39: Conversion of acetonitrile to diboryl amine using 1 mol% catalyst **20** in benzene-*d*₆ after 2 h.

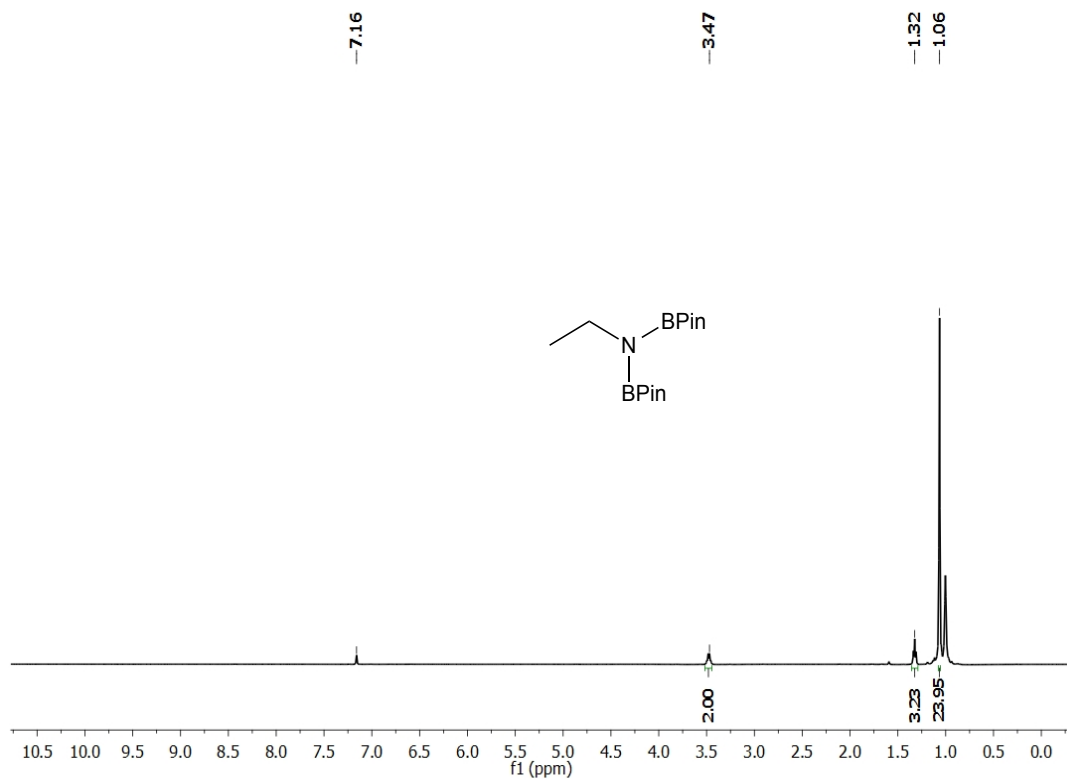


Figure 4.40: ^1H NMR spectrum of $\text{CH}_3\text{CH}_2\text{N}(\text{BPin})_2$ in benzene- d_6 .

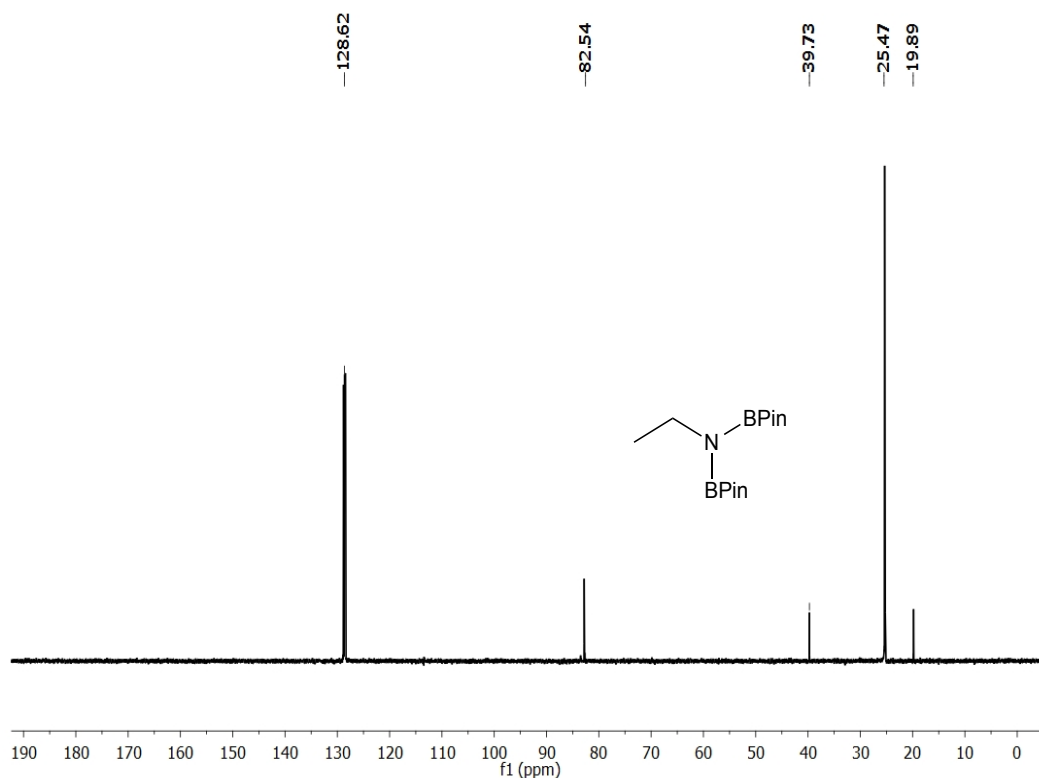


Figure 4.41: ^{13}C NMR spectrum of $\text{CH}_3\text{CH}_2\text{N}(\text{BPi})_2$ in benzene- d_6 .

NMR scale dihydroboration of propionitrile (1 mol% **20):**

In the nitrogen filled glove box, a benzene- d_6 solution of propionitrile (42.9 μL , 0.603 mmol) and pinacolborane (0.19 mL, 1.326 mmol) was added to a vial containing 2.6 mg (0.0060 mmol) of **20**. The resulting solution immediately changed color from green to dark purple, which was transferred to a J. Young tube and remained at ambient temperature for 2 h. Based on the integration of methyl peak of the nitrile vs. product in ^1H NMR spectrum, 74% conversion was observed after 2 h, and it took 24 h for complete conversion to $\text{CH}_3\text{CH}_2\text{N}(\text{BPi})_2$. ^1H NMR (400 MHz, benzene- d_6) δ 3.27 (t, $J = 6.8$ Hz, 2H, $-\text{NCH}_2$), 1.64 (dd, $J = 14.5, 7.2$ Hz, 2H, $-\text{NCH}_2\text{CH}_2$), 1.03 (s, 24H, $-\text{C}(\text{CH}_3)_2$), 0.88

(t, $J = 7.3$ Hz, 3H, $-CH_3$). ^{13}C NMR (126 MHz, benzene- d_6) δ 82.57 ($-C(CH_3)_2$), 46.58 ($-NCH_2$), 27.28 ($-NCH_2CH_2$), 25.46 ($-C(CH_3)_2$), 12.10 ($-CH_3$).

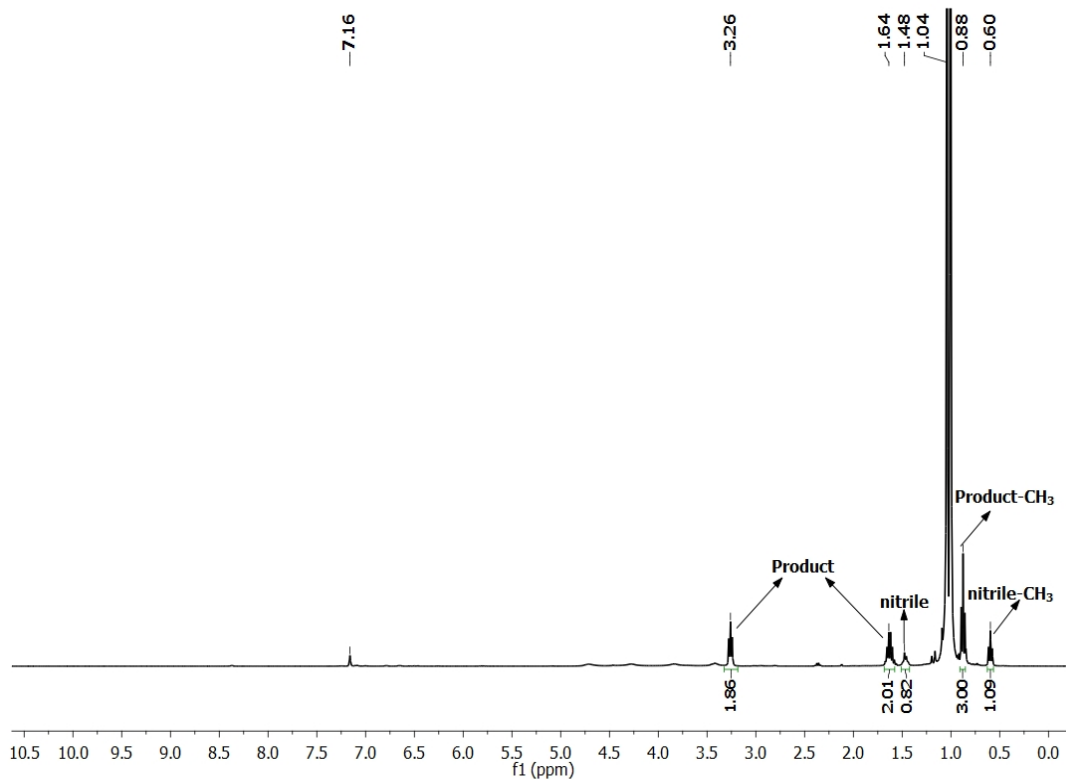


Figure 4.42: Conversion of propionitrile to diboryl amine using 1 mol% catalyst **20** in benzene- d_6 after 2 h.

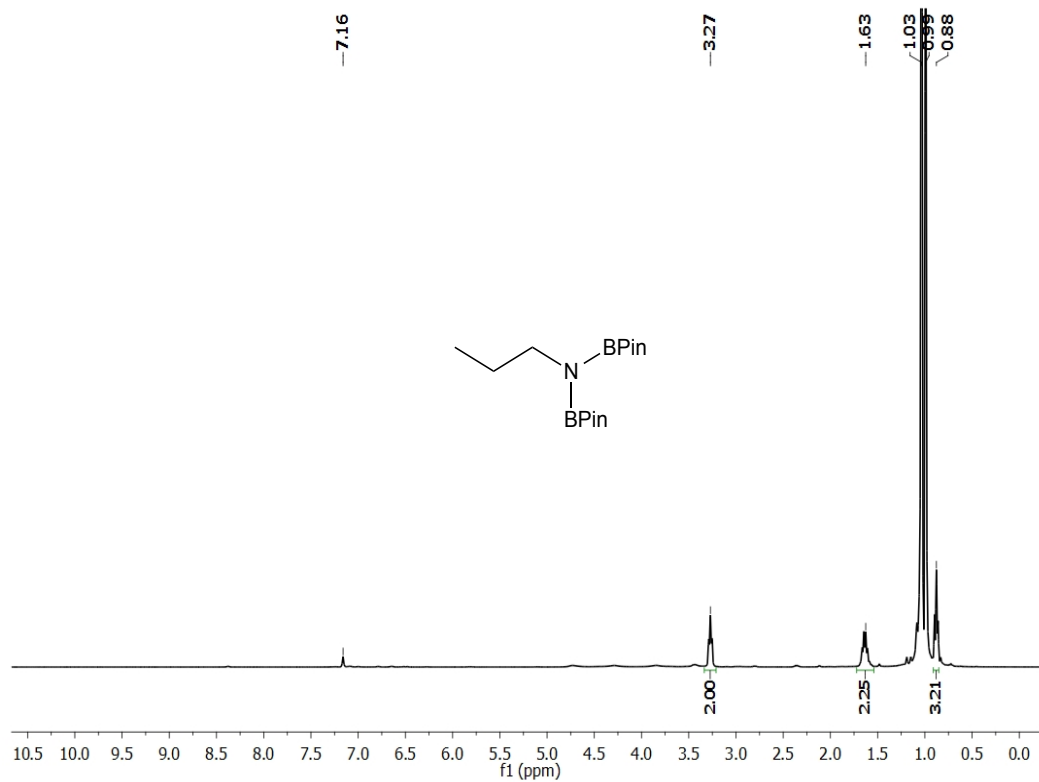


Figure 4.43: Conversion of propionitrile to diboryl amine using 1 mol% catalyst **20** in benzene- d_6 after 24 h.

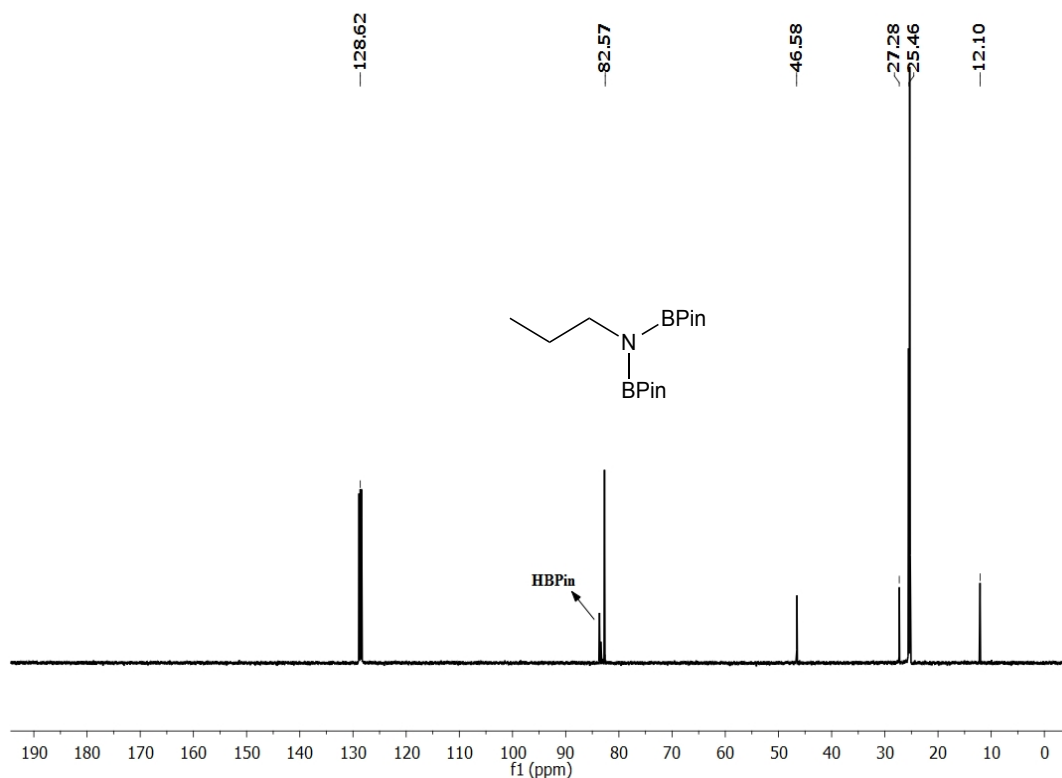


Figure 4.44: ^{13}C NMR spectrum for the conversion of propionitrile to diboryl amine using 1 mol% catalyst **20** in benzene- d_6 after 24 h.

NMR scale dihydroboration of isobutyronitrile (1 mol% **20**):

In the nitrogen filled glove box, a benzene- d_6 solution of isobutyronitrile (60.3 μL , 0.672 mmol) and pinacolborane (0.21 mL, 1.479 mmol) was added to a vial containing 2.9 mg (0.0070 mmol) of **20**. The resulting solution immediately changed color from green to dark purple, which was transferred to a J. Young tube and remained at ambient temperature for 2 h. Based on the integration of methyl peak of the nitrile vs. product in ^1H NMR spectrum, 52% conversion was observed after 2 h, 84% after 24 h, and it required 4 days for complete conversion to $(\text{CH}_3)_2\text{CHCH}_2\text{N}(\text{BPin})_2$. ^1H NMR (400 MHz, benzene- d_6) δ 3.12 (d, $J = 7.2$ Hz, 2H, $-\text{NCH}_2$), 1.91 (dt, $J = 13.6, 6.8$ Hz, 1H, $-\text{CH}(\text{CH}_3)_2$), 1.03 (s, 24H, $-\text{C}(\text{CH}_3)_2$), 0.91 (d, $J = 6.7$ Hz, 6H, $-\text{CH}_3$). ^{13}C NMR (126

MHz, benzene- d_6) δ 82.57 (-C(CH₃)₂), 52.21 (-NCH₂), 31.70 (-CH), 25.46 (-C(CH₃)₂), 20.83 (-CHCH₃).

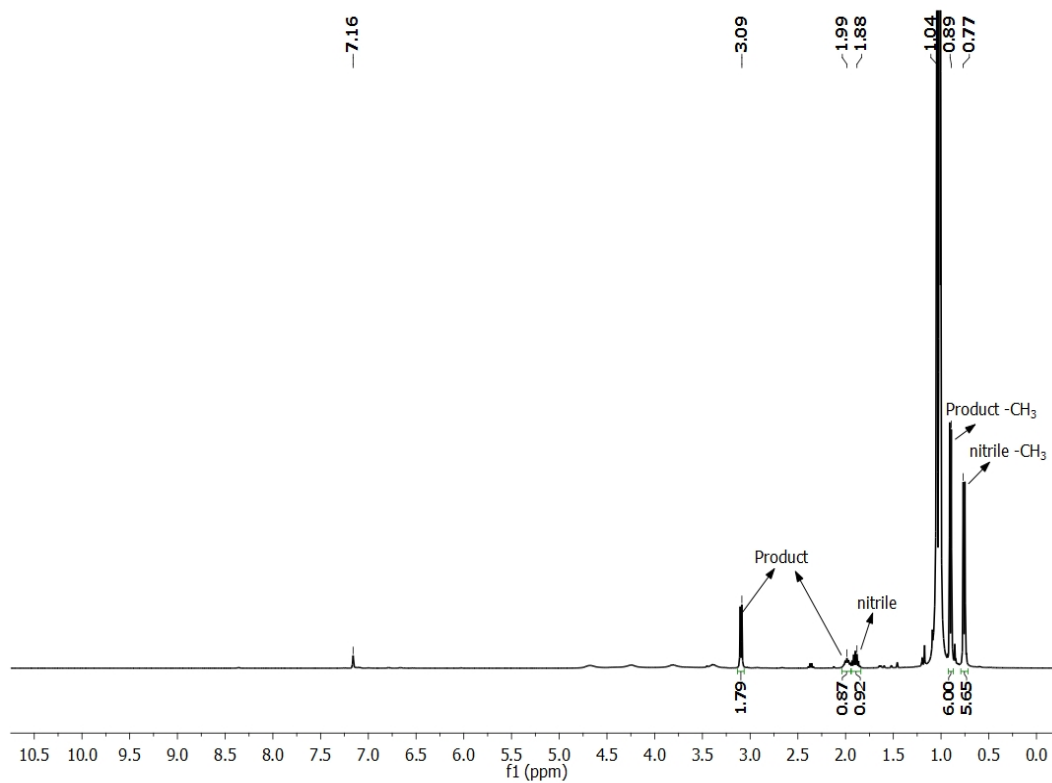


Figure 4.45: Conversion of isobutyronitrile to diboryl amine using 1 mol% catalyst **20** in benzene- d_6 after 2 h.

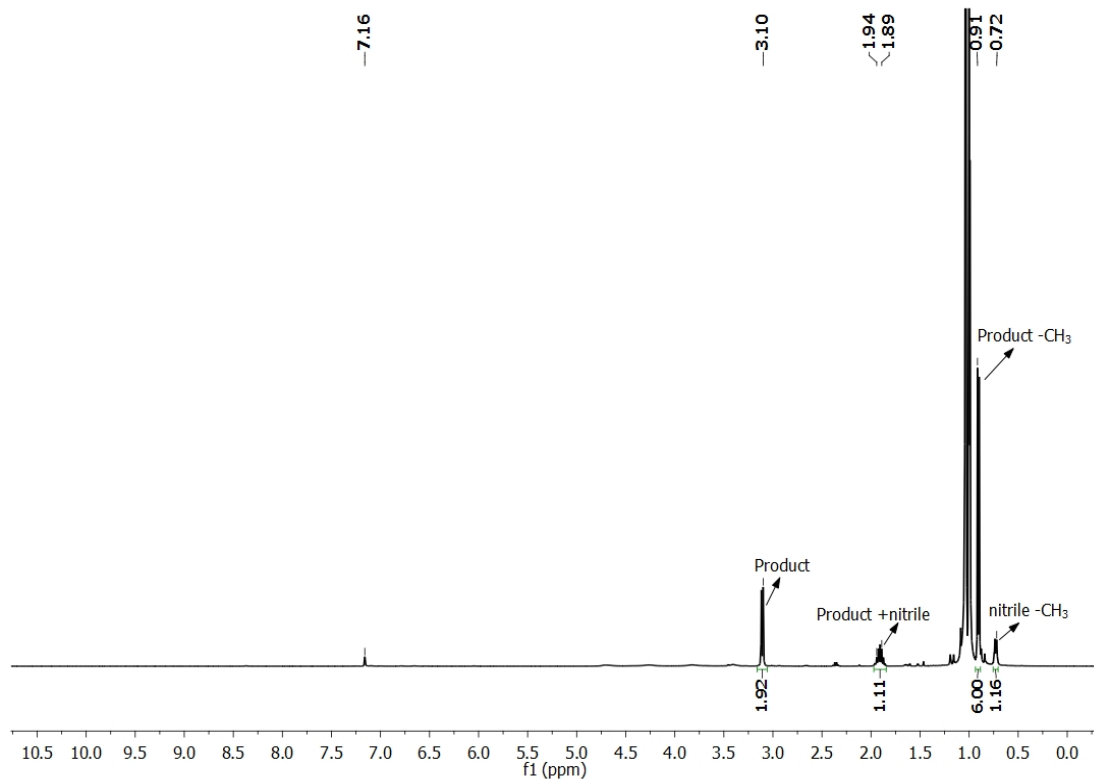


Figure 4.46: Conversion of isobutyronitrile to diboryl amine using 1 mol% catalyst **20** in benzene-*d*₆ after 24 h.

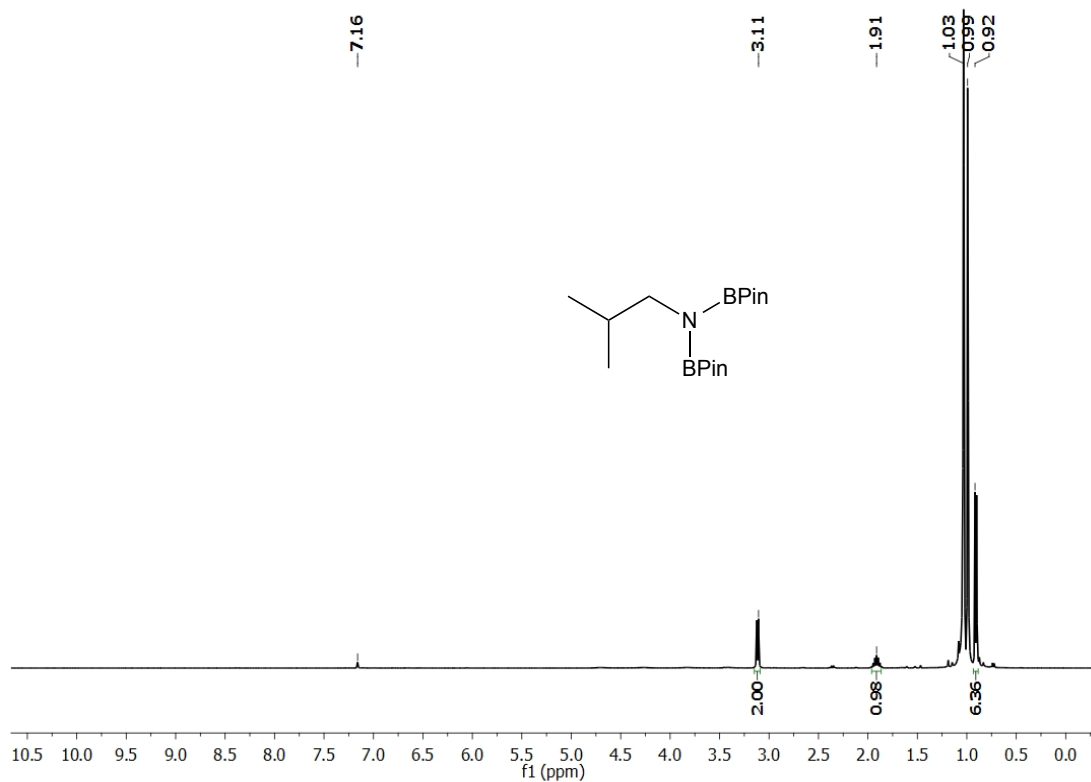


Figure 4.47: Conversion of isobutyronitrile to diboryl amine using 1 mol% catalyst **20** in benzene- d_6 after 4 d.

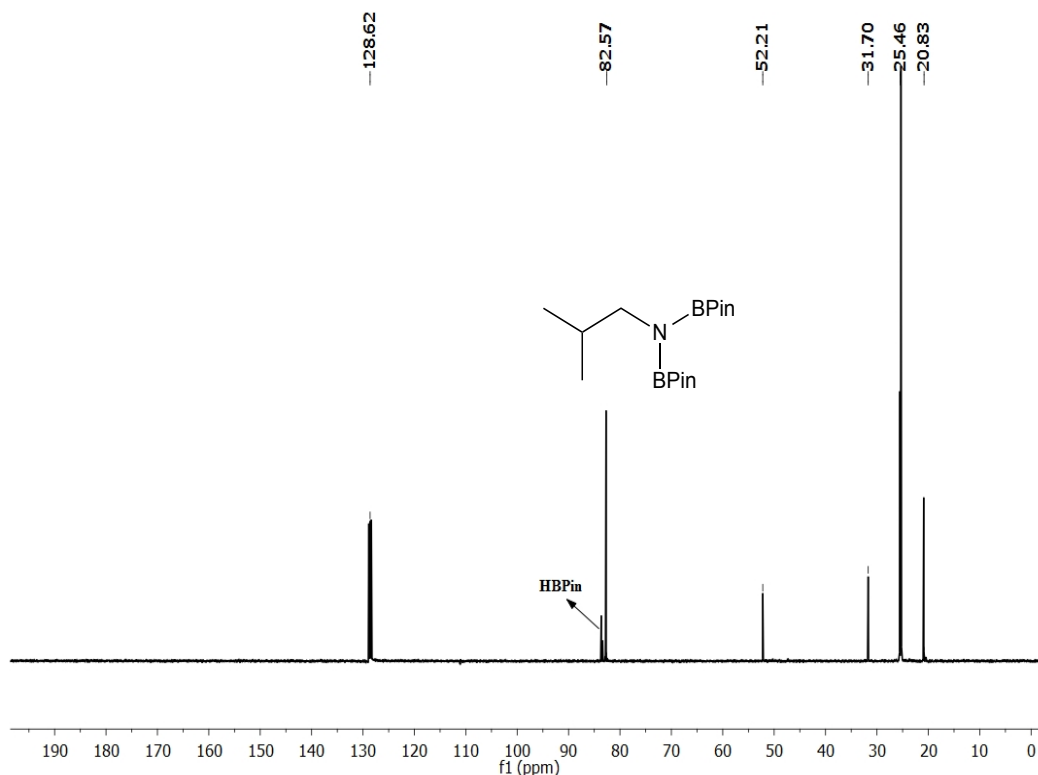


Figure 4.48: ^{13}C NMR spectrum for the conversion of isobutyronitrile to diboryl amine using 1 mol% catalyst **20** in benzene- d_6 after 4 d.

NMR scale dihydroboration of (*N,N*-dimethylamino) propionitrile (1 mol% **20):**

In the nitrogen filled glove box, a benzene- d_6 solution of (*N,N*-dimethylamino) propionitrile (67.9 μL , 0.6026 mmol) and pinacolborane (0.19 mL, 1.3258 mmol) was added to a vial containing 2.6 mg (0.0060 mmol) of **20**. The resulting solution immediately changed color from green to dark purple, which was transferred to a J. Young tube and remained at ambient temperature for 2 h. Based on the integration of methyl peak of the nitrile vs. product in the ^1H NMR spectrum, 43% conversion was observed after 2 h, 85% after 24 h, and it required 4 days for complete conversion to $(\text{CH}_3)_2\text{NCH}_2\text{CH}_2\text{CH}_2\text{N}(\text{BPin})_2$. ^1H NMR (400 MHz, benzene- d_6) δ 3.35 (t, $J = 7.2$ Hz, 2H, $-\text{N}(\text{BPin})_2\text{CH}_2$), 2.23 (t, $J = 7.2$ Hz, 2H, $-\text{N}(\text{BPin})_2\text{CH}_2\text{CH}_2$), 2.08 (s, 6H, $-\text{N}(\text{CH}_3)_2$),

1.84 – 1.74 (m, 2H, $-\text{NMe}_2\text{CH}_2$), 1.02 (s, 24H, $-\text{C}(\text{CH}_3)_2$). ^{13}C NMR (101 MHz, benzene- d_6) δ 82.72 ($-\text{C}(\text{CH}_3)_2$), 58.34 ($-\text{CH}_2\text{N}(\text{BPin})_2$), 46.15 ($-\text{N}(\text{CH}_3)_2$), 43.18 ($-\text{N}(\text{CH}_3)_2\text{CH}_2$), 32.73 ($-\text{CH}_2\text{N}(\text{BPin})_2$), 25.33 ($-\text{C}(\text{CH}_3)_2$).

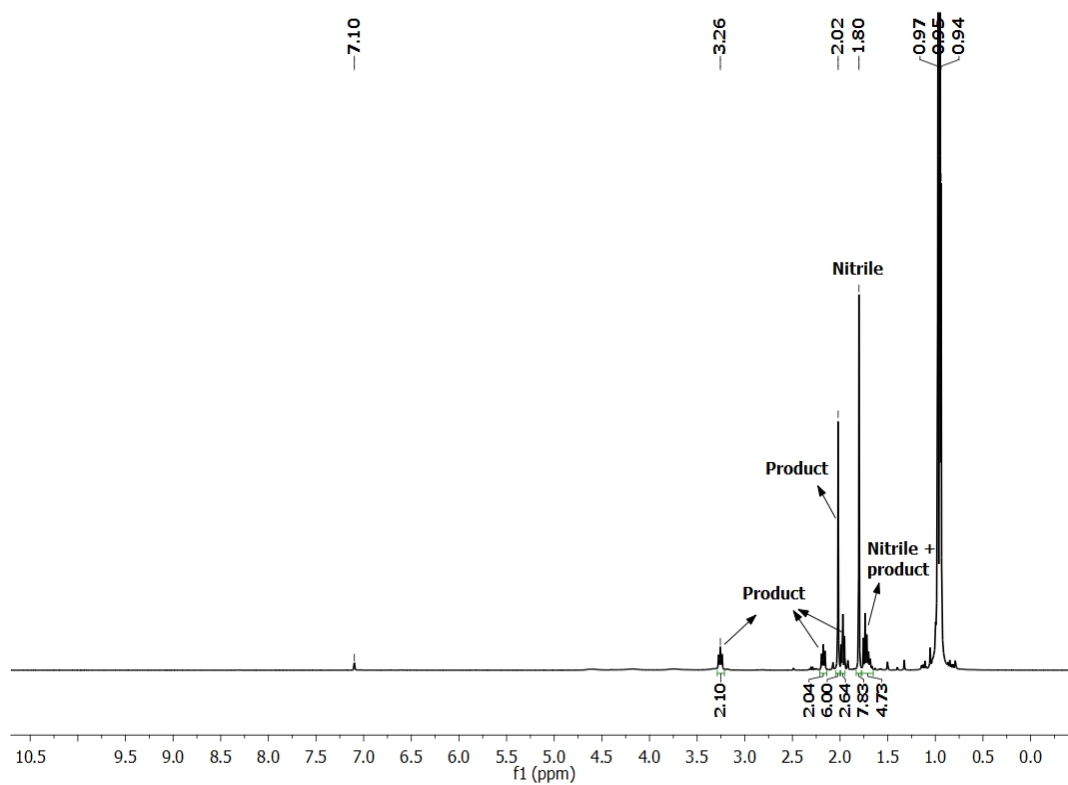


Figure 4.49: Conversion of (*N,N*-dimethylamino) propionitrile to diboryl amine using 1 mol% catalyst **20** in benzene- d_6 after 2 h.

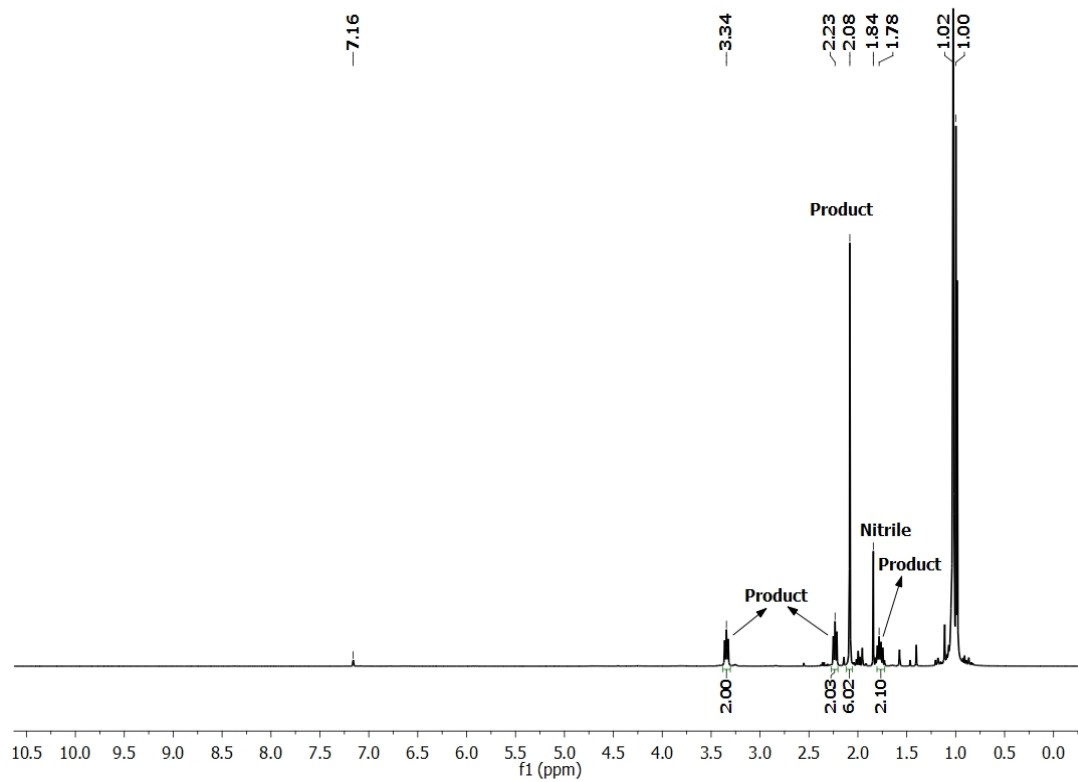


Figure 4.50: Conversion of (*N,N*-dimethylamino) propionitrile to diboryl amine using 1 mol% catalyst **20** in benzene-*d*₆ after 24 h.

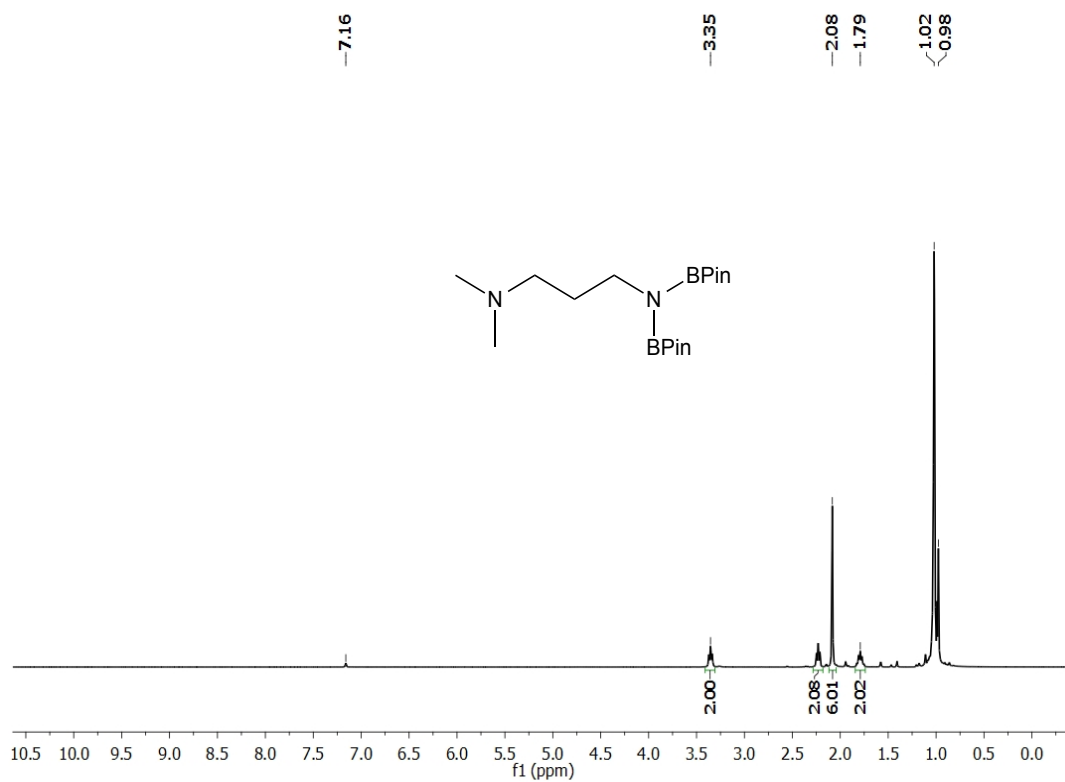


Figure 4.51: Conversion of (*N,N*-dimethylamino) propionitrile to diboryl amine using 1 mol% catalyst **20** in benzene-*d*₆ after 4 d.

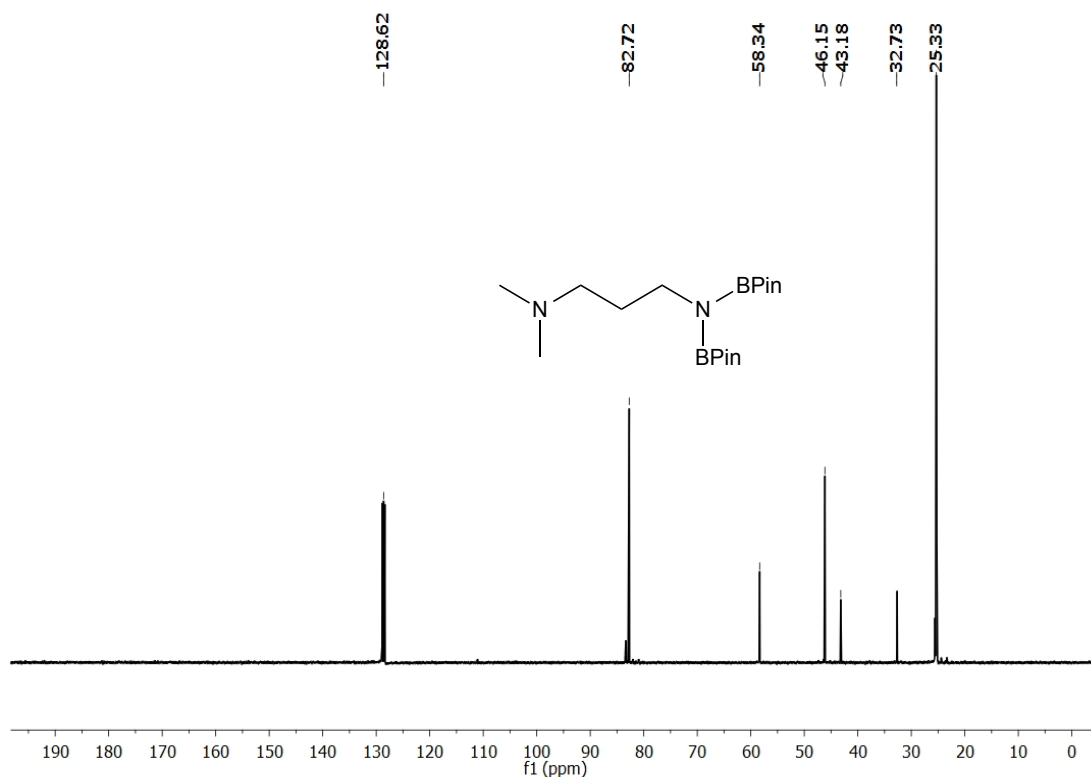


Figure 4.52: ^{13}C NMR spectrum for the conversion of (*N,N*-dimethylamino) propionitrile to diboryl amine using 1 mol% catalyst **20** in benzene- d_6 after 4 d.

NMR scale dihydroboration of (3-diphenylphosphino) propionitrile (1 mol% **20):**

In the nitrogen filled glove box, a benzene- d_6 solution of (3-diphenylphosphino)propionitrile (127.5 mg, 0.5331 mmol) and pinacolborane (0.17 mL, 1.1728 mmol) was added to a vial containing 2.3 mg (0.0053 mmol) of **20**. The reaction mixture turned red in color and it was transferred to a J. Young tube and then heated to 60 °C in a pre-heated oil bath. Immediately, the color changed from red to orange. Both ^1H NMR and ^{13}C NMR spectroscopy confirmed >99% conversion of the starting nitrile compound to diboryl amine, 3-PPH $_2$ CH $_2$ CH $_2$ CH $_2$ N(BPin) $_2$ after 2 h at 60 °C. After removal of the solvent under vacuum, the product was recrystallized from ether at -35 °C to obtain a pale orange solid compound (0.214 g, yield = 81 %). ^1H NMR (400 MHz,

benzene- d_6) δ 7.47 (t, $J = 7.5$ Hz, 4H, *phenyl*), 7.14 – 7.02 (m, 6H, *phenyl*), 3.54 (s, 2H, - CH_2), 2.14 – 2.07 (m, 2H, - CH_2), 1.93 (s, 2H, - CH_2), 1.05 (s, 24H, - $C(CH_3)_2$). ^{13}C NMR (126 MHz, benzene- d_6) δ 140.65 (*phenyl*), 133.88 (*phenyl*), 133.69 (*phenyl*), 129.18 (*phenyl*), 83.01 (- $C(CH_3)_2$), 46.08 (- CH_2), 30.59 (- CH_2), 26.28 (- CH_2), 25.32 (- $C(CH_3)_2$).

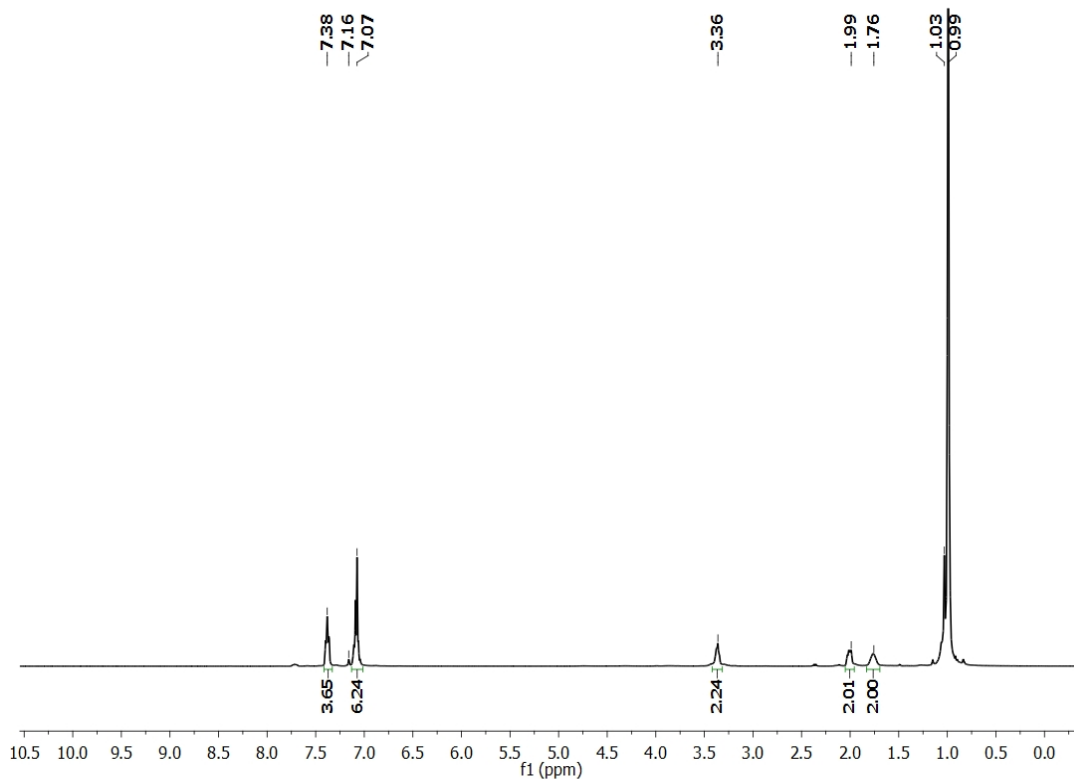


Figure 4.53: Conversion of (3-diphenylphosphino) propionitrile to diboryl amine using 1 mol% catalyst **20** in benzene- d_6 after 2 h at 60 °C.

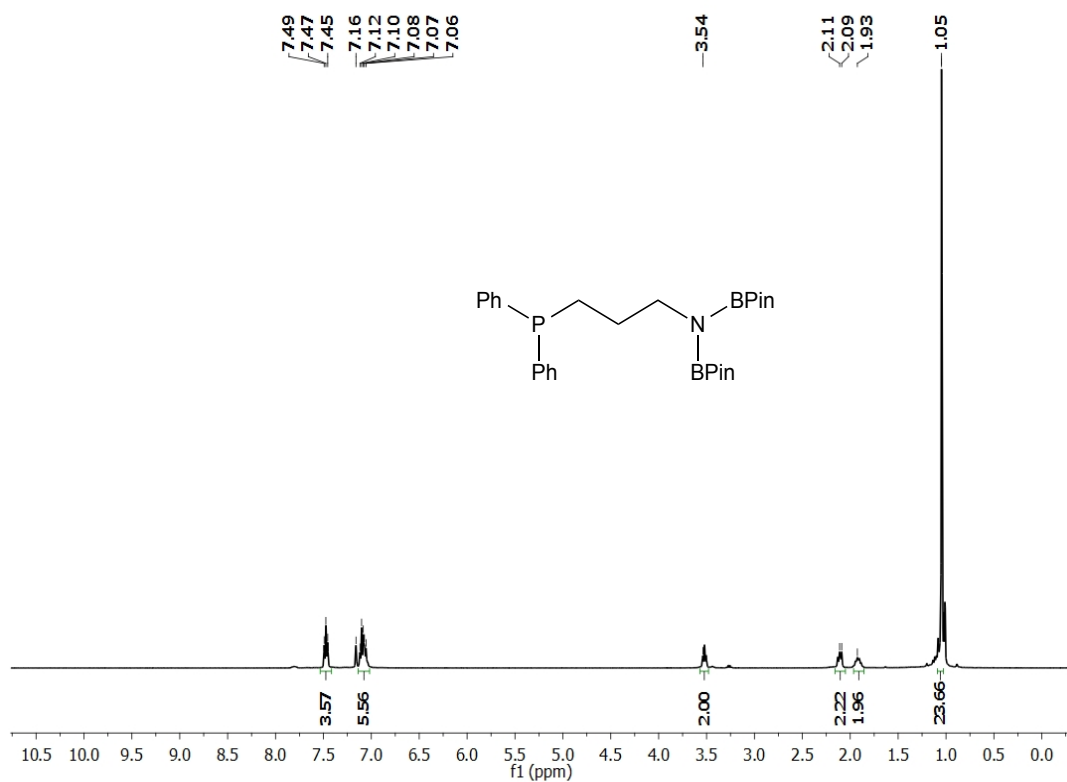


Figure 4.54: ¹H NMR spectrum of 3-PPh₂CH₂CH₂CH₂N(BPin)₂ in benzene-*d*₆ at 25 °C.

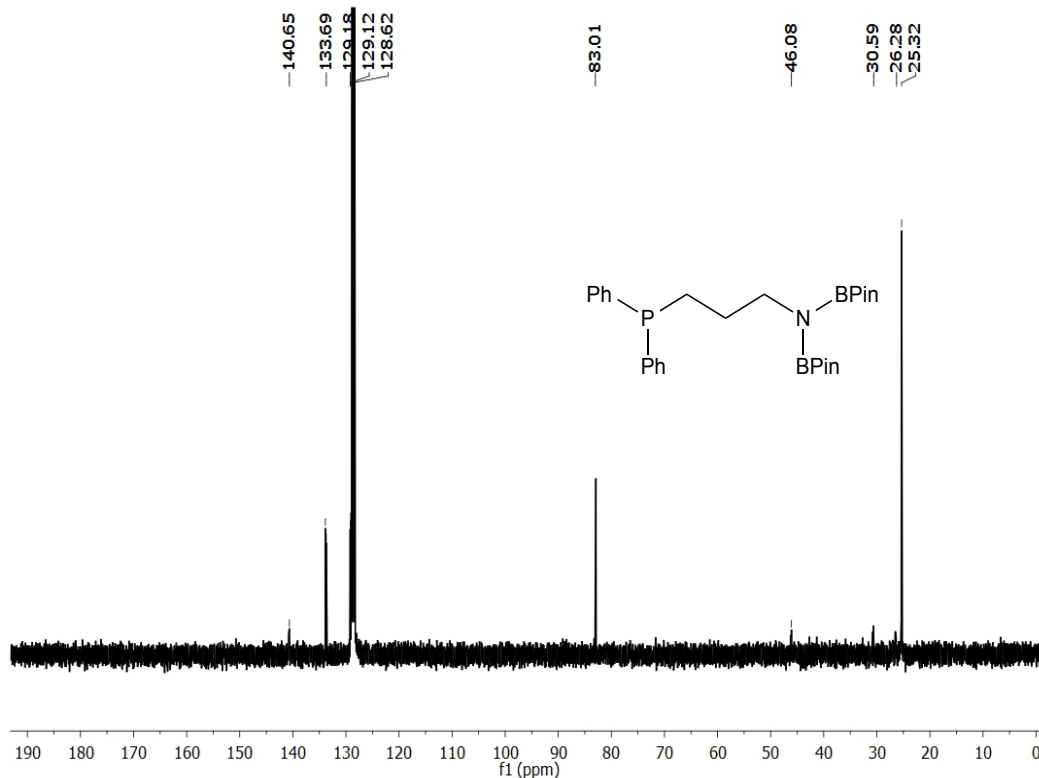


Figure 4.55: ^{13}C NMR spectrum of 3-PPh₂CH₂CH₂CH₂N(BPin)₂ in benzene-*d*₆ at 25 °C.

4.8.4. Catalytic Imine Hydroboration Using Complex **20**:

NMR scale hydroboration of *N*-benzylidenebenzylamine (1 mol% **20**):

In the nitrogen filled glove box, a benzene-*d*₆ solution of *N*-Benzylidenebenzylamine (113.1 mg, 0.579 mmol) and pinacolborane (100.9 μL , 0.695 mmol) was added to a vial containing 2.5 mg (0.0058 mmol) of **20**. The resulting solution immediately changed color from green to dark brown, which was transferred to a J. Young tube and remained at ambient temperature for 2 h. Both ^1H NMR and ^{13}C NMR spectroscopy confirmed >99% conversion of the starting imine compound to mono-boryl amine, (PhCH₂)₂N(BPin) after 2 h at room temperature. ^1H NMR (400 MHz, benzene-*d*₆)

δ 7.18 (d, $J = 7.4$ Hz, 4H, *phenyl*), 7.13 (t, $J = 7.5$ Hz, 4H, *phenyl*), 7.04 (t, $J = 7.1$ Hz, 2H, *phenyl*), 4.04 (s, 2H, -NCH₂), 1.12 (s, 12H, -C(CH₃)₂).

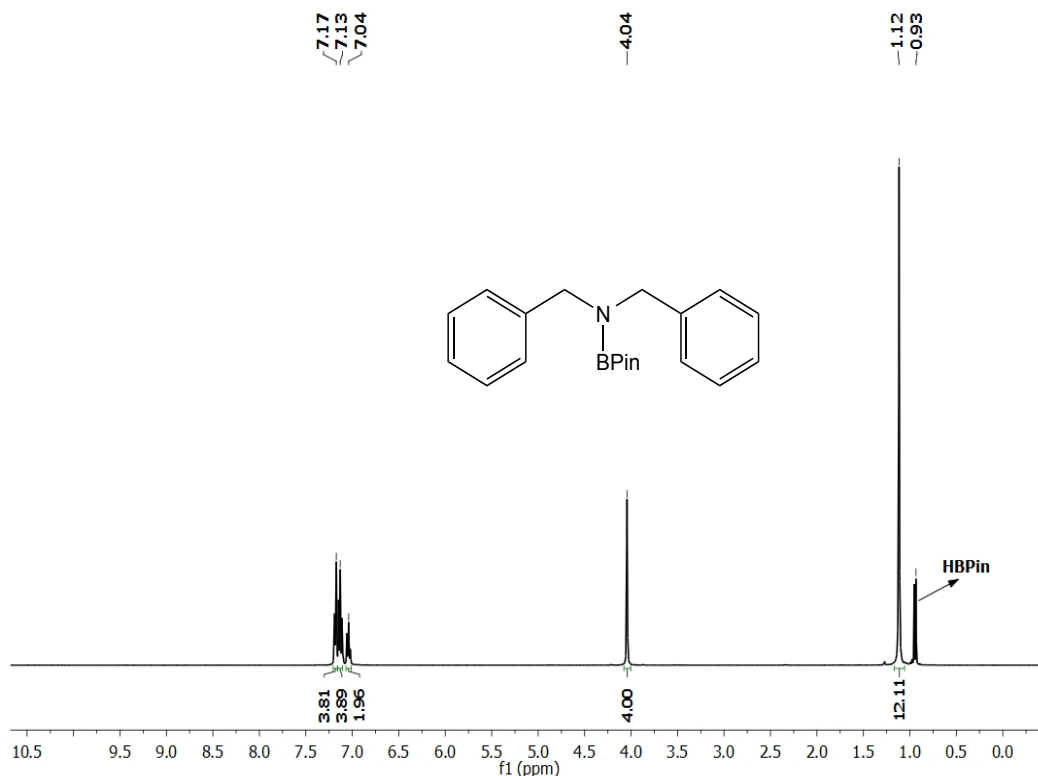


Figure 4.56: Hydroboration of *N*-benzylidenebenzylamine using 1 mol% catalyst **20** in benzene-*d*₆ after 2 h.

NMR scale hydroboration of 4-chloro-*N*-(phenylmethylene) benzenamine (1 mol% **20):**

In the nitrogen filled glove box, a benzene-*d*₆ solution of 4-chloro-*N*-(phenylmethylene) benzenamine (134.9 mg, 0.626 mmol) and pinacolborane (0.11 mL, 0.751 mmol) was added to a vial containing 2.7 mg (0.0062 mmol) of **2**. The resulting solution immediately changed color from green to dark brown, which was transferred to a J. Young tube and remained at ambient temperature for 2 h. Both ¹H NMR and ¹³C NMR spectroscopy confirmed >99% conversion of the starting imine compound to mono-boryl amine, (PhCH₂)(4-ClPh)N(BPin) after 2 h at room temperature. ¹H NMR (400 MHz,

benzene- d_6) δ 7.27 (d, $J = 8.8$ Hz, 2H, *phenyl*), 7.22-7.14 (m, 4H, *phenyl*), 7.06 (d, $J = 8.8$ Hz, 3H, *phenyl*), 4.68 (s, 2H, -NCH₂), 1.14 (s, 12H, -C(CH₃)₂).

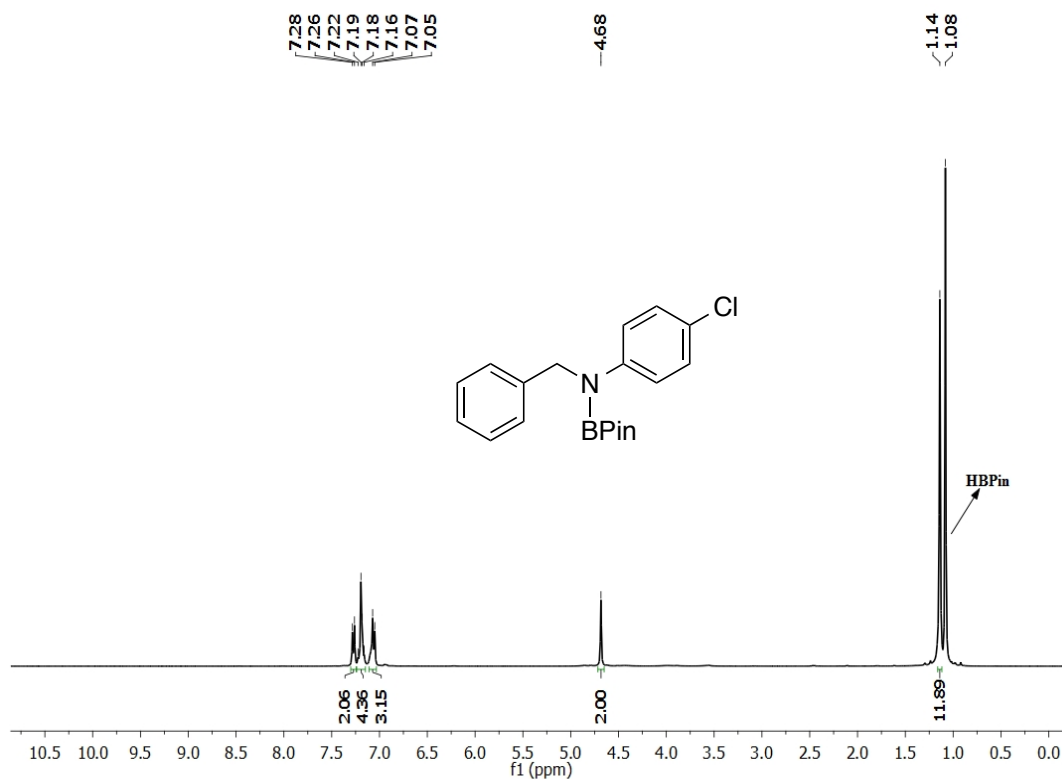


Figure 4.57: Hydroboration of 4-chloro-*N*-(phenylmethylene) benzenamine using 1 mol% catalyst **20** in benzene- d_6 after 2 h.

NMR scale hydroboration of 2,6-difluoro-*N*-(phenylmethylene) benzenamine (1 mol% **20):**

In the nitrogen filled glove box, a benzene- d_6 solution of 2,6-difluoro-*N*-(phenylmethylene) benzenamine (105.7 mg, 0.487 mmol) and pinacolborane (77.7 μ L, 0.535 mmol) was added to a vial containing 2.1 mg (0.0049 mmol) of **2**. The resulting solution immediately changed color from green to dark brown, which was transferred to a J. Young tube and remained at ambient temperature for 2 h. Both ¹H NMR and ¹³C NMR spectroscopy confirmed >99% conversion of the starting imine compound to mono-boryl amine, (PhCH₂)(2,6-difluoro-Ph)N(BPin) after 2 h at room temperature. ¹H NMR (400

MHz, benzene- d_6): δ 7.31 (d, $J = 7.5$ Hz, 2H), 7.06 (t, $J = 7.6$ Hz, 2H), 6.97 (t, $J = 7.3$ Hz, 1H), 6.34-6.32 (m, 3H), 4.73 (s, 2H), 1.12 (s, 12H, $-C(CH_3)_2$).

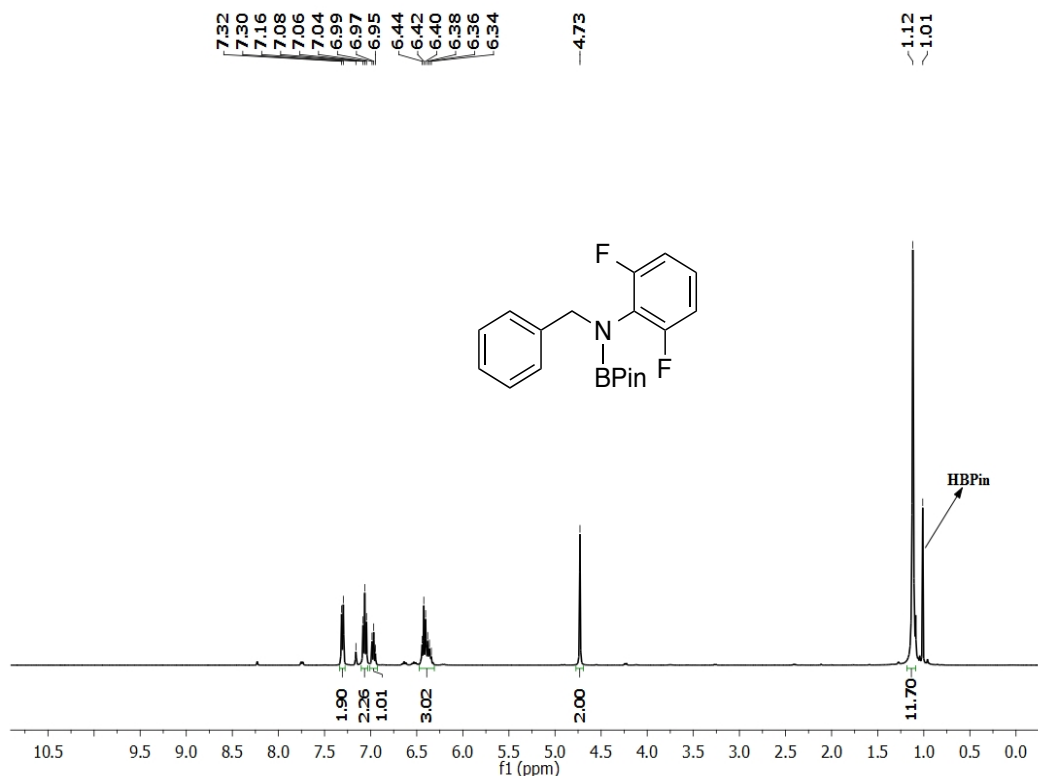


Figure 4.58: Hydroboration of 2,6-difluoro-*N*-(phenylmethylene) benzenamine using 1 mol% catalyst **20** in benzene- d_6 after 2 h.

NMR scale hydroboration of 4-methyl-*N*-(phenylmethylene) benzenamine (1 mol% **20):**

In the nitrogen filled glove box, a benzene- d_6 solution of 4-methyl-*N*-(phenylmethylene) benzenamine (113.1 mg, 0.579 mmol) and pinacolborane (100.9 μ L, 0.695 mmol) was added to a vial containing 2.5 mg (0.0058 mmol) of **20**. The resulting solution immediately changed color from green to dark brown, which was transferred to a J. Young tube and remained at ambient temperature for 2 h. Both ^1H NMR and ^{13}C NMR spectroscopy confirmed >99% conversion of the starting imine compound to mono-boryl

amine, (PhCH₂)(4-MePh)N(BPin) after 2 h at room temperature. ¹H NMR (400 MHz, benzene-*d*₆) δ 7.31 (d, *J* = 8.4 Hz, 2H, *phenyl*), 7.22 (d, *J* = 7.5 Hz, 2H, *phenyl*), 7.12 (t, *J* = 7.5 Hz, 2H, *phenyl*), 7.01 (t, *J* = 7.3 Hz, 1H, *phenyl*), 6.89 (d, *J* = 8.3 Hz, 2H, *phenyl*), 4.73 (s, 2H, -NCH₂), 2.05 (s, 3H, -CH₃Ph), 1.10 (s, 12H, -C(CH₃)₂).

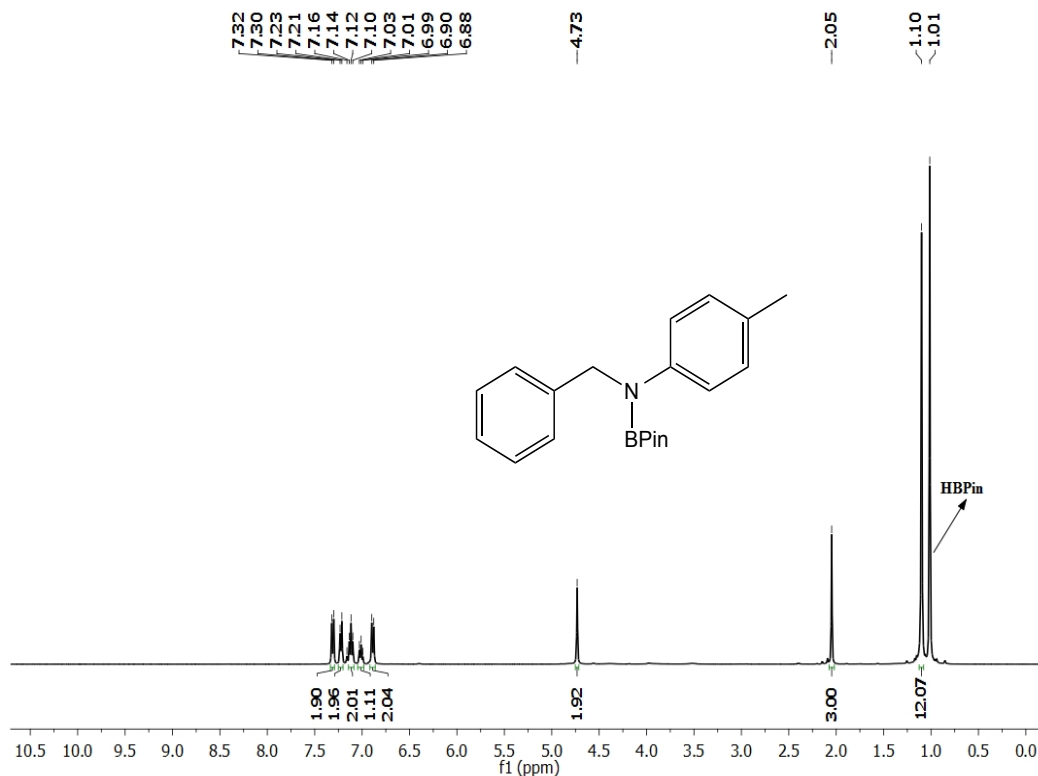


Figure 4.59: Hydroboration of 4-methyl-*N*-(phenylmethylene) benzenamine using 1 mol% catalyst **20** in benzene-*d*₆ after 2 h.

NMR scale hydroboration of 2,4,6-trimethyl-*N*-(phenylmethylene) benzenamine (1 mol% **20):**

In the nitrogen filled glove box, a benzene-*d*₆ solution of 2,4,6-trimethyl-*N*-(phenylmethylene) benzenamine (113.8 mg, 0.5099 mmol) and pinacolborane (88.8 μL, 0.6119 mmol) was added to a vial containing 2.2 mg (0.0051 mmol) of **20**. The resulting solution immediately changed color from green to dark brown, which was transferred to a

J. Young tube. Integration of the $-CH$ peak of the imine at 7.83 ppm vs. the $-CH_2$ resonance of the product at 4.30 ppm indicated 85% conversion after 2 h and complete conversion to its corresponding mono-boryl amine, $(Ph_2CH)(2,4,6\text{-trimethyl-Ph})N(\text{BPin})$ at room temperature after 24 h. $^1\text{H NMR}$ (400 MHz, benzene- d_6) δ 7.22 (d, $J = 5.7$ Hz, 2H, *phenyl*), 7.07 (d, $J = 6.1$ Hz, 3H, *phenyl*), 6.72 (s, 2H, *phenyl*), 4.36 (s, 2H, $-NCH_2$), 2.07 (s, 3H, $-CH_3$), 2.01 (s, 6H, $-CH_3$), 1.15 (d, $J = 44.8$ Hz, 12H, $-C(CH_3)_2$).

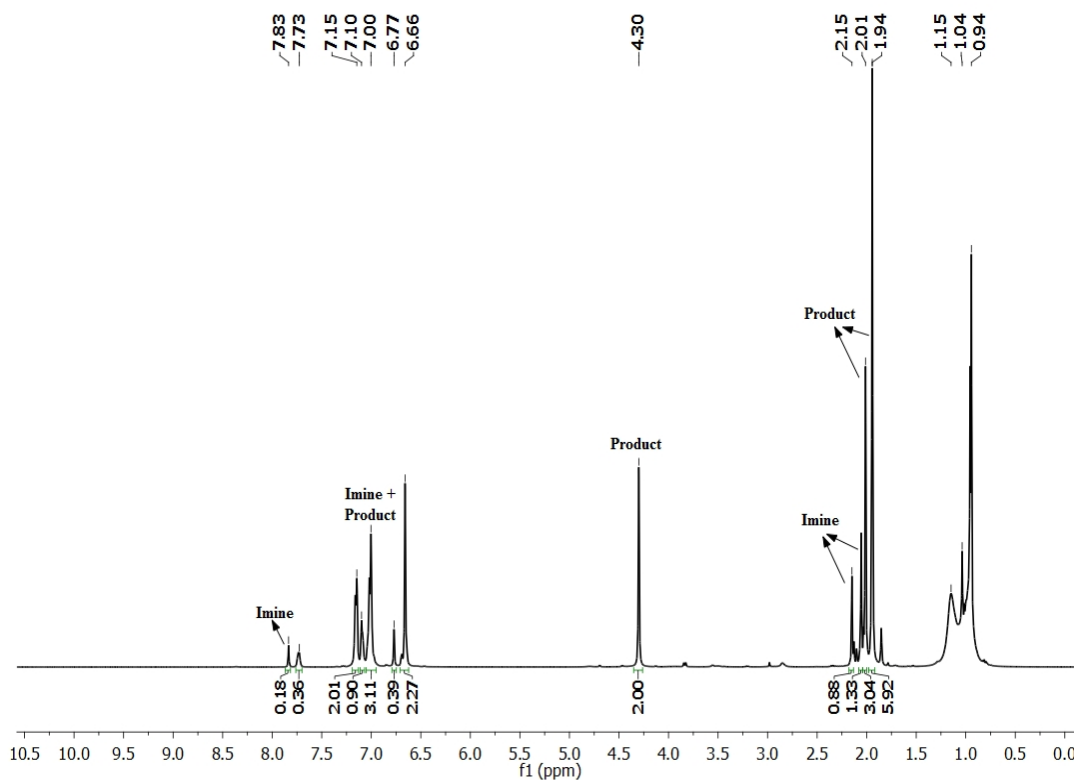


Figure 4.60: Partial hydroboration (85%) of 2,4,6-trimethyl-*N*-(phenylmethylene) benzenamine using 1 mol% catalyst **20** in benzene- d_6 after 2 h.

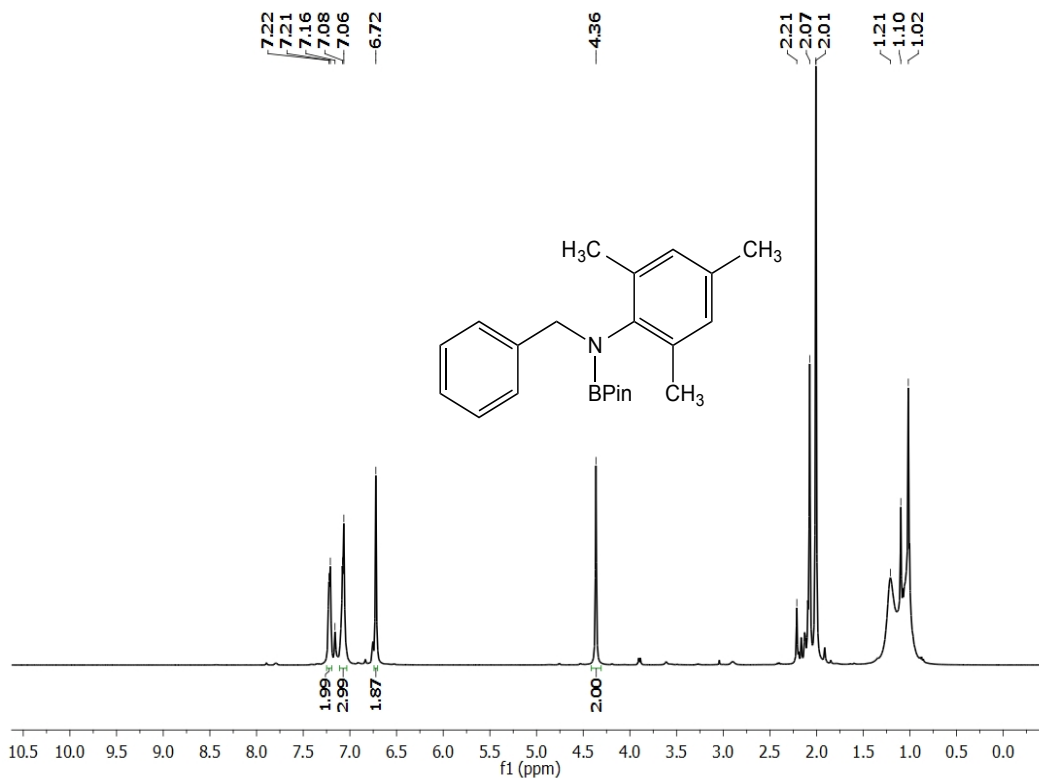


Figure 4.61: Hydroboration of 2,4,6-trimethyl-*N*-(phenylmethylene) benzenamine using 1 mol% catalyst **20** in benzene- d_6 after 24 h.

NMR scale hydroboration of α -methyl-*N*-(phenylmethylene) benzenemethanamine (1 mol% **20):**

In the nitrogen filled glove box, a benzene- d_6 solution of α -methyl-*N*-(phenylmethylene) benzenemethanamine (116.4 mg, 0.5563 mmol) and pinacolborane (96.9 μ L, 0.6675 mmol) was added to a vial containing 2.4 mg (0.0056 mmol) of **20**. The resulting solution immediately changed color from green to dark brown, which was transferred to a J. Young tube. Integration of the hydrogen resonance (-NCHMePh) at 4.29 ppm (imine) vs. 4.48 ppm (product) indicated 34% conversion after 2 h and it took 24 h to reach complete conversion to the corresponding mono-boryl amine, (PhCH₂)(CHMePh)N(BPin) at room temperature. ¹H NMR (400 MHz, benzene- d_6) δ 7.34 (d, J = 7.1 Hz, 2H, *phenyl*), 7.27 (d, J = 6.9 Hz, 2H, *phenyl*), 7.23 – 7.15 (m, 4H,

phenyl), 7.13 – 7.04 (m, 2H, *phenyl*), 4.48 (s, 2H, -NCH₂), 4.10 (dd, *J* = 78.4, 15.7 Hz, 1H, -CHMePh), 1.45 (d, *J* = 6.9 Hz, 3H, -CHCH₃Ph), 1.15 (s, 12H, -C(CH₃)₂).

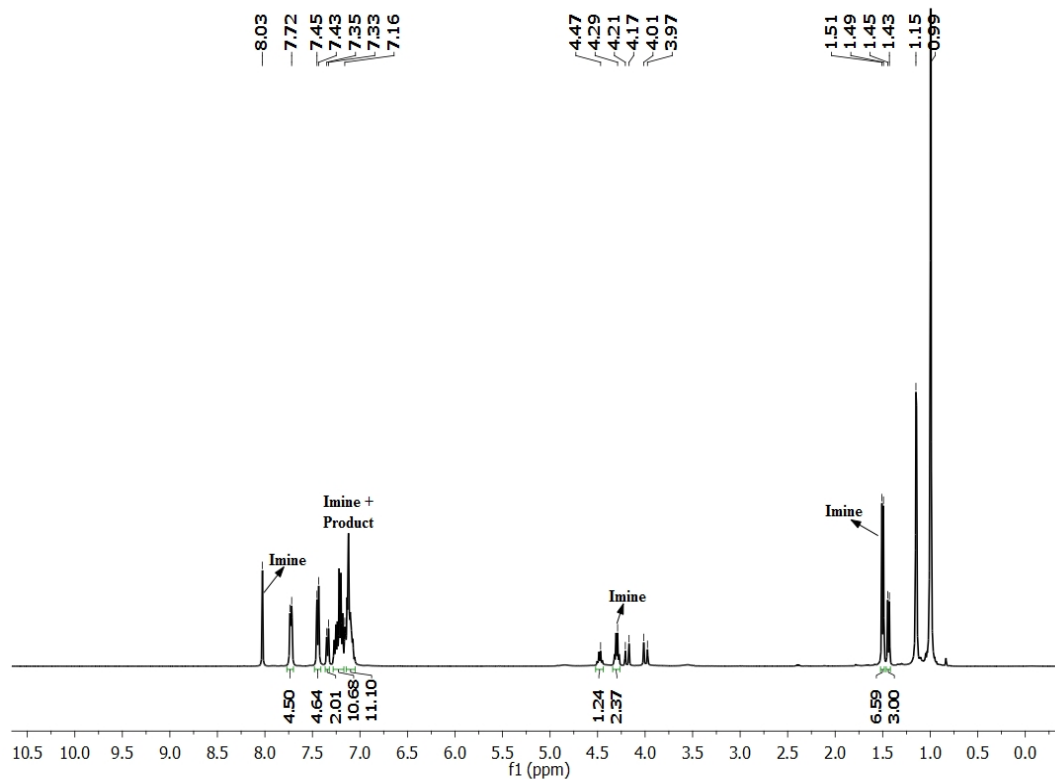


Figure 4.62: Partial hydroboration (34%) of α -methyl-*N*-(phenylmethylene) benzenemethanamine using 1 mol% catalyst **20** in benzene-*d*₆ after 2 h.

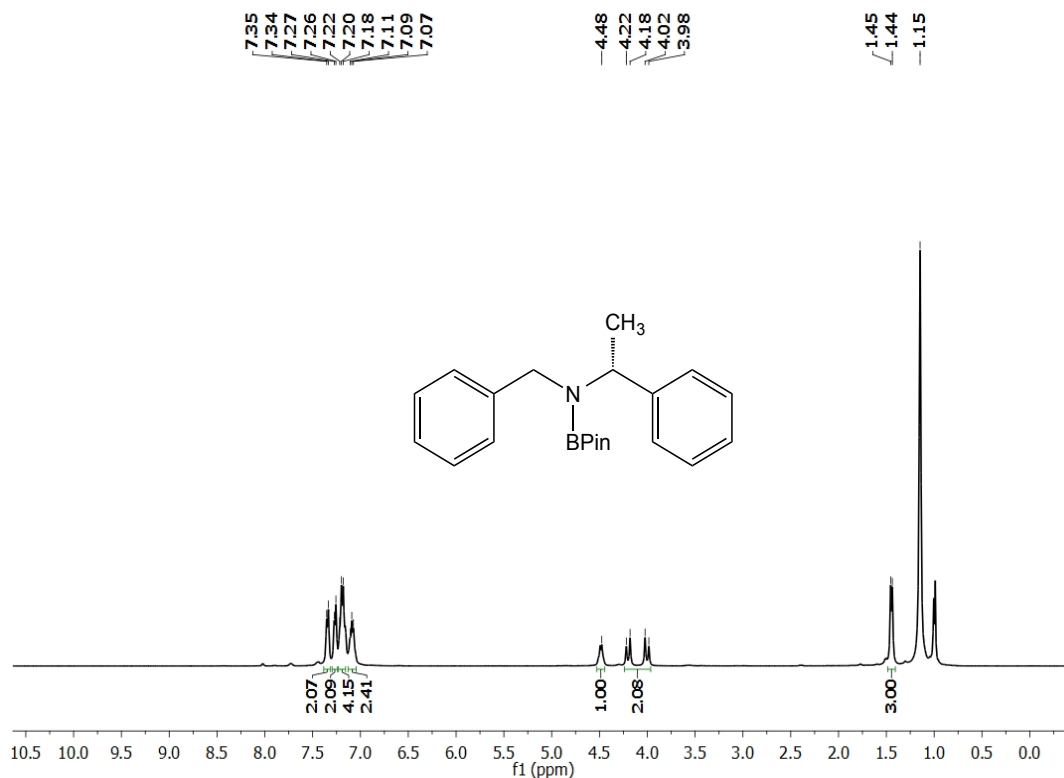


Figure 4.63: Hydroboration of α -methyl-*N*-(phenylmethylene) benzenemethanamine using 1 mol% catalyst **20** in benzene- d_6 after 24 h.

NMR scale hydroboration of *N*-(phenylmethylene)-2-propanamine (1 mol% **20):**

In the nitrogen filled glove box, a benzene- d_6 solution of *N*-(phenylmethylene)-2-propanamine (81.9 mg, 0.556 mmol) and pinacolborane (96.9 μ L, 0.667 mmol) was added to a vial containing 2.4 mg (0.0056 mmol) of **20**. The resulting solution immediately changed color from green to dark brown, which was transferred to a J. Young tube and remained at ambient temperature for 2 h. Integration of the ^1H NMR peak at 8.01 ppm (imine-H) vs. 4.18 ppm (product-NCH $_2$) confirmed 72% conversion after 2 h and it took 24 h to reach complete conversion to the corresponding mono-boryl amine, (PhCH $_2$)(i Pr)N(BPin) at room temperature. ^1H NMR (400 MHz, benzene- d_6) δ

7.33 (d, $J = 7.5$ Hz, 2H, *phenyl*), 7.21 (d, $J = 7.4$ Hz, 2H, *phenyl*), 7.09 (dd, $J = 14.3, 6.9$ Hz, 2H, *phenyl*) (combined imine and product), 4.19 (s, 2H, $-NCH_2Ph$), 3.40 (m, 1H, $-CH$), 1.14 (s, 12H, $-C(CH_3)_2$), 1.10 (d, $J = 6.7$ Hz, 6H, $-CH(CH_3)_2$).

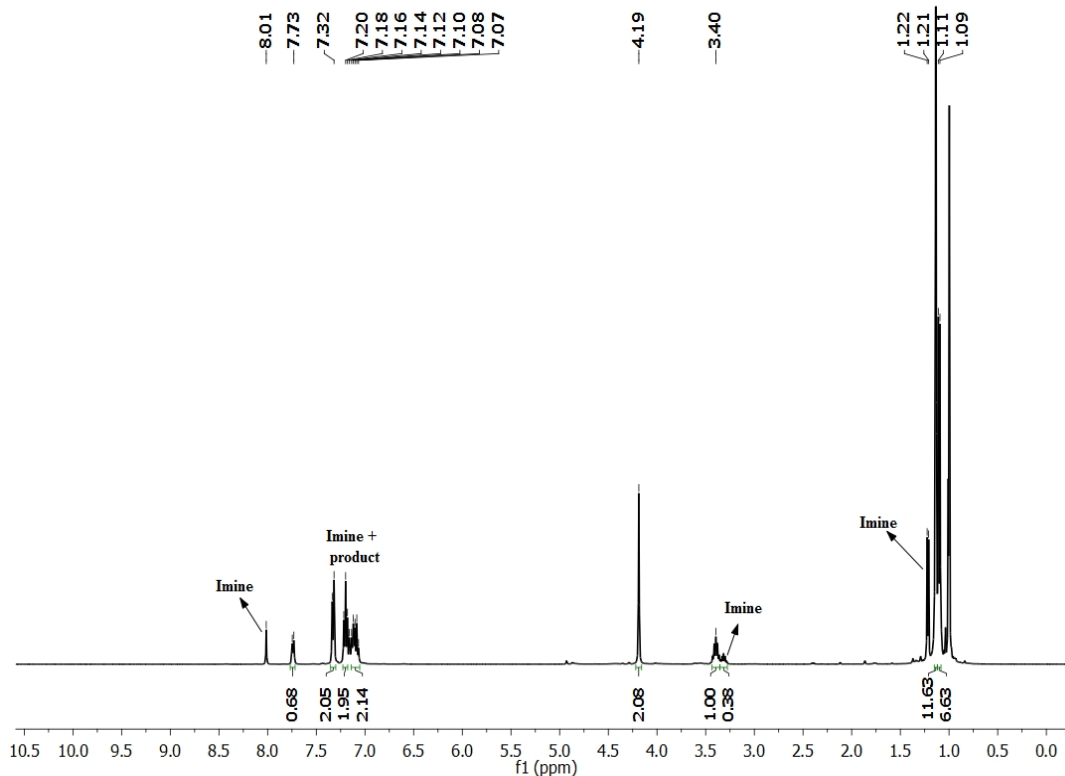


Figure 4.64: Partial hydroboration (72%) of *N*-(phenylmethylene)-2-propanamine using 1 mol% catalyst **20** in benzene- d_6 after 2 h.

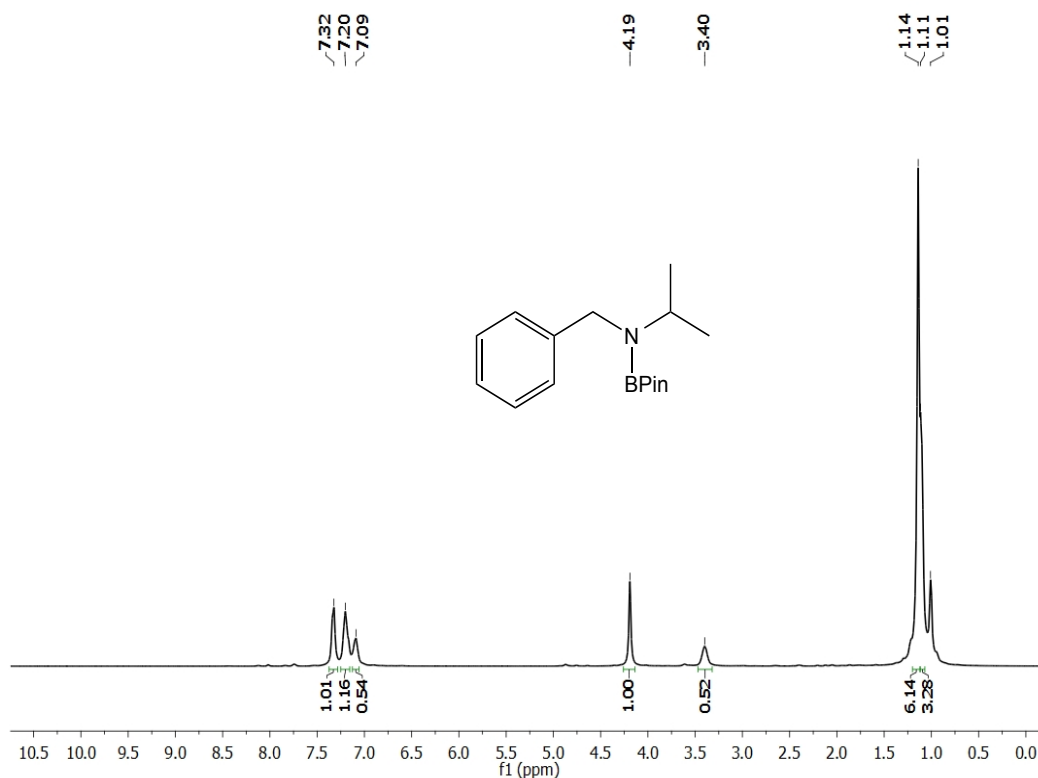


Figure 4.65: Hydroboration of *N*-(phenylmethylene)-2-propanamine using 1 mol% catalyst **20** in benzene-*d*₆ after 3 d.

NMR scale hydroboration of *N*-(phenylmethylene)-1-butanamine (1 mol% **20):**

In the nitrogen filled glove box, a benzene-*d*₆ solution of *N*-(phenylmethylene)-1-butanamine (119.6 mg, 0.742 mmol) and pinacolborane (0.13 mL, 0.890 mmol) was added to a vial containing 3.2 mg (0.0074 mmol) of **20**. The resulting solution immediately changed color from green to dark brown, which was transferred to a J. Young tube and remained at ambient temperature for 2 h. Integration of the ¹H NMR peak at 8.04 ppm (imine-H) vs. 4.17 ppm (product-NCH₂) confirmed 86% conversion of the starting imine compound to mono-boryl amine, (PhCH₂)(ⁿBu)N(BPin) after 2 h at room temperature. ¹H NMR (400 MHz, benzene-*d*₆) δ 7.27 (d, *J* = 7.4 Hz, 2H, *phenyl*), 7.21 (d, *J* = 7.4 Hz, 2H, *phenyl*), 7.10 (t, *J* = 7.2 Hz, 1H, *phenyl*), 4.17 (s, 2H, -NCH₂Ph),

2.93 (t, $J = 7.0$ Hz, 2H, $-CH_2$), 1.43 – 1.34 (m, 2H, $-CH_2$), 1.23 (m, 2H, $-CH_2$), 1.16 (s, 12H, $-C(CH_3)_2$), 0.85 (t, $J = 7.3$ Hz, 3H, $-CH_3$).

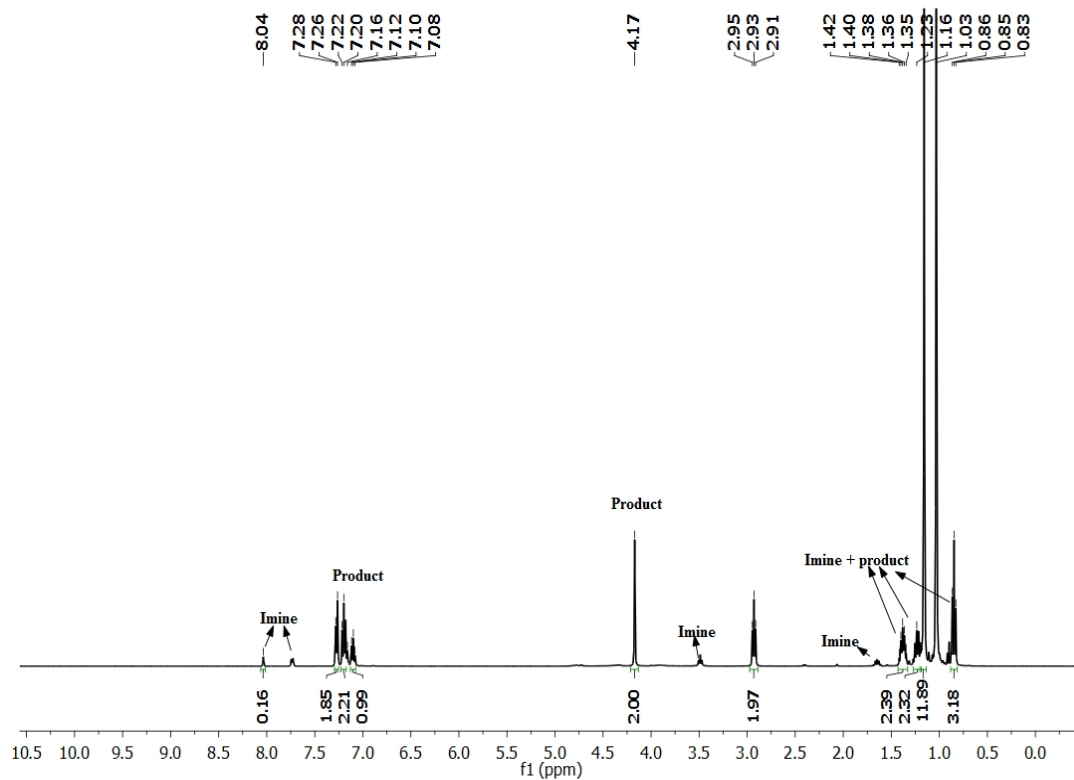


Figure 4.66: Partial hydroboration (86%) of *N*-(phenylmethylene)-1-butanamine using 1 mol% catalyst **20** in benzene- d_6 after 2 h.

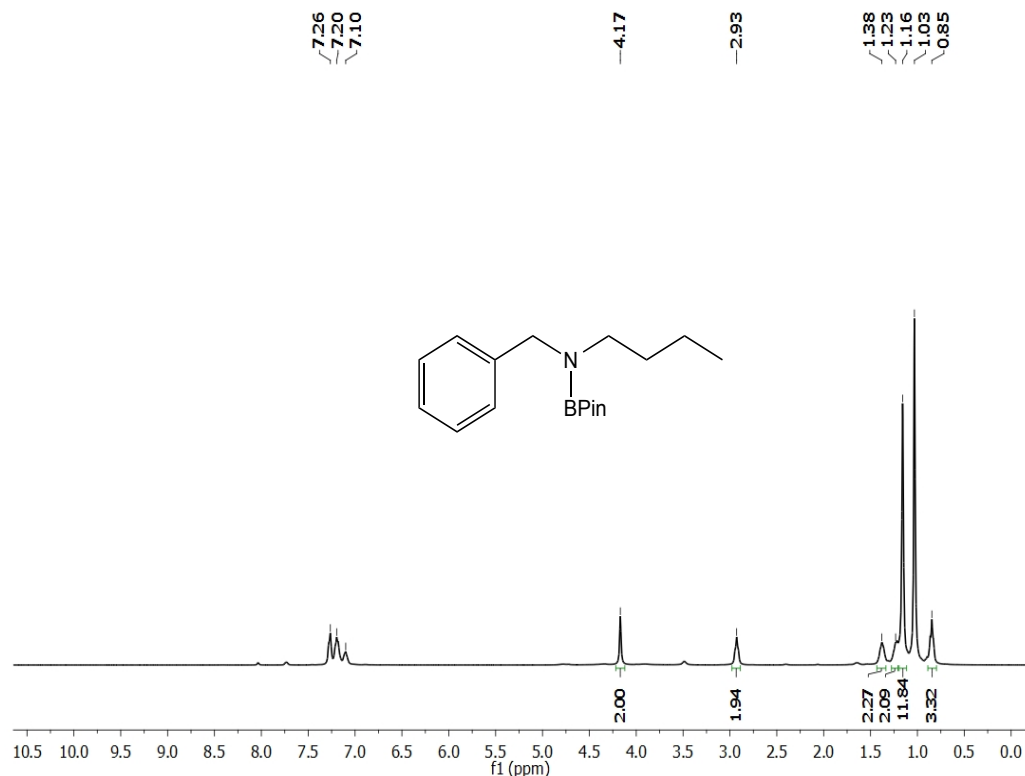


Figure 4.67: Hydroboration of *N*-(phenylmethylene)-1-butanamine using 1 mol% catalyst **20** in benzene-*d*₆ after 2 d.

NMR scale hydroboration of *N*-[(4-fluorophenyl)methylene] benzenemethanamine (1 mol% **20):**

In the nitrogen filled glove box, a benzene-*d*₆ solution of *N*-[(4-fluorophenyl)methylene] benzenemethanamine (118.6 mg, 0.556 mmol) and pinacolborane (96.8 μ L, 0.667 mmol) was added to a vial containing 2.4 mg (0.0056 mmol) of **20**. The resulting solution immediately changed color from green to dark brown, which was transferred to a J. Young tube and remained at ambient temperature for 2 h. Both ¹H NMR and ¹³C NMR spectroscopy confirmed >99% conversion of the starting imine compound to mono-boryl amine, (4-FPhCH₂)(PhCH₂)N(BPin), after 2 h at room temperature. ¹H NMR (400 MHz, benzene-*d*₆) δ 7.23 – 7.10 (m, 4H, *phenyl*), 7.06 (t, *J* = 6.5 Hz, 1H, *phenyl*), 6.97 (dd, *J* =

8.3, 5.6 Hz, 2H, *phenyl*), 6.78 (t, $J = 8.6$ Hz, 2H, *phenyl*), 3.99 (s, 2H, $-NCH_2$), 3.93 (s, 2H, $-NCH_2$), 1.12 (s, 12H, $-C(CH_3)_2$).

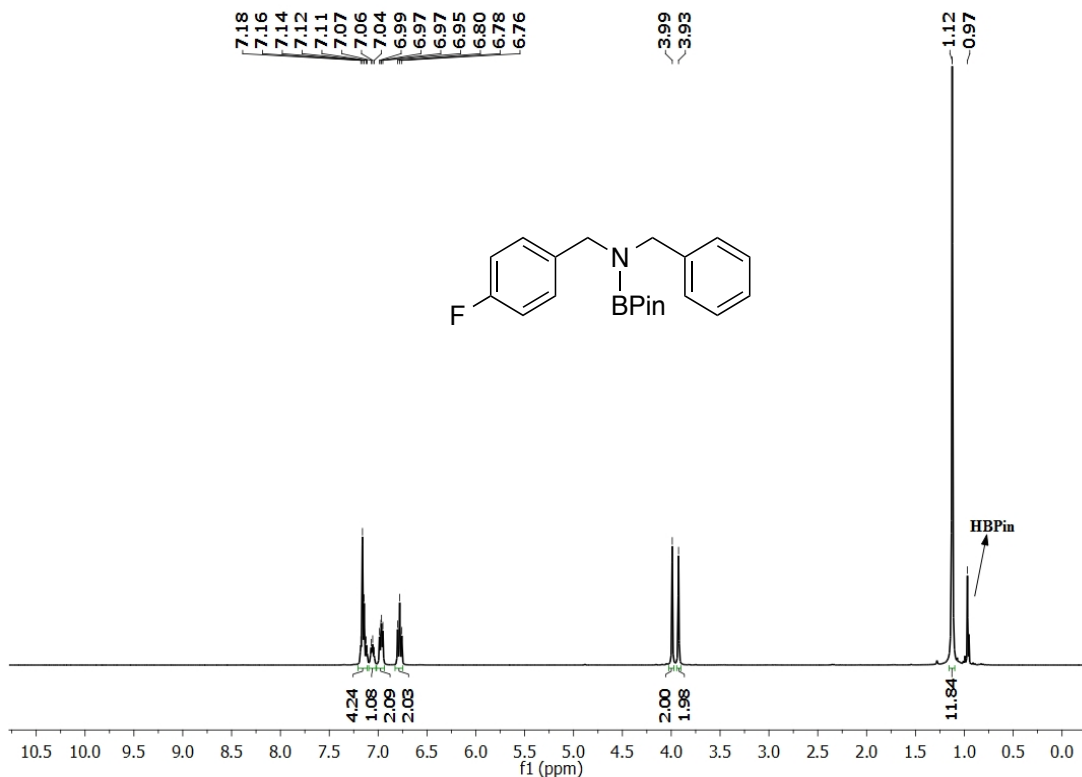


Figure 4.68: Hydroboration of *N*-[(4-fluorophenyl)methylene] benzenemethanamine using 1 mol% of catalyst **20** in benzene- d_6 after 2 h.

NMR scale hydroboration of (*p*-methoxybenzylidene) benzylamine (1 mol% **20):**

In the nitrogen filled glove box, a benzene- d_6 solution of (*p*-methoxybenzylidene) benzylamine (113.1 mg, 0.579 mmol) and pinacolborane (100.9 μ L, 0.695 mmol) was added to a vial containing 2.5 mg (0.0058 mmol) of **20**. The resulting solution immediately changed color from green to dark brown, which was transferred to a J. Young tube and remained at ambient temperature for 2 h. Both ^1H NMR and ^{13}C NMR spectroscopy confirmed >99% conversion of the starting imine compound to mono-boryl amine, (4-OMePhCH $_2$)(PhCH $_2$)N(BPin) after 2 h at room temperature. ^1H NMR (400 MHz, benzene- d_6) δ 7.25 (d, $J = 7.4$ Hz, 2H), 7.19 (d, $J = 7.4$ Hz, 2H), 7.16 (d, $J = 2.9$

Hz, 1H), 7.13 (b, 1H), 7.08 (t, $J = 7.2$ Hz, 1H), 7.08 (t, $J = 7.2$ Hz, 1H), 6.77 (d, $J = 8.4$ Hz, 2H), 4.10 (s, 2H), 4.05 (s, 2H), 3.33 (s, 3H), 1.16 (s, 12H).

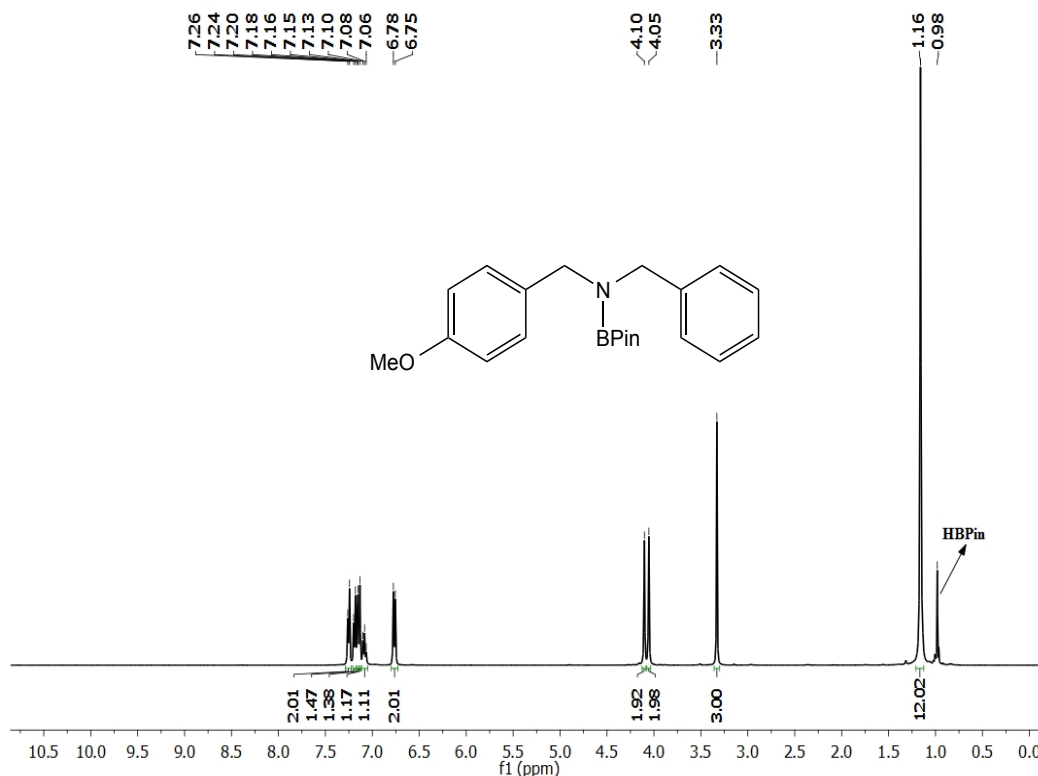


Figure 4.69: Hydroboration of (*p*-methoxybenzylidene) benzylamine using 1 mol% catalyst **20** in benzene-*d*₆ after 2 h.

NMR scale hydroboration of *N*-(2-furanylmethylene) benzenemethanamine (1 mol% **20):**

In the nitrogen filled glove box, a benzene-*d*₆ solution of *N*-(2-furanylmethylene) benzenemethanamine (128.8 mg, 0.695 mmol) and pinacolborane (0.12 mL, 0.834 mmol) was added to a vial containing 3.0 mg (0.0069 mmol) of **20**. The resulting solution immediately changed color from green to dark brown, which was transferred to a J. Young tube and remained at ambient temperature for 2 h. Both ¹H NMR and ¹³C NMR spectroscopy confirmed >99% conversion of the starting imine compound to mono-boryl

amine, (2-furylCH₂)(PhCH₂)N(BPin), after 2 h at room temperature. ¹H NMR (400 MHz, benzene-*d*₆) δ 7.17 (d, *J* = 7.4 Hz, 2H, *phenyl*), 7.11 (t, *J* = 7.4 Hz, 2H, *phenyl*), 7.07 (s, 1H, *furyl*), 7.02 (t, *J* = 7.0 Hz, 1H, *phenyl*), 6.03 (s, 1H, *furyl*), 5.91 (s, 1H, *furyl*), 4.07 (s, 2H, -NCH₂), 3.97 (s, 2H, -NCH₂), 1.09 (s, 12H, -C(CH₃)₂).

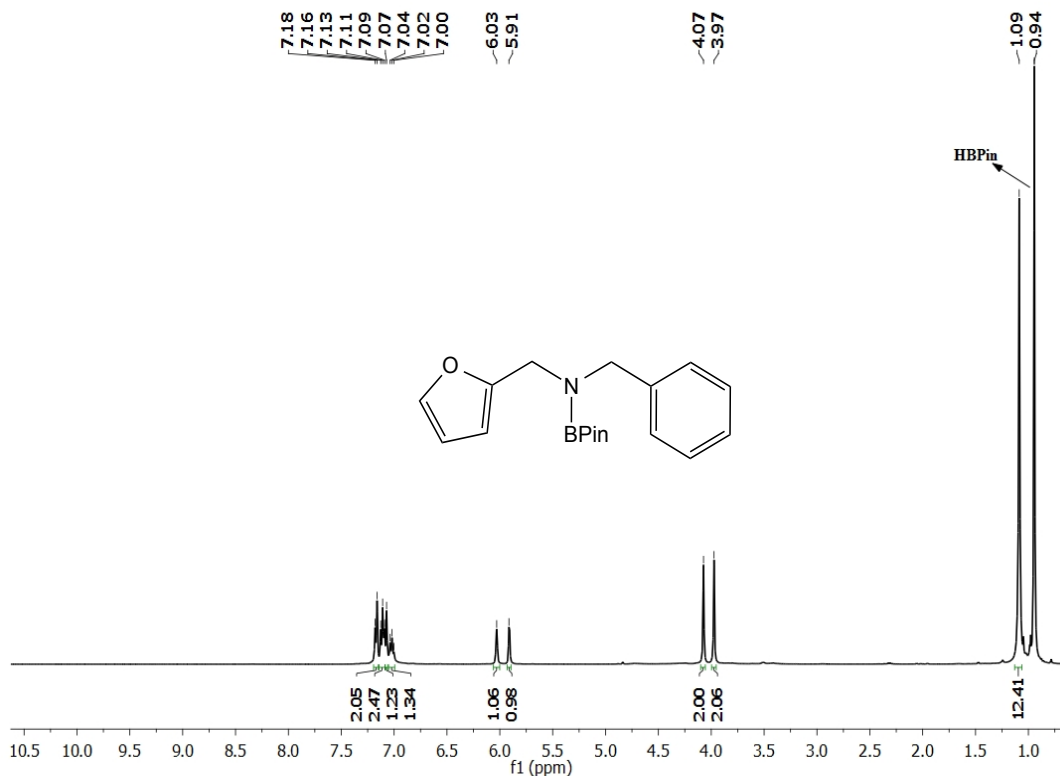


Figure 4.70: Hydroboration of *N*-(2-furylmethylene) benzenemethanamine using 1 mol% catalyst **20** in benzene-*d*₆ after 2 h.

NMR scale hydroboration of *N*-(1-phenylethylidene) benzenemethanamine (1 mol% **20):**

In the nitrogen filled glove box, a benzene-*d*₆ solution of *N*-(1-phenylethylidene) benzenemethanamine (169.8 mg, 0.8113 mmol) and pinacolborane (0.14 mL, 0.9735 mmol) was added to a vial containing 3.5 mg (0.0081 mmol) of **20**. The resulting solution immediately changed color from green to dark brown, which was transferred to a J.

Young tube and remained at ambient temperature for 2 h. Integration of the methyl resonance (-CHCH₃Ph) of the imine at 1.75 ppm (imine) vs. the doublet methyl resonance of the product at 1.35 ppm indicated 55% conversion after 2 h and 88% conversion after 24 h. Complete conversion to the corresponding mono-boryl amine, (PhCH₂)(CHMePh)N(BPin) took 48 h at room temperature. ¹H NMR (400 MHz, benzene-*d*₆) δ 7.26 (d, *J* = 5.6 Hz, 3H, *phenyl*), 7.21 – 7.06 (m, 7H, *phenyl*), 7.03 (m, 3H, *phenyl*), 4.39 (s, 1H, -CH), 4.00 (dd, *J* = 77.8, 15.5 Hz, 2H, -NCH₂), 1.36 (d, *J* = 6.0 Hz, 3H, -CH₃), 1.09 (s, 12H, -C(CH₃)₂).

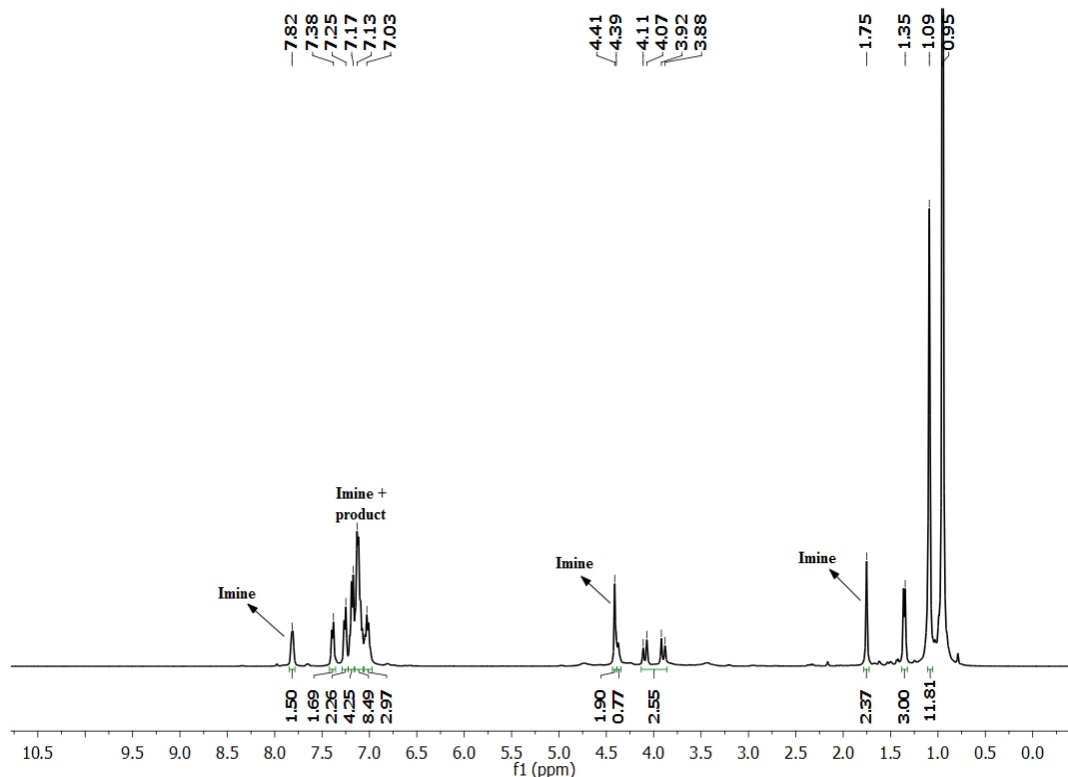


Figure 4.71: Partial hydroboration (55%) of *N*-(1-phenylethylidene)benzenemethanamine using 1 mol% catalyst **20** in benzene-*d*₆ after 2 h.

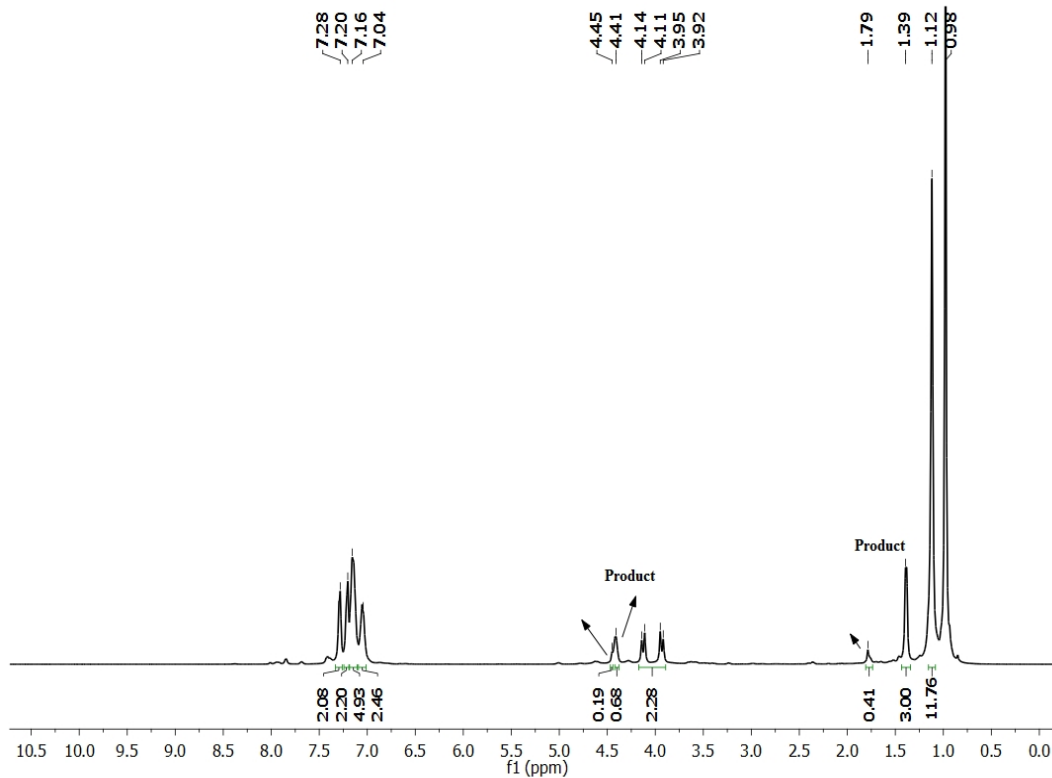


Figure 4.72: Partial hydroboration (88%) of *N*-(1-phenylethylidene)benzenemethanamine using 1 mol% of catalyst **20** in benzene-*d*₆ after 24 h.

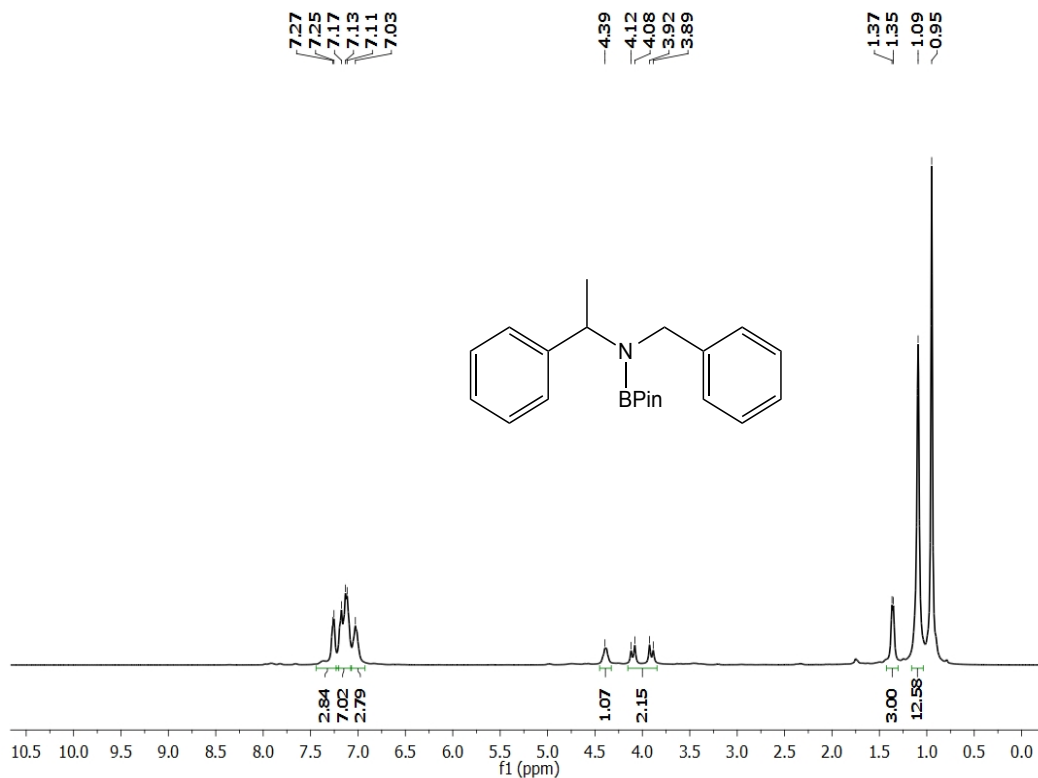


Figure 4.73: Hydroboration of *N*-(1-phenylethylidene) benzenemethanamine using 1 mol% catalyst **20** in benzene-*d*₆ after 48 h.

NMR scale hydroboration of *N*-(diphenylmethylene) benzenemethanamine (1 mol% **20):**

In the nitrogen filled glove box, a benzene-*d*₆ solution of *N*-(diphenylmethylene) benzenemethanamine (144.7 mg, 0.5331 mmol) and pinacolborane (92.8 μ l, 0.6397 mmol) was added to a vial containing 2.3 mg (0.0053 mmol) of **20**. The resulting solution immediately changed color from green to dark brown, which was transferred to a J. Young tube. Integration of the -CH₂ resonances of imine at 4.59 ppm vs 1.35 ppm the product indicated 18% conversion to the corresponding mono-boryl amine, (Ph₂CH)(CH₂Ph)N(BPin) at room temperature. Complete conversion was not even observed after 7 days.

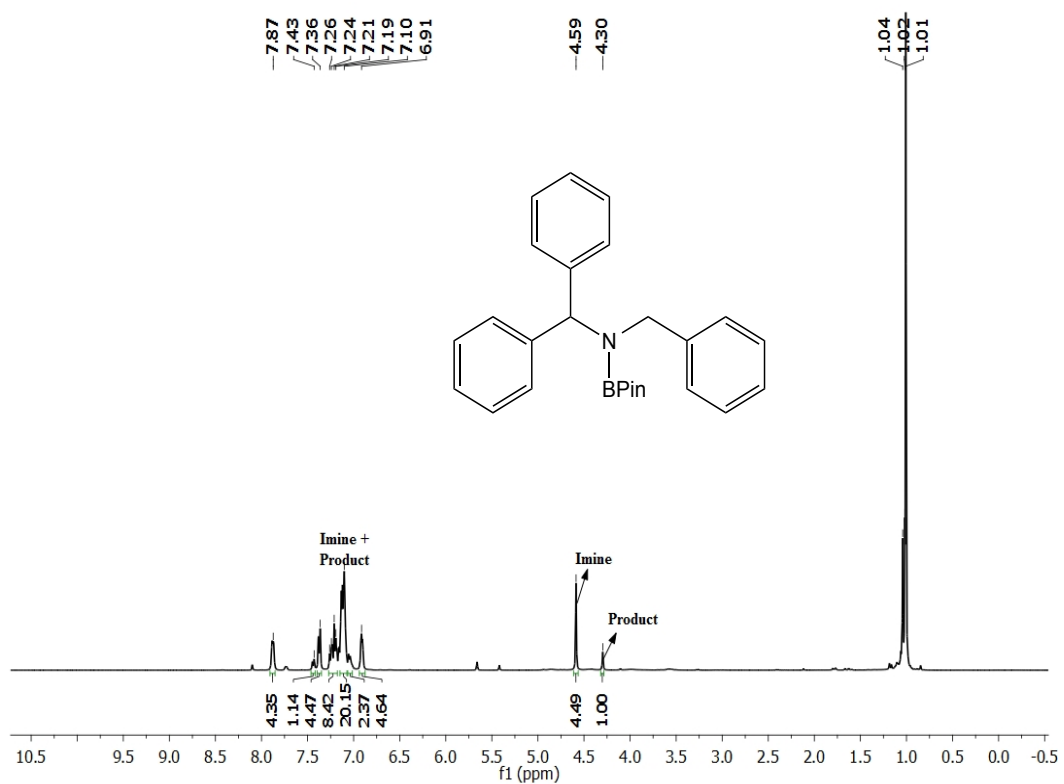


Figure 4.74: Partial hydroboration (18%) of *N*-(diphenylmethylene)benzenemethanamine using 1 mol% catalyst **20** in benzene- d_6 after 2 h.

4.9. References:

1. (a) The Handbook of Homogeneous Hydrogenation, ed. J. G. de Vries and C. J. Elsevier, Wiley-VCH, Weinheim, **2007**; (b) L. A. Oro, D. Carmona and J. M. Fraile, in Metal-Catalysis in Industrial Organic Processes, ed. G. P. Chiusoli and P. M. Maitlis, RSC Publishing, London, **2006**; pp. 79-113.
2. (a) Gomez, S.; Peters, J. A.; Maschmeyer, T. *Adv. Synth. Catal.* **2002**, *344*, 1037-1057. (b) Reguillo, R.; Grellier, M.; Vautravers, N.; Vendier, L.; Sabo-Etienne, S. *J. Am. Chem. Soc.* **2010**, *132*, 7854-7855.
3. (a) Gunanathan, C.; Hölscher, M.; Leitner, W. *Eur. J. Inorg. Chem.* **2011**, *2011*, 3381-3386. (b) Li, T.; Bergner, I.; Haque, F. N.; Zimmer-De Iuliis, M.; Song, D.; Morris, R. H. *Organometallics* **2007**, *26*, 5940-5949. (c) Reguillo, R.; Grellier, M.; Vautravers, N.; Vendier, L.; Sabo-Etienne, S. *J. Am. Chem. Soc.* **2010**, *132*, 7854-7855. (d) Rajesh, K.; Dudle, B.; Blacque, O.; Berke, H. *Adv. Synth. Catal.* **2011**, *353*, 1479-1484. (e) Yoshida, T.; Okano, T.; Otsuka, S. *J. Chem. Soc., Chem. Commun.* **1979**, *0*, 870-871. (f) Chin, C., S.; Lee, B. *Catal. Lett.* **1992**, *14*, 135-140.
4. (a) Lange, S.; Elangovan, S.; Cordes, C.; Spannenberg, A.; Junge, H.; Bachmann, S.; Scalone, M.; Topf, C.; Junge, K.; Beller, M. *Catal. Sci. Technol.*, **2016**, *6*, 4768-4772. (b) Mukherjee, A.; Srimani, D.; Chakraborty, S.; Ben-David, Y.; Milstein, D. *J. Am. Chem. Soc.* **2015**, *137*, 8888-8891. (c) Chakraborty, S.; Leitus, G.; Milstein, D. *Chem. Commun.* **2016**, *52*, 1812-1815.
5. Nixon, T. D.; Whittlesey, M. K.; Williams, J. M. J. *Tetrahedron Lett.* **2011**, *52*, 6652.
6. Khalimon, A. Y.; Farha, P.; Kuzmina, L. G.; Nikonov, G. I. *Chem. Commun.* **2012**, *48*, 455-457.
7. Suginome, M.; Uehlin, L.; Murakami, M. *J. Am. Chem. Soc.* **2004**, *126*, 13196-13197.
8. (a) Beguerie, M.; Faradji, C.; Vendier, L.; Sabo-Etienne, S.; Alcaraz, G. *ChemCatChem* **2017**, *9*, 3303-3306. (b) Beguerie, M.; Dinoi, C.; Rosal, I.; Faradji, C.; Alcaraz, G.; Vendier, L.; Sabo-Etienne, S. *ACS Catal.* **2018**, *8*, 939-948.
9. Geri, J. B.; Szymczak, N. K. *J. Am. Chem. Soc.* **2015**, *137*, 12808-12814.
10. Kaithal, A.; Chatterjee, B.; Gunanathan, C. *J. Org. Chem.* **2016**, *81*, 11153-11161.
11. Weetman, C.; Anker, M. D.; Arrowsmith, M.; Hill, M. S.; Kociok-Köhn, G.; Liptrot, D. L.; Mahon, M. F. *Chem. Sci.* **2016**, *7*, 628-641.

12. Nakamura, G.; Nakajima, Y.; Matsumoto, K.; Srinivas, V.; Shimada, S. *Catal. Sci. Technol.* **2017**, *7*, 3196-3199.
13. Ito, M.; Itazaki, M.; Nakazawa, H. *Inorg. Chem.* **2017**, *56*, 13709-13714.
14. Examples for hydrogenation: (a) Yuwen, J.; Chakraborty, S.; Brennessel, W. W.; Jones, W. D. *ACS Catal.* **2017**, *7*, 3735-3740. (b) Adam, R.; Cabrero-Antonino, J. R.; Spannenberg, A.; Junge, K.; Jackstell, R.; Beller, M. *Angew. Chem. Int. Ed.* **2017**, *56*, 3216-3220. (c) Friedfeld, M. R.; Shevlin, M.; Hoyt, J. M.; Krska, S. W.; Tudge, M. T.; Chirik, P. J. *Science* **2013**, *342*, 1076-1080. (d) Chen, C.; Zhang, Z.; Dong, X.-Q.; Zhang, X. *Chem. Commun.* **2017**, *53*, 4612-4615. Examples for hydrosilylation: (e) Chen, C.; Hecht, M. B.; Kavara, A.; Brennessel, W. W.; Mercado, B. Q.; Weix, D. J.; Holland, P. L. *J. Am. Chem. Soc.* **2015**, *137*, 13244-13247. (f) Chen, C.; Dugan, T., R.; Brennessel, W. W.; Weix, D. J.; Holland, P. L. *J. Am. Chem. Soc.* **2014**, *136*, 945-955. (g) Teo, W. J.; Wang, C.; Tan, Y. W.; Ge, S. *Angew. Chem. Int. Ed.* **2017**, *56*, 4328-4332. (h) Raya, B.; Biswas, S.; RajanBabu, T. V. *ACS Catal.* **2016**, *6*, 6318-6323. Examples for hydroboration: (i) Zhang, L.; Zuo, Z.; Leng, X.; Huang, Z. *Angew. Chem.* **2014**, *126*, 2734-2738. (j) Zhang, L.; Zuo, Z.; Wan, X.; Huang, Z. *J. Am. Chem. Soc.* **2014**, *136*, 15501-15504. (k) Guo, J.; Cheng, B.; Shen, X.; Lu, Z. *J. Am. Chem. Soc.* **2017**, *139*, 15316-15319.
15. Ibrahim, A. D.; Entsminger, S. W.; Fout, A. R. *ACS Catal.* **2017**, *7*, 3730-3734.
16. Ben-Daat, H.; Rock, C. L.; Flores, M.; Groy, T. L.; Bowman, A. C.; Trovitch, R. J. *Chem. Commun.* **2017**, *53*, 7333-7336.
17. (a) Werkmeister, S.; Junge, K.; Beller, M. *Org. Process Res. Dev.* **2014**, *18*, 289-302. (b) Nishimura, S. *Handbook of Heterogeneous Catalytic Hydrogenation for Organic Synthesis*; Wiley-VCH: New York. 2001.
18. (a) Gribble, G. W. *Chem. Soc. Rev.* **1998**, *27*, 395-404. (b) Seyden-Penne, J. *Reductions by Alumino and Borohydrides in Organic Synthesis*, 2nd ed.; Wiley-VCH: New York, 1997. (c) Lu, Z.; Williams, T. J. *Chem. Commun.* **2014**, *50*, 5391-5393. (d) Haddenham, D.; Pasumansky, L.; DeSoto, J.; Eagon, S.; Singaram, B. *J. Org. Chem.* **2009**, *74*, 1964-1970.
19. (a) Fleury-Brégeot, N.; Fuente, V.; de la Castellón, S.; Claver, C. *ChemCatChem* **2010**, *2*, 1346-1371. (b) Nugent, T. C.; El-Shazly, M. *Adv. Synth. Catal.* **2010**, *352*, 753-819. (c) Fabrello, A.; Bachelier, A.; Urrutigoity, M.; Kalck, P. *Coord. Chem. Rev.* **2010**, *254*, 273-287. (d) Xie, J.-H.; Zhu, S.-F.; Zhou, Q.-L. *Chem. Rev.* **2011**, *111*, 1713-1760. (e) Bartoszewicz, A.; Ahlsten, N.; Martín-Matute, B. *Chem. -Eur. J.* **2013**, *19*, 7274-7302. (f) Tang, W.; Xiao, J. *Synthesis* **2014**, *46*, 1297-1302.
20. Koren-Selfridge, L.; Londino, H. L.; Vellucci, J. K.; Simmons, B. J.; Casey, C. P.;

- Clark, T. B. *Organometallics* **2009**, *28*, 2085-2090.
21. Arrowsmith, M.; Hill, M. S.; Kociok-Köhn, G. *Chem. Eur. J.* **2013**, *19*, 2776-2783.
22. King, A. E.; Stieber, S. C. E.; Henson, N. J.; Kozimor, S. A.; Scott, B. L.; Smythe, N. C.; Sutton, A. D.; Gordon, J. C. *Eur. J. Inorg. Chem.* **2016**, 1635-1640.
23. (a) Yin, Q.; Soltani, Y.; Melen, R. L.; Oestreich, M. *Organometallics* **2017**, *36*, 2381-2384. (b) Eisenberger, P.; Bailey, A. M.; Crudden, C. M. *J. Am. Chem. Soc.* **2012**, *134*, 17384-17387.
24. Lin, Y.-C.; Hatzakis, E.; McCarthy, S. M.; Reichl, K. D.; Lai, T. Y.; Yennawar, H. P.; Radosevich, A. T. *J. Am. Chem. Soc.* **2017**, *139*, 6008-6016.
25. Wu, J.; Zeng, H.; Cheng, J.; Zheng, S.; Golen, J. A.; Manke, D. R.; Zhang, G. *J. Org. Chem.* ASAP.
26. Ghosh, C.; Mukhopadhyay, T. K.; Flores, M.; Groy, T. L.; and Trovitch, R. J. *Inorg. Chem.* **2015**, *54*, 10398-10406.
27. Small, L. B.; Brookhart, M.; Bennett, A. M. A. *J. Am. Chem. Soc.* **1998**, *120*, 4049-4050.
28. Khusnutdinova, J. R.; Milstein, D. *Angew. Chem. Int. Ed.* **2015**, *54*, 12236-12273.
29. (a) Knijnenburg, Q.; Gambarotta, S.; Budzelaar, P. H. M. *Dalton Trans.* **2006**, 5442-5448. (b) Muresan, N.; Chlopek, K.; Weyhermüller, T.; Neese, F.; Wieghardt, K. *Inorg. Chem.* **2007**, *46*, 5327-5337.
30. (a) Lam, C. H.; L.-Li, S.; Zhang, Z.; Mak, T. C. W.; Lee, H. K. *Inorg. Chem.* **2001**, *40*, 4691-4695. (b) Yao, S.; Tam, D. Y. S.; Cheung, P. S.; Lam, C.-K.; Guo, P.; Lam, S. L.; Lee, H. K. *Dalton Trans.* **2015**, *44*, 17950-17959.
31. (a) Kleigrewe, N.; Steffen, W.; Blömker, T.; Kehr, Fröhlich, R.; Wibbeling, B.; Erker, G.; C.-Wasilke, J.; Wu, G.; Bazan, G. C. *J. Am. Chem. Soc.* **2005**, *127*, 13955-13968. (b) Bowman, A. C.; Milsmann, C.; Atienza, C. C. H.; Lobkovsky, E.; Wieghardt, K.; Chirik, P. J. *J. Am. Chem. Soc.* **2010**, *132*, 1676-1684.
32. (a) Zhang, L.; Zuo, Z.; Leng, X.; Huang, Z. *Angew. Chem., Int. Ed.* **2014**, *53*, 2696-2700. (b) Obligacion, J. V.; Chirik, P. J. *J. Am. Chem. Soc.* **2013**, *135*, 19107-19110.
33. (a) Gunanathan, C.; Hölscher, M.; Pan, F.; Leitner, W. *J. Am. Chem. Soc.* **2012**, *134*, 14349-14352. (b) Ohmura, T.; Yamamoto, Y.; Miyaura, N. *J. Am. Chem. Soc.* **2000**, *122*, 4990-4991.

34. Schaefer, B. A.; Margulieux, G., W.; Small, B. L.; Chirik, P. J. *Organometallics* **2015**, *34*, 1307-1320.
35. (a) Obligacion, J. V.; Semproni, Chirik, P. J. *J. Am. Chem. Soc.* **2014**, *136*, 4133-4136. (b) Obligacion, J. V.; Semproni, S. P.; Pappas, I.; Chirik, P. J. *J. Am. Chem. Soc.* **2016**, *138*, 10645-10653.
36. Wang, H.; Wang, C.; Huang, K.; Liu, L.; Chang, W.; Li, J. *Org. Lett.* **2016**, *18*, 2367-2370.

BIBLIOGRAPHY

CHAPTER 1

1. Labinger, J. A.; Bercaw, J. E. *Nature* **2002**, *417*, 507-514.
2. For leading examples see: (a) Jia, C.; Kitamura, T.; Fujiwara, Y. *Acc. Chem. Res.* **2001**, *34*, 633-639. (b) van der Boom, M. E.; Milstein, D. *Chem. Rev.* **2003**, *103*, 1759-1792. (c) Colby, D. A.; Bergman, R. G.; Ellman, J. A. *Chem. Rev.* **2010**, *110*, 624-655.
3. Sun, C.-L.; Li, B.-J.; Shi, Z.-J. *Chem. Rev.* **2011**, *111*, 1293-1314.
4. For leading examples see: (a) Chen, M. S.; White, M. C. *Science* **2007**, *318*, 783-787. (b) Chen, M. S.; White, M. C. *Science* **2010**, *327*, 566-571.
5. For leading examples see: (a) Sarhan, A. A. O.; Bolm, C. *Chem. Soc. Rev.* **2009**, *38*, 2730-2744, and references therein; (b) Baran, P. S.; Hafensteiner, B. D.; Ambhaikar, N. B.; Guerrero, C. A.; Gallagher, J. D. *J. Am. Chem. Soc.* **2006**, *128*, 8678-8693.
6. For leading examples see: (a) Vierling, P.; Riess, J. G. *J. Am. Chem. Soc.*, **1984**, *106*, 2432-2434. (b) Garrou, P. E. *Chem. Rev.* **1985**, *85*, 171-185. (c) Grohmann, A. *Dalton Trans.* **2010**, *39*, 1432-1440, and references therein.
7. Uddin, M. N.; Begum, N.; Hassan, M. R.; Hogarth, G.; Kabir, S. E.; Miah, M. A.; Nordlander, E.; Tocher, D. A. *Dalton Trans.* **2008**, 6219-6230.
8. Rahman, M. A.; Begum, N.; Ghosh, S.; Hossain, M. K.; Hogarth, G.; Tocher, D. A.; Nordlander, E.; Kabir, S. E. *J. Organomet. Chem.* **2011**, *696*, 607-612.
9. Yeh, W.-Y.; Tsai, K.-Y. *Organometallics* **2010**, *29*, 604-609.
10. Carty, A. J.; Hogarth, G.; Enright, G. D.; Steed, J. W.; Georganopoulou, D. *Chem. Commun.* **1999**, 1499-1500.
11. Alcaez, C. M.; Galán, B.; García, M. E.; Riera, V.; Ruiz, M. A.; Vaissermann, J. *Organometallics* **2003**, *22*, 5504-5512.
12. Porter, T. M.; Hall, G. B.; Groy, T. L.; Trovitch, R. J. *Dalton Trans.* **2013**, *42*, 14689-14692.
13. (a) Gardiner, M. G.; Hanson, G. R.; Henderson, M. J.; Lee, F. C.; Raston, C. L. *Inorg. Chem.* **1994**, *33*, 2456-2461. (b) Rijnberg, E.; Richter, B.; Thiele, K.-H.; Boersma, J.; Veldman, N.; Spek, A. L.; van Koten, G. *Inorg. Chem.* **1998**, *37*, 56-63.
14. (a) Khusniyarov, M. M.; Harms, K.; Burghaus, O.; Sundermeyer, J. *Eur. J. Inorg. Chem.* **2006**, 2985-2996. (b) Muresan, N.; Chlopek, K.; Weyhermüller, T.; Neese, F.;

Wieghardt, K. *Inorg. Chem.*, **2007**, *46*, 5327-5337.

15. Accepted isomer shift ranges: high-spin Fe(III), 0.1 to 0.5 mm s⁻¹; high spin Fe(II), 0.6 to 1.7 mm s⁻¹; low-spin Fe(III), -0.1 to 0.5 mm s⁻¹; low-spin Fe(II), -0.2 to 0.5 mm s⁻¹. See: D. P. E. Dickson and F. J. Berry, *Mössbauer Spectroscopy*, Cambridge University Press, 1986, p. 22.

16. Crossland, J. L.; Tyler, D. R. *Coord. Chem. Rev.* **2010**, *254*, 1883-1894.

17. Mukhopadhyay, T. K.; Feller, R. K.; Rein, F. N.; Henson, N. J.; Smythe, N. C.; Trovitch, R. J.; Gordon, J. C. *Chem. Commun.* **2012**, *48*, 8670-8672.

18. Mukhopadhyay, T. K.; Flores, M.; Feller, R. K.; Scott, B. L.; Taylor, R. D.; Paz-Pasternak, M.; Henson, N. J.; Rein, F. N.; Smythe, N. C.; Trovitch, R. J.; Gordon, J. C. *Organometallics* **2014**, *33*, 7101-7112.

19. For examples see: Trovitch, R. J.; Lobkovsky, E.; Chirik, P. J. *J. Am. Chem. Soc.* **2008**, *130*, 11631-11640.

20. (a) Miller, T. M.; Whitesides, G. M. *Organometallics* **1986**, *5*, 1473-1480. (b) Chappell, S. D.; Cole-Hamilton, D. J. *Polyhedron* **1982**, *1*, 739-777.

21. Tondreau, A. M.; Atienza, C. C. H.; Darmon, J. M.; Milsman, C.; Hoyt, H. M.; Weller, K. J.; Nye, S. A.; Lewis, K. M.; Boyer, J.; Delis, J. G. P.; Lobkovsky, E.; Chirik, P. J. *Organometallics* **2012**, *31*, 4886-4893.

22. Neese, F. Orca, an Ab Initio, Density Functional and Semiempirical Electronic Structure Program Package, version 2.9.1; Max Planck Institute for Bioinorganic Chemistry: Mülheim an der Ruhr, Germany, 2012.

23. (a) Becke, A. D. *J. Chem. Phys.* **1993**, *98*, 5648-5652. (b) Lee, C. T.; Yang, W. T.; Parr, R. G. *Phys. Rev.* **1988**, *37*, 785-789.

24. Grimme, S. *J. Comput. Chem.* **2006**, *27*, 1787-1799.

25. Pantazis, D. A.; Chen, X. Y.; Landis, C. R.; Neese, F. *J. Chem. Theory Comput.* **2008**, *4*, 908-919.

26. Molekel, Advanced Interactive 3D-Graphics for Molecular Sciences; Swiss National Supercomputing Center; [http:// www.cscs.ch/molekel](http://www.cscs.ch/molekel).

CHAPTER 2

1. Egorova, K. S.; Ananikov, V. P. *Angew. Chem., Int. Ed.* **2016**, *55*, 12150-12162.
2. European Medicines Agency, Guideline on the Specification Limits for Residues of Metal Catalysts or Metal Reagents, EMEA/CHMP/SWP/4446/2000, London, February 21, 2008.
3. Fürstner, A. *ACS Cent. Sci.* **2016**, *2*, 778-789.
4. Bertini, I.; Gray, H. B.; Lippard, S. J.; Valentine, J. S., Eds. *Bioinorganic Chemistry*; University Science Books: Mill Valley, CA, 1994.
5. (a) Lyaskovskyy, V.; Bruin, de; B. *ACS Catal.* **2012**, *2*, 270-279. (b) Luca, O.; R.; Crabtree, R.; H. *Chem. Soc. Rev.* **2013**, *42*, 1440-1459.
6. Bart, S. C.; Lobkovsky, E.; Chirik, P. J. *J. Am. Chem. Soc.* **2004**, *126*, 13794-13807.
7. (a) Bouwkamp, M. W.; Bowman, A. C.; Lobkovsky, E.; Chirik, P. J. *J. Am. Chem. Soc.* **2006**, *128*, 13340-13341. (b) Hoyt, O. M.; Schmidt, V. A.; Tondreau, A. M.; Chirik, P. J. *Science* **2015**, *349*, 960-963.
8. (a) Bart, S. C.; Hawrelak, E. J.; Lobkovsky, E.; Chirik, P., *J. Organometallics* **2005**, *24*, 5518-5527. (b) Schmidt, V. A.; Rose, K. C.; Bezdek, M.; Chirik, P. J. *J. Am. Chem. Soc.* **2018**, *140*, 3443-3453. (c) Lee, H.; Campbell, M. G.; Sánchez, R. H.; Börgel, J.; Raynaud, J.; Parker, S. E.; Ritter, T. *Organometallics* **2016**, *35*, 2923-2929. (d) Wang, H.; Yan, W.; Jiang, T.; Liu, B.; Xu, W.; Ma, J.; Hu, Y. *Chinese Science Bulletin* **2002**, *47*, 1616-1618.
9. Bauer, G.; Hu, X. *Inorg. Chem. Front.* **2016**, *3*, 741-765.
10. (a) Trovitch, R. J.; Lobkovsky, E.; Chirik, P. J. *Inorg. Chem* **2006**, *45*, 7252-7260. (b) Srimani, D.; Diskin-Posner, Y.; Ben-David, Y.; Milstein, D. *Angew. Chem. Int. Ed.* **2013**, *52*, 14131-14134. (c) (i) Langer, R.; Leitus, G.; Ben-David, Y.; Milstein, D. *Angew. Chem. Int. Ed.* **2011**, *50*, 2120-2124. (ii) Langer, R.; Iron, M. A.; Konstantinovski, L.; Diskin-Posner, Y.; Leitus, G.; Ben-David, Y.; Milstein, D. *Chem. – Eur. J.* **2012**, *18*, 7196-7209. (iii) Zell, T.; Ben-David, Y.; Milstein, D. *Catal. Sci. Technol.* **2015**, *5*, 822-826. (iv) Chakraborty, S.; Bhattacharya, P.; Dai, H.; Guan, H. *Acc. Chem. Res.* **2015**, *48*, 1995-2003. (v) Chakraborty, S.; Dai, H.; Bhattacharya, P.; Fairweather, N. T.; Gibson, M. S.; Krause, J. A.; Guan, H. *J. Am. Chem. Soc.* **2014**, *136*, 7869-7872. (vi) Werkmeister, S.; Junge, K.; Wendt, B.; Alberico, E.; Jiao, H.; Baumann, W.; Junge, H.; Gallou, F.; Beller, M. *Angew. Chem. Int. Ed.* **2014**, *53*, 8722-8726. (d) (i) Bornschein, C.; Werkmeister, S.; Wendt, B.; Jiao, H.; Alberico, E.; Baumann, W.; Junge, H.; Junge, K.; Beller, M. *Nat. Commun.* **2014**, *5*, 4111. (ii) Chakraborty, S.; Milstein, D. *ACS Catal.*, **2017**, *7*, 3968-3972. (e) Mazza, S.; Copelliti, R.; Hu, X. *Organometallics* **2015**, *34*, 1538-1545. (f) Bleith, T.; Wadepohl, H.; Gade, L. H. *J. Am. Chem. Soc.* **2015**, *137*,

- 2456-2459. (g) (i) Chakraborty, S.; Lagaditis, P. O.; Förster, M.; Bielinski, E. A.; Hazari, N.; Holthausen, M. C.; Jones, W. D.; Schneider, S. *ACS Catal.* **2014**, *4*, 3994-4003. (ii) Pena-Lopez, M.; Neumann, H.; Beller, M. *ChemCatChem* **2015**, *7*, 865-871. (h) Chakraborty, S.; Brennessel, W.; Jones, W. D.; *J. Am. Chem. Soc.* **2014**, *136*, 8564-8567.
11. Dötz, K. H.; Stendel, J. *Chem. Rev.* **2009**, *109*, 3227-3274.
12. West, N. M.; Miller, A. J. M.; Labinger, J. A.; Bercaw, J. E. *Coord. Chem. Rev.* **2011**, *255*, 881-898.
13. (a) Suess, D. L. M.; Peters, J. C. *J. Am. Chem. Soc.* **2013**, *135*, 12580-12583. (b) Buss, J. A.; Agapie, T. *Nature* **2016**, *529*, 72-75. (c) Buss, J. A.; Agapie, T. *J. Am. Chem. Soc.* **2016**, *138*, 16466-16477.
14. Ghosh, C.; Groy, T. L.; Bowman, A. C.; Trovitch, R. J. *Chem. Commun.* **2016**, *52*, 4553-4556.
15. Muresan, N.; Chlopek, K.; Weyhermüller, T.; Neese, F.; Wieghardt, K. *Inorg. Chem.* **2007**, *46*, 5327-5337.
16. (a) Cutler, A. R.; Hanna, P. K.; Vites, J. C. *Chem. Rev.* **1988**, *88*, 1363-1403. (b) Wolczanski, P. T.; Bercaw, J. E. *Acc. Chem. Res.* **1980**, *13*, 121-127. (c) Gladysz, J. A. *Adv. Organomet. Chem.* **1982**, *20*, 1-38.
17. Rock, C. L.; Groy, T. L.; Trovitch, R. J. *Dalton Trans.* **2018**, *47*, 8807-8816.
18. Mukhopadhyay, T. K.; Ghosh, C.; Flores, M.; Groy, T. L.; Trovitch, R. J. *Organometallics* **2017**, *36*, 3477-3483.
19. Bart, S. C.; Lobkovsky, E.; Chirik, P. J. *J. Am. Chem. Soc.* **2004**, *126*, 13794-13807.
20. Ben-Daat, H.; Hall, G. B.; Groy, T. L.; Trovitch, R. J. *Eur. J. Inorg. Chem.* **2013**, 4430-4442.
21. Mukhopadhyay, T. K.; Flores, M.; Groy, T. L.; Trovitch, R. J. *J. Am. Chem. Soc.* **2014**, *136*, 882-885.
22. (a) Bhattacharya, P.; Krause, J. A.; Guan, H. *J. Am. Chem. Soc.* **2014**, *136*, 11153-11161. (b) Zhao, H.; Sun, H.; Li, X. *Organometallics* **2014**, *33*, 3535-3539.

CHAPTER 3

1. (a) Junge, K.; Schröder, K.; Beller, M. *Chem. Commun.* **2011**, *47*, 4849-4859. (b) Le Bailly, B. A. F.; Thomas, S. P. *RSC Adv.* **2011**, *1*, 1435. (c) Bullock, R. M. *Catalysis without Precious Metals*; Wiley-VCH: Weinheim, Germany, 2010. (d) Gosmini, C.; Bégouin, J.-M.; Moncomble, A. *Chem. Commun.* **2008**, 3221-3233. (e) Gaillard, S.; Renaud, J.-L. *ChemSusChem* **2008**, *1*, 505-509.
2. Haynes, W. M. *CRC Handbook of Chemistry and Physics: A Ready reference Book of Chemical and Physical Data*, 94th ed.; Taylor & Francis: Boca Raton, FL, 2013-2014.
3. (a) Enthaler, S.; Junge, K.; Beller, M. *Angew. Chem. Int. Ed.* **2008**, *47*, 3317-3321. (b) Plietker, B. *Iron Catalysis in Organic Chemistry*; Wiley-VCH: Weinheim, Germany, 2008.
4. (a) Hitchcock, P. B.; Lappert, M. F.; Warhurst, N. J. W. *Angew. Chem., Int. Ed. Engl.* **1991**, *30*, 438-440. (b) Speier, J. L.; Webster, J. A.; Barnes, G. H. *J. Am. Chem. Soc.* **1957**, *79*, 974-979.
5. (a) Srinivas, V.; Nakajima, Y.; Ando, W.; Sato, K.; Shimada, S. *Catal. Sci. Technol.* **2015**, *5*, 2081-2084. (b) Peng, D.; Zhang, Y.; Du, X.; Zhang, L.; Leng, X.; Walter, M. D.; Huang, Z. *J. Am. Chem. Soc.* **2013**, *135*, 19154-19166. (c) Tondreau, A. M.; Atienza, C. C. H.; Darmon, J. M.; Milsmann, C.; Hoyt, H. M.; Weller, K. J.; Nye, S. A.; Lewis, K. M.; Boyer, J.; Delis, J. G. P.; Lobkovsky, E.; Chirik, P. J. *Organometallics* **2012**, *31*, 4886-4893. (d) Hojilla Atienza, C. C.; Tondreau, A. M.; Weller, K. J.; Lewis, K. M.; Cruse, R. W.; Nye, S. A.; Boyer, J. L.; Delis, J. G. P.; Chirik, P. J. *ACS Catal.* **2012**, *2*, 2169-2172. (e) Tondreau, A. M.; Atienza, C. C. H.; Weller, K. J.; Nye, S. A.; Lewis, K. M.; Delis, J. G. P.; Chirik, P. J. *Science* **2012**, *335*, 567-570. (f) Troegel, D.; Stohrer, J. *Coord. Chem. Rev.* **2011**, *255*, 1440-1459.
6. For leading Fe examples, see: (a) Blom, B.; Enthaler, S.; Inoue, S.; Irran, E.; Driess, M. *J. Am. Chem. Soc.* **2013**, *135*, 6703-6713. (b) Ruddy, A. J.; Kelly, C. M.; Crawford, S. M.; Wheaton, C. A.; Sydora, O. L.; Small, B. L.; Stradiotto, M.; Turculet, L. *Organometallics* **2013**, *32*, 5581-5588. (c) Bhattacharya, P.; Krause, J. A.; Guan, H. *Organometallics* **2011**, *30*, 4720-4729. (d) Yang, J.; Tilley, T. D. *Angew. Chem. Int. Ed.* **2010**, *49*, 10186-10188. (e) Kandepi, V. V. K. M.; Cardoso, J. M. S.; Peris, E.; Royo, B. *Organometallics* **2010**, *29*, 2777-2782. (f) Tondreau, A. M.; Darmon, J. M.; Wile, B. M.; Floyd, S. K.; Lobkovsky, E.; Chirik, P. J. *Organometallics* **2009**, *28*, 3928-3940. (g) Tondreau, A. M.; Lobkovsky, E.; Chirik, P. J. *Org. Lett.* **2008**, *10*, 2789-2792.
7. For leading Co examples, see: (a) Zhou, H.; Sun, H.; Zhang, S.; Li, X. *Organometallics* **2015**, *34*, 1479-1486. (b) Niu, Q.; Sun, H.; Li, X.; Klein, H.-F.; Flörke, U. *Organometallics* **2013**, *32*, 5235-5238. (c) Sauer, D. C.; Wadepohl, H.; Gade, L. H. *Inorg. Chem.* **2012**, *51*, 12948-12958. (d) Yu, F.; Zhang, X.-C.; Wu, F.-F.; Zhou, J.-N.; Fang, W.; Wu, J.; Chan, A. S. C. *Org. Biomol. Chem.* **2011**, *9*, 5652. (e) Brunner, H.;

- Amberger, K. *J. Organomet. Chem.* **1991**, *417*, C63–C65. (f) Nesbit, M. A.; Suess, D. L. M.; Peters, J. C. *Organometallics* **2015**, *34*, 4741.
8. For leading Ni examples, see: (a) Porter, T. M.; Hall, G. B.; Groy, T. L.; Trovitch, R. J. *Dalton Trans.* **2013**, *42*, 14689-14692. (b) Bheeter, L. P.; Henrion, M.; Brelot, L.; Darcel, C.; Chetcuti, M. J.; Sortais, J.-B.; Ritleng, V. *Adv. Synth. Catal.* **2012**, *354*, 2619-2624. (c) Postigo, L.; Royo, B. *Adv. Synth. Catal.* **2012**, *354*, 2613-2618. (d) Tran, B. L.; Pink, M.; Mindiola, D. J. *Organometallics* **2009**, *28*, 2234-2243. (e) Chakraborty, S.; Krause, J. A.; Guan, H. *Organometallics* **2009**, *28*, 582-586 and references cited therein. (f) MacMillan, S. N.; Harman, H. W.; Peters, J. C. *Chem. Sci.* **2014**, *5*, 590-597. (g) Steiman, T. J.; Uyeda, C. *J. Am. Chem. Soc.* **2015**, *137*, 6104-6110.
9. For leading Cu examples, see: (a) Roy, S. R.; Sau, S. C.; Mandal, S. K. *J. Org. Chem.* **2014**, *79*, 9150-9160. (b) Albright, A.; Gawley, R. E. *J. Am. Chem. Soc.* **2011**, *133*, 19680-19683. (c) Yu, F.; Zhou, J.-N.; Zhang, X.-C.; Sui, Y.-Z.; Wu, F.-F.; Xie, L.-J.; Chan, A. S. C.; Wu, J. *Chem. - Eur. J.* **2011**, *17*, 14234-14240. (d) Zhang, X.-C.; Wu, F.-F.; Li, S.; Zhou, J.-N.; Wu, J.; Li, N.; Fang, W.; Lam, K. H.; Chan, A. S. C. *Adv. Synth. Catal.* **2011**, *353*, 1457-1462. (e) Díez-González, S.; Escudero-Adán, E.; Benet-Buchholz, J.; Stevens, E. D.; Slawin, A. M. Z.; Nolan, S. P. *Dalton Trans.* **2010**, *39*, 7595-7606. (f) Fujihara, T.; Semba, K.; Terao, J.; Tsuji, Y. *Angew. Chem. Int. Ed.* **2010**, *49*, 1472-1476. (g) Mostefai, N.; Sirol, S.; Courmarcel, J.; Riant, O. *Synthesis* **2007**, *2007*, 1265–1271. (h) Díez-González, S.; Scott, N. M.; Nolan, S. P. *Organometallics* **2006**, *25*, 2355-2358. (i) Lipshutz, B. H.; Lower, A.; Kucejko, R. J.; Noson, K. *Org. Lett.* **2006**, *8*, 2969-2972. (j) Díez-González, S.; Kaur, H.; Zinn, F. K.; Stevens, E. D.; Nolan, S. P. *J. Org. Chem.* **2005**, *70*, 4784–4796. (k) Wu, J.; Ji, J.-X.; Chan, A. S. C. *Proc. Natl. Acad. Sci. U. S. A.* **2005**, *102*, 3570-3575. (l) Lee, D.; Yun, J. *Tetrahedron Lett.* **2004**, *45*, 5415-5417. (m) Kaur, H.; Zinn, F. K.; Stevens, E. D.; Nolan, S. P. *Organometallics* **2004**, *23*, 1157-1160. (n) Lipshutz, B. H.; Noson, K.; Chrisman, W.; Lower, A. *J. Am. Chem. Soc.* **2003**, *125*, 8779-8789. (o) Lipshutz, B. H.; Noson, K.; Chrisman, W. *J. Am. Chem. Soc.* **2001**, *123*, 12917-12918. (p) Sirol, S.; Courmarcel, J.; Mostefai, N.; Riant, O. *Org. Lett.* **2001**, *3*, 4111-4113. (q) Brunner, H.; Miehl, W. *J. Organomet. Chem.* **1984**, *275*, C17-C21.
10. For leading Zn examples, see: (a) Rit, A.; Zanardi, A.; Spaniol, T. P.; Maron, L.; Okuda, J. *Angew. Chem. Int. Ed.* **2014**, *53*, 13273-13277. (b) Lummis, P. A.; Momemi, M. R.; Lui, M. W.; McDonald, R.; Ferguson, M. J.; Miskolzie, M.; Brown, A.; Rivard, E. *Angew. Chem. Int. Ed.* **2014**, *53*, 9347-9351. (c) Łowicki, D.; Bezlada, A.; Mlynarski, J. *Adv. Synth. Catal.* **2014**, *356*, 591-595. (d) Boone, C.; Korobkov, I.; Nikonov, G. I. *ACS Catal.* **2013**, *3*, 2336-2340. (e) Pang, S.; Peng, J.; Li, J.; Bai, Y.; Xiao, W.; Lai, G. *Chirality* **2013**, *25*, 275-280. (f) Enthaler, S.; Schröder, K.; Inoue, S.; Eckhardt, B.; Junge, K.; Beller, M.; Drieß, M. *Eur. J. Org. Chem.* **2010**, *2010*, 4893-4901. (g) Gajewy, J.; Kwit, M.; Gawroński, J. *Adv. Synth. Catal.* **2009**, *351*, 1055-1063. (h) Gérard, S.; Pressel, Y.; Riant, O. *Tetrahedron: Asymmetry* **2005**, *16*, 1889–1891. (i) Bette, V.; Mortreux, A.; Savoia, D.; Carpentier, J.-F. *Adv. Synth. Catal.* **2005**, *347*, 289-302. (j) Bette, V.; Mortreux, A.; Savoia, D.; Carpentier, J.-F. *Tetrahedron* **2004**, *60*, 2837-2842. (k) Mastranzo, V. M.; Quintero, L.; Anaya de Parrodi, C. A.; Juaristi, E.; Walsh, P. J.

- Tetrahedron* **2004**, *60*, 1781-1789. (l) Mimoun, H. *J. Org. Chem.* **1999**, *64*, 2582-2589. (m) Sattler, W.; Ruccolo, S.; Rostami Chaijan, M.; Nasr Allah, T.; Parkin, G. *Organometallics* **2015**, *34*, 4717.
12. For leading examples, see: (a) Bleith, T.; Wadepohl, H.; Gade, L. H. *J. Am. Chem. Soc.* **2015**, *137*, 2456-2459. (b) Darwish, M.; Wills, M. *Catal. Sci. Technol.* **2012**, *2*, 243-255. (c) Inagaki, T.; Ito, A.; Ito, J.; Nishiyama, H. *Angew. Chem. Int. Ed.* **2010**, *49*, 9384-9387. (d) Inagaki, T.; Phong, L. T.; Furuta, A.; Ito, J.; Nishiyama, H. *Chem. - Eur. J.* **2010**, *16*, 3090-3096. (e) Morris, R. H. *Chem. Soc. Rev.* **2009**, *38*, 2282-2291. (f) Langlotz, B. K.; Wadepohl, H.; Gade, L. H. *Angew. Chem. Int. Ed.* **2008**, *47*, 4670-4674. (g) Shaikh, N. S.; Enthaler, S.; Junge, K.; Beller, M. *Angew. Chem, Int. Ed.* **2008**, *47*, 2497-2501. (h) Nishiyama, H.; Furuta, A. *Chem. Commun.* **2007**, 760-762.
13. (a) Valyaev, D. A.; Lavigne, G.; Lugan, N. *Coord. Chem. Rev.* **2015**. (b) Trovitch, R. J. *Synlett* **2014**, *25*, 1638-1642.
14. Pratt, S. L.; Faltynek, R. A. *J. Organomet. Chem.* **1983**, *258*, C5-C8.
15. Hilal, H. S.; Abu-Eid, M.; Al-Subu, M.; Khalaf, S. *J. Mol. Catal.* **1987**, *39*, 1-11.
16. Mao, Z.; Gregg, B. T.; Cutler, A. R. *J. Am. Chem. Soc.* **1995**, *117*, 10139-10140.
17. DiBiase Cavanaugh, M.; Gregg, B. T.; Cutler, A. R. *Organometallics* **1996**, *15*, 2764-2769.
18. Son, S. U.; Paik, S.-J.; Lee, I. S.; Lee, Y.-A.; Chung, Y. K.; Seok, W. K.; Lee, H. N. *Organometallics* **1999**, *18*, 4114-4118.
19. Son, S. U.; Paik, S.-J.; Chung, Y. K. *J. Mol. Catal. A: Chem.* **2000**, *151*, 87-90.
20. Igarashi, M.; Fuchikami, T. *Tetrahedron Lett.* **2001**, *42*, 1945-1947.
21. Zheng, J.; Chevance, S.; Darcel, C.; Sortais, J.-B. *Chem. Commun.* **2013**, *49*, 10010-10012.
22. Chidara, V. K.; Du, G. *Organometallics* **2013**, *32*, 5034-5037.
23. Zheng, J.; Elangovan, S.; Valyaev, D. A.; Brousses, R.; César, V.; Sortais, J.-B.; Darcel, C.; Lugan, N.; Lavigne, G. *Adv. Synth. Catal.* **2014**, *356*, 1093-1097.
24. Mukhopadhyay, T. K.; Flores, M.; Groy, T. L.; Trovitch, R. J. *J. Am. Chem. Soc.* **2014**, *136*, 882-885.
25. Pal, R.; Groy, T. L.; Bowman, A. C.; Trovitch, R. J. *Inorg. Chem.* **2014**, *53*, 9357-9365.
26. Reardon, D.; Aharonian, G.; Gambarotta, S.; Yap, G. P. A. *Organometallics* **2002**, *21*, 786-788.

27. Knijnenburg, Q.; Gambarotta, S.; Budzelaar, P. H. M. *Dalton-Trans.* **2006**, 5442-5448.
28. Palmer, G. In *Physical Methods in Bioinorganic Chemistry. Spectroscopy and Magnetism*; Que, L. J., Ed.; University Science Books: Sausalito, CA, **2000**; pp 145-153.
29. Ben-Daat, H.; Hall, G. B.; Groy, T. L.; Trovitch, R. J. *Eur. J. Inorg. Chem.* **2013**, 2013, 4430-4442.
30. Bart, S. C.; Chlopek, K.; Bill, E.; Bouwkamp, M. W.; Lobkovsky, E.; Neese, F.; Wieghardt, K.; Chirik, P. J. *J. Am. Chem. Soc.* **2006**, 128, 13901-13912.
31. (a) Khusniyarov, M. M.; Harms, K.; Burghaus, O.; Sundermeyer, J. *Eur. J. Inorg. Chem.* **2006**, 2006, 2985-2996. (b) Muresan, N.; Chlopek, K.; Weyhermüller, T.; Neese, F.; Wieghardt, K. *Inorg. Chem.* **2007**, 46, 5327-5337.
32. Mukhopadhyay, T. K.; Rock, C. L.; Ashley, D. C.; Hong, M.; Groy, T. L.; Baik, M. H.; Trovitch, R. J. *J. Am. Chem. Soc.* **2017**, 139, 4901-4915.
33. Valyaev, D. A.; Wei, D.; Elangovan, S.; Cavailles, M.; Dorcet, V.; Sortais, J.-B.; Darcel, C.; Lugan, N. *Organometallics* **2016**, 35, 4090-4098.
34. LeBlanc, F. A.; Piers, W.; Parvez, M. *Angew. Chem. Int. Ed.* **2014**, 53, 789-792.
35. Berk, S. C.; Kreutzer, K. A.; Buchwald, S. L. *J. Am. Chem. Soc.* **1991**, 113, 5093-5095.
36. Le Bideau, F.; Henique, J.; Samuel, E.; Elschenbroich, C. *Chem. Commun.* **1999**, 1397-1398.
37. In a prior assessment of Ni-mediated carbonyl hydrosilylation, catalysts in refs 8e (ref 23) and 8b (ref 12b) were cited as the most active for this transformation. However, TOFs of up to 2,304 h⁻¹ have been reported in ref 8c.
38. Weil, J. A.; Bolton, J. R. *Electron paramagnetic resonance: Elementary theory and practical applications*; Wiley: Hoboken, NJ, **2007**.

CHAPTER 4

1. (a) *The Handbook of Homogeneous Hydrogenation*, ed. J. G. de Vries and C. J. Elsevier, Wiley-VCH, Weinheim, **2007**; (b) L. A. Oro, D. Carmona and J. M. Fraile, in *Metal-Catalysis in Industrial Organic Processes*, ed. G. P. Chiusoli and P. M. Maitlis, RSC Publishing, London, **2006**; pp. 79-113.

2. (a) Gomez, S.; Peters, J. A.; Maschmeyer, T. *Adv. Synth. Catal.* **2002**, *344*, 1037-1057. (b) Reguillo, R.; Grellier, M.; Vautravers, N.; Vendier, L.; Sabo-Etienne, S. *J. Am. Chem. Soc.* **2010**, *132*, 7854-7855.
3. (a) Gunanathan, C.; Hölscher, M.; Leitner, W. *Eur. J. Inorg. Chem.* **2011**, *2011*, 3381-3386. (b) Li, T.; Bergner, I.; Haque, F. N.; Zimmer-De Iuliis, M.; Song, D.; Morris, R. H. *Organometallics* **2007**, *26*, 5940-5949. (c) Reguillo, R.; Grellier, M.; Vautravers, N.; Vendier, L.; Sabo-Etienne, S. *J. Am. Chem. Soc.* **2010**, *132*, 7854-7855. (d) Rajesh, K.; Dudle, B.; Blacque, O.; Berke, H. *Adv. Synth. Catal.* **2011**, *353*, 1479-1484. (e) Yoshida, T.; Okano, T.; Otsuka, S. *J. Chem. Soc., Chem. Commun.* **1979**, *0*, 870-871. (f) Chin, C., S.; Lee, B. *Catal. Lett.* **1992**, *14*, 135-140.
4. (a) Lange, S.; Elangovan, S.; Cordes, C.; Spannenberg, A.; Junge, H.; Bachmann, S.; Scalone, M.; Topf, C.; Junge, K.; Beller, M. *Catal. Sci. Technol.*, **2016**, *6*, 4768-4772. (b) Mukherjee, A.; Srimani, D.; Chakraborty, S.; Ben-David, Y.; Milstein, D. *J. Am. Chem. Soc.* **2015**, *137*, 8888-8891. (c) Chakraborty, S.; Leitner, G.; Milstein, D. *Chem. Commun.* **2016**, *52*, 1812-1815.
5. Nixon, T. D.; Whittlesey, M. K.; Williams, J. M. J. *Tetrahedron Lett.* **2011**, *52*, 6652.
6. Khalimon, A. Y.; Farha, P.; Kuzmina, L. G.; Nikonov, G. I. *Chem. Commun.* **2012**, *48*, 455-457.
7. Suginome, M.; Uehlin, L.; Murakami, M. *J. Am. Chem. Soc.* **2004**, *126*, 13196-13197.
8. (a) Beguerie, M.; Faradji, C.; Vendier, L.; Sabo-Etienne, S.; Alcaraz, G. *ChemCatChem* **2017**, *9*, 3303-3306. (b) Beguerie, M.; Dinoi, C.; Rosal, I.; Faradji, C.; Alcaraz, G.; Vendier, L.; Sabo-Etienne, S. *ACS Catal.* **2018**, *8*, 939-948.
9. Geri, J. B.; Szymczak, N. K. *J. Am. Chem. Soc.* **2015**, *137*, 12808-12814.
10. Kaithal, A.; Chatterjee, B.; Gunanathan, C. *J. Org. Chem.* **2016**, *81*, 11153-11161.
11. Weetman, C.; Anker, M. D.; Arrowsmith, M.; Hill, M. S.; Kociok-Köhn, G.; Liptrot, D. L.; Mahon, M. F. *Chem. Sci.* **2016**, *7*, 628-641.
12. Nakamura, G.; Nakajima, Y.; Matsumoto, K.; Srinivas, V.; Shimada, S. *Catal. Sci. Technol.* **2017**, *7*, 3196-3199.
13. Ito, M.; Itazaki, M.; Nakazawa, H. *Inorg. Chem.* **2017**, *56*, 13709-13714.
14. Examples for hydrogenation: (a) Yuwen, J.; Chakraborty, S.; Brennessel, W. W.; Jones, W. D. *ACS Catal.* **2017**, *7*, 3735-3740. (b) Adam, R.; Cabrero-Antonino, J. R.; Spannenberg, A.; Junge, K.; Jackstell, R.; Beller, M. *Angew. Chem. Int. Ed.* **2017**, *56*, 3216-3220. (c) Friedfeld, M. R.; Shevlin, M.; Hoyt, J. M.; Krska, S. W.; Tudge, M. T.; Chirik, P. J. *Science* **2013**, *342*, 1076-1080. (d) Chen, C.; Zhang, Z.; Dong, X.-Q.; Zhang,

- X. *Chem. Commun.* **2017**, 53, 4612-4615. Examples for hydrosilylation: (e) Chen, C.; Hecht, M. B.; Kavara, A.; Brennessel, W. W.; Mercado, B. Q.; Weix, D. J.; Holland, P. L. *J. Am. Chem. Soc.* **2015**, 137, 13244-13247. (f) Chen, C.; Dugan, T., R.; Brennessel, W. W.; Weix, D. J.; Holland, P. L. *J. Am. Chem. Soc.* **2014**, 136, 945-955. (g) Teo, W. J.; Wang, C.; Tan, Y. W.; Ge, S. *Angew. Chem. Int. Ed.* **2017**, 56, 4328-4332. (h) Raya, B.; Biswas, S.; RajanBabu, T. V. *ACS Catal.* **2016**, 6, 6318-6323. Examples for hydroboration: (i) Zhang, L.; Zuo, Z.; Leng, X.; Huang, Z. *Angew. Chem.* **2014**, 126, 2734-2738. (j) Zhang, L.; Zuo, Z.; Wan, X.; Huang, Z. *J. Am. Chem. Soc.* **2014**, 136, 15501-15504. (k) Guo, J.; Cheng, B.; Shen, X.; Lu, Z. *J. Am. Chem. Soc.* **2017**, 139, 15316-15319.
15. Ibrahim, A. D.; Entsminger, S. W.; Fout, A. R. *ACS Catal.* **2017**, 7, 3730-3734.
16. Ben-Daat, H.; Rock, C. L.; Flores, M.; Groy, T. L.; Bowman, A. C.; Trovitch, R. J. *Chem. Commun.* **2017**, 53, 7333-7336.
17. (a) Werkmeister, S.; Junge, K.; Beller, M. *Org. Process Res. Dev.* **2014**, 18, 289-302. (b) Nishimura, S. *Handbook of Heterogeneous Catalytic Hydrogenation for Organic Synthesis*; Wiley-VCH: New York. 2001.
18. (a) Gribble, G. W. *Chem. Soc. Rev.* **1998**, 27, 395-404. (b) Seyden-Penne, J. *Reductions by Alumino and Borohydrides in Organic Synthesis*, 2nd ed.; Wiley-VCH: New York, 1997. (c) Lu, Z.; Williams, T. J. *Chem. Commun.* **2014**, 50, 5391-5393. (d) Haddenham, D.; Pasumansky, L.; DeSoto, J.; Eagon, S.; Singaram, B. *J. Org. Chem.* **2009**, 74, 1964-1970.
19. (a) Fleury-Brégeot, N.; Fuente, V.; de la Castellón, S.; Claver, C. *ChemCatChem* **2010**, 2, 1346-1371. (b) Nugent, T. C.; El-Shazly, M. *Adv. Synth. Catal.* **2010**, 352, 753-819. (c) Fabrello, A.; Bachelier, A.; Urrutigoity, M.; Kalck, P. *Coord. Chem. Rev.* **2010**, 254, 273-287. (d) Xie, J.-H.; Zhu, S.-F.; Zhou, Q.-L. *Chem. Rev.* **2011**, 111, 1713-1760. (e) Bartoszewicz, A.; Ahlsten, N.; Martín-Matute, B. *Chem. -Eur. J.* **2013**, 19, 7274-7302. (f) Tang, W.; Xiao, J. *Synthesis* **2014**, 46, 1297-1302.
20. Koren-Selfridge, L.; Londino, H. L.; Vellucci, J. K.; Simmons, B. J.; Casey, C. P.; Clark, T. B. *Organometallics* **2009**, 28, 2085-2090.
21. Arrowsmith, M.; Hill, M. S.; Kociok-Köhn, G. *Chem. Eur. J.* **2013**, 19, 2776-2783.
22. King, A. E.; Stieber, S. C. E.; Henson, N. J.; Kozimor, S. A.; Scott, B. L.; Smythe, N. C.; Sutton, A. D.; Gordon, J. C. *Eur. J. Inorg. Chem.* **2016**, 1635-1640.
23. (a) Yin, Q.; Soltani, Y.; Melen, R. L.; Oestreich, M. *Organometallics* **2017**, 36, 2381-2384. (b) Eisenberger, P.; Bailey, A. M.; Crudden, C. M. *J. Am. Chem. Soc.* **2012**, 134, 17384-17387.
24. Lin, Y.-C.; Hatzakis, E.; McCarthy, S. M.; Reichl, K. D.; Lai, T. Y.; Yennawar, H. P.; Radosevich, A. T. *J. Am. Chem. Soc.* **2017**, 139, 6008-6016.

25. Wu, J.; Zeng, H.; Cheng, J.; Zheng, S.; Golen, J. A.; Manke, D. R.; Zhang, G. *J. Org. Chem.* ASAP.
26. Ghosh, C.; Mukhopadhyay, T. K.; Flores, M.; Groy, T. L.; and Trovitch, R. J. *Inorg. Chem.* **2015**, *54*, 10398-10406.
27. Small, L. B.; Brookhart, M.; Bennett, A. M. A. *J. Am. Chem. Soc.* **1998**, *120*, 4049-4050.
28. Khusnutdinova, J. R.; Milstein, D. *Angew. Chem. Int. Ed.* **2015**, *54*, 12236-12273.
29. (a) Knijnenburg, Q.; Gambarotta, S.; Budzelaar, P. H. M. *Dalton Trans.* **2006**, 5442-5448. (b) Muresan, N.; Chlopek, K.; Weyhermüller, T.; Neese, F.; Wieghardt, K. *Inorg. Chem.* **2007**, *46*, 5327-5337.
30. (a) Lam, C. H.; L.-Li, S.; Zhang, Z.; Mak, T. C. W.; Lee, H. K. *Inorg. Chem.* **2001**, *40*, 4691-4695. (b) Yao, S.; Tam, D. Y. S.; Cheung, P. S.; Lam, C.-K.; Guo, P.; Lam, S. L.; Lee, H. K. *Dalton Trans.* **2015**, *44*, 17950-17959.
31. (a) Kleigrewe, N.; Steffen, W.; Blömker, T.; Kehr, Fröhlich, R.; Wibbeling, B.; Erker, G.; C.-Wasilke, J.; Wu, G.; Bazan, G. C. *J. Am. Chem. Soc.* **2005**, *127*, 13955-13968. (b) Bowman, A. C.; Milsmann, C.; Atienza, C. C. H.; Lobkovsky, E.; Wieghardt, K.; Chirik, P. J. *J. Am. Chem. Soc.* **2010**, *132*, 1676-1684.
32. (a) Zhang, L.; Zuo, Z.; Leng, X.; Huang, Z. *Angew. Chem., Int. Ed.* **2014**, *53*, 2696-2700. (b) Obligacion, J. V.; Chirik, P. J. *J. Am. Chem. Soc.* **2013**, *135*, 19107-19110.
33. (a) Gunanathan, C.; Hölscher, M.; Pan, F.; Leitner, W. *J. Am. Chem. Soc.* **2012**, *134*, 14349-14352. (b) Ohmura, T.; Yamamoto, Y.; Miyaura, N. *J. Am. Chem. Soc.* **2000**, *122*, 4990-4991.
34. Schaefer, B. A.; Margulieux, G., W.; Small, B. L.; Chirik, P. J. *Organometallics* **2015**, *34*, 1307-1320.
35. (a) Obligacion, J. V.; Semproni, Chirik, P. J. *J. Am. Chem. Soc.* **2014**, *136*, 4133-4136. (b) Obligacion, J. V.; Semproni, S. P.; Pappas, I.; Chirik, P. J. *J. Am. Chem. Soc.* **2016**, *138*, 10645-10653.
36. Wang, H.; Wang, C.; Huang, K.; Liu, L.; Chang, W.; Li, J. *Org. Lett.* **2016**, *18*, 2367-2370.

APPENDIX A
COPYRIGHT AND PERMISSIONS

Part of the chapter 1 has been taken from “Ghosh, C.; Groy, T. L.; Bowman, A. C.; Trovitch, R. J. *Chem. Commun.* **2016**, *52*, 4553-4556.”

Reproduced by permission of The Royal Society of Chemistry-
<http://pubs.rsc.org/en/content/articlelanding/2016/cc/c5cc09167e#!divAbstract>



Chandrani Ghosh <cghosh1@asu.edu>

Permission request for copyrights

2 messages

Chandrani Ghosh <cghosh1@asu.edu>
To: contracts-copyright@rsc.org

Sun, Jul 15, 2018 at 4:00 PM

Dear RSC Personnel,

This is Chandrani Ghosh and I am writing this to request permission to reuse one of my published articles in my Ph.D. thesis.

Here is the article that I published as a first author in Chemical Communication -
Ghosh, C.; Groy, T. L.; Bowman, A. C.; Trovitch, R. J. "Two-step C–H, C–P bond activation at an a-diimine iron dinitrogen complex" *Chem. Commun.* **2016**, *52*, 4553-4556.

I have carefully reviewed the copyright information on RSC journal website, but it will be helpful if you can guide me how to get the permission for reusing the article information in my thesis.

I really appreciate your time and consideration.

- Sincerely,
Chandrani Ghosh
6th year Graduate Student
Advisor: Prof. Ryan J. Trovitch
School of Molecular Science
Arizona State University
Tempe, AZ 85287

CONTRACTS-COPYRIGHT (shared) <Contracts-
Copyright@rsc.org>
To: Chandrani Ghosh <cghosh1@asu.edu>

Mon, Jul 16, 2018 at 5:01
AM

Dear Chandrani Ghosh,

Many thanks for sending the permissions request below. The Royal Society of Chemistry

(RSC) hereby grants permission for the use of your paper(s) specified below in the printed and microfilm version of your thesis. You may also make available the PDF version of your paper(s) that the RSC sent to the corresponding author(s) of your paper(s) upon publication of the paper(s) in the following ways: in your thesis via any website that your university may have for the deposition of theses, via your university's Intranet or via your own personal website. We are however unable to grant you permission to include the PDF version of the paper(s) on its own in your institutional repository. The Royal Society of Chemistry is a signatory to the STM Guidelines on Permissions (available on request).

Please note that if the material specified below or any part of it appears with credit or acknowledgement to a third party then you must also secure permission from that third party before reproducing that material.

Please ensure that the thesis states the following:

Reproduced by permission of The Royal Society of Chemistry

and include a link to the paper on the Royal Society of Chemistry's website.

Please ensure that your co-authors are aware that you are including the paper in your thesis.

Best wishes,

Chloe Szebrat
Contracts and Copyright Executive
Royal Society of Chemistry
Thomas Graham House
Science Park, Milton Road
Cambridge, CB4 0WF, UK
Tel: +44 (0) 1223 438329

www.rsc.org

From: Chandrani Ghosh <cghosh1@asu.edu>
Sent: 16 July 2018 00:01
To: CONTRACTS-COPYRIGHT (shared) <Contracts-Copyright@rsc.org>
Subject: Permission request for copyrights

[Quoted text hidden]

This communication is from The Royal Society of Chemistry, a company incorporated in England by Royal Charter (registered number RC000524) and a charity registered in England and Wales (charity number 207890). Registered office: Burlington House, Piccadilly, London W1J 0BA. Telephone: 0207 4378 6556, Facsimile: 0207 4490 3393 (Head Office). This communication (including any attachments) may contain confidential, privileged or copyright material. It may not be relied upon or disclosed to any person other than the intended recipient(s) without the consent of The Royal Society of Chemistry. If you are not the intended recipient(s), please (1) notify us immediately by replying to this email and delete all copies from your system and (2) note that disclosure, distribution, copying or use of this communication is strictly prohibited. Any advice given by The Royal Society of Chemistry has been carefully formulated but is necessarily based on the information available, and The Royal Society of Chemistry cannot be held responsible for accuracy or completeness. In this respect, any views or opinions presented in this email are solely those of the author and may not represent those of The Royal Society of Chemistry. The Royal Society of Chemistry owes no duty of care and shall not be liable for any resulting damage or loss as a result of the use of this email and/or attachments. The Royal Society of Chemistry acknowledges that a disclaimer cannot restrict liability at law for personal injury or death arising through a finding of negligence. The Royal Society of Chemistry does not warrant that its emails or attachments are Virus-free: Please rely on your own screening.

Part of the chapter 3 has been taken from (a) “Ghosh, C.; Mukhopadhyay, T. K.; Flores, M.; Groy, T. L.; Trovitch, R. J. *Inorg. Chem.* **2015**, *54*, 10398-10406.” (b) “Mukhopadhyay, T. K.; Ghosh, C.; Flores, M.; Groy, T. L.; Trovitch, *Organometallics* **2017**, *36*, 3477-3483.”

7/15/2018

Rightslink® by Copyright Clearance Center



RightsLink®

Home

Create Account

Help



Title: A Pentacoordinate Mn(II) Precatalyst That Exhibits Notable Aldehyde and Ketone Hydrosilylation Turnover Frequencies
Author: Chandrani Ghosh, Tufan K. Mukhopadhyay, Marco Flores, et al
Publication: Inorganic Chemistry
Publisher: American Chemical Society
Date: Nov 1, 2015
Copyright © 2015, American Chemical Society

LOGIN
If you're a copyright.com user, you can login to RightsLink using your copyright.com credentials.
Already a RightsLink user or want to [learn more?](#)

PERMISSION/LICENSE IS GRANTED FOR YOUR ORDER AT NO CHARGE

This type of permission/license, instead of the standard Terms & Conditions, is sent to you because no fee is being charged for your order. Please note the following:

- Permission is granted for your request in both print and electronic formats, and translations.
- If figures and/or tables were requested, they may be adapted or used in part.
- Please print this page for your records and send a copy of it to your publisher/graduate school.
- Appropriate credit for the requested material should be given as follows: "Reprinted (adapted) with permission from (COMPLETE REFERENCE CITATION). Copyright (YEAR) American Chemical Society." Insert appropriate information in place of the capitalized words.
- One-time permission is granted only for the use specified in your request. No additional uses are granted (such as derivative works or other editions). For any other uses, please submit a new request.

BACK

CLOSE WINDOW

Copyright © 2018 Copyright Clearance Center, Inc. All Rights Reserved. [Privacy statement](#). [Terms and Conditions](#).
Comments? We would like to hear from you. E-mail us at customercare@copyright.com

**RightsLink®**[Home](#)[Create Account](#)[Help](#)**ACS Publications**
Most Trusted. Most Cited. Most Read.**Title:** Hydrosilylation of Aldehydes and Formates Using a Dimeric Manganese Precatalyst**Author:** Tufan K. Mukhopadhyay, Chandrani Ghosh, Marco Flores, et al**Publication:** Organometallics**Publisher:** American Chemical Society**Date:** Sep 1, 2017

Copyright © 2017, American Chemical Society

LOGIN

If you're a **copyright.com** user, you can login to RightsLink using your copyright.com credentials. Already a **RightsLink** user or want to [learn more?](#)

PERMISSION/LICENSE IS GRANTED FOR YOUR ORDER AT NO CHARGE

This type of permission/license, instead of the standard Terms & Conditions, is sent to you because no fee is being charged for your order. Please note the following:

- Permission is granted for your request in both print and electronic formats, and translations.
- If figures and/or tables were requested, they may be adapted or used in part.
- Please print this page for your records and send a copy of it to your publisher/graduate school.
- Appropriate credit for the requested material should be given as follows: "Reprinted (adapted) with permission from (COMPLETE REFERENCE CITATION). Copyright (YEAR) American Chemical Society." Insert appropriate information in place of the capitalized words.
- One-time permission is granted only for the use specified in your request. No additional uses are granted (such as derivative works or other editions). For any other uses, please submit a new request.

[BACK](#)[CLOSE WINDOW](#)

Copyright © 2018 [Copyright Clearance Center, Inc.](#) All Rights Reserved. [Privacy statement](#). [Terms and Conditions](#). Comments? We would like to hear from you. E-mail us at customercare@copyright.com

BIOGRAPHICAL SKETCH

Chandrani Ghosh was born in Kolkata, which is the capital of West Bengal state in India. After schooling, she got admitted to Presidency College, under Calcutta University, which is one of the prestigious colleges in India. During her B.Sc., she was introduced to different aspects of chemistry and its applications. There she achieved her Bachelor's degree with honors in Chemistry with a First class. Then she went to IIT Madras after qualifying the entrance examination (JAM), for her Masters' degree. She was awarded for merit scholarship being a top 10 students. During her one-year Masters' project in organic chemistry, she worked on the synthesis of 1-aryl tetrahydroisoquinoline using Weinreb amide building blocks while she gathered knowledge on synthetic chemistry and characterization techniques. From then, she nurtured herself to pursue her future career as a research chemist. Her dream came true when she got the chance to do research at Arizona State University, USA. She joined as a Ph.D. student in an organometallic chemistry research lab under the supervision of Prof. Ryan J. Trovitch. During her tenure of doctoral research, she gained extensive knowledge in inorganic and organometallic chemistry concepts, synthesis, handling air-sensitive compounds, catalysis, and various characterization techniques. She mainly worked on the development of homogeneous first row metal complexes (Fe, Co, Mn) and their applications in bond activation, carbonyl hydrosilylation, and nitrile hydroboration. Besides, she has also sharpened her presentation and communication skills. She was fortunate to teach different undergraduate level organic lab courses, which allowed to improve her teaching skills. With all these, she aspires to apply her acquired knowledge in her future career as a postdoctoral fellow, while learning new concepts and skills.